SECRET

UNCLASSIFIED

ORNL-2422 (Del.)

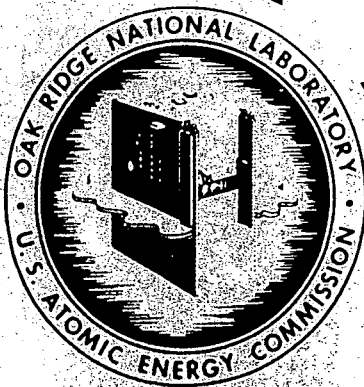C-84 – Reactors–Special Features
of Aircraft Reactors
M-3679 (20th ed. Rev.)

AEC RESEARCH AND DEVELOPMENT REPORT

METALLURGY DIVISION

ANNUAL PROGRESS REPORT

FOR PERIOD ENDING OCTOBER 10, 1957

OAK RIDGE NATIONAL LABORATORY
OPERATED BY
UNION CARBIDE NUCLEAR COMPANY
Division of Union Carbide Corporation

UCC

POST OFFICE BOX X · OAK RIDGE, TENNESSEE

UNCLASSIFIED

ORNL-2422
C-84 — Reactors—Special Features
of Aircraft Reactors
M-3679 (20th ed. Rev.)

This document consists of 263 pages.

Copy 278 of 303 copies. Series A.

Contract No. W-7405-eng-26

METALLURGY DIVISION

ANNUAL PROGRESS REPORT

for Period Ending October 10, 1957

J. H. Frye, Jr., Director
W. D. Manly, Associate Director
J. E. Cunningham, Assistant Director

DATE ISSUED

DEC 13 1957

Reports previously issued in this series are as follows:

ORNL-28	Period Ending March 1, 1948
ORNL-69	Period Ending May 31, 1948
ORNL-407	Period Ending July 31, 1949
ORNL-511	Period Ending October 31, 1949
ORNL-583	Period Ending January 31, 1950
ORNL-754	Period Ending April 30, 1950
ORNL-827	Period Ending July 31, 1950
ORNL-910	Period Ending October 31, 1950
ORNL-987	Period Ending January 31, 1951
ORNL-1033	Period Ending April 30, 1951
ORNL-1108	Period Ending July 31, 1951
ORNL-1161	Period Ending October 31, 1951
ORNL-1267	Period Ending January 31, 1952
ORNL-1302	Period Ending April 30, 1952
ORNL-1366	Period Ending July 31, 1952
ORNL-1437	Period Ending October 31, 1952
ORNL-1503	Period Ending January 31, 1953
ORNL-1551	Period Ending April 10, 1953
ORNL-1625	Period Ending October 10, 1953
ORNL-1727	Period Ending April 10, 1954
ORNL-1875	Period Ending October 10, 1954
ORNL-1911	Period Ending April 10, 1955
ORNL-1988	Period Ending October 10, 1955
ORNL-2080	Period Ending April 10, 1956
ORNL-2217	Period Ending October 10, 1956

ORNL-2422
C-84 – Reactors–Special Features
of Aircraft Reactors
M-3679 (20th ed. Rev.)

INTERNAL DISTRIBUTION

1. G. M. Adamson, Jr.
2. S. E. Beall
3. R. J. Beaver
4. D. S. Billington
5. F. F. Blankenship
6. E. P. Blizard
7. E. G. Bohlmann
8. E. S. Bomar
9. G. E. Boyd
10. M. A. Bredig
11. R. B. Briggs
12. F. R. Bruce
13. W. D. Burch
14. D. W. Cardwell
15. C. E. Center (K-25)
16. R. A. Charpie
17. R. D. Cheverton
18. R. E. Clausing
19. J. H. Coobs
20. E. L. Compere
21. F. L. Culler
22. J. S. Culver
23. J. E. Cunningham
24. J. H. DeVan
25. R. R. Dickison
26. L. M. Doney
27. D. A. Douglas, Jr.
28. W. K. Eister
29. L. B. Emlet (K-25)
30. D. E. Ferguson
31. E. Franco-Ferreria
32. J. H. Frye, Jr.
33. C. H. Gabbard
34. W. R. Gall
35. R. J. Gray
36. J. C. Griess
37. W. R. Grimes
38. E. Guth
39. J. P. Hammond
40. P. H. Harley
41. C. S. Harrill
42. P. N. Haubenreich
43. R. L. Heestand
44. T. Hikido
45. J. W. Hill
46. M. R. Hill

47. E. E. Hoffman
48. A. Hollaender
49. A. S. Householder
50. H. Inouye
51. G. H. Jenks
52. L. K. Jetter
53. W. H. Jordan
54. S. I. Kaplan
55. P. R. Kasten
56. C. P. Keim
57. T. M. Kegley, Jr.
58. M. T. Kelley
59. R. B. Korsmeyer
60. K. A. Kraus
61. J. A. Lane
62. C. F. Leitten
63. W. J. Leonard
64. R. E. Leuze
65. S. C. Lind
66. R. B. Lindauer
67. R. S. Livingston
68. M. I. Lundin
69. R. N. Lyon
70. H. G. MacPherson
71. F. C. Maienschein
72. W. D. Manly
73. J. P. McBride
74. H. F. McDuffie
75. C. J. McHargue
76. R. A. McNees
77. R. P. Milford
78. A. J. Miller
79. E. C. Miller
80. K. Z. Morgan
81. E. J. Murphy
82. J. P. Murray (Y-12)
83. M. L. Nelson
84. E. O. Nurmi
85. R. B. Oliver
86. W. W. Parkinson
87. L. F. Parsly
88. P. Patriarca
89. A. M. Perry
90. D. Phillips
91. M. L. Picklesimer
92. J. J. Prislinger

EXTERNAL DISTRIBUTION

SECRET

CONTENTS

HIGH-TEMPERATURE METALLURGY

SECRET

HRP METALLURGY

APPLIED METALLURGY

FUNDAMENTAL METALLURGY

METALLURGY DIVISION
AT
THE OAK RIDGE NATIONAL LABORATORY

JULY 1, 1957

DIRECTOR — J. H. FRYE, JR.
B. BYRUM, SEC.
ASSOCIATE DIRECTOR — W. D. MANLY*
J. MORRISON,* SEC.
ASSISTANT DIRECTOR — J. E. CUNNINGHAM*
M. WHITE,* SEC.

ADMINISTRATIVE ASSISTANT
L. E. BANKER*
M. BOLINGER, SEC.

FUNDAMENTAL METALLURGY

PHYSICO-METALLURGICAL RESEARCH
L. K. JETTER
B. BALLARD,* SEC.

STRUCTURE OF METALS
C. J. McHARGUE
J. C. OGLE

THEORY OF ALLOYING
J. O. BETTERTON, JR.
G. D. KNEIP, JR.
D. S. EASTON
E. B. NUNN (CO-OP)
J. O. SCARBROUGH
D. O. WELCH (CO-OP)

X-RAY DIFFRACTION
H. L. YAKEL, JR.
B. BALLARD,* SEC.
R. M. STEELE
J. C. RICHTER

HRP METALLURGY
G. M. ADAMSON
F. LOVING,*¹ SEC.

ENGINEERING
E. S. BOMAR
F. W. COOK
W. J. LEONARD
J. J. PRISLINGER
C. M. SMITH, JR.
J. J. WOODHOUSE, JR.

RESEARCH
M. L. PICKLESIMER
M. BOND,* SEC.
P. L. RITTENHOUSE
R. L. STEPHENSON
P. J. JONES
G. C. NELSON
M. A. WHEELER

ADMINISTRATION
L. E. BANKER*

PROCUREMENT
R. J. STEERE
B. BOTHWELL
R. P. BAYNE
C. E. DUNN

BUDGET ANALYST
R. G. CARDWELL

TIMEKEEPING
O. POE*

HIGH-TEMPERATURE METALLURGY
W. D. MANLY*
J. MORRISON,* SEC.
T. HIKIDO, USAF

METALLURGY REPORTS OFFICE
W. R. HILL
W. DIXON
F. FINN
L. PYATT

GENERAL CORROSION
E. E. HOFFMAN
D. POE,* SEC.
W. H. COOK
D. H. JANSEN
D. L. GRIFFITH
J. W. HENDRICKS
J. L. POPE
L. R. TROTTER

DYNAMIC CORROSION
J. H. DEVAN
E. Q. TAYLOR,* SEC.
J. R. DiSTEFANO
G. D. BRADY
E. J. LAWRENCE
M. A. REDDEN

HIGH-TEMPERATURE REACTIONS
G. P. SMITH, JR.
M. BOND,* SEC.
C. R. BOSTON
J. V. CATHCART
J. J. McBRIDE
G. F. PETERSEN
J. J. CAMPBELL
J. E. EPPERSON
W. M. EWING

NONDESTRUCTIVE TEST DEVELOPMENT
R. B. OLIVER
M. BOND,* SEC.
J. W. ALLEN
R. W. McCLUNG
R. A. NANCE
J. K. WHITE²
D. H. BOWMAN³
W. O. CARDEN³
O. E. CONNER
R. A. CUNNINGHAM, JR.
W. J. MASON
W. A. POSTON³
A. C. SMITH³
B. J. YOUNG³

INSPECTION
A. TABOADA
E. Q. TAYLOR,* SEC.
R. L. HEESTAND
G. M. TOLSON
R. H. EVANS
E. A. NICHOLS²
J. B. PHILLIPS

FABRICATION
J. H. COOBS
B. BALLARD,* SEC.
D. O. HOBSON
H. INOUYE
R. E. McDONALD (PWA)
T. K. ROCHE
J. L. COOK (CO-OP)
W. R. JOHNSON
J. F. NEWSOME
J. E. SPRUIELL (CO-OP)

WELDING AND BRAZING
P. PATRIARCA
M. BOND,* SEC.
R. E. CLAUSING
G. M. SLAUGHTER
B. McDOWELL
R. G. SHOOSTER
C. E. SHUBERT
C. C. WILLIAMS

CPR METALLURGY
E. A. FRANCO-FERREIRA

CHEM. TECH. COORDINATOR
A. E. GOLDMAN

MECHANICAL PROPERTIES
D. A. DOUGLAS, JR.
J. MORRISON,* SEC.
C. R. KENNEDY (PWA)
R. W. SWINDEMAN
J. W. WOODS
F. L. BEELER
R. W. BOLING
E. BOLLING
J. T. EAST
J. D. HUDSON
V. G. LANE
B. McNABB, JR.
E. B. PATTON, JR.
C. W. WALKER

SERVICE LABORATORY
C. W. DOLLINS
C. K. THOMAS

FUNDAMENTAL LIQUID-METAL MASS TRANSFER
J. L. SCOTT
B. BALLARD,* SEC.
J. W. BARNETT

PROCESS METALLURGY
R. J. BEAVER
M. WHITE,* SEC.
L. L. HALL

METAL FABRICATION
J. H. ERWIN*
G. D. GOLDSTON
T. W. COFFEY

FUEL ELEMENT FABRICATION
J. H. ERWIN*
G. H. CALLAWAY
N. H. FLICKINGER
J. H. NIX
C. M. HOLLAND
W. W. PROAPS
H. J. WALLACE

ALLOY PREPARATION
W. C. THURBER
G. E. ANGEL
J. B. FLYNN
C. QUEENER

FUEL ELEMENT DEVELOPMENT
C. F. LEITTEN
W. J. KUCERA
J. W. GEER
C. HAMBY
E. R. TURNBILL

METALLURGICAL MATERIALS AND PROCESSING
R. C. WAUGH
M. WHITE,* SEC.
B. ADAMS
D. T. BOURGETTE
J. H. CHERUBINI
J. I. FEDERER
T. S. LUNDY
R. A. PADGETT, JR.
J. H. TERRY

APPLIED METALLURGY
J. E. CUNNINGHAM*
M. WHITE,* SEC.

LONG RANGE PLANNING
J. P. HAMMOND
M. WHITE,* SEC.

CERAMICS RESEARCH
L. M. DONEY
A. HOBBS, SEC.

GENERAL CERAMICS
C. E. CURTIS
S. D. FULKERSON
F. P. JEFFERS

FUNDAMENTAL CERAMICS RESEARCH
A. G. THARP

FUEL ELEMENT DEVELOPMENT
A. J. TAYLOR
R. L. HAMNER

ANP MATERIALS
L. A. HARRIS
R. A. POTTER
G. D. WHITE
J. A. GRIFFIN

WASTE DISPOSAL
M. P. HAYDON
J. M. KERR

METALLOGRAPHY
R. J. GRAY
W. SHOCKLEY, SEC.
R. S. CROUSE
E. L. LONG, JR.

X-10 LABORATORY
W. H. BRIDGES
J. R. RIDDLE
J. E. VAN-CLEVE, JR.
M. D. ALLEN
L. A. AMBURN, JR.
M. W. ATCHLEY
R. A. BOWMAN
W. E. DENNY
C. K. H. DuBOSE
W. H. FARMER
R. L. FITZGERALD
J. C. GOWER
E. P. GRIGGS
T. J. HENSON
J. T. HOUSTON
E. H. LEE
B. C. LESLIE
C. D. MATHES
C. E. ZACHARY

Y-12 LABORATORY
T. M. KEGLEY, JR
D. F. STONEBURNER
W. J. WERNER
E. R. BOYD
B. F. DAY
B. J. REECE
L. G. SHRADER

*MULTIPLE LISTING
¹ON LOAN FROM REED
²ON LOAN FROM HRP METALLURGY
³ON LOAN FROM INSPECTION ENGINEERING

PUBLICATIONS

E. E. Hoffman, P. Patriarca, C. F. Leitten, Jr., and G. M. Slaughter, *An Evaluation of the Corrosion and Oxidation Resistance of High-Temperature Brazing Alloys*, ORNL-1934 (Oct. 23, 1956).

G. P. Smith and E. E. Hoffman, *The Action of Sodium Hydroxide Melts on Alloys of Nickel, Molybdenum, and Iron at 815°C*, ORNL-2131 (May 2, 1957).

H. Insley, T. N. McVay, R. E. Thoma, and G. D. White, *Optical Properties and X-ray Diffraction Data for Some Inorganic Fluoride and Chloride Compounds*, ORNL-2192 (May 3, 1957).

H. Inouye, *High-Thermal-Conductivity Fin Material for Radiators*, ORNL-2065 (Jan. 2, 1957).

R. B. Oliver, R. W. McClung, and J. K. White, *Immersed Ultrasonic Inspection of Pipe and Tubing*, ORNL-2254 (May 2, 1957); *J. Soc. Nondestructive Testing* 15, 140–144 (1957). Paper presented before the 16th Annual Convention of the Nondestructive Testing Society, Cleveland, Ohio, Oct. 11, 1956.

G. P. Smith, M. E. Steidlitz, and E. E. Hoffman, *Two-Phase Product Formed in the Reaction Between Fused Sodium Hydroxide and Inconel*, ORNL-2129 (March 11, 1957).

J. W. Allen and R. B. Oliver, *Inspection of Small Diameter Tubing by Eddy-Current Methods*, ORNL-2253 (May 2, 1957); *J. Soc. Nondestructive Testing* 15, 104–109 (1957). Paper presented before the 16th Annual Convention of the Nondestructive Testing Society, Cleveland, Ohio, Oct. 11, 1956.

E. E. Hoffman and W. D. Manly, *Corrosion Resistance of Metals and Alloys to Sodium and Lithium*, ORNL-2271 (March 19, 1957); "Handling and Uses of the Alkali Metals," *Advances in Chem. Ser.* 19, 82–91 (1957). Paper presented before the American Corrosion Society, Dallas, April 11, 1956.

P. Patriarca, G. M. Slaughter, and W. D. Manly, *Electroless-Plated Brazing Alloys*, ORNL-2243 (May 2, 1957).

G. P. Smith and E. E. Hoffman, *Corrosion Products Formed in the Reaction Between Fused Sodium Hydroxide and Iron-Rich Alloys of Iron, Chromium, and Nickel*, ORNL-2156 (April 26, 1957).

M. L. Picklesimer, *Anodizing as a Metallographic Technique for Zirconium Base Alloys*, ORNL-2296 (April 26, 1957).

J. R. Weir, Jr., D. A. Douglas, and W. D. Manly, *Inconel as a Structural Material for a High-Temperature Fused-Salt Reactor*, ORNL-2264 (June 4, 1957).

R. J. Beaver, R. C. Waugh, and C. F. Leitten, *Specifications for Army Power Package Reactor (APPR-1) Fuel and Control Rod Components*, ORNL-2225 (July 24, 1957).

J. L. Scott, *A Calorimetric Investigation of Zirconium, Titanium, and Zirconium Alloys from 60 to 960°C*, ORNL-2328 (July 24, 1957).

R. E. Clausing, P. Patriarca, and W. D. Manly, *Aging Characteristics of Hastelloy B*, ORNL-2314 (July 30, 1957).

J. O. Betterton, Jr., J. H. Frye, Jr., and D. S. Easton, *Phase Diagram of Zirconium with Silver, Indium, and Antimony*, ORNL-2344 (Aug. 12, 1957).

J. P. Page, *The Annealing Behavior of Cold-Rolled Niobium*, ORNL-2372 (Sept. 19, 1957).

W. D. Manly, G. M. Adamson, Jr., J. H. Coobs, J. H. DeVan, D. A. Douglas, E. E. Hoffman, and P. Patriarca, *Aircraft Reactor Experiment — Metallurgical Aspects*, ORNL-2349 (Sept. 17, 1957) (Secret).

W. C. Thurber, J. A. Milko, and R. J. Beaver, *Boron-Aluminum and Boron-Uranium-Aluminum Alloys for Reactor Application,* ORNL-2149 (Sept. 26, 1957).

R. J. Beaver, R. C. Waugh, C. F. Leitten, Jr., and W. R. Burt, Jr., *Investigation of the Factors Affecting Sensitization of Army Package Power Reactor (APPR-1) Fuel Elements,* ORNL-2312 (Sept. 18, 1957).

G. D. Kneip, Jr., and J. O. Betterton, Jr., "Floating Zone Purification of Zirconium," *J. Electrochem. Soc.* **103,** 12, 684–689, (1956).

C. E. Curtis and J. R. Johnson, "Properties of Thorium Oxide Ceramics," *J. Am. Ceram. Soc.* **40,** 63–68 (1957).

L. K. Jetter and C. J. McHargue, "Preferred Orientation in Extruded Uranium Rod," *J. Metals* **9,** 291 (1957); *Trans. Am. Inst. Mining Met. Engrs.* **209,** 291 (1957).

C. E. Curtis and J. R. Johnson, "Ceramic Properties of Samarium Oxide and Gadolinium Oxide; X-ray Studies of Other Rare Earth Oxides and Some Compounds," *J. Am. Ceram. Soc.* **40,** 15–19 (1957).

J. R. Johnson, S. D. Fulkerson, and A. J. Taylor, "Technology of Uranium Dioxide, A Reactor Material," *Am. Ceram. Soc. Bull.* **36,** 112–117 (1957).

J. V. Cathcart, L. L. Hall, and G. P. Smith, "The Oxidation Characteristics of the Alkali Metals – I. The Oxidation Rate of Sodium Between 79 and 48°C," *Acta Met.* **5,** 245–248 (1957).

G. M. Slaughter, C. F. Leitten, Jr., P. Patriarca, E. E. Hoffman, and W. D. Manly, "Sodium Corrosion and Oxidation Resistance of High-Temperature Brazing Alloys," *Welding J. (N.Y.)* **36,** 217s–225s (1957).

J. H. Frye, Jr., J. L. Scott, and J. W. Woods, "Effect of Strain and Temperature on the Yielding of Copper and Nickel," *J. Metals* **9,** 708 (1957); *Trans. Am. Inst. Mining Met. Engrs.* **209,** 708 (1957).

C. E. Curtis, "Properties of Yttrium Oxide," *J. Am. Ceram. Soc.* **40,** 274–278 (1957).

G. P. Smith, M. E. Steidlitz, and E. E. Hoffman, "Corrosion and Metal Transport in Fused Sodium Hydroxide. Part 1—Experimental Procedures," *Corrosion* **13,** 561t–564t (1957); "Corrosion and Metal Transport in Fused Sodium Hydroxide. Part 2—Corrosion of Nickel-Molybdenum-Iron Alloys," *Corrosion* **13,** 627t–630t (1957).

E. E. Hoffman and W. D. Manly, "Comparison of Sodium, Lithium, and Lead as Heat Transfer Media from a Corrosion Standpoint," in *Problems in Nuclear Engineering,* vol 1, p 128 (ed. by D. J. Hughes, S. McLain, and C. Williams), Pergamon Press, New York, 1957.

R. B. Oliver, "Recommendations for Technical Development and Standardization," *J. Soc. Nondestructive Testing* **15,** 294–297 (1957).

A. G. Tharp, "Some Uses of Thermodynamics in Ceramics," *Ceramic Information Meeting Held at Oak Ridge National Laboratory on October 1, 2, and 3, 1956,* TID-7530 (Pt. 1) p 38–45 (April 1957).

W. J. Leonard and J. C. Thompson, Jr., "Peripheral Welding of Internally-Clad Steel for Nuclear Reactor Application," *Welding J. (N.Y.)* **36,** 243–251 (1957).

E. G. Bohlman and G. M. Adamson, "Stress-Corrosion Cracking Problems in the Homogeneous Reactor Test," Paper No. 57-NESC-111, *2nd Nuclear Engineering and Science Conference,* March 11–14, 1957, Pergamon Press, New York, 1957.

The following papers were published in *Metallurgy Information Meeting, Ames Laboratory, Iowa State College, May 2, 3, and 4, 1956:*

W. C. Thurber, J. A. Milko, and R. J. Beaver, "Aluminum-Boron and Aluminum-Uranium-Boron Alloys for Improved Reactor Performance," TID-7526 (Pt. 1) p 116–128 (Feb. 1957).

L. K. Jetter and C. J. McHargue, "Preferred Orientation in Extruded Thorium Rod," TID-7526 (Pt. 1) p 150–164 (Feb. 1957).

M. L. Picklesimer and G. M. Adamson, Jr., "Morphology of Zircaloy-2," TID-7526 (Pt. 1) p 165–185 (Feb. 1957).

G. B. Wadsworth, M. L. Picklesimer, and G. M. Adamson, Jr., "The Microstructural Appearance and Identification of Hydrides in Zirconium and Zircaloy-2 Hydrogen Alloys," TID-7526 (Pt. 1) p 186–208 (Feb. 1957).

J. W. Allen and R. B. Oliver, "Inspection of Small Diameter Tubing by Eddy-Current Methods," TID-7526 (Pt. 1) p 209–226 (Feb. 1957).

R. B. Oliver and R. W. McClung, "Application of the Immersed Ultrasonic Technique for the Inspection of Small Diameter Tubes," TID-7526 (Pt. 1) p 227–243 (Feb. 1957).

E. E. Hoffman and L. R. Trotter, "Corrosion and Mass Transfer by Lithium at Elevated Temperatures," TID-7526 (Pt. 1) p 244–267 (Feb. 1957).

R. C. Waugh and J. E. Cunningham, "The Application of Low-Enrichment Uranium Dioxide to Aluminum Plate-Type Fuel Elements," TID-7526 (Pt. 2a) p 28–41 (March 1957).

H. Inouye and J. P. Page, "Clad Niobium," TID-7526 (Pt. 2b) p 368–383 (March 1957).

M. R. D'Amore and H. Inouye, "The Extrusion of Composite Tubes," TID-7526 (Pt. 2b) p 384–401 (March 1957).

H. Inouye, M. R. D'Amore, and T. K. Roche, "Nickel-Base Alloys for High-Temperature Service," TID-7526 (Pt. 3) p 133–154 (Feb. 1957).

G. M. Slaughter, C. F. Leitten, P. Patriarca, E. E. Hoffman, and W. D. Manly, "Sodium Corrosion and Oxidation Resistance of High-Temperature Brazing Alloys," TID-7526 (Pt. 3) p 273–305 (Feb. 1957).

H. Inouye, "High-Conductivity Fin Material for Heat Exchangers," TID-7526 (Pt. 5) p 58–75 (Feb. 1957).

R. J. Beaver, J. E. Cunningham, and M. J. Feldman, "Radiation Damage to Solid Fuel Elements. The Effect of Particle Size on the Mechanical Behavior of Irradiated Stainless Steel Uranium Dioxide Fuel Elements," TID-7526 (Pt. 6) (Feb. 1957).

METALLURGY DIVISION ANNUAL PROGRESS REPORT

SUMMARY

HIGH-TEMPERATURE METALLURGY

General Corrosion

Corrosion tests, in several high-temperature baths, of Inconel specimens joined by various welding and brazing techniques are discussed. Results of tests on various refractory metals, cermets, and ceramic specimens in fused-salt and liquid-metal media are included. Interactions between metal couples such as Inconel-beryllium and molybdenum-beryllium have been studied. The progress made in the study of corrosion by lithium in various systems is outlined. Lithium purification by vacuum distillation has been investigated. Casting and fabrication techniques on a new lead-lithium shielding alloy have been developed. Corrosion tests of several metals in contact with boiling rubidium are discussed.

Dynamic Corrosion

Studies have been made in order to determine the effects of operating time, flow rate, and temperature drop on the corrosion of Inconel forced-circulation loops by the fuel mixture (No. 30) $NaF-ZrF_4-UF_4$ (50-46-4 mole %). A comparison of several loops which operated for various test durations at 1600°F showed a rapid increase in attack within the first 15 hr, followed by a gradual increase in attack at a constant rate of 1 mil per 280 hr. Flow rate appeared to have no effect on attack in Inconel—fuel No. 30 systems. A variation in the loop temperature gradient, however, was seen to increase attack as the gradient increased above 200°F, but did not appreciably decrease attack as the gradient was lowered below 200°F.

An Inconel pump loop which operated for 1000 hr with fuel No. 30 at a maximum fluid temperature of 1700°F was attacked to a depth of 9 mils, with some deposits occurring in the cold-leg sections. Attack in this loop was approximately 4 to 5 mils greater than has been observed in loops operated at 1500°F.

Unusually deep intergranular voids resulted from the circulation of fuel No. 30 in an Inconel pump loop in which the hot-leg sections had been grain-coarsened prior to the test. The loop was operated for 1000 hr at a maximum temperature of 1600°F and was attacked to a depth of 12 mils. A test of the fuel mixture (No. 70) $NaF-ZrF_4-UF_4$ (56-39-5 mole %) was conducted in an Inconel pump loop operated at 1510°F. Attack in this loop after 716 hr was similar in appearance and depth to that experienced in fuel No. 30 systems under comparable test conditions. However, a thin metallic layer, which is normally not found in fuel No. 30 loops, was present in the cold leg of the fuel No. 70 loop.

Three Hastelloy B pump loops which circulated the fluoride mixture (No. 107) $NaF-LiF-KF-UF_4$ (11.2-45.3-41.0-2.5 mole %) were examined after operation at 1650°F. Two of the loops, which operated with a 1750°F maximum wall temperature, showed no evidence of mass transfer after 407 and 1000 hr, respectively. The third loop, which operated with a 1710°F maximum temperature and a relatively low flow rate, showed slight evidence of deposits throughout the pump. The hot legs of all loops were found to be badly pitted after test, but much of the surface roughness could be attributed to the condition of the inside surfaces of the tubing before test.

A nickel-molybdenum alloy forced-circulation loop, composed of 17% Mo, 6% Fe, bal Ni, completed 1000 hr of operation with fuel No. 107 at a maximum temperature of 1760°F. Hot-leg sections of the loop revealed intergranular attack to a maximum depth of 4 mils. Metal deposits were present in cold-leg sections of the loop, and analysis indicated that they contained sizable quantities of nickel and iron.

Two Inconel-sodium pump loops, which operated at flow rates of 1.5 and 3.0 gpm, were examined after 1000 hr at 1500°F. The temperature difference between hot- and cold-leg sections was 300°F in both loops. Operation of the loops produced

a deposit weight of 14 g at the higher flow rate, compared with 10.4 g at the lower flow rate. The average thickness of the deposits was also higher at the higher flow rate.

A series of Inconel forced-circulation loops was also operated with sodium in order to evaluate the effectiveness of certain oxide formers added to sodium for inhibiting mass transfer. All loops were operated at 1500°F with a 300°F temperature drop. A loop to which magnesium chips were added showed no differences in the amount of mass transfer, as compared with a normal sodium loop. A zirconium hot-leg insert, which was operated in a standard Inconel pump loop, reduced the amount of mass-transfer deposit slightly, as compared with a normal Inconel pump loop. A titanium insert, employed in a manner identical with that for the zirconium insert, produced no apparent effect on mass transfer.

The rate of mass transfer in Inconel pump loops operated for 1000 hr with sodium was found to vary linearly with temperature drop between hot- and cold-leg sections. The composition of metal deposits resulting from mass transfer was not affected by changes in temperature drop.

An experiment to evaluate the flow resistance resulting from mass transfer at 1250°F was carried out in an Inconel forced-circulation loop. Although it was necessary to increase the pump speed in order to maintain a constant flow rate during operation of this loop, no change was observed in pressure-measuring devices placed across the heater and the cooler. However, upon examination of the loop after 1508 hr of operation, some evidence of deposit was found in the cold-leg sections of the loop. A bend immediately ahead of the heater also showed deposits and may have interfered with the pressure-drop readings obtained.

An Inconel forced-circulation loop was operated with sodium for 2000 hr in order to evaluate the rate of mass transfer of Inconel by sodium over a relatively long-time period. The maximum sodium temperature in the loop was 1500°F, and a 300°F temperature drop was maintained between hot- and cold-leg sections. Deposit weight in this loop was approximately one and one-half times that normally observed in 1000-hr loops and three times that of 500-hr loops.

An evaluation was made of the effect of cold-trap operation on the removal of oxide impurities and its resultant effect on mass transfer in Inconel-NaK forced-circulation loops. Cold traps, maintained at temperatures of 100, 300, 600, and 800°F, respectively, were utilized in conjunction with pump loops operating at a maximum NaK temperature of 1500°F and a 300°F fluid temperature drop. A noticeable increase in the amount of mass transfer was observed in the test in which an 800°F cold-trap temperature was employed, as compared with a test having a 600°F cold-trap temperature; however, a smaller change in the amount of deposit was noted between the latter test and tests operated at lower cold-trap temperatures. The average size of particles comprising the deposits also varied with cold-trap temperature, becoming coarser as the cold-trap temperature increased. These Inconel-NaK tests reveal that the weight of deposits is less than one-half those of Inconel-sodium tests operated under similar temperature and time conditions.

Long-duration tests of Inconel were made in both NaK and sodium loops operating at a maximum fluid temperature of 1500°F. Tests in NaK, which utilized a temperature gradient of 600°F, were terminated after 2760 hr. The cooler of this loop, upon examination, was found to contain extensive crystalline deposits ranging to 14 mils in thickness. A loop which operated with sodium for 4000 hr with a temperature gradient of 800°F revealed considerably more deposits, reaching a thickness of 50 mils in some areas.

Forced-circulation loop tests of both types 347 and 304 stainless steel were completed with sodium at a maximum temperature of 1500°F and a temperature drop of 300°F. Visual examination of the loops revealed only slight traces of mass-transfer particles in the cold-leg sections. The hot leg of the loop revealed slight surface pitting and void formation to 2 mils.

An Incoloy (34% Ni, 20% Cr, bal Fe) pump loop was operated for 1000 hr with sodium at a maximum fluid temperature of 1500°F. Mass-transfer deposits and maximum hot-leg attack were similar to those observed in the Inconel loop. The deposits, in contrast with Inconel loops, did not adhere to the loop wall.

A series of Inconel thermal convection loops was operated for 500 hr with special fluoride mixtures at 1500°F. Results from loops containing the salt mixture NaF-ThF_4 (74-26 mole %) indicated attacks from 4 to 6 mils. The addition of

2 mole % UF_4 to this mixture increased the depth of attack to 12 to 15 mils. An attack of 12 mils resulted from the operation of the salt mixture LiF-BeF_2-UF_4-ThF_4 (71-16-1-12 mole %). Results of tests with fluoride mixtures of BeF_2 complexed with LiF and/or NaF indicated that attack decreased as the ratio of BeF_2 to alkali-metal constituents decreased. Mixtures of these salts containing 3 mole % UF_4 resulted in attacks to depths 3 to 6 mils greater than those in the counterpart mixture without uranium. In the uranium-bearing salts, attack again was decreased by decreasing the ratio of BeF_2 to LiF and/or NaF. Metallic layers were observed along the cold-leg regions of all loops operated with uranium-bearing mixtures of these salts.

A study was made in order to compare the rate of void migration in Inconel thermal convection loops with the rate of chromium removal by fuel No. 30 in such loops. Results from loops operated at 1500°F showed that the migration of voids into Inconel is rate-limited by the rate of chromium removal in the corrosion process. Corrosion studies of Inconel castings were continued in thermal convection loops. Various casting compositions, differing in the amounts of Si, Nb, Mn, and C additions, were evaluated in both fuel No. 30 and in sodium. No difference was found in the attack experienced in these castings, compared with wrought Inconel sections of the loops.

Three stainless-steel-clad niobium loops revealed only slight hot-leg attack in tests with fuel No. 107 at 1500°F. However, some cold-leg deposits were observed in niobium loops which operated for 1000 hr or longer. A niobium loop was also operated for 1000 hr with sodium at 1500°F and was found to have negligible attack. Cold-leg deposits containing Fe, Ni, and Cr, as well as Nb, were observed in the loop and indicated that the loop had leaked to the cladding.

The corrosion resistance of Hastelloy B in sodium was also evaluated by means of forced-circulation loops operated at 1300 and 1500°F. At the lower temperature, mass-transfer deposits were relatively slight, comparing in amount to those in Inconel loops operated under similar conditions. At 1500°F, metallic crystals, composed principally of nickel, were deposited in cold-leg sections at a rate which was slightly higher than in Inconel loops after 1000 hr and which was comparable with Inconel loops after 2000 hr.

A Hastelloy W pump loop in which sodium was circulated at a maximum temperature of 1500°F was examined after 1000 hr of operation. Mass-transfer deposits found in this loop were approximately 17% greater by weight than the weight of deposits observed in a Hastelloy B loop under similar conditions. The deposits contained 97% Ni and 3% Cr by analysis. Attack occurred to a depth of $1\frac{1}{2}$ mils along hot-leg sections of the loop.

Thermal convection loops fabricated from various experimental nickel-molybdenum alloys were tested in fuel No. 107 for 1000 and for 500 hr. All tests were conducted at 1500°F. Fluoride attack averaged $1\frac{1}{2}$ mils in all loops except those constructed of alloys containing aluminum, tungsten, or vanadium additions. In the latter alloys, attacks were in the range of 2 to $4\frac{1}{2}$ mils. Chromium in amounts up to 10% in these alloys and niobium in amounts up to 5% had little effect on the depth of attack, although their presence as corrosion products in the fuel increased as their percentage in the base metal increased.

Mechanical Properties

Design data were obtained for the structural, moderator, and shielding metals to be used in the construction of the ART. The effects of the important variables of environment, section size, grain size, and temperature on the creep properties of Inconel were investigated, and the limitations of stress and temperature on life can be determined from the data presented.

A lead-copper alloy is shown to be the strongest reactor-grade lead for use at 230°F. However, it does not achieve the level of creep resistance desired by the engineers.

The strength properties of beryllium in sodium were compared with data obtained in argon, and no serious deleterious effects were noted. Mechanically induced strain reversals were imposed on beryllium to simulate the effects of thermal stresses. Although life expectancy for this metal is somewhat shorter than for Inconel under similar test conditions, the metal does exhibit sufficient ductility at 1250°F to survive a reasonable number of strain reversals.

The effects of thermal stresses resulting from temperature fluctuations were studied by relaxation and dynamic strain tests. The usual

variables were investigated, and grain size, environment, and frequency appear to have the greatest effect on life expectancy. In addition, preliminary data show that prior strain cycling markedly reduces rupture life in subsequent creep tests.

A program to evaluate the effect of stress distribution on deformation rates was initiated. The results indicate that rupture life may range from 200 to 2000 hr, depending on the stress conditions.

Substantial advancement has been made in the development of new alloys to contain fused salts at high temperatures. Although further improvements are expected, a composition has been tested which would enable the reactor to be operated at a 200°F higher temperature than when constructed of Inconel and with a much reduced corrosive attack.

Nondestructive Testing

Eddy-current methods of inspection have received most of the developmental effort. Considerable effort has been expended both to improve the instrumentation for the eddy-current methods of inspection of tubing and to apply eddy-current methods to thickness measurements. Eddy-current methods of measurement are particularly suited to determining cross-section thickness in sections less than 0.020 in. thick. This is the only method currently available for measuring cladding thickness. Eddy-current probe-coil methods have also been used to identify alloys, thus preventing the inadvertent substitution of the wrong alloy in reactor construction. Fundamental mathematical studies have been made of the effect of flat metallic sections on the impedance of probe-type coils. This study has given a rational basis for the selection of test parameters to solve specific testing problems.

Both eddy-current and ultrasonic methods were used to inspect over 50,000 ft of pipe and tubing for reactor construction. In addition, ultrasonic methods were employed to inspect about 1500 ft^2 of plate, several of the ARE and ETU core shells, and the large hot-pressings of beryllium intended for reactor construction. On several occasions the resonance ultrasonic method was successfully employed to detect non-bond areas in clad composites.

Inspection

Materials for construction of ETU, ART, and test components have been inspected with the intended use as the acceptance criterion. Quantities and rejection rates for tubing, pipe, plate, sheet, and bar are reported. Descriptions of five methods of inspecting tubing are given, including types of defects found by each method.

Descriptions of weld classifications used in ANP welding and the welding performance are reported. A table listing the welding procedures used is included, and the work performed for vendors is discussed.

Three methods of fabricating shells have been evaluated, and the criteria for acceptability are included.

Methods of salvaging tubing and the effects of residual penetrant materials on Inconel at high temperatures were investigated. Development work on inspection techniques has been performed in order to ensure that material of adequate quality is furnished. These include radiographic film evaluation, inspection of weldments in beryllium-containing vessels, crack detection in tubing with radiography, and radiography of tube-to-header welds.

Welding and Brazing

The results of mechanical property tests on commercial and experimental nickel-molybdenum alloy weldments are reported. Similar results are presented for Inconel weldments. Welding experiments with a boron-containing stainless steel have indicated that the welds are brittle and notch sensitive. A study of Inconel weld-metal corrosion in fused salts has been made.

The NaK-to-air radiator fabrication development and sodium-to-NaK heat exchanger fabrication development are described. The effects of various brazing variables upon the grain growth observed in Inconel tubing were determined and correlated. Fabrication procedures for producing the tube-to-header joints of the ART fill-and-drain tank are recommended.

Thermal expansion and oxidation tests on brazing alloys are reported, and procedures for fabricating cermet valve components are described. The status of subcontract work is presented.

Fabrication

The development of alloys of the nickel-molybdenum system for use with fuel 107 has been continued. These alloys have shown exceptional promise as container materials. The production of commercial quantities of the alloys was accomplished during the year without serious difficulty.

A series of standards for evaluation of the alloys was developed, with the ideal properties being a summation of the desirable qualities of Inconel and Hastelloy B. The general status of the alloy development is discussed in terms of potential operating temperature, fabricability, corrosion resistance, mechanical properties, and weldability. Laboratory heats of alloy INOR-8 have acceptable fabricability and weldability, and sufficient corrosion resistance and mechanical strength to permit operation at 1650 to 1700°F for 1000 hr.

A series of alloys designated as INOR-9 are being developed as possible substitutes for INOR-8. The chromium content of INOR-8, which exhibits rapidly increasing corrosion tendencies above 1650°F, is replaced by 3 to 5% of niobium. It is expected that even higher metal-salt interface temperatures will be possible with this alloy.

Sufficient experimental alloy tubing was produced from laboratory heats for the operation of several forced-circulation loops in order to secure test results before the receipt of tubing from commercial heats.

The alloy program at the Battelle Memorial Institute has concentrated on the development of compositions containing aluminum and having a high carbon content. These compositions were outstanding in creep strength but were subject to fabrication difficulties and showed excessive corrosion tendencies in fuel 107.

In the phase-diagram studies at the University of Tennessee, the transformation temperatures as a function of molybdenum content have been determined for the Ni-Mo binary system, and preliminary data have been obtained on the ternary Ni-Mo-Cr system.

Creep testing of five special alloys and of the six commercial heats prepared by the International Nickel Company was conducted at various temperatures by the New England Materials Laboratory. Extruded tube shells of the six commercial heats were tube-reduced by the International Nickel

Company and are being redrawn at the Superior Tube Company.

A 10,000-lb air-melted heat of INOR-8 was prepared by the Haynes Stellite Company, and various forged and rolled products have been received and are being evaluated. Three air-melted heats of INOR-8 were also prepared by the Westinghouse Electric Corporation. The various changes in mold design and melting practice necessary to overcome the forging difficulties are described. A sound 3-in.-dia forging of the initial heat was received, and the fabricability and the physical and mechanical properties of the heat were determined.

The interface reactions and extent of diffusion between INOR-8 and type 316 stainless steel were studied to determine the problems associated with fabrication of composite tubing.

The recrystallization characteristics of niobium were investigated, primarily to compare the annealing behavior and mechanical properties of arc-cast and powder-metallurgy niobium. No significant differences between the two materials were found. The properties of niobium-clad Nb-UO$_2$ fuel plates and of an 80% Nb–20% U alloy were also investigated.

Experimental rod and tube-blank extrusions of niobium and molybdenum were prepared. The niobium was consolidated from pellets, while the molybdenum was in the form of arc-cast billets.

A shield plug assembly to protect the fuel pump motors of the ART was developed and fabricated. The assembly consisted of three components designed to limit heat transfer from the impellers. Much evaluation and coordination work was required in assisting the vendor to fabricate the Cu-B$_4$C shield layer for the ART.

Successful 3- and 5-ply extruded control rods were prepared containing a core of 70% nickel–30% Lindsay oxide. The strength and ductility of the core material were determined from extruded rods.

Equipment for the production of yttrium metal has been installed, and a new reduction process was developed in which lithium is used as the reductant. The yield on several reduction runs varied from 60 to 83%. Arc melts of the product, after removal of magnesium and lithium by vacuum distillation, were quite ductile.

Fundamental Liquid-Metal Studies

A new group was established this year to study the mechanisms involved in the mass-transport phenomenon in liquid-metal flow systems. A distillation apparatus was designed and constructed to purify the sodium to be used in these studies. Since liquid-metal diffusion is one of the mass-transport mechanisms, a program was begun to measure the rates of diffusion of various solutes in different liquid metals. Results are reported for the nickel-lead system.

High-Temperature Reactions

An electron-optical investigation of the micro-topography of oxide films formed on niobium, tantalum, and zirconium was undertaken in an effort to gain an understanding of the phenomena leading to nonprotective oxide formation on metals. It was found that initially protective oxide films on niobium became nonprotective when small, blister-like cracks formed in the oxide films. The changes which were observed during the development of niobium oxide films suggested that an oxidation process, which is maintained primarily by anion diffusion, produces, by itself, stresses in the oxide film which eventually cause the rupture of the film. On the basis of this postulate, an oxidation model was proposed in order to explain the results obtained with niobium. Tantalum oxide exhibited many of the same characteristics as did niobium, and it was shown that the oxidation mechanism proposed for niobium could also be applied to tantalum. Preliminary studies of the oxidation of zirconium showed that there was the development of nodular growths on the oxide, and further work is in progress to determine whether or not cracks also eventually form in zirconium oxide films.

A brief survey was also made of the micro-topography of sulfide films on niobium, tantalum, and zirconium in order to contrast the sulfurization and oxidation processes for these metals. Many of the details of the surface texture of the tantalum sulfide films were similar to those found on tantalum oxide, but no crack formation was observed. Niobium and zirconium sulfide films, on the other hand, showed features markedly different from those exhibited by the corresponding oxides.

A study is in progress of the effect of radiation on the gaseous oxidation of metals. In-pile oxidation experiments with niobium are scheduled to begin in the near future, the standard for the oxidation of niobium in the absence of radiation having now been established.

The oxidation of copper is also being investigated in order that the effect of radiation on an oxidation process (that for copper) controlled by cation-vacancy diffusion may be compared with an oxidation process (that for niobium) in which anion-vacancy diffusion appears to be the rate-controlling step. A preliminary study designed to characterize the oxidation of copper in terms of the microtexture of its oxide films is in progress. Thin oxide films stripped from the (100), (111), (110), and (311) faces of copper single crystals have been examined by utilizing electron-optical techniques. The early stages of oxidation appeared to involve the formation of oxide films exhibiting large thickness inhomogeneities, but as oxidation proceeded, the films became more uniform in character. Because of several still-unresolved experimental problems, further work on the out-of-pile oxidation of copper is considered to be desirable before an attempt is made to determine the effects of radiation on the oxidation process.

Absorption spectra were measured for solutions of $NiCl_2$ in fused LiCl-KCl mixtures near the eutectic composition over the wavelength range of 220 to 750 mμ and at temperatures of 360 to 550°C. In the ultraviolet region an absorption band was found with a maximum at 260 mμ and with a molar absorbancy index of $(3.6 \pm 0.2) \times 10^3$ at 395°C. The visible spectrum consisted of four overlapping bands with maximums at 512, about 590, 625, and 695 mμ at 398°C. The highest of these bands (625 mμ) had a molar absorbancy index of 61 ± 3 at a temperature of 398°C and a solvent salt composition of 41.0 mole % KCl. The absorbancy indices of all bands changed considerably with temperature. Furthermore, the ultraviolet band broadened, and its maximum shifted to longer wavelengths with increasing temperature. It was shown that these absorption bands were caused by two light-absorbing species which were probably two different chloronickel(II) complexes. With increasing temperature the concentration of one species decreased while the concentration of the other species increased. At a constant temperature the concentration of both species was proportional to the concentration of total nickel. The spectra were changed by a small but measurable amount

with small changes in the composition of the solvent salt.

An investigation of the application of nuclear magnetic resonance techniques at high temperatures, particularly as a means of elucidating the structure of fused electrolytes, has continued. During the past year a high-resolution nuclear magnetic resonance spectrometer designed for high-temperature investigations was constructed.

Studies of the growth of large single crystals of MgO from melts were conducted by using a modified Czochralski method. Difficulties were encountered in maintaining resistive heating. Therefore an extremely modified Verneuil method is now under investigation.

HRP METALLURGY

It has been shown that under some conditions zirconium-base niobium alloys possess better in-pile corrosion resistance to uranyl sulfate than do the standard Zircaloy alloys. An alloy development study of the Zr-Nb-X alloys has determined considerable information on the transformation kinetics, mechanisms, and products by using beta-quench and reheat-aging studies. At least three transformation products have been identified. While under many circumstances these alloys rapidly harden to a brittle condition, by proper selection of ternary additions and heat treatments, alloys with high strengths and moderate ductilities have been obtained.

Morphological studies have continued with Zircaloy-2. A mechanism has been developed which explains the apparently brittle behavior of some impact samples. A fabrication procedure that eliminates some of the difficulties has been successfully demonstrated.

Charpy V-impact tests and drop-weight tests have been conducted on a variety of zirconium and titanium alloys. The nil-ductility-transition temperature for most of the alloys was surprisingly low. Differences between the results obtained with these hexagonal metals and with steels are noted. No adverse effects were found when Zircaloy-2 tensile and impact specimens were exposed to an oxygenated uranyl sulfate solution in in-pile corrosion testing loops.

Welding procedures have been developed for both type 347 stainless steel and for titanium which use preplaced simple ring-type inserts for the root pass. Such techniques yield more consistent quality in the welds and use an easily formed insert.

It has been shown that both titanium and zirconium will ignite and burn to completion if fractured at room temperature in high-pressure oxygen. No reaction was found in oxygenated water.

A successful technique has been developed by which either steel or stainless steel may be clad with titanium. In order to prevent excessive diffusion, vanadium and copper are used as barrier materials.

APPLIED METALLURGY

Process Metallurgy

The major effort during the past year has been centered on further development of the Army Package Power Reactor components, investigation of a suitable alloy and powder metallurgy techniques for manufacturing plate-type aluminum fuel elements containing uranium enriched in the U^{235} isotope at the 20% level, and the establishment of procedures for processing composite aluminum fuel plates for the Tower Shielding Reactor No. 2 core.

Further development of the APPR components has revealed that type 347 stainless steel wrought and powder material can be substituted for the type 304 cladding and type 304 stainless steel powder utilized in manufacturing fuel elements for the first reactor loading. The finer grain size of the type 347 stainless steel cladding results in greater potential corrosion protection, and the stabilized condition of the material offers additional integrity compared to the sensitized type 304 stainless steel.

The concept of enclosing a flux suppressor at the tip end of the fuel core in the APPR-1 control-rod fuel plate has been pursued, and fuel plates containing a 17 wt % dispersion of rare earths in stainless steel have been successfully fabricated.

Irradiation testing of miniature stainless steel composites, containing a core of 3 wt % B^{10} in iron, indicated that the material will withstand at least an estimated 11% burnup of the B^{10} atom. The material was successfully fabricated into absorber sections for the APPR-1 control rods. Investigations have been conducted to develop a similar absorber section containing a 30 wt % Eu_2O_3 dispersion in stainless steel. Compatibility

tests reveal that Eu_2O_3 reacts with high-silicon stainless steel, but appears stable in iron and nickel.

Development has continued on the selection of materials for aluminum plate-type fuel elements containing uranium, enriched in the U^{235} isotope at the 20% level. A 40 wt % U-Al alloy, containing 3 wt % Si, was developed in order to improve fabricability of alclad fuel plates.

Examination of a Materials Testing Reactor fuel element containing the unmodified 48 wt % U-Al alloy, irradiated to an estimated burnup of 25% of the U^{235} atoms, failed to reveal any indication of irradiation damage.

The application of uranium oxides and carbides for aluminum fuel elements containing the 20% enriched uranium has been pursued. Fused UO_2 and the hydrothermal-type UO_2, prepared in a helium atmosphere, reacted with aluminum at 600°C with severe volume changes and distortion. On the other hand, U_3O_8 showed negligible dimensional changes after extensive heating at 600°C. However, it was observed that some of the U_3O_8 converted to UO_2. Compatibility testing of uranium carbides with aluminum at 600°C showed that monocarbide reacted quite drastically and that, as the carbon content of the carbide increased, the carbide became less reactive. Uranium dicarbide showed traces of reaction after 96 hr at 600°C, but was dimensionally stable. The difficulty experienced in the blistering of aluminum fuel plates containing UC_2, hot rolled in air, was resolved by either vacuum sintering of the cores prior to hot rolling or by degassing fuel billets under vacuum at 600°C.

Investigations have indicated the feasibility of using forming rolls to form plates for the core of the Tower Shielding Reactor No. 2, a spherical core containing segmental fuel elements. Joining the plates into the segmental elements by peening and tack welding, instead of brazing, proved feasible.

Additional efforts to improve the strength of plate-type aluminum elements have been directed toward substitution of type 5050 aluminum for type 1100. An element, containing nineteen 50-mil-thick plates, was shown to have a greater resistance to permanent deflection of the outer plates than the present Mark XI fuel element.

Efforts to roll-clad cadmium with aluminum revealed that hot rolling at 290°C resulted in a very weak bond.

Reactor components which were manufactured during this period included 80 high-strength aluminum elements for SPERT "B", 63 stainless steel components for the APPR-1, 72 aluminum elements for the ORR, and 18 aluminum elements for the LITR.

Metallurgical Materials and Processing

Experiments have been continued on the use of metallurgical treatments to assist chemical methods for recovery of uranium from difficulty dissolvable reactor fuel elements. Carburized APPR fuel material of type 347 stainless steel responds as well as type 304 when treated to develop either extensive dissolution or intergranular corrosion. Limited experiments indicate that air sparging can replace the urea previously used for controlling passivation. Liquation experiments have been made on carburized APPR stainless steel fuel material, but were not successful in concentrating the uranium dioxide in the lower part of the melt. Magnesium diffuses into zirconium intergranularly and embrittles the zirconium. Preliminary experiments have indicated that this behavior might be developed into techniques which will allow removal of zirconium cladding.

Metallography

In a service capacity, the Metallography Group has concentrated its efforts primarily on the Aircraft Nuclear Propulsion, the Homogeneous Reactor, and the Reactor Fabrication Programs. Some programs have required considerable study in post-failure examinations and the accumulation of statistical data on corrosion tests. Special problems of hot-stage microscopy, polishing techniques, etc., have originated and are under investigation as the result of unanswerable questions which arise from the metallographic studies for the various programs.

Five radiators and five heat exchangers have been examined in Metallography. Four of the radiators had failed in service, and examinations were made to determine the cause of failure. Other examinations included the fin-to-tube braze-joint-integrity, corrosion, and mass-transfer studies.

None of the heat exchangers apparently failed in operation; however, metallographic examination revealed that four heat exchangers had fissures completely penetrating the tube walls.

One hundred and eleven thermal-convection loops have been examined. This number represents eight materials and six fluids. Twenty-five thermal-cycle tests have been examined.

Pump loops composed of several designs, constructed of different alloys, and containing different fluids have been examined.

Considerable metallographic service has been conducted for the Homogeneous Reactor Program in the examination of flanges, leak-detector tubing, bellows, and valves for evidence of stress-corrosion cracking.

Uranium carbides (UC and UC_2) have been studied metallographically as a possible fuel material in MTR-type reactors.

A new polishing method utilizing vibratory polishing machines has been tried successfully. This method appears to be applicable for remote metallography.

Considerable development work has been done in electron microscopy in the study of microstructure requiring ultra-high magnifications.

A direct-reading dilatometer has been developed and is operating. Both vacuum and argon atmospheres can be used.

A metallographic study of Hastelloy B has been completed and a report will be published soon.

A hot-stage microscope has been completed and will be used to study the microstructures of metals and alloys up to 1100°C.

Ceramics Research

Several rare-earth silicides have been prepared and studied. The transition temperature of europium oxide from the cubic to the monoclinic phase was determined. A study of the thermodynamic properties of several refractory compounds of thorium and of uranium has been started.

The diffusion coefficient of calcium in titanium oxide and thorium oxide has been determined for two temperatures.

A preliminary phase diagram of the thoria-silica system has been determined. Techniques used in the study are described.

The fabrication of various beryllium oxide powders by hot-pressing has been studied; den-

sities as high as 96% of theoretical were obtained. The use of $BeSO_4 \cdot nH_2O$ and $Be(OH)_2$ as sources of beryllium oxide of high surface activity for hot-pressing of high-density beryllium oxide is also being studied.

The production of zirconium hydride for the high-temperature moderator program of ANP has been successfully worked out so that experimental shapes are easily produced.

The incorporation of larger amounts of UO_2 into the Si-SiC fuel-element matrix has been the object of further study. Several factors which cause the failure of the compacts are discussed; also, some radiation damage results for low-level exposure are reported.

Research work on Al_2O_3-Cr and other ceramic materials for fuel elements is reported.

The synthesis and property study of zirconium disilicide, tantalum diboride, zirconium diboride, and hafnium carbide are reported.

The fabrication of boron nitride and zirconium oxide by hot-pressing is reported.

The properties of ceramic compositions of various rare-earth oxides are reported.

Preliminary results of a study of zirconium niobate ceramics are reported.

Various procedures for the calcination of low-calcined thoria are described.

The electrical phenomena associated with thoria suspensions and the causes of settling of these slurries have been studied.

The Knoop hardness of ThO_2 and UO_2 was determined.

A series of experiments on mixtures of ThO_2 and UO_2 was completed. Results are reported on various property determinations which were made.

A method of spheroidizing various ceramic powders has been developed.

The retention of the radioactivity from both Hope and Purex-type wastes by sintered ceramic mixtures has been greatly increased by the use of several highly absorbent clays in the ceramic mixes.

The retention of radioactivity by porous ceramics and porous concrete which are sintered subsequent to the pores being filled with salts from the Hope waste is discussed.

Phase determinations with the petrographic microscope for the fluoride fuels program have been continued during the past year, with one man engaged full-time in the work.

The thermal analysis and thermal expansion work carried out on equipment in the Ceramic Laboratory is discussed.

A rather large and difficult shape which was produced from samarium oxide is described.

Various ceramics which were fabricated for the Critical Experiments Group are described.

Fabrication studies of various refractory oxides are reported.

A literature survey on thermal diffusivity has been compiled.

A study of the ability of various clays to prevent the settling of thoria slurries has been made.

FUNDAMENTAL METALLURGY

Physicometallurgical Research

Data are presented on the crystal structures found in high-purity cerium metal between 77 and 450°K. The high-temperature face-centered cubic form transforms either to a double-hexagonal structure (c/a = 3.23) or to a denser face-centered cubic phase at low temperatures. Both transformations appear to be athermal in nature and show large hysteresis. Plastic deformation at any temperature suppresses the cubic-to-hexagonal transformation; however, deformation below the M_s temperature promotes the cubic-to-collapsed-cubic transformation.

The effects of fabricating conditions (temperature, extrusion speed, and amount of deformation) on the preferred orientation in extruded aluminum rods are described. At relatively low temperatures (below 450°F) or slow extrusion speeds (1 to 2 fpm) duplex <111> – <001> textures are developed; however, the relative amount of these components may vary by a factor of two. At high temperature and high speeds (650°F and above, 600 to 700 fpm) such unusual textures as <115> or <118> may be developed.

The low-temperature specific heats of 99.95% zirconium and a zirconium alloy with 8 at. % indium have been measured. An increase in the electronic specific heat, and hence in the density of states at the Fermi surface, occurs which may correspond to the Brillouin zone overlaps which have been assumed to be responsible for the expansion of the axial ratio of zirconium with indium additions. The variation of the lattice specific heat with the indium addition was small.

Investigation of the $\alpha/(\alpha+\beta)$ and $\beta(\alpha+\beta)$ phase boundaries of Zr-Cd shows that these boundaries rise only slightly, and within the accuracy of the earlier valency scheme of the α/β boundaries, are consistent with this hypothesis. A preliminary result on the vapor pressure of a zirconium alloy with 7.5% indium is given.

X-Ray Diffraction

A resumé of activities of the Metallurgy Division X-Ray Laboratory during the past year is given. Besides a large number of service problems, several more detailed investigations have been made of problems involving, among others, metal-hydrogen systems, martensitic phase transitions, and aging alloys.

The thermally induced structure transitions in the titanium-hydrogen system have been followed from compositions of $TiH_{1.98}$ to $TiH_{1.79}$. A reasonable pattern is emerging from these studies, and experiments with intermediate hydrogen concentrations in titanium and other metals are contemplated.

The Unicam high-temperature x-ray diffraction camera has been used to verify the martensitic character of the monoclinic $\rightleftharpoons$ rhombohedral phase transition in sodium nickelate(III). This is now one of the more concrete cases of such transitions in inorganic materials as a result of these experiments.

High-temperature diffraction data have also been obtained for several rare-earth–transition-metal perovskitic oxides which show interesting magnetic properties at low temperatures. Transitions to less distorted lattices have been found which support current theories of bond ordering in such systems.

Preliminary x-ray diffraction studies of the aging phenomena in zirconium-niobium alloys suggest that a complex aging mechanism may be operative. Indications of a "modulated" structure have been found. A preliminary precipitate, previously called the "hardening phase" in Ti-Cr and Zr-Mo alloys, has been identified although it is not the hardening phase in this case. Extensive single-crystal experiments are being carried out in an effort to understand the aging reactions.

HIGH-TEMPERATURE METALLURGY

W. D. Manly

GENERAL CORROSION

E. E. Hoffman

W. H. Cook   D. H. Jansen

J. L. Griffith   J. E. Pope

J. W. Hendricks   L. R. Trotter

The bulk of the work reported in this section was done either in support of the Aircraft Reactor Test or as preliminary investigations on advanced aircraft nuclear propulsion systems.

CORROSION TESTS ON BRAZING ALLOYS

Brazing Alloys Tested in Bath No. 44 and NaK

From a series of ten high-nickel-content brazing alloys seesaw-corrosion-tested in the $NaF-ZrF_4-UF_4$ (53.5-40.0-6.5 mole %, fuel 44) and NaK (56-44 wt %) media for 100 hr at 1500°F, the Handy-Harmon No. 91 (91.25 Ni–4.5 Si–2.9 B) and No. 93 (93.25 Ni–3.5 Si–1.9 B) alloys have the best corrosion resistance to both baths.[1] The alloys were tested to determine the possibility of using them for high-temperature heat exchanger applications. Brazed Inconel tube-to-header joints were used for test specimens.

Brazing Alloys Tested in Bath No. 107

In view of the increased interest in the mixture $NaF-KF-LiF-UF_4$ (11.2-41.0-45.3-2.5 mole %, fuel 107), brazing alloys that have shown promising corrosion resistance to other fuel mixtures have been tested in this medium. The Handy-Harmon Nos. 91 and 93 alloys and the Coast Metals No. 52 (89% Ni–5% Si–4% B–2% Fe) alloy showed good corrosion resistance to this fuel mixture during 100-hr seesaw tests at 1500°F. A 3- to 4-mil-deep depleted region with accompanying subsurface voids was observed on these alloys. The chromium-containing Coast Metals No. 53 (81% Ni–8% Cr–4% Si–4% B–3% Fe) alloy showed limited resistance to fuel 107; a stringer-type attack to a maximum depth of 10 mils was found on the surface of the alloy.

CORROSION TESTS ON WELDED INCONEL

D. H. Jansen

Corrosion Characteristics of Resistance-Welded Inconel to Bath No. 30 and NaK

Results of seesaw corrosion tests on resistance-welded Inconel tube-to-header joints in $NaF-ZrF_4-$

UF_4 (56-40-4 mole %, fuel 30) and NaK (56-44 wt %) show that the recrystallized portion of these welds was attacked to no greater extent than the other Inconel components of the specimens.[2,3] Both the conventional "flange-during-welding" joint with an additional fusion weld and the pre-chamfer type[4] of resistance-welded joints were corrosion-tested.

Corrosion Resistance of Inconel Welds Made with Nitrogen as the Shield Gas

Inconel welds in which nitrogen was substituted for helium as shield gas showed about the same corrosion resistance to $NaF-ZrF_4-UF_4$ (50-46-4 mole %, fuel 30) and NaK (56-44 wt %) as did the conventional Heliarc welds when corrosion-tested under seesaw conditions. A maximum attack of 2 mils was observed on the weld.

COMPATIBILITY OF MOLYBDENUM AND NICKEL-MOLYBDENUM ALLOYS IN BATH NO. 107

D. H. Jansen

Dissimilar-metal mass transfer occurred between molybdenum and nickel-molybdenum alloys that were exposed to the mixture $NaF-KF-LiF-UF_4$ (11.2-41.0-45.3-2.5 mole %, fuel 107) in a seesaw apparatus operated for 500 hr. The systems were composed of nickel-molybdenum capsules (15% Mo–6% Cr–Bal Ni, hot-zone temperature 1650°F and 17% Mo–2% V–bal Ni, hot-zone temperature 1600°F) with a pure molybdenum strip confined to the hot zone of each. The presence of nickel on

[1] D. H. Jansen, *ANP Quar. Prog. Rep. Sept. 30, 1957,* ORNL-2387 (in press).

[2] D. H. Jansen, *ANP Quar. Prog. Rep. Dec. 31, 1956,* ORNL-2221 (Parts 1–5), p 184.

[3] D. H. Jansen, *ANP Quar. Prog. Rep. March 31, 1957,* ORNL-2274 (Parts 1–5), p 164.

[4] J. J. Mueller *et al., Special Welding Techniques, Final Summary Report,* ER-7205 (Jan. 1956).

the molybdenum strips could not be seen by metallographic examination, but was found by microspark spectrographic examination to be of the order of a few per cent.[5]

VANADIUM CORROSION-TESTED IN BATH NO. 107 AND LITHIUM

D. H. Jansen

Vanadium mass-transferred rather heavily in bath No. 107 in a seesaw corrosion test of 100 hr duration.[6] A sample of the mass-transfer crystals analyzed as follows: 97% vanadium, 1.5% iron, 0.8% chromium, 0.34% nickel (adjusted to 100%).

A 100-hr static test of the vanadium-lithium system at 1500°F showed no attack on the vanadium. A seesaw test of this system will be conducted later.

EFFECT OF BATH NO. 44 ON BORON CARBIDE

W. H. Cook

A specimen of B_4C was exposed to static NaF-ZrF_4-UF_4 (53.5-40-6.5 mole %) at 1500°F for 100 hr.[7] The quantity of boron found in the fuel at the conclusion of the test indicated that the specimen had lost 30% of its weight. Metallographic examination showed an irregular reaction layer, which is as yet unidentified, surrounding the specimen.

BORON CARBIDE AND BORON NITRIDE CORROSION-TESTED IN MOLTEN SODIUM

W. H. Cook

Boron carbide specimens with densities 85 and 90% of theoretical were found to have fair resistance to attack by static sodium at 1500°F.[8] A dense (2.15 g/cc, 98% of theoretical) boron nitride specimen was severely attacked in a 100-hr exposure to sodium at 1500°F in a seesaw furnace.

POROUS RARE-EARTH OXIDES EXPOSED TO MOLTEN SODIUM IN INCONEL CAPSULES

W. H. Cook

Four rare-earth-oxide samples fabricated in the same configuration as that to be used in the ART control rod were tested in sodium for 500-, 1000-, 2000-, and 3000-hr periods while the temperature was cycled between 1100 and 1350°F.[9] These specimens had an average bulk density of 4.10 g/cc and an apparent porosity of 46.3%. Chemical analysis of a sodium sample taken from the bottom of the test capsule of the 2000-hr test showed a total of 129 ppm of rare earths in the alcohol-insoluble residue. The majority of the analyses of sodium samples from the other tests showed totals of rare earths less than 15 ppm and never greater than 20 ppm.

EFFECT OF MOLTEN SODIUM ON SEVERAL NITRIDE, BORIDE, AND SILICIDE CERMETS

W. H. Cook

Standard screening corrosion tests were made on BN, BN + Si_3N_4, ZrB_2, ZrB_2 + BN, $MoSi_2$, and $MoSi_2$ + BN in sodium at 1500°F.[10] Metallographic data indicated: (1) ZrB_2 and $MoSi_2$ were not attacked, and (2) the presence of BN in ZrB_2, $MoSi_2$, or Si_3N_4 directly or indirectly decreases their corrosion resistance to molten sodium.

SiC-Si CORROSION-TESTED IN MOLTEN SODIUM

W. H. Cook

Exposure of a pure SiC-Si specimen for 100 hr to sodium at 1500°F in a seesaw furnace resulted in complete removal of the silicon phase so that only SiC particles remained.[11]

TITANIUM CARBIDE–NICKEL CERMETS IN MOLTEN SODIUM AT 1500°F

W. H. Cook

Four titanium carbide–nickel cermets, three with 10, 20, and 30% nickel and one with 25% Ni plus 5% Mo, were attacked to a depth of approximately 0.5 mil during a 100-hr exposure to sodium at

[5]D. H. Jansen, *ANP Quar. Prog. Rep. March 31, 1957,* ORNL-2274 (Parts 1–5), p 165.

[6]D. H. Jansen, *ANP Quar. Prog. Rep. Sept. 30, 1957,* ORNL-2387 (in press).

[7]W. H. Cook and E. E. Hoffman, *ANP Quar. Prog. Rep. June 30, 1957,* ORNL-2340 (Parts 1–5), p 234.

[8]W. H. Cook, *ANP Quar. Prog. Rep. March 31, 1957,* ORNL-2274 (Parts 1–5), p 173.

[9]W. H. Cook, *ANP Quar. Prog. Rep. Dec. 31, 1956,* ORNL-2221 (Parts 1–5), p 189.

[10]W. H. Cook and E. E. Hoffman, *ANP Quar. Prog. Rep. June 30, 1957,* ORNL-2340 (Parts 1–5), p 234.

[11]W. H. Cook, *ANP Quar. Prog. Rep. March 31, 1957,* ORNL-2274 (Parts 1–5), p 174.

1500°F in a seesaw-furnace apparatus.[12] In previous similar tests these cermets were not attacked by NaF-ZrF_4-UF_4(53.5-40-6.5 mole %, fuel 44).[13]

TUNGSTEN CARBIDE- AND TITANIUM CARBIDE-BASE CERMETS IN SODIUM AT 1200°F

W. H. Cook

Cermet specimens of WC-Co, $WTiC_2$, and TiC-Ni-Mo were not attacked in a 100-hr exposure to sodium at 1200°F in a seesaw-furnace apparatus.[14]

TUNGSTEN-NICKEL-COPPER ALLOY TESTED IN MOLTEN SODIUM AND BATH NO. 30

W. H. Cook

Tungsten-nickel-copper alloy (90 W–6 Ni–4 Cu wt %) specimens lost 1.3% by weight and were completely penetrated ($\frac{1}{4}$ in.^{2} in cross section) in 100-hr exposures to sodium at 1500°F in a seesaw-furnace apparatus.[15] Heat-treating the alloy at 1920°F for one-half hour before the exposure to sodium did not alter its corrosion resistance. Specimens of the same kind were not attacked when given a similar exposure to bath No. 30 (NaF-ZrF_4-UF_4, 50-46-4 mole %).

MOLYBDENUM-BERYLLIUM COMPATIBILITY IN MOLTEN SODIUM

R. Carlander   E. E. Hoffman

Molybdenum and beryllium specimens were held in contact for 100 and 500 hr at 1500°F while immersed in sodium in order to study the extent of intermetallic compound formation between these two metals. The various compounds formed and their thicknesses have been reported.[16]

INCONEL-BERYLLIUM COMPATIBILITY IN MOLTEN SODIUM

E. E. Hoffman   L. R. Trotter

Effect of Various Platings on Inconel

The effect of chromium plating and nickel-plus-chromium plating of Inconel on the extent of reaction of this material with beryllium at 1300°F has been investigated.[17] The results indicate that chromium platings of at least 5 mils thickness are required to protect the Inconel from embrittlement for test periods of 1000 hr.

Beryllium-Inconel Staple Tests

It has been proposed that Inconel staples be placed in the beryllium moderator sections used in the construction of the Aircraft Reactor Test in order to act as sacrificial spacers to protect the Inconel core shells. This proposed configuration has been tested at 1300°F for 1000 hr, and the results have been reported.[18]

EFFECT OF ZIRCONIUM ON CORROSION IN AN INCONEL-SODIUM SYSTEM

R. Carlander   E. E. Hoffman

Standpipe tests were conducted to determine the effect of the presence of zirconium on the corrosion and mass transfer of Inconel by sodium. Although the zirconium was found to have picked up oxygen from the sodium, no effect on the extent of mass transfer was detected.[19]

HASTELLOY B–SODIUM THERMAL CONVECTION LOOP TEST

E. E. Hoffman   L. R. Trotter

A thermal convection loop of Hastelloy B containing sodium at a hot-leg temperature of 1600°F (cold leg, 990°F) was operated for 1008 hr. The test revealed a slight amount of mass transfer. The performance of Hastelloy B was found to be quite similar to that of Inconel tested under the same conditions.[20]

[12]W. H. Cook, *ANP Quar. Prog. Rep. March 31, 1957*, ORNL-2274 (Parts 1–5), p 171.

[13]E. E. Hoffman, W. H. Cook, and C. F. Leitten, Jr., *ANP Quar. Prog. Rep. March 10, 1955*, ORNL-1864, p 77, esp 84.

[14]W. H. Cook and E. E. Hoffman, *ANP Quar. Prog. Rep. Sept. 30, 1957*, ORNL-2387 (in press).

[15]W. H. Cook and E. E. Hoffman, *ANP Quar. Prog. Rep. Sept. 30, 1957*, ORNL-2387 (in press).

[16]R. Carlander, *ANP Quar. Prog. Rep. March 31, 1957*, ORNL-2274 (Parts 1–5), p 169.

[17]E. E. Hoffman and L. R. Trotter, *ANP Quar. Prog. Rep. March 31, 1957*, ORNL-2274 (Parts 1–5), p 166.

[18]E. E. Hoffman, *ANP Quar. Prog. Rep. Dec. 31, 1956*, ORNL-2221 (Parts 1–5), p 190.

[19]R. Carlander, *ANP Quar. Prog. Rep. March 31, 1957*, ORNL-2274 (Parts 1–5), p 169.

[20]E. E. Hoffman and L. R. Trotter, *ANP Quar. Prog. Rep. March 31, 1957*, ORNL-2274 (Parts 1–5), p 166.

LITHIUM CORROSION STUDIES

E. E. Hoffman   L. R. Trotter

A summary of recent findings of the lithium corrosion testing program was given at the Lithium Symposium held at the Oak Ridge National Laboratory on August 7 and 8, 1957.[21] An inert-atmosphere chamber for thermal-convection-loop testing of non-oxidation-resistant materials has been described in a previous report.[22] Seesaw-furnace tests have indicated that niobium and molybdenum have excellent corrosion resistance to molten lithium.[23] Three thermal-convection-loop tests on niobium at hot-leg temperatures of 1500°F and 1550°F were recently conducted. These loops failed in weld areas after operating for 155, 24, and 44 hr. No evidence of attack or mass transfer has been found in the preliminary examinations conducted to date. These loops were operated in a vacuum of less than 5 microns, and the loops were bright and ductile after the test. Further tests will be conducted on niobium and other refractory metals in the near future.

A lithium distillation rig has been in operation for several months. Four distillations of approximately 600 g each have been carried out at a distillation temperature of 625°C. The details of these purification attempts have been reported.[24]

SUBCONTRACT STUDIES WITH MOLTEN LITHIUM

E. E. Hoffman

The progress made by the Nuclear Development Corporation of America during the past twelve months has been summarized in topical re-ports.[25-28] Type 316 stainless steel was found to be unsatisfactory for containing lithium in dynamic systems at hot-leg temperatures of 1600°F. The present program calls for tests on refractory metals and will attempt to discover whether inhibitors exist which would permit utilization of the more common structural alloys.

LEAD-LITHIUM SHIELDING ALLOY

D. H. Jansen   E. E. Hoffman

Some metallurgical studies including alloying, casting, rolling, and segregation were conducted on a lead–0.7% lithium alloy.[29] This alloy is a potential material for use in the construction of shields for a gamma-ray spectrometer.[30]

The lithiated lead is mechanically superior to ordinary lead but is attacked quite rapidly when exposed to moisture. The information obtained in this study was used to make a lithiated lead slab (36 in. square by 4 in. thick) for experimental determination of the neutron and gamma-ray shielding characteristics of the alloy.[31]

RUBIDIUM CORROSION TESTS

R. Carlander   E. E. Hoffman

Molybdenum and Hastelloy B have been corrosion-tested in contact with boiling rubidium for 500-hr test periods under various temperature conditions. Hastelloy B was found to be attacked to a depth of 1 mil at 1600°F, while molybdenum was unattacked at 1900°F.[32]

[21] *Proceedings of the Lithium Symposium — Analytical Procedures and High-Temperature Corrosion*, Aug. 7–8, 1957, TID-7544 (to be published).

[22] E. E. Hoffman and L. R. Trotter, *ANP Quar. Prog. Rep. Sept. 30, 1957*, ORNL-2387 (in press).

[23] E. E. Hoffman and L. R. Trotter, *ANP Quar. Prog. Rep. Sept. 30, 1957*, ORNL-2387 (in press).

[24] E. E. Hoffman, paper presented in *Proceedings of the Lithium Symposium — Analytical Procedures and High-Temperature Corrosion*, Aug. 7–8, 1957, TID-7544 (to be published).

[25] N. I. Sax, *Determination of Nitrogen in Lithium*, NDA-38 (June 14, 1957).

[26] W. Arbiter and S. Lazerus, *Purification of Lithium by Vacuum Distillation*, NDA-39 (June 14, 1957).

[27] J. M. McKee, *Effect of Nitrogen on Corrosion by Lithium*, NDA-40 (June 14, 1957).

[28] M. Kolodney and B. Minushkin, *A Method for Determining the Solution Rate of Container Metals in Lithium*, NDA-41 (June 14, 1957).

[29] D. H. Jansen and E. E. Hoffman, *ANP Quar. Prog. Rep. Dec. 31, 1956*, ORNL-2221 (Parts 1–5), p 194–198.

[30] R. W. Peelle, T. A. Love, and F. C. Maienschein, *ANP Quar. Prog. Rep. March 31, 1957*, ORNL-2274 (Part 6), p 27.

[31] E. E. Hoffman *et al.*, *Lead-Lithium Shielding Alloy — Metallurgical Studies*, ORNL-2404 (to be published).

[32] R. Carlander, *ANP Quar. Prog. Rep. Dec. 31, 1956*, ORNL-2221 (Parts 1–5), p 193.

DYNAMIC CORROSION

J. H. DeVan

J. R. DiStefano   R. S. Crouse

FORCED-CIRCULATION LOOP STUDIES OF FLUORIDE FUELS

J. H. DeVan   R. S. Crouse

Fuel Mixtures in Inconel

Effect of Time on Depth of Corrosion. — A series of Inconel loops having identical temperature conditions and variable test durations has been operated to study the effect of time on corrosion by the fuel mixture (No. 30) NaF-ZrF_4-UF_4 (50-46-4 mole %). This series supplements an earlier series of tests which was operated for similar purposes but at a lower system temperature.[1] Table 1 lists the conditions and the results of operation of the latest test series.

Figure 1 shows the variations in attack as a function of the test durations employed, which were 15, 50, 100, 300, 1000, and 3000 hr. Attack may be seen to increase rapidly within the first 15 hr of operation and to level off at a slower and

relatively constant rate thereafter. The slope of the straight-line portion of the attack is approximately 1 mil per 280 hr. Typical hot-leg sections taken at several time intervals are shown in Fig. 2. Chromium pickup by the fuel increased up to a value of approximately 400 ppm during the first 50 hr of operation and did not change appreciably in tests of longer duration.

Effect of Flow Rate on Corrosion. — Experiments to further evaluate flow rate as a factor in the corrosion of Inconel by fuel No. 30 were carried out in Inconel pump loops in which temperature conditions remained constant while the Reynolds number was varied. The tests encompassed a range in Reynolds number values from 5000 to 14,000 and were intended to operate for 1000 hr under the conditions shown in Table 2. An additional test was run at the highest Reynolds number value, following an instrument failure in the first test after only 515 hr of operation.

In comparing the corrosion results listed in Table 2, it appears that a slight increase in attack has occurred in the test with the highest Reynolds number value. However, an inverse relation of attack with flow rate exists between the 5000 and 10,000 Reynolds number tests. If the attacks are averaged for the three tests which operated for 1000 hr, a value approximating 5 mils results; the deviations from this value among the tests are quite small and very probably lie within the inherent scatter band for such test results. Hence the effect of flow rate on corrosion does appear to be small.

Effect of Temperature Drop on Corrosion. — Previous efforts to study the effect of temperature drop on attack in Inconel–fuel No. 30 pump loops gave rise to questionable results because of operational difficulties encountered in two of the tests involved.[2] The tests in question have been repeated and appear as loops 7425-16 and 7425-10 in Table 3. Loop 4950-6, which also is included in this table, was operated as part of the earlier series and, in view of its satisfactory operation

---

[1]J. H. DeVan, *Met. Semiann. Prog. Rep. April 10, 1956*, ORNL-2080, p 53.

Table 1. Operating Conditions of Time-Series Pump Loops

Maximum loop fluoride temp	1600°F
Maximum loop wall temp	1700°F
Fluoride ΔT	300°F
Reynolds number of fuel	6000
Ratio of hot-leg surface to total loop volume	2.15 in.^{2}/in.^{3}

Loop No.	Operating Time (hr)	Maximum Attack (mils)
7425-23B	15	3
7425-23A	50	3
7425-23C	100	4
7425-21	304	4
7425-25	500	5
7425-22	1000	7
7425-9	3000	14

---

[2]J. H. DeVan, *Met. Semiann. Prog. Rep. April 10, 1956*, ORNL-2080, p 53, esp 61.
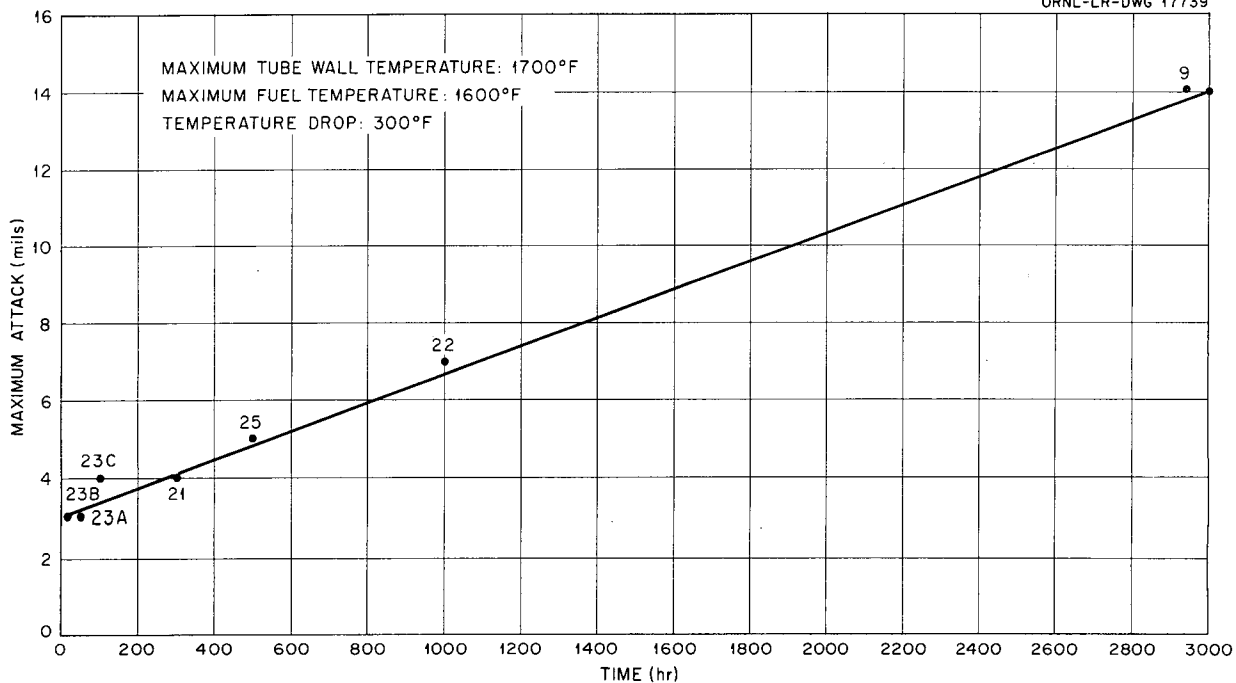
Fig. 1. Depth of Attack as a Function of Time for Fuel No. 30 in Inconel Pump Loops.

Table 2. Operating Conditions of Inconel Pump Loops with Variable Reynolds Numbers

Fluoride fuel No. 30
Fluid temperature drop, 150°F

Operating Conditions	Loop No.			
	7425-17	7425-18	7425-19	7425-24
Operating time, hr	1000	1000	515*	981**
Maximum fluoride mixture temp, °F	1520	1510	1510	1515
Maximum tube wall temp, °F	1565	1565	1560	1570
Reynolds number of fuel	5200	9620	13,835	14,258
Fluid velocity, fps	3.49	6.49	9.32	9.61
Flow rate, gpm	1.44	2.68	3.85	3.97
Maximum depth of attack, mils	4	3	3	$6\frac{1}{2}$

*Terminated by instrument failure.

**Terminated by pump failure.
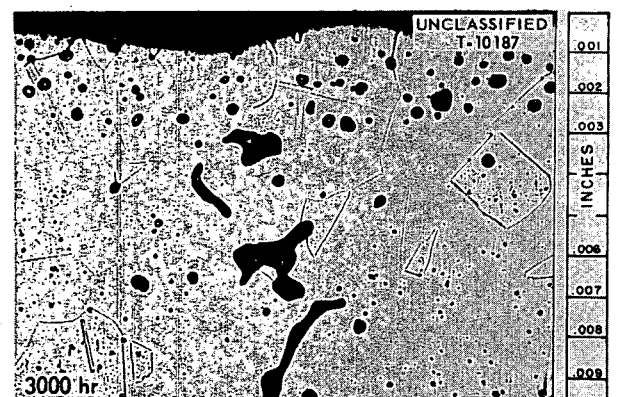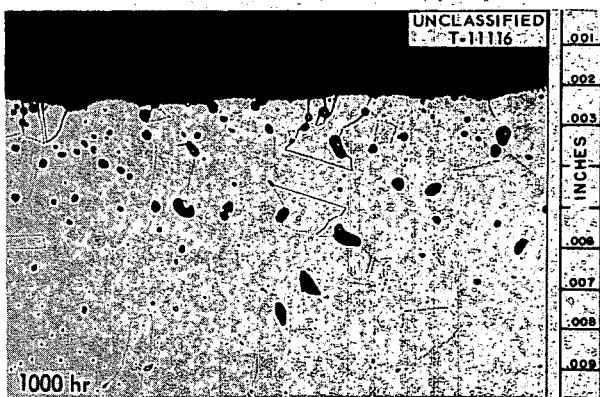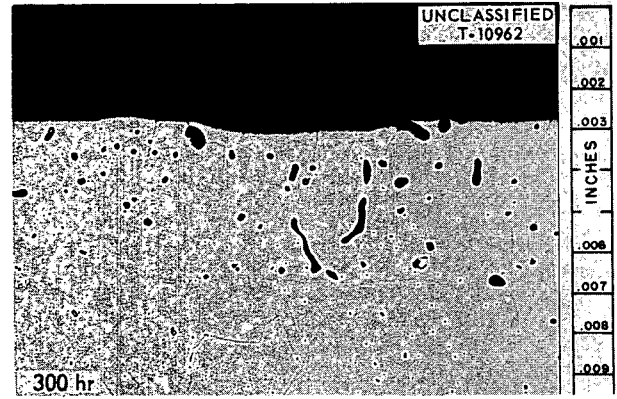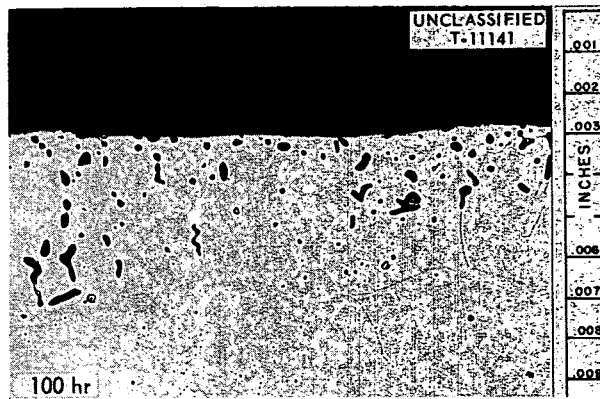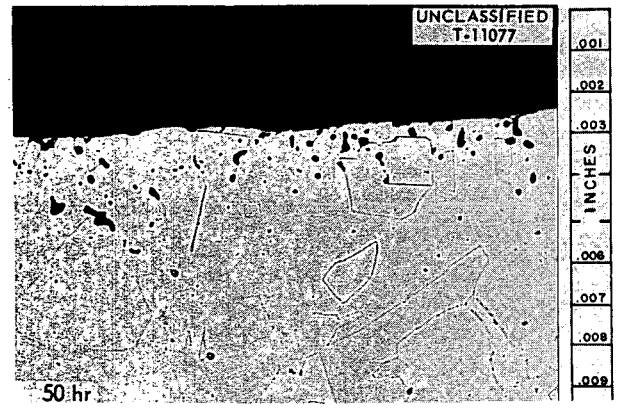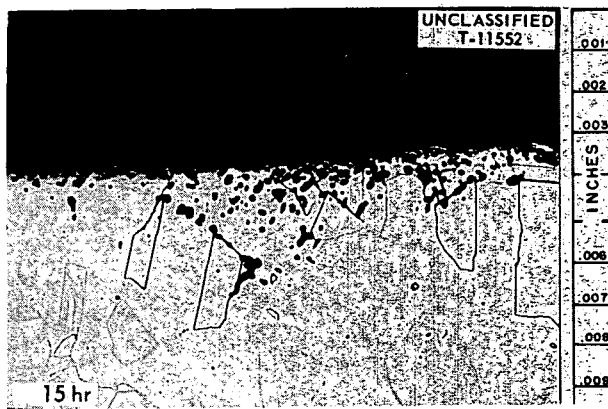
Fig. 2. Changes in Attack with Increasing Operating Time in Forced-Circulation Inconel Loops. 250X. Reduced 13%. (Secret with caption)

history, was not repeated. Since varying of the Reynolds number or the flow rate, as discussed above, has not been seen to appreciably affect corrosion results, differences in the corrosion behavior among the loops are assumed to correspond directly to changes in temperature drop.

The temperature drops employed for the series were 145, 200, and 300°F, respectively. As seen in Table 3, attacks recorded for the lower two values were quite similar and were significantly lower than the value obtained at a temperature drop of 300°F. This would suggest that at the temperature levels employed, increases in temperature drop above 200°F noticeably increase the attack,

Table 3. Operation Conditions for Inconel Pump Loops with Variable Temperature Drops

Fluoride fuel No. 30

Operating Conditions	Loop No.		
	7425-16	7425-10	4950-6
Operating time, hr	1040	1000	1000
Maximum fluoride mixture temp, °F	1540	1500	1520
Maximum tube wall temp, °F	1600	1580	1620
Temperature gradient, °F	145	200	300
Reynolds number of fuel	10,000	10,000	8000
Fluid velocity, fps	5.9	5.9	5.22
Maximum depth of attack, mils	4	$4\frac{1}{2}$	8

but that decreases in temperature drop below 200°F do not correspondingly reduce the attack. Such a conclusion supports a statement made previously[3] that the leaching of chromium from the hot leg is rate-controlled by the diffusion of chromium into the cold leg. At the higher cold-leg temperatures, which accompanied the smaller system temperature drops, the rate of diffusion of chromium into the cold leg would become proportionately greater. The increase in this diffusion step may have compensated for the loss in driving force toward mass

[3]J. H. DeVan, *Met. Semiann. Prog. Rep. Oct. 10, 1956,* ORNL-2217, p 45, esp 46.

transfer brought about by the lower temperature drop.

Effect of Test Temperature on Fluoride Attack. — The operation of an Inconel pump loop (7425-20) at a maximum fuel temperature of 1700°F was carried out to complete studies of temperature effects on Inconel corrosion by fuel mixture No. 30. Loop operating conditions appear in Table 4. Void formation following 1000 hr of operation was observed to reach a maximum depth of 9 mils. This attack was accompanied by the deposition of a few scattered particles of metal on cold-leg surfaces. The deposits are known to contain chromium and may also, on the basis of etching characteristics, be composed of some uranium or zirconium components. The attack in this loop is 4 to 5 mils higher than the attack recorded in Inconel loops operating with a fuel temperature of 1500°F and a wall temperature[4] of 1600°F.

Effect of Grain Size on Attack. — During the examination of the fuel circuit of the NaK-to-fuel heat exchanger ORNL-1, type IHE-3, unusually deep intergranular voids were evident in tubes near the tube-to-header joints of the NaK outlet header.[5]

[4]J. H. DeVan, *Met. Semiann. Prog. Rep. Oct. 10, 1956,* ORNL-2217, p 45.

[5]R. J. Gray and P. Patriarca, *Met. Semiann. Prog. Rep. Oct. 10, 1956,* ORNL-2217, p 99, esp 109.

Table 4. Conditions of Operation of Two Inconel Forced-Circulation Loops with Fuel Mixtures

Operating Conditions	Loop No.	
	7425-20	7425-26
Fuel mixture	30*	70**
Maximum fuel mixture temp, °F	1715	1510
Maximum tube wall temp, °F	1840	1615
Reynolds number of fuel	23,700	14,000
Velocity of fuel, fps	5.0	4.79
Operating time, hr	1000	716.5
Ratio of hot-leg surface to loop volume, in.$^{-1}$	2.21	2.15
Temperature gradient, °F	300	200

*Composition: $NaF-ZrF_4-UF_4$ (50-46-4 mole %).
**Composition: $NaF-ZrF_4-UF_4$ (56-39-5 mole %).

The Inconel tubing in this area, because of the furnace-brazing heat treatment used to back-braze the tube-to-header joints, was associated with a relatively large grain size. It was thus desired to determine whether the metallurgical changes accompanying the grain-coarsening heat treatment of Inconel could affect the corrosion resistance in molten fluorides. Accordingly, an Inconel pump loop was prepared with hot-leg sections which had been annealed at 1940°F, and it was operated with fuel No. 30. The annealing treatment was carried out for 2 hr in hydrogen and was intended to reproduce a grain diameter similar to that obtained during the furnace brazing of heat exchanger and radiator tubes. The test was operated for 1000 hr with a maximum fluoride-metal interface temperature of 1600°F and with a minimum fluoride temperature of 1300°F. Under similar conditions, a standard Inconel loop (ASTM grain size 4 to 8) shows 5 to 7 mils of general and intergranular subsurface void formation.

The grain size of the annealed sections, measured in both before-test and after-test samples, was very random, ranging from ASTM No. 5 to greater than 1 within a single sample. After-test samples taken from the point of maximum wall temperatures revealed heavy general and intergranular void formation to $5\frac{1}{2}$ mils. In addition, a few scattered intergranular voids were visible to depths of 12 mils, which are shown in Fig. 3. Thus preferential grain-boundary attack, which has been noted in the examination of heat exchanger units, was seen to exist to a limited extent in the coarse-grained sections of this pump loop.

Thermal convection loop tests were operated several years ago to evaluate grain-size effects, although little difference in the depth of attack was noted between as-received and annealed alloys.[6] In reviewing these tests, however, it is quite apparent that subsurface voids became much more concentrated in the grain boundaries of coarse-grain tubing than in fine-grain tubing. While the depth of these intergranular voids in the coarse-grain tubing did not greatly exceed the depth of voids in the grain matrix of fine-grained samples, such tests indicate the possibility of relatively deep attacks under certain conditions of grain-boundary orientations in coarse-grained material.

Fig. 3. Intergranular Voids Formed During Operation of Inconel Pump Loop for 1000 hr with Fuel No. 30 ($NaF-ZrF_4-UF_4$, 50-46-4 Mole %). Heater sections of loop were annealed at 1940°F prior to operation. Etchant: aqua regia. Reduced 10%. (Secret with caption)

Tests in Fuel No. 70. — A third Inconel forced-circulation loop has been operated with the fuel mixture (No. 70) $NaF-ZrF_4-UF_4$ (56-39-5 mole %). The results of two other pump loop tests which compared the corrosion properties of this fuel mixture with the more commonly used mixture No. 30, $NaF-ZrF_4-UF_4$ (50-46-4 mole %), were reported previously.[7] Operating conditions for this loop, 7425-26, appear in Table 4. Although intended for 1000-hr operation, the loop was terminated after only 716 hr because of a pump pulley failure. Void formation during this time period progressed to a depth of 5 mils. A thin metallic layer was noted in the cold leg which was similar to layers seen in the earlier Inconel loops operated with this fuel mixture. This layer was too thin to provide a

[6]G. M. Adamson, *ANP Quar. Prog. Rep. Sept. 10, 1954*, ORNL-1771, p 98.

[7]J. H. DeVan, *Met. Semiann. Prog. Rep. Oct. 10, 1956*, ORNL-2217, p 45, esp 47.

sufficient sample for chemical analysis and could not be resolved by using spectrographic techniques.

The attack of 5 mils in this loop agrees closely with attacks of 7 mils in each of the two loops operated previously with fuel No. 70 for 1000 hr. One of these latter loops operated under temperature conditions identical to those for loop 7425-26, while the other operated with a maximum fluid temperature of 1650°F. The depth and type of attack in these loops resemble very closely the attack which results in Inconel–fuel No. 30 tests under similar conditions; however, the presence of a thin layer in the fuel No. 70 systems is in contrast with fuel No. 30 systems, where visible layers or deposits have normally not been observed.

Fuel Mixtures in Hastelloy B

Three Hastelloy B pump loops which circulated the fluoride mixture (No. 107) NaF-LiF-KF-UF$_4$ (11.2-41.0-45.3-2.5 mole %) were examined following operation at 1650°F. Operating conditions for the loops are shown in Table 5. Two of the loops completed 1000 hr of operation, but the third loop, 7641-3, was terminated by a pump failure after 407 hr of operation.

The hot legs of all three loops were seen to be badly pitted after test, the worst areas ranging to 4 mils. Unfortunately, considerable surface roughness was already present in the as-received samples of this tubing, as seen in Fig. 4, and accounted for a large measure of the pitting observed. Cold-leg sections of loops 7641-1B and 7641-3 were entirely free of metal deposits, but revealed deeper surface imperfections than were found in hot-leg

sections. In some areas of the coolers, pitting reached a depth of 7 mils; however, as seen in Fig. 5, which shows a cold-leg section of loop 7641-1B, these imperfections appear to be the result of a combination of corrosion and surface pits present in the tubing before test.

The examination of loop 7641-2B likewise revealed greater pitting in the cold leg than in the hot leg. However, unlike the loops reported above, a few small metal crystals were found in the cold leg of the loop. These crystalline deposits occurred in clumps approximately 2 mils in thickness and were confined to a short section of the loop near the cooler outlet. The quantity of the deposits was insufficient for a chemical analysis, and it is not known whether the buildups resulted from grains which became detached from the extremely rough as-received surfaces or from mass transfer. Loop 7641-2B operated with the lowest Reynolds number among the three tests, and it is doubtful that mass transfer would take place in this test and not in the others. Analyses of the fluorides used in these tests for metal constituents showed no significant changes in any of these constituents during the test period. These analyses are shown in Table 6.

Fuel Mixtures in Nickel-Molybdenum Alloys

The first forced-circulation loop test of an experimental nickel-molybdenum composition with fuel No. 107 was successfully operated for 1000 hr at a maximum fuel-metal temperature of 1760°F. The loop was composed of 17% Mo, 6% Fe, bal Ni.

Table 5. Conditions of Operation of Three Hastelloy B Forced-Circulation Loops with Fuel Mixture No. 107

Temperature gradient, 300°F

Ratio of hot-leg surface to loop volume, 2.2 in.$^{-1}$

Operating Conditions	Loop No.		
	7641-1B	7641-2B	7641-3
Maximum fuel mixture temperature,°F	1635	1640	1660
Maximum tube wall temperature, °F	1767	1710	1750
Reynolds number of fuel	10,000	5500	10,000
Velocity of fuel, fps	2.61	1.16	2.61
Operating time, hr	1000	1000	407

Other operating conditions for the loop, 7641-9, are shown below:

Maximum fuel-metal interface temp	1760°F
Maximum bulk fuel temp	1610°F
Fuel temperature drop	300°F
Reynolds number	10,000
Flow rate	1.4 gpm
Ratio of heater section surface to total loop volume	2.2 in.^{2}/in.^{3}

An examination of hot-leg sections of this loop indicated fluoride attack to be confined almost entirely to grain boundaries, reaching a maximum depth of 4 mils at the point of maximum wall temperature. Attack appeared generally in the form of small, discontinuous voids, although shallow surface pitting also was evident along exposed surfaces. Considerable oxidation had taken place on the outer surfaces of the hot leg which had been in contact with air. In addition to a heavy uniform oxide film, oxidation proceeded preferentially along grain boundaries to depths of 9 mils.

Cold-leg sections showed numerous surface pits and some areas of intergranular attack to 2 mils. A very thin deposit of tiny metal crystals was present over most of the cold-leg surface, and, in addition, widely dispersed clumps of metal deposits were seen to thicknesses of 6 mils. The presence of these deposits interfered with drainage of the fuel from the walls of the loop along
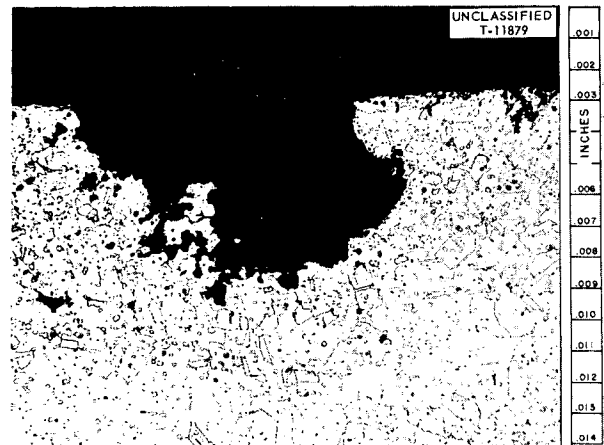
Fig. 5. Area of Deep Pitting in Cooling Coil from Loop 7641-1B. 250X. Reduced 33%.
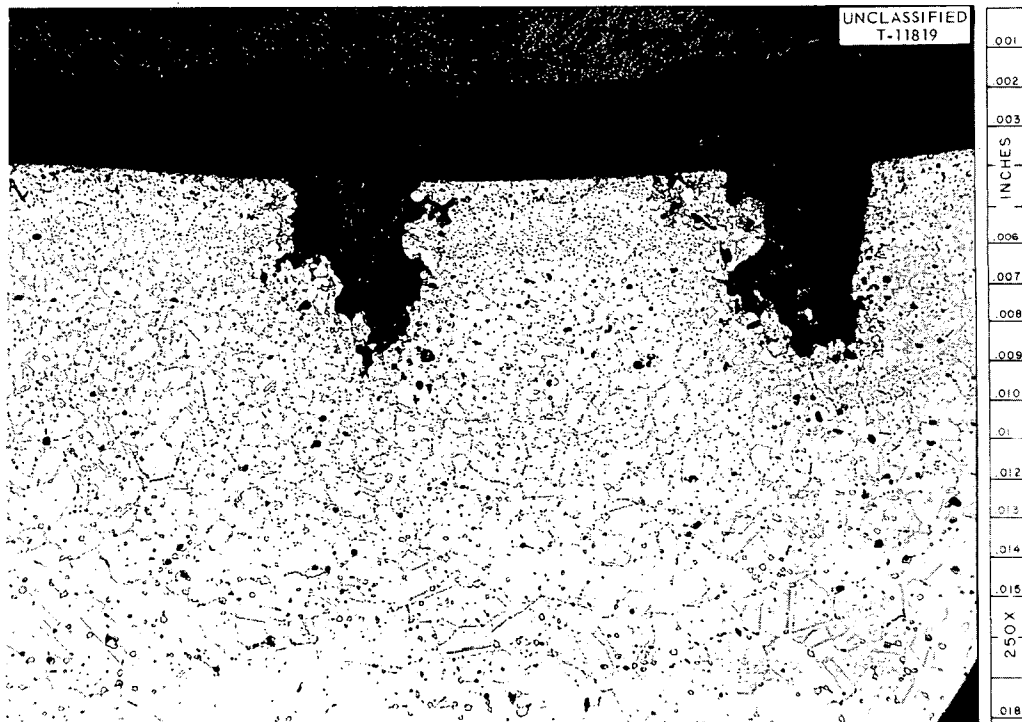
Fig. 4. Surface of As-Received Hastelloy B Tubing. Reduced 17%.

Table 6. Analyses of Fuel No. 107 Mixtures Circulated in Hastelloy B Pump Loops

Loop No.	Fuel Sample	U (%)	Ni (ppm)	Cr (ppm)	Fe (ppm)	Mo (ppm)
7641-1B	Fill	13.7	160	125	150	<2
	Termination	12.4	85	330	95	<2
7641-2B	Fill	13.0	195	110	165	<2
	Termination	12.8	185	325	120	2
7641-3	Fill	13.0	20	35	55	15
	Termination	12.6	205	270	75	9

these portions, and as a result the deposits were partially covered by a heavy fluoride film. Samples of this film which contained sizable quantities of metal crystals were analyzed and were found to contain the following elements:

Fuel Constituents		Contaminants	
K	5–10%	Al	0.05%
Na	2–5%	Fe	0.3%
Li	2–5%	Cr	0.1%
U	10%	Mo	0.1%

It was possible to make a separation of the metal crystals from the residuum of fuel by use of an ammonium oxalate solution, and a spectrographic analysis of the metal particles indicated the following major constituents: 70% Ni, 15.8% Fe, and 7% Mo.

Before-test and after-test samples of fuel from this loop showed no change in nickel and iron contamination, but a slight increase in chromium contamination during the test was noted. It is assumed that Hastelloy W, which was used as a filler wire in making the loop welds, served as the source of this chromium.

FORCED-CIRCULATION LOOP STUDIES OF SODIUM AND NaK

J. H. DeVan   R. S. Crouse

Sodium in Inconel

Three Inconel-sodium forced-circulation loops in which variable temperature drops were employed were examined after they had been operating for 1000 hr at 1500°F. Each loop was of similar construction and incorporated an oxide cold trap maintained at 300°F. Table 7 shows the metallographic results for the series. A definite increase in the amount of mass transfer with increasing temperature drop is evident. A plot of this increase is shown in Fig. 6 and is seen to approximate a linear relationship with temperature drop. In all cases the deposits were composed of approximately 90% Ni and 10% Cr.

A similar series of Inconel loops was operated to evaluate the effectiveness of certain oxide formers added to sodium in order to inhibit mass transfer. Operating conditions of these loops and test results appear in Table 8. An addition of magnesium was tested by exposing sodium to magnesium chips at a temperature of 800°F before introducing the sodium into the test loop. The magnesium concentration anticipated was approximately 1%. Two analyses of the sodium which

Table 7. Variation in Rate of Mass Transfer with Temperature Drop in Inconel-Sodium Pump Loops

Time of operation, 1000 hr

Loop No.	ΔT (°F)	Maximum Thickness of Mass Transfer Deposits (mils)	Total Weight of Loop Deposits* (g)
7426-19	150	12	5.5
7426-6	300	18	13.5
7426-12	400	20	21.2

*Measured by scraping deposits from loop wall.

were made during filling indicated magnesium concentrations to be 2.27 wt %; this high reading possibly indicates carry-over of magnesium chips with the sodium. An oxide cold trap maintained at 300°F was used in the system, but was valved off during the first 50 hr of operation. Flow through the cold trap decreased throughout the test run because of a magnesium buildup at the entrance to the trap. After 1000 hr of operation at a hot-leg temperature of 1500°F and a temperature drop of 300°F, no difference could be seen in the amount of mass transfer in this loop compared with a normal sodium loop.

Two loops which operated under similar temperature conditions with inserts of titanium and zirconium in the hot legs likewise showed little difference in mass transfer compared with a standard loop. The inserts, which were in the

Fig. 6. Effect of Temperature Drop on Mass Transfer in Inconel-Sodium Pump Loops.

form of rods produced by the crystal-bar process, were composed of many incompletely joined crystals and provided a relatively high surface area. The test incorporating a titanium insert resulted in 15 g of mass transfer, while the test with a zirconium insert produced deposits slightly less in extent, comprising a total weight of 13 g. These tests are comparable with standard loops in which deposits in the amount of 15 g are encountered. Hot-leg attack in the loops was intergranular in nature and reached a maximum depth of 1 mil.

Additions of zirconium and titanium, in addition to providing a means of oxide gettering, have been found in certain other liquid-metal systems to result in the formation of corrosion-resistant surface products on the loop wall. Metallographic examination of the loops failed to show any surface layers which could be attributed to the presence of the inserts. Further experiments with these additions are planned, in which finely divided powders will be added directly to the liquid sodium.

Two Inconel forced-circulation loops have been operated with sodium at different velocities in order to evaluate the effect of flow rate on mass transfer. Sodium temperatures ranged from a maximum of 1500°F in the hot leg to a minimum of 1200°F in the cold leg. Pumps were operated at different power levels in order to establish sodium flows of 1.5 and 3.0 gpm, respectively. Both loops contained bypass cold traps for maintaining low oxide levels. Examination of the loops following 1000-hr operation revealed a substantial difference in the amount of deposits recovered

Table 8. Effect of Elemental Additions to Sodium on Mass Transfer in Inconel-Sodium Systems

Maximum fluid temperature, 1500°F

ΔT, 300°F

Loop No.	Type of Addition	Maximum Thickness of Mass Transfer Deposits (mils)	Total Weight of Loop Deposits (g)
7426-16	1% Mg added directly to sodium	14	16
7426-20	Titanium insert added in loop hot leg	23	13
7426-21	Zirconium insert added in loop hot leg	$13\frac{1}{2}$	15
7426-6	Standard loop; cold trap maintained at 300°F	11	15

15

from the cold leg of both tests. At a flow rate of 1.5 gpm (loop 7426-22) the amount of deposit was 10.4 g. Doubling the flow rate to 3.0 gpm (loop 7426-23) resulted in an increase in the amount of deposits to 14.0 g. Hot-leg attack in both loops appeared as intergranular penetrations and reached maximum depths of 2 mils in each test. The average thickness of the deposit also varied as flow rate was changed. The thickness at the lower flow rate was 12 mils, while at the higher flow rate the thickness increased to 22 mils.

Several other sodium loops have operated at flow rates of 2.5 gpm and can be compared with the above tests. While the majority of such tests have incorporated some test variable which introduces a slight difference from the above loops, an average value of deposit weight for those which most closely simulate the conditions of the above loops is 13 g. The resultant plot showing the effect of flow rate when the latter value is included is given in Fig. 7.
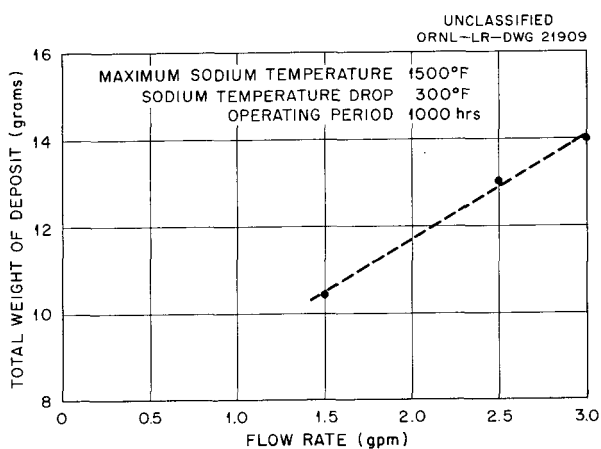
Fig. 7. **Effect of Flow Rate on Mass Transfer in Inconel-Sodium Pump Loops.**

An Inconel pump loop of the design illustrated in Fig. 8 has been operated with sodium for 1508 hr. Test conditions are shown below:

Operating time	1508 hr
Maximum Na temperature	1250°F
Maximum wall temperature	1276°F
Approximate Reynolds number	40,000 (increased to 60,000 after 900 hr)
Temperature gradient	200°F
Ratio of hot-leg surface to total loop volume (in.^{2}/in.^{3})	0.275

This experiment was intended to provide an indication of the flow resistance resulting from mass transfer at sodium temperatures of 1250°F. To evaluate this flow resistance, pressure-measuring instruments were placed across the heater and the cooler of the loop, and changes in pressure drop were measured during the course of the test.

After 900 hr of loop operation, no changes in pressure-drop readings across the heater and the cooler had occurred, although flow had decreased slightly from its value at the original pump speed setting. Flow rate was increased slightly at this time, but no further changes in flow were observed during the remainder of the test. The test was terminated after 1508 hr by a pump failure. On examination of the loop after test, very light deposits were evident in the $\frac{3}{16}$-in.-OD cooler section and also in the loop bend immediately ahead of the heater. It is believed that the deposits which occurred in the bend ahead of the heater may have prevented the correlation of pressure-drop measurements with the buildup of deposits in the cooler section. Thus, although the resistance to flow through the cooler did increase, the pressure-drop measurement ahead of the cooler section changed concurrently with the measurement downstream from the cooler section, so that a pressure-drop increase was not registered.

In conventional Inconel pump loops, operated with sodium under similar temperature conditions, deposits have normally not been observed. Possible explanations for this difference may lie with difference in flow rate or in oxide contamination of the sodium. The mass flow rate in conventional sodium loops is approximately 132 lb·ft^{-2}·sec^{-1}, as compared with 605 lb·ft^{-2}·sec^{-1} in the above loop. Also, a diffusion-type cold trap was incorporated in the above loop for oxide removal, whereas conventional loop tests have employed bypass cold traps of larger capacity.

An Inconel forced-circulation loop was operated with sodium for 2000 hr in order to measure the amount of mass transfer in the system over a relatively long time period. The maximum sodium temperature in the loop was 1500°F, and a 300°F temperature drop was maintained between hot- and cold-leg sections. The loop also contained a bypass cold trap for establishing a low level of oxide contamination in the sodium. A measurement of the weight of crystalline deposits resulting from mass transfer over a 2000-hr period in the
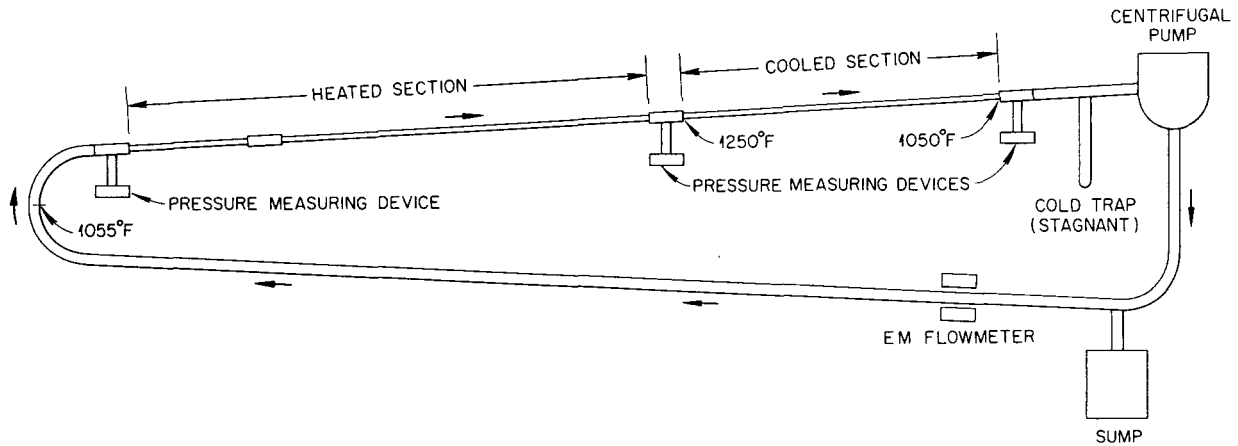
Fig. 8. Inconel Pump Loop Which Circulated Sodium at 1250°F.

loop revealed a deposit buildup of approximately 20 g. It is interesting to compare this value with the results of earlier Inconel loops operated for shorter test durations.[8] The variation in the weight of deposit as a function of test time can be seen in Fig. 9. In tests operated for 1000 hr, the deposit weight was almost twice that of tests operated for 500 hr. However, in the test conducted for 2000 hr, the deposit weight was only $1\frac{1}{2}$ times that of the 1000-hr test. Thus, for times in excess of 1000 hr, the rate of mass transfer appears to decrease somewhat from the almost linear variation below 1000 hr.

[8]J. H. DeVan, *Met. Semiann. Prog. Rep. April 10, 1956,* ORNL-2080, p 53, esp 64.
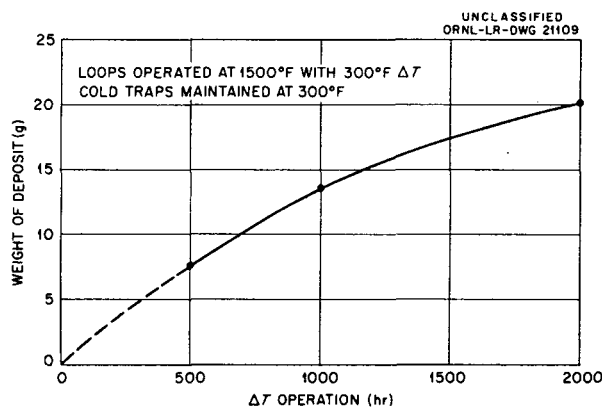
Fig. 9. Variation of Mass Transfer in Inconel-Sodium Forced-Circulation Loops as a Function of Time.

NaK in Inconel

Studies have been made of two Inconel-NaK (56% Na–44% K) forced-circulation loops which contained oxide cold traps operated at 600 and 800°F, respectively. These loops, together with two previous NaK loops having cold-trap temperatures of 100 and 300°F reported previously,[9] provide an analysis of the effect of cold-trap operation on corrosion and mass transfer in Inconel systems. The maximum fluid temperature of each loop was 1500°F, and the temperature drop across the cold-leg section was 300°F. All tests were operated for 1000 hr.

An investigation of the cold-trap design used in these loops had been made prior to the beginning of these studies in order to determine the effectiveness of such a trap in controlling oxide level. In a special test loop containing a bypass cold trap and a device known as a plugging meter,[10] NaK was circulated isothermally at 1500°F, and measurements were made of the oxide concentration of the NaK under various conditions of cold-trap temperatures and flow rates. The plugging meter was used to indicate the saturation temperature of

[9]J. H. DeVan, *Met. Semiann. Prog. Rep. April 10, 1956,* ORNL-2080, p 53, esp 66.

[10]J. W. Mausteller and B. G. Voorhees, in *Liquid-Metals Handbook, Sodium-NaK Supplement,* p 103, ed. by C. B. Jackson, GPO, Washington, 1955.

sodium oxide in the NaK under each of the cold-trap operating conditions. The saturation temperature, together with published information[11] on the solubility limits of sodium oxide in NaK as a function of temperature, was used to establish the oxide concentration. These tests demonstrated that the cold-trap operating temperature in the range from 100 to 1200°F accurately reflected the oxide concentration; that is, the oxide concentration which existed in the NaK corresponded to the limit of solubility for sodium oxide in NaK at the cold-trap temperature.

Table 9 summarizes the effect of the various cold-trap operating temperatures on mass transfer. Samples taken from the coolers at similar locations in each of the loops are compared in Fig. 10.

Table 9. Effect of Cold-Trap Operation on Mass Transfer in Inconel-NaK Pump Loops

Loop No.	Minimum Cold-Trap Temperature (°F)	Maximum Deposit Thickness (mils)	Weight of Metal Deposited (g)*
7439-3	100	7	
7439-1	300	12	
7426-18	600	$11\frac{1}{2}$	3.86
7426-17	800	20	6.29

*Measured by scraping cold-leg deposits from loop wall.

Difficulties in removing deposits from the walls of the earlier NaK loops, 7439-1 and -3, as cited previously,[12] made it impossible to obtain weight determinations of the deposits in these tests. However, in the tests with higher cold-trap temperatures (loops 7426-17 and -18) the deposits were comprised of larger crystals which were more easily separated from the loop walls. The weight determination made of the deposits in these latter tests shows that a noticeable increase in the

amount of deposit was brought about by an increase in cold-trap temperatures from 600 to 800°F. This increase is also reflected in the deposit thickness. A smaller difference in deposit thickness is apparent in comparing the test having a cold-trap temperature of 600°F with the two tests at lower cold-trap temperatures. Metallographic examination of cold-leg sections from these loops also indicates that the change in the amount of deposited material accompanying a decrease in cold-trap temperature below 600°F is less than the change from 800 to 600°F.

As mentioned above, the particle size comprising the deposits is apparently affected by the cold-trap temperature and the oxide concentration. Figures 11 and 12 show deposits taken from similar sections of the loops having cold-trap temperatures of 100 and 800°F. As can be seen, the average particle size has increased considerably at the higher cold-trap temperature. No difference in the composition of the deposits with the variations in cold-trap temperature was noticed. In all tests, deposits were found to contain approximately 90% Ni and 10% Cr.

The results of these studies on the effect of oxides in Inconel-NaK systems show trends quite similar to those found in Inconel-sodium tests. The latter tests, which were discussed previously,[13] were carried out by making oxide additions directly to the sodium. The effects on mass transfer were small at oxide concentrations of 0.05 wt % and below, but became significant at higher concentrations. The deposit particle size also increased as the oxide level increased. A difference in the amount of mass transfer deposits in Inconel-sodium systems, as compared with Inconel-NaK systems, however, has now become apparent. The results of weight determinations made of the deposits in the two more recent Inconel-NaK loops represent somewhat less than one-half the amount of deposits found in sodium systems under similar temperature conditions. This difference in deposit weight was not obvious on the basis of earlier NaK tests, since, as mentioned above, deposit weight determinations had not been available for these first NaK systems. The deposit thicknesses found in the two test media are comparable, although, as discussed in conjunction with the first NaK tests,

[11]R. M. Adams and M. Sittig, *Liquid-Metals Handbook, Sodium-NaK Supplement*, p 8, ed. by C. B. Jackson, GPO, Washington, 1955.

[12]J. H. DeVan, *Met. Semiann. Prog. Rep. April 10, 1956*, ORNL-2080, p 53, esp 66.

[13]J. H. DeVan, *Met. Semiann. Prog. Rep. April 10, 1956*, ORNL-2080, p 53, esp 62.
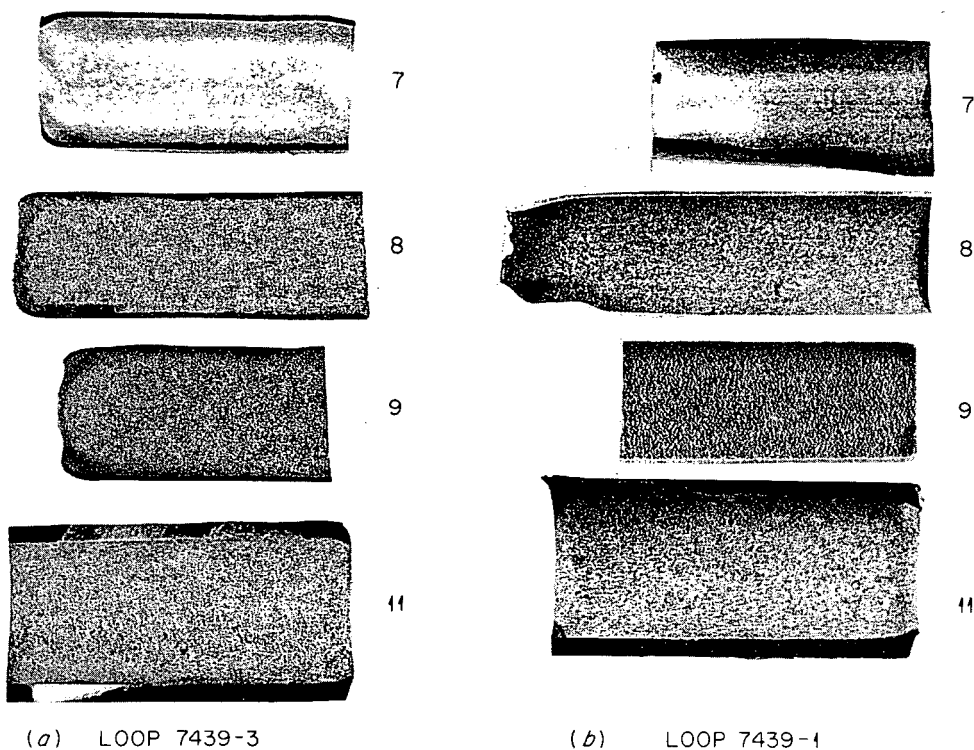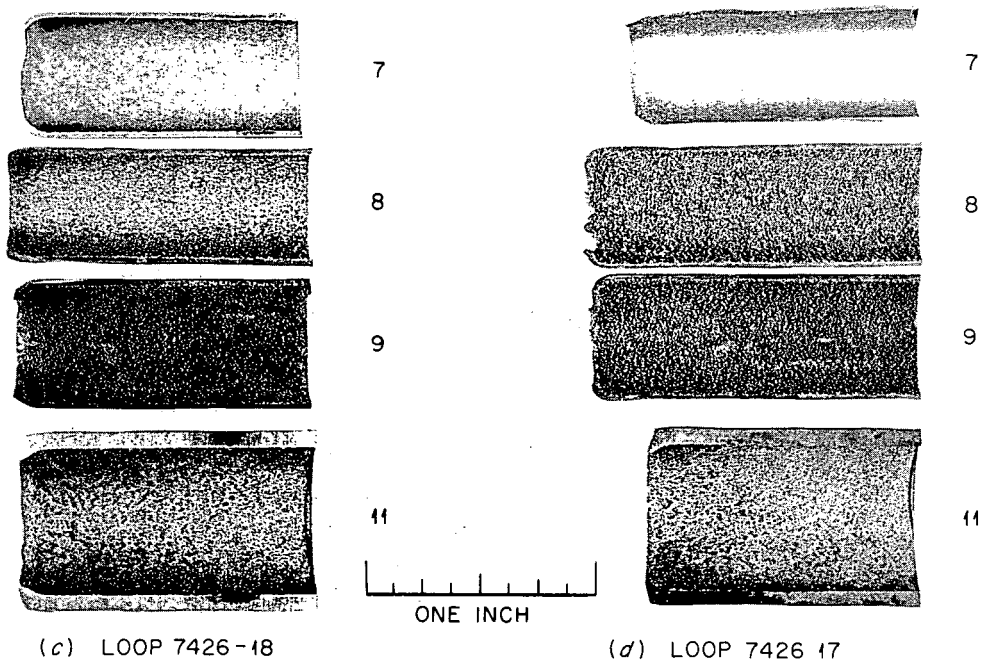
Fig. 10. Effect of Cold-Trap Operation on Mass Transfer in Inconel Pump Loops in Which NaK (56% Na—44% K) Was Circulated at a Maximum Temperature of 1500°F and a Temperature Differential of 300°F. (a) Cold trap at 100°F; (b) 300°F; (c) 600°F; (d) 800°F. (Confidential with caption)

19
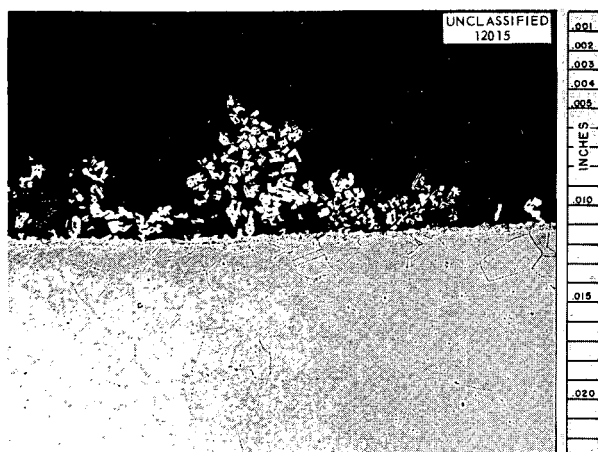
Fig. 11. Appearance of Mass Transfer Deposits in Inconel Loop 7439-3, Which Circulated NaK at 1500°F. Cold trap was maintained at 100°F. 150X. Reduced 31%.

Fig. 12. Appearance of Mass Transfer Deposits in Inconel Loop 7426-17, Which Circulated NaK at 1500°F. Cold trap was maintained at 800°F. 150X. Reduced 31.5%.

this measurement does not accurately reflect the weight of deposits, since the crystals comprising the deposits build up quite randomly and in discontinuous patches.

The composition and the manner of deposition of deposits in the two systems appear to be identical. The average crystallite size comprising the deposits in both systems also is similar. Thus it would appear that the same mechanism for mass transfer exists in both test media, but that the process proceeds slower in Inconel-NaK systems than in Inconel-sodium systems.

Long-Duration Tests of Inconel in NaK and Sodium

An Inconel pump loop, 7439-51, was operated with NaK for 2760 hr to determine the long-range effects of a high thermal gradient on mass transfer and corrosion in an Inconel-NaK system. The loop was of the design shown in Fig. 13 and operated with a thermal gradient of 650°F and a maximum bulk fluid temperature of 1500°F. Fluid flow was maintained at 1.28 gpm. After 2480 hr of operation, a leak developed in the heater coil of the loop, requiring the loop to be dumped. The heater coil was replaced and the loop was again put into operation. After 280 hr of additional operation the loop was terminated when a similar leak developed in the new heater coil.

Metallographic examination of the hot leg which was removed from the loop after 2480 hr revealed light to heavy intergranular attack to a depth of $1\frac{1}{2}$ mils. A needlelike deposit, 7 mils in depth, was also observed in the section just beyond the heater coil, where the loop first experienced a thermal gradient. The cooler coil, which operated for an additional 280 hr, showed only light to moderate pitting, with intergranular attack to a depth of 1 mil. Metal deposits reached a maximum depth of 14 mils in the section entering the cooling coil.

A loop similar to the one mentioned above was also operated with sodium as the test fluid. This loop, 7426-51, was terminated after 4000 hr when a leak developed near the pump. Operating conditions, with the exception of temperature gradient, were similar to those for loop 7439-51. Because of the better heat transfer properties of sodium, a higher thermal gradient of 800°F was achieved. Typical sodium attack in the loop reached a depth of 5 mils. A heavy deposit of metal crystals to a maximum depth of 50 mils was found in the section entering the cooling coil. A photomicrograph of this deposit appears in Fig. 14. Carbide precipitation was also evident along the inside surfaces of all sections of tubing which had been exposed to sodium. This loop operated with a mechanical pump, and a slight passage of the pump lubricating oil through the pump seal could have been responsible for the carburization found.

These long-duration loops were of a unique design and cannot be compared directly with other NaK or sodium tests of shorter duration. The extensive deposits observed in the sodium loop
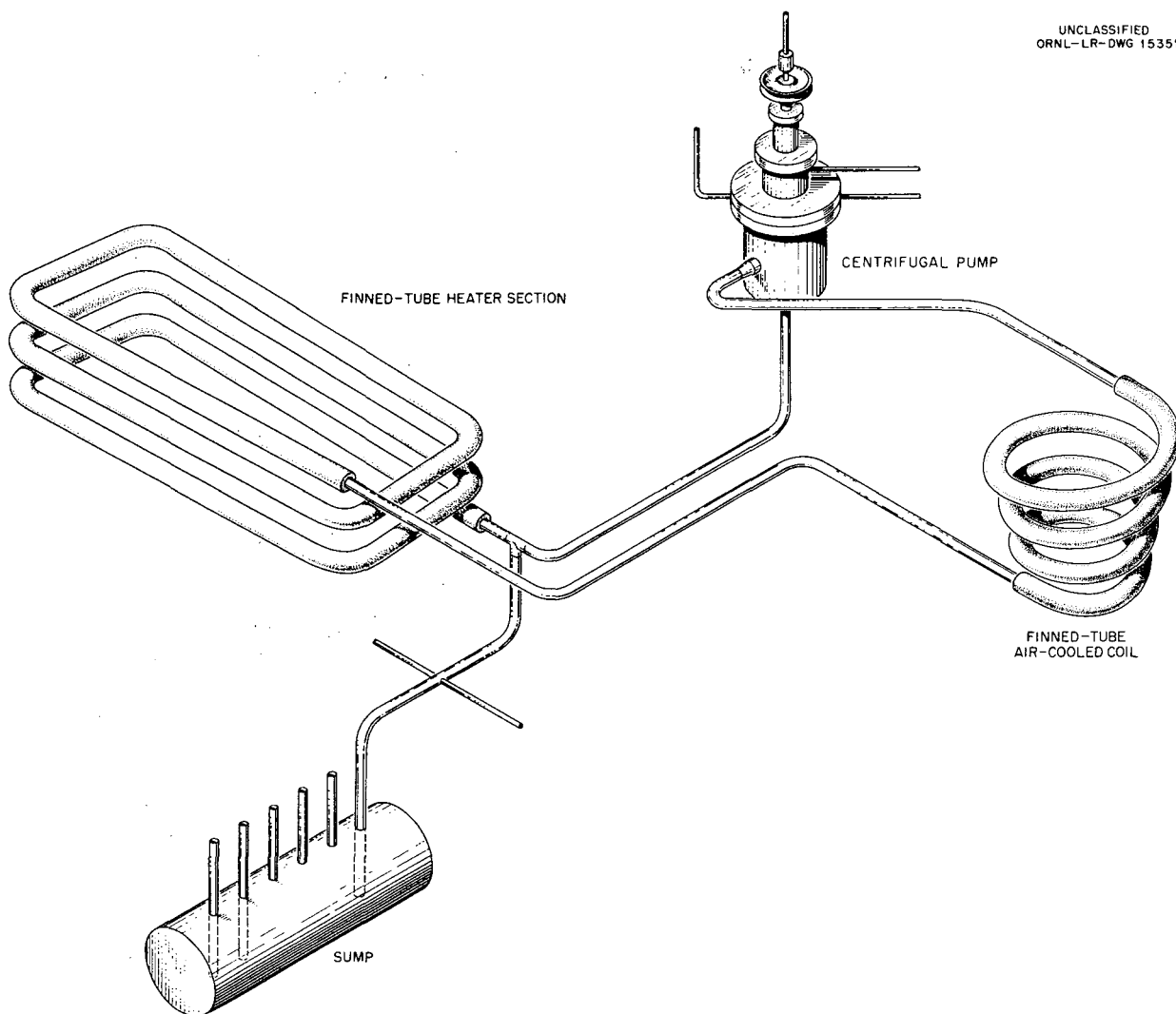
Fig. 13. Schematic Drawing of Gas-Fired Inconel Loop Used for Long-Time Liquid Metals Test.

would indicate that mass transfer proceeds at a rate which is not significantly diminished with time, although, based on the carburization observed in this loop, impurities may also have contributed a major part to the mass transfer process.

Sodium in Stainless Steel

Forced-circulation loop tests of both types 347 and 304 stainless steel were completed with sodium at a maximum temperature of 1500°F and a temperature drop of 300°F. Both loops operated for 1000 hr and contained an oxide cold trap maintained at 300°F. Visual examination of the loops revealed only slight traces of mass transfer particles in cold-leg sections. A typical cold-leg section is shown in Fig. 15. Deposits were similar in extent and appearance to those which have been observed in type 316 stainless steel loops operating under similar conditions,[14] and were much less in amount than deposits found in comparable Inconel loops. The hot leg of the loop revealed slight surface pitting and void formation to 2 mils.

[14]J. H. DeVan and E. A. Kovacevich, *Met. Semiann. Prog. Rep. April 10, 1956*, ORNL-2080, p 67.
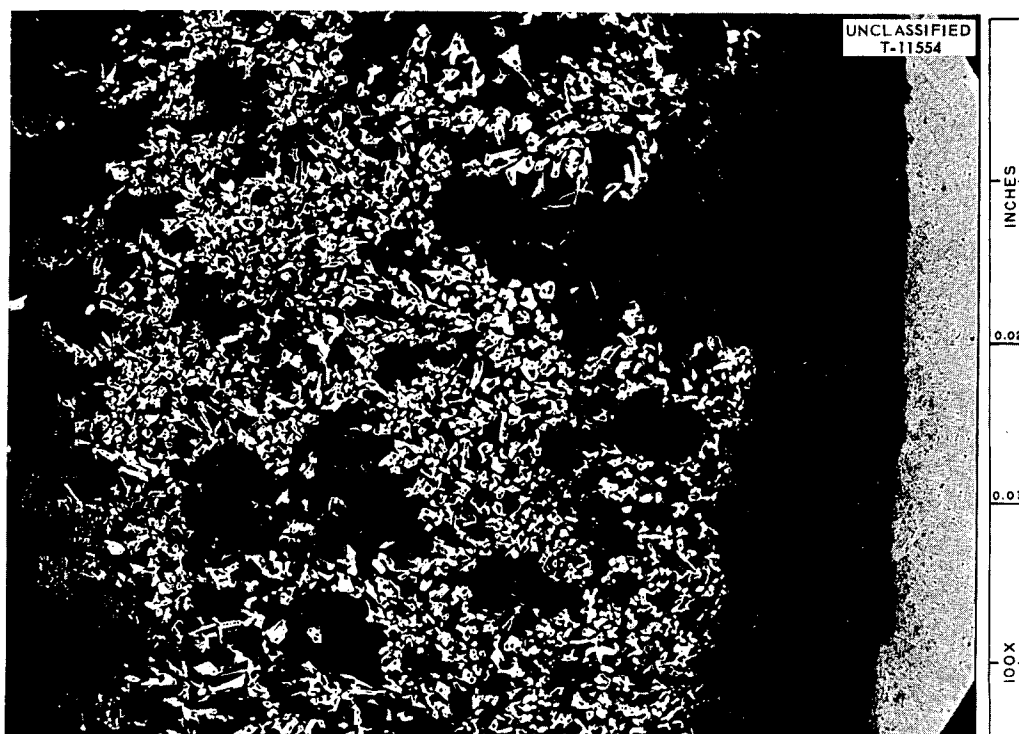
Fig. 14. Deposit Found in Cooler Coil of Inconel Loop 7426-51, Which Circulated Sodium for 4000 hr at 1500°F. Reduced 17%.

Sodium in Incoloy

A sodium pump loop constructed of Incoloy (34% Ni−20% Cr−bal Fe) tubing was operated for 1000 hr at a maximum fluid temperature of 1500°F. The loop employed a temperature drop of 300°F and contained an oxide cold trap. Examination of the loop revealed that mass transfer in colder portions of the loop had taken place in a manner similar to that in Inconel loops. The deposits, however, in contrast with Inconel loops, did not adhere to the loop wall and fell off immediately upon sectioning of the loop. Metallographic specimens therefore did not accurately reveal the extent of such deposits, and a thickness measurement was not obtained. Chemical analysis of the deposits showed them to be comprised predominantly of nickel and chromium (in approximately equal amounts), with 1 to 4% iron. Hot-leg attack was similar to that found in Inconel loops, appearing as intergranular corrosion to depths of 2 mils.

Sodium in Hastelloys B and W

Forced-circulation loops constructed of Hastelloy B have been operated with sodium in order to provide a comparison of the mass transfer properties of this alloy in sodium with the properties established for Inconel. Two such loop tests have been operated with temperature drops of 300°F and with maximum fluid temperatures of 1500 and 1300°F, respectively. Test times employed were 1000 hr. Cold traps were utilized in conjunction with both loops in order to keep the oxide content of the sodium below the saturation value which exists in sodium at 300°F (~50 ppm).

The loop which operated with a maximum fluid temperature of 1500°F (7642-1) contained a somewhat larger mass of cold-leg deposits than did Inconel loops operated under similar temperature conditions. The total weight of deposit resulting from mass transfer over 1000-hr periods (determined by mechanically removing the deposits from the cold leg and weighing them) was 17.3 g in the case of the Hastelloy B loop, as compared with 13 to 14 g in the case of Inconel loops. A chemical analysis of the deposits obtained from both Inconel and Hastelloy B loops is presented in Table 10. Note that the deposits are composed primarily of nickel in the case of both alloys.

At 1300°F the amount of mass transfer occurring in a Hastelloy B loop (7642-2) was very slight, the total weight of deposit measuring only 0.4 g. This compares quite closely with the rate of mass transfer in Inconel-sodium loops at 1300°F. Thus

UNCLASSIFIED
T-11650

7426-25
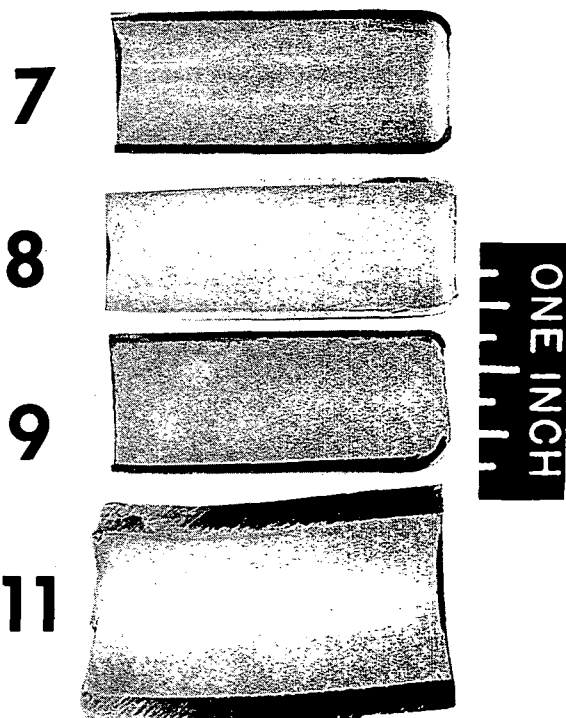
Fig. 15. Cold-Leg Section of Type 304 Stainless Steel Pump Loop Which Circulated Sodium for 1000 hr at 1500°F.

Table 10. Analyses of Mass Transfer Deposits in Inconel- and Hastelloy B—Sodium Pump Loops

Element	Amount Present (%)	
	Inconel Loop	Hastelloy B Loop
Ni	87 to 95	97.5
Cr	4.8 to 10	0.26
Fe	0.005 to 3	0.43
Mo		0.50

a marked increase in the rate of mass transfer as the temperature is increased above 1300°F, which has been well established in Inconel-sodium systems, seems to occur in like manner in sodium–Hastelloy B systems. However, at 1500°F the rate of mass transfer appears to have shown a greater increase in Hastelloy B loops than in comparable Inconel loops.

Microscopic examination of crystals occurring in the Hastelloy B loop operated at 1500°F showed them to be fairly large hexagonal platelets growing out of clusters of smaller crystals of undetermined morphology. The lattice parameter of the crystals was somewhat higher than that of pure nickel and probably reflects the presence of small amounts of iron, chromium, and molybdenum in solid solution. A transmission Laue photograph of one of the platelets showed the plane of the platelet to be of the (111) type.

Hot-leg attack in both Hastelloy B loops occurred as heavy surface pitting to $1\frac{1}{2}$ mils.

A third forced-convection loop of Hastelloy B was operated with sodium for a test duration of 2000 hr. The maximum temperature in the hot leg was 1500°F, and a temperature drop of 300°F was maintained between the hot leg and the cold leg. The loop, 7642-3, showed a weight buildup of 21 g, which compares closely with the 20 g of mass transfer found in an Inconel loop (7426-11) operated for the same time period. Over a 1000-hr period the deposit weight of a Hastelloy B loop of similar design and under similar operating conditions was 17 g. It is evident that mass transfer deposits in the Hastelloy B systems with sodium form at a substantially faster rate during the initial 1000-hr operating period than during the subsequent 1000-hr period. A similar condition is also found to exist in the case of Inconel in sodium (see Fig. 9).

A Hastelloy W pump loop, 7642-4, has been examined after 1000 hr of operation with sodium at 1500°F. Mass transfer deposits found in this loop were approximately 17% greater by weight than the weight of deposits observed in a Hastelloy B loop (7642-1) under identical conditions. A spongy, heavily attacked area approximately $1\frac{1}{2}$ mils deep was seen metallographically along the hot-leg surfaces exposed to sodium. These corroded areas were quite brittle, and in many cases had pulled away from the metal underneath. The cold-leg deposits in this loop contained, by analysis, 97% Ni and 3% Cr.

THERMAL CONVECTION LOOP STUDIES

J. H. DeVan   J. R. DiStefano

Experimental Nickel-Molybdenum Alloys in Fuel No. 107

A test program has been under way for evaluating the corrosion resistance of nickel-molybdenum alloys in the presence of the fluoride mixture (No. 107) NaF-LiF-KF-UF_4 (11.2-45.3-41.0-2.5 mole %). The experiments have been directed toward an understanding of the effects on corrosion behavior resulting from various alloy additions to the binary nickel-molybdenum system. Several alloy heats of varying compositions were prepared by vacuum melting and were fabricated into $\frac{1}{2} \times 0.045$ in. tubing for operation in the form of thermal convection loops. Where sufficient material was available, two loops were operated with each alloy composition in order to permit evaluations at 500 and 1000 hr of operation, respectively. The maximum loop wall temperature was maintained at 1670°F for all tests, and a fluid temperature drop of 250°F existed between hot- and cold-leg sections of the loops.

The results of tests which operated for a 500-hr period are listed in Table 11, and the results for those which operated for 1000 hr are listed in Table 12. It is seen that at the shorter time period only those alloys containing relatively large quantities of aluminum, tungsten, or vanadium have been attacked to depths greater than 2 mils. After a 1000-hr test period, these same alloy additions are again seen to be associated with the heaviest attacks, in this case ranging to $4\frac{1}{2}$ mils. Chromium in amounts up to 10% and niobium in amounts up to 5% in these loop tests did not appear to seriously affect corrosion resistance from the standpoint of total depth of attack. However, the presence of chromium as a corrosion product in the fuel increased noticeably as the percentage of the element in the base metal increased. This effect is shown in Fig. 16, which illustrates both the attack and the chromium concentration in the fuel for alloys containing chromium in the range from 3 to 9%. The cold legs of all loops showed very limited attack and no evidence of metallic deposits, except where noted.

Special Fuels

A test program utilizing standard thermal convection loops has been in progress for evaluating
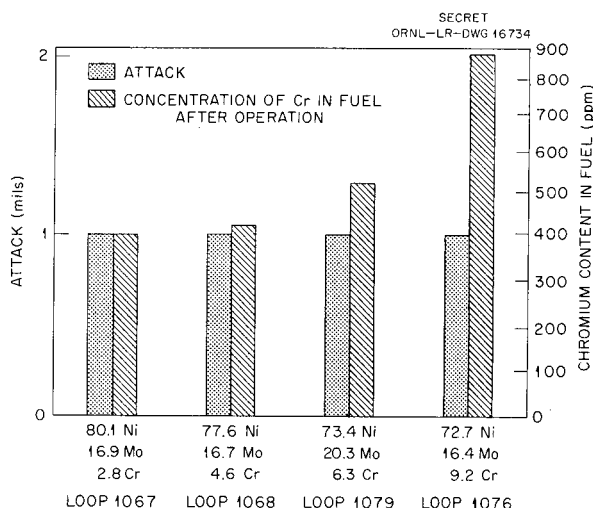
Fig. 16. Corrosion Results of Nickel-Chromium-Molybdenum Alloys in Fuel No. 107 (NaF-KF-LiF-UF$_4$, 11.2-41-45.3-2.5 Mole %).

the corrosion properties of various fluoride mixtures in conjunction with Inconel. Several of these tests were discussed in a previous progress report.[15] Results of subsequent tests are shown in Table 13.

The maximum fluoride mixture temperature in all tests was 1500°F, and the test duration was 500 hr. Standard thermal convection loop-filling procedures were followed, but, due to the limited availability of salt, the precleaning steps, which normally utilize an extra fluoride fill, were omitted.

The first group of tests listed in Table 13 is comprised of loops in which a thorium-bearing salt mixture was circulated. The examination of three loops which contained the salt mixture NaF-ThF_4 (74-26 mole %) revealed attack along hot-leg sections to depths of 5, 4, and 6 mils, respectively. The addition of 2 mole % uranium fluoride to this mixture increased the resultant hot-leg attack in three tests to depths of 12 and 15 mils, and was accompanied by a metallic layer in the cold leg. An attack of 12 mils resulted from operation with a third thorium-bearing salt of the composition LiF-BeF_2-UF_4-ThF_4 (71-16-1-12 mole %).

Test results are shown under group 2 of Table 13 for fuels containing beryllium fluoride complexed with lithium fluoride and/or sodium fluoride. In

---

[15] E. A. Kovacevich, *Met. Semiann. Prog. Rep. Oct. 10, 1956,* ORNL-2217, p 51, esp 58.

Table 11. Test Results of Ni-Mo Thermal Convection Loops Operated for 500 hr in Fuel No. 107

Loop No.	Alloy Composition (wt %)	Metallographic Results	
		Hot-Leg Attack (mils)	Cold-Leg* Attack
1067	17 Mo—3 Cr—bal Ni	1	None
1069	20 Mo—3 Cr—bal Ni	1	Few voids to 1 mil
1068	17 Mo—5 Cr—bal Ni	1	Few voids to 1 mil
1093	17 Mo—7 Cr—bal Ni	2	Light surface roughening, few voids to 2 mils in one spot
1079	20 Mo—7 Cr—bal Ni	1	None
1076	17 Mo—10 Cr—bal Ni	1	Light surface roughening
1113	17 Mo—2 W—bal Ni	1.25	Few voids to 1 mil
1120	17 Mo—4 W—bal Ni	1	Moderate surface roughening, few voids to 1 mil
1100	17 Mo—2 V—bal Ni	<1	Light surface roughening and surface pitting
1123	17 Mo—4 V—bal Ni	2	Light surface roughening
1126	17 Mo—3 Nb—bal Ni	<1	Moderate surface roughening
1131	17 Mo—5 Nb—bal Ni	<1	Light surface roughening
1070	17 Mo—0.5 Al—bal Ni	<1	None
1108	17 Mo—2 Al—bal Ni	3	Light surface roughening
1098	17 Mo—2 Ti—bal Ni	<1	None
1119	17 Mo—4 Fe—bal Ni	<1	Moderate surface roughening
1080	15 Mo—1 Al—1.5 Ti—bal Ni	1	Light surface roughening
1103	16 Mo—1 Al—1.5 Ti—bal Ni	1	Light surface roughening
1105	16 Mo—2 Al—1.5 Ti—bal Ni	3	None
1094	20 Mo—7 Cr—2 Nb—1 Fe—bal Ni	2	None
1082	15 Mo—0.5 Al—3 Nb—3 W—bal Ni	<1	None
1133	16 Mo—6 Cr—1 Nb—1 Al—bal Ni	3	Light surface roughening, subsurface voids to 1 mil
1078	20 Mo—1 Nb—2 Ti—0.8 Mn—bal Ni	1	None
1101	16 Mo—5 Cr—1.5 Ti—1 Al—bal Ni	2	Light surface roughening, subsurface voids to 1 mil
1081	15 Mo—5 Cr—3 Nb—3 W—bal Ni	2.5	None
1099	20 Mo—7 Cr—1 Al—2 Nb—1 Fe—bal Ni	1.5	None
1156**	15 Mo—6 Cr—0.5 Al—5 Fe—0.5 Mn—bal Ni	2	Very light surface roughening

*The cold leg of all loops appeared to be free of metallic deposit.
**Operated for 123 hr.

Table 12. Test Results of Ni-Mo Thermal Convection Loops Operated for 1000 hr in Fuel No. 107

Loop No.	Alloy Composition (wt %)	Metallographic Results	
		Hot-Leg Attack (mils)	Cold-Leg* Attack
1075	17 Mo—5 Cr—bal Ni	1	Light surface roughening
1122**	17 Mo—4 W—bal Ni	2	Heavy but shallow surface roughening, few voids to 2.5 mils
1125	17 Mo—4 V—bal Ni	4	Heavy but shallow surface roughening
1128	17 Mo—3 Nb—bal Ni	3	Heavy but shallow surface roughening, heavy subsurface voids to 1 mil
1130	17 Mo—5 Nb—bal Ni	4	Light surface roughening
1024	11 Mo—2 Al—bal Ni	2	Light surface roughening
1025	11 Mo—2 Al—bal Ni	2	Light surface roughening
1114	17 Mo—2 Al—bal Ni	4	Light surface roughening
1115	17 Mo—2 Ti—bal Ni	1	Light surface roughening
1136	16 Mo—2 Al—1.5 Ti—bal Ni	4.5	Light surface roughening
1135	16 Mo—6 Cr—1 Nb—bal Ni	4.5	Light surface roughening
1087	20 Mo—1 Nb—2 Ti—0.8 Mn—bal Ni	2.5	Very light surface roughening
1137	20 Mo—7 Cr—1 Al—2 Nb—1 Fe—bal Ni	2.5	None
1155	15 Mo—6 Cr—0.5 Al—5 Fe—0.5 Mn—bal Ni	3	Moderate surface roughening
1159***	17 Mo—8 Cr—1 Al—7 Fe—0.5 Mn—bal Ni	12	Light surface roughening, metallic deposit to depth of 1 mil

*The cold legs of all loops appeared to be free of metallic deposits, except where noted.

**Operated for 791 hr.

***Operated at 1650°F.

non-uranium-bearing fuels of this type, it is evident that decreasing the ratio of the beryllium fluoride to the alkali-metal fluoride constituents causes a corresponding decrease in attack. The addition of 3 mole % uranium fluoride to these mixtures generally was accompanied by a 3- to 6-mil increase in attack, although the total depth of attack still decreased as BeF_2 was reduced in proportion to NaF and/or LiF. Metallic layers and finely dispersed metal crystals were observed along the cold-leg regions of loops operated with all uranium-bearing mixtures.

Void Migration Studies in Inconel—Fuel No. 30 System

An analysis of the corrosion process in Inconel thermal convection loops containing fluorides indicates that the rate of attack (i.e., void formation) becomes constant when the test period exceeds 250 hr. This linear relationship of attack with time is reached after an initial period of rapid attack resulting from the equilibration of the fluorides with the Inconel. It would be assumed that the linear migration of voids into Inconel with time represents a constant rate of chromium removal with time. However, some question has existed as to whether, even in the absence of further chromium removal, some void formation might continue as a result of the rapid attack represented by the equilibration of fluorides. Accordingly, a series of standard Inconel thermal convection loops was operated with the fuel (No. 30) NaF-ZrF_4-UF_4 (50-46-4 mole %) at a bulk fluid temperature of 1500°F following the schedule illustrated in Fig. 17. One loop, 1085, was terminated after 277 hr of operation, while the fuel in a second

Table 13. Test Results of Thermal Convection Loops Operated for 500 hr with Fluoride Mixtures at 1500°F

Fuel No.	Fuel Composition (mole %)					Loop No.	Metallographic Results	
	NaF	LiF	BeF$_2$	UF$_4$	ThF$_4$		Hot-Leg Attack (mils)	Cold Leg
Group 1								
WR-23	74				26	969	5	No layer or crystals
						1026	4	No layer or crystals
						1027	6	No layer or crystals
WR-24	74			2	24	970	12	Metallic layer
						1028	15	Metallic layer
						1029	15	Metallic layer
WR-25		71	16	1	12	972	8	Metallic layer
Group 2								
WR-27	50		50			1042	11	Metallic layer
						1043	9	No layer or crystals
WR-28	48.5		48.5	3		1044	14	Metallic layer
						1045	12	Metallic layer
WR-18		50	47	3		959	12	No layer or crystals
						982	14	Metallic layer
WR-30	55		42	3		1151	11	Metallic layer and crystals
						1152	11	Metallic layer
WR-31	70.		30			1050	6	No layer or crystals
						1051	4	No layer or crystals
WR-32	68		29	3		1052	12	No layer or crystals
						1053	12	Metallic layer
WR-22	33	33	31	3		966	8½	Metallic layer
						967	9	Metallic layer
WR-33	53	24	23			1054	5	No layer or crystals
WR-34	52	23	22	3		1056	12½	Metallic layer and crystals
WR-35	49	36	15			1046	3	No layer or crystals
						1047	4	No layer or crystals
WR-36	48	35	14	3		1060	10	Metallic crystals
WR-25		71	16	1	12	972	8	Metallic layer

SECRET
ORNL-LR-DWG 25171
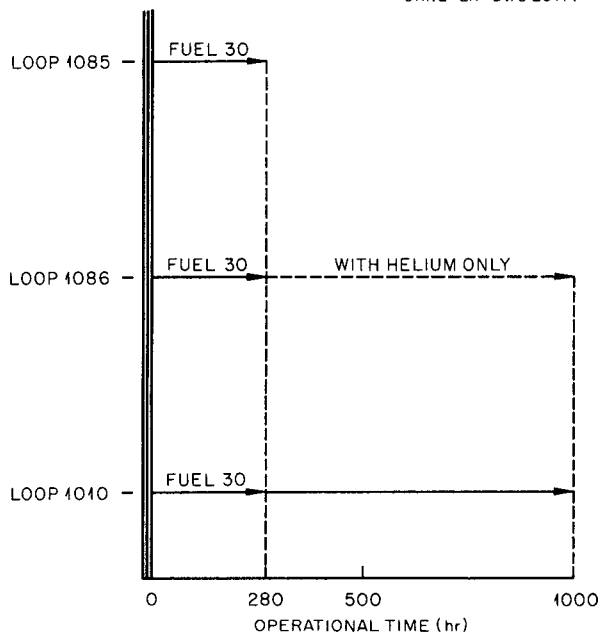
Fig. 17. Schedule of Thermal Convection Loops Operated to Study Void Migration in Inconel Exposed to Fuel No. 30 (NaF-ZrF$_4$-UF$_4$, 50-46-4 Mole %).

loop, 1086, was replaced with helium after 280 hr, and the loop was then held at test temperature for the remaining scheduled 1000 hr. A third loop, 1010, was included as a standard loop; this loop completed 1000 hr with another batch of fuel under similar temperature conditions.

Metallographic examination of loop 1085 revealed a maximum hot-leg attack of 8 mils, which occurred as heavy surface roughening with heavy general subsurface void formation to 1 mil, accompanied by heavy intergranular subsurface void formation to a depth of 8 mils. The cold leg showed only heavy roughening. Comparison of the hot-leg attacks found in loops 1085 and 1086, as shown in Fig. 18, indicates the attacks in both loops to be identical in depth, size, and type of void formation. Further metallographic examination throughout both loops revealed similar corrosion profiles for respective metallographic samples. In the standard 1000-hr loop, 1010, which operated with a different batch of fuel, the maximum attack observed was 12 mils.

The results of these tests provide evidence that the migration of voids into Inconel, instituted by

the leaching of chromium during the corrosion process, does not continue if the loop is left at the test temperature without fuel. Thus the coalescence of vacancies in the metal to form visible voids must proceed at a rate at least commensurate with the rate at which vacancies
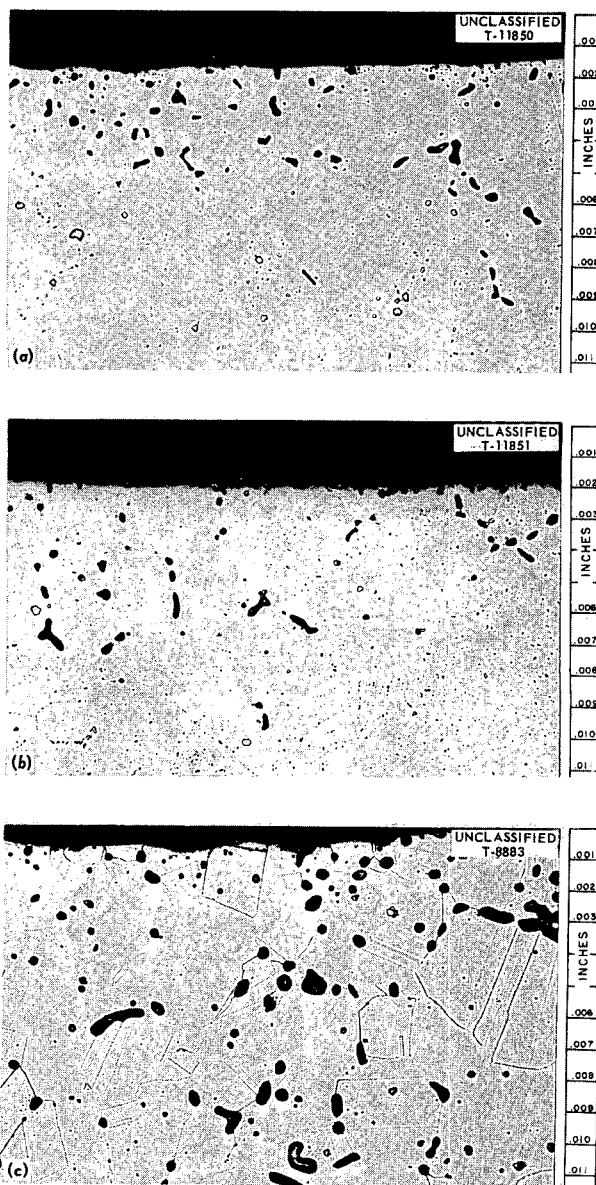
Fig. 18. Comparison of Hot-Leg Attacks Found in (a) Loop 1085, (b) Loop 1086, and (c) Loop 1010. Loop 1085 operated 277 hr with fuel No. 30 at 1500°F; loop 1086 operated 280 hr with fuel No. 30 but was allowed to continue 720 hr with helium at test temperatures; loop 1010 operated 1000 hr with fuel No. 30 at 1500°F. 250X. Reduced 32.5%. (Secret with caption)

are formed. If the removal of chromium from the metal surface is stopped, void formation is also stopped.

Inconel Castings

Corrosion studies were continued with Inconel castings in order to determine their suitability for applications involving large intricate shapes, difficult to fabricate by ordinary machining methods. Earlier experiments indicated that Inconel in the cast form was highly susceptible to attack in fuel No. 30, while showing no visible attack in sodium.[16] In contrast with the previous set of experiments in fuel No. 30, later studies have shown comparable attack in the wrought and cast Inconel sections examined. The compositions which were evaluated in more recent experiments are listed in Table 14.

Two specimens, each 1 in. in outside diameter by ½ in. in inside diameter by 6 in. long, were procured for each of these compositions. For fuel No. 30 tests, one specimen was welded into the hot leg of a wrought Inconel thermal convection loop, and a section approximately 1 in. long was removed from the other specimen for radiographic and metallographic inspection. When sodium was the coolant, two loops containing cast inserts

---

[16]E. A. Kovacevich, *Met. Semiann. Prog. Rep. Oct. 10, 1956*, ORNL-2217, p 51.

were operated for each composition, and no as-received specimen was obtained. The location of the casting was at the point of maximum wall temperature in the loop. The results of the thermal convection loop tests operated in fuel No. 30 at 1500°F for 500 hr have been summarized in Table 15. The maximum depth of attack noted in these castings was much less than in the first set of experiments with Inconel castings and, in general, was comparable with the attack in wrought Inconel sections. A major factor contributing to this result was the soundness of the as-received casting, which was considerably better in the latter set of castings than in the first.

No significant difference in attack was noted among the castings, even though the compositions varied considerably from the standpoint of Nb, Mn, Si, and C. Maximum depths of attack noted in all loops ranged normally from 6 to 8 mils. In the case of loop No. 1143, the weld interface between the cast and the wrought sections revealed relatively large intergranular cracks to a depth of 20 mils. It is believed that these cracks developed during welding, however, rather than as a result of corrosion.

Table 16 lists the results of thermal convection loop tests operated in sodium for 500 hr at 1500°F. The four loops which circulated sodium (1138, 1139, 1140, and 1141) revealed only slight attack in the cast specimens examined. In general, the cast areas showed heavy surface roughening and

---

Table 14. Compositions of Inconel Castings

Loop No.	Heat No.	Composition (wt %)								Test Fluid
		Ni	Cr	Fe	Cu	Nb	Mn	Si	C	
1138	1G	71.2	15.1	7.89	0.13	3.1	0.89	1.42	0.21	Na
1139	1G									
1140	2H	70.6	14.7	7.62	0.13	4.02	0.97	1.13	0.22	Na
1141	2H									
1142	3A	74.4	15.7	8.5	0.13	0.13	0.51	0.41	0.08	30
1143	4B	75.0	15.6	8.1	0.12	0.06	0.53	0.34	0.13	30
1144	5C	72.1	15.0	7.96	0.13	3.4	0.37	0.51	0.13	30
1145	6D	73.5	16.0	8.21	0.14	0.12	0.47	1.13	0.13	30
1146	7E	73.8	15.7	8.25	0.14	<0.1	1.55	0.43	0.12	30
1147	8F	72.9	15.8	7.62	0.14	1.8	0.33	1.23	0.12	30

Table 15. Test Results of Inconel Castings in Fuel No. 30

Loop No.	Heat No.	Metallographic Results			Constituents in Fuel (ppm)				
		Hot Leg	Attack (mils)	Cold-Leg Attack (mils)	Ni	Cr	Fe	Nb	Mn
1142	3A	Cast section	6		60	620	75	135	50
		Weld interface	7						
		Wrought	4	<1					
1143	4B	Cast section	8		25	635	80	50	50
		Weld interface	11*						
		Wrought	8	<1					
1144	5C	Cast section	8		40	860	75	50	40
		Weld interface							
		Wrought	$6\frac{1}{2}$	<1					
1145	6D	Cast section	7		30	750	55	80	45
		Weld interface	$5\frac{1}{2}$						
		Wrought	$6\frac{1}{2}$	<1					
1146	7E	Cast section	7		40	700	60	85	45
		Weld interface							
		Wrought	$7\frac{1}{2}$	<1					
1147	8F	Cast section	8		55	860	60	2	45
		Weld interface	$7\frac{1}{2}$						
		Wrought	$8\frac{1}{2}$	<1					

*Cracks to 20 mils were observed in the weld bead; these resulted most probably during fabrication rather than from corrosion.

Table 16. Metallographic Results of Inconel Castings Tested in Sodium

Loop No.	Heat No.	Metallographic Results		
		Hot Leg	Attack (mils)	Cold-Leg Attack (mils)
1138	1G	Cast section	<1	
		Weld interface		
		Wrought	<1	Moderate surface roughness
1139	1G	Cast section	1	
		Weld interface		
		Wrought	<1	Moderate surface roughness
1140	2H	Cast section	1	
		Weld interface		
		Wrought	<1	<1
1141	2H	Cast section	1	
		Weld interface		
		Wrought	<1	<1

surface pitting with a few general subsurface voids to depths of less than 1 mil. Moderate porosity was noticed, as well as a heavy intergranular second phase believed to be niobium carbide.

Niobium with Fuel No. 107 and Sodium

The compatibility of niobium with fuel No. 107 and sodium has been studied in thermal convection loops operating at 1500°F. The loops, which were fabricated by Battelle Memorial Institute, were somewhat smaller than standard loops employed for corrosion studies of more common materials. The niobium tubing was formed from 0.020-in. sheet stock and had an inside diameter of 0.53 in. To eliminate the oxidation problem which exists for niobium at the test temperatures, the niobium was encased with an outer sheath of stainless steel (type 321). Fabrication of a sound loop of this design was difficult, in that cracks often developed in the niobium tubing when the cladding was assembled.

Three niobium loops, 1072, 1073, and 1022, were operated for 1664, 1000, and 775 hr, respectively, at 1500°F with fuel No. 107. The fuel analysis after operation for loop 1022 revealed a high buildup of chromium, 715 ppm, and points to the probability of a leak to the stainless steel clad. The examination of this loop showed an absence of cold-leg deposits and only slight hot-leg attack in the form of shallow pitting. Loops 1072 and 1073, on the other hand, apparently remained sound during operation, since no elements other than niobium were found in the fuel after test. However, in a microscopic examination of the loops, metallic crystals were detected in the fuel layer bordering the loop wall. These crystals were also picked up metallographically and can be seen in Fig. 19, which shows a cold-leg section from loop 1072. Hot-leg attack in these loops also occurred as shallow pitting to less than 1 mil. A typical after-test specimen from the hot leg of loop 1072 is shown in Fig. 20.

An additional niobium loop, 1091, was operated for 1000 hr with sodium at 1500°F. Examination of the hot leg of this loop showed little evidence

of attack other than possible uniform surface removal. Cold-leg deposits were, however, observed macroscopically. Chemical analysis of this deposit indicates that the loop probably leaked to the cladding during operation, since large amounts of Fe, Ni, and Cr, in addition to Nb, were present in the deposit.
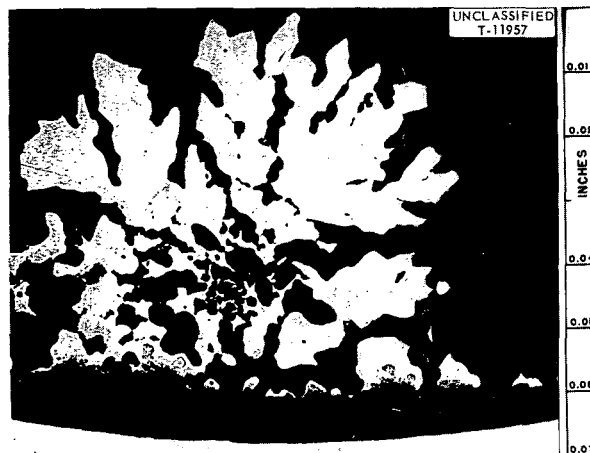
Fig. 19. Metallic Crystals in Fuel of Cold-Leg Sections from Niobium Loop 1072, Which Operated 1664 hr with Fuel No. 107 at 1500°F. 50X. Reduced 32%. (Secret with caption)

Fig. 20. Maximum Hot-Leg Attack Observed in Niobium Loop 1072, Which Operated 1664 hr with Fuel No. 107 at 1500°F. 250X. Reduced 32%. (Secret with caption)

MECHANICAL PROPERTIES

D. A. Douglas

C. R. Kennedy[1]   J. W. Woods

J. R. Weir   R. W. Swindemann

The work of the High-Temperature Mechanical Properties Section during the past year has been directed towards several goals. The primary effort was concerned with evaluating, for design purposes, the behavior of materials under the various conditions of stress, temperature, and environment which will be encountered during operation of the ART. In this regard, studies were conducted on the structural alloy Inconel, the moderator material beryllium, and the shielding metals, lead and lithium-containing alloys. A second portion of the endeavor was directed towards gathering the type of basic information on high-temperature metal behavior which would make possible a prediction of the safe operating life of the various component parts of the reactor under a variety of operating conditions. Finally, attention was given to the problem of developing improved alloys which would permit substantial gains in power through higher operating temperatures and a greater margin of safety through better strength and corrosion resistance. The progress made during the past year is reported in sections corresponding to these three general categories.

DESIGN DATA

Inconel

Creep and stress-rupture properties were obtained for Inconel in the temperature range from 1300 to 1650°F in sodium and in the fused salt (No. 30) NaF-ZrF_4-UF_4 (50-46-4 mole %). Data in argon were used for purposes of comparison. Variables such as grain size, section thickness, and heat consistency were investigated. It was found that in the fused salt environment fine grain metal is stronger than coarse grain metal at 1300°F but weaker at 1500°F and above. However, in argon and sodium the fine grain Inconel maintains its superiority up to 1650°F, where metallurgical instabilities begin to introduce adverse effects. A comparison of three heats of Inconel showed that quite wide variations in properties may be expected. There are not large enough differences in the major alloying elements to account for this lack of uniformity; so, apparently, the source lies in the variations of the minor additions or the residual elements which are difficult to control in air-melting practice. The detailed information mentioned above has been compiled and reported.[2]

Since the strength properties of Inconel render it a very marginal material for use at the peak operating temperatures, some thought has been given to a modification which would increase the strength without impairing the material's excellent fabricating characteristics. Carbon is a very potent strengthening agent because of the effect of dispersed carbides through the matrix and in the grain boundaries; unfortunately, such a structure is difficult to draw into tubing. It was believed feasible, however, to fabricate the tubing and then add carbon through carburization. Several creep specimens were pack carburized and tested in fused salt and argon. As anticipated, a very marked improvement in creep properties was realized.

Recrystallization of Inconel

A stable metallurgical microstructure is required if optimum strength properties are to be obtained in an alloy. Tests have demonstrated that metals which have undergone various amounts of cold work may recrystallize under certain conditions of stress and temperature and that a deleterious effect on the creep properties results.[3] Since many reactor components are fabricated by pressure-forming methods, and assembled by welding and brazing, portions of the structural metal will have experienced a variety of thermal treatments prior to operation. This program was undertaken in order to establish the temperatures required for recrystallization after varying amounts of cold work and to determine the stable grain size achieved after high-temperature anneals.

[1]Pratt & Whitney Aircraft.

[2]J. R. Weir, Jr., D. W. Douglas, and W. D. Manly, *Inconel as a Structural Material for a High-Temperature Fused-Salt Reactor*, ORNL-2264 (June 18, 1957).

[3]D. A. Douglas *et al.*, *ANP Quar. Prog. Rep. Dec. 31, 1956*, ORNL-2221 (Parts 1–5), p 244.

The report,[4] ORNL-2406, describes the testing procedures used and presents photomicrographs illustrating the grain size produced in the recrystallized structure. It was noted that the recrystallization temperature ranged from 1200 to 1650°F, depending on the amount of cold work and the time held at temperature. Initially, fine grain Inconel recrystallized about 100°F lower than the coarse grain material for the same amount of prior deformation and time at temperature. Up to temperatures of 1800°F, the grain size resulting from high-temperature treatments was found to be dependent on the degree of working prior to recrystallization. However, at 1900°F only a very small difference in grain sizes could be seen regardless of the prior treatment.

Beryllium

In the Metallurgy Semiannual Progress Report for October 1956, it was reported that an extensive mechanical testing program for beryllium from 800 to 1500°F was conducted by the Brush Beryllium Company under Subcontract P.O. W34X-75581 (ref 5). During the past year additional tests were conducted by the same company on samples trepanned from the actual moderator blocks prepared for the ART. These results have shown excellent consistency with values obtained in the prior test program for material of like composition. Thus, it appears that data from the test program can be reliably applied to large scale production pressings.

SHIELDING MATERIAL

Creep-rupture testing of an 80% Mg–20% Li alloy proposed as a neutron-shielding material has been completed. Additional data to those previously obtained[6] at 200°F on specimens that were given a chemical surface treatment[7] are summarized below:

Stress (psi)	Time to Per Cent Strain (hr)		
	0.2%	0.5%	1.0%
100	3579	6647	
200	862	2284	3484

Tests were also run on untreated specimens for comparative purposes and are summarized in the following table:

Stress (psi)	Time to Per Cent Strain (hr)					
	0.2%	0.5%	1%	2%	5%	10%
600	3.6	25	72	121	420	940
			0.5		1	71

An alloy of very pure lead containing 0.06% copper has been proposed as a gamma-ray shielding material. As no mechanical property data were available at a temperature of 230°F, the expected maximum operating temperature of the lead shield, a creep-rupture testing program was initiated to determine the strength of this alloy. The design criteria were established at a creep rate of 0.5% strain, at a stress of 100 psi. Tolerable deformation was estimated to be 0.5%/yr. However, the test results in air show that this alloy has a deformation rate of about 2%/yr at 100 psi. Specimens tested at 50 and 20 psi show a deformation of 0.08%/yr and 0.05%/yr, respectively. A lead-lithium alloy was also investigated in the hope that its excellent room-temperature strength would be reflected in good high-temperature strength also. However, it has been found that the lead-copper alloy has the greater creep strength at 230°F (ref 8).

As the temperature of the tests in air was difficult to control because of ambient temperature fluctuations, three testing machines were designed and built to test the lead alloys in an oil bath. Tests have been in progress for only a short time, but it is indicated that both alloys will have a higher creep rate in oil than was obtained from tests in air.

[4]D. A. Douglas and J. R. Weir, *Recrystallization and Grain Growth of Inconel*, ORNL-2406 (to be published).

[5]D. A. Douglas *et al.*, *Met. Semiann. Prog. Rep. Oct. 10, 1956*, ORNL-2217, p 65; R. G. O'Rourke, *Mechanical Properties of Reactor-Grade Beryllium at Elevated Temperatures*, COO-312 (Aug. 1956).

[6]D. A. Douglas *et al.*, *ANP Quar. Prog. Rep. Sept. 10, 1956*, ORNL-2157 (Parts 1–5), p 205.

[7]R. E. McDonald and C. F. Leitten, Jr., *ANP Quar. Prog. Rep. June 10, 1956*, ORNL-2106 (Parts 1–5), p 173.

[8]E. E. Hoffman *et al.*, *Lead-Lithium Shielding Alloy — Metallurgical Study*, ORNL-2404 (to be published).

DEFORMATION STUDIES

Extrapolation of Inconel Data

One of the problems associated with mechanical testing work is that there are frequent needs for data under conditions outside the range of temperature or stress that has been explored. Thus, the first step toward being able to anticipate the behavior of metals under service conditions is to develop a reliable method of interpolating and extrapolating the data at hand. There has been much work done in this field and there are several relationships which appear to have merit. However, the multitude of metallurgical variables involved in high-temperature deformation processes makes it advisable to derive empirical equations based on fairly specific data. This has been done for Inconel, and the method and limitations are described in a recent report.[9]

THERMAL STRESSES

The thermal cycles which occur in a reactor during its operation at various power levels induce into the structural members corresponding stress and strain cycles. For the purpose of design and estimation of reactor lifetime, it is essential to know the effect of these strain cycles on the life expectancy of the reactor materials. In order to furnish design data in this regard, the Mechanical Testing Group has conducted tests to determine the strain-cycle and stress-relaxation properties of Inconel. Important factors which have been investigated in conjunction with this program are the effects of temperature, grain size, environment, specimen geometry, and cycle frequency. Rigs have been constructed for testing of both tube and rod specimens. However, to gain a clear picture of the true influence of strain reversals, the rigs have been designed to mechanically strain the specimens, whereas under true operating conditions, the strains are generally produced by thermal fluctuations. Support work, therefore, has been subcontracted to the University of Alabama where thermally induced strain-cycle investigations are being conducted.

Strain-cycle investigations in argon at 1300, 1500, and 1600°F have been completed and data

are given in two reports.[10,11] Curves have been drawn which show the number of strain cycles to failure (N) as a function of plastic strain per cycle (ϵp). An empirical equation,

$$N^{\alpha} \epsilon p = C ,$$

has been formulated to relate the data, which fall on a straight line when plotted as log ϵp vs log N. Similar behavior has been observed by Coffin[12] in his work on thermally induced cyclic strains in type 347 stainless steel.

At 1500 and 1600°F, fine-grained Inconel is superior to coarse-grained material. Data indicate that fine-grained specimens endure a greater number of cycles (N) at a given strain-cycle level (ϵp) before failure. At 1300°F, however, the difference in cycles-to-rupture between coarse- and fine-grained Inconel is negligible.

The influence of geometry is not great. Rod specimens appear to endure slightly more cycles before failure than do the tube specimens. However, this improvement may be attributed to a less sensitive method of detecting the initiation of failure in the case of rod specimens.

The effect of temperature on these properties is not appreciable over the temperature range studied. Specimens cycled at 1600°F exhibit only a slightly greater number of cycles-to-failure than specimens tested under comparable conditions at 1300 and 1500°F.

Tests have also been conducted on Inconel tubes in the liquid fuel (No. 30) NaF-ZrF_4-UF_4 (50-46-4 mole %), at 1500 and 1600°F. Results from these tests have been reported in two of the ANP reports.[13,14] The effect of fuel is to reduce the number of cycles to failure. Depending on the plastic strain per cycle and the grain size, this reduction ranges from approximately 40 to 66% of the values in argon.

[9]C. R. Kennedy and D. A. Douglas, *Use of a Rate Equation for the Extrapolation of Creep Data*, ORNL CF-57-8-119 (Aug. 20, 1957).

[10]C. R. Kennedy and D. A. Douglas, *Plastic Strain Absorption as a Criterion for High-Temperature Design*, ORNL-2360 (to be published).

[11]D. A. Douglas *et al.*, *ANP Quar. Prog. Rep. Dec. 31, 1956*, ORNL-2221 (Parts 1–5), p 246; C. R. Kennedy and D. A. Douglas, *ANP Quar. Prog. Rep. June 30, 1957*, ORNL-2340 (Parts 1–5), p 190.

[12]L. F. Coffin, Jr., *Trans. Am. Soc. Mech. Engrs.* **76**, 931–950 (1954).

[13]C. R. Kennedy and D. A. Douglas, *ANP Quar. Prog. Rep. June 30, 1957*, ORNL-2340 (Parts 1–5), p 190.

[14]D. A. Douglas *et al.*, *ANP Quar. Prog. Rep. Sept. 30, 1957*, ORNL-2387 (in press).

Since the frequency of induced strain cycles within the reactor will not be uniform, a program has been set up to determine the effect of frequency on the strain-cycle properties. Previously, all tests have been conducted employing 2 min/cycle. Present investigations are being conducted at 30 min/cycle on Inconel tube specimens at 1500°F. The modified apparatus and test conditions have been described in the two reports previously cited.[13,14] There are some indications that frequency may be an important factor in determining the rupture life. Specimens cycled at small strains at 30 min/cycle do not endure as many cycles as are observed in the case of the 2 min/cycle period. Further investigations, however, must be completed before this effect can be entirely clarified.

Results from the tests at the University of Alabama indicate that mechanical strain-cycle data at 1300°F correlate well with thermally induced strain-cycle behavior at the same mean temperature.[14]

Additional programs have been aimed at the determination of the effect of carburization and of weld-metal and braze-metal coatings on the strain-cycle properties of Inconel tubes. Tests conducted on carburized Inconel tubes were performed in conjunction with the alloy modification program. Results shown in an ANP report[14] reveal no reduction in strain-cycle properties resulting from the carburization treatment. The test series on all-weld-metal tubes has not yet been completed; however, some information was given on this subject also in an ANP report.[14] Several Inconel tube specimens were coated with brazing metal (92% Ni–3% Si–3% B–2% Fe) in order to determine whether or not boron penetration of the base material would affect the strain-cycle properties. Rupture data from these tests at 1500°F agree closely with the design curve for coarse-grained Inconel at 1500°F. Consequently, it may be assumed that no detectable loss in strain-cycle properties will be produced by the presence of the braze-metal coating.

A test series intended to evaluate the effect of prior strain cycling upon the creep properties of Inconel has also been in progress. The procedure and initial results are described in an ANP report.[14] Available data indicate that the creep strength and rupture life are significantly reduced by prior strain cycling, and that with increasing consumption of strain-cycle life, the creep-life expectancy is correspondingly reduced. The inference is that design calculations based on only one of these conditions would be optimistic for instances where both strain-cycling and creep could be operative.

The only reactor material besides Inconel which has been investigated in regard to its strain-cycle properties is beryllium. A test series at 1250°F has been conducted on hot-pressed, reactor-grade beryllium. Results from these tests are reported in an ANP report.[14] Test data reveal that beryllium, although much inferior to Inconel, does exhibit ductility and the ability to withstand cyclic strains at this elevated temperature.

Relaxation

Stresses induced by a thermal cycle in a constrained structural member of a reactor generally undergo some degree of decay or relaxation if the temperature is sufficiently high. This relaxation of stress occurs through a conversion, by creep, of the elastic strain into plastic strain. In order to establish the true plastic strain induced by a thermal loading, relaxation characteristics of a material must be known and taken into consideration.

Relaxation tests on Inconel have been completed. Tests have been conducted on coarse- and fine-grained specimens at 1100, 1300, 1500, and 1650°F. Procedure, apparatus, and results have been described in an earlier report.[15]

Data indicate that, at temperatures greater than 1300°F, relaxation of stress occurs rapidly. The relaxation rate at these temperatures varies only when the initial strain is below the elastic limit. Moreover, induced plastic strains do not significantly increase the elastic limit, since recovery appears to be rapid above 1300°F. Stresses are reduced to low residual values after a few minutes. The maximum plastic strain which could occur, as given by the elastic limit, is very small.

Below 1300°F, however, relaxation occurs less rapidly. At 1100°F high initial strains produce work hardening which results in larger elastic strains and higher stress values. These, in turn, relax slowly.

Results also give indications of a grain-size effect. Relaxation rates for coarse-grained Inconel at all temperatures were lower than for the fine-grained material.

---

[15]C. R. Kennedy, D. A. Douglas, and W. D. Manly, *Relaxation Characteristics of Inconel at 1100 to 1650°F*, ORNL-2407 (to be published).

Fatigue

Under a subcontract to Battelle Memorial Institute, a program has been initiated to investigate the effect of cyclic stresses imposed on a statically loaded system. The aim of this program is to define the stress conditions under which fatigue is the dominant failure mechanism, and the stress conditions under which creep may be regarded as the controlling mechanism for failure.

Preliminary tests, intended to check performance of apparatus and reproducibility of results, have been satisfactorily completed. At present, tests are being conducted to determine the influence of stress-cycle frequency on the fatigue properties.

Biaxial Creep

Very little is known concerning the influence of stress distribution on deformation rates. The fact that structures normally are subject to multiaxial stresses emphasizes the need for additional research in this area. A test program is being conducted in which tubes are subjected to various ratios of axial and tangential stresses and the resultant creep rates are measured. A considerable change in rupture life is observed ranging from 200 to 2000 hr, and significant variations on creep rates are noted.[14] A considerable quantity of data must be accumulated before it will be possible to determine which of the various mechanical theories of failure appear to control fracture under these test conditions.

ALLOY DEVELOPMENT

Commercial Alloys

Commercial nickel-base molybdenum alloys, such as Hastelloy B or W, have always attracted much attention because of their excellent resistance to chemical corrosion and their relatively high strength at elevated temperatures. Because such alloys showed promise as structural materials for a circulating fuel reactor, an extensive investigation of the mechanical properties of the Hastelloy alloys was carried out.[16] It was found that these alloys are not single phase and that they exhibit a serious loss of ductility resulting from the precipitation of a brittle beta phase at design temperatures.

---

[16]C. R. Kennedy, D. A. Douglas, and W. D. Manly, *High-Temperature Mechanical Properties of Hastelloy B and W*, ORNL-2402 (to be published).

These alloys also presented fabrication difficulties, and, as seamless tubing was preferred, the only apparent solution was to change the composition. Therefore, special alloys, designed to retain the inherent advantages of the Hastelloy-type alloys and to eliminate their objectionable behavior, were studied.

New Alloys

Screening tests were made of the creep-rupture properties of the various experimental alloys exposed to the fuel mixture (No. 107) NaF-KF-LiF-UF_4 (11.2-41-45.3-2.5 mole %). For comparison, each alloy was tested with a stress of 8000 psi at 1500°F in two conditions: annealed at 2000°F for 1 hr, and annealed at 2000°F for 1 hr and aged for 50 hr at 1300°F.

Results of the creep-rupture testing program, previously reported,[17-20] included data from air-melted heats prepared by Battelle Memorial Institute, International Nickel Company, Inc., Westinghouse Electric Corporation, Superior Tube Co., and Haynes Stellite Company as well as from vacuum-melted heats produced at the Oak Ridge National Laboratory.

Attempts were made to increase the strength of the Ni-Mo alloys by the addition of elements that form complex precipitates and by the addition of elements that are simple carbide formers. Additions of very small amounts (<1%) of aluminum and titanium did not seem to increase the strength, but they did increase the final elongation. Fabrication difficulties were encountered when additions of aluminum and titanium exceeded 1.5%. However, it has been possible to improve the creep characteristics by additions of carbide-forming elements, such as niobium and tungsten, without seriously compromising the other good characteristics. The Battelle alloys, containing carbon in excess of 0.1%, exhibited high-strength properties, but tended to fracture when subjected to tube fabricating

---

[17]D. A. Douglas *et al.*, *ANP Quar. Prog. Rep. Dec. 31, 1956*, ORNL-2221 (Parts 1–5), p 249.

[18]J. W. Woods, *ANP Quar. Prog. Rep. March 31, 1957*, ORNL-2274 (Parts 1–5), p 220.

[19]H. Inouye, T. K. Roche, and J. H. Coobs, *ANP Quar. Prog. Rep. June 30, 1957*, ORNL-2340 (Parts 1–5), p 176.

[20]D. A. Douglas *et al.*, *ANP Quar. Prog. Rep. Sept. 30, 1957*, ORNL-2387 (in press).

processes. Additional alloying elements, such as chromium (7%) and iron (4%), were found to enhance the creep properties of the basic nickel-molybdenum binary alloy.

The Haynes Stellite alloy (INOR-8) (nominal composition in wt %, 16 Mo—7 C—5 F—0.02 C—bal Ni) appears to be the best alloy produced to date. It has good corrosion resistance and fabricating characteristics. As a result of its low carbon content the strength properties are merely fair.

It is considered feasible to substantially increase the strength of the alloy after the difficult fabrication processes are completed by adding more carbon through gas carburizing. Tests of specimens to which 0.2% carbon was added by this means showed greatly improved strength properties.

Although INOR-8 does not represent the ultimate in mechanical properties which can be obtained from this alloy system, it has better strength than type 316 stainless steel. Tensile tests of this alloy in air, at a temperature of 1500°F, indicated a tensile strength of 46,000 psi with 20% elongation. The maximum corrosive attack observed corresponds to the corrosion noted in Hastelloy B in the same fuel environment. It is indicated that this alloy system will meet the container requirements for high-temperature fused-salt reactors.

NONDESTRUCTIVE TESTING

R. B. Oliver   R. A. Nance   R. W. McClung
J. W. Allen   J. K. White   M. O. Chester[1]

EDDY-CURRENT DEVELOPMENT: TUBING

J. W. Allen

Eddy-current methods[2] are rapid, versatile, and economical, but they are not sufficiently sensitive and definitive for the complete inspection of reactor-grade tubing. Continued efforts have been made to develop an instrument featuring both a continuously variable frequency and phase separation with a dual-channel read-out. A prototype instrument, the Impedograph,[3] was constructed and evaluated. It has been demonstrated that the instrument can separate the effects of varying diameter and varying wall thickness with the dual-channel read-out. Although the Impedograph is still in the process of development and is somewhat difficult to operate, it has been used successfully for the inspection of a large quantity of small-diameter tubing. Another approach to obtaining a definitive and sensitive eddy-current inspection of reactor-grade tubing is being studied. This approach involves the use of multiple operating frequencies which cover the entire range of frequencies suitable for the inspection of a particular size and material. Some experimental electronic circuitry has been constructed to investigate the use of an instrument simultaneously applying ten different frequencies, but no conclusive results have been obtained.

EDDY-CURRENT DEVELOPMENT: METAL IDENTIFICATION METER

J. W. Allen

An extremely stable instrument,[4] which is almost completely free of drift, has been developed to sort nonferromagnetic metals and alloys on the basis of conductivity. The Metal Identification Meter (MIM-1) was developed to positively identify

Inconel parts in the presence of both the austenitic stainless steels and the Hastelloy alloys. It has been established that, in addition to satisfying the design requirements, the instrument will positively identify a metal or alloy in any system of nonferromagnetic materials in which the conductivity of the particular metal is unique. Also, the instrument has recently[5] been successfully adapted to the measurement of thicknesses of thin metal sections.

EDDY-CURRENT DEVELOPMENT: MATHEMATICAL ANALYSIS OF EDDY-CURRENT PROBE COILS

J. W. Allen   M. O. Chester

Since mathematical studies of the impedance of a coil surrounding a cylindrical rod or a tubular object have been extremely helpful in establishing a rational basis for the selection of test parameters, similar analyses are being conducted[6] on eddy-current probe coils. An analytical expression for the impedance of a probe coil near metal plates of apparently infinite thickness has been obtained, and impedance curves generated from these expressions have been correlated with experimental data. The impedance of a probe coil near thin metal sheets of finite thickness has also been studied. The results of these investigations should be invaluable in the future application of eddy-current probe-coil methods to the measurement of metal thickness and the thickness of cladding layers.

EDDY-CURRENT DEVELOPMENT: THICKNESS MEASUREMENTS

R. A. Nance

Currently the eddy-current probe-coil technique appears to be the only nondestructive method for measuring the thickness of the protective cladding on solid fuel elements. An instrument was designed for developing inspection methods in which

[1]Summer employee from Cornell University.

[2]J. W. Allen and R. B. Oliver, *Inspection of Small Diameter Tubing by Eddy-Current Methods*, ORNL-2253 (Feb. 19, 1957).

[3]R. B. Oliver and J. W. Allen, *ANP Quar. Prog. Rep. March 31, 1957*, ORNL-2274 (Parts 1–5), p 225.

[4]R. B. Oliver, J. W. Allon, and R. A. Nance, *ANP Quar. Prog. Rep. June 30, 1957*, ORNL-2340 (Parts 1–5), p 256.

[5]R. B. Oliver, J. W. Allen, and R. A. Nance, *ANP Quar. Prog. Rep. Sept. 30, 1957*, ORNL-2387 (in press).

[6]J. W. Allon and M. O. Chester, *ANP Quar. Prog. Rep. Sept. 30, 1957*, ORNL-2387 (in press).

this technique is utilized.[7] The prototype instrument was not sufficiently sensitive and stable to make accurate measurements, and, therefore, an improved instrument was designed.[8] An inspection procedure for the measurement of the cladding thickness on the MTR-type fuel elements is currently being developed with an indicated accuracy of approximately 0.002 in. The accuracy of measurement of a simple clad composite involving only the cladding and the core materials is about 0.001 in. When a third component is added for the purpose of forming a bond layer or a diffusion barrier, the problem is much more complicated, as indicated by the MTR-type element. Laboratory studies will be continued in order to develop this technique into a production-type inspection method.

Complex-impedance-plane plots describing the effects of thin sections on the impedance of a probe coil have been plotted for several different conditions.[9] The interrelated effects of conductivity, thickness, and test frequency on the coil impedance have been studied, as well as the effect of lift-off or coil coupling. Similar studies were made in which the impedance change was plotted as a function of the thickness of a layer of one material covering a second material. These studies will lay a foundation for the application of eddy-current measurements to thin sheet, to the measurement of outer-ply thickness of duplex tubing, and to the evaluation of thin sections of shrouded assemblies.

INSPECTION OF PIPE AND TUBING

R. W. McClung   J. K. White

Both the immersed, pulse-echo ultrasonic method and the encircling-coil eddy-current method were used to inspect approximately 57,000 ft of Inconel and Hastelloy pipe and tubing. In general, the ultrasonic inspection detects longitudinal discontinuities such as cracks, laps, folds, seams, gouges, and laminations.[10] The eddy-current

method, as applied to the inspection of small-diameter tubing, detects the presence of larger cracks, intergranular corrosion, and small particles of high-permeability material, and continuously gages the dimensional variations along the length of the tube.[11] The small-diameter Inconel and Hastelloy tubing was inspected to reactor-grade specifications and was intended for use in the construction of radiators and heat exchangers. The tubing ranged in size from $\frac{3}{16}$-in. OD × 0.025-in. wall and $\frac{1}{4}$-in. OD × 0.017-in. wall up to $\frac{5}{8}$-in. OD and 0.065-in. wall. Most of this tubing was either the 42-in. lengths of $\frac{3}{16}$-in.-OD tubing or the 78-in. lengths of the 0.229-in.-OD tubing. The rejection rate for all tubing by both inspection methods averaged less than 10%, although some individual lots had a rejection rate as high as 99% for Hastelloy tubing and as low as 1% for the CX-900 Inconel tubing.

The pipe inspected by the immersed-ultrasonic technique[10] ranged in size from $\frac{1}{4}$-in. schedule 40 up to and including 6-in. schedule 40. The common defects detected were cracks, large pits, seams, physical mismatch at the weld bead, and severe eccentricity. The rejection rates for the 2200 ft of pipe inspected averaged 10%. Approximately one-third of the total quantity of pipe was also examined with the resonance ultrasonic method to determine wall thickness or eccentricity.[12] Approximately 95% of this pipe was acceptable if a ±10% wall thickness variation was allowed, but if a ±5% tolerance was applied the acceptance ranged from 10% to as high as 90%.

ULTRASONIC INSPECTION: PLATE

R. W. McClung

The immersed-ultrasonic method is the only reliable technique for the detection of small laminations in large flat plates.[13] It has been used to inspect approximately 1500 sq ft of Inconel plate ranging in thickness from $\frac{1}{4}$ in. to 1 in., with an average rejection rate of five per cent. The rejection was based on both the presence of

[7]J. W. Allen and R. A. Nance, *ANP Quar. Prog. Rep. March 31, 1957,* ORNL-2274 (Parts 1–5), p 227.

[8]R. B. Oliver, J. W. Allen, and R. A. Nance, *ANP Quar. Prog. Rep. Sept. 30, 1957,* ORNL-2387 (in press).

[9]R. B. Oliver, J. W. Allen, and R. A. Nance, *ANP Quar. Prog. Rep. June 30, 1957,* ORNL-2340 (Parts 1–5), p 257.

[10]R. B. Oliver, R. W. McClung, and J. K. White, *Immersed Ultrasonic Inspection of Pipe and Tubing,* ORNL-2254 (Feb. 15, 1957).

[11]J. W. Allen and R. B. Oliver, *Inspection of Small Diameter Tubing by Eddy-Current Methods,* ORNL-2253 (Feb. 19, 1957).

[12]R. B. Oliver and R. W. McClung, *ANP Quar. Prog. Rep. June 30, 1957,* ORNL-2340 (Parts 1–5), p 259.

[13]R. B. Oliver and R. W. McClung, *ANP Quar. Prog. Rep. June 30, 1957,* ORNL-2340 (Parts 1–5), p 261.

lamination-like defects and upon indication of excessive ultrasonic attenuation by the plate.

ULTRASONIC INSPECTION: BERYLLIUM HOT-PRESSINGS

R. B. Oliver   J. W. Allen
R. W. McClung

Four large beryllium hot-pressings were inspected by the immersed-ultrasonic technique. Three of the hot-pressings were inspected in the Brush Beryllium Company's plant, and the fourth was inspected under laboratory conditions at ORNL.[14]   The purpose of the laboratory-type inspection was twofold: to determine the quality of the object and to evaluate the column-coupled ultrasonic technique as compared with the conventional immersed method. The laboratory inspection proved that the inspection method used in the field was adequate. Only one defect was located in the four pressings, and that defect was in a region that would be removed by subsequent machining; hence, all four pieces were acceptable.

ULTRASONIC INSPECTION: CORE SHELLS

R. W. McClung   R. B. Oliver

A "ringing" technique was developed for the immersed-ultrasonic inspection of thin sheets for the detection of both cracks and laminations.

This technique was adapted to the inspection of the Inconel core shells for the ART and ETU.[15] Only one of the three core shells inspected was rejected.   The rejection was due to a localized thin section which was detected by the ultrasonic "ringing" technique and confirmed by the use of the ultrasonic resonance method.

ULTRASONIC INSPECTION: DETECTION OF NON-BOND AREAS

R. B. Oliver

The ultrasonic resonance method was successfully used to detect non-bond areas as small as 0.4 in.^{2} in a stainless steel–clad boron carbide–copper plate. The boron carbide–copper core was separated from the type 430 stainless steel cladding by a copper diffusion barrier. The non-bonding appeared to result from an oxide film on the interface between the copper diffusion barrier and the stainless steel cladding.   The non-bond areas could be detected from either side of the plate, although the best detection and the best evaluation were accomplished if the non-bond area was on the opposite side of the plate from the transducer.[16]

[14]R. W. McClung, *ANP Quar. Prog. Rep. March 31, 1957,* ORNL-2274 (Parts 1–5), p 238.

[15]R. B. Oliver and R. W. McClung, *ANP Quar. Prog. Rep. Sept. 30, 1957,* ORNL-2387 (in press).

[16]R. B. Oliver, J. W. Allen, and R. A. Nance, *ANP Quar. Prog. Rep. Sept. 30, 1957,* ORNL-2387 (in press).

INSPECTION

A. Taboada

R. L. Heestand   G. M. Tolson

MATERIAL INSPECTION

G. M. Tolson   A. Taboada

The inspection of materials for reactor service was performed, with the intended use as the criterion for acceptability. Several salvaging operations and procedures were established to eliminate detrimental conditions in order that losses from rejections can be kept to a minimum. These operations and procedures included polishing of tubing at intermediate steps of inspection, centerless grinding of pipe, pickling for removal of oxides, hand grinding of individual conditions, and, in cases where complete rejection occurred, downgrading for less critical use. The types and quantities of material which were inspected during the period and the results are reported in Table 17. Comments pertaining to the individual items are as follows.

Tubing

The majority of the CX-900 Inconel tubing listed in the table was inspected for use in radiators, heat exchangers, and dump tanks. Of the amount rejected, approximately 25% was returned to the vendor for credit, approximately 25% was held for salvage operation (see the section, "Related Development Work"), and the remainder, approximately 50%, was downgraded for less critical use. Much of the regular Inconel inspected was material of unknown origin and specification and was obtained for reasons of expedience. Handling and fabrication defects comprised the major reasons for rejection of this tubing. The rejection rate as shown for Hastelloy B and INOR-8 tubing is not truly indicative of the quality received, as only the most gross type of defect was rejected. Seventy-five feet of the type 430 stainless steel shown as rejected was found to contain cracks which extended completely through the wall at the seam weld.

Seven hundred fifty-four feet of experimental Inconel-clad type 316 stainless steel tubing was inspected for the purpose of obtaining sufficient material to build a test heat exchanger. Numerous surface pits and gouges were detected on approximately 500 ft of this tubing by dye-penetrant inspection. Radiography revealed no serious internal conditions, and a good bond was noted on metallographic examination.

Pipe

The rejection of regular Inconel pipe included 130 ft for which the wall thicknesses were too low. The high Hastelloy B rejection rate was principally due to defects in the seam weldments.

Plate and Sheet

In most cases inspection was performed prior to cutting of the material. The areas found with defective conditions which could not be cleared up within tolerance by grinding were identified, and, by proper orientation of the layout by the fabricator, loss was kept to a minimum.

INSPECTION OF TUBING FOR HEAT EXCHANGER APPLICATION

G. M. Tolson   A. Taboada

Complete integrity is required for thin-wall tubing for reactor heat exchanger application, since one failure in the tube could result in the destruction of the unit. To obtain the desired quality of tubing, material is required to meet the conditions of metallurgy specifications MMS-1 and IPS-2, which allow no discontinuity greater than 2% of the wall thickness. Five different methods of inspection have been instituted. Discussed below is a description of each method and the types of defects most prone to detection by each method.

Visual Inspection

Visual inspection is used both as a preliminary check to cull out any obvious defects and as a final inspection to find tube damage occurring during processing. In addition, minor conditions often missed by other methods are readily seen by this method. These include small pits (see Fig. 21) caused by foreign material being pressed into the tube during fabrication, and handling

Table 17. Summary of Material Inspected

Item	Type	Amount Inspected (ft)	Amount Rejected (ft)	Per Cent
Tubing	CX-900 Inconel	51,265	11,251	22.0
	Regular Inconel	2,023	1,464	48.0
	Hastelloy B	250	3	1.2
	Type 430 stainless steel	169	90	53.0
	INOR-8	128	5	4.0
		Total 54,835	Total 12,813	23.4
Pipe	CX-900 Inconel	1,473	79	5.0
	Regular Inconel	2,215	402	18.5
	Hastelloy B	1,063	808	76.0
	Hastelloy W	77	5	6.5
		Total 4,828	Total 1,294	26.7
Plate and sheet	CX-900 Inconel	1,215 ft^2	197 ft^2	16.0
	Regular Inconel	4,372 ft^2	481 ft^2	11.0
		Total 5,587 ft^2	Total 678 ft^2	12.0
Rod and bar	CX-900 Inconel	50	0	0
	Regular Inconel	903	96	10.5
		Total 953	Total 96	10
Fittings	Inconel	267 pieces	5 pieces	1.8
Miscellaneous parts		11 pieces	0	0

defects such as dents (Fig. 22), scratches (Fig. 23), and nicks. Visual inspection is carried out while the tube is being rotated under a light of approximately 10 cp. When a discontinuity is seen, it is more closely examined with 10X magnification in order to determine its magnitude. The defect is removed by polishing the questionable area with 400-grit sandpaper until the defect is no longer visible. The depth of the material removed is then determined by measuring the change in the outside diameter of the tube. Any change in the tube outside diameter of over $\frac{1}{2}$ mil is cause for rejection of the tube.

Fluorescent-Penetrant Inspection

An evaluation of the available penetrant inspection methods resulted in the replacement of a dye-penetrant method with postemulsification-fluorescent penetrant for the inspection of critical tubing. Figure 24 shows examples of a small crack which was not seen by other methods but which was found by using fluorescent penetrant. There are several additional advantages to fluorescent-penetrant inspection. The method is less dependent on human variables, inherently more rapid, and more easily controlled than the dye-penetrant

(a)

(b)
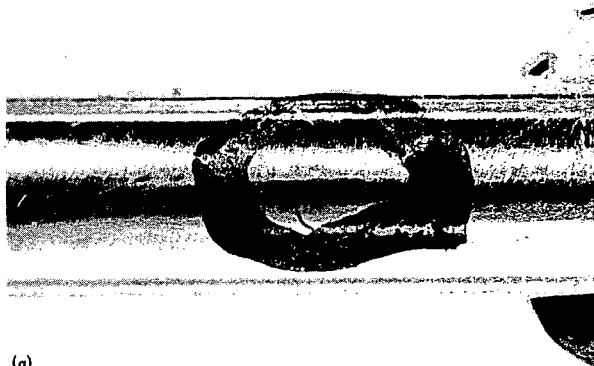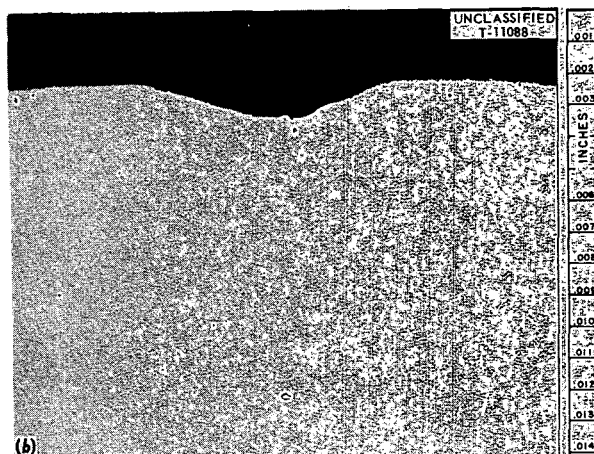
Fig. 21. Small Pit Found Visually on Small-Diameter Tubing. (*a*) 6.5X, reduced 32%; (*b*) 250X, reduced 32%; photomicrograph not etched.

Fig. 23. Scratch Found Visually on Small-Diameter Tubing. 8X. Reduced 32%.
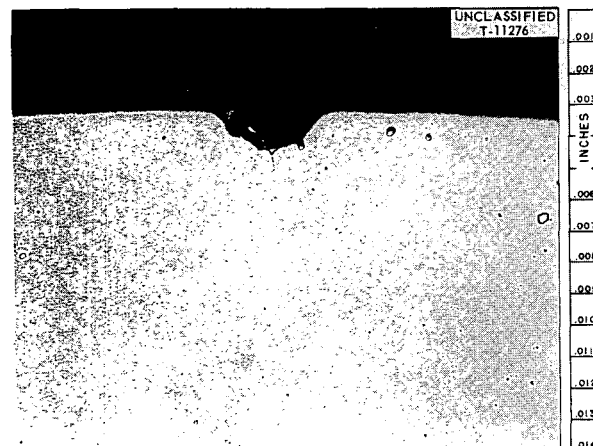
Fig. 24. Pit Containing Microcracks Found on Zyglo Inspection. Unetched. 250X. Reduced 32%.

Fig. 22. Dent Found Visually on Small-Diameter Tubing. 6X. Reduced 32%.

method, and the defects are seen more easily because of higher contrast. The disadvantages of this method are the difficulty in differentiating the actual defects from false indications and the possibility of contaminating the final stages of penetrant developing to give these "false indications." Shallow pitlike defects have not been found with this method.

Figures 25 and 26 show equipment used for fluorescent-penetrant inspection. Important variables in this technique are the cleanliness of the material, the time-interval control for various

43
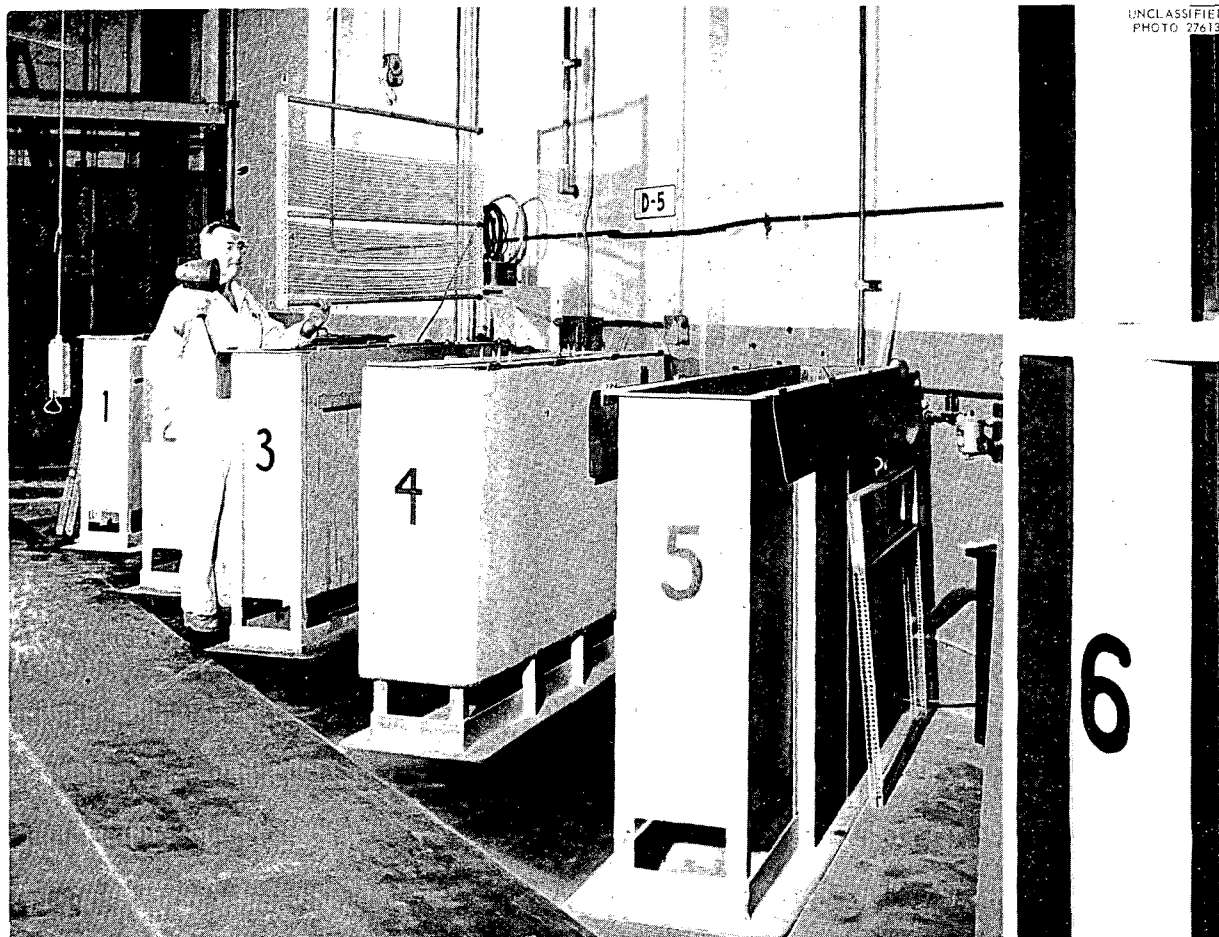
Fig. 25. Equipment Used for the Processing of Small-Diameter Tubing Through Zyglo Inspection.

stages of the operation, the intermediate washing operation, and the ability to keep the developer from being contaminated with fluorescent material. The time in the emulsifier appears to be the controlling factor in evaluating the sensitivity of this method. Test runs show that when the time was decreased from 5 min to 1 min the ability to detect small shallow defects increased about 33%. To minimize contamination, the powder developer is applied by enclosing the tubing in a chamber and applying the powder by aeration. A technique has been developed for determining false indications, which involves inspecting the area under the indication, marking the area, and reinspecting the tube.[1]

Radiographic Inspection

Radiographic techniques have been developed for the rapid inspection of large quantities of tubing with a minimum sacrifice of quality of inspection. These techniques have been used to locate defects of less than 2% of wall thickness; however, determining the location of these defects is dependent upon their general shape, orientation with the x-ray beam, and location in the tube. Determination of the last two variables is facilitated by making three exposures of the same

[1] R. B. Oliver, G. M. Tolson, and A. Taboada, "The Use of Penetrants in the Inspection of Small Diameter Tubing," submitted to *Am. Soc. Testing Materials, Proc.*

Fig. 26. Rack of Small-Diameter Tubes Being Inspected with Use of Black Lights.

section of the tubing 120 deg apart. This method gives three views with different orientations at the same location on each tube. Figure 27 shows a group of tubes being prepared for radiography. The conditions used for radiographing tubing are given in Table 18. Interpretation of the x-ray film and defect location is extremely tedious and critical work. To facilitate the interpretation and eliminate error, the three radiographs of each section of tubing are compared and the defects are matched. This method seems to be more sensitive to defects on the inside of the tube. Gouge marks such as are shown in Fig. 28 are easily detected with this method. Cracks are detected with some difficulty (see the section, "Development of Inspection Methods").

Ultrasonic Inspection of Tubing

An immersion-ultrasonic test has been developed for highly critical tubing by the Nondestructive Testing Group. This method shows extreme sensitivity in the detection of cracks or sharp discontinuities in the tubing. Gouges which have no sharp discontinuity are difficult to detect by this method, but the method is very sensitive to the surface condition of the tube, and care must be exercised in its interpretation.[2]

Eddy-Current Inspection

An eddy-current method of inspection of high-performance tubing has also been developed by the Nondestructive Testing Group. This method[3] has been used for dimensional checks and to detect foreign particles of magnetic materials on the inside surface as shown in Fig. 29.

[2]R. B. Oliver, R. W. McClung, and J. K. White, *Immersed Ultrasonic Inspection of Pipe and Tubing,* ORNL-2254 (Feb. 15, 1957).

[3]J. W. Allen and R. B. Oliver, *Inspection of Small Diameter Tubing by Eddy-Current Methods,* ORNL-2253 (Feb. 15, 1957).
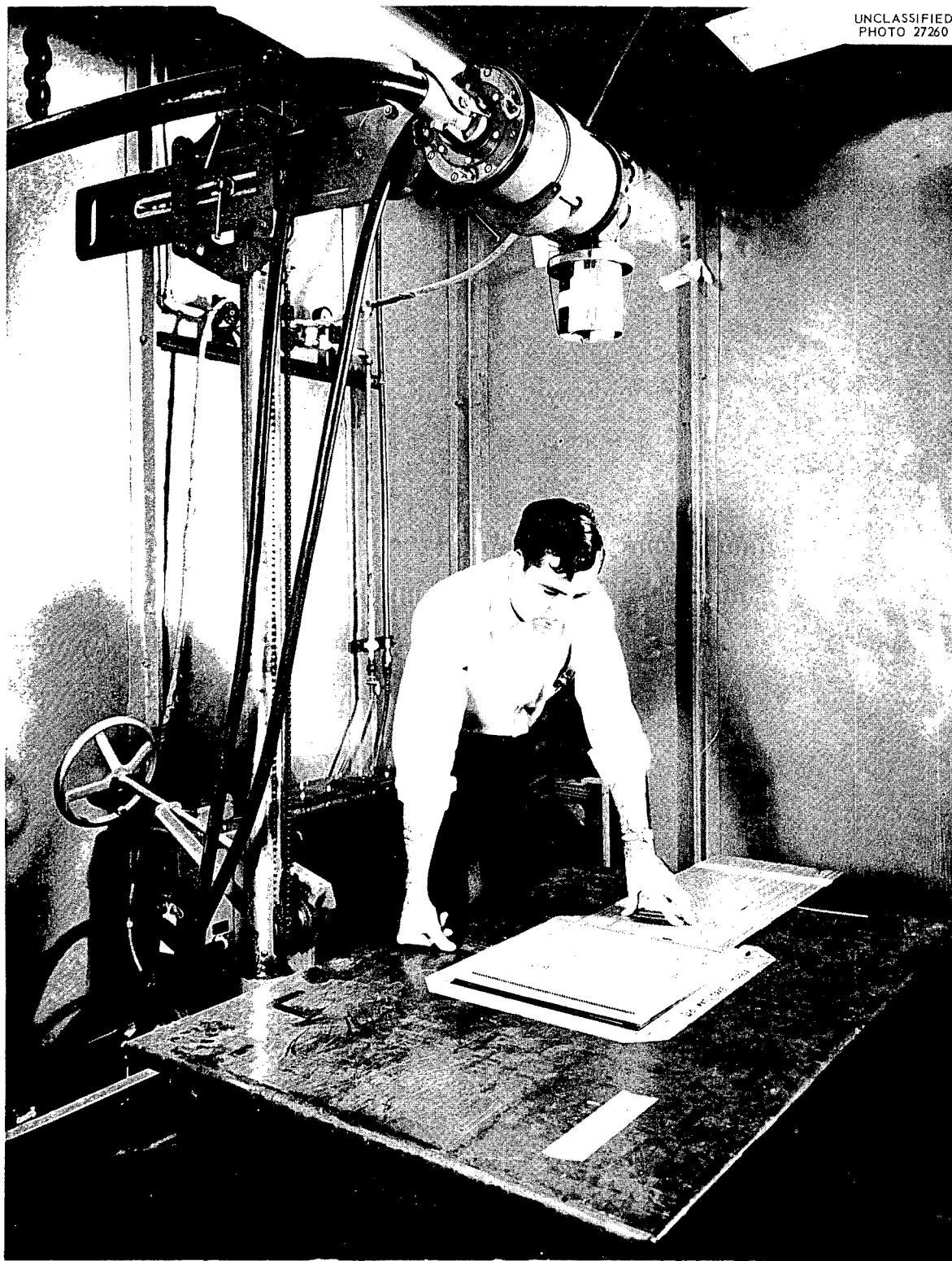
Fig. 27. Small-Diameter Tubing Being Prepared for Radiographic Inspection.

Table 18. Conditions for Radiographing Tubing

Condition	Outside Diameter of Tubing (in.)	
	0.187	0.229
Tube voltage	120 kv	120 kv
Tube current	6 ma	6 ma
Tube-to-target distance	60 in.	60 in.
Number of tubes per group	68	54
Film density	2.4	2.4
Exposure time	2 min, 15 sec	2 min, 15 sec
Filter at film	0.025-in. Al	0.025-in. Al
Intensifying screen	0.005-in. Pb	0.005-in. Pb
Backup screen	0.010-in. Pb	0.010-in. Pb
Machine	Norelco 150	Norelco 150
Film	Type M	Type M

UNCLASSIFIED
T-11704

Fig. 28. Gouge Found Radiographically on Small-Diameter Tubing. (a) 7½X, reduced 36%; (b) 150X, reduced 36%; photomicrograph etchant: glyceria regia.

WELD INSPECTION

R. L. Heestand   A. Taboada

Weld Classifications

Since experimental tests were being conducted which present a range of metallurgical considerations both during fabrication and during the operation of the tests, a need for more specific inspection standards was indicated. A criterion was established which would fulfill these requirements in most instances. At the time of the design review, factors such as corrosive environment, temperature gradient, strength, length of operation, and accessibility for welding are considered. A designation is then given to each weld as to the type of inspection it is to receive. Basically, there are three classifications of welds; they are as follows:

1. *"C" type* includes all welds requiring optimum soundness. Fabrication is in accordance with the applicable Metallurgy Welding Procedure (see Table 19) and Metallurgy Inspection Procedure (Table 20). These procedures require that the weld be inspected by visual, dye-penetrant, and radiographic techniques.

2. *"CN" type* includes those welds requiring high integrity which will be in less severe operating conditions than those classified as "C" type. This designation also includes welds which would be classified as "C" type but which are not x-rayed. Fabrication on these welds requires

47

Fig. 29. Inside Surface of CX-900 Inconel Tube Containing Magnetic Particles. 8X. Reduced 17%.

Table 19. Metallurgy Welding Procedures

PS-1	Inert Arc Welding of Inconel Pipe, Plate, and Fittings
PS-2	Inert Arc Welding of Inconel Tubing for High Corrosion Applications
PS-3	Inert Arc Welding of 61ST-6 and 63ST-6 Aluminum Pipe and Plate
PS-4	Inert Arc Welding of 61ST-6 and 63ST to 54S Aluminum Pipe, Plate, qnd Fittings
PS-5	Inert Arc Welding of 54S Aluminum Pipe and Plate
PS-6	Inert Arc Welding of 54S to 3S Aluminum Pipe, Plate, and Fittings
PS-7	Inert Arc Welding of 61ST-6 and 63ST-6 to 3S Aluminum Pipe, Plate, and Fittings
PS-8	Inert Arc Welding of Nickel and Low Carbon Nickel Pipe, Plate, and Fittings
PS-9	Inert Arc Welding of Nickel, and Low Carbon Nickel Pipe, Plate, and Fittings to Inconel Pipe, Plate, and Fittings
PS-12	Metal Arc Welding of Inconel Plate
PS-14	Inert Arc Welding of Inconel Pipe, Plate, and Fittings to Type 304, 316, 321, and 347 Stainless Steel Pipe, Plate, and Fittings
PS-15	Inert Arc Welding of Hastelloy B and Hastelloy C Pipe, Plate, and Fittings
PS-18	Inert Arc Welding of Hastelloy B and Hastelloy C Tubing for High Corrosion Applications

that all the caution exercised on "C" type be used in order to ensure a sound weld. Inspection procedure requires that the welds be examined only by visual and dye-penetrant methods.

3. "S" *type* includes structural and other noncritical welds. Inspection is confined to visual and dye-penetrant methods, and the cause for rejection is limited to cracks.

Weld Inspection

Several welds were examined which had been fabricated on core shells for test purposes. In general, these welds were found to be acceptable for the intended use; however, in most cases they were not of reactor quality.

Initial inspection of welds fabricated on the NaK piping manifold of the ETU manifold resulted in a rejection rate of 20%. Examination of the defects revealed most problems to be associated with obtaining an adequate purge for the welds.

An investigation of the use of argon as the purging gas on the weldments was conducted in order to determine whether the welds could be made more expediently and whether a reduction in the rejection rate could be attained. Records were maintained on the volume and flow rate of argon required to remove the air and to drop the dew point to an acceptable level prior to the welding operation. A portable Beckman oxygen analyzer and a portable dew-point meter were used as indicators. Results showed that, while argon is more expensive than helium, a much shorter purging time, less total volume, and a lower rejection rate (currently 8%) could be attained by minimizing porosity.[4] The results of inspections performed on weldments during the period are shown in Table 21.

[4] *General Welding and Purging Procedures for ETU Construction,* Intra-Laboratory Memorandum from D. K. Davis to G. D. Whitman, May 28, 1957.

Table 20. Metallurgy Inspection Procedures

IPS-1	For Weldments of Inconel Pipe, Plate, and Fittings
IPS-2	For Small Thin-Wall Seamless Tubing
IPS-2-1	For 0.065-in. Wall Seamless Tubing
IPS-3	Tentative Inspection Procedure for Mass Spectrometer Leak Detection
IPS-4a	Tentative Inspection Procedure for the Ultrasonic Inspection of Inconel Plate by Pulse Echo Longitudinal Wave Method
IPS-5	Emergency Procedure for the Ultrasonic Inspection of Thick Sections of Hot-Pressed Beryllium
IPS-6	For Insuring Cleanliness of Pipe Systems
IPS-7	For Formed Inconel Parts
IPS-8	Radiographic Procedure for Inconel Pipe Manifold Weldments
IPS-9	Fluorescent Penetrant Inspection Procedure for Thin-Wall Tubing

Table 21. Weld Inspection Results

	"C" Type			"CN" and "S" Types		
	Total Inspected	Number Rejected	Per Cent	Total Inspected	Number Rejected	Per Cent
Test Loops and Fabricated Parts	3244	573	17.5	11,292*	130	1.0
ETU Manifold	256	40	15.5			

*Included in this number were 1346 welds fabricated on fuel sample units and 363 welds on NaK filter units.

VENDOR WORK PERFORMED

R. L. Heestand   G. M. Tolson
A. Taboada

Throughout the past year, evaluation of procedures, test specimens, and component hardware has been carried out for 16 vendors. In addition to the evaluation of vendors' efforts, several trips to the vendors' plants have been made in order to give technical assistance. In many instances the technical assistance given has required investigation of a limited nature in the division. Table 22 shows a brief summary of all vendor work performed.

SHELL FABRICATION EVALUATION

A. Taboada   G. M. Tolson

Inconel shells of various thicknesses and configurations and fabricated by three different methods have been evaluated to determine their acceptability for use in high-temperature, high-stress application. The following requirements were considered necessary for an acceptable shell:

1. There should be no surface cracks or ruptures and no other material discontinuity greater than 5% of the wall thickness.
2. The shell would have to meet rigid tolerance requirements as specified by design prints.
3. A uniform small grain size was required for good strain-cycling properties.

Material and inspection specifications were prepared for determining the shell quality. These included destructive examination of sample pieces and nondestructive examination of the actual part. Specimens of finished shells were obtained, where possible, from the trim areas. Metallography was performed in order to determine the grain size, wall thickness, surface conditions, and general integrity of the material.

Nondestructive tests were performed on parts in the intermediate and finished stages. These tests included visual and penetrant techniques for inspection of the surfaces, and ultrasonic and radiographic methods for inspection of wall thicknesses and of the material in general.

Hydrospin Method

Initial attempts to get shells of $\frac{1}{8}$-in. thickness were made by using the hydrospin method. Although still an experimental fabricating method, hydrospin had the advantages of good tolerance

control and a resulting one-piece shell which required no final machining. Experimental attempts to make shells revealed that the condition of the initial material was important. Uniform thickness of closer thickness tolerance than was commercially available was required to meet design dimensions, and a smooth, sound surface was necessary to eliminate surface rupturing. Both overpickling and improper annealing were found to result in surface rupturing. Although final shells were approaching the dimensional and grain requirements and had acceptable surfaces, the work was discontinued because of the high cost and because of alternate methods which looked more promising.

Forming, Welding, and Machining Methods

Shells that complied with surface and dimensional requirements were readily made by cold forming of sections of thicker dimensions in order to approximate certain shapes. These were then welded into a shell and machined to final dimensions. Inspection was made at intermediate points of the operations to ensure that no repair would be required on the finished part. The questionable feature of this method of making shells was the excessive size grain formed at the heat-affected zones of the weldments; in particular at the junction of two weldments, which would result in lower strain-cycling strengths. The severity of this effect is presently being investigated.

Hot-Forged Method

Thicker shells were all made by the hot-forged and machined methods. All shells that were made in this manner were found to be acceptable at inspection.

RELATED DEVELOPMENT WORK

A. Taboada   R. L. Heestand
G. M. Tolson

Salvaging of Tubing by Removal of Magnetic Particles

The destructive examination of defects found during cyclograph inspection revealed the existence of magnetic particles, as shown in Fig. 29, which had become attached to the inside surface during the manufacturing process. Since tubing affected with conditions of this nature is not returnable to the vendor for credit, a method

Table 22. Vendor Items Inspected

Vendor	Item	Disposition
Air Research Mfg. Co.	9 welder qualification specimens	All rejected
Allis-Chalmers Mfg. Co.	Radiator job sample — 9 welder qualification specimens	Information only, all rejected
Black, Sivalls & Bryson, Inc.	Welder qualification specimens; 4 each	All accepted; 2 welders qualified, PS-1
	Dump valve parts	Accepted
	Punch valve No. 1	Accepted
	Fusion welding techniques	Accepted
	Prototype shutoff valve	Accepted
	Stellite hard facing	Accepted
	Bellows adapter assembly	Accepted
	Two $\frac{1}{2}$-Mw radiators	Accepted
	Intermediate heat exchanger No. 6	Accepted
	Main heat exchanger	
	Tube bend samples	Accepted
	Tube sheet—to—bulkhead weld	Rejected
	Tube sheet—to—bulkhead weld	Accepted
	Resistance heating bending	Accepted
	Technique for main heat exchanger tubes	Accepted
	Welding procedures	Accepted
	Tube—to—tube sheet fusion welds	Accepted
	Channel leg—to—web weld	Accepted
	3 braze specimens	Accepted
	North and south stress header units	Accepted
	North and south experimental units	Pending
Coast Metals, Inc.	Braze powder	Rejected
Erco Mfg. Co.	Load ring cover plate	Pending
Fulton Sylphon Co.	Sodium expansion bellows	Rejected, defective welds
General Electric Co.	Liquid level indicators	Several repairs necessitated due to defective welds
General Plate Co.	3-lot sample of fin material	Accepted
Griscom-Russell Co.	Welder qualifications, 25 specimens	13 accepted, 3 welders qualified
	Intermediate heat exchanger units Nos. 2 and 3	Accepted
	Drawings of R U "K" fins	Rejected, insufficient information

Table 22 (continued)

Vendor	Item	Disposition
Griscom-Russell Co.	Special radiator, tube—to—tube sheet job sample	Pending
	Intermediate heat exchanger braze sample	Accepted
	Auxiliary heat exchanger	
	Tube bending techniques	Accepted
	300 tube braze samples	Accepted
	Radiography of tube—to—header welds	Accepted
	Tube sheet—to—bulkhead weldments	2 rejected, 1 accepted
	Tube—to—tube sheet fit-up	Accepted
	10 tube—to—header welder qualification samples	2 rejected, 8 accepted
	Dummy braze sample	Accepted
	Stress analysis header	Accepted
	Auxiliary heat exchanger units Nos. 1 and 2	Accepted
Hoke, Inc.	102 NaK-type valves received, of which 2 welds on each were examined	Several repairs were made due to defective welds
Ladish Co.	Lower shell VII forging (intermediate stage)	Pending
	Lower deck skirt	Accepted
	Fuel expansion tank top	Accepted
Kaiser Metal Products, Inc.	Can bottoms	3 accepted
Midwest Piping Company, Inc.	Welder qualification, 7 specimens	5 accepted
	Forged reducers, 4 specimens	3 rejected due to large grains and defects
	Saddle welding technique	Approved
	Pipe bending technique	Approved
Norton Company	X rays of boron carbide tiles	Accepted
Process Engineering, Inc.	Welder qualification, 16 specimens	7 accepted
	8 fill and drain tanks	Accepted
	Junction panel bellows, 3 specimens	2 accepted
	3 standard NaK tanks	Accepted
	12 junction panel bellows	Rejected, welds were of very poor quality
York Corp.	Welder qualification, 13 specimens	5 accepted, 5 welders qualified

Table 22 (continued)

Vendor	Item	Disposition
York Corp.	4 lots of fin material with edge treatment	Accepted
	Inspection reports, x-ray film and control samples on radiator fin sections Nos. 1—16	Several repairs necessitated due to porosity in tube-to-header welds; 4 units rejected due to poor brazing
	Tube—to—header welder qualification, 11 specimens	2 rejected due to porosity
	$\frac{1}{2}$-Mw radiators 15, 16, 17, 18, 19, and 20	No. 15 rejected for damage during transportation, remainder accepted
	1-Mw test radiators 1, 2, and 3	No. 1 rejected because of a poor tube—to—tube sheet braze, Nos. 2 and 3 accepted
	8 radiator job samples	6 rejected, poor braze; 2 accepted
	11 lots of braze rings	Information only
	Header material for analysis	Accepted
	Radiographic procedures	Accepted
	Procedure for using "stop-off" to limit braze flow	Accepted
Miscellaneous	Tubing for three 20-tube wrap-around test heat exchangers	1 group rejected due to handling defects
	Welded and hydroformed hemispheres	Accepted
	$\frac{1}{16}$-in.-OD thermocouple walls	Accepted
	7212 ft of electrode Calrods	Radiographed for determining position of conduit

of removal was found by pickling the tubing in a 10% solution of phosphoric acid for approximately 1 hr. Test specimens metallographically examined after pickling in this solution for 168 hr revealed no attack whatever.

Effect of Penetrant Materials on Inconel at High Temperature

An experiment was conducted in order to determine if the sulfur-bearing materials used in penetrant inspection would be detrimental to Inconel at elevated temperatures. Metallographic examination of specimens which had been contaminated with these materials and heated to 1500°F for 50 hr did not reveal any embrittlement or attack.

Investigation of Overpickled Redraw Material

Samples from 2618 lb of CX-900 Inconel redraw material, which had been inadvertently overpickled, were submitted by the manufacturer for ORNL examination. Metallographic examination revealed microcracks 0.003 in. in depth; consequently, the entire amount was rejected. An attempt to eliminate the condition by sandblasting was not successful, since examination of finished tubing revealed microcracks 0.0005 in. in depth. The manufacturer indicated that the material would be reamed and that additional samples would be submitted for approval.

DEVELOPMENT OF INSPECTION METHODS

A. Taboada   G. M. Tolson

Radiographic Film Evaluation

An evaluation of available x-ray film was made for various inspection conditions on Inconel pipe. Eastman types "A," "AA," and "M" film were used for material up to $\frac{3}{4}$ in. thick that had been exposed to both x rays and an iridium source.

Results indicated that the greatest sensitivity could be obtained on material thicknesses less than $\frac{1}{2}$ in. by using fine-grain type "M" film. For thicker materials, an excessive exposure time was required when using type "M" film, thus resulting in inferior resolution. The higher speed film, type "AA," was found to be more acceptable for thicker materials. Sensitivities of less than 2% could be obtained with x rays. Iridium source sensitivity with the use of "M" film was approximately 2.5%.

Inspection of Weldments in Beryllium-Containing Vessels

A radiographic-inspection technique was developed for inspecting Inconel weldments in vessels containing beryllium. Tests were made on $\frac{1}{8}$-in. Inconel weldments through a combined thickness of 10 in. of beryllium and $\frac{1}{4}$ in. of Inconel to simulate actual conditions. Drilled holes varying from 0.010 to 0.030 in. in diameter and depth were used as sensitivity standards. A 300-kv x-ray machine, a million-volt x-ray machine, and iridium were tried as irradiation sources in order to find the optimum voltage range.

The method considered most acceptable involved the use of the 300-kv machine at a position as close to the vessel as possible but on the opposite side of the weldment (Fig. 30). The x-ray beam was collimated by filters, shown in Fig. 30, to minimize scatter by the beryllium and fogging of the film. Exposure time was minimized by using the faster

UNCLASSIFIED
ORNL—LR—DWG 25172

MACHINE: NORELCO 300 kv

TECHNIQUES USED IN ATTAINING OPTIMUM SENSITIVITY :
1 200 kv
2 15 ma
3 8 min
4 TARGET-OPENING FILTER: 0.005-in. Cu
5 "AA" FILM
6 DEVELOPING TIME: 8 min

CROSS SECTION SHOWING FABRICATED DEFECTS AND PENETROMETERS
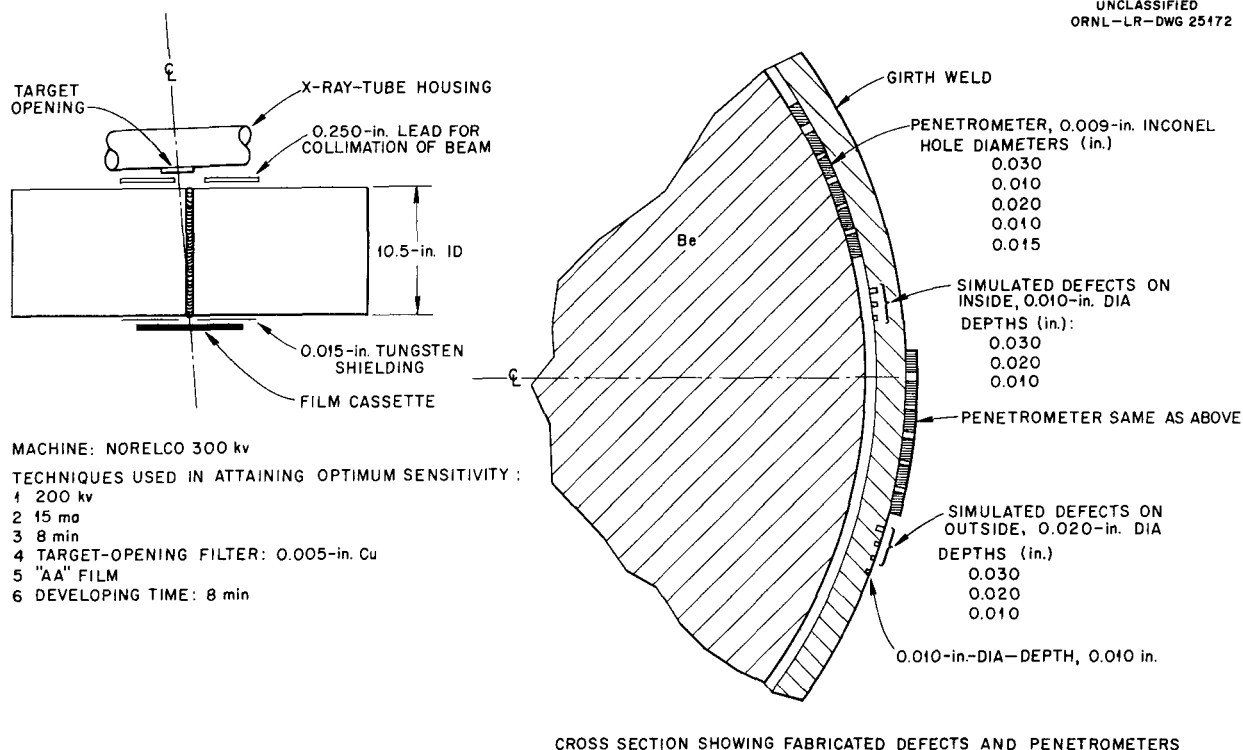
Fig. 30. Method for Radiographic Inspection of Girth Weld on Inconel Cylinder of $\frac{1}{8}$-in. Wall Thickness Containing Beryllium.

Eastman type "AA" film and a 15-ma setting on the machine. Optimum voltages were found in the range of 210 to 280 kv. With the optimum technique, it was possible to resolve the 0.010-in.-dia by 0.010-in.-depth hole.

Crack Detection in Tubing with Radiography

The inspection of tubing for reactor application involves five different methods: visual, penetrant, eddy current, ultrasonic, and radiography, each of which is sensitive to particular types of defects and is insensitive to others. Radiography will detect internal conditions which have depths as little as 1.0% of the material thickness being inspected, if the discontinuity has reasonable length and width. Discontinuities, with narrow widths but large in other directions, such as cracks, are found when orientation is in a direction approximately normal to the x-ray beam. However, as the direction of the crack and the x-ray beam diverge, it becomes more difficult to detect the cracks. The angle at which the cracks will not be seen depends on the dimensions of the cracks, the angle being most sensitive to the crack width.

The technique used for radiographing tubing includes x-raying of the tubes at three different orientations in order to locate random defects in the areas of optimum inspection (as shown in in Fig. 31). During routine tubing inspection, cracks have frequently been observed by means of radiography because they had randomly fallen within the proper range of these positions. In order to determine how well the method of radiography would perform in detecting cracks, an in-

vestigation was established in which $\frac{1}{2}$-in. × 0.045-in.-wall tubes with known cracks were radiographed at 16 evenly spaced locations. The conditions shown in Fig. 32 were used, and the exposures were interpreted by 11 people. The results were averaged to minimize any human error. The exposures were evaluated into three categories: resolved, not resolved, and questionable.
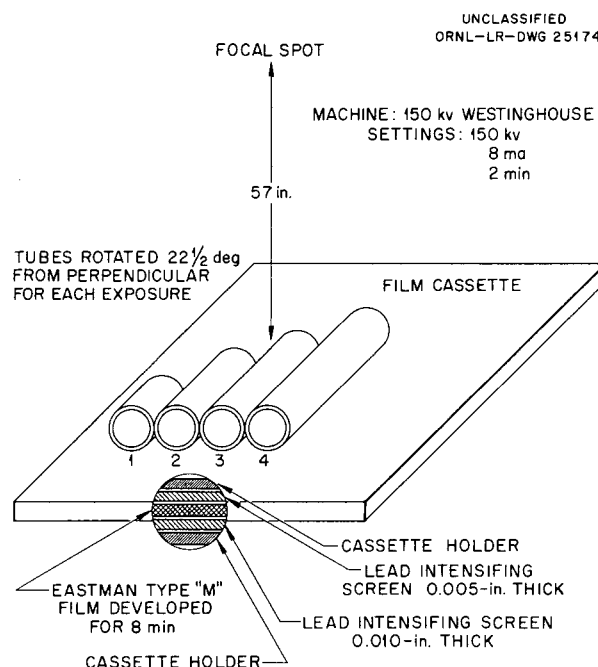
Fig. 32. Method of Radiography Used in the Inspection of INOR-8 Tubing $\frac{1}{2}$-in. OD × 0.045-in. Wall Thickness.

Metallographic cross sections of the four cracks are shown in Fig. 33, and their descriptions are as follows.

Tube No. 1. — The crack in the first tube (Fig. 33*a*) was approximately 25 mils in depth and approximately $1\frac{1}{2}$ mils in width. This crack could be found by using three exposures 120 deg apart, and probably would also be found by using only two exposures 90 deg apart.

Tube No. 2. — The crack in tube No. 2, as shown in Fig. 33*b*, was approximately 20 mils in depth and close to $\frac{1}{2}$ mil in width, running at almost a 45-deg angle with the surface of the tube. As would be expected, this crack was resolved more easily at a slight angle to the x-ray beam than

Fig. 31. Method Used for the Radiographic Inspection of Tubing.

if the beams were perpendicular to the wall of the tube. Four exposures would be necessary in order to detect this crack.

Tube No. 3. — The crack in tube No. 3 (Fig. 33c) was approximately 19 mils in depth and less than $\frac{1}{4}$ mil in width. Four exposures would also be needed on this crack to ensure detection.

Tube No. 4. — The crack in tube No. 4 (Fig. 33d) was approximately 28 mils in depth and approximately 1 mil in width. Three x-ray exposures should detect this crack in almost all instances. However, to be absolutely sure of detection, four exposures should be used. Cross sections of this crack were taken in order to determine the extent to which it ran longitudinally beyond that which was shown on the radiographs. The crack was

resolved all along the tube to its shallowest point, which was approximately 9 mils in depth and $\frac{1}{4}$ mil in width.

The results of this experiment, as shown in Fig. 34, indicated that cracks in tubing of the sizes investigated could be detected by using radiography if sufficient exposures were made. In this case four exposures, 45 deg apart, would be sufficient for a complete inspection of the tubing. The width, orientation, and position of the cracks appear to be the most influencing factors in determining the angle for resolution. The section closest to the x-ray film is resolved to a slightly greater extent than that area 180 deg away.
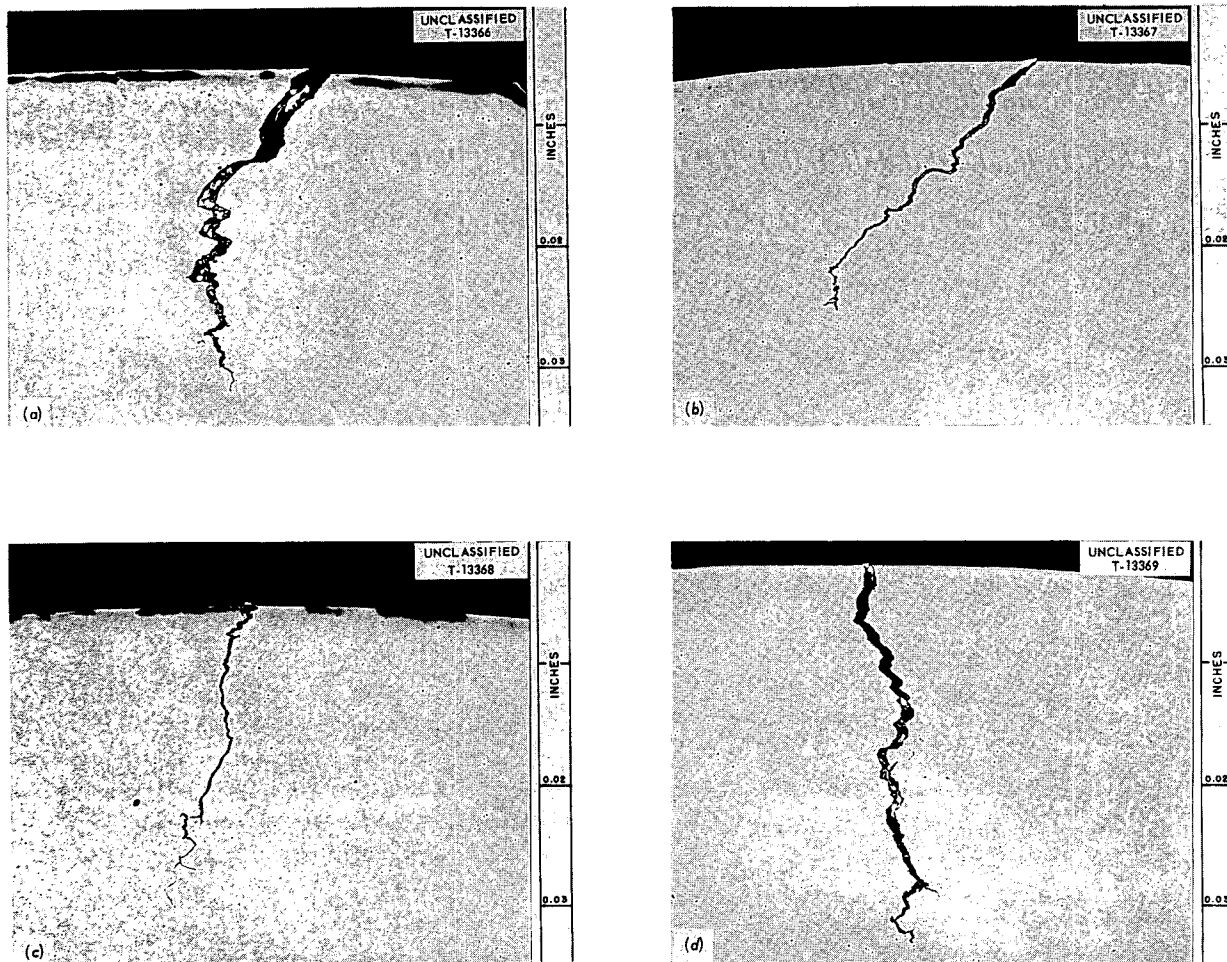
Fig. 33. Cracks in INOR-8 Tubing Used in Experiments of Crack Detection by Radiography. Note angle of crack to the surface in (b). Unetched. 100X. Reduced 35.5%.

80 deg

85 deg

TUBE NO. 1 (SEE Fig. 33a)

55 deg

54 deg

TUBE NO. 2 (SEE Fig. 33b)

AREA OF CRACK RESOLUTION

AREA OF QUESTIONABLE RESOLUTION

AREA OF NO RESOLUTION

DIRECTION OF XRAY

56 deg

58 deg

TUBE NO. 3 (SEE Fig. 33c)

76 deg

73 deg

TUBE NO. 4 (SEE Fig. 33d)
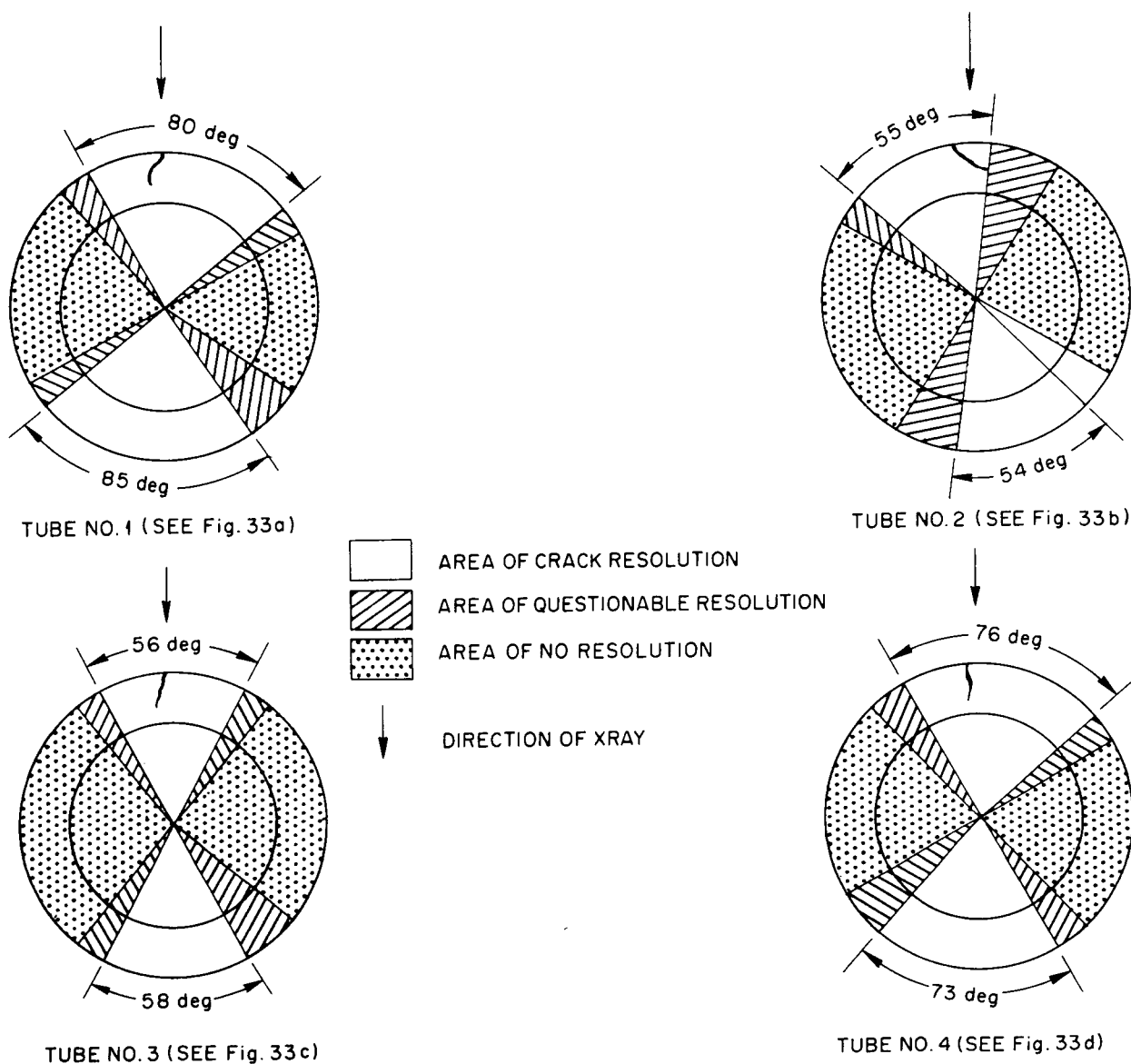
Fig. 34. Areas of Crack Resolution by Radiographic Methods for Varying Positions of Cracks with Respect to X-Ray Beam.

Radiography of Tube-to-Header Welds

The destructive examination of small tube-to-header test specimens, such as those shown in Fig. 35, revealed the existence of defects, which indicates the need for nondestructive inspection on weldments of this type. Radiographic experiments were performed with the use of specimens of various configurations in order to determine the best techniques. These techniques were then recommended to the vendor as a method for the inspection of such welds on radiators and heat exchangers. Figure 36 is a photomicrograph showing a porosity-type defect which had been detected radiographically. While defects 0.009 in. and greater are detected very easily during routine inspection, defects as small as 0.003 in. have been found under optimum conditions. Where noted, defects are removed by grinding and then re-welding.
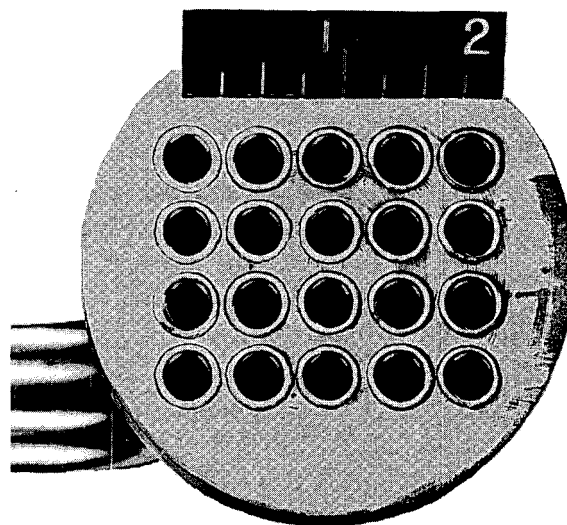
Fig. 35. Tube-to-Header Welds as Fabricated on Radiator and Heat Exchangers. $1\frac{1}{2}$X. Reduced 23%.
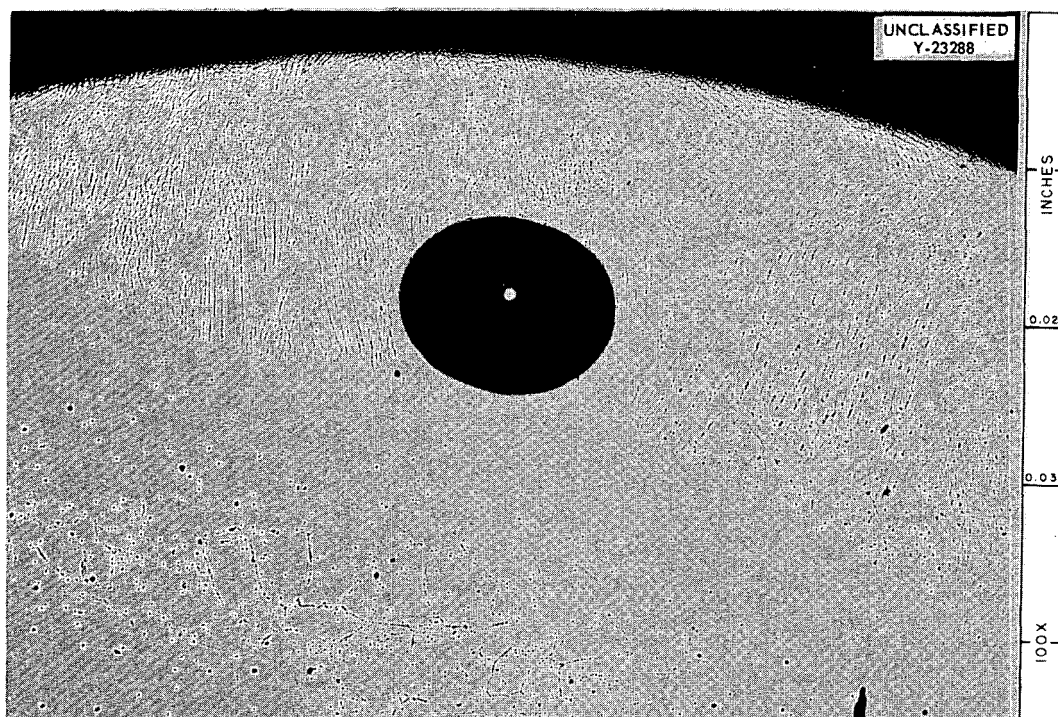
Fig. 36. Porosity Found by Radiographic Inspection. Approximately 0.012 in. in diameter. Etchant: oxalic acid. Reduced 16%.

WELDING AND BRAZING

P. Patriarca

R. E. Clausing   E. A. Franco-Ferreira

G. M. Slaughter

B. McDowell   R. G. Shooster

L. C. Williams

The progress of the Welding and Brazing Group during the past year has been published in the ANP Project Quarterly Progress Reports and in various topical reports. The investigations have been highly diversified in scope and cannot be summarized under a general subject. Hence, the pertinent results of each study have been abstracted, and these are presented under individual headings.

WELDABILITY OF NICKEL-MOLYBDENUM ALLOYS

R. E. Clausing

Aging Characteristics of Hastelloy B Base Metal

A study[1] was made of the elevated-temperature precipitation occurring in Hastelloy B, and the resulting microstructures were related to the room- and elevated-temperature mechanical properties. In general, aging resulted in a relatively minor improvement in the room- and elevated-temperature tensile strength, accompanied by a marked reduction in room- and elevated-temperature ductility.

Mechanical Properties of Hastelloy B and Hastelloy W Weldments

The results of tensile tests on Hastelloy B and Hastelloy W welds on ½-in. plate have been summarized.[2-4] Hastelloy B welds have good ductility in the as-welded condition when tested at room temperature but poor ductility at 1500°F. Hastelloy W weld metal exhibits a comparable strength with a higher ductility. Aging at 1300

and 1500°F, however, results in a significant decrease in ductility in both alloys.

Hardness traverses of weld joints after aging at various temperatures[5] indicated that aging at 1300°F produced the highest hardness value. Hardening was most pronounced along the interface between the weld metal and base metal.

Mechanical Properties of Experimental Nickel-Molybdenum Alloys

Preliminary weldability tests have been conducted on several experimental nickel-molybdenum alloy compositions, and observations have been made.[6] The INOR-8 composition was studied extensively, and tensile, hardness, and hot-bend-test results have been summarized.[7] At the temperatures investigated, the INOR-8 composition appears to be a compromise between the properties of Inconel and Hastelloy B. Generally, the strength is less than that of Hastelloy B but greater than that of Inconel, while the ductility lies between that of Inconel and Hastelloy B.

Hot-ductility tests[8] on INOR alloys 1 through 6 were conducted at Rensselaer Polytechnic Institute, and the results were compared with similar results for Inconel, Inconel X, and Hastelloy B. Alloys INOR-1, -2, and -3 behave in a manner which appears to be superior to that of Hastelloy B (by virtue of high as-heated ductility), whereas alloys INOR-4, -5, and -6 are definitely inferior to Hastelloy B.

[1]R. E. Clausing, P. Patriarca, and W. D. Manly, *Aging Characteristics of Hastelloy B*, ORNL-2314 (July 30, 1957).

[2]P. Patriarca and R. E. Clausing, *ANP Quar. Prog. Rep. Dec. 31, 1956*, ORNL-2221 (Parts 1–5), p 221.

[3]R. E. Clausing, *ANP Quar. Prog. Rep. March 31, 1957*, ORNL-2274 (Parts 1–5), p 201–204.

[4]R. E. Clausing, G. M. Slaughter, and P. Patriarca, *ANP Quar. Prog. Rep. June 30, 1957*, ORNL-2340 (Parts 1–5), p 184.

[5]P. Patriarca, R. E. Clausing, and G. M. Slaughter, *ANP Quar. Prog. Rep. Dec. 31, 1956*, ORNL-2221 (Parts 1–5), pp 221, 222, 224.

[6]R. E. Clausing, G. M. Slaughter, and P. Patriarca, *ANP Quar. Prog. Rep. June 30, 1957*, ORNL-2340 (Parts 1–5), p 182.

[7]R. E. Clausing, *ANP Quar. Prog. Rep. Sept. 30, 1957*, ORNL-2387 (in press).

[8]G. M. Slaughter, *ANP Quar. Prog. Rep. March 31, 1957*, ORNL-2274 (Parts 1–5), p 205–207.

RELATIVE TENSILE PROPERTIES OF INCONEL PLATE AND INCONEL WELD DEPOSITS

R. E. Clausing

An investigation was conducted in order to determine the room- and elevated-temperature properties of Inconel weld deposits.[9] The weld metal was found to be significantly stronger than the base metal at temperatures from 1400 to 1800°F, while its ductility was lower. The weld should, therefore, not readily deform at these temperatures in structures of uniform stress distribution, provided that the service conditions are comparable with the test conditions.

WELDING OF BORON-CONTAINING STAINLESS STEELS

P. Patriarca

Experiments were conducted in order to determine the properties of welded joints in a type 304 stainless steel containing 1% boron, which is of interest in shielding applications.[10] The weldments exhibited extremely poor ductility and were exceptionally notch sensitive. In view of the results obtained, it appears that the use of this alloy for load-carrying components is inadvisable.

BRAZING ALLOY DEVELOPMENT

Thermal Expansion Studies

R. E. Clausing

Thermal expansion data for several high-temperature brazing alloys were obtained[11] in the range from room temperature to 900°C. Mean coefficients of expansion were calculated for different temperature ranges, and typical curves were plotted. While most alloys exhibited a nearly linear curve, the curve for the 82% Au–18% Ni alloy revealed a deviation associated with a solid-phase reaction.

High-Temperature Oxidation Studies

G. M. Slaughter

Static and cyclic oxidation tests on joints brazed with approximately 20 commercial and developmental alloys have been performed, and the results have been tabulated.[12] The oxidation resistance of most of these alloys at both 1500 and 1700°F is excellent.

NaK-TO-AIR RADIATOR FABRICATION

G. M. Slaughter

An extensive investigation[13] was conducted in order to study the influence of several brazing variables upon the melting characteristics of Coast Metals alloy No. 52 brazing rings. Rate-of-temperature-rise experiments indicated that a minimum heating rate of 300°F/hr was necessary to obtain adequate flow of the ring on type 310 stainless steel–clad copper fins. On the other hand, the brazing alloy rings melted completely at a 100°F/hr rate of rise when Inconel-clad copper fins were substituted. The improvement in flow characteristics was attributed to the minimization of braze liquation upon the Inconel. Dry-helium-atmosphere brazing also resulted in good flowability of the rings on stainless steel–clad copper fins at the slower heating rates.

A statistical analysis of the fin adherence obtained with varying rates of temperature rise was made, and the results were tabulated.[14] At 100°F/hr the ORNL cast ring exhibited much better flow than the Coast Metals sintered ring. However, at 300°F/hr the two were comparable.

Numerous trips were made this year to the York Corporation to provide assistance in the solution of difficulties in the fabrication of high-conductivity-fin NaK-to-air radiators. A variety of recommendations was made[15] and a cooperative research program was established[16] and carried out.

[9]R. E. Clausing, *ANP Quar. Prog. Rep. Sept. 30, 1957*, ORNL-2387 (in press).

[10]P. Patriarca, *ANP Quar. Prog. Rep. Dec. 31, 1956*, ORNL-2221 (Parts 1–5), p 239–240.

[11]R. E. Clausing, *ANP Quar. Prog. Rep. Dec. 31, 1956*, ORNL-2221 (Parts 1–5), p 232–233; E. J. Wilson and G. M. Slaughter, *ANP Quar. Prog. Rep. Dec. 31, 1956*, ORNL-2221 (Parts 1–5), p 233–236.

[12]G. M. Slaughter, *ANP Quar. Prog. Rep. Sept. 30, 1957*, ORNL-2387 (in press).

[13]P. Patriarca and G. M. Slaughter, *ANP Quar. Prog. Rep. Dec. 31, 1956*, ORNL-2221 (Parts 1–5), p 224–232.

[14]G. M. Slaughter, *ANP Quar. Prog. Rep. March 31, 1957*, ORNL-2274 (Parts 1–5), pp 205, 207.

[15]G. M. Slaughter, *ANP Quar. Prog. Rep. March 31, 1957*, ORNL-2274 (Parts 1–5), p 208.

[16]G. M. Slaughter, *ANP Quar. Prog. Rep. June 30, 1957*, ORNL-2340 (Parts 1–5), p 223.

STUDIES OF GRAIN GROWTH IN INCONEL TUBING

G. M. Slaughter   E. J. Wilson

A detailed study was undertaken to determine the influence of the important variables on the grain growth characteristics of Inconel tubing.[17-19] Samples of tubing were heated for 30 min at various temperatures, and the grain size was studied metallographically. After the 30-min heat treatment at temperatures as low as 1814°F and up to and including 1904°F, the grain growth was found predominantly in the grains along the outer surface of the tube. After heat treatment at 1922°F and above, general grain growth was evident. The influence of time-at-temperature was also investigated, and, as was expected, the growth increased with increasing time. The influence of the straightening and polishing operations on the tubing was determined and was found to be only minor.

The grain coarsening obtained with actual brazing cycles (slow rate of rise and rate of cooling) was also determined. Significantly increased grain growth was obtained in this type of cycle as compared with the simple isothermal cycle.

A study of the grain growth obtained in $\frac{1}{8}$- and $\frac{1}{4}$-hard tubing was also conducted. The cold work was noticeably beneficial in reducing the grain growth upon thermal treatment.

FABRICATION OF CERMET VALVE COMPONENTS

G. M. Slaughter

Suitable procedures have been developed for fabricating valve components containing titanium carbide and tungsten carbide cermets. A report has been prepared[20] describing the various brazing and high-temperature-bonding procedures for several compositions of cermets. This report also discusses the metallographic studies which were made on the various types of joints investigated.

ART SODIUM-TO-NaK HEAT EXCHANGER FABRICATION

G. M. Slaughter

Brazing procedures were developed for use in the fabrication of ART sodium-to-NaK heat exchangers by the Griscom-Russell Company. Experiments indicated that a 300°F/hr heating rate, which should be readily attainable with most industrial equipment, provides a high degree of assurance of successful brazing.[21]

Several trips were made to the vendor's plants to provide assistance with actual fabrication problems.

INVESTIGATION OF RAPID HEATING CYCLES

E. A. Franco-Ferreira

Tests were run to investigate the feasibility of using very short heating cycles (of the order of 5 min) for the back-brazing of heat exchanger tube-to-header joints.[22] This method of brazing should minimize grain growth in the tubes, reduce tube-wall dilutions, and avoid distortion and the jigging problems associated with conventional furnace-brazing of entire assemblies.

ART FILL-AND-DRAIN-TANK FABRICATION

E. A. Franco-Ferreira   G. M. Slaughter

A procedure has been developed for welding and back-brazing the tube-to-header joints of the ART fill-and-drain tanks.[23,24] A trepanned weld joint minimizes root cracking resulting from the restraint of the $1\frac{1}{2}$-in. Inconel tube sheet. A trepanned annulus with small feeder holes provides a suitable method of brazing alloy preplacement in which reliable filleting is assured.

[17]E. J. Wilson and G. M. Slaughter, *ANP Quar. Prog. Rep. Dec. 31, 1956*, ORNL-2221 (Parts 1–5), pp 233, 236–238.

[18]E. J. Wilson and G. M. Slaughter, *ANP Quar. Prog. Rep. March 31, 1957*, ORNL-2274 (Parts 1–5), p 208–215.

[19]G. M. Slaughter and P. Patriarca, *ANP Quar. Prog. Rep. June 30, 1957*, ORNL-2340 (Parts 1–5), p 214.

[20]G. M. Slaughter, P. Patriarca, and W. D. Manly, *Bonding of Cermet Valve Components to Metals*, ORNL-2322 (in press).

[21]G. M. Slaughter, *ANP Quar. Prog. Rep. March 31, 1957*, ORNL-2274 (Parts 1–5), p 195–197.

[22]E. A. Franco-Ferreira, *ANP Quar. Prog. Rep. March 31, 1957*, ORNL-2274 (Parts 1–5), pp 195, 198.

[23]E. A. Franco-Ferreira, *ANP Quar. Prog. Rep. June 30, 1957*, ORNL-2340 (Parts 1–5), p 225.

[24]E. A. Franco-Ferreira and G. M. Slaughter, *ANP Quar. Prog. Rep. Sept. 30, 1957*, ORNL-2387 (in press).

CORROSION OF INCONEL WELDS

E. A. Franco-Ferreira

A metallographic study was made of Inconel heat exchanger welds after they were subjected to elevated-temperature service in fused salts.[25] Severe intergranular corrosion was evident in welds in which the surface layer was removed by machining. In the as-welded condition the surface layer is generally such as to minimize the depth of corrosive attack.

SUBCONTRACT STATUS

1. The University of Florida subcontract for an investigation of the diffusion of boron and silicon from high-temperature brazing alloys was completed, and a final report is being prepared.

2. The Glenn L. Martin Company subcontract for a study of electric resistance welding of tube-to-header joints was also completed, and a final report is being prepared.

3. The progress made by Rensselaer Polytechnic Institute in their hot-ductility studies is covered in this report (see "Weldability of Nickel-Molybdenum Alloys").

4. The Battelle Memorial Institute subcontract for molybdenum welding studies has continued. The variables being studied include atmosphere purity, prior surface treatment, and type of shielding.

[25]E. A. Franco-Ferreira, *ANP Quar. Prog. Rep. June 30, 1957,* ORNL-2340 (Parts 1–5), p 247.

FABRICATION

J. H. Coobs

H. Inouye	M. R. D'Amore[1]
T. K. Roche	R. E. McDonald[1]
D. O. Hobson	V. M. Kolba[2]
J. P. Page	T. Hikido[3]

NICKEL-MOLYBDENUM ALLOY DEVELOPMENT

H. Inouye   T. K. Roche

The development of the alloys of the nickel-molybdenum system was continued during the period, with the major effort being devoted toward the evaluation of experimental alloys containing as the principal alloying addition between 15 and 20 wt % molybdenum. On the basis of the requirements for an ideal container material for fluoride fuel 107, these experimental alloys have shown exceptional promise. During this period the production of these alloys was increased from experimental heats to commercial quantities without serious difficulties.

Alloy Evaluation Norms

In coordinating the effort to develop and produce a suitable alloy, a system of evaluation was developed.[4] Optimum criteria for the acceptability of an alloy were established as *combinations of the favorable properties of Inconel and Hastelloy B.* The various alloys were rated on such qualities as oxidation resistance, creep strength and rupture life, corrosion resistance, fabricability, joining and aging characteristics, and nuclear properties.

Status of Development Program

A preliminary summary of the status of the alloy development effort was presented previously.[5] The alloys which have been studied fall into three general categories: solution-hardening, precipitation-hardening, and dispersion-hardening alloys. The solution-hardening alloys are represented by alloys INOR-1 and -8; the precipitation-hardening alloys by INOR-3, -4, -6, and -7; and the dispersion-hardening alloys by INOR-5 and -9. Preliminary

[1] Pratt & Whitney Aircraft.

[2] The Glenn L. Martin Co.

[3] USAF.

[4] H. Inouye and T. K. Roche, *ANP Quar. Prog. Rep. Dec. 31, 1956,* ORNL-2221 (Parts 1–5), p 199.

[5] H. Inouye and T. K. Roche, *ANP Quar. Prog. Rep. Dec. 31, 1956,* ORNL-2221 (Parts 1–5), p 199–203.

properties of the INOR alloys 1 through 8 have been presented previously, along with the composition ranges of each alloy studied.[6] These properties show that, of the three categories of alloys, the solid-solution-hardening alloys offer the best compromise. On this basis, the INOR-8 alloy was selected as having the best combination of properties, and much of the effort has been directed toward establishing the final composition and producing commercial quantities of the alloys.

However, it is felt that the full potential of the alloys of the nickel-molybdenum system definitely has not been developed. For the immediate future, these alloys appear to be the only structural materials which show the possibility of bridging the gap between Inconel and the refractory metals niobium and molybdenum.

The most attractive feature of the nickel-base alloys containing 15–20% molybdenum as the principal alloying element is their versatility. From the studies of numerous alloy combinations and types, it has been determined that a particular property of interest can be enhanced, but usually at the expense of some other property. Inasmuch as the property variations are derived largely from additions of a third, fourth, or fifth alloying element, the principal properties of importance, such as strength and corrosion resistance, can be balanced to give an alloy composition which is best suited for a particular application. As the severity of the service conditions is increased (e.g., higher temperatures and longer times), the freedom of modification becomes narrower, and thus many of the alloys are eliminated for various reasons. In short, for every temperature or application, there appears to be an optimum alloy composition.

For 1000 hr of operation, the alloys as presently developed appear to permit peak temperatures of 1650–1700°F at the metal-salt interface. This limitation has been tentatively set because of the

[6] H. Inouye and T. K. Roche, *ANP Quar. Prog. Rep. March 31, 1957,* ORNL-2274 (Parts 1–5), p 177–182.

rapid increase of the corrosion tendency of the alloys containing chromium and the deterioration of the strength above these temperatures.

Fabricability. — Alloys which are solid solutions at the forging temperatures should present no unusual difficulties. Forging difficulties have been encountered with large heats of the INOR alloys, as reported previously,[7-9] but these difficulties have been associated with poor melting and forging techniques. It is anticipated that further problems encountered will be those normally associated with the development of reduction schedules for a new material. The alloy INOR-8, which meets the initial alloy requirements, should soon be considered a commercial item.

A serious limitation which exists in the production of tubing, which has been discussed previously,[10] is the tendency toward longitudinal splitting exhibited by alloys containing over 0.10% carbon. This tendency has not been encountered during hot-forging operations or during cold-rolling of plate and sheet products.

Mechanical Properties. — The mechanical properties of the nickel-molybdenum alloys are reported elsewhere in this report. In general, available data on INOR-8 show that an increase of up to 200°F in operating temperature should be realized by substituting it for Inconel. Thus, operation at temperatures between 1650 and 1700°F with fuel 107 appears possible.

The correlation between microstructure and creep rupture showed that those microstructures which exhibited a grain boundary network of fine carbides had the best strength. Carbide-precipitation studies have shown that the desired microstructure could be obtained by high annealing temperatures (2300°F). Improvements in the rupture life and ductility have been realized by minor additions of malleableizers and by vacuum-remelting of air melts.

Corrosion Resistance. — Within certain limitations, the corrosion resistance of the nickel-molybdenum alloys approaches the optimum for service in environments of fused salts, sodium, and air. The corrosion behavior of these alloys in fused salts and in sodium is discussed elsewhere in this report.

The oxidation of the nickel-molybdenum alloys has been found to vary from excessive to slight, the rate depending upon the composition. The element having the largest effect is chromium, and its critical level at a temperature of 1800°F was ascertained to be 6%. Alloys containing less than this amount show about 4 mils of oxidation in 170 hr, while those containing over 6% show an attack of less than 1 mil.

The extent of oxidation, for all compositions studied, in 1000 hr at temperatures as high as 1750°F has been tolerable. This conclusion is based upon the fact that approximately 75 loops have been operated without special coatings or protection. The probable maximum service temperature in each environment for alloys of current interest is given in Table 23.

Weldability. — The status of welding development on these alloys is described elsewhere in this report. However, it is felt that the weldability will not be a serious problem, since approximately 40 alloy compositions representing various modifications of the nickel-molybdenum base material have been welded satisfactorily. These welds have been placed in service for periods up to 1000 hr at temperatures as high as 1850°F without deleterious effects.

The incidence of poor weldability and cracking tendencies under restraint in various heats of alloys has shown good correlation with heats which were not properly melted.

Aging Characteristics. — Of the elements, titanium, aluminum, and beryllium, which cause the basic nickel-molybdenum to respond to an aging heat treatment, beryllium was found to be the most potent. Alloys containing amounts as low as 0.25% exhibited strong aging tendencies at 1300°F. At a temperature of 1300°F, the aging response of alloys containing titanium and aluminum was significant, while at 1500°F these alloys either overaged in a short time or showed no effect.[11]

[7]H. Inouye and T. K. Roche, *ANP Quar. Prog. Rep. March 31, 1957,* ORNL-2274 (Parts 1–5), p 183–186.

[8]H. Inouye, T. K. Roche, and J. H. Coobs, *ANP Quar. Prog. Rep. June 30, 1957,* ORNL-2340 (Parts 1–5), p 175–176.

[9]H. Inouye and T. K. Roche, *ANP Quar. Prog. Rep. Sept. 30, 1957,* ORNL-2387 (in press).

[10]H. Inouye and T. K. Roche, *Met. Semiann. Prog. Rep. Oct. 10, 1956,* ORNL-2217, p 129–131.

[11]H. Inouye and T. K. Roche, *ANP Quar. Prog. Rep. Dec. 31, 1956,* ORNL-2221 (Parts 1–5), p 203.

Table 23. Maximum Permissible Interface Temperature of Nickel-Molybdenum Alloys

Alloy Designation	Composition (wt %)	Maximum Temperature (°F)*		
		In Fuel 107	In Sodium	In Air
INOR-1	Ni—20 Mo	1850**	1650	1300
	Ni—17 Mo—6 Fe	1800**	1650	1300
INOR-9	Ni—17 Mo—3 Cb—5 Fe	1800**	1650	1300
Hastelloy W	Ni—24 Mo—5 Cr—5 Fe	1800**	1650	1400
INOR-8	Ni—17 Mo—7 Cr—5 Fe	1700**	1650	1800
INOR-8 (mod.)	Ni—17 Mo—7 Cr—5 Fe—3 Cb	1700**	1650	1800
	Ni—17 Mo—10 Cr	1650	1650	1800

*Based upon 4 mils of corrosion in 1000 hr of operation.
**Estimates based upon tests at 1650°F or 1750°F.

Properties of INOR-8

It appears at this time that the alloy INOR-8, which is based on the Ni-Mo-Cr-Fe system, will offer the best compromise of properties for fulfilling the requirements of a structural material compatible with fused fluorides. The current optimum composition range of this alloy is 15–18% Mo, 6–8% Cr, 4–5% Fe, 0.04–0.08% (max) Mn, 0.5% (max) Si, bal Ni. The properties of this alloy have been summarized and discussed in previous reports.[12,13]

A program is in progress that is concerned with an investigation of the effect of varying composition on the mechanical properties of alloys of the INOR-8 type.[14] Eighteen alloys have been prepared and tested in creep rupture at a stress of 10,000 psi and a temperature of 1500°F in argon. Results of these tests, although incomplete, show that (1) increasing the molybdenum content is the most effective means of improving the creep properties, (2) increasing the chromium content from 5 to 7% without changing the molybdenum and iron content produces only a slight improvement in the

creep properties, and (3) there is no obvious correlation of the rupture life of the material with the total content of alloying elements in the nickel base.

Properties of INOR-9

Alloys designated as INOR-9 have been studied[15] to determine whether they may be suitable as a possible substitute for INOR-8. The base composition of these alloys is INOR-1 (nickel-molybdenum binary) with niobium and carbon added for strength. Since the alloys of this group do not contain elements exhibiting corrosive tendencies in fuel 107, it is expected that higher metal-salt interface temperatures will be permissible.

The heats of INOR-9 under investigation have as a nominal composition range 12–19% Mo, 3–5% Nb, 2–5% Fe, 0.06–0.30% C, bal Ni. The present studies showed that (1) the maximum permissible niobium content for forgeability is about $7\frac{1}{2}$%, (2) the solid solubility of niobium up to 1700°F in the nickel-molybdenum base is 5%, (3) the creep strength is about equal to that of INOR-8, and (4) the oxidation rates of the alloys are slightly higher than those observed for Hastelloy B.[13,16]

[12]H. Inouye and T. K. Roche, *ANP Quar. Prog. Rep. March 31, 1957,* ORNL-2274 (Parts 1–5), p 182–183.

[13]H. Inouye and T. K. Roche, *ANP Quar. Prog. Rep. Sept. 30, 1957,* ORNL-2387 (in press).

[14]H. Inouye, T. K. Roche, and J. H. Coobs, *ANP Quar. Prog. Rep. June 30, 1957,* ORNL-2340 (Parts 1–5), p 175–176.

[15]H. Inouye and T. K. Roche, *ANP Quar. Prog. Rep. March 31, 1957,* ORNL-2274 (Parts 1–5), p 183–186.

[16]H. Inouye, T. K. Roche, and J. H. Coobs, *ANP Quar. Prog. Rep. June 30, 1957,* ORNL-2340 (Parts 1–5), p 176–177.

Fabrication of ORNL Alloys

To bridge the gap between the present and the time when tubing will be available from commercial heats of nickel-molybdenum-base alloys, several alloys were produced on a laboratory scale, extruded into tube blanks, and redrawn into seamless tubing at Superior Tube Company.[17] It was intended that pump loops of these alloys would be operated to determine their corrosion resistance in fuel 107. Sufficient tubing of these alloys was obtained for the intended purpose, with the exception of one alloy (heats 30-46 and 30-47), on which the conditioning of the extruded tube blanks prior to tube reducing was excessive and resulted in a low yield of tubing. Consequently, three thermal convection loops of this alloy were operated instead of a pump loop.

Studies at Battelle Memorial Institute, Subcontract No. 979

The semiannual ANP meeting on materials was held at Battelle Memorial Institute on June 17, 1957. The progress made during the preceding six months was presented.[18] In general, their effort, which was fairly comprehensive, stressed the development of alloy compositions which had superior strength; as such, much of their effort was devoted to a study of alloys containing aluminum and molybdenum as the principal strengtheners.

Several compositions, of which B-3277 (20% Mo–7% Cr–2% Nb–1.5% Al–0.15% C–bal Ni) showed outstanding creep strength, were evaluated. Thermal convection loop tests of this alloy in fuel 107 showed that it was prone to attack by the salt by virtue of its aluminum and chromium content.

It was the intention of Battelle to round out their program with pump loop studies on several of their promising alloys in fuel 107. The Laboratory assisted this effort by preparing tube blank extrusions from billets of these alloys; however, these could not be redrawn to tubing because of splitting which occurred on the tube reducer. The relatively high carbon content was undoubtedly

responsible for the failures, as was noted previously.[19] The alloys were remade by Battelle with a lower carbon content (0.02%), and seamless tubing was processed; however, defects in this tubing caused early failure of the loops, and, therefore, the corrosion data were inconclusive.

This contract has been terminated, and a final report is being prepared by Battelle.

Fabrication of Alloy Tubing at Superior Tube Company, Subcontract No. 1112

The principal effort by Superior Tube Company under Subcontract No. 1112 is concerned with the processing of nickel-molybdenum alloy tubing from material supplied by ORNL, International Nickel Company, Haynes Stellite Company, and Westinghouse Electric Corporation. This work is referred to under the contributions of the individual companies to the over-all alloy development program.

In addition to the above support work, a series of alloys of the INOR-8 type was prepared by Superior by air-melting. These compositions were intended for investigation of the effect of zirconium additions to the alloy. Strip and tubing of these compositions have been received for testing.[13]

Phase Diagram Studies at the University of Tennessee, Subcontract No. 582

This investigation is being conducted for the purpose of establishing phase relationships and characteristic transformations in the binary Ni-Mo and ternary Ni-Mo-Cr systems. In the binary system, the three secondary phases have been identified, and their transformation temperatures have been redetermined.[20]

The present work is concerned with determining the solubility limits of molybdenum plus chromium in nickel and identifying the phases observed. The compositions studied range from 20 to 35% Mo and 3 to 15% Cr. Apparently the addition of chromium suppresses the formation of the beta phase (Ni_4Mo), since it was not observed in any of the ternary compositions.

A report in the form of a thesis is being prepared on these studies.

[17]H. Inouye, T. K. Roche, and J. H. Coobs, *ANP Quar. Prog. Rep. June 30, 1957*, ORNL-2340 (Parts 1–5), p 177–178.

[18]E. M. Simons, *Semi-annual ANP Meeting, Battelle Memorial Institute — Agenda*, ORNL CF-57-6-77 (June 17, 1957).

[19]H. Inouye and T. K. Roche, *Met. Semiann. Prog. Rep. Oct. 10, 1956*, ORNL-2217, p 129–131.

[20]H. Inouye and T. K. Roche, *ANP Quar. Prog. Rep. March 31, 1957*, ORNL-2274 (Parts 1–5), p 186–187.

Testing of Nickel-Molybdenum Alloys by The New England Materials Laboratory, Inc., Subcontract No. 584

Two nickel-base alloys containing 22 and 27% Mo plus fixed additions of manganese, chromium, iron, and vanadium were tested in stress-rupture and tensile tests. The composition and stress-rupture life of these alloys are summarized in Tables 24 and 25. Details regarding the effect of aging on the mechanical properties have been reported.[21]

The production heats INOR-1 through -6, which were prepared by the International Nickel Company, were tested in stress-rupture tests at 1350, 1500, and 1650°F in air. A final report is being prepared in accordance with the terms of the contract. The stress-rupture strengths of these alloys are summarized in Table 26.

Status of Production Heats of Nickel-Molybdenum Alloys

International Nickel Company. — A purchase order was placed with the International Nickel Company for the preparation of 4800-lb heats of six nickel-molybdenum-base alloys in order that production experience might be gained with this type of material. The alloy compositions are shown in Table 27. Phase I of the order[22] covered melting, casting, and ingot forging to produce billet stock suitable for conversion to seamless tubing, plate, sheet, wire, and rod for carrying out an evaluation program on each alloy. The results

Table 25. The 1000-hr Stress-Rupture Strength (psi) of Alloys Studied by the New England Materials Laboratory

Test bars 0.225-in. in diameter, annealed $\frac{1}{2}$ hr at 2000°F, air-cooled

Alloy	Test Temperature		
	1350°F	1500°F	1650°F
A	9,200	3,000	2,000
B	13,500	5,400	2,800
C	27,500	12,500	3,200
D	19,000	7,500	2,900
E	27,500	13,000	3,700

of the billet conversion (phase II) as well as a listing of products which have been received at ORNL were given in a previous report.[23]

In general, billet conversion was only moderately successful. Difficulties were encountered with cracking during the rolling of the Ti- and Al-bearing INOR alloys 4 and 6. INOR alloys 1, 2, and 5 were processed with considerably more success. Strength and weldability studies were conducted on the converted products which were received at ORNL. Recently, after some delay, the tube reducing of the tube shells which were extruded under phase II was completed, and these shells are presently being redrawn to small-diameter seamless tubing.[24] This tubing, if successfully processed, will

[21]O. Preston, N. J. Grant, and C. F. Floe, *Final Report — Development and Testing of Vacuum Melted Nickel—Molybdenum Alloys with Minor Alloying Additions*, ORNL-2181 (Oct. 3, 1956).

[22]H. Inouye and T. K. Roche, *Met. Semiann. Prog. Rep. Oct. 10, 1956*, ORNL-2217, p 136.

[23]H. Inouye and T. K. Roche, *ANP Quar. Prog. Rep. March 31, 1957*, ORNL-2274 (Parts 1–5), p 183–186.

[24]H. Inouye and T. K. Roche, *ANP Quar. Prog. Rep. Sept. 30, 1957*, ORNL-2387 (in press).

Table 24. Composition of Alloys Studied by the New England Materials Laboratory

Alloy	Constituent (wt %)								
	C	S	Cr	Mo	Fe	V	Mn	Nb	Ni
A	0.02	0.004	0.65	22.3	0.43	0.38	0.72		Bal
B	0.02	0.005		22.5	0.70		0.74	1.30	Bal
C	0.02	0.005	0.65	28.5	0.16	0.34	0.66		Bal
D	0.02	0.006	0.62	26.5	4.80	0.37	0.65		Bal
E	0.03	0.005		26.5	0.82		0.65	1.29	Bal

Table 26. The 1000-hr Stress-Rupture Strength of INOR Alloys 1 Through 6

1 hr at 2000°F, air-cooled; 16 hr at 1500°F, air-cooled

| Alloy | Test Temperature | | | | | |
| | 1350°F | | 1500°F | | 1650°F | |
	Stress-Rupture Strength (psi)	Elongation* (%)	Stress-Rupture Strength (psi)	Elongation* (%)	Stress-Rupture Strength (psi)	Elongation* (%)
INOR-1	13,000	18	3,900	19	1,800	19
INOR-2	8,000	11	3,600	12	1,600	20
INOR-3	15,000	5	5,100	19	2,800	9
INOR-4	17,000	1	6,300	5	3,400	11
INOR-5	15,000	22	4,500	26	1,700	32
INOR-6	18,000	5	11,000	8	2,600	20

*Interpolated values at a 100-hr rupture life.

Table 27. Experimental Nickel-Molybdenum Alloys Prepared by International Nickel Company

Alloy	Nominal Composition (wt %)
INOR-1	20 Mo—bal Ni
INOR-2	16 Mo—5 Cr—bal Ni
INOR-3	16 Mo—1 Al—1.5 Ti—bal Ni
INOR-4	16 Mo—2 Al—1.5 Ti—bal Ni
INOR-5	13 Mo—5 Cr—2 W—2 Nb—0.1 C—bal Ni
INOR-6	16 Mo—5 Cr—1 Al—1.5 Ti—bal Ni

provide material for additional corrosion studies in fluoride fuel 107. Currently, the International Nickel Company is engaged in the last phase (phase III) of this order, which is the conversion of the remaining billet stock to items identical with those received under phase II.

Haynes Stellite Company. – A 10,000-lb air-melted heat of the alloy INOR-8 has been purchased from the Haynes Stellite Company to supply the immediate material needs for conducting test programs in corrosion, welding, and creep.[24] Casting and fabrication of the alloy by hot- and cold-working to bar, plate, sheet, and strip products was accomplished with little or no difficulty.

Various shapes of this material have been received, including forged bar, hot-rolled plates, hot-rolled sheet, hot-rolled bar, six production-size extrusion billets, and rolled strip for the processing of Weldrawn tubing.

Westinghouse Electric Corporation, Subcontract No. 1067. – A contract was signed with the Westinghouse Electric Corporation which covers the melting, casting, and fabrication of large pilot heats of nickel-molybdenum-base alloys at their Blairsville, Pennsylvania, metals plant. Details on the work to be accomplished under this subcontract have been reported previously.[23,25,26] Recently, a review was made of the progress to date, and the first periodic report on this development work was submitted to ORNL.

In summary, this report states that three air-induction-melted heats of the specified composition for INOR-8 (see "Properties of INOR-8") were prepared. Difficulties were encountered in forging castings of these heats due to internal flaws formed during cooling. Various changes in mold design and melting practice were made to overcome this, as described in detail previously.[24]

[25]H. Inouye and T. K. Roche, ANP Quar. Prog. Rep. Dec. 31, 1956, ORNL-2221 (Parts 1–5), p 206–207.

[26]H. Inouye, T. K. Roche, and J. H. Coobs, ANP Quar. Prog. Rep. June 30, 1957, ORNL-2340 (Parts 1–5), p 175–176.

A sound 3-in.-dia forging from the initial high-carbon heat of INOR-8 prepared by Westinghouse was received for evaluation. The material was successfully worked by extrusion and by hot- and cold-rolling. Specimens were prepared for creep-rupture studies and for density and thermal expansion measurements. The density of the material, determined by weighing a machined specimen, was found to be 8.795 g/cm³. Thermal-expansion measurements were made from room temperature to 1832°F through the cooperation of the Ceramics Group. The data are shown in Fig. 37. A creep-rupture test was run on the material, the results of which are reported in Table 28, together with the results obtained on the same material after vacuum-remelting. These data show that a definite improvement in rupture life and elongation was realized through vacuum-remelting. However, the creep rate of the air-melted alloy was superior to that of the vacuum-remelted material.

Composite Tubing and Plate

To take advantage of the corrosion resistance of the nickel-molybdenum alloys in fuel 107 at temperatures exceeding 1650°F, it would be necessary to isolate the nickel-base alloy from the sodium through the use of a composite tube of nickel-base and iron-base alloys. Preliminary studies of diffusion couples composed of INOR-8 and type 316 stainless steel show that one or more unknown phases precipitate at the interface as a result of diffusion. The extent of the interface reaction is negligible after a diffusion time of 500 hr at 1300°F. As was expected, the severity of reaction increases rapidly as the temperature is increased to 1800°F. The precipitate is confined to the nickel-base side of the interface and occurs as a

grain boundary phase rather than as a continuous layer. Room-temperature tensile tests of composite sheet showed that strengthening occurred after diffusion heat treatments at 1300 and 1500°F. A weakening effect was observed in those specimens heat-treated at 1650 and 1800°F. A minimum
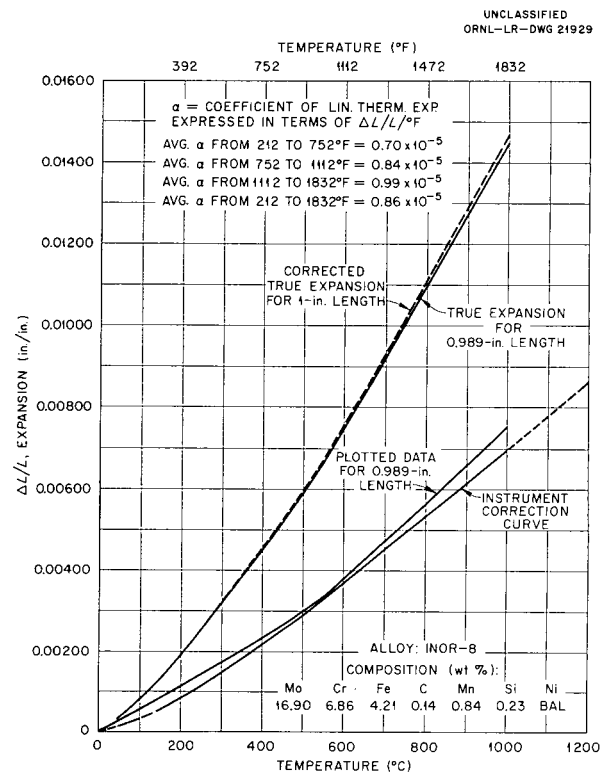
Fig. 37. **Linear Thermal Expansion for 1-in. Length of INOR-8 Alloy as Determined by Vacuum Atcotron Differential Transformer Recorder.** Sample used was only 0.989 in. long, and data were interpolated to a value for a 1-in. length.

Table 28. **Results of Creep-Rupture Tests of Initial Heat of INOR-8 Prepared by Westinghouse**

Temperature: 1500°F
Stress: 10,000 psi
Atmosphere: Argon

Type of Melt	Time to Specified Strain (hr)			Rupture Life (hr)	Elongation (%)
	1%	5%	10%		
As air-melted	32	120		135	6.25
Vacuum-remelted	25	80	125	214	54.5

fracture ductility of 28% elongation was observed in the specimens heat-treated at 1650°F (ref 24).

The feasibility of fabricating composite tubing of Inconel and type 316 stainless steel has been reported previously.[27] It is anticipated that similar procedures can be applied to the fabrication of composites of INOR-8 and type 316 stainless steel.

NIOBIUM RESEARCH

J. P. Page   V. M. Kolba   D. O. Hobson

Recrystallization of Niobium

A comprehensive investigation of the recrystallization characteristics of niobium was carried out, primarily to compare the annealing behavior and mechanical properties of arc-cast niobium with the standard powder-base product. The results should also be useful in understanding the creep behavior of niobium and as a basis for comparing niobium alloys.

A fabrication schedule was devised for producing materials of the two types having a comparable grain size. From these starting materials, samples were cold-rolled to total reductions varying from 20 to 97% and annealed at temperatures from 900 to 1350°C for times varying from 0.1 to 100 hr. The resulting specimens were analyzed by x-ray and microscopic techniques. An additional study was made on the effects of recovery and recrystallization on the room-temperature mechanical properties of niobium.

Except for the larger recrystallized grain size of the arc-cast material, no significant differences were found between the two types of niobium. A topical report describing the complete investigation of the recrystallization of niobium has been published.[28]

Niobium-Base Fuel Components

Several small fuel plates containing an Nb-UO$_2$ core and clad with niobium were prepared in order to demonstrate the metallurgical feasibility of such fuel elements. The distribution of UO$_2$ and the bonding of core to cladding were good in all cases. An attempt to extrude a rod of Nb-UO$_2$ core material canned in steel failed when the core material did not reduce proportionately and the can ruptured.

The fabricability and tensile properties of an alloy of 80% Nb–20% U were investigated. Selective oxidation of the uranium to produce a dispersion of UO$_2$ was partly successful.[29]

Extrusion of Niobium

An experimental quantity of niobium pellets produced by the Electro Metallurgical Company was consolidated into a rod by extrusion. After being stripped from the stainless steel can, this rod was cold-swaged to a reduction of 97% without annealing.

On the basis of this success, eight rod and tube extrusions of niobium pellets were processed, both the compacted and extruded pellets being used. Four of these are shown in Fig. 38. The first rod in this picture had been stripped from the extrusion can, while the remainder are shown as extruded. A summary of the extrusion data on these billets is given in Table 29. The extrusions are now being evaluated for workability and recovery.

Table 29. Extrusion Data for Canned Niobium Billets

Number of Extrusions	Type	Reduction Ratio	Extrusion Pressure (tsi)
3	Rod	10:1	53–64
4	Tube	13:1	45–51
1	Tube	7:1	28

SHIELDING MATERIALS DEVELOPMENT

J. P. Page   M. R. D'Amore

Shield Plug for the ART Fuel Pumps

A shield plug assembly was devised to protect the fuel pump motors of the Aircraft Reactor Test. This shield plug was required to fulfill certain conditions with respect to density and heat transfer properties which are necessary for successful operation of the fuel pumps.

The shield plug consists of three components assembled into an Inconel container. These consist of a dense gamma-ray shield composed of

[27] H. Inouye and T. K. Roche, *ANP Quar. Prog. Rep. March 31, 1957*, ORNL-2274 (Parts 1–5), p 188.

[28] J. P. Page, *The Annealing Behavior of Cold-Rolled Niobium*, ORNL-2372 (Sept. 19, 1957).

[29] V. M. Kolba, *ANP Quar. Prog. Rep. Dec. 31, 1956*, ORNL-2221 (Parts 1–5), p 214–218.
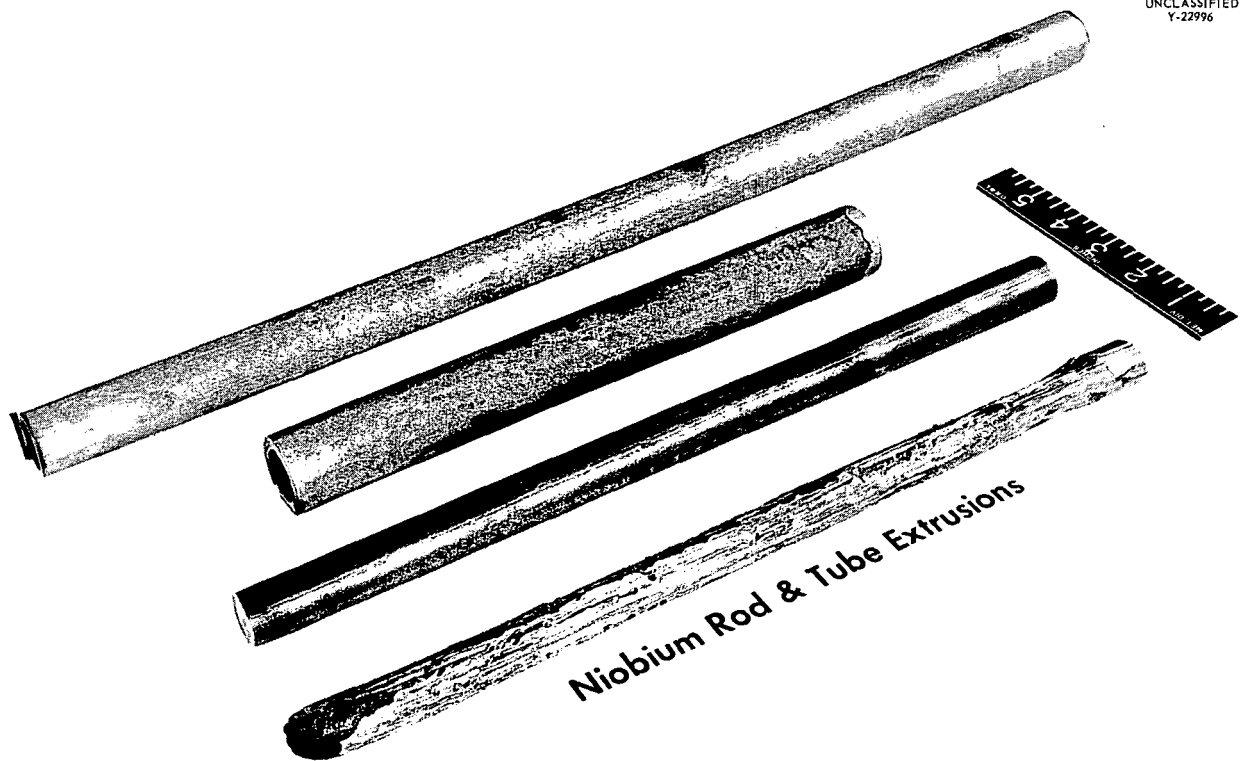
Fig. 38. Niobium Rod and Tube Extrusions Produced from Canned Pellets.

tungsten carbide bonded with Hastelloy C, a thermal shield of low-density zirconia, and a neutron shield composed of boron carbide dispersed in copper. The development work leading to the final components and the fabrication of a full-sized assembly have been reported in detail previously.[30-32] A topical report describing the work has also been written.[33]

Neutron Shielding Materials

The previous report summarized the materials development for the ART shield and the decisions concerning the use of these materials. Certain other investigations on alternative materials were also summarized.[34]

Activity during the year was largely confined to cooperation with the Procurement Section as needed in evaluating and coordinating the work of vendors. Much difficulty was experienced on the part of the Allegheny Ludlum Steel Corporation in producing the stainless steel–clad $Cu-B_4C$ shield material. Numerous batches of material from rolled packs were examined and evaluated, and a considerable amount of coordination was required to resolve the difficulties. Procedures based on recommendations by ORNL personnel were finally established, and good yields of sound material were obtained.[35,36]

[30]J. P. Page, *ANP Quar. Prog. Rep. Dec. 31, 1956,* ORNL-2221 (Parts 1–5), p 207–209.

[31]J. P. Page, *ANP Quar. Prog. Rep. March 31, 1957,* ORNL-2274 (Parts 1–5), p 188.

[32]J. P. Page, *ANP Quar. Prog. Rep. June 30, 1957,* ORNL-2340 (Parts 1–5), p 239.

[33]J. P. Page and J. H. Coobs, *The Shield Plug Assembly for the ART Fuel Pumps,* ORNL-2353 (to be published).

[34]M. R. D'Amore and J. H. Coobs, *Met. Semiann. Prog. Rep. Oct. 10, 1956,* ORNL-2217, p 138–140.

[35]M. R. D'Amore and J. H. Coobs, *ANP Quar. Prog. Rep. Dec. 31, 1956,* ORNL-2221 (Parts 1–5), p 209.

[36]M. R. D'Amore, *ANP Quar. Prog. Rep. March 31, 1957,* ORNL-2274 (Parts 1–5), p 188–189.

In addition to this work, two large rings, 14 in. and 19 in. in diameter, respectively, of stainless steel–clad Cu-B$_4$C were produced for use in a hot critical experiment.

TUBULAR CONTROL RODS

M. R. D'Amore

The strength of the 70% nickel–30% Lindsay oxide[37] material for the control rods was determined at 1500°F. None of the samples exhibited appreciable ductility, primarily because of stringering and agglomeration of the oxide particles.[38] Several three-ply extrusions with Inconel as cladding were prepared, but they cracked badly during cooling.

A technique was developed for producing hard, dense particles of the Lindsay oxide. Three extrusions prepared with the use of this dense oxide were successful.[39,40] Tensile bars cut from two of the extrusions were tested at room temperature and at 1500°F; they exhibited elongations of up to 5.0 and 2.0%, respectively, as compared with elongations of less than 0.1% for the specimens mentioned above.

HIGH-TEMPERATURE HYDRIDE MODERATORS

T. Hikido   R. E. McDonald

Yttrium Metal Production and Hydriding Equipment

The development of suitable solid moderators for use at very high temperatures is quite necessary for realizing the potential performance of nuclear propulsion systems. Of the various materials only beryllium oxide and hydrided yttrium show promise for the temperatures of interest (1800°F).

A capsule containing zirconium hydrided to an N_H of 3.5 ($N_H \times 10^{22}$ = number of hydrogen atoms per cubic centimeter) was fabricated for tests in the MTR. Useful data on hydride moderators are expected, since hydrided zirconium has favorable properties at the test temperature of 1600°F. Hydriding equipment based on designs used at the General Electric Company was completed and was used for preparing hydrided zirconium.

Equipment for the production of yttrium metal was installed and was used for several reduction runs. A new reduction process was developed in which lithium metal is used as reductant. The yield in four runs with the lithium reductant varied from 60 to 83% of the theoretical quantity of yttrium-magnesium alloy.

Vacuum distillation equipment has been set up, and distillation of the magnesium and lithium from the alloy product has yielded good quality sponge. Several arc melts prepared from this sponge were quite ductile. Analytical data on these melts are incomplete.[41–43]

Hydrogen Diffusion Studies

The use of hydride moderators at high temperatures requires a suitable barrier or can material to prevent gradual loss of the hydrogen. Development work directed toward finding a suitable barrier was initiated under subcontract No. 390 by Metal Hydrides, Inc. A scheme was evolved for using a test specimen machined from bar stock or cast ingots. Measurements of diffusion constants were made on copper and nickel, but termination of the contract led to cancellation of further work planned on molybdenum and on nickel-molybdenum alloys.

Equipment has been set up at ORNL for measuring the diffusion of hydrogen through a heavy-walled tube having a short sample section of reduced thickness.[43,44]

FABRICATION OF MOLYBDENUM

M. R. D'Amore   D. O. Hobson

The fabrication of molybdenum tubing for use in corrosion tests is being investigated. Several billets of molybdenum and molybdenum alloys were extruded into rods and tube shells. The alloys with various additions of titanium and zirconium were difficult to extrude at a ratio of 10:1, while unalloyed molybdenum billets were extruded into rods at a ratio of 16:1, and one billet was extruded into a tube shell at 13:1 (ref 45).

[37] J. A. Griffin and L. M. Doney, *ANP Quar. Prog. Rep. June 10, 1956,* ORNL-2106 (Parts 1–5), p 213.

[38] M. R. D'Amore, *ANP Quar. Prog. Rep. Dec. 31, 1956,* ORNL-2221 (Parts 1–5), p 210–211.

[39] M. R. D'Amore, *ANP Quar. Prog. Rep. March 31, 1957,* ORNL-2274 (Parts 1–5), p 189–190.

[40] M. R. D'Amore, *ANP Quar. Prog. Rep. June 30, 1957,* ORNL-2340 (Parts 1–5), p 242.

[41] R. A. Potter, T. Hikido, and R. E. McDonald, *ANP Quar. Prog. Rep. March 31, 1957,* ORNL-2274 (Parts 1–5), p 192–194.

[42] T. Hikido and R. E. McDonald, *ANP Quar. Prog. Rep. June 30, 1957,* ORNL-2340 (Parts 1–5), p 240–241.

[43] T. Hikido and R. E. McDonald, *ANP Quar. Prog. Rep. Sept. 30, 1957,* ORNL-2387 (in press).

[44] E. A. Sullivan and S. Johnson, *ANP Quar. Prog. Rep. June 30, 1957,* ORNL-2340 (Parts 1–5), p 241–242.

[45] M. R. D'Amore, *ANP Quar. Prog. Rep. June 30, 1957,* ORNL-2340 (Parts 1–5), p 242.

FUNDAMENTAL LIQUID-METAL STUDIES

J. L. Scott

H. W. Leavenworth, Jr.[1]   J. W. Barnett

The purpose of the Fundamental Liquid-Metal Studies Group is to study the mechanisms associated with the phenomenon of mass transport in liquid-metal flow systems. The phenomenon of mass transport is the combination of the effects of solution of container components in the hot zone of the system and the subsequent nucleation and growth of acicular crystals, or the diffusion of the solute out of the solution as it becomes supersaturated in the cold zone. When acicular crystals form, they tend to plug the flow channels in the regions where they occur. This phenomenon constitutes a serious problem in the design of liquid-metal heat-transfer systems, for, if mass transport could be prevented, liquid metals with their excellent heat-transfer characteristics of high thermal conductivity, high heat capacity, and high boiling points would serve as excellent reactor coolants.

One task of the Fundamental Liquid-Metal Studies Group was to determine the approach and the systems to be used. After a study of the literature on the subject and a consideration of the skills distinctive to the Oak Ridge National Laboratory, it was decided that particular emphasis would be placed on the alkali metals in this work. The metals mercury, bismuth, and lead were also selected for study to the extent that they would complete the scope of the program. The solutes to be emphasized were iron, chromium, and nickel, although studies of periodic-table sequences of elements were also anticipated. Because of the fundamental nature of the program the systems were to be simple binary or possibly ternary ones with geometries which are amenable to mathematical analysis.

THE PURIFICATION OF SODIUM

J. L. Scott

The purity of the alkali metals which were to be used in this research had to be very high; otherwise, any data which were obtained would have been open to question. Several investigators[2-4] have shown that oxygen in sodium will markedly increase the rate of mass transfer of iron in an iron-sodium system. Horsley[2] has suggested that the accelerating influence of oxygen on the mass transfer in stainless steel—sodium systems is due to a shift, with temperature, of the reaction

$$3\ Na_2O + Fe \rightleftharpoons 2\ Na_2O{\cdot}FeO + 2\ Na$$
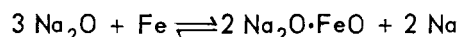
with $Na_2O{\cdot}FeO$ being formed in the hot zone and reduced in the cold zone. Thus, in the study of mass transfer in liquid sodium, materials which are very low in oxygen content must be used. Both oxygen and nitrogen are believed to affect the rate of mass transport in lithium systems.[5]

There are two methods currently being used for purifying alkali metals: filtration with filters made by the Micro Metallic Corp., and vacuum distillation. Theoretically, filtration would remove all oxygen not in solution, that is, the oxygen present in Na_2O. Since the solubility is reportedly 30 ppm at the melting point of sodium,[6] this purity should be attainable. There is the concern, however, that small particles of oxide will penetrate the filter and thus lower the efficiency of the purification process. Distillation has been used by Horsley,[7] who produced sodium with less than 9 ppm of oxygen. Because this latter method seemed to be more reliable and reproducible, a vacuum still for producing sodium was designed and constructed.

The sodium vacuum distillation apparatus, which is shown in Fig. 39, consists of three primary components: the still, the condenser, and the receiver. The still and receiver are constructed of 8-in.-dia,

[2]G. W. Horsley, *The Corrosion of Iron by Oxygen-Contaminated Sodium*, AERE-MR-1441 (April 1954).

[3]S. J. Rodgers, J. W. Mausteller, and E. F. Batutis, *Iron and Nickel Concentrations in Sodium*, MSA-TR-27 (June 30, 1954).

[4]A. D. Bogard, *The Solubility of Iron in Sodium Metal, Sodium—Sodium Oxide, and Sodium—Sodium Oxide—Sodium Hydroxide*, NRL-4131 (March 9, 1953).

[5]J. M. McKee, *Effect of Nitrogen on Corrosion by Lithium*, NDA-40 (June 14, 1957).

[6]R. M. Adams and M. Sittig, in *Liquid Metals Handbook, Sodium-NaK Supplement*, p 6, ed. by C. B. Jackson, GPO, Washington, 1955.

[7]G. W. Horsley, *The Purification of Sodium by Vacuum Distillation*, AERE-M/R-1152 (May 12, 1953).

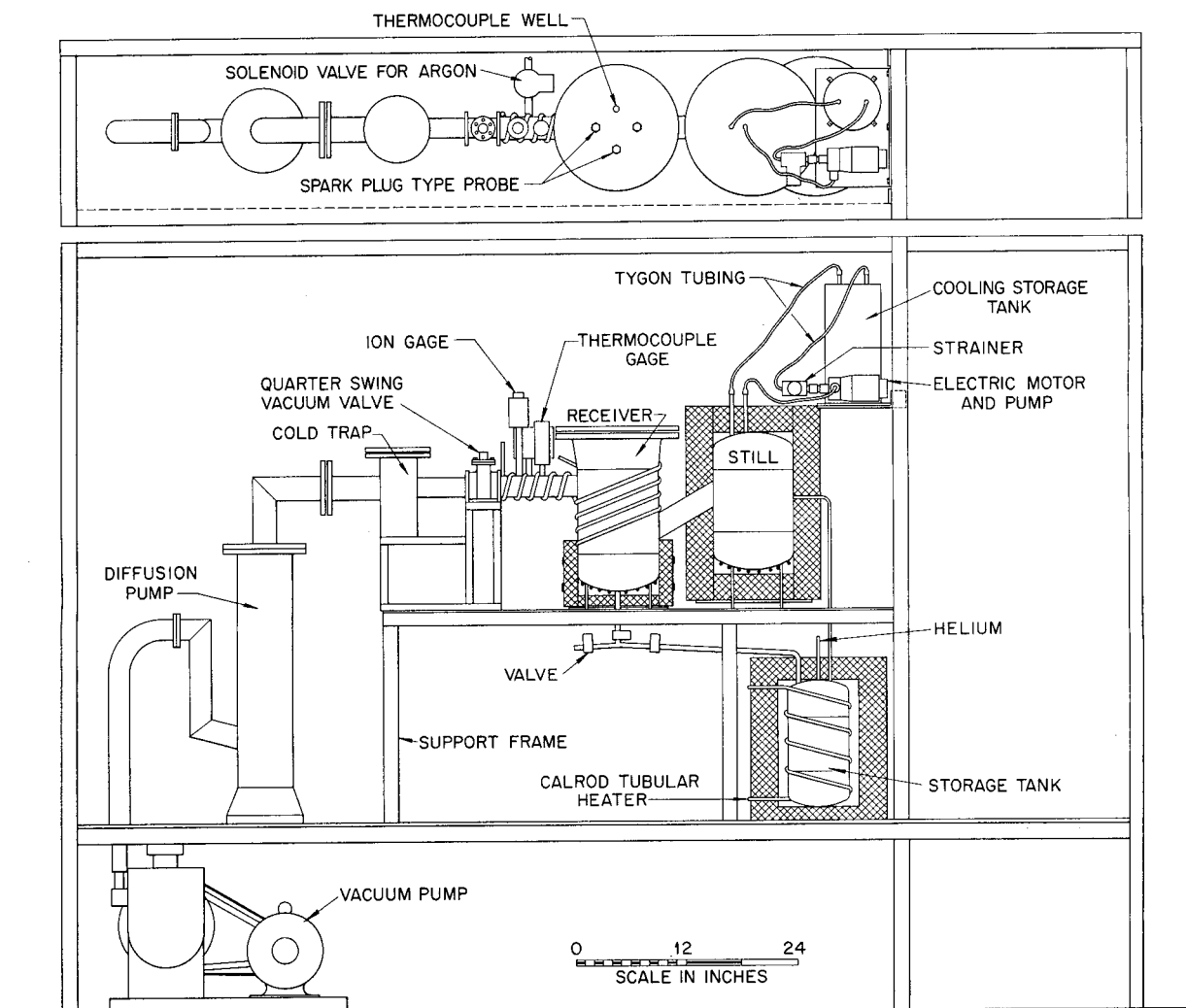[1]On assignment from Pratt & Whitney Aircraft.

Fig. 39. Sodium Distillation Apparatus.

schedule 40, type 347 stainless steel pipe, and each is about 12 in. high. The condenser consists of a coil of $\frac{1}{4}$-in.-dia, 45-mil-wall, type 347 stainless steel tubing wound inside the tube which connects the still and the receiver. Cooling for the condenser is provided by a circulation system which pumps ethylene glycol through the condenser tube.

The vacuum system consists of a Welch Duo-seal 25 fore-pump and a Consolidated Vacuum MC-500 diffusion pump, a cold trap, and thermocouple and ion vacuum gages. A 2-in. quarter-swing vacuum valve separates the still from the vacuum system. Preliminary tests have shown that a vacuum of 2×10^{-5} mm Hg may be attained in the system by a thorough outgassing treatment.

There are several auxiliary components to the still. Several heaters are required to supply the heat for distillation and to maintain the sodium in a molten condition. Included in this category are several small heaters not shown in Fig. 39, which maintain the temperature of all the transfer tubes above 100°C. A storage tank is included in the system in order to increase the total capacity. Spark plug probes for determining liquid levels and thermocouples for temperature measurement are essential to the operation of the still. The sodium

is pumped around the system by applying a positive argon or helium pressure to the full container and a vacuum to the empty one. Finally, a safety device is included which shuts off the power to the system and floods it with argon whenever the pressure rises above 50 μ.

The principal advantage of the present design over previous ones[7] is that the sodium may be re-circulated from the receiver to the still any number of times and redistilled to remove the contamination picked up in the receiver. Since the installation has just been completed, no analysis of the efficiency of the system for purification has yet been made.

RATE OF DIFFUSION OF NICKEL IN LIQUID LEAD

J. L. Scott   H. W. Leavenworth, Jr.[1]

One of the possible mechanisms which determines the rate of mass transfer in a liquid-metal system is the diffusion of the solute in the solvent through a "boundary layer" adjacent to the wall. For this reason, the gaining of a better understanding of the process of diffusion in liquid metals is an essential part of the study of the mass-transport process. In systems where the rate of the surface-solution process is quite high there is a relatively large concentration gradient across the laminar layer which varies from a saturated solution at the liquid-solid interface to a highly unsaturated solution at the laminar-turbulent boundary. If the diffusion coefficient for the diffusion of the solute in the liquid varies with composition, theoretical analyses of the mass-transport process, which are based on the assumption that the diffusion coefficient is independent of concentration, may lead to predictions which are in serious error. Consequently, the following question must be answered: Is the diffusion coefficient for a slightly soluble solute a function of concentration in a liquid-metal system?

In order to acquire good diffusion data on liquid-metal systems and to determine the effect of concentration on the diffusion coefficients, a study was initiated on the rate of diffusion of nickel in liquid lead. Lead was picked as the liquid metal because of its ease of handling and its inertness to pyrex. Nickel was selected as the solute because it is a component of most of the high-temperature alloys and because data for the rate of mass transfer of nickel in a lead thermal convection

loop have been reported.[8] The object of the study was to determine the diffusion coefficients of nickel in lead at a series of temperatures and over a range of concentrations.

The capillary-reservoir technique, which was used in these studies for measuring diffusion coefficients in liquid metals, has been described previously.[8] Typical data, computational methods, and diffusion coefficients for saturated solutions of nickel in lead were also given in this same report.[8] Diffusion coefficients for unsaturated solutions were given in a later report.[9]

The following conclusions were reached in this investigation:

1. If only the saturated solutions of nickel in lead, which vary in composition from 0.15 to 0.50 wt % nickel over the temperature range studied, are considered, the apparent diffusion coefficient for nickel in liquid lead may be written as:

$$D = 7.41 \times 10^{-1} e^{-10,300/RT} \; .$$

2. The diffusion coefficient for nickel in liquid lead changes slightly with composition over the composition range studied. The change appears to be the result of a shift in the entropy of activation rather than the enthalpy of activation, but further work will be required to prove this conclusively.

3. The diffusion coefficient for nickel in liquid lead is an order of magnitude higher than the co-efficient for self-diffusion of lead at any temperature. This result is in agreement with the results of Strauss,[10] who has given evidence that some of the nickel atoms may occupy interstitial sites in liquid lead. The rate of diffusion of interstitial atoms is generally much higher than the rate of diffusion of substitutional atoms. These observations may be associated with the fact that the radius of the nickel atom is 27% smaller than the radius of the lead atom.[11]

---

[8]J. L. Scott and H. W. Leavenworth, Jr., *ANP Quar. Prog. Rep. June 30, 1957*, ORNL-2340 (Parts 1–5), p 236.

[9]J. L. Scott and H. W. Leavenworth, Jr., *ANP Quar. Prog. Rep. Sept. 30, 1957*, ORNL-2387 (in press).

[10]S. W. Strauss, Naval Research Laboratory, private communication.

[11]L. Pauling, "The Electronic Structure of Metals and Alloys," in *Theory of Alloy Phases*, p 220, American Society for Metals, Cleveland, 1956.

HIGH-TEMPERATURE REACTIONS

G. P. Smith, Jr.

C. R. Boston   J. J. McBride
J. V. Cathcart   G. F. Petersen
G. W. Clark[1]   J. B. Wagner[2]

MICROTOPOGRAPHY OF OXIDE FILMS FORMED ON NIOBIUM, TANTALUM, AND ZIRCONIUM

J. V. Cathcart

A previous investigation of the oxidation characteristics of the alkali metals[3] indicated that all metals probably formed protective oxide films, provided that the oxidation temperature was sufficiently low. Such films may be expected to become nonprotective if for some reason the lattice of the covering layer of oxide becomes disrupted. In an effort to determine the nature of these disruptions and to understand the phenomena which produce them, this study has been extended to include an investigation of the oxidation of several of the structurally important metals in groups IV and V of the periodic table. Niobium, in particular, and, to a lesser extent, tantalum and zirconium have been studied.

The main emphasis in the research has been placed on an electron-microscopic examination of the surface topography of the oxide films formed on these metals. The results thus far obtained suggest that the mode of diffusion of the reacting species in the oxide film during oxidation may be very important in determining the degree of protectiveness of the oxide film.

A discussion of the results obtained with each of the three metals is given below.

Niobium

An electron-optical investigation was made of the microtopography of oxide films formed on niobium at temperatures from 325 to 450°C. It was found that small blister-like cracks tended to form in the oxide while the film was still relatively thin and that the onset of this blistering could be correlated with an increase in the oxidation rate.

As a preliminary to the main study, a series of rate measurements was made on niobium at temperatures in the vicinity of 400°C. A typical result is shown in Fig. 40. Characteristically, these oxidation rate curves showed an initial protective stage of oxidation followed by a transition period in which the oxidation rate increased. Finally, a nonprotective stage of oxidation ensued in which the oxidation rate became essentially constant. A manometric technique similar to that used in a previous study of the oxidation of alkali metals[4] was utilized for these rate measurements.
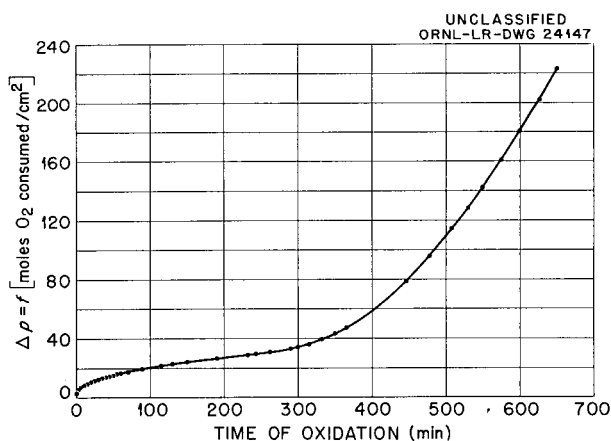

Fig. 40. Oxidation Rate Curve for Niobium at 400°C.

The above results are in general agreement with the data of Inouye[5] and of Gulbransen and Andrew.[6] The latter authors reported that protective oxidation continued for at least 7 hr at 375°C. At higher temperatures, however, their rate curves had the same qualitative form as that shown in Fig. 40, the protective stage of oxidation becoming shorter and shorter as the temperature

[1]Consultant, Virginia Institute for Scientific Research, Richmond, Virginia.

[2]Summer research participant from the Pennsylvania State University.

[3]J. V. Cathcart, *Met. Semiann. Prog. Rep. Oct. 10, 1956*, ORNL-2217, p 145.

[4]J. V. Cathcart, L. L. Hall, and G. P. Smith, *Acta Met.* 5, 245–248 (1957).

[5]H. Inouye, *Scaling of Columbium in Air*, ORNL-1565 (Sept. 24, 1953).

[6]E. A. Gulbransen and K. F. Andrew (to be published).

was increased to 500°C. At 600°C and above, Inouye reported the existence of linear rate curves throughout his experiment.

Procedure and Results. — Electron-microscope specimens were prepared from niobium coupons 1 × 2 cm on a side and 0.05 cm thick. The coupons were hand-ground through 4/0 emery, polished with 0.3-μ levigated alumina, and electrolytically polished in a 90% H_2SO_4–10% HF solution. Prior to oxidation the polished specimens were annealed in a pyrex apparatus overnight at the oxidation temperature under a pressure of approximately 10^{-6} mm Hg. All specimens were oxidized in purified oxygen at a pressure of 1 atm. Carbon replicas preshadowed with a gold-Manganin alloy were made of the surfaces of most of the oxidized specimens, but in a few instances Formvar replicas were prepared.

The changes in oxide topography as a function of time at a constant temperature are illustrated in Figs. 41(a–d). These electron micrographs show the surface topography of the oxide film after times ranging from 30 to 240 min for oxidation at 400°C. Optical examination of the specimen which had been oxidized for 30 min, corresponding to the protective stage of oxidation, revealed only the presence of the oxide interference colors usually associated with protective oxide films. In the related electron micrograph (Fig. 41a), the oxide film appeared to be smooth and coherent; no cracks could be observed in the film. The most striking feature of the specimen was a variation of oxidation rate with crystal plane, as is shown by the different thicknesses of oxide over different grains in the metal.

The 120-min specimen corresponded to the beginning of the transition zone in the oxidation rate curve. Again, optical examination showed only interference colors in the oxide film. However, a few cracked blisters were apparent in the electron micrograph, Fig. 41b, although most of the oxide still appeared to be quite coherent.

The approximate center of the transition zone in the oxidation rate curve was reached with the 210- and 240-min specimens. Optical examination of these specimens revealed areas of oxide interference colors interspersed with small rough areas of white oxide. Electron micrographs (see Figs. 41c and 41d) showed that these white areas were regions of the oxide in which a large increase in blister density had occurred.

When oxidation was continued until the linear portion of the oxidation rate curve had been reached, the entire specimen surface became covered with a rough white oxide. These surfaces were too rough to permit replication, since particles of oxide adhered to the replica. For this reason, the electron-optical portion of this study had to be limited to cases where the oxidation of the specimens had not proceeded beyond the approximate center of the transition zone of the rate curves. It should be noted, however, that even in cases where considerable oxide adhered to the replica, something of the topography of the oxide could be inferred from the shadows cast by the oxide patches (see Fig. 41d).

The surface topography of the niobium oxide films also reflected the decrease, reported by Gulbransen and Andrew,[6] in the duration of the initial protective stage of oxidation with increase in temperature. As judged on the basis of blister density, the transition region between the protective and nonprotective stages of oxidation occurred after 10, 60, 240, 480, and 2900 min for oxidation temperatures of 450, 420, 400, 380, and 350°C, respectively. A typical result from these experiments is illustrated in Fig. 42, which shows the surface topography of the oxide film formed in 480 min at 380°C. At 325°C, no blisters were seen in the oxide films in experiments lasting up to 144 hr (see Fig. 43).

It was also observed that as the oxide films thickened, their surfaces tended to become rougher. This phenomenon occurred at all temperatures investigated, but it can be most clearly seen in Fig. 43. The oxide surface had a "rippled" texture, the direction of the ripples varying with crystallographic direction. As discussed below, this effect may be related to plastic deformation of the oxide film.

A few metal specimens were anodically oxidized in order to contrast the topography of the oxide thus formed with that produced during gaseous oxidation. A 0.1% solution of sodium sulfate was used in these experiments. Results typical of anodizations at 25, 75, and 100 v are shown in Figs. 44(a–c), respectively. As is evident from the photographs, no variation of oxidation rate with crystallographic plane was observed for the anodically oxidized specimens. Many blisters were formed in the film, however, and blister size and density increase with anodizing voltage.
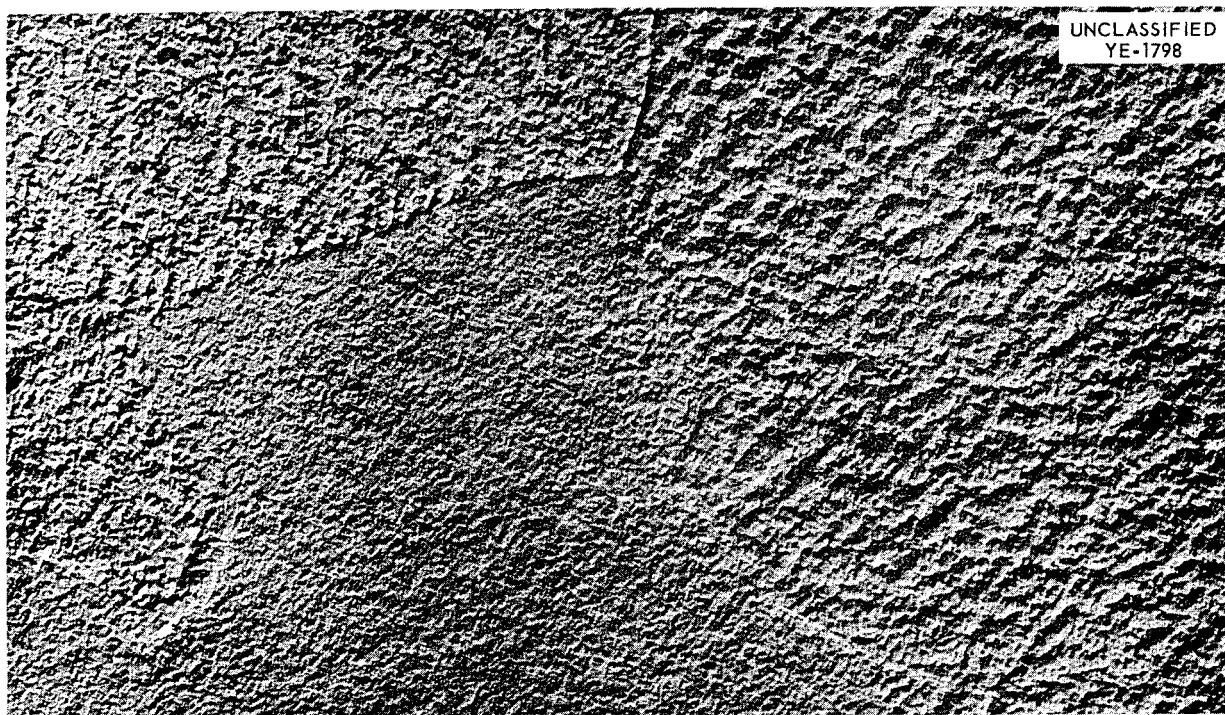
Fig. 41*a*. Carbon Replica, Preshadowed with Gold-Manganin, of Niobium Specimen Oxidized for 30 min at 400°C. 12,000X.
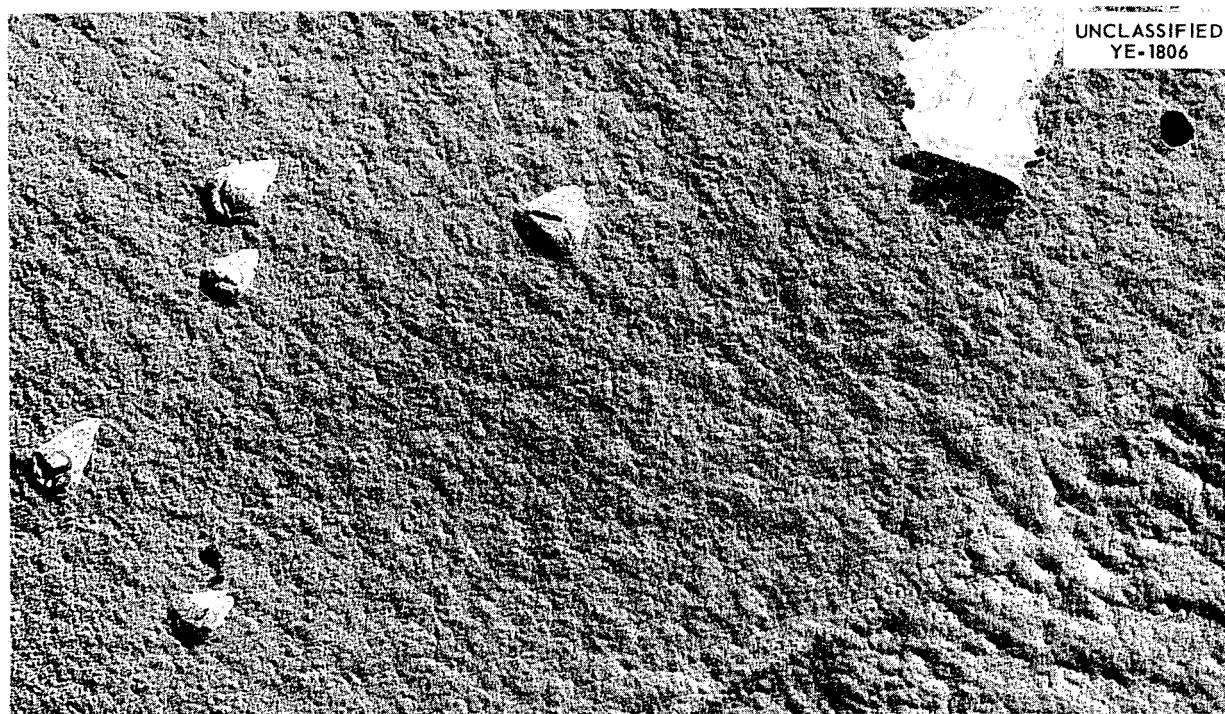

Fig. 41*b*. Carbon Replica, Preshadowed with Gold-Manganin, of Niobium Specimen Oxidized for 120 min at 400°C. The irregular white area in the lower right of the photograph is due to a small tear produced when the replica was removed from the Nb specimen. This area was originally occupied by a blister, as is indicated by the adjacent shadowed region. 22,700X.
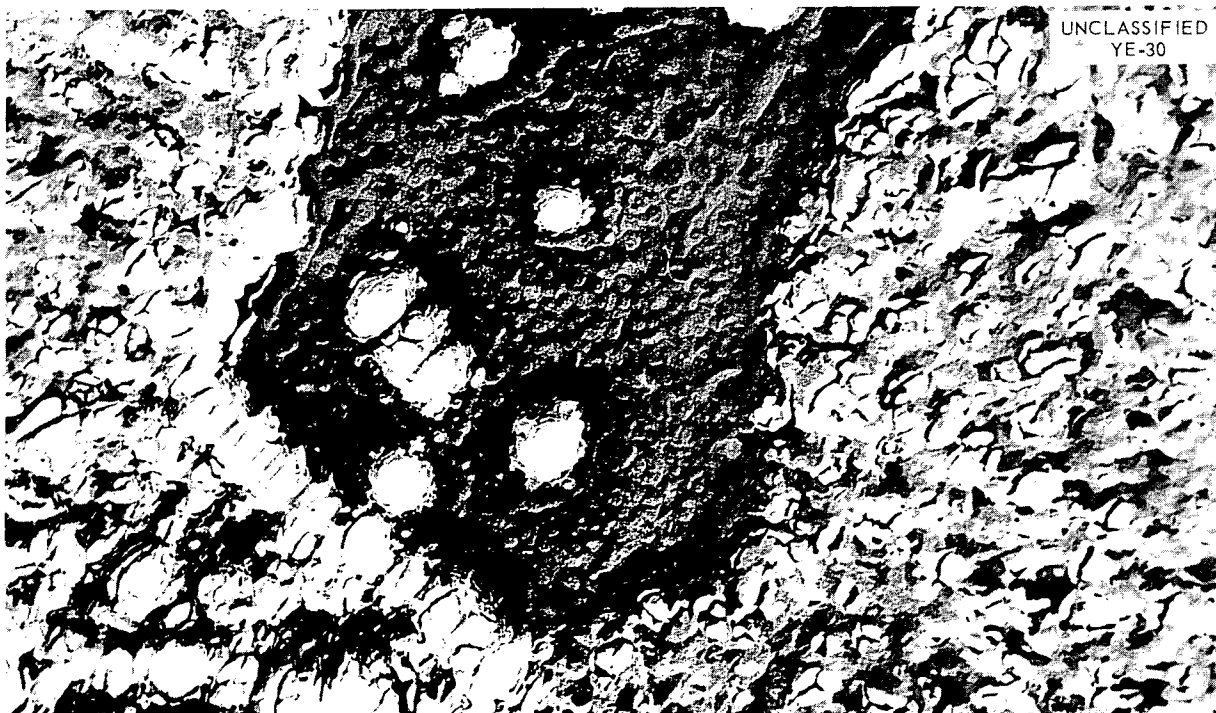
Fig. 41c. Formvar Replica, Shadowed with Gold-Manganin, of Niobium Specimen Oxidized for 210 min at 400°C. 5000X.
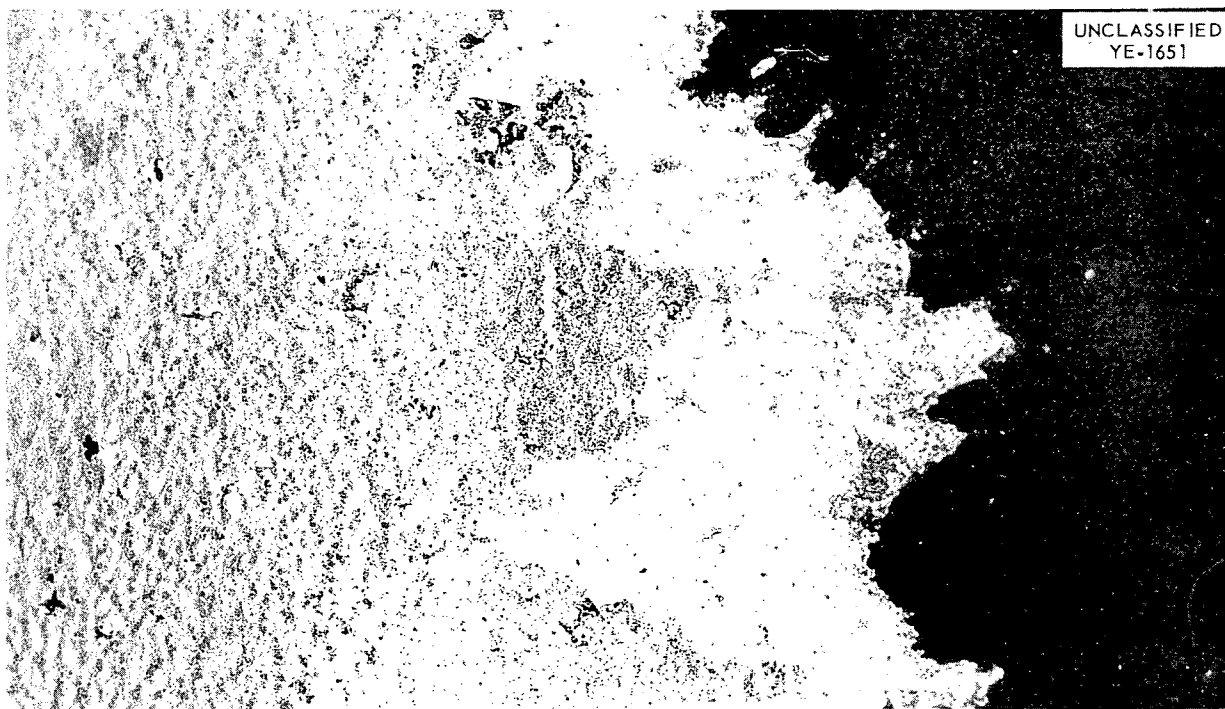

Fig. 41d. Carbon Replica, Preshadowed with Gold-Manganin, of Niobium Specimen Oxidized for 240 min at 400°C. 12,000X.

Fig. 42. Carbon Replica, Preshadowed with Gold-Manganin, of Niobium Specimen Oxidized for 8 hr at 380°C. 7500X.
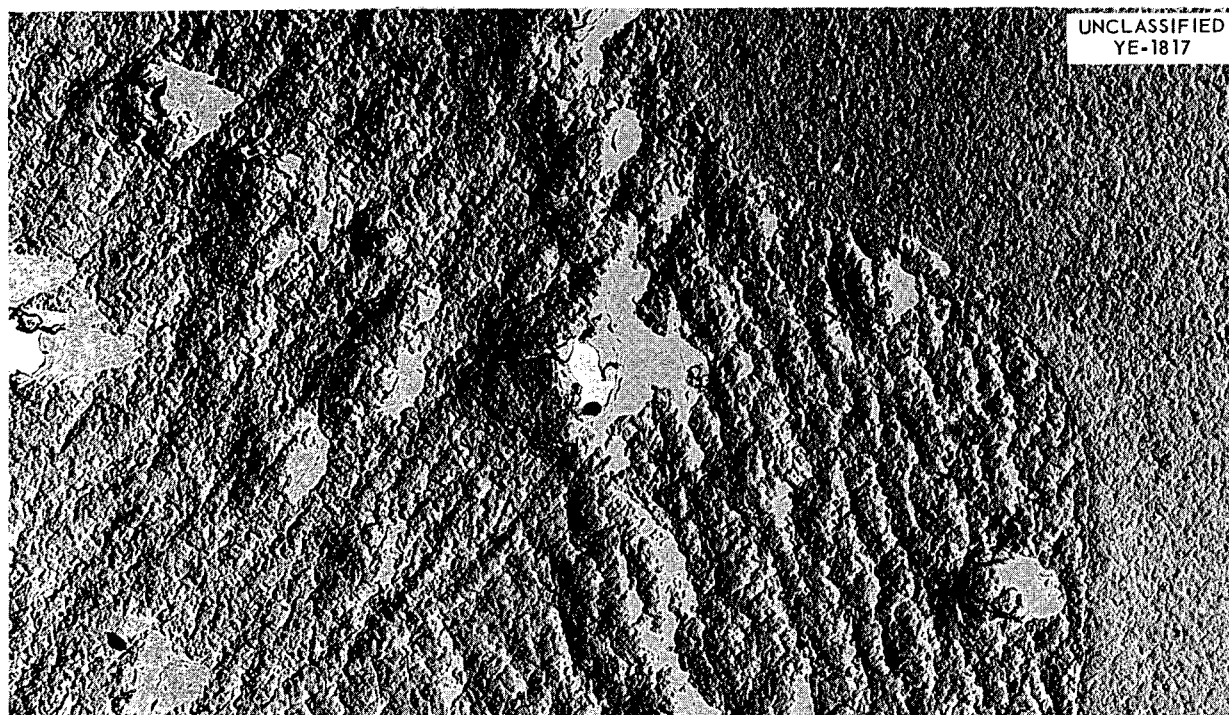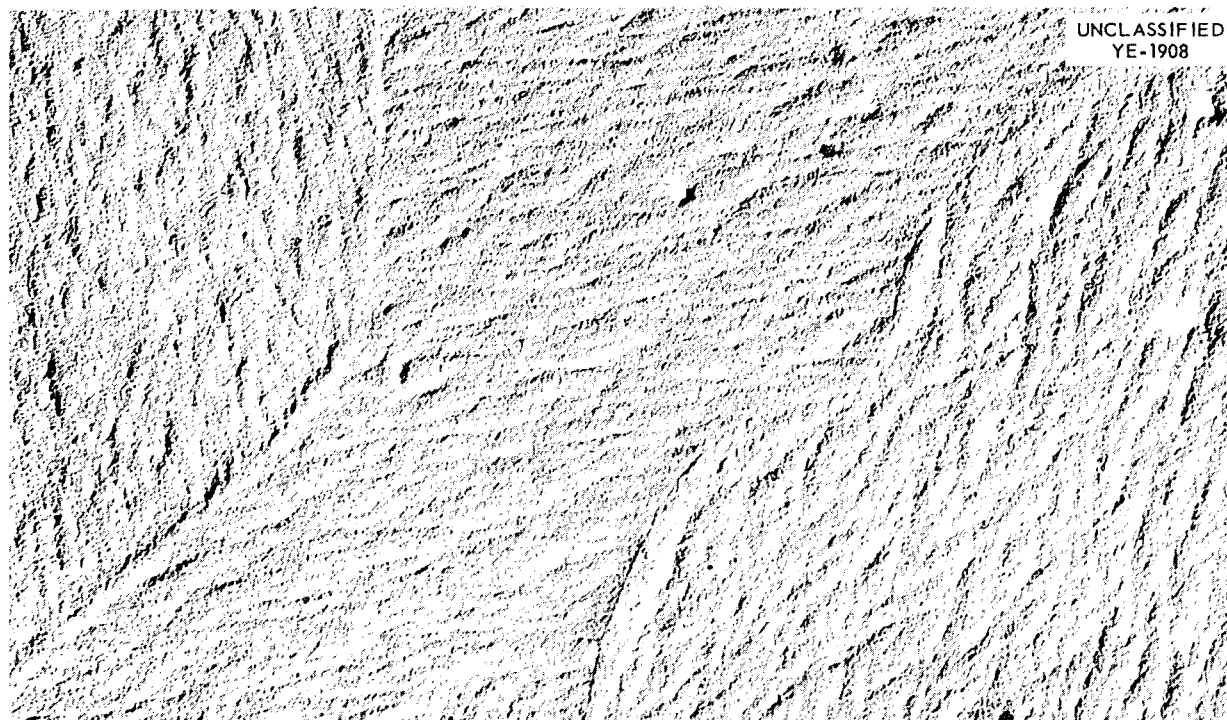

Fig. 43. Carbon Replica, Preshadowed with Gold-Manganin, of Niobium Specimen Oxidized for 48 hr at 325°C. 12,000X.
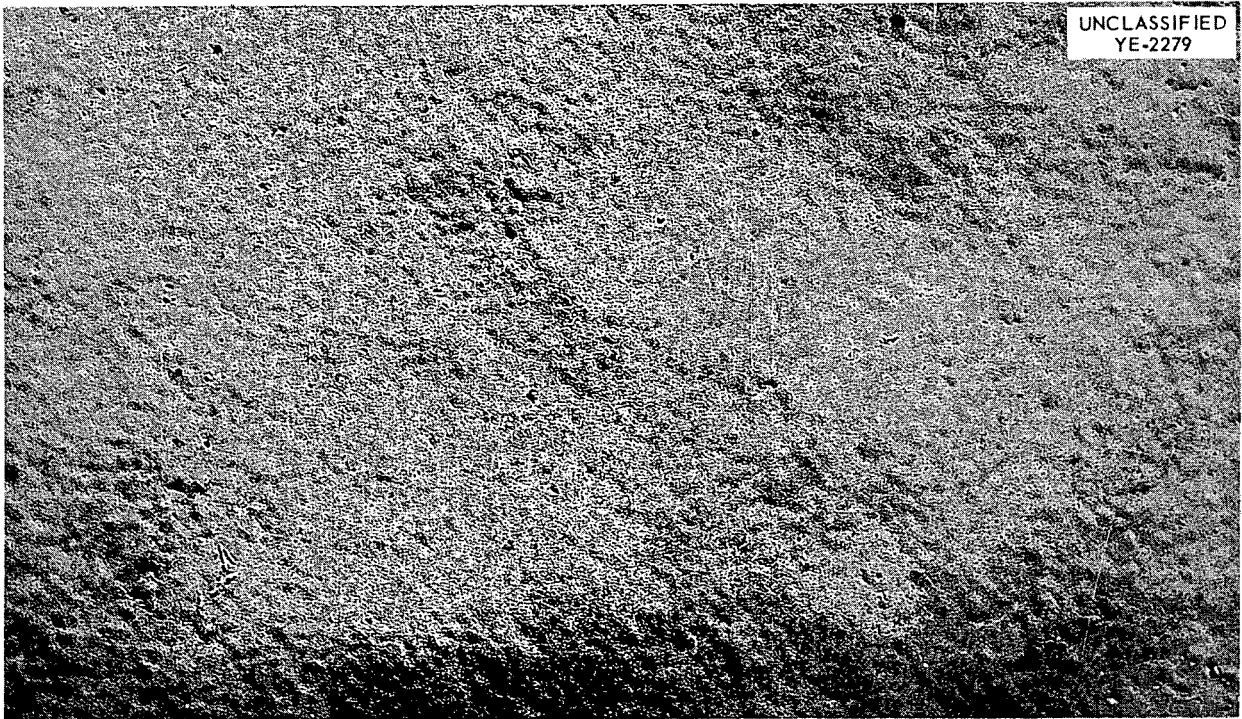
Fig. 44a. Carbon Replica, Preshadowed with Gold-Manganin, of Niobium Specimen Anodized at 25 v. 12,000X.
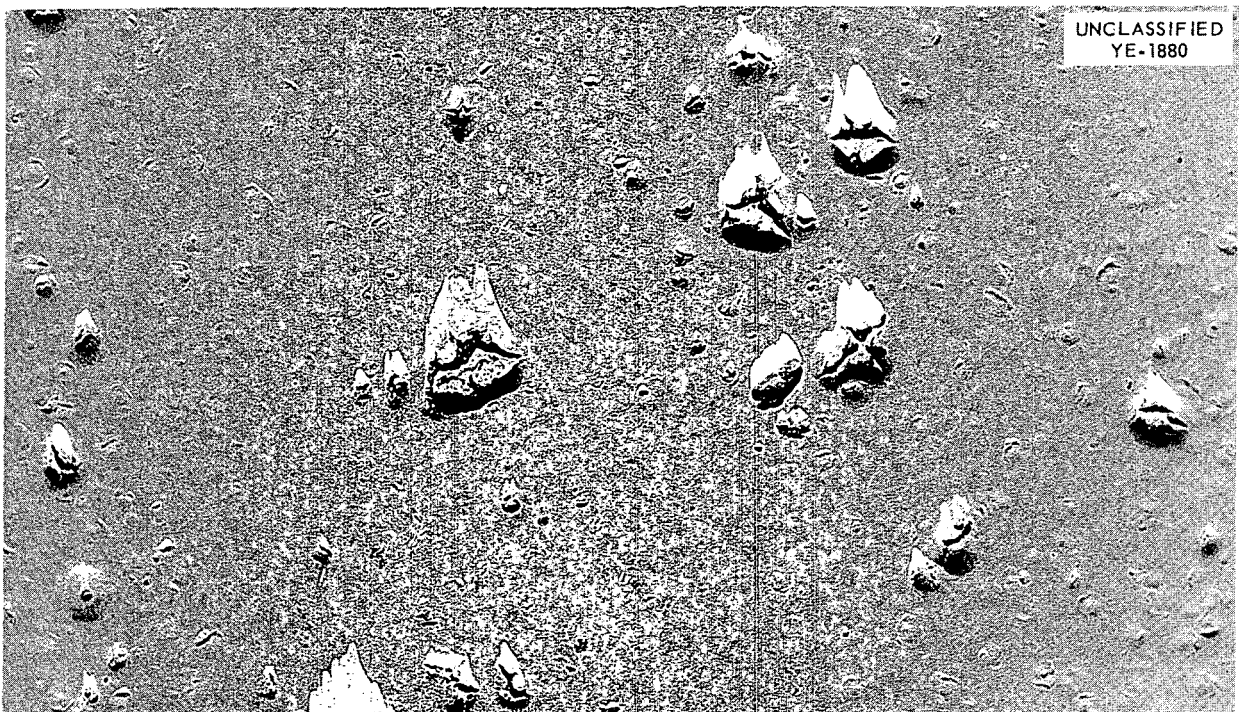

Fig. 44b. Carbon Replica, Preshadowed with Gold-Manganin, of Niobium Specimen Anodized at 75 v. 12,000X.
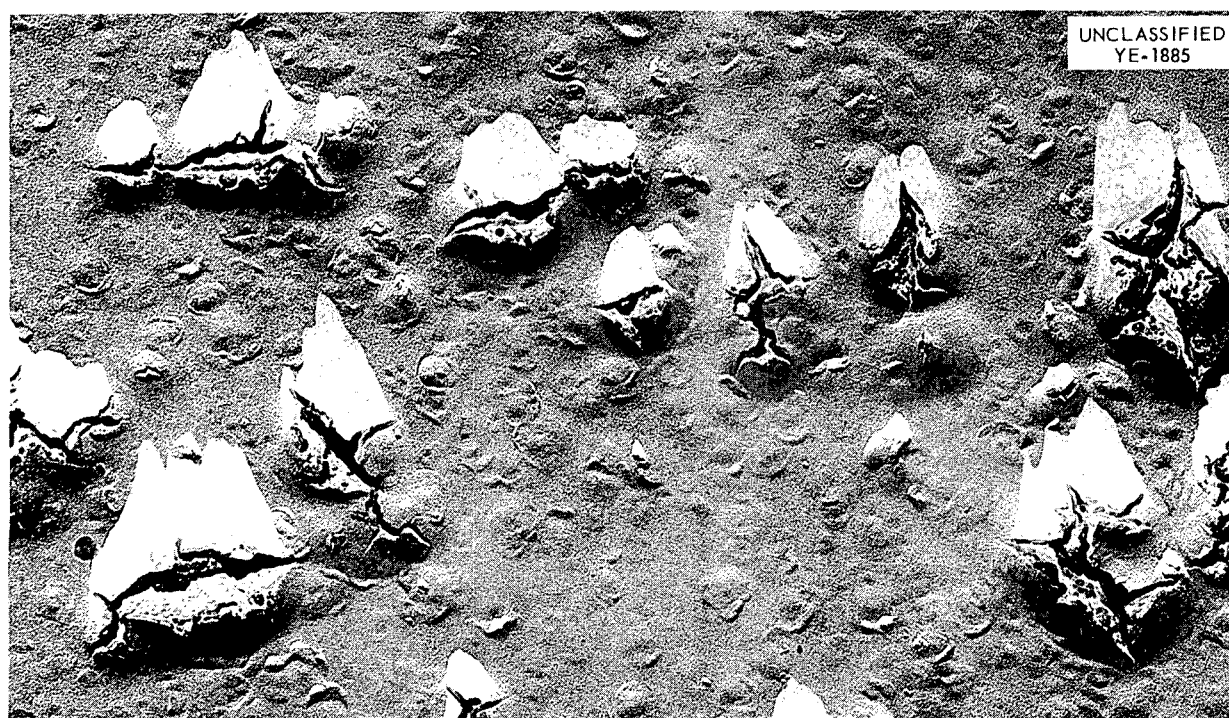
UNCLASSIFIED
YE-1885

Fig. 44c. Carbon Replica, Preshadowed with Gold-Manganin, of Niobium Specimen Anodized at 100 v. 12,000X.

The oxide films formed during the gaseous oxidation of niobium were studied both by x-ray and electron diffraction methods. Only the low-temperature form of niobium oxide (Nb_2O_5) was detected. However, this result does not preclude the presence of one of the lower oxides of niobium, especially if such an oxide were present as a thin layer on the oxide-metal interface.

Discussion. — A clear correlation appeared to exist between oxide topography and the oxidation rate curves (see Figs. 40 and 41). Both the rate curves and the electron micrographs showed that in the initial stages the oxide film was nonporous and protective. After a period of time which depended inversely on the temperature of oxidation, cracked blisters formed in the oxide, and the film became less protective. A further increase in blister density produced a corresponding increase in the oxidation rate, until, finally, a steady-state condition was attained in which the rate curve was linear. Thus it is evident that blister formation was related to an increase in the porosity in the oxide film, and, in the later stages where a linear rate curve was observed, the oxidation was either an interface control process or else the rate of oxidation was determined by diffusion across a

thin layer of oxide which maintained a statistically constant thickness.

While it is plain that the nonprotective stage of the oxidation of niobium is related to the formation of cracked blisters in the oxide, the source of the stress which leads to such blister formation is much less obvious. The oxide-to-metal volume ratio for Nb_2O_5/Nb is high (2.7), but it is to be expected that any stresses produced in the oxide due to its epitaxial misfit with the substrate metal should be confined to a very thin layer at the oxide-metal interface as a result of the formation of an array of dislocations or other lattice defects at this interface. If such be the case, differences in volume of equivalent amounts of oxide and parent metal cannot, per se, produce a significant stress in any but the thinnest oxide films.

A possible explanation of the results observed is provided by a consideration of the diffusion mechanism associated with the oxidation of niobium. A marker experiment was performed in which a fine platinum wire was tied securely around a 0.25-in.-dia niobium rod, and the rod was oxidized for 4 hr at 450°C. The specimen was then sectioned and examined metallographically. The oxide-metal interface had receded from the

marker, indicating that oxidation had proceeded by either anion-vacancy or anion-interstitial diffusion. It was concluded, therefore, that new oxide was formed at the oxide-metal interface rather than at the oxide-gas interface.

On the basis of this observation, a model for the oxidation of niobium has been devised. A basic assumption made is that cation diffusion within the oxide film is insignificant compared with anion diffusion. It follows then that the new oxide must be formed at the oxide-metal interface. When a segment of the metal lattice at this interface is converted to oxide, a three-dimensional expansion of the metal lattice is required to bring the metal ions into their new positions in the oxide. This expansion is resisted by the overlying layer of previously formed oxide and can occur only through the deformation of this layer. Thus in an oxidation reaction where new oxide is formed at the oxide-metal interface, the oxidation process itself continually produces stresses in the oxide film. The observed increase in surface roughness of the oxide with film thickness may be cited in support of this argument. The surface topography of the niobium oxide film (see especially Fig. 43)

resembles in many respects the type of surface texture which might be expected for a highly deformed film.

Sufficient plastic deformation would, of course, eventually lead to fracturing of the oxide. However, the blister-like nature of the cracks actually observed suggests that the stresses producing them were much more highly localized than the stresses discussed in connection with the plastic deformation of the entire oxide film. The development of a locally highly stressed region leading ultimately to blister formation can be rationalized in terms of any mechanism which would produce a localized acceleration of oxidation. Such a condition would lead to the formation of a pit in the metal at the oxide-metal interface. Then, due to the volume difference between equivalent amounts of oxide and metal, the oxide produced in forming the pit would exert a substantial stress normal to the surface of the oxide film. When the stress so generated exceeded the fracture strength of the oxide, a cracked blister would form.

Figure 45 shows an optical micrograph of the edge of a transverse section through a niobium
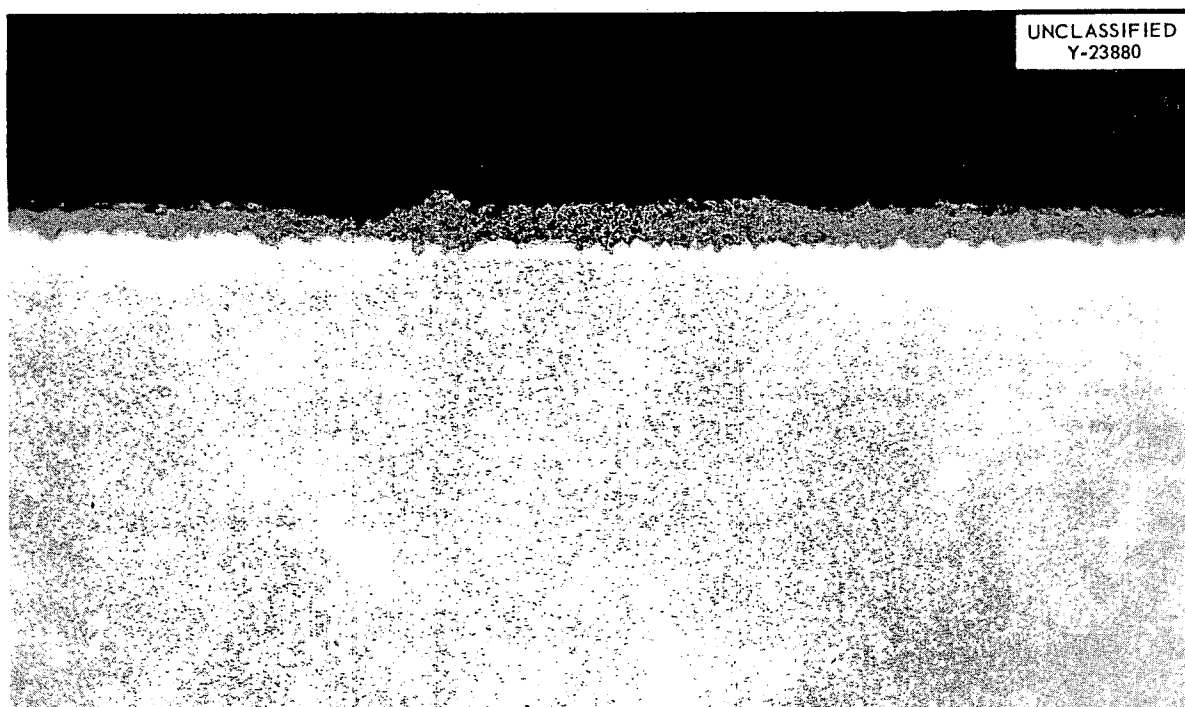

UNCLASSIFIED
Y-23880

Fig. 45. Edge of Transverse Section of Niobium Specimen Oxidized for 4 hr at 400°C. Note formation of pits in metal surface under thick layer of oxide. 500X.

specimen which had been oxidized for 4 hr at 400°C. The white area at the bottom of the photograph is a portion of the unoxidized part of the metal specimen, while a cross section through a heavily blistered region of the oxide film appears as a narrow, slightly irregular band of gray just above the metal. As may be seen, the metal surface under this blistered area was badly pitted, in agreement with the mechanism outlined above.

It should be noted that once the oxide-metal interface becomes rough, any new oxide formed is initially confined by the walls of the pits in the surface of the metal. When the thickness of oxide lining a pit approximates the diameter of the pit, the difference in volume of equivalent amounts of oxide in metal should provide a means for the continual generation of stresses sufficient to produce extensive cracking in the oxide. At best, a very thin film of nonporous oxide could exist at the interface. Under these circumstances, the oxidation process should approach, after prolonged periods of oxidation, the steady-state condition indicated by the development of linear rate curves.

It is realized that much of the argument presented here is speculative, and the author regards this oxidation model only as a working hypothesis. It is a hypothesis which has, nevertheless, proved to be very helpful in suggesting a promising new approach to the problem of determining the factors which produce nonprotective oxide formation on many metals.

Tantalum

The oxidation behavior of tantalum is similar to that of niobium. At temperatures below 500°C, the oxide films formed on tantalum exhibit interference colors typical of a protective oxide film.[7] Above 500°C, however, a linear oxidation rate curve has been reported for tantalum.[8] Thus it appears that with temperatures in the immediate vicinity of 500°C the oxidation of tantalum is probably a two-stage process in which the oxide film is initially protective but becomes nonprotective as the time of oxidation increases.

As in the case of niobium, a qualitative correlation was shown to exist between the oxidation

rate behavior of tantalum and the microtopography of the oxide films. Tantalum oxidation specimens were prepared in a manner identical with that described above for niobium, and oxidation experiments have thus far been performed at 400, 450, and 500°C. At the two lower temperatures, where the oxide film is protective, the oxide was found to be coherent and nonporous even after 24 hr of oxidation (see Figs. 46 and 47). After 4 hr of oxidation at 500°C, however, many cracked blisters were observed in the film (Fig. 48), indicating that the oxidation process had entered the nonprotective stage. In some respects there were significant differences between the details of the tantalum and the niobium films. For example, a close examination of Figs. 46, 47, and 48 will reveal background texture consisting of many tiny bubble-like protuberances. The texture is shown at a very high magnification in Fig. 49. These bubble-like features appeared to originate during the preparation of the specimen surfaces. They were observed on all specimens which had been either chemically polished or electropolished, regardless of whether or not these specimens had been oxidized. They were not observed, however, even on oxidized specimens, if their surfaces had previously received only a mechanical polishing.

On oxidized tantalum specimens a much grosser pattern of needle-like formations was observed to be superimposed on the bubble texture described above (see Figs. 46, 47, and 48). The pattern was produced by three sets of parallel ridges in the oxide, each set making an angle of about 60 deg with the other two. As may be seen in Fig. 46, the orientation of these ridges changed from grain to grain in the metal substrate. This needle pattern was formed on specimens which had been either chemically polished or electropolished prior to oxidation, but, like the bubble texture, it did not occur on specimens which had been only mechanically polished before oxidation. In the latter case the crystal structure of the underlying metal was, of course, masked by a surface layer of cold-worked metal, while both chemical polishing and electropolishing removed this layer. Furthermore, no phase change has been reported for either the metal or the oxide in the temperature range covered by these experiments. Therefore it was concluded that the needle pattern was related to the crystal structure of the substrate metal.

A critical factor in assessing the degree of similarity between the oxidation mechanisms for

---

[7]H. H. Uhlig (ed.), *The Corrosion Handbook*, p 720–721, Wiley, New York, 1948.

[8]W. McKewan and W. M. Fassell, Jr., *The Parabolic-Linear Oxidation Rate Transition Theory*, AECU-1918 (Feb. 1, 1952).

Fig. 46. Carbon Replica, Preshadowed with Gold-Manganin, of Tantalum Specimen Oxidized for 24 hr at 400°C. 12,000X.
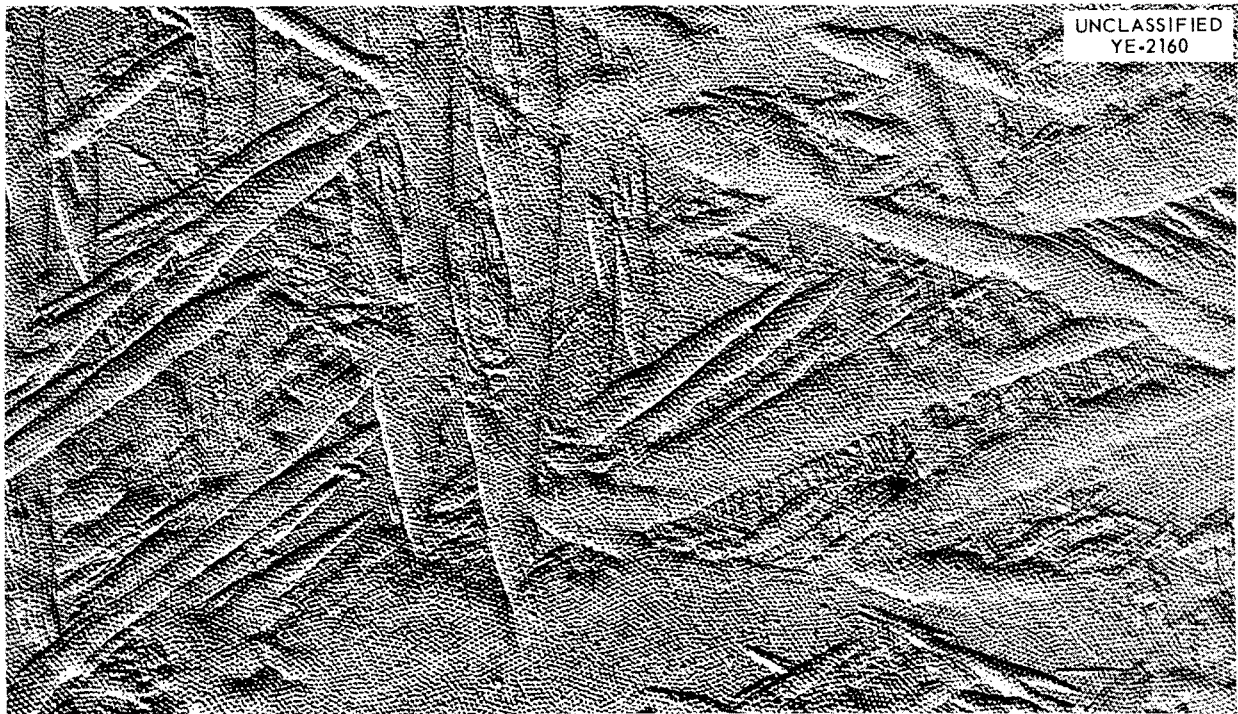

Fig. 47. Carbon Replica, Preshadowed with Gold-Manganin, of Tantalum Specimen Oxidized for 8 hr at 450°C. 12,000X.
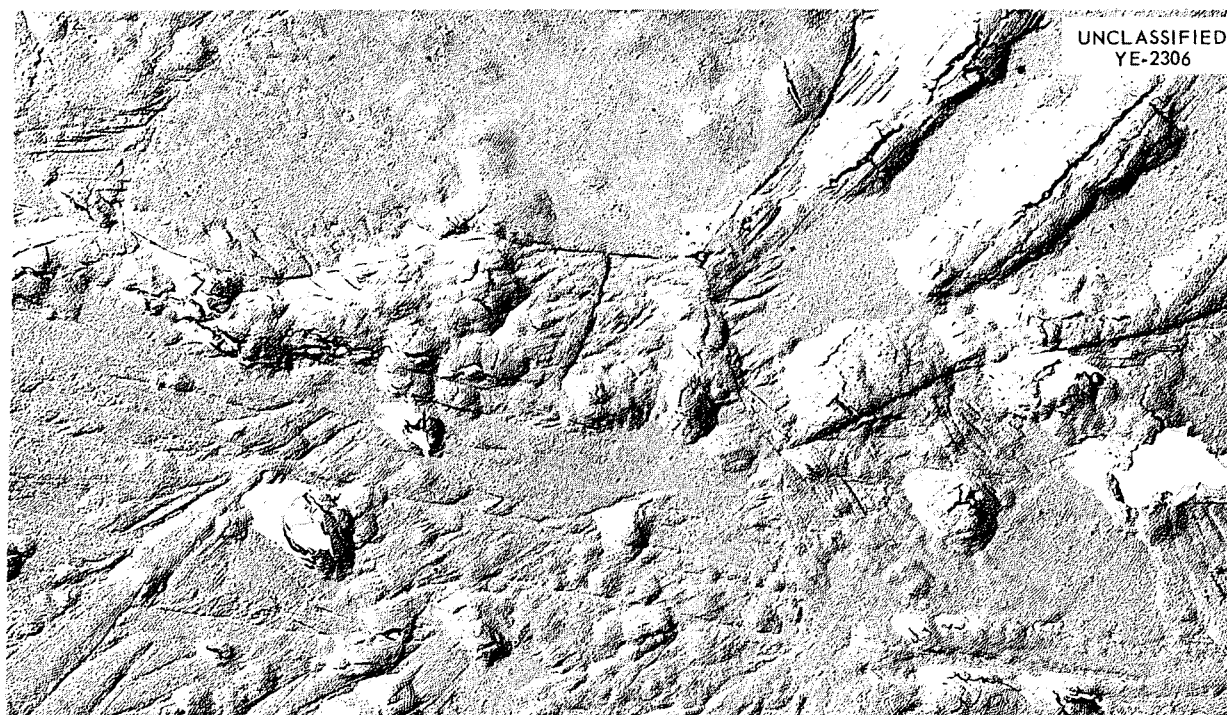
Fig. 48. Carbon Replica, Preshadowed with Gold-Manganin, of Tantalum Specimen Oxidized for 4 hr at 500°C. 7500X.
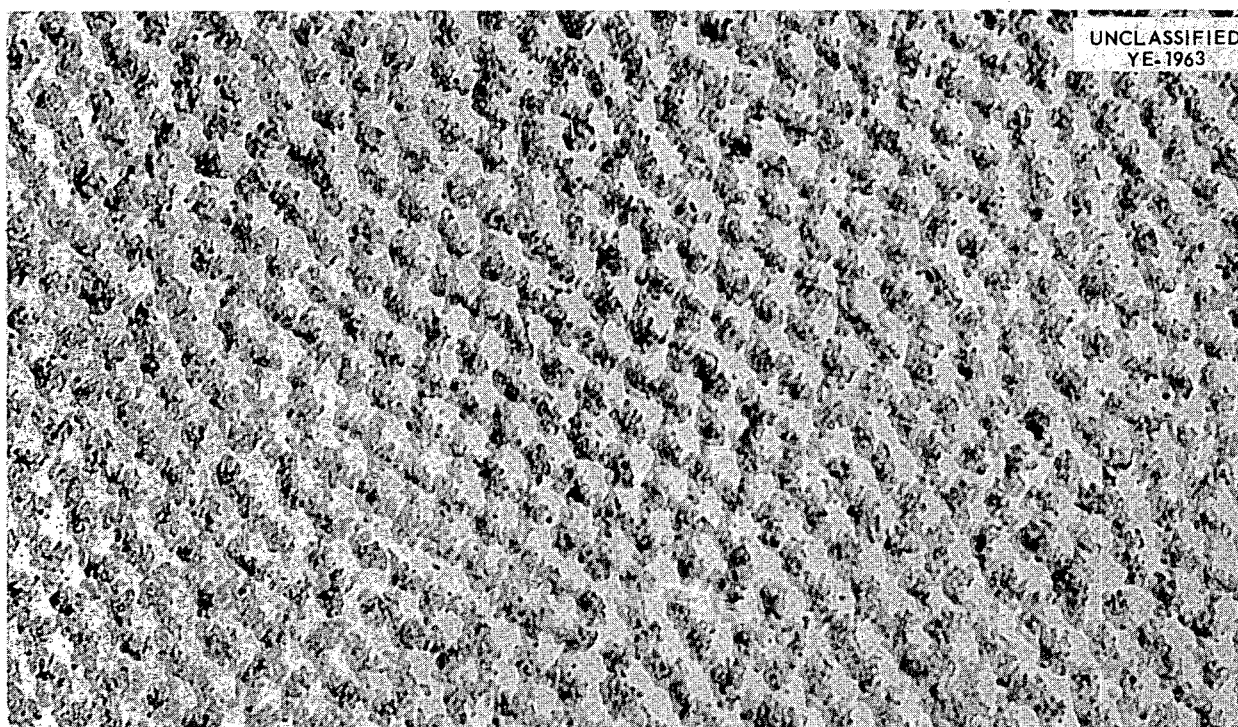

Fig. 49. Carbon Replica, Preshadowed with Gold-Manganin, Showing Bubble-Like Background Texture on Electropolished Tantalum Specimen. 120,000X.

tantalum and niobium is the mode of diffusion which predominates in tantalum oxide. Unfortunately, no unequivocal information is available concerning this point. Semiconductor data show that Ta_2O_5 contains an excess of metallic ions,[9] but it is not known whether this fact is attributable to the presence of interstitial cations or anion vacancies. All that can be said for the present is that from the point of view of its oxidation rate behavior, the structure and composition of its oxides,[10] and its general chemical and physical properties, tantalum is entirely comparable with niobium. This similarity also extends to the microtopography of the oxides of the two metals. Thus the available data suggest that the oxidation mechanisms for the two metals are analogous and involve anion-vacancy diffusion. If this be true, the oxidation behavior of tantalum can be explained in terms of the oxidation model proposed for niobium.

Zirconium

The oxidation of zirconium has been reported to be a two-stage process in which the first formed oxide films are protective but become nonprotective as oxidation proceeds.[11] However, the reported oxidation characteristics of zirconium may be complicated by the fact that zirconium reacts with nitrogen and even more readily with minor atmospheric constituents such as carbon dioxide and water.[12] Furthermore, the solubility of oxygen in zirconium may serve to make the oxidation of zirconium different from that of niobium or tantalum.

The mode of diffusion in zirconium oxide films involves predominantly anion diffusion, presumably anion-vacancy diffusion.[13] In this respect, zirconium, niobium, and tantalum appear to be comparable with one another.

[9]W. Hartmann, Z. *Physik* 102, 709–733 (1936).

[10]W. H. Zachariasen, in *Physics Division Report for Month Ending April 15, 1945,* CF-2926.

[11]J. J. Polling and A. Charlesby, *The Inhibition of Gas Phase Reactions of Zirconium by Anodic Oxide Films.* Part 1, AERE-M/R-1040 (Nov. 13, 1952); *The Inhibition of Gas Phase Reactions of Zirconium by Anodic Oxide Films. Part 2,* AERE-M/R-1040A (May 27, 1953).

[12]O. Kubaschewski and B. E. Hopkins, *Oxidation of Metals and Alloys,* p 210, Academic Press, New York, 1953.

[13]J. Chirigos and D. E. Thomas, in *Proceedings of the Spring Metallurgy Conference, March 24–26, 1952,* vol 2, p 377–400, TID-5084.

The study of the microtopography of oxide films on zirconium is still in a preliminary stage. Zirconium specimens, $1 \times 2 \times 0.05$ cm, were mechanically polished and then chemically polished in a solution consisting of 50 parts of nitric acid, 8 parts of hydrofluoric acid, and 45 parts of water. The grain boundaries in the zirconium surface were sharply delineated by this treatment (see Fig. 50), and care had to be exercised in interpreting electron micrographs of oxidized zirconium specimens in order to distinguish between features due to the oxidation process and those attributable to the substrate metal.

Zirconium specimens were oxidized for periods up to 24 hr at 400, 450, and 600°C. Typical of the results obtained are the electron micrographs shown in Figs. 51(a–c), which illustrate the oxide topography on zirconium specimens after oxidation for 2, 4, and 6 hr at 600°C. As may be seen, the development of the oxide films was characterized chiefly by the formation of small nodular growths on the oxide surface. No cracks or blisters were observed in the oxide films formed under the experimental conditions described above.

The significance of the nodular growths on the zirconium oxide films is not yet understood, and further work will be required to clarify the oxidation behavior of zirconium.

MICROTOPOGRAPHY OF SULFIDE FILMS FORMED ON NIOBIUM, TANTALUM, AND ZIRCONIUM

J. V. Cathcart　　　J. B. Wagner

A brief survey was made of the microtopography of sulfide films formed on niobium, tantalum, and zirconium. In view of the similarity between the oxidation and sulfurization processes, it was hoped that this investigation would provide a better understanding of the oxidation study described above.

Small coupons of niobium, tantalum, and zirconium were given the same surface treatments as in the oxidation experiments and were placed in the reaction chamber shown in Fig. 52. The system was then evacuated, the samples were annealed overnight at 425°C under a pressure of 10^{-6} mm Hg, and finally the reaction chamber was sealed off in a vacuum. The apparatus was inserted into a two-stage furnace in which the specimens were held at 425°C while the sulfur reservoir was at 380°C. After the specimens had reached the

12,000X.

Fig. 51a. Carbon Replica, Preshadowed with Gold-Manganin, of Zirconium Specimen Oxidized for 2 hr at 600°C.

UNCLASSIFIED
YE-2755

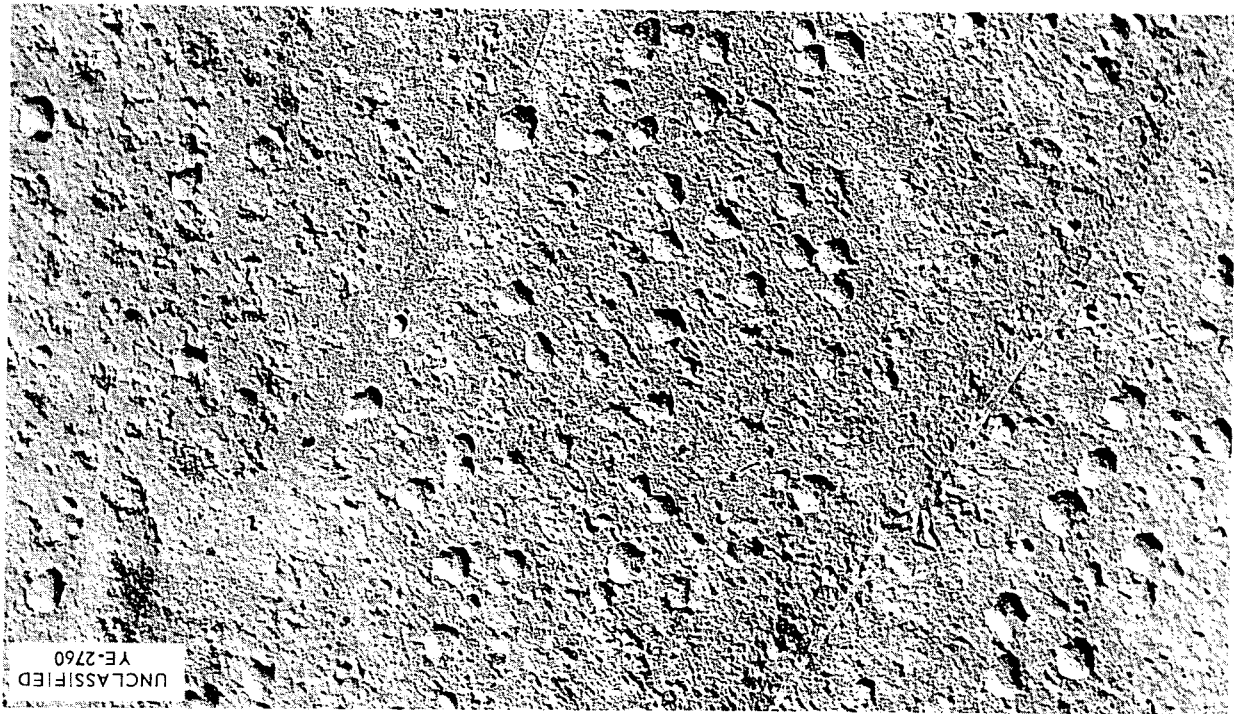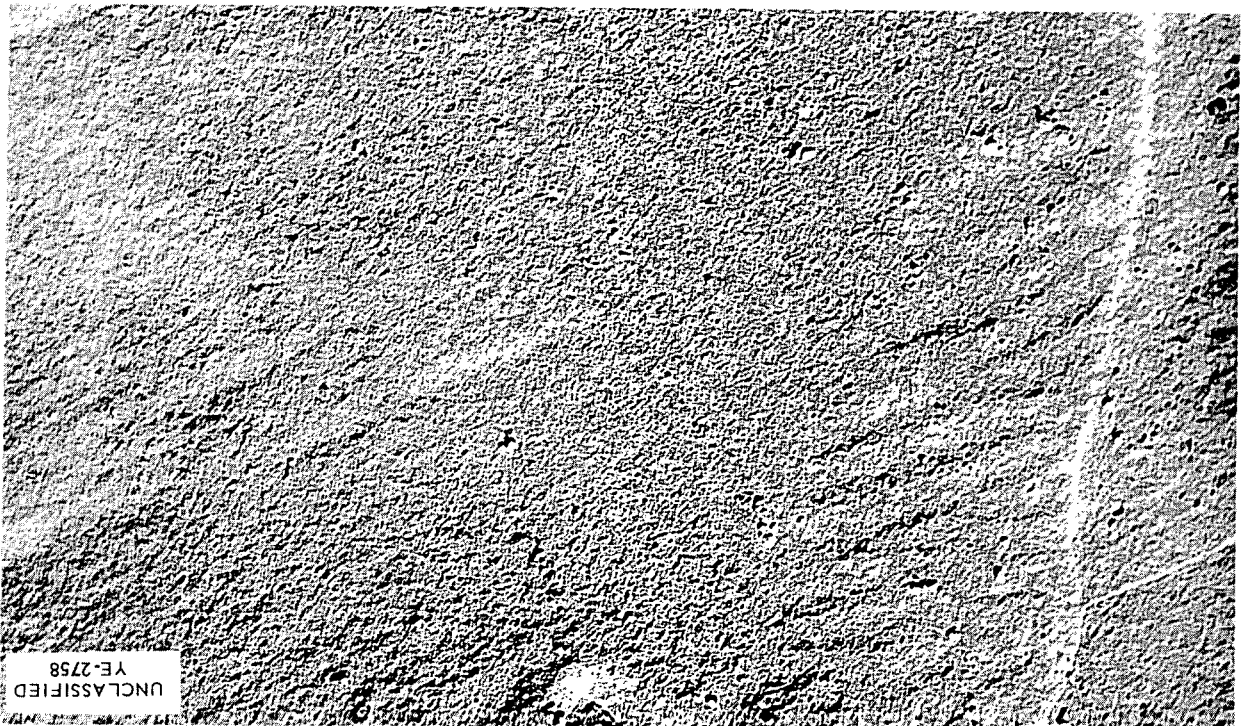Specimen. 12,000X.

Fig. 50. Carbon Replica, Preshadowed with Gold-Manganin, of a Chemically Polished, Unoxidized Zirconium

UNCLASSIFIED
YE-2692

temperature, the breakoff tip separating the sulfur reservoir and the reaction chamber was crushed, allowing sulfur vapor at a pressure of about 300 mm Hg to fill the reaction chamber. At the end of predetermined sulfurization times, the apparatus was partially withdrawn from the furnace so that the reaction chamber could be maintained at temperature while the sulfur reservoir was cooled in an air jet. By using this procedure, all the excess sulfur on the specimens was vaporized and caused to recondense in the sulfur reservoir. The entire apparatus was then allowed to cool to room temperature, and the specimens were removed.

UNCLASSIFIED
ORNL-LR-DWG 25176
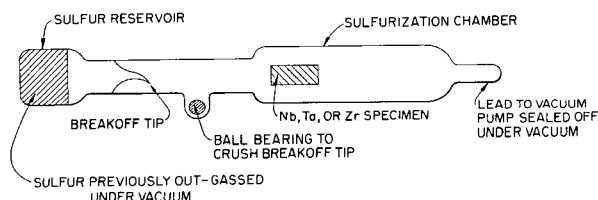
Fig. 52. Sulfurization Apparatus.

Specimens were sulfurized for various periods up to 72 hr at 425°C, and estimates of the quantity of sulfur consumed per square centimeter of metal surface were made from weight-gain measurements. The rate of sulfurization of tantalum was slower than that of either niobium or zirconium. The weight change for zirconium was rather erratic, but its rate of sulfurization was roughly an order of magnitude greater than that for tantalum.

The surfaces of the films formed on niobium and zirconium were too rough to permit replications for electron-micrographic examination. The film on niobium consisted of a relatively smooth base covered by crystals of needle-like projections (see Fig. 53) which in some respects resemble the "whisker" growths reported for many metals.

The zirconium specimens were covered with a fluffy white film which appeared to consist of at least two phases. Prolonged sulfurization tended to cause the upper portion of the film to peel off, exposing a second layer of sulfide which was also white. The composition of neither of these layers has yet been determined.

Unlike niobium and zirconium, tantalum formed a coherent sulfide film which exhibited deep-blue interference colors for the sulfurization times
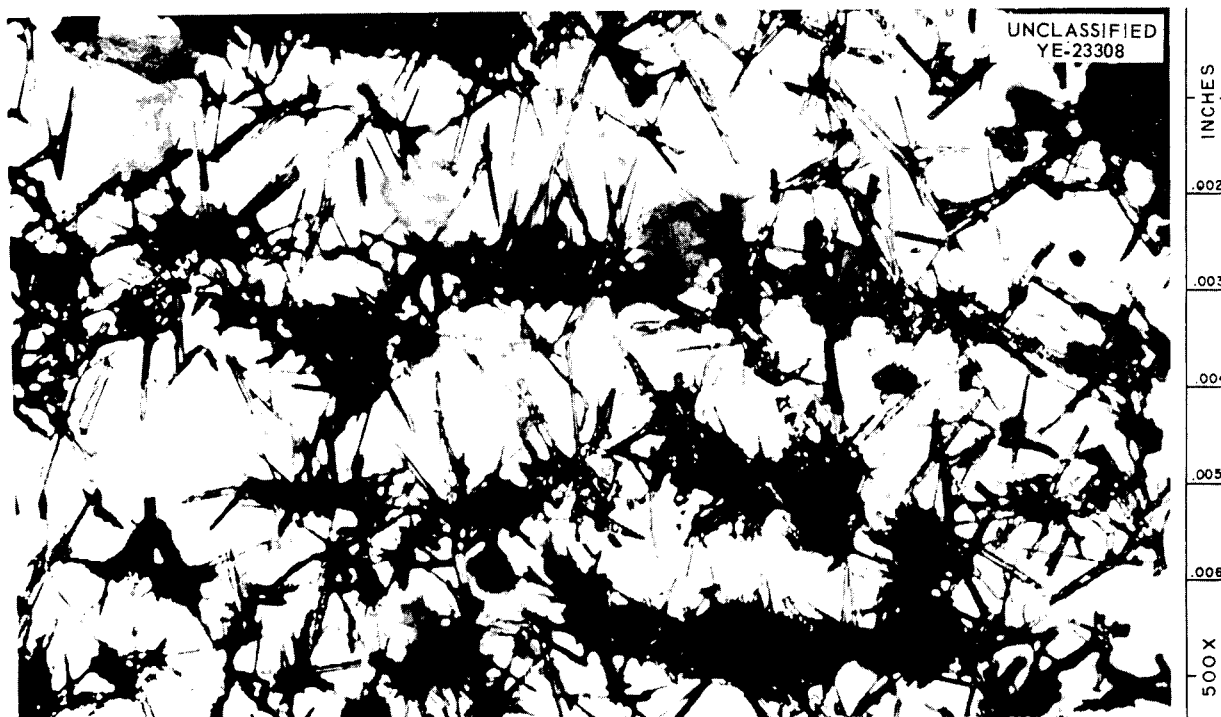
Fig. 53. Sulfide Film Formed on Niobium in 24 hr at 425°C.

described above. Optical examination revealed a needle-like pattern in the sulfide very similar to that observed in the oxide. The analogy between the oxide and the sulfide was even more pronounced in electron micrographs of films formed in the early stages of sulfurization. Figure 54 shows the topography of the oxide film formed after 1 hr at 425°C. Both the "bubble texture" and the "needle pattern" previously observed in the corresponding oxide films (see Figs. 46, 47, and 48) were clearly evident. After long sulfurization times, no cracks formed in the tantalum sulfide films, but the development of nodules on the surface of these films was observed [see Figs. 55(a–b)].

EFFECT OF RADIATION ON THE OXIDATION OF METALS[14]

J. V. Cathcart

A research program has been undertaken with the aim of determining the effect of reactor radiation on the gaseous oxidation of metals. The need for such information has been accentuated by recent advances in both operating temperatures and

radiation intensities in new reactor designs. It is the goal of this investigation to establish, from a fundamental point of view, the nature of the changes produced in the oxidation mechanism by various radiation fields. It is believed that the data which will be obtained may also be of value in understanding the influence of radiation on the aqueous corrosion of metals.

As yet, no in-pile experiments have been performed, since it was deemed to be essential to establish, in the absence of a radiation field, a standard for the oxidation of the metals to be tested. Such a standardization of the oxidation behavior of niobium (see section on "High-Temperature Reactions") has now been virtually completed, both in terms of oxidation rate curves and the microtopography of the oxide films formed on niobium. A study of the in-pile oxidation of niobium is scheduled to begin in the near future.

UNCLASSIFIED
YE-2636

Fig. 54. Carbon Replica, Preshadowed with Gold-Manganin, of Tantalum Specimen Sulfurized for 1 hr at 425°C. 16,400X.

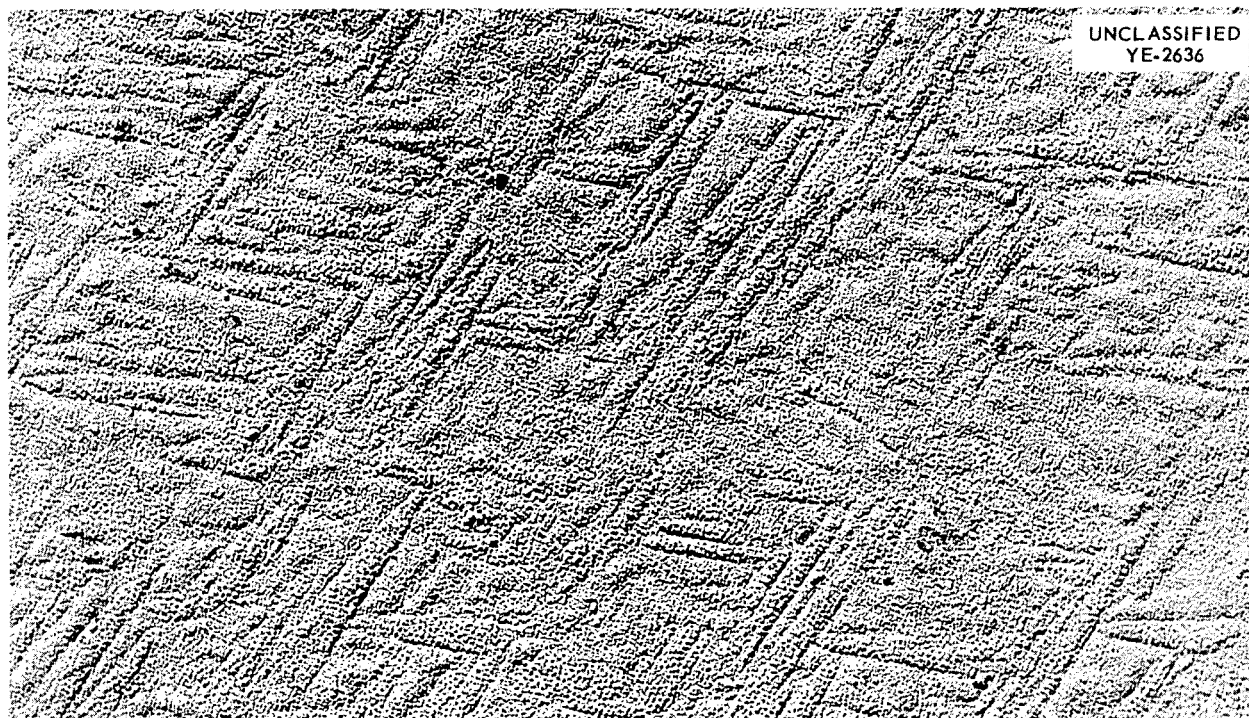Fig. 55a. Carbon Replica, Preshadowed with Gold-Manganin, of Tantalum Specimen Sulfurized for 24 hr at 425°C. 12,000X.
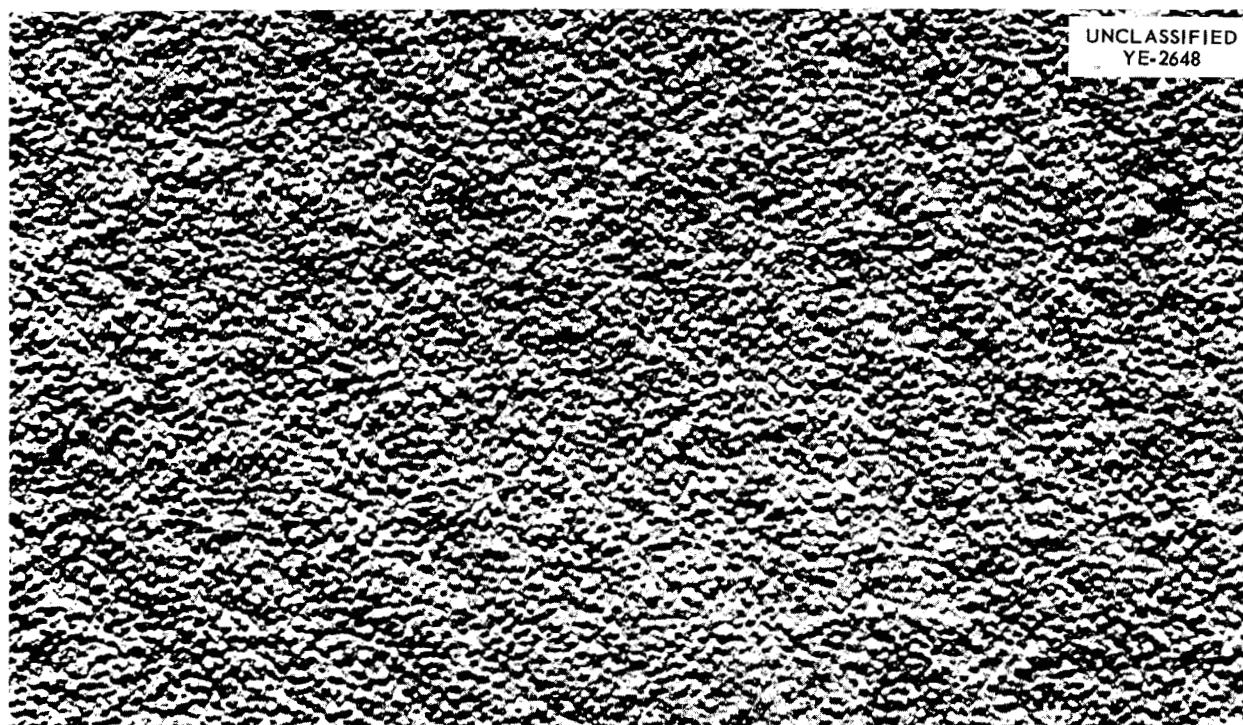

Fig. 55b. Carbon Replica, Preshadowed with Gold-Manganin, of Tantalum Specimen Sulfurized for 36 hr at 425°C. 12,000X.

In addition to the research with niobium, the effect of radiation on the oxidation of copper will be studied. Copper was chosen as a typical example of a metal whose oxidation mechanism, in contrast with that for niobium, involves cation-vacancy diffusion. Thus the two investigations will permit a comparison to be made of the effect of radiation on oxidation mechanisms controlled, on the one hand, by cation diffusion and, on the other, by anion diffusion.

A rather extensive set of preliminary experiments has been undertaken to establish the standard for the oxidation of copper in the absence of radiation. A precise determination of the oxidation rate curves for several crystallographic planes of copper is already available for the temperature range[15] 70 to 170°C, and the present work has been aimed at characterizing the microtexture of cuprous oxide films, utilizing electron microscopy and diffraction techniques.

Single crystals of copper, grown from 99.999% copper, have been used throughout this research. The crystals were grown in the form of $\frac{5}{8}$-in.-dia spheres to which were attached cylindrical stems $\frac{1}{8}$ in. in diameter and 1 in. long. Flat surfaces were cut on the spheres parallel to particular crystallographic planes in order that the oxide films formed on these planes might be studied.

Prior to oxidation, a crystal was mechanically polished through 3-μ levigated alumina and polished electrolytically in a solution of H_3PO_4. The crystal was then washed for about 10 min in a stream of distilled water, dried in a jet of oxygen, and placed directly in an all-glass oxidation chamber. The crystal was then annealed in hydrogen for 1 hr at 500°C, the hydrogen evacuated with a mechanical vacuum pump, and purified oxygen admitted to the system.

The method[16] used for preparing electron-microscope specimens from oxidized crystals consisted in the electrolytic stripping of the oxide film from the copper crystal in a bath of saturated KCl. Small squares of the stripped film were then mounted on standard microscope screen and given a thorough wash.

The method proved to be very sensitive to the amperage and the voltage of the stripping current.

A very low current density caused the films to strip very unevenly, if at all. The use of a higher current density improved the quality of the stripping but also led to the formation in the stripping bath of a substance, probably a Cu-KCl complex,[17] which tended to adhere to the stripped films. A current of 7 ma and 0.6 v was found to produce the best results obtained thus far, but the operating characteristics of the stripping bath are still somewhat erratic and are not regarded as entirely satisfactory.

A second problem associated with the stripping bath was the possibility that additional oxide was formed anodically on the copper crystal during stripping. In order to test this question, a copper crystal was sulfurized and a portion of the resulting sulfide film was stripped by the usual procedure and examined with the electron microscope. None of the reflections in the electron diffraction pattern from this film could be identified as oxide reflections, and certainly none of the strong reflections were due to the presence of oxide. This result is regarded as a strong indication that the stripping process did not produce any additional oxide.

The presence of trace quantities of certain impurities, either as gaseous or surface contaminants, has been shown to alter the oxidation characteristics of copper markedly.[15] Both the relative and the absolute rates of the different crystallographic planes of copper may be changed by large factors. Considerable changes also occur in the microtexture of the oxide film. In the discussion that follows, the expression "contamination" will be used to refer to the collective effects of these trace impurities on the oxidation of copper.

One criterion used to judge the extent of contamination in any given experiment was the pattern of interference colors which is formed over the surface of an oxidized, spherical single crystal of copper. The pattern arises from the fact that different crystallographic planes of the copper crystal oxidize at different rates, thus producing a variation in the thickness of the oxide films formed. Since both the relative and the absolute rates of oxidation of different crystal planes are greatly changed by the presence of trace contaminants, the oxidation pattern offers a convenient

[15]F. W. Young, Jr., J. V. Cathcart, and A. T. Gwathmey, *Acta Met.* 4, 145–152 (1956).

[16]R. T. Phelps, E. A. Gulbransen, and J. W. Hickman, *Ind. Eng. Chem. Anal. Ed.* 18, 391–400 (1946).

[17]M. C. Sneed and J. L. Maynard, *General Inorganic Chemistry*, p 821, Van Nostrand, New York, 1942.

but highly sensitive test for "contamination." Only one consistently reproducible oxidation pattern has been discovered, and when this "standard pattern" was obtained on the crystal, it was assumed that in the experiment in question the impurities present had been minimized and that their effect on the thickness of the oxide films developed was at least reproducible. Thus in order for the results of a particular experiment to be considered acceptable, it was necessary that the oxidation pattern on the spherical part of the crystal used correspond to the "standard pattern."

As a further precaution, immediately prior and subsequent to the oxidation of a crystal for the purpose of obtaining electron-microscope specimens, a spherical copper crystal was oxidized in the oxidation chamber for 30 min at 250°C. Variations in the oxidation pattern formed at 250°C were much more easily detected than changes in a pattern formed at lower temperatures. It was felt that the formation of a "standard pattern" at 250°C both immediately before and after the oxidation of a crystal provided additional evidence that in the intervening experiment the crystal was not contaminated.

Oxide films formed in the (100), (111), (110), and (311) faces of a copper single crystal have been studied at oxidation temperatures of 25, 130, 150, and 160°C for oxidation times ranging up to 45 min. In most of these experiments the thicknesses of the oxide films were measured with a polarizing spectrometer. For all cases reported these thickness values agreed to within 10 to 20 Å with the thicknesses determined from the previously cited oxidation rate curves for copper.[15]

The oxide formed on copper crystals in uncontaminated experiments consisted entirely of cuprous oxide, as was indicated by transmission electron diffraction patterns of the stripped oxide films. Except for the very thinnest films observed (those produced by room-temperature oxidations), the Cu_2O films were highly oriented. For the (110) and (311) faces of the copper crystal, the oxide formed with its (110) planes parallel to the substrate. For the (111) and (100) planes of copper, the (111) plane of the oxide was parallel to the substrate. These results are in agreement with the data of Lawless and Gwathmey[18] and Harris, Ball, and Gwathmey.[19]

The texture of the oxide films formed on the (311) face of a copper crystal in 1 hr at 25°C is illustrated in Fig. 56. The corresponding electron diffraction pattern is shown in Fig. 57. The average thickness of this film was only 10 Å, but the nonuniformity of the film is apparent. It consisted of almost filament-like regions of thicker oxide superimposed on a thinner base film. As may be seen from Fig. 57, the film was at best only weakly oriented.

The oxide film formed in short oxidation times at higher temperatures exhibited a "loose," nonuniform texture somewhat similar to that observed in films formed at room temperature. Figure 58a shows an oxide film formed in 30 sec at 150°C on the (311) face of a copper crystal. The filament-like structure of the oxide is still apparent, but the filaments are relatively thick.

The films formed in 15 and 30 min at 150°C on the (311) face are shown in Figs. 58b and c, respectively. As may be seen, the nonuniformity of the films was somewhat less than that observed after 1 min of oxidation. Lateral growth of the filament-like regions of thicker oxide appeared to occur. A diffraction pattern typical of the patterns obtained from all films formed on the (311) face at 150°C is shown in Fig. 58d. The high degree of orientation of the film is evident.

The development of oxide films on the (110), (111), and (100) planes of copper at 150°C appeared to parallel that illustrated for the (311) face. Short oxidation times produced films with the "loose" texture characteristic of thin oxide films formed on the (311) face. An increase of the oxidation time likewise produced a general thickening of the films. The electron micrographs shown in Figs. 59 and 60 are typical of the results from a 45-min oxidation at 150°C of the (110) and (111) faces, respectively. The film stripped from the (100) face after 15 min of oxidation at 150°C is illustrated in Fig. 61. The origin of the irregular dark patches which appear in Figs. 60 and 61 is not fully understood, but it is believed that the patches are artifacts produced during the stripping process.

[18]K. R. Lawless and A. T. Gwathmey, *Acta Met.* 4, 153–163 (1956).

[19]W. W. Harris, F. L. Ball, and A. T. Gwathmey, *Acta Met.* (in press).

Fig. 56. Oxide Film Stripped from the (311) Face of a Cu Crystal After 1 hr of Oxidation at 25°C. Film thickness: 10 Å. 37,500X.
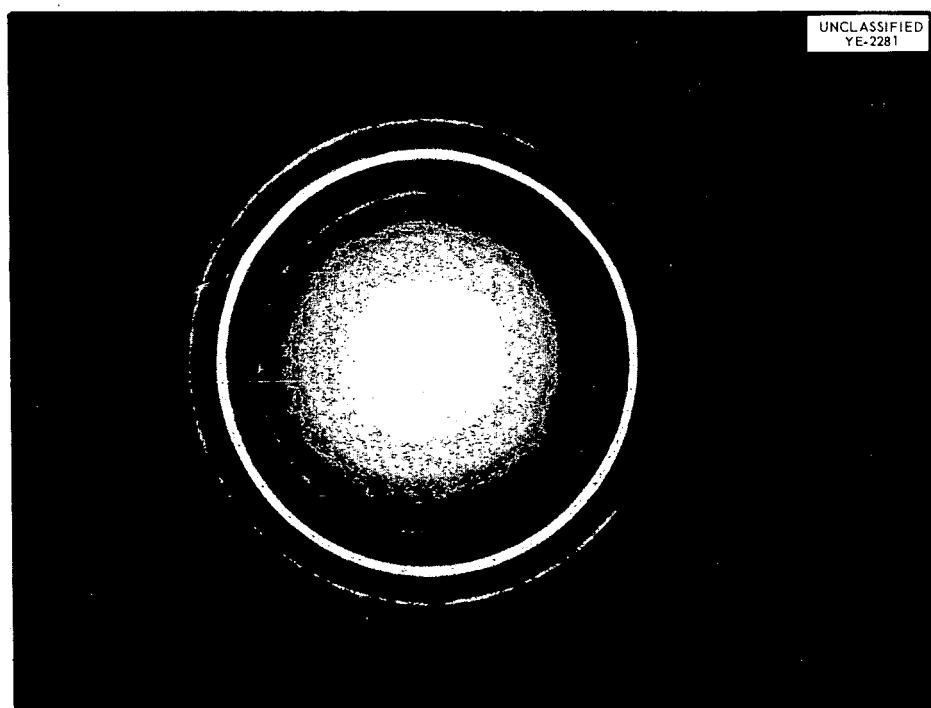
Fig. 57. Transmission Electron Diffraction Pattern from Cu_2O Film Shown in Fig. 56.
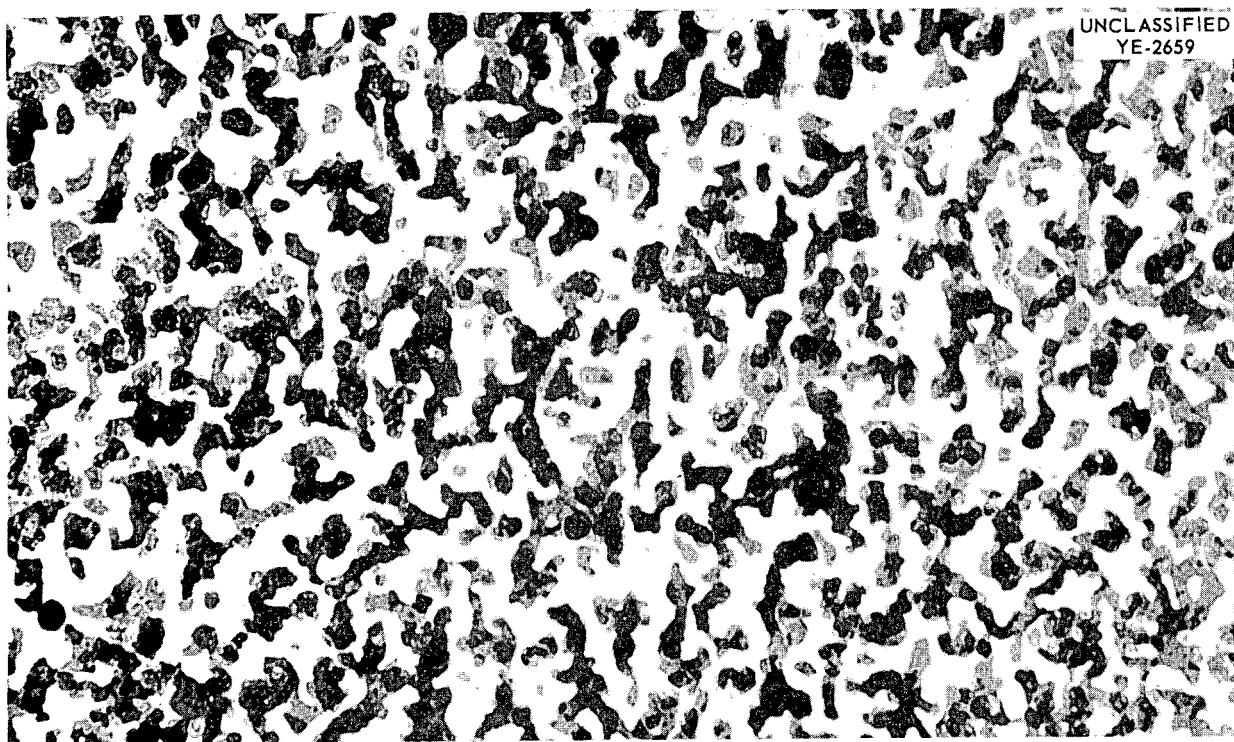
Fig. 58*a.* Oxide Film Stripped from the (311) Face of a Cu Crystal After 30 sec of Oxidation at 150°C. Film thickness: 64 Å. 37,500X.
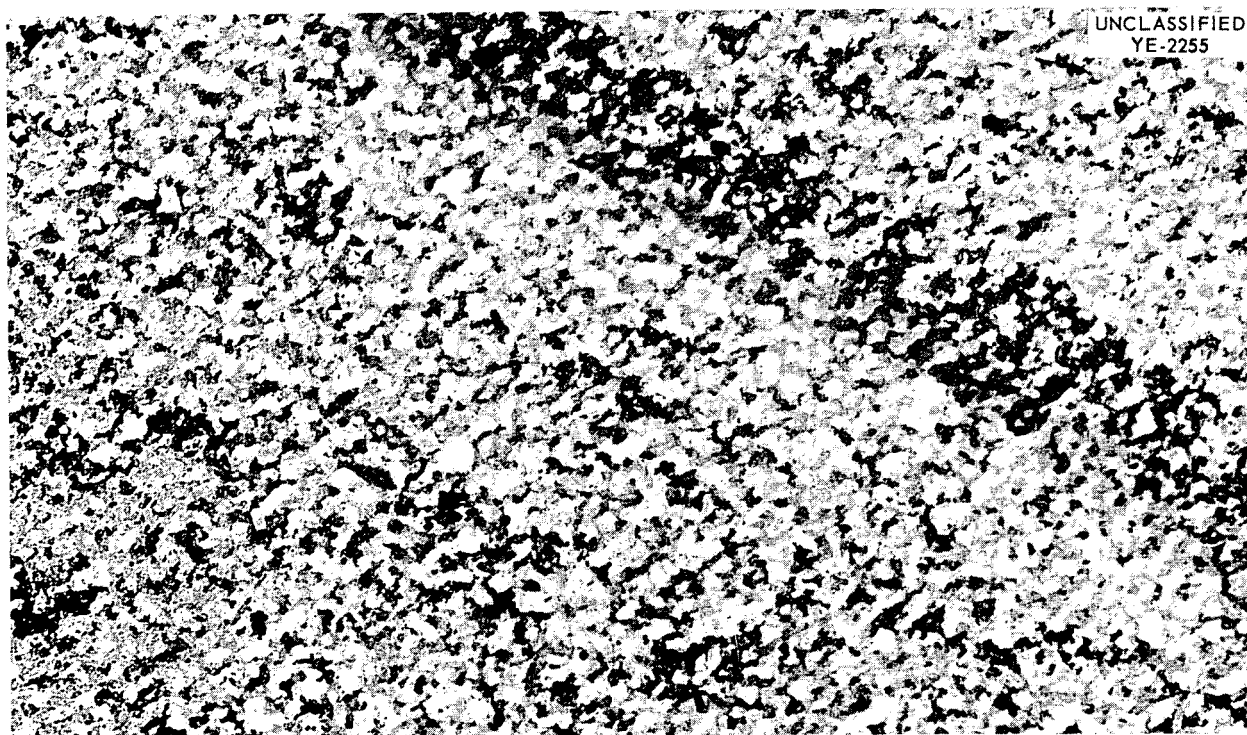
Fig. 58*b.* Oxide Film Stripped from the (311) Face of a Cu Crystal After 15 min of Oxidation at 150°C. Film thickness: 80 Å. 37,500X.

Fig. 58c. Oxide Film Stripped from the (311) Face of a Cu Crystal After 30 min of Oxidation at 150°C. 13,400X.

Fig. 58d. Typical Transmission Electron Diffraction Pattern for Cu₂O Film Formed on the (311) Face of a Cu Crystal at 150°C.

Fig. 59. Oxide Film Stripped from the (110) Face of a Cu Crystal After 45 min of Oxidation at 150°C. Film thickness: 90 Å. 37,500X.
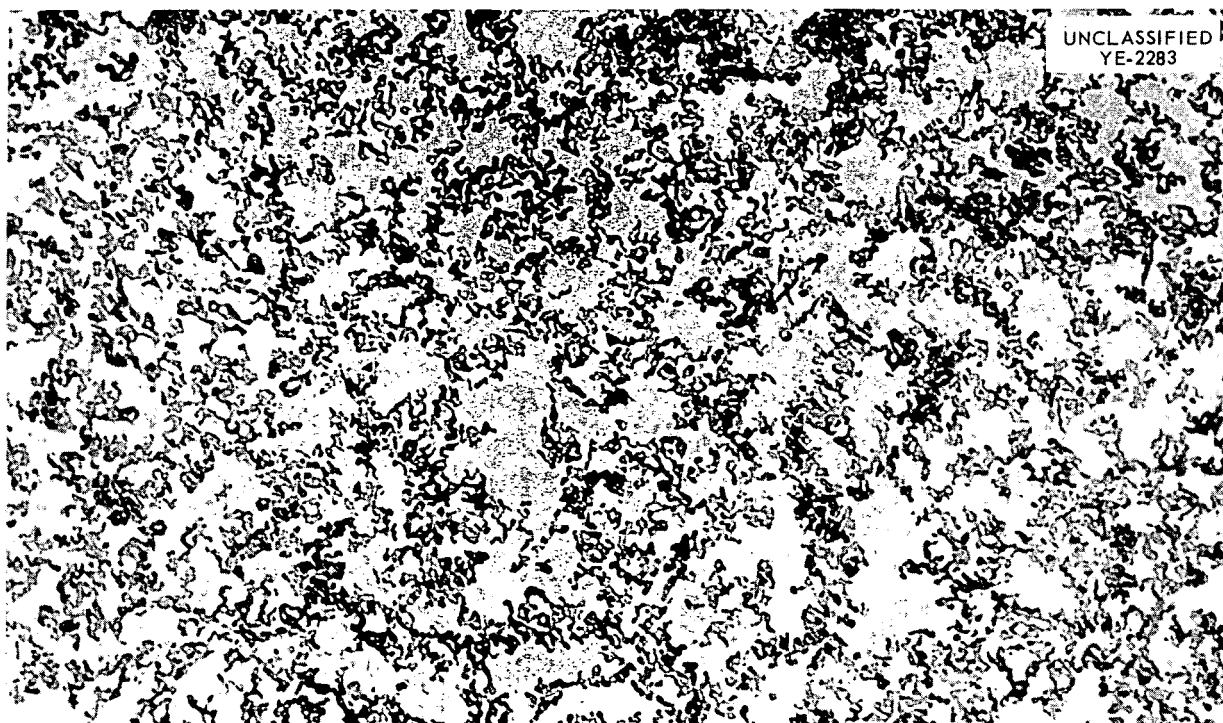

Fig. 60. Oxide Film Stripped from the (111) Face of a Cu Crystal After 45 min of Oxidation at 150°C. Film thickness: 132 Å. 62,000X.
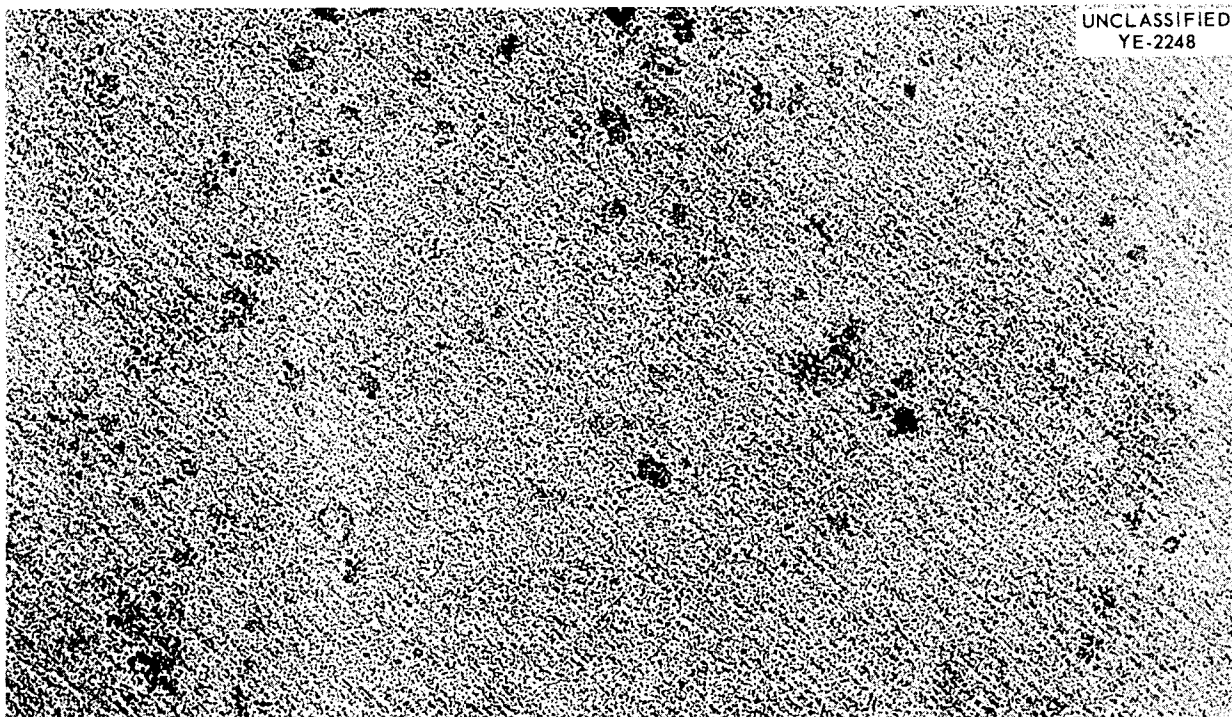
Fig. 61. Oxide Film Stripped from the (100) Face of a Cu Crystal After 15 min of Oxidation at 150°C. Film thickness: 193 Å. 12,000X.

Electron diffraction patterns typical of the oxide films formed on the (110), (111), and (100) faces of copper at 150°C are shown in Figs. 62, 63, and 64, respectively. Again, the high degree of orientation of the films may be clearly seen.

The oxide films formed at 130°C exhibited many of the same characteristics observed in the 150°C experiments. The same "loose" filament-like texture in the oxide films was observed in the early stages of oxidation, and longer oxidations produced a thickening of this texture. In addition, the films formed on the (111) and (100) faces frequently exhibited regions of thicker oxide in geometric shapes which reflected the symmetry of the substrate. Examples of this phenomenon are given in Figs. 65 and 66 for the (111) and (100) faces, respectively. An array of triangular shapes such as are shown in Fig. 65 was also occasionally observed in oxide films formed at 150°C on the (111) face.

The diffraction patterns obtained for all the films formed at 130°C were identical with those produced by films formed on the corresponding crystal planes at 150°C (cf. Figs. 58*d*, 62, 63, and 64). Thus the degree of orientation of the films formed at 130°C was also very high.

The oxide textures described above are typical of the results obtained in experiments in which it was believed that contamination had been reduced to a minimum. These data are, however, still considered to be tentative, since the degree of reproducibility of the oxide textures is still not entirely satisfactory. Furthermore, the problems discussed in connection with the procedure for stripping the oxide films have not yet been completely solved. For these reasons it is planned to continue the investigation of the oxidation characteristics of copper in the absence of radiation fields and, for the time being, to devote most of the effort in the in-pile work to studies of the effect of radiation on the oxidation of niobium and, perhaps later, tantalum and zirconium.
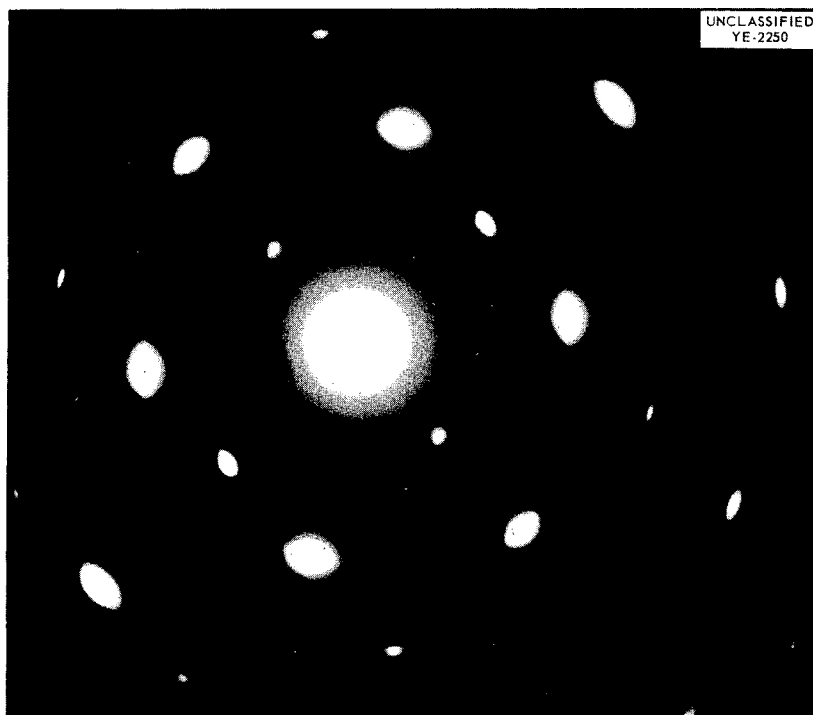
Fig. 62. Typical Transmission Electron Diffraction Pattern of Oxide Film Formed on the (110) Face of a Cu Crystal at 150°C.
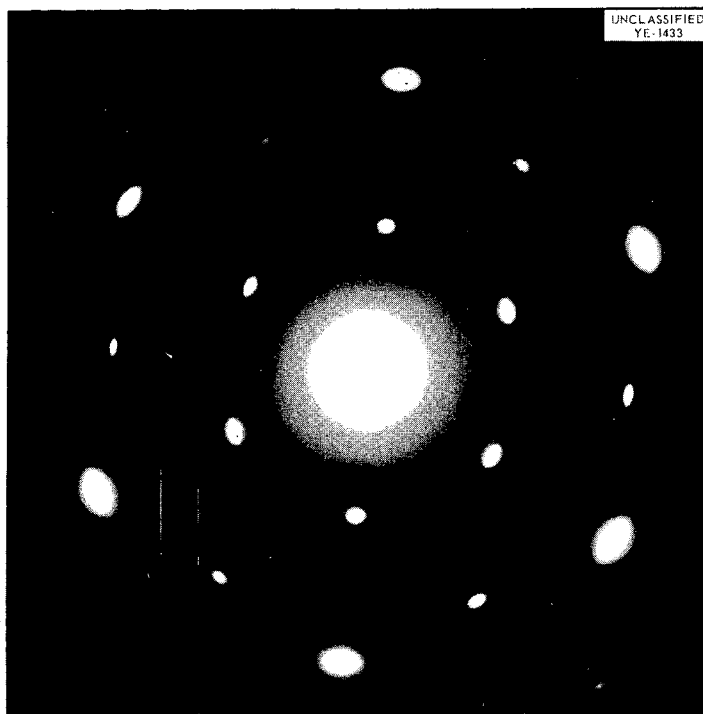
Fig. 63. Typical Transmission Electron Diffraction Pattern of Oxide Film Formed on the (111) Face of a Cu Crystal at 150°C.
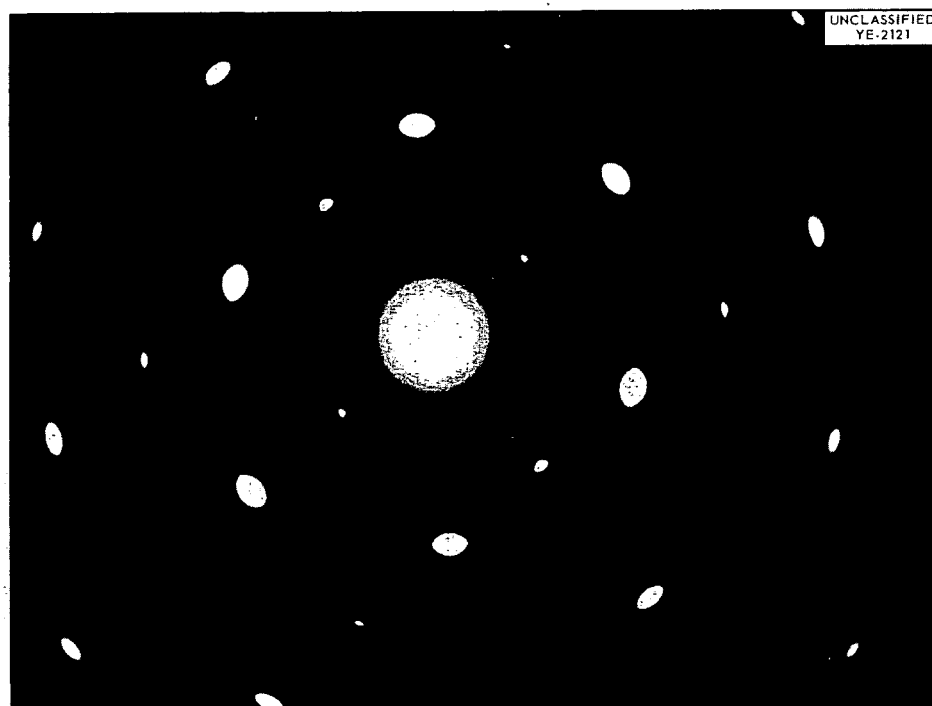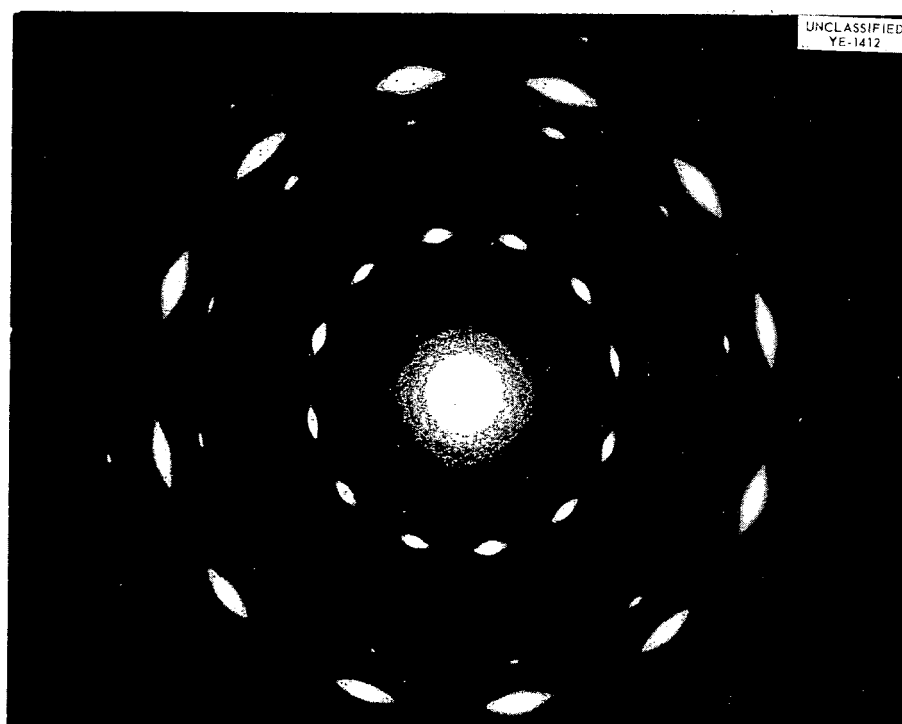
Fig. 64. Typical Transmission Electron Diffraction Pattern of Oxide Film Formed on the (100) Face of a Cu Crystal at 150°C.

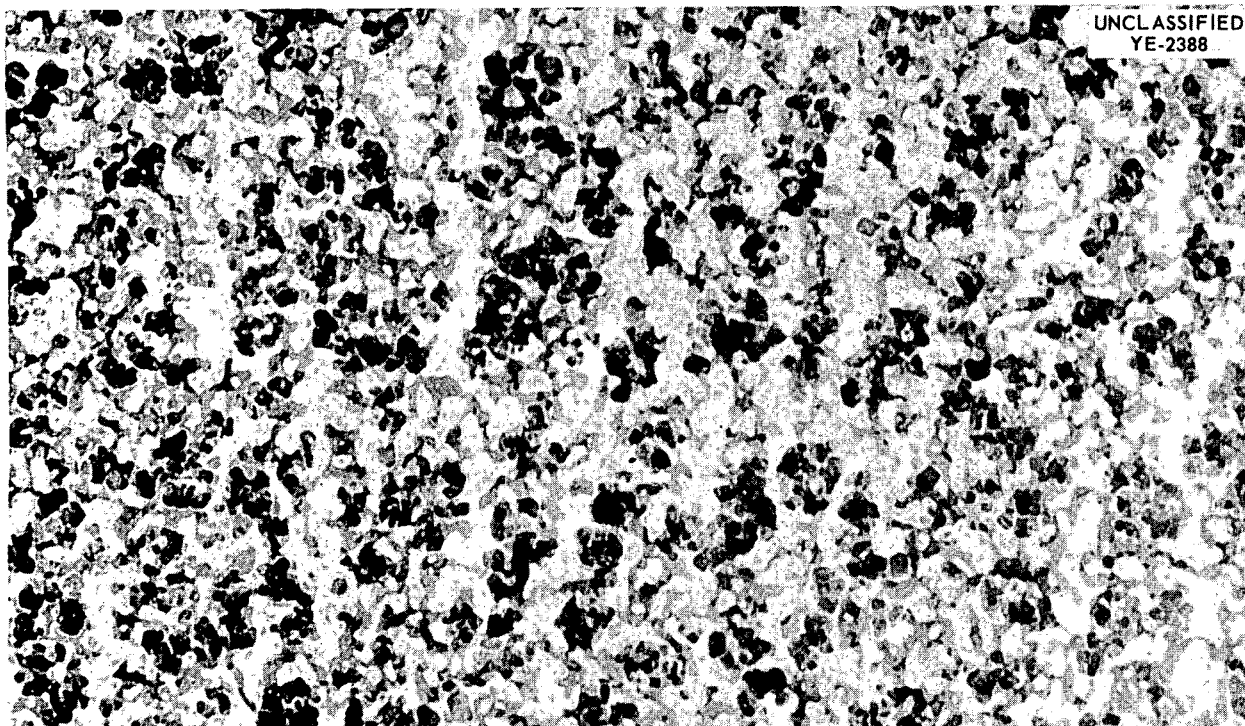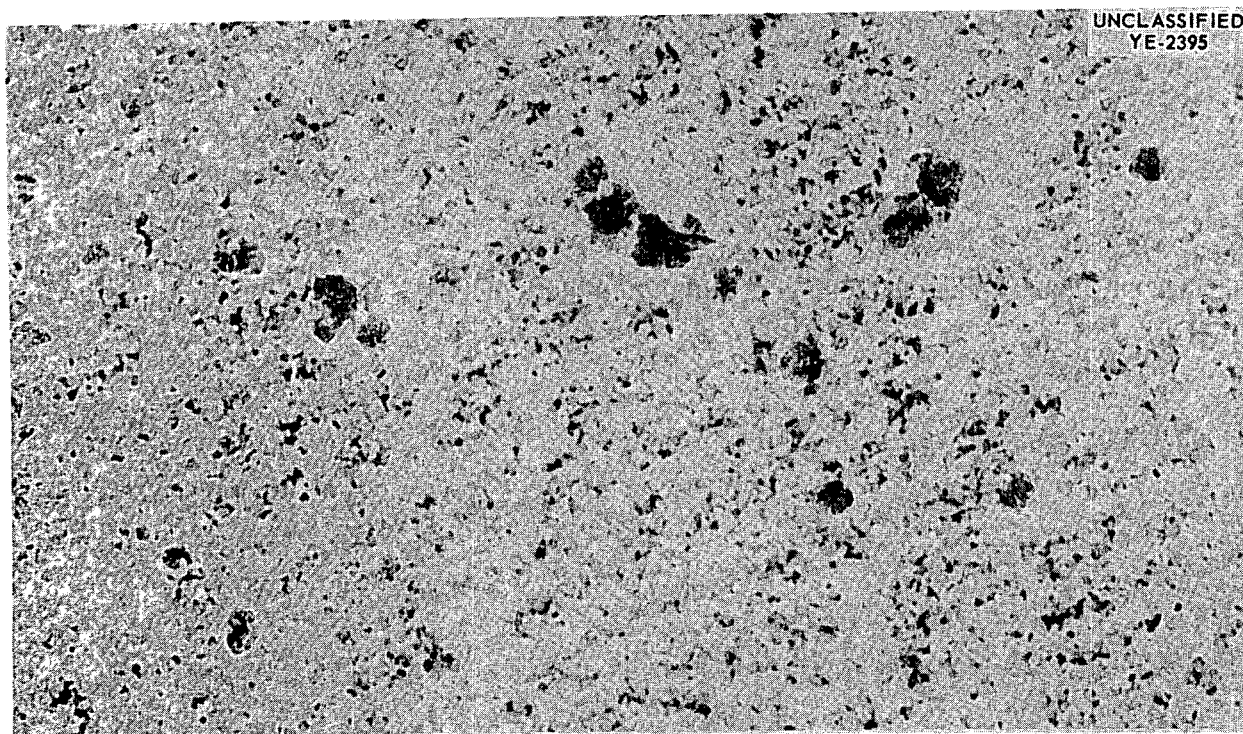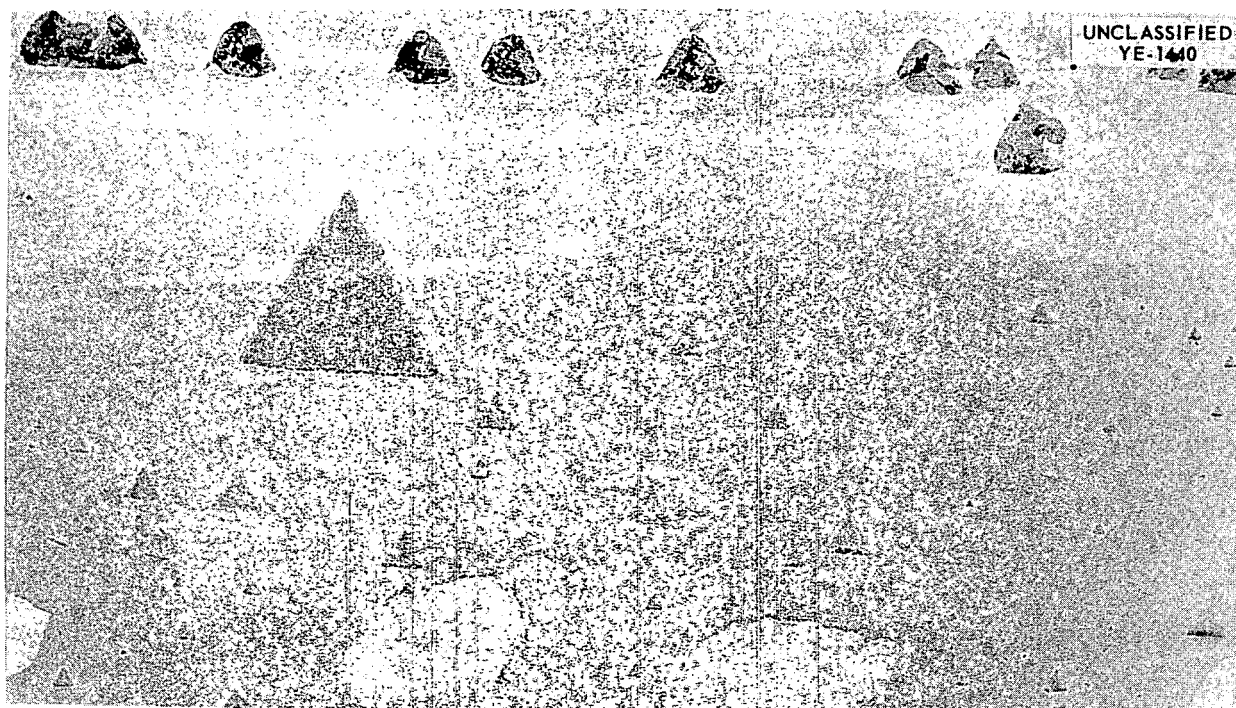Fig. 65. Oxide Film Stripped from the (111) Face of a Cu Crystal After 30 min of Oxidation at 130°C. The white areas in the photograph are due to holes produced in the oxide film during the stripping process.
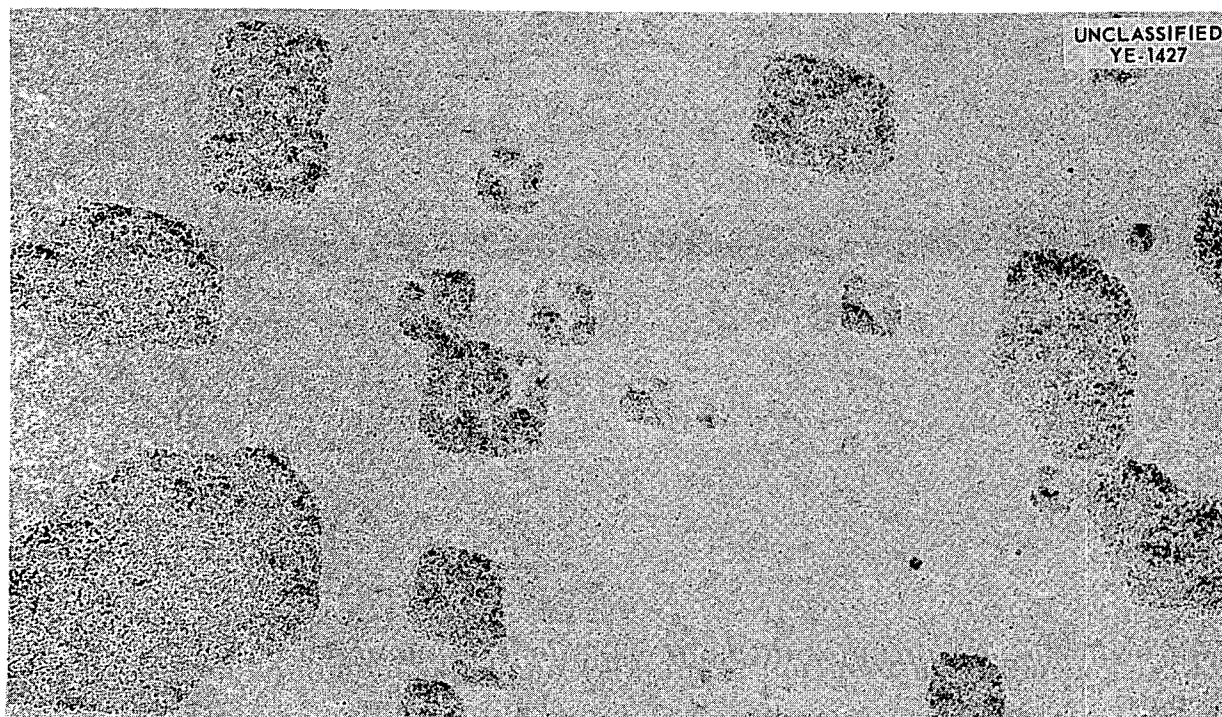
Fig. 66. Oxide Film Stripped from the (100) Face of a Cu Crystal After 30 min of Oxidation at 130°C.

DENSITY OF FUSED SALTS
G. F. Petersen

In order to provide data needed for the quantitative evaluation of absorption spectra (see next section, "Absorption Spectra of Fused Salts"), measurements are being made of the densities of fused salt mixtures. However, it should be pointed out that such density data are of intrinsic fundamental interest because they provide boundary values which any structural theory of the fused state must satisfy.

The present studies are being made for the reciprocal salt system $LiCl-KCl-LiNO_3-KNO_3$. Work reported here is for the binary system $KCl-KNO_3$. Preliminary measurements were made on salts of known density,[20] $NaNO_3$ and KNO_3, in order to check the experimental apparatus. Density measurements were made from 10°C above the melting point of the salt mixture to a maximum of about 600°C. Since the alkali nitrates decompose at lower temperatures, measurements on salt

mixtures with a high nitrate concentration may be terminated at lower temperatures. The $NaNO_3$, KNO_3, and KCl were purified by recrystallization, and then were fused under vacuum and held slightly above the melting point for a short time. Each salt was checked for chemical neutrality and found to be satisfactory.

The densities are determined from the difference in weight of a platinum bob, weighed first in air and then while immersed in the fused salt. The platinum bob is attached to an Ainsworth analytical balance by means of a 38-gage platinum wire. Density values obtained have a maximum deviation from literature values of less than 0.5%. Since most of the salts used are hygroscopic, design of the apparatus permits evacuation of room atmosphere and replacement with high-purity nitrogen. Density weighings are made under a flowing nitrogen atmosphere.

A calibrated Pt, Pt–10% Rh single-junction thermocouple enclosed in a quartz tube was used as the temperature sensing element. The thermocouple junction was placed near the middle of the melt. The thermocouple output was measured with a high-precision Rubicon potentiometer in conjunction with a Leeds & Northrup Pointerlite

[20]E. W. Washburn (ed.), *International Critical Tables of Numerical Data, Physics, Chemistry and Technology*, vol 3, p 28, McGraw-Hill, New York, 1928.

galvanometer. Temperature control was achieved by using a standard Marshall furnace with a 6-in. constant-temperature zone, the power for which was governed by an L&N model G Speedomax coupled to a DAT.

Temperature was measured to $\pm 0.1^\circ C$, weighings were made to ± 0.1 mg, and separate determinations of density had a maximum deviation from a straight line of less than 0.1%. The results of these measurements are plotted in Fig. 67. As might be expected, the density of a molten salt varied linearly as a function of temperature in the range measured. The method of least squares was used to transform the experimental results into equation form. These results are listed below:

Composition (mole %)	Density Function	Temperature Range ($^\circ C$)
Pure KNO_3	$\rho = 2.1101 - 0.00073_3 t$	340–510
10% $KCl-KNO_3$	$\rho = 2.1053 - 0.00073_6 t$	340–540
20% $KCl-KNO_3$	$\rho = 2.0898 - 0.00071_2 t$	425–585
30% $KCl-KNO_3$	$\rho = 2.0691 - 0.00068 t$	485–635

ABSORPTION SPECTRA OF FUSED SALTS[21]

C. R. Boston

The absorption spectra of fused salts have been of interest for some time as aids in studying the chemical constitution and the electronic structure of these media.[22-27] This paper is concerned with the determination of molar absorbancy indices from the spectra of solutes existing in dilute solutions in fused salt media. Such measurements should give useful information concerning the chemical nature of species in fused salt solution. The particular system chosen for initial study was a solution of $NiCl_2$ in mixtures of LiCl and KCl. Measurements of this sort have recently been reported by Lux and Niedermaier,[24] who measured absorbancy values for manganese oxysalts dissolved in NaOH and KOH fusions, and by Gruen,[26] who determined absorbancy values for a variety of metal chlorides in fused $LiNO_3$-KNO_3 eutectic.

Experimental

Preparation of Materials. — Commercial, anhydrous HCl gas was purified by passing it over activated charcoal and silica gel. Stopcocks through which the HCl passed were lubricated with low-vapor-pressure, fluorinated hydrocarbons. Pressure regulators were made of monel. Argon was purified by passing it first over hot copper and then over P_2O_5.

Anhydrous $NiCl_2$ was made from reagent-grade, "cobalt-free" $NiCl_2 \cdot 6H_2O$. This material was first heated slowly to $450^\circ C$ over a period of 4 hr under an atmosphere of flowing HCl gas. Then it was sublimed at 800 to $900^\circ C$ under an HCl atmosphere. The cobalt content of the final product was 0.0037%, as determined by spectroscopic analysis.

Most of the LiCl-KCl mixtures used had a composition close to that of the eutectic (about 41 mole % KCl). The most troublesome contaminants were water, which is difficult to remove from LiCl, and small amounts of a black residue which formed on melting of the reagent-grade salts. The purification procedure for the LiCl-KCl mixtures consisted in removing most of the water in a vacuum; reversing the hydrolysis, due to the remaining water, with anhydrous HCl; and, finally, removing the black residue by filtration of the melt through a fritted pyrex disk. A convenient method was devised for carrying out these operations. This procedure is described below in detail, inasmuch as it is applicable to the preparation of a variety of low-melting halide mixtures in a form suitable for quantitative spectral measurements.

The apparatus used for the purification of LiCl-KCl mixtures is schematically illustrated in Fig. 68. The pyrex fritted disk was of a "fine" porosity. By maintaining a suitable pressure differential on either side of the fritted disk, the melt could be supported on the disk or filtered through at will. The apparatus was heated over the distance from the bottom of the 11-mm tube to

---

[21]Throughout this paper the nomenclature and symbols recommended by K. S. Gibson, *Nat. Bur. Standards (U.S.) Circ.* 484 (1949), are used where applicable.

[22]K. Schaum and M. Funk, *Z. wiss. Phot.* 23, 73 (1924).

[23]E. Mollwo, *Z. Physik* 124, 118 (1947).

[24]H. Lux and T. Niedermaier, *Z. anorg. u. allgem. Chem.* 285, 246 (1956).

[25]B. R. Sundheim and J. Greenberg, *Rev. Sci. Instr.* 27, 703 (1956).

[26]D. M. Gruen, *J. Inorg. & Nuclear Chem.* 4, 74 (1957).

[27]K. Sakai, *J. Phys. Chem.* 61, 1131 (1957).

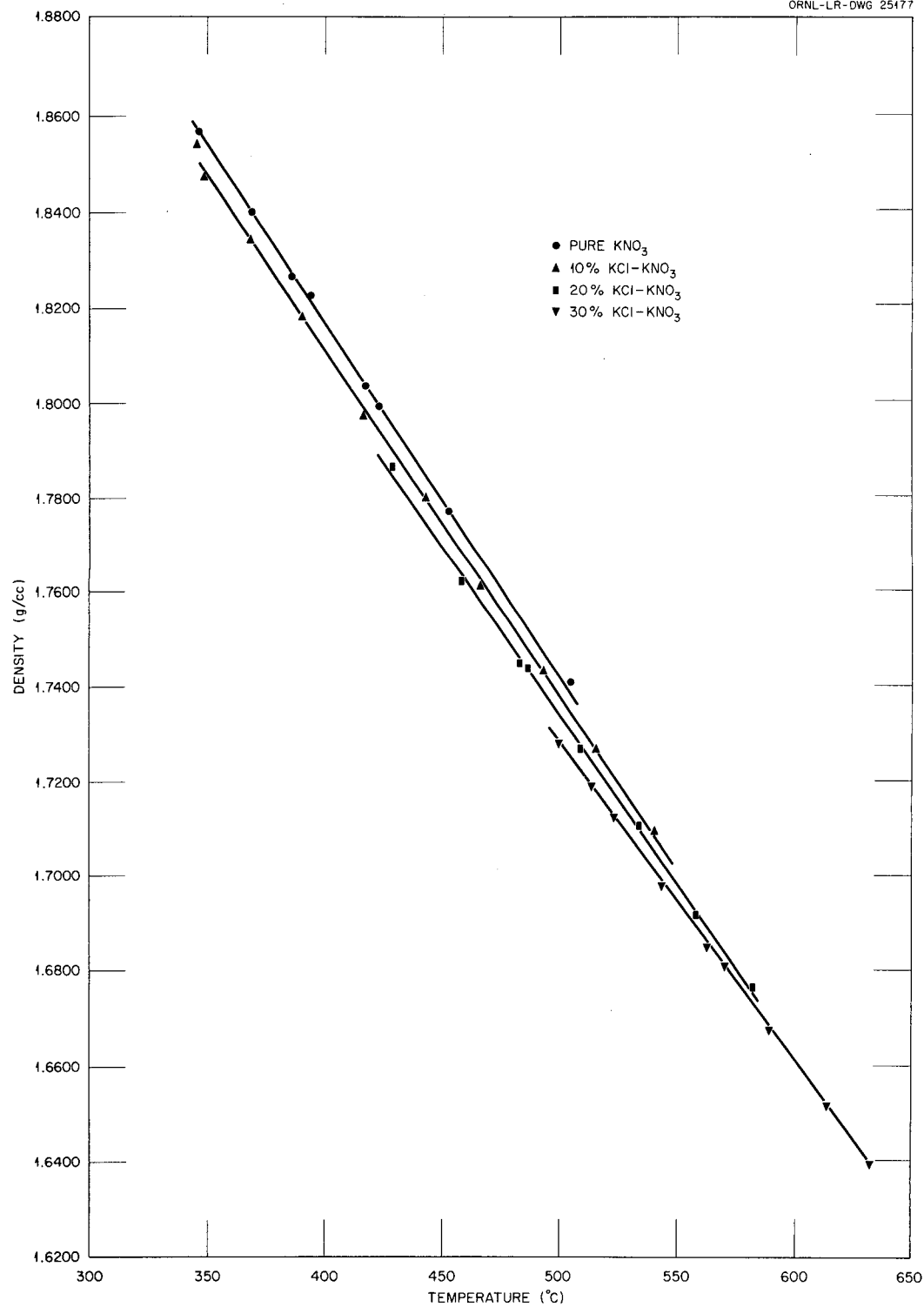**Fig. 67. Results of Density Measurements.**

UNCLASSIFIED
ORNL-LR-DWG 23743
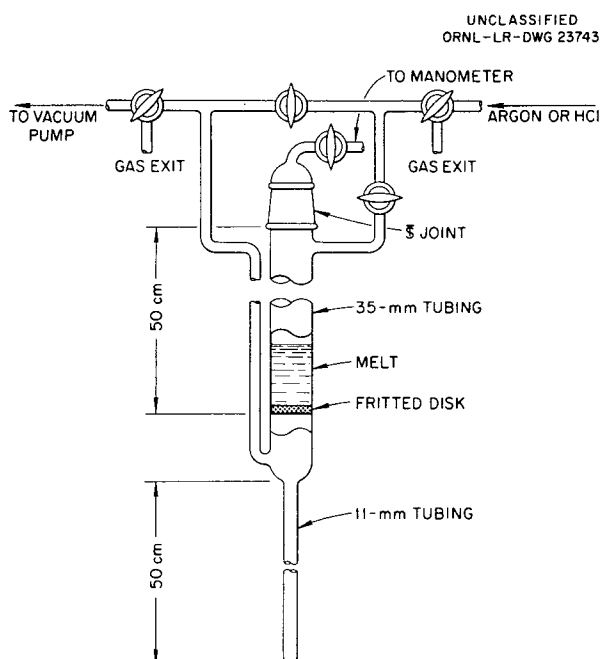
Fig. 68. Apparatus Used for the Purification of LiCl-KCl Mixtures.

a position well above the top of the melt in the 35-mm tube. Heating was by means of two electric tube furnaces stacked so as to give a continuous hot-zone length of 85 cm. The upper furnace had a window which permitted visual observation of the melt during the purification procedure. The lower furnace, which heated the 11-mm tube, was of the split-core type and could be opened to permit rapid cooling.

A mixture of reagent-grade LiCl and KCl was placed on the fritted disk, and the entire apparatus was evacuated with a mechanical pump. Exposure time of the LiCl to room air was held to a minimum. The solid was heated under vacuum to 300°C by gradually raising the temperature over a period of 2 hr. At 300°C, argon, followed by anhydrous HCl, was admitted. While HCl passed through the filter disk and the solid salt mixture, the temperature was raised over a period of $\frac{1}{2}$ hr to 500°C in order to fuse the mixture. Initially, the melt was cloudy. The HCl, dispersed as fine bubbles by the fritted disk, was then passed through the melt until the cloudiness disappeared and for about 10 min thereafter. The argon was bubbled through the melt for 5 min in order to remove excess HCl.

Next, a vacuum was applied to the lower side arm, and the melt was filtered through the disk in order to remove the solid impurities. The molten salt flowed into the lower, 11-mm, tube, where it was quickly frozen by opening the lower furnace. The tube containing the purified mixture was then sealed off under vacuum, checked for vacuum leaks, and stored until needed. The material in the tube was of a fairly uniform composition only if the LiCl-to-KCl ratio was near that of the eutectic and only if solidification took place simultaneously at a number of sites along the length of the tube.

The salt mixtures prepared by this method unavoidably varied in composition by a few mole per cent from one preparation to another. These small variations in solvent composition were found to have a small but measurable effect on the absorption spectra. For that reason the solvents used here are not referred to as "the eutectic."

The mixture was easily removed from these tubes in a dry box by cracking the glass tubing and sliding out the solid rod of mixture, which was then broken into segments and loaded into optical absorption cells. The purity of the solvent mixture prepared in this way was evidenced by the complete absence of etch on the highly polished cell windows after 20 hr of exposure and by the reproducibility of the absorption spectra.

Spectrophotometer and Furnace. – Measurements of absorption spectra were made with a Cary model 11 MS recording spectrophotometer which was modified for high-temperature work by replacing the cell compartment with a furnace assembly described below. Furnace radiation did not interfere with the spectral measurements reported. This absence of interference was ensured by two design features of the Cary instrument. First, the light beam was pulsed at a low audio-frequency, and the output current was filtered so that only the fundamental frequency of the pulses was passed. Second, the light-sensing units were a pair of matched 1P28 multiplier phototubes which had a low sensitivity to light of wavelengths greater than 750 mμ.

The furnace assembly is shown in Fig. 69. It consisted of two silver blocks which held the optical cells, a furnace, and a supporting rod made from stainless steel pipe. This supporting rod was screwed into the lower silver block and carried a brass platform on which the furnace

105

OPTICAL CELL

WATER COOLING COILS

UPPER SILVER BLOCK

SAMPLE COMPARTMENT

RUBBER LIGHT-SEAL

LOWER SILVER BLOCK

REFERENCE COMPARTMENT

LIGHT-BEAM PORTS

SUPPORTING ROD OF STEEL

VERTICAL ADJUSTMENT SET SCREW

1 0 1 2 3 4
SCALE IN INCHES
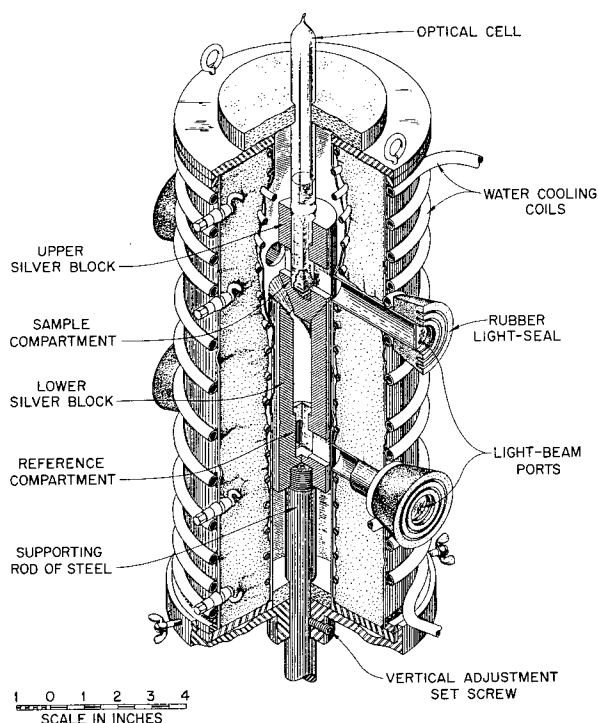
**Fig. 69. Furnace Assembly Used as a Cell Compart-
ment in the Spectrophotometer.**

rested. The furnace could be unbolted from its platform and raised to give easy access to the silver blocks. The furnace assembly and the phototube housing were held on carriages which rode on a lathe-bed type of optical bench. This optical bench was accurately aligned with the light beams from the monochromator. Hence the furnace assembly and the phototube housing could be moved laterally without tedious optical re-alignment. Such lateral motion was required for adjustment and servicing of the components.

The lower silver block, shown in Fig. 69, was designed to hold an optical cell containing a reference material. This cell was omitted in the measurements reported here and is not illustrated in the diagram. The upper silver block held the optical cell which contained the sample material. A cone on the bottom of the upper block rested in a precisely mating conical socket at the top of the lower block. Rotary alignment of the two blocks was ensured by means of a steel pin. Silver shims in the upper block held each cell in a reproducible position in the light beam.

In order to prevent heating of other components, the furnace shell was cooled with water, and the light-beam ports were closed off with optical-grade fused-silica windows. In order to prevent volatile products from the furnace insulation and the refractory cement from reaching and condensing on the furnace windows, the interior of the furnace and the adjacent light-beam ports were lined throughout with an all-welded Inconel shield.

The furnace winding was provided with shunts so that different power in-puts could be applied to the top, middle, and lower sections in order to help reduce thermal gradients. Further reduction in thermal gradients was provided by the silver blocks which held the optical cells. Inasmuch as a reference cell was not placed in the lower silver block in the research described here, the elimination of a thermal gradient between the two silver blocks was not important. However, such a gradient can be reduced to a very small value with this apparatus when it is desired to measure absorbancy directly.

The gradients that existed, together with the temperature of each cell compartment, were measured by means of five calibrated Pt, Pt-Rh thermocouples placed into holes drilled at suitable positions in the silver blocks and read with an L&N model K-3 universal potentiometer. The temperature level was controlled by means of a Chromel-Alumel thermocouple which actuated an L&N model G Speedomax coupled with an L&N DAT controller. Temperature control was within a precision of 0.5°C, as measured by couples adjacent to the optical cells. The temperature of a melt was calibrated with a platinum-sheathed thermocouple immersed therein. It is estimated that the absolute temperature of a melt was known to within 1°C.

The absorbance range of the spectrophotometer, as supplied by the manufacturer, was 0 to 3.5 absorbance units. For a few high absorbance measurements this range was increased to about 5.5 by the insertion, in the reference light beam, of screens made from accurately perforated steel plates supplied by the Pyramid Screen Co. This extension of the absorbance range was permissible because of the very low level of stray light achieved by the Cary double monochromator. The absorbances of the screens were accurately measured.

Optical Cells. — The types of optical cells used in this work are illustrated in Fig. 70. (Cells were supplied by the Pyrocell Manufacturing Company.) The cell shown in Fig. 70a was used largely for preliminary work in which some risk of atmospheric contamination was accepted in order to gain experimental flexibility. This type of cell will be referred to as a "stoppered" cell. The other type of cell, shown in Fig. 70b, initially had a standard-taper joint on the upper end, as shown. However, after being loaded it was sealed off under vacuum by fusing the glass several centimeters above the melt so as to avoid any chance of atmospheric contamination during a run. This type of cell is referred to as a "sealed" cell.

GAS INLET

JOINT

QUARTZ CAPILLARY TUBING

GAS EXIT

PYREX TUBING

MELT

GRADED SEAL

QUARTZ INSERT

(a)   (b)

FUSED SILICA WINDOWS
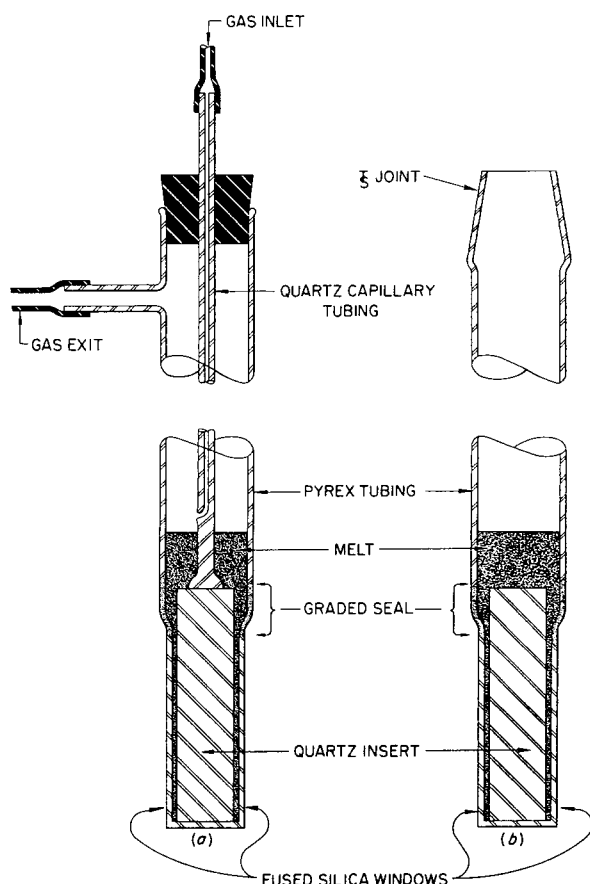
Fig. 70. Types of Optical Cells Used. (a) "Stoppered" cell. (b) "Sealed" cell; after loading, this cell was sealed off under vacuum at a point below the standard-taper joint.

The lower end of both types of cells consisted of a square-cross-section, Beckman optical cell made of fused silica. This Beckman cell was fastened to the upper pyrex tubing by means of a graded seal. The cell windows were 40 mm high by 10 mm wide, and the inside distance between the windows was 10 mm. For some measurements the light-path length through the melt was reduced to 0.5 mm. This was accomplished with precision-grade quartz inserts, supplied by Pyrocell Manufacturing Company, which are shown in place in Fig. 70. Values of the average path length for each measurement were determined to within 1% by micrometer measurements on the cell and the insert.

In the stoppered cells, purified argon was admitted through a quartz capillary tube which had a side opening near the liquid level. Below this side opening the capillary tube was collapsed to form a rod which was fused to a quartz insert. Argon left the cell through a side arm that was closed with a valve that permitted gas to leave but not to enter the cell.

Procedure. — Optical cells were loaded with salt in a vacuum-type dry box under a high-purity nitrogen atmosphere. The cells were weighed on an analytical balance before and after loading in order to obtain the weight of the LiCl-KCl mixture. The $NiCl_2$ was added in the dry box from a weighing bottle which was likewise weighed before and after the addition. After loading, the cells of the sealed type were pumped down to about 10^{-5} mm Hg and sealed off.

Absorption spectra measurements were made at a series of temperatures between 360 and 550°C for each cell loading. At the end of such a series, repeat measurements were made at one or more of the previously used temperatures. Inasmuch as all the spectra for a given cell loading were recorded in an overlapping fashion on the same strip of chart paper, it was possible to obtain an accurate check on reproducibility. This reproducibility was generally found to be within the width of a pen line, except for some of the high absorbance measurements, where a moderate noise level was encountered. During the course of each spectral measurement the temperature adjacent to the optical cell was monitored in order to verify the absence of significant thermal cycling or drift. Spectra were measured at a wavelength scanning speed of 1.0 mμ/sec in the visible region and 0.4 mμ/sec in the ultraviolet region. In all cases,

air was the reference material, and spectra were corrected for absorbance due to solvent by determining the solvent spectrum independently, at various temperatures, and subtracting it from the corresponding solution spectrum. Light absorption by the solvent over the range 280 to 750 mμ was small and did not change much with temperature. However, at wavelengths approaching 220 mμ the light absorption of the solvent rose rapidly and changed considerably with temperature.

In measurements made with the stoppered type of optical cell, weighed amounts of $NiCl_2$ were added as desired by momentarily unstoppering the cell. After each addition the cell was flushed with argon, and the $NiCl_2$ was mixed with the melt by raising and lowering the quartz insert a number of times. It is to be noted that anhydrous $NiCl_2$ is not hygroscopic. Following each addition of $NiCl_2$, adequate time was allowed for thermal equilibration.

The vaporization of $NiCl_2$ was appreciable only for a few melts containing a high concentration of this material, and then only after a prolonged time at temperature. In these instances the contents of the cell, including vapor-deposited $NiCl_2$, were remixed before each spectral measurement.

At the termination of measurements on a given sample contained in a sealed cell, the cell was inverted and allowed to cool. Then the cell was cut open, the entire contents dissolved in 0.1 M HNO_3, and portions of the solution submitted for analytical determination of lithium and potassium. If the cell was not inverted before cooling, the square-cross-section part of the cell usually cracked as the salt solidified.

Values for the molar absorbancy index a_M (also known as the molar extinction) were computed from weights of $NiCl_2$ and LiCl-KCl mixture added to the optical cell, and from the density of the fused LiCl-KCl mixture at the temperature and KCl concentration involved. It is not unlikely that a small amount of $NiCl_2$ was lost in the loading operation. This would cause the absolute values of a_M reported here to be too great. However, the precision in the a_M values for different weighings of $NiCl_2$ was very good (standard deviation <2%), considering sources of error other than weighing. The absolute values of a_M are estimated to be within 5%. The density of the solutions was taken to be the density of the solvent. The error involved in this assumption is considered to be less than experimental errors, inasmuch as the

$NiCl_2$ concentrations were for the most part very small. Density values of the LiCl-KCl mixtures were obtained from the work of Van Artsdalen and Yaffe.[28] They gave empirical equations in two constants, a and b, which express density as a function of temperature at several fixed concentrations of KCl. In the measurements reported here, density values were needed at intermediate concentrations in the neighborhood of the eutectic composition. For this purpose the constants of Van Artsdalen and Yaffe were represented by the following equations:

$$a = 1.860 + 0.00225(X - 30) ,$$

$$b \times 10^3 = 0.5073 + 0.0018(X - 30) ,$$

where X = mole % KCl, and $30 < X < 60$.

Results and Discussion

Typical results of the spectral measurements are illustrated for the ultraviolet region in Fig. 71 and for the visible region in Fig. 72. The data shown were obtained with sealed cells. Along the ordinates in these figures is plotted the molar absorbancy index computed in terms of the molar concentration of nickel atoms without regard to the chemical composition of the light-absorbing species. Five absorption bands were found over the range of 220 to 750 mμ, and these will be designated as bands I through V, taken in the order of increasing wavelength. Band I is shown in Fig. 71, and bands II through V are indicated in Fig. 72. The shape of the short-wavelength side of band I indicates the presence of another absorption band at shorter wavelengths. With increasing temperature, bands I and II decreased in molar absorbance index, while bands III, IV, and V increased. The temperature coefficient of the molar absorbance index was found to have the same value for all wavelengths between the maximums of bands III and V. The spectra for different temperatures were found to intersect twice between bands I and II and once between bands II and III. The two intersections between bands I and II were caused by a broadening and a shift toward the longer wavelengths of band I, whereas the intersection between bands II and III was caused by the simultaneous downward

[28]E. R. Van Artsdalen and I. S. Yaffe, *J. Phys. Chem.* 59, 118 (1955).
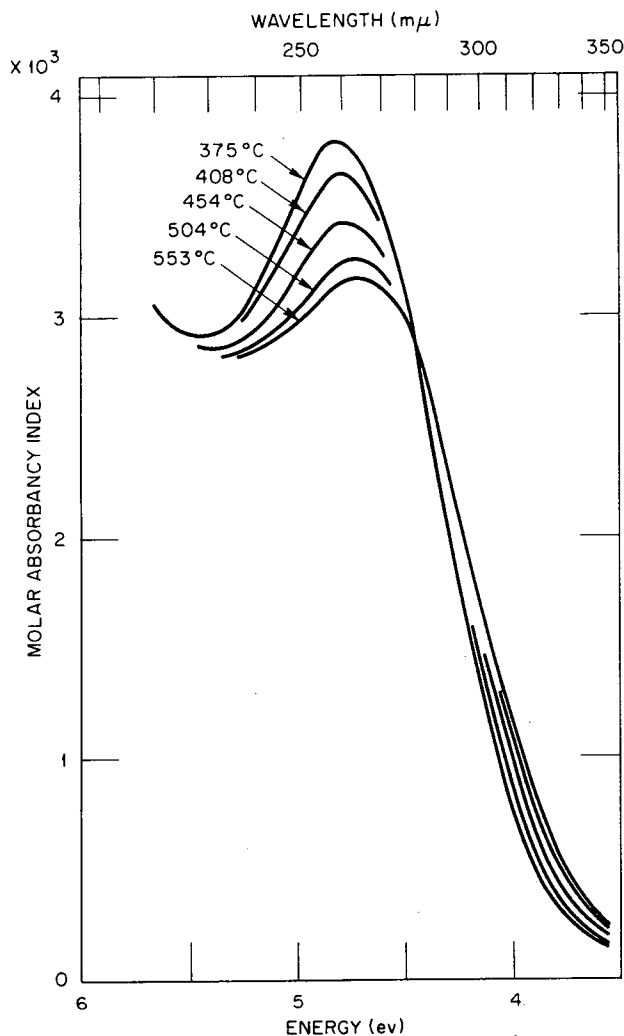
Fig. 71. Ultraviolet Absorption Spectra of a Solution of $NiCl_2$ in a Fused LiCl-KCl Mixture at Several Temperatures. Measurements made in sealed optical cells. Melt contained 1.11×10^{-3} g of $NiCl_2$ per gram of solution. Molar absorbancy indices computed from concentration of total nickel.

Fig. 72. Visible Absorption Spectra of a Solution of $NiCl_2$ in a Fused LiCl-KCl Mixture at Several Temperatures. Measurements made in a sealed optical cell. Melt contained 0.0246 g of $NiCl_2$ per gram of solution, and solvent salt contained 41.0 mole % KCl.

movement of band II and the upward movement of band III. At 398°C the band maximums occurred as follows: I at 260 mμ, II at 512 mμ, III at about 590 mμ, IV at 625 mμ, and V at 695 mμ. As may be seen, there was a considerable overlapping of bands, so that the above values are somewhat different from those of the true band centers.

The temperature dependence of the absorption curves showed that there were two light-absorbing species in equilibrium such that, with increasing temperature, one species, associated with bands I and II, decreased in concentration. Both species were, of course, derived from $NiCl_2$, as shown below by the linear dependence of absorbancy on total nickel concentration. These species were probably two different chloronickel(II) complexes.

Any quantitative interpretation of a change in shape of an absorption curve with a large change in temperature must be made with caution. It is to be expected, in general, that an increase in temperature will cause a given absorption band to broaden and may cause a shift in the wavelength of the band maximum. These effects are caused by thermal motions of the light-absorbing species, and the magnitude of these effects is determined in a complex way by the electronic structures of the ground and the excited states. As a consequence of these changes in band shape, the absorbancy per unit path length will change for each wavelength in a way which is independent of any change in concentration of the light-absorbing species; that is, the absorbancy index will be a function of temperature. In principle this difficulty can be avoided in large measure by use of the integrated absorbancy index, defined as $(1/bc)$ $\int A_s(\bar{\nu}) \, d\bar{\nu}$, where b is the path length, c is the concentration of light-absorbing species, and $A_s(\bar{\nu})$

is the absorbancy as a function of wave number $\bar{\nu}$. The integration is taken over all values of $\bar{\nu}$ for which A_s is not negligible. The integrated absorbancy index will be independent of temperature-induced changes in band shape provided that the oscillator strength associated with the absorption band does not change. Changes in oscillator strength are expected to be quite small. For the spectra reported here, band overlap is too great to permit a reliable evaluation of the change in integrated absorbancy index with temperature. Qualitatively, however, these effects are in the wrong direction to account for the marked increase of the molar absorbancy indices of bands III, IV, and V with increasing temperature. Furthermore, estimates can be made of the contribution of band broadening to the decrease in molar absorbancy index of band I, and these estimates show that band broadening can account for no more than one-half the observed decrease. Consequently, it is concluded that the changes in the shapes of the absorption curves show the presence of two light-absorbing species which are in equilibrium, such that one species increases in concentration while the other decreases in concentration with increasing temperature.

Further evidence that the observed absorption bands arise from transitions associated with chloronickel(II) complexes is given by the work of Gruen.[29] The author has conducted similar studies in which spectra were measured for a solution of $NiCl_2$ in fused KNO_3 to which additions of KCl were made. With increasing additions of KCl the 440-mμ absorption band of $NiCl_2$ in pure KNO_3 disappeared, and there appeared the complex of overlapping bands reported here for the visible absorption spectrum of $NiCl_2$ in fused LiCl-KCl mixtures. Studies in the ultraviolet region were impossible because of the intense absorption of the nitrate ion in that region. Details of this study will be reported later.

Small changes in the composition of the solvent salt were found to have a small but measurable effect on the absorption spectra. This effect is best shown in terms of the ratio of the absorbancy values of bands II and IV, that is, $(A_s)_{II}/(A_s)_{IV}$. In Fig. 73 this ratio is plotted against mole % KCl at two temperatures, 364 and 398°C. These temperatures are near the freezing point of the

[29]D. M. Gruen, *J. Inorg. & Nuclear Chem.* **4,** 74 (1957).
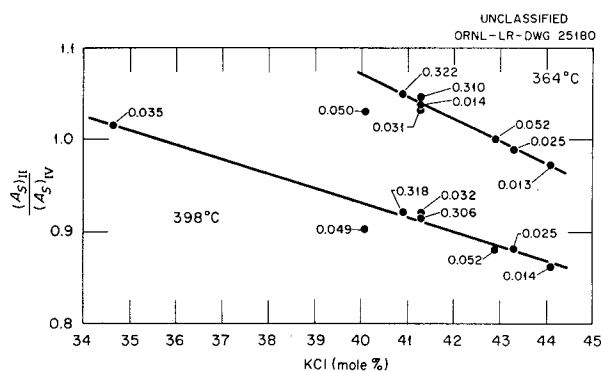
Fig. 73. Effect of Small Changes in Solvent Composition on the Visible Absorption Spectrum as Measured by Changes in the Ratio of the Absorbancy of Band II to That of Band IV at Each of Two Temperatures. The number by each point indicates the molar concentration of total nickel in the melt. The point at 34.4 mole % KCl on the 398°C line was obtained by extrapolation from data obtained at 416°C and above.

eutectic, so that the accessible composition range for LiCl-KCl mixtures was quite small. Values of the molar concentration of $NiCl_2$ are indicated for each point in Fig. 73. It will be noted that, to within experimental error, the effect of solvent composition is independent of the $NiCl_2$ concentration for the range of compositions measured. The absorbancy ratio for the 34.4 mole % KCl mixture was extrapolated from measurements at 416°C and above. This extrapolation was necessary because this mixture freezes at the lower temperature, while for mixtures near the eutectic at temperatures above 400°C, band II is obliterated by overlap of band III.

It is not surprising that the cation ratio of the solvent salt has an effect on the relative absorbancy values of bands II and III. At a constant temperature these relative absorbancies are a measure of the relative concentration of the two species which give rise to the bands, and this relative concentration would be expected to shift with a change in the cation ratio of the solvent salt because of a corresponding shift either in the activity coefficients of the two species or in the equilibrium constant. On the other hand, chloronickel(II) complex anion should be surrounded by Li^+ and K^+ cations, which differ greatly in their ability to polarize neighboring ions. Consequently, a change in the average of the ratio of Li^+ to K^+ ions surrounding a chloronickel(II)

complex anion might well be expected to have some effect on the width or even on the oscillator strength of the absorption bands of the anion. The existing experimental data do not permit a separation of the contribution of the latter effects from that of a change in concentration. However, if the latter effects are small compared with the change in concentration, then a decrease in the KCl concentration of the solvent salt is equivalent to a decrease in temperature in its effect on the equilibrium between the light-absorbing species.

It was found that at constant temperature and constant solvent salt composition the molar absorbancy index computed from the molar concentration of nickel atoms was a constant independent of nickel atom concentration over the range of about 0.01 to 0.4 M. This result, the experimental evidence for which is described below, shows, first, that the concentrations of the two light-absorbing species are proportional to the total concentration of nickel atoms and, second, that the molar absorbancy index computed as described could be employed for analytical purposes in the way which is customary for more conventional solutions at ordinary temperatures. Experimental verification of the constancy of the molar absorbancy index computed by using the total concentration of nickel is described in the following paragraphs.

Spectra were measured over the visible range after each of seven successive additions of NiCl$_2$ to an LiCl-KCl melt contained in a stoppered cell at 409°C. Some results of these measurements are shown in Fig. 74, in which absorbancy per unit path length is plotted as a function of the molarity of NiCl$_2$ for the maximums of bands II and IV. It will be seen that these data may be represented reasonably well by straight lines. Furthermore, molar absorbancy indices were computed at 10-mμ intervals over the range of 350 to 750 mμ for all seven spectra. The resultant values obtained at the same wavelengths but at different NiCl$_2$ concentrations were in agreement to within the accuracy to be expected from the behavior of the two maximums illustrated in Fig. 74.

Similar measurements were made in the ultraviolet range. The results of measurements on two melts at 407°C are shown in Fig. 75. The data for the run marked by closed circles in Fig. 75 lie on a fairly smooth curve which shows a negative deviation from a straight line at large values of absorbance. A small shift in band maximums

toward longer wavelengths was likewise observed at the high absorbance values. These systematic deviations were probably caused by stray light.

In order to determine the constancy of the molar absorbancy index over a wide range of temperatures, visible spectra were measured for five sealed absorption cells. Each cell contained a

Fig. 74. Maximum Absorbance per Unit Path Length for Bands II and IV as a Function of Concentration of Total Nickel in Melt. All data are for a single melt measured in a stoppered cell. Data denoted by O measured with 1.00-cm path length; ■ measured with 1.00-cm path length and calibrated screen in reference beam; ● measured with 0.050-cm path length.
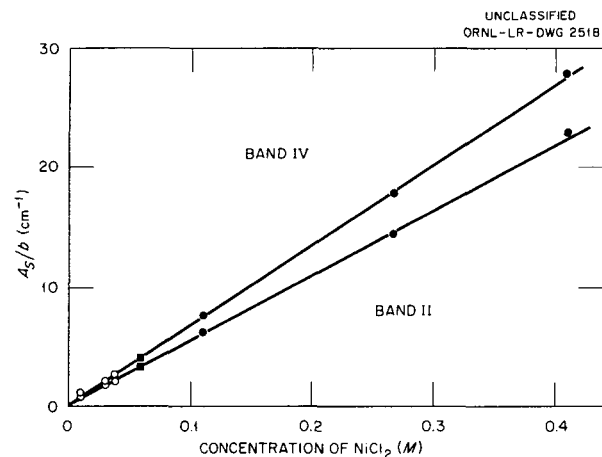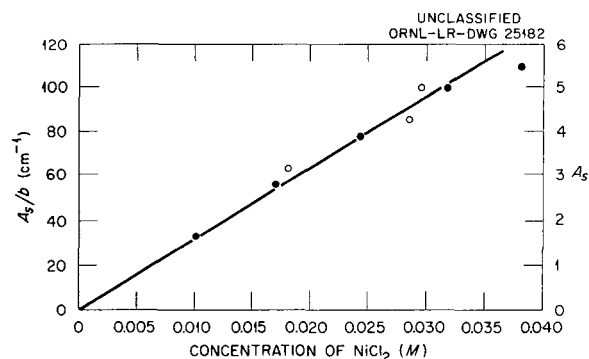

Fig. 75. Maximum Absorbance per Unit Path Length for Band I as a Function of Concentration of Total Nickel in Melt. Open and closed circles represent results from each of two melts in stoppered cells. Temperature for both melts was 407°C, and path length was 0.0501 cm.

different concentration of $NiCl_2$ over the range of about 0.013 to 0.32 M, and each was measured at five temperatures from 364 to 540°C. The results of these measurements are shown in Fig. 76, in which molar absorbancy indices for bands II and IV are plotted against temperature. In each of these five sets of measurements the composition of the solvent salt was unavoidably somewhat different. As would be expected from the results described above, these variations in solvent composition had a small effect on the molar absorbancy indices. Consequently, the data given in Fig. 76 were corrected to 41.0 mole % KCl, the eutectic composition, on the basis of plots of a_M vs mole % KCl for each of the two band maximums. These corrections were small. The vertical bars in Fig. 76 show the spread in the five values at each point expressed as the average deviation from the mean value.

Absorption spectra measurements will be continued on this system and on other fused salt systems. In addition, consideration is being given

UNCLASSIFIED
ORNL—LR—DWG 25183
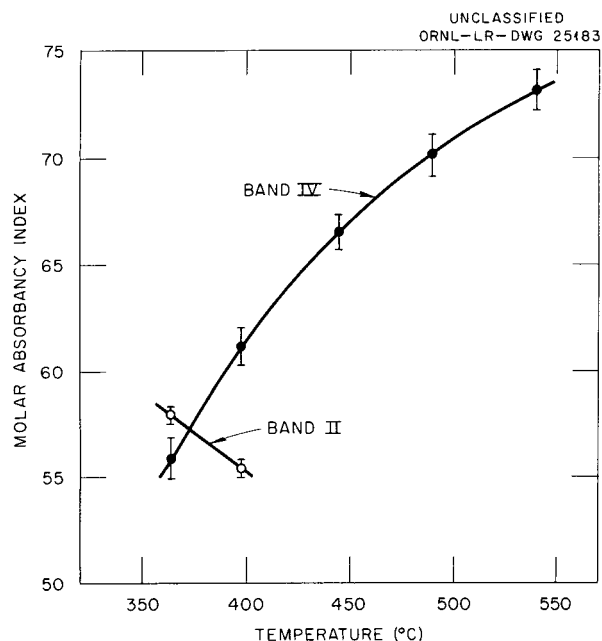
Fig. 76. Maximum Molar Absorbancy Indices Corrected to a Solvent Composition of 41.0 Mole % KCl for Bands II and IV as a Function of Temperature. Each point is the average of measurements with five sealed cells, including concentrations of total nickel from about 0.013 through 0.32 M. Vertical bars represent average deviation from the mean value.

to measurements of paramagnetic susceptibility for fused salt systems. Such measurements, particularly in the case of nickel, should provide information regarding the electronic and spatial configurations of the complex species present.

NUCLEAR MAGNETIC RESONANCE STUDIES AT HIGH TEMPERATURES

J. J. McBride

The investigation into the use of nuclear magnetic resonance (NMR) techniques as a means of elucidating the structure of fused electrolytes has continued. This work has had the invaluable assistance of R. Livingston's group of the Chemistry Division, whose NMR apparatus has been used. They have also been generous in making their time and experience available in the running of these experiments.

Although some preliminary observations of the H^1 and Na^{23} resonances in fused NaOH were made with a broad-line spectrometer, it became obvious that higher-resolution apparatus would be necessary for detailed study of these lines, and, for this reason, the principal activities in the past year have been apparatus development and refinement, aimed mainly at converting the NMR spectrometer to one of higher resolution and high sensitivity.

In addition to the apparatus development, some experiments were made with the now nearly completed high-resolution spectrometer. Attempts were made to find an ion which would exist as a paramagnetic entity in molten NaOH. This would be detected by a broadening of the H^1 resonance in molten NaOH, as compared with the H^1 line with no paramagnetic ions present. The compounds Na_2CrO_4, $NiSO_4$, Na_2O_2, and $Ce(NO_3)_3$ were added individually to batches of molten NaOH. No H^1 line broadening was observed.

STUDIES OF THE GROWTH OF LARGE SINGLE CRYSTALS OF MAGNESIUM OXIDE FROM MELTS[30]

G. W. Clark

An effort is being made to develop suitable techniques for the growth of large single crystals of magnesium oxide. These single crystals will

---

[30]Work performed under subcontract No. 934 under contract W-7405-eng-26.

be machined into optical absorption cells for the study of the absorption spectra of alkaline fused salts.

Most of the research to date has been conducted by using a modified Czochralski method. A controlled electric current passing through the charge material was used to melt the magnesium oxide, and attempts were made to pull single-crystal material from this melt. Difficulties were encountered in obtaining and maintaining resistive heating. There was a tendency for an arc to be established between one of the electrodes and the charge material. Such an arc is of lower impedance and hence creates an unstable system.

The problem has been attacked most recently by using an extremely modified Verneuil process. Such a system has been assembled and is now being adjusted. It is possible that this modified process will need to be contained in a pressurized system at a few atmospheres.

HRP METALLURGY

G. M. Adamson

HRP METALLURGY

G. M. Adamson

E. S. Bomar   M. L. Picklesimer
F. W. Cooke   J. J. Prislinger
J. P. Hammond   P. L. Rittenhouse
W. J. Leonard   R. L. Stephenson

J. K. White

HRP PHYSICAL METALLURGY

M. L. Picklesimer   P. L. Rittenhouse
R. L. Stephenson

Zirconium Alloy Development

Zirconium-niobium alloys have shown promise in having an in-pile corrosion resistance superior to that of Zircaloy-2 in the uranyl sulfate solutions of interest to HRP. An alloy development program has been under way for the past year with the objective of improving the corrosion resistance of zirconium-niobium alloys and of determining the transformation kinetics and mechanisms of the alloy system.[1-5] Beta-quench and reheat studies of the transformation kinetics, products, and mechanisms are being made by using the techniques of hardness measurements, metallography, and x-ray diffraction. The principal effort has been on Zr–15% Nb and Zr–15% Nb–X alloys. Ternary additions of Al, Cu, Th, Pd, Pt, Mo, Fe, Ni, and Cr have been made in amounts from 0.5 wt % for Cu, up to 5 wt % for Pd, Pt, and Mo. A small quantity of in-pile corrosion data has been obtained for some of the ternary alloys, and for binary alloys containing 15 and 20 wt % Nb.[6-8] While insuffi-

cient corrosion data have been obtained to determine completely the effects of heat treatment and alloy content, the trend is such as to indicate that the beta-quenched condition is the best and that additions of palladium and platinum improve the corrosion resistance of the Zr–15% Nb alloy. Most of the effort to date has been expended on the physical metallurgy of the alloy systems since a complete knowledge and understanding of the morphology and transformation kinetics of the alloy are necessary in order to properly select and prepare the alloy specimens for in-pile corrosion experiments.

The following are the major conclusions reached to date:

1. Three major transformation products are observed in the Zr-Nb eutectoid decomposition.

2. A Widmanstätten type platelet precipitate forms in a retained beta matrix on quenching. This platelet precipitate will redissolve in the beta matrix, when heated to subcritical temperatures, without the decomposition of the beta phase.

3. At all temperatures of transformation below 550°C an age hardening transformation occurs in which the retained beta phase, a body-centered cubic structure with $a_0 = 3.5435$ Å for the Zr–15% Nb alloy, transforms into two body-centered cubic structures, one of which is zirconium rich and the other niobium rich, whose compositions and lattice constants change with aging time and temperature toward Zr–5% Nb and Nb–15% Zr (see "An X-ray Diffraction Study of Aging in Zirconium-Niobium Alloys" this report). At least two, and possibly three, aging peaks occur. Maximum hardening occurs within 8 min at 400°C for the beta-quenched and reheated Zr–15% Nb alloy; less hardening occurs at higher temperatures and much longer times are required to reach a given hardness at lower temperatures. Overaging has been observed only at and above 500°C in two weeks.

4. At temperatures above 550°C, but below the eutectoid temperature of about 615°C, the transformation occurs sluggishly by a precipitation of

[1]M. L. Picklesimer, G. B. Wadsworth, and O. Zmeskal, *Met. Semiann. Prog. Rep. Oct. 10, 1956*, ORNL-2217, p 153ff.

[2]G. M. Adamson *et al., HRP Quar. Prog. Rep. Oct. 31, 1956*, ORNL-2222, p 114ff.

[3]G. M. Adamson *et al., HRP Quar. Prog. Rep. Jan. 31, 1957*, ORNL-2272, p 119ff.

[4]G. M. Adamson *et al., HRP Quar. Prog. Rep. April 30, 1957*, ORNL-2331, p 124ff.

[5]G. M. Adamson *et al., HRP Quar. Prog. Rep. July 31, 1957*, ORNL-2379, p 122.

[6]G. H. Jenks *et al., HRP Quar. Prog. Rep. Jan. 31, 1957*, ORNL-2272, p 102, esp 115.

[7]G. H. Jenks *et al., HRP Quar. Prog. Rep. July 31, 1956*, ORNL-2148, p 93ff.

[8]G. H. Jenks *et al., HRP Quar. Prog. Rep. July 31, 1957*, ORNL-2379, p 92.

alpha platelets at the grain boundary (in a fashion similar to that of bainite in steels) with a consequent enrichment of the neighboring beta phase in niobium, followed by a precipitation of Nb–15% Zr (approximately) between the alpha needles, and with the remainder of the transformation occurring by the formation of alpha-zirconium and Nb–15% Zr (approximate) platelets from the retained beta matrix. The transformation is very sluggish (a Zr–15% Nb specimen contained 50% retained beta phase after two weeks at 600°C).

5. Increasing the niobium content slows down the rate of reaction and increases the incubation time for all of the transformations with the exception of the Widmanstätten platelet phase formed on quenching from the beta field.

6. Ternary alloying additions of palladium, platinum, and molybdenum to the Zr–15% Nb alloy speed up the transformation occurring at and above 550°C, but delay or inhibit the aging transformation occurring below 550°C. Iron, nickel, and chromium have similar tendencies but are not as potent. Aluminum and copper delay the hardening appreciably as well as decrease the temperature for the maximum rate of hardening to below 400°C.

7. Sponge-base alloys (containing oxygen from the sponge zirconium) transform faster at all temperatures.

8. High strengths with some ductility can be obtained by proper aging treatments. A sponge Zr–15% Nb alloy beta quenched and aged at 550°C for two weeks had, at room temperature, a 0.2% offset yield strength of 140,000 psi, an ultimate tensile strength of 150,000 psi, and an elongation of 9% in 1 in.; at 300°C it had a yield strength of 90,000 psi, an ultimate strength of 108,000 psi, and an elongation of 16% in 1 in.

A representative series of microstructures of the Zr–15% Nb alloy system is shown in Fig. 77. Aging curves for the Zr–15% Nb alloy are given in Fig. 78 for specimens aged in Vycor capsules, where the heating rates are not very fast, and in Fig. 79 for specimens aged in the isothermal transformation machine, where the specimens reached the aging temperature in $2\frac{1}{2}$ sec. Aging curves and structures for the ternary alloys have been presented in previous reports.[1-5] Isothermal transformation studies have also been initiated for the Zr–15% Nb–X alloys but the data are too few to report at the present time.

Morphology of Zircaloy-2

Studies on the morphology and properties of Zircaloy-2 have continued on a reduced scale. An embrittlement of the Zircaloy-2 impact specimens exposed in in-pile loop "GG" and a metallographic examination of the broken specimens resulted in a series of heat treatment tests to determine if the microstructure and impact brittleness of the specimens could be caused by heat treatment alone. Specimens were capsulated in Vycor in purified argon and heat treated at 810, 820, and 830°C for 5, 10, and 15 min, and broken by impact. The resulting impact curve and the microstructures of the specimens resulting from the heat treatment showed that the embrittlement and microstructures observed in the loop "GG" impact specimens were caused by a damaging heat treatment sometime during their history and not by the irradiation exposure.[9]

Fabrication of $\frac{3}{16}$-, $\frac{1}{4}$-, $\frac{3}{8}$-, and $\frac{1}{2}$-in. Zircaloy-2 plate and of Zircaloy-2 rod with diameters ranging from $\frac{3}{8}$ in. to $1\frac{1}{4}$ in. by commercial fabricators has shown that (1) the fabrication schedule developed and reported[10] can be followed successfully in commercial practice, and (2) the resulting material is free of intermetallic stringers but not of gas stringers, is much "cleaner" in its microstructure in that very little grain boundary or grain matrix precipitate is visible at any magnification under the optical microscope, and the degree of preferred orientation of the fabricated material is much less than that resulting from prior fabrication schedules.[11] Mechanical property studies will be performed in the near future on some of the plate fabricated to the new schedule.

The Effect of Alloying Elements on the Alpha-Zirconium Solubility for Hydrogen

The effect of several alloying elements on the alpha-zirconium solubility for hydrogen at temperatures above 450°C has been studied, under a research contract, by O. Zmeskal[12] at the University

[9]G. M. Adamson *et al.*, *HRP Quar. Prog. Rep. Oct. 31, 1956*, ORNL-2222, p 114ff.

[10]M. L. Picklesimer and G. M. Adamson, *Development of a Fabrication Procedure for Zircaloy-2*, ORNL CF-56-11-115 (Nov. 21, 1956).

[11]M. L. Picklesimer, G. B. Wadsworth, and O. Zmeskal, *Met. Semiann. Prog. Rep. Oct. 10, 1956*, ORNL-2217, p 153.

[12]G. M. Adamson *et al.*, *HRP Quar. Prog. Rep. July 31, 1957*, ORNL-2379, p 122.
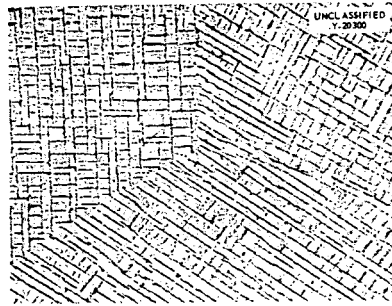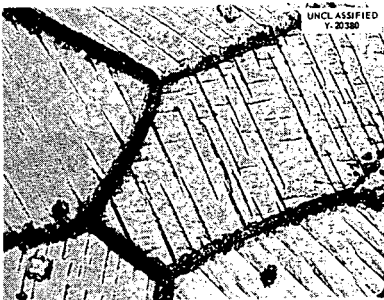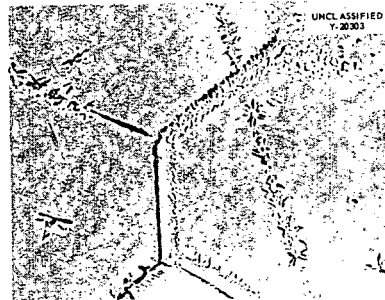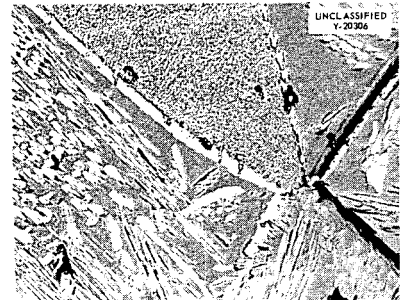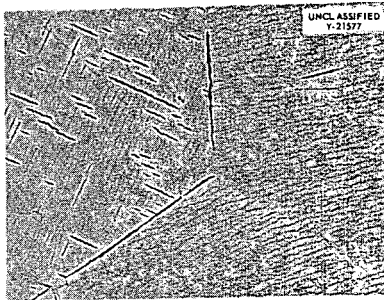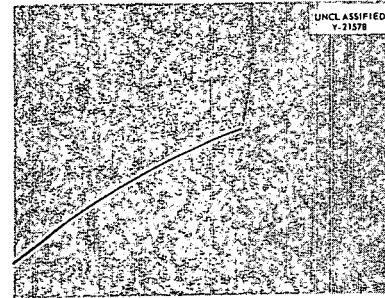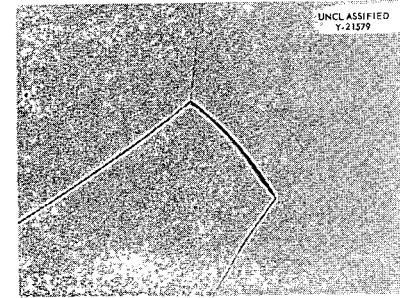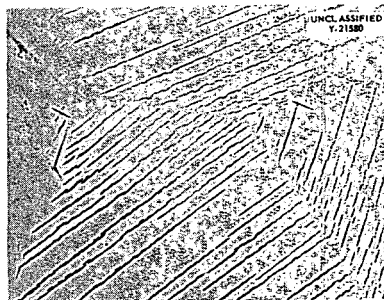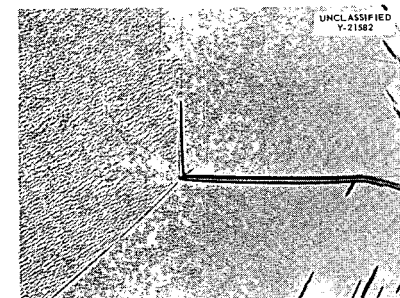
Fig. 77. Microstructures of Aged Quench-and-Reheat Specimens of Zr–15% Nb Alloy, Capsulated. 750X. Reduced 52%.
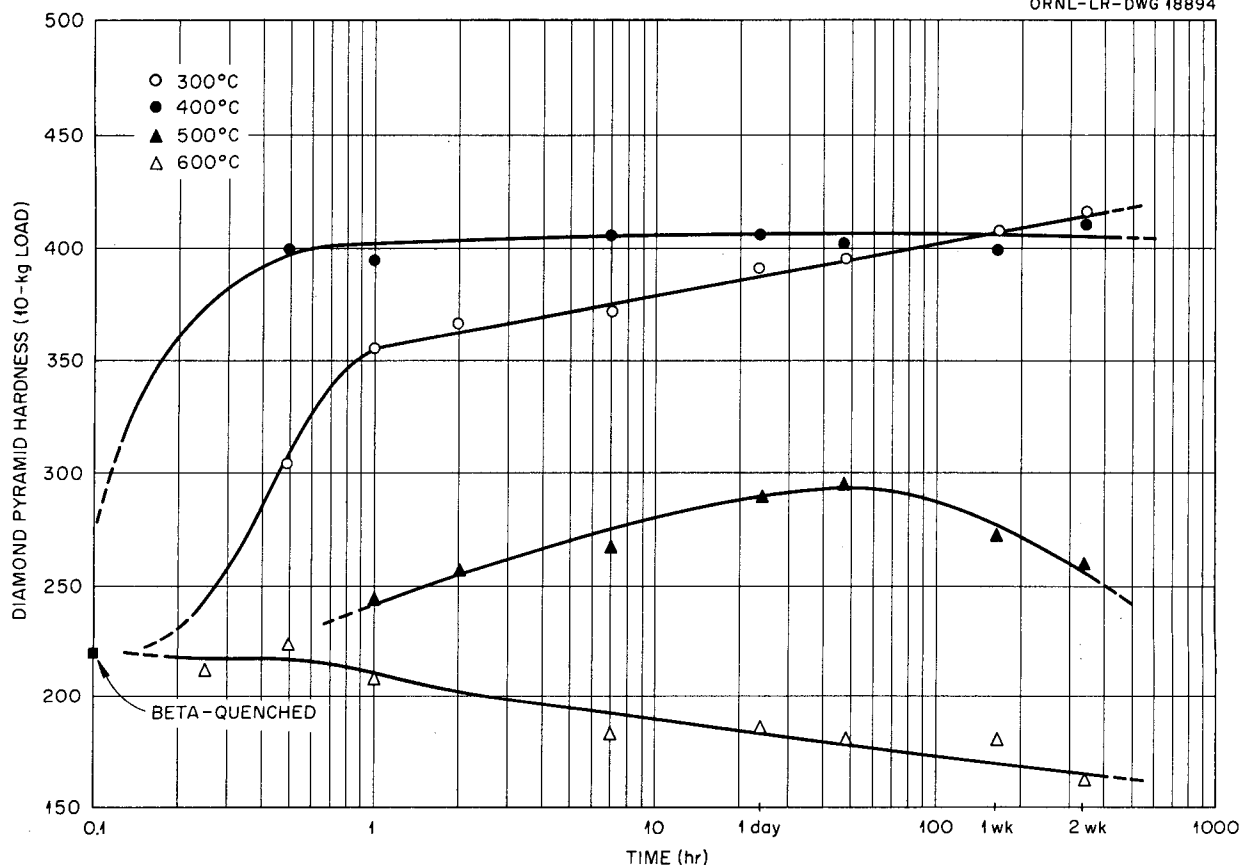
Fig. 78. Time-Temperature-Hardness Curves for Zr—15% Nb Alloy, Beta Quenched from 900°C and Reheated in Capsules.

of Florida. A modified Sievert's apparatus was used to determine the equilibrium hydrogen overpressure as a function of temperature, hydrogen content, and alloying elements. Results on high-purity zirconium used to test the apparatus and procedure have agreed quite well with published data. Considerable difficulty was encountered in reaching equilibrium conditions for the alloys because the time required for equilibrium to be established was so long that the virtual leak rate of the system began to interfere seriously with the pressure measurements. Several experiments involving various means of speeding up the rate of approach to equilibrium were tried without success. Results were obtained for some of the alloys at temperatures above 600°C. The contract has been terminated and a final report is expected shortly.

Special Zirconium Alloys —Mechanical Properties

The Armour Research Foundation of the Illinois Institute of Technology has been investigating, under a research contract, the stability of weldable beta- and alpha-zirconium-base alloys for applications under stress at temperatures up to approximately 300°C. The tensile ductility and the deterioration of impact strength are being studied as functions of time at operating temperatures, of stresses, and of heat treatment.

The work on the all-alpha alloys was summarized in a prior report as was a small amount of work performed on the Zr—15% Nb—X alloys.[13] Recent results on the tensile properties of the Zr-Nb-X

[13]G. M. Adamson *et al., HRP Quar. Prog. Rep. Jan. 31, 1957,* ORNL-2272, p 119ff.
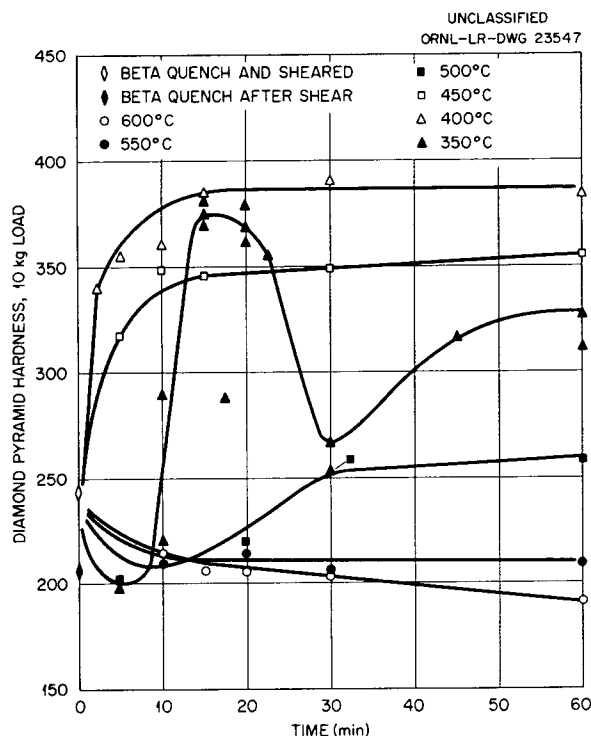
Fig. 79. Time-Temperature-Hardness Curves for Zr–15% Nb Alloy, Beta Quenched and Aged in Transformation Machine.

alloys have also been reported.[12] No tensile impact results have been reported but will be reported in the final summarizing report to be received shortly. Ultimate tensile strengths as high as 200,000 psi with elongations of 2% have been obtained. Certain heat treatments have resulted in brittle fracture, no elongation, and low fracture strengths.

MECHANICAL METALLURGY

J. J. Prislinger

The Effect of Hydrogen on the Embrittlement of Titanium at 300°C

This study was initiated as a result of commercially pure titanium failing in an apparently brittle manner under test loop conditions. The various details involving impact specimen geometry and orientation, vacuum-annealing, and hydrogenation have been reported previously.[14]

[14]G. M. Adamson et al., HRP Quar. Prog. Rep. Jan. 31, 1957, ORNL-2272, p 114, esp 124.

The room-temperature impact strength of as-received, commercially pure A-55 titanium (containing 30 ppm hydrogen) was not impaired upon aging at 300°C for times up to 5040 hr,[14,15] as is indicated in Fig. 80. Upon altering the hydrogen content of the as-received material from 30 ppm to a range of values from 10 to 140 ppm, as is shown in Fig. 80, there was no indication of embrittlement due to aging at 300°C for times up to 5040 hr; however, the room-temperature impact strength fell quite rapidly with increasing hydrogen content.

Brittle Fracture Study

A brittle fracture with the usual rapid and extensive cracking would be extremely serious if it occurred in a reactor system. The mechanics of brittle failure have just recently begun to be understood in steels and practically no information is available on the hexagonal metals. A joint program with the Solid State Division has been set up to study brittle failure. The present studies on this program are with the V-notch impact test and with the drop-weight test.

The drop-weight test is accomplished by dropping a known weight from a predetermined height upon a plate of standard size. A crack is started in the base metal by welding brittle crack-starter material to the tension or under side of the test plate.[16] It is desirable to know the particular temperature (the nil-ductility-transition or NDT temperature) at which, with limited deformation, the crack will propagate through the plate. The NDT temperature may be defined as the temperature at which the metal being tested loses its ability to deform in the presence of a sharp crack.[17]

This study is being coordinated with full-size Charpy V-notch and subsize Izod impact tests in order to better understand the various relationships influencing brittle fracture and ultimately how these various testing techniques can forecast the temperature, or temperature range, where a transition from ductile to brittle behavior occurs for present or tentative reactor materials.

[15]G. M. Adamson et al., HRP Quar. Prog. Rep. July 31, 1957, ORNL-2379, p 127.

[16]P. P. Puzak, M. E. Schuster, and W. S. Pellini, Welding J. 33, 4815 (1954).

[17]Rem-Cru Titanium Data Sheet, Rem-Cru Titanium Inc., Midland, Pa., 1956.
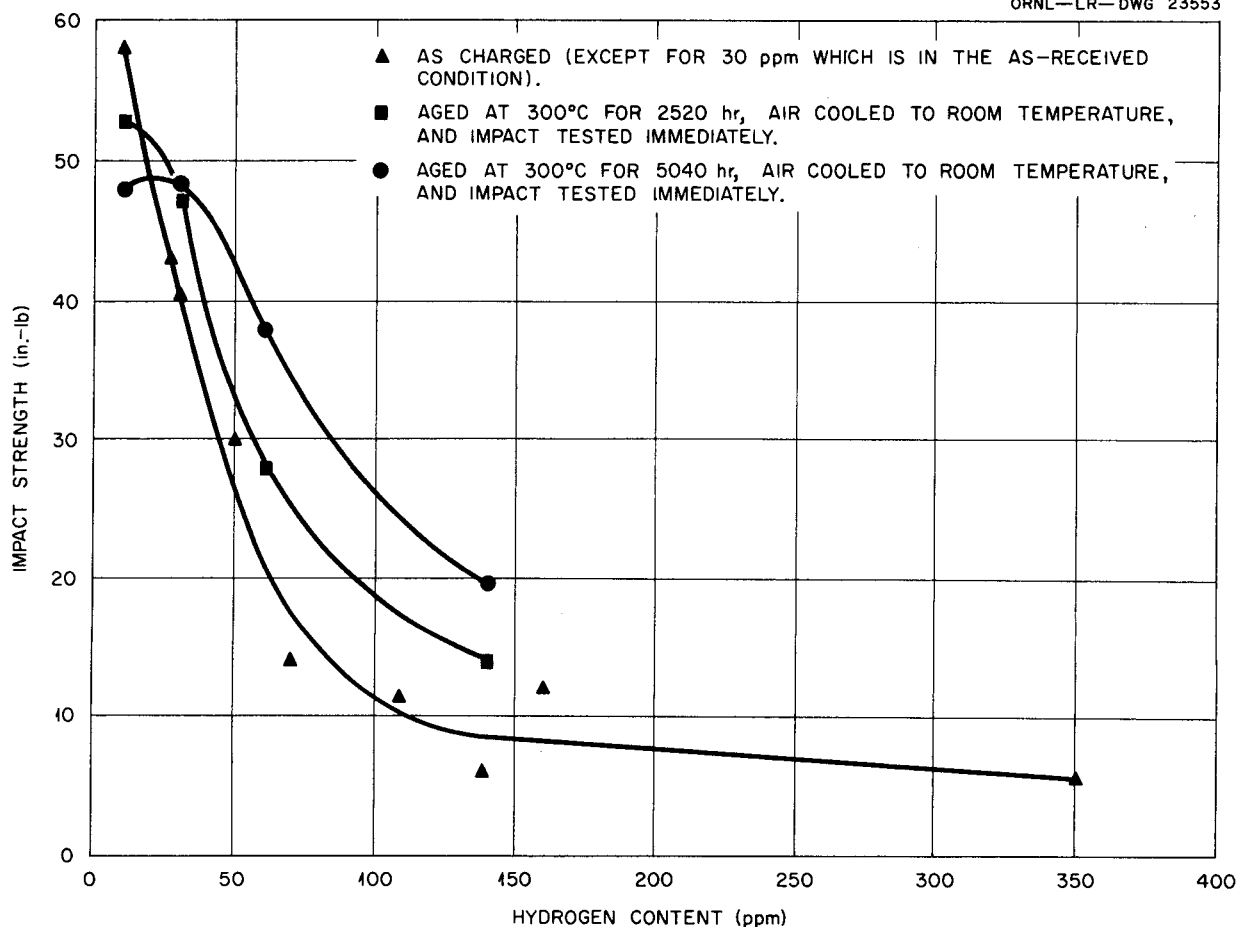
Fig. 80. Change in Impact Strength of A-55 Titanium with Hydrogen Content and Aging Time.

Titanium Alloys

For the drop-weight study of titanium alloys the brittle crack-starter material was made by hydrogenating welding wire or strips cut from the metal.

A Charpy V-notch impact curve for MST Grade 3 (high-purity commercial) titanium is shown in Fig. 81. This curve confirms the data found in the literature for similar alloys.[16] This material was shown to have an unexpectedly low NDT temperature, below −320°F. In all the drop-weight specimens broken at room temperature or lower a small crack propagated about $\frac{1}{8}$ in. into the base metal. It has not yet been determined whether these small cracks are caused by contamination during welding or indicate a brittle zone in the heat-affected area. The thermal cycling of this material ten times from room temperature to 575°F, such as

would occur in a heat exchanger, was shown to have no effect on the shape of the curve or on the impact values.[18] Also shown on Fig. 81 is a curve in which per cent of lateral expansion, as measured on the side opposite the notch, is plotted against fracture temperature. While the significance of this measurement is not understood, it would seem to indicate an increase in ductility in the range of 450 to 550°F where the impact curve had indicated a small decrease.

The possible danger in using titanium alloys of questionable history is shown by the impact curve in Fig. 82. This curve was obtained from some old A-75 (moderate-purity commercial) titanium which

---

[18]G. M. Adamson *et al., HRP Quar. Prog. Rep. April 30, 1957,* ORNL-2331, p 124, esp 132–133.
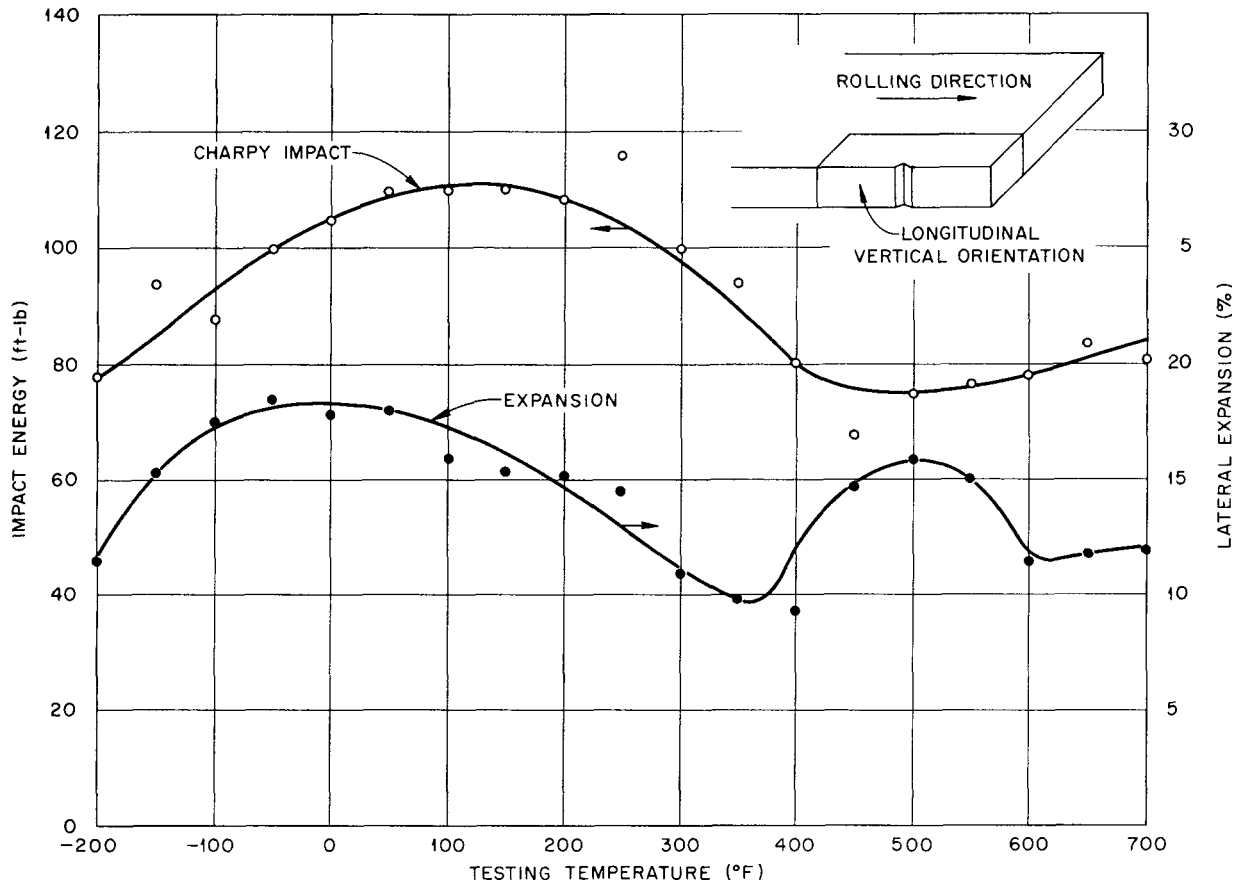
Fig. 81. Charpy V-Notch Impact Strength and Change in Lateral Expansion for High-Purity Commercial Titanium.

contained 400 ppm of hydrogen. With this material the NDT temperature has increased to 220°F and the shape of the impact curve is completely changed. Such material could very easily fail in a brittle manner under impact loading.

The relationship between the Charpy impact curve and the NDT temperature for a 6% Al–4% V titanium alloy, an alpha + beta alloy, is shown in Fig. 83. With this alloy, containing 95 ppm of hydrogen, the NDT temperature was found to be –140°F. This material exhibited a very pronounced shear lip whose size decreased with decreasing fracture temperature but was still visible at the lowest temperature studied. The persistence of this lip below the NDT temperature is contrary to what is found with steels, and since it indicates some ductility below the NDT temperature, it is inconsistent with the definition. These differences will be resolved by additional testing.

Zirconium Alloys

All mechanical property work with zirconium alloys has been with Zircaloy-2 (1.5% Sn–0.1% Cr–0.15% Fe–0.05% Ni), which is the alloy used for the HRT core tank. With present fabrication procedures this material is very anisotropic as shown by Charpy V impact tests. Charpy impact values from samples cut from two directions in the same plate are shown in Fig. 84. These curves are thought to be the extremes, but the complete data for other orientations are not yet available. Even with the poor impact strengths the NDT temperature for this material was found to be low, –250°F.

Steels

An understanding of the phenomena of brittle fracture in steels is necessary so that adequate design criteria may be developed for reactor pressure vessels.
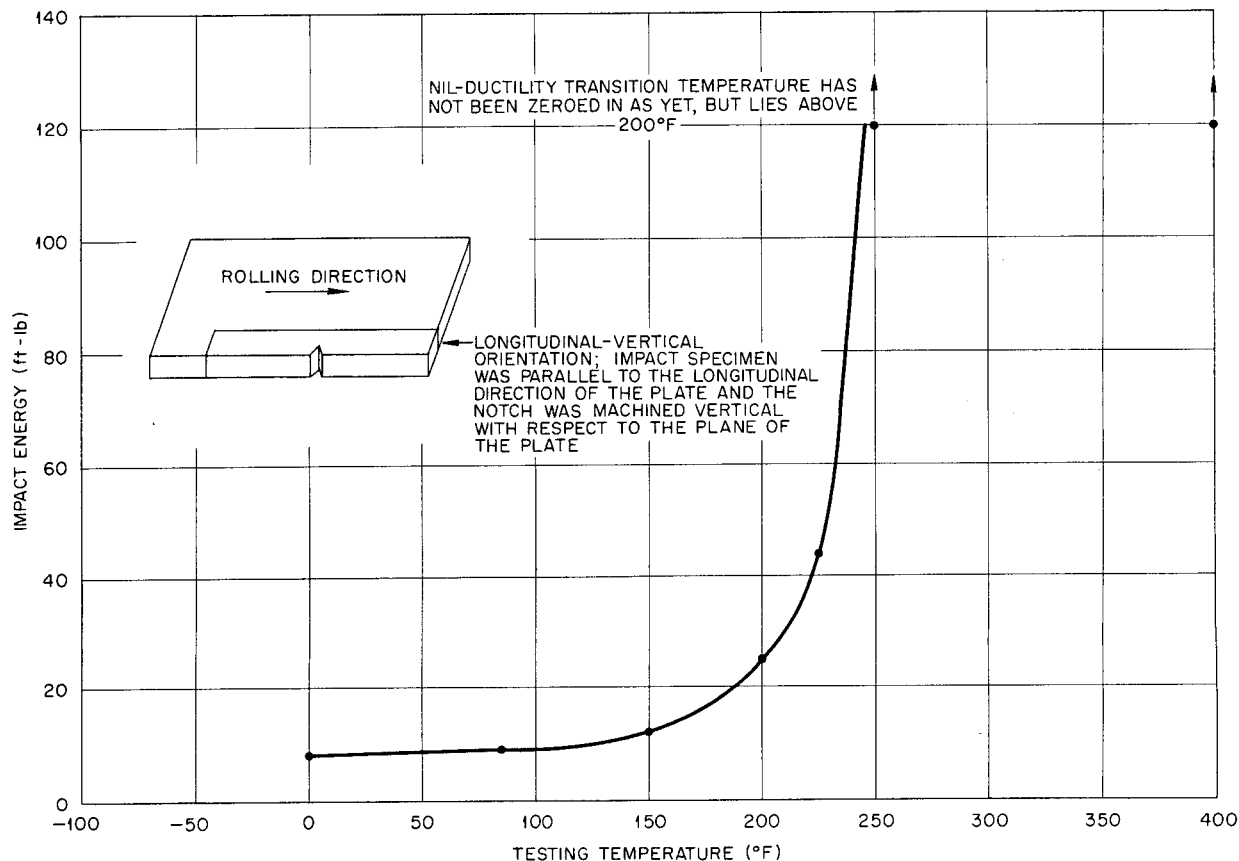
Fig. 82. Charpy V Impact Strengths of A-75 Titanium.
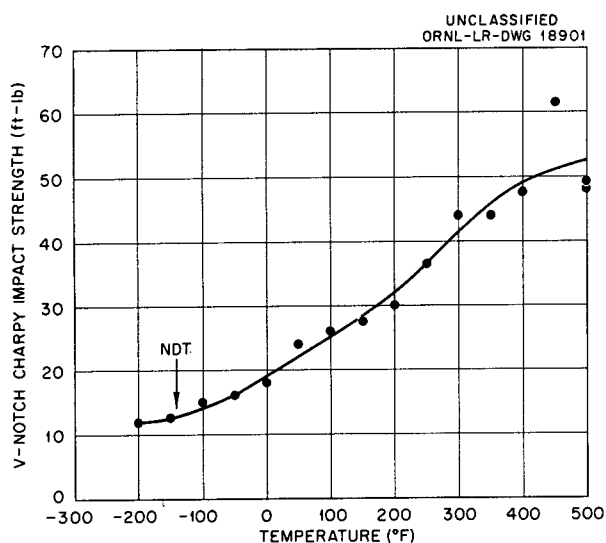
Fig. 83. Charpy V Impact Strengths of 6 Al–4 V Titanium.

The curves in Fig. 85 illustrate the danger in the commonly accepted practice of basing brittle-fracture data on impact curves. The upper curve was obtained from the same plate material used for the lower curve, except that it had been normalized at 1700°F for 1 hr and air-cooled to room temperature. The NDT temperatures indicate that the normalized material is brittle below –20°F with impact values of 30 ft-lb, while the as-received material is brittle below 10°F but has impact values of only 4 ft-lb at slightly higher temperatures.[19]

Drop-weight tests were performed on three pressure vessel steels with the results tabulated in Table 30.

[19]G. M. Adamson *et al., HRP Quar. Prog. Rep. Jan. 31, 1957,* ORNL-2272, p 114, esp 124.
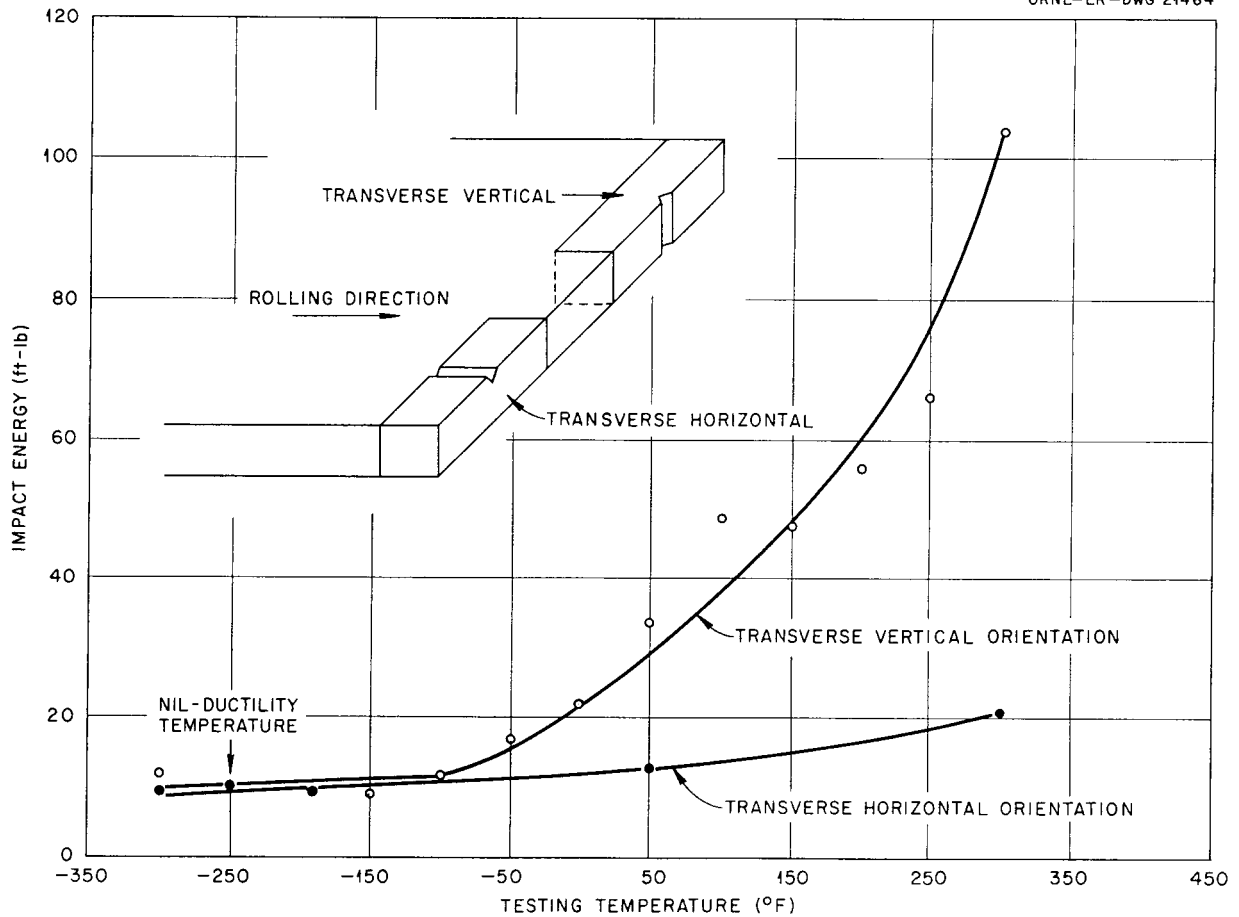
Fig. 84. Effect of Specimen Orientation on Charpy V Impact Strength of Zircaloy-2.
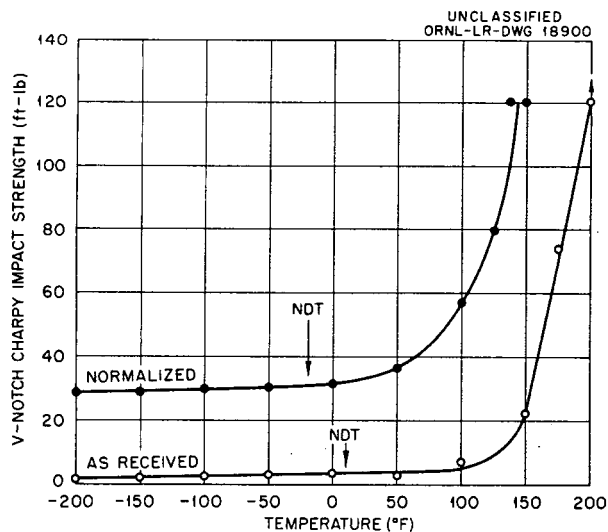
Fig. 85. Charpy V Impact Curves for Ferro-Vac-10 Steel.

Loop Radiation Effects on Zirconium Alloys

Subsize, multibreak tensile and impact specimens of Zircaloy-2[20,21] were irradiated in corrosion loops built and operated by the Corrosion Group of the Reactor Experimental Engineering Division. These tests were to determine if any harmful mechanical property changes occurred in Zircaloy-2 through neutron irradiation or from changes resulting from the loop environment, that is, hydrogen.

The tensile specimens were exposed in loop L-2-10, which circulated oxygenated uranyl sulfate solution for 1672 hr at 280°C for a total reactor exposure of 3765 Mwhr with an integrated fast-neutron

[20]M. L. Picklesimer, G. B. Wadsworth, and O. Zmeskal, *Met. Semiann. Prog. Rep. Oct. 10, 1956,* ORNL-2217, p 153ff.

[21]G. M. Adamson *et al., HRP Quar. Prog. Rep. April 30, 1957,* ORNL-2331, p 124ff.

Table 30. Nil-Ductility-Transition Temperatures for Pressure Vessel Steels

Type Steel	Condition	NDT Temperature (°F)	Maximum Temperature with Partial Cracking (°F)
A212-B	As received	−100	−65
	Normalized	− 80	−45
A285-A	As received	0	15
	Normalized	− 10	20
A301-B	1660°F for 1½ hr, furnace cooled to 1100°F, air cooled	− 10	10

dose varying with sample position from 1.7 to 3.2 × 10^{19} *nvt*. Under conditions of exposure in this loop, no significant change in tensile properties was found between specimens exposed to the full flux (core samples), those exposed to the same solution but at very low flux (in line samples), and the control specimens.[22] For comparative purposes, the data are summarized in Table 31.

Subsize Zircaloy-2 V-notch impact specimens were irradiated in in-pile loop L-4-12. This loop circulated oxygenated uranyl sulfate for 2020 hr at 250°C for a total reactor exposure of 4386 Mwhr. The fast-neutron flux is not known in this facility but it is lower than that for the other loop. The curve plotted in Fig. 86 shows no difference between the control and the irradiated samples either in values or in the shape of the curve.

WELDING DEVELOPMENT

W. J. Leonard

Stainless Steel

Corrosion studies using thorium oxide slurries have shown increased attack where excessive push-through occurs in a weld. Proposed HRP slurry systems will therefore require even closer welding control than has been previously required. In an attempt to consistently obtain high quality welds while using production techniques, considerable work has been done in which preplaced

inserts have been used for the root pass. Such studies have been made with both stainless steel and titanium weldments.

With type 347 stainless steel, satisfactory techniques have been developed by using the Electric Boat (EB) type of insert, a washer type, and with a round wire insert.[23] With the EB-type insert the procedures have been qualified and a

---

[23]G. M. Adamson *et al.*, *HRP Quar. Prog. Rep. April 30, 1957*, ORNL-2331, p 124, esp 136–138.

UNCLASSIFIED
ORNL-LR-DWG 25185
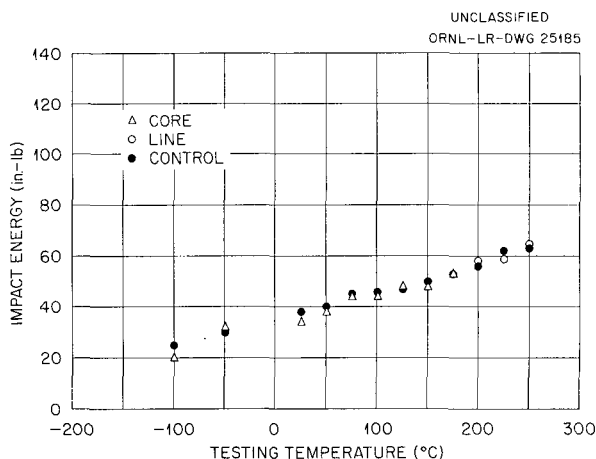
Fig. 86. Comparison of Impact Strengths of Irradiated and Control Samples of Zircaloy-2. Rod was ⅜ in. drawn to 0.250 in.; vacuum annealed at 750°C for 2 hr and furnace cooled; machined to 0.200 × 0.200 in. impact specimens; run in conditions of loop L-4-12.

---

[22]G. M. Adamson *et al.*, *HRP Quar. Prog. Rep. July 31, 1957*, ORNL-2379, p 127.

welding specification written.[24] Subsequent work has shown that a simple round wire insert is much cheaper to make, and easier to fit up than the other type. Welding with this simple insert requires slightly more skill and control than does an EB insert, but it is still easier and the results are more reproducible than when the filler wire is hand fed. A welding procedure for the simple O-ring insert is now being written. These results with stainless steel closely parallel those previously reported for titanium.[25]

Titanium Alloys

The air-welding procedure developed for welding high-purity titanium,[25,26] A-40, has been extended

---

[24]HRP Welding Specification No. 9 — Inert Gas-Shielded Arc Welding of Chromium Nickel Stainless Steels Using Pre-Placed Root Insert Rings.

[25]W. J. Leonard and C. H. Wodtke, *Met. Semiann. Prog. Rep. Oct. 10, 1956,* ORNL-2217, p 162—164.

[26]HRP Welding Specification No. 7.

Table 31. Tensile Data from Subsize Zircaloy-2 Samples Irradiated in
Uranyl Sulfate in an In-Pile Corrosion Loop L-2-10

Specimen No.	Loop Position	Temperature (°F)	Strain Rate $(in.\cdot in.^{-1}\cdot min^{-1})$	Tensile Strength (psi)	Proportional Limit (psi)	Reduction in Area (%)
17	Core	*	2.0	89,225	72,550	44.7
21	Line	*	2.0	88,225	63,725	33.9
23	Control	*	2.0	88,225	60,800	44.3
19	Control	*	2.0	87,450	60,400	40.0
1	Core	*	0.05	77,650	62,350	48.0
5	Line	*	0.05	79,600	53,925	40.0
3	Control	*	0.05	80,000	55,875	42.7
7	Control	*	0.05	79,200	62,750	46.1
13	Core	*	0.002	72,950	47,050	44.0
9	Line	*	0.002		47,050	45.9
11	Control	*	0.002	68,625	41,175	43.1
15	Control	*	0.002	63,725	35,300	45.1
18	Core	600	2.0	48,400	33,725	73.0
22	Line	600	2.0	47,050	30,600	74.9
24	Control	600	2.0	43,375	29,400	73.1
20	Control	600	2.0	42,750	27,050	68.9
2	Core	600	0.05	38,825	21,575	71.2
6	Line	600	0.05	41,175	28,625	70.7
4	Control	600	0.05	42,600	25,500	69.4
8	Control	600	0.05	42,500	25,100	66.2
14	Core	600	0.002	36,475	21,950	79.5
10	Line	600	0.002	34,500	23,525	69.9
12	Control	600	0.002	36,850	25,500	68.2
16	Control	600	0.002	28,475	21,575	73.8

*Room temperature.

to include more common materials such as A-70.[27] When the impure alloys are welded in air with high-purity filler metal, the resultant welds are sound and will have mechanical strengths equivalent to those of the base metal.

The only commercial alpha-titanium alloy, A-110AT (5% Al—2.5% Sn), has been investigated as to its weldability. Samples $\frac{1}{8}$ in. thick were welded, with filler metal strips cut from the plate, using the air-welding procedure specified in HRP-11. Although this alloy is designated as an all-alpha alloy with present commercial practices, as shown in Fig. 87, it actually contains two phases. In an A-110AT weldment the heat-affected zone contains three structures. One is an area that has been completely transformed by being in the beta region and contains large grains with Widmanstätten plates. Only a small transition region is found which shows a slightly larger amount of second phase than was found in the base metal, and in the hottest portion a few matrix grains are found with the Widmanstätten pattern. The remaining large portion shows no change from the base metal.

---

[27]G. M. Adamson *et al.*, *HRP Quar. Prog. Rep. July 31, 1957*, ORNL-2379, p 122, esp 131.

UNCLASSIFIED
Y-23315
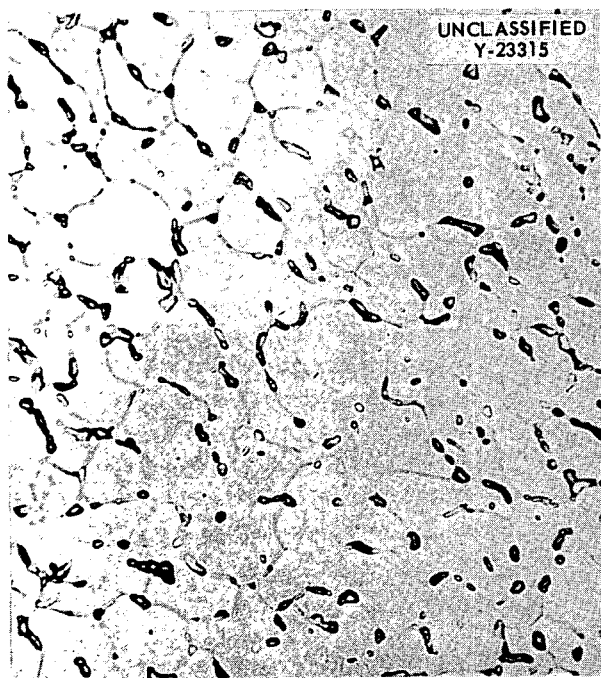
Fig. 87. Microstructure of Titanium A-110AT Base Plate. 750X.

These welds do not show nearly as much duplex structure as would be predicted from samples heated in the laboratory. It is thought that the kinetics of the reaction are not sufficiently rapid for the transformations to occur in the short time a weld zone is in the required temperature range. The effects on multipass welds have not been determined.

Figure 88 is a plot of a microhardness survey of a weldment cross section. Figure 89 is a photograph of guided bend tests taken from the weldment (etched for photographic results). All these tests indicate that the welds are sound and that they have not suffered from contamination or harmful transformations. No evidence of cracking was found even in the narrow transition region.

METALLURGICAL DEVELOPMENT AND SERVICE

J. P. Hammond   G. M. Adamson

Active-Metal Aqueous-Solution Reactions

In an HRP valve testing program two sets of titanium alloy valve trims failed by a rapid burning.[28] The first failure occurred while oxygenated uranyl sulfate was circulated through a 6% Al—4% V titanium alloy and the second while oxygenated wash water was circulated through a 4% Al—4% Mn titanium alloy.

A project-sponsored program was initiated at Stanford Research Institute to determine the conditions essential for initiating and sustaining such reactions. It was shown that titanium will ignite and be completely consumed if ruptured at room temperature in an atmosphere containing 350 psi or greater oxygen pressure. The rupture may occur either in a $\frac{1}{4}$-in. tensile bar or in a thin rupture disk. If the temperature is increased to 300°C, the oxygen pressure required for ignition decreases to 250 psi. No reaction has been obtained with rupture in water saturated with oxygen. In a series of comparison tests, titanium and zirconium ignited after being ruptured in 1000 psi oxygen, while magnesium, aluminum, and stainless steel did not.

Under another subcontract Aerojet General Corporation is endeavoring to determine if differences exist between the reactions of molten

---

[28]J. P. Hammond, T. M. Kegley, Jr., and G. M. Adamson, *Failures of Titanium Alloy Trim in HRP Dump Valve Loop*, ORNL CF-56-8-214 (Aug. 15, 1956).
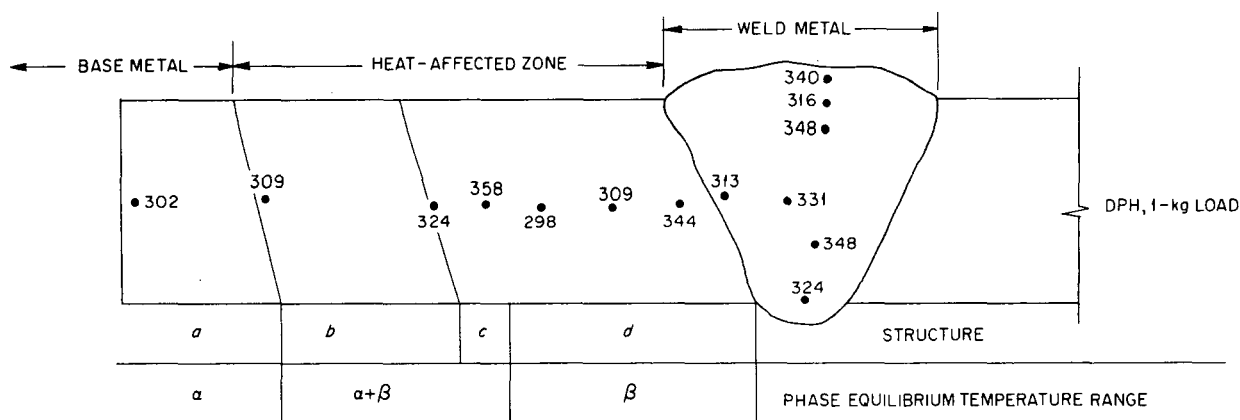
Fig. 88. Microhardness Traverse Across Titanium A-110AT Weldment. (a) Alpha matrix with prior beta within grains adjacent to grain boundaries and corners; (b) same as a with slight increase of 2nd phase near c; (c) transition structure combination of b and d; (d) Widmanstätten pattern similar to beta-quenched material.

1/8" A-110AT Ti Alloy Plate Weld
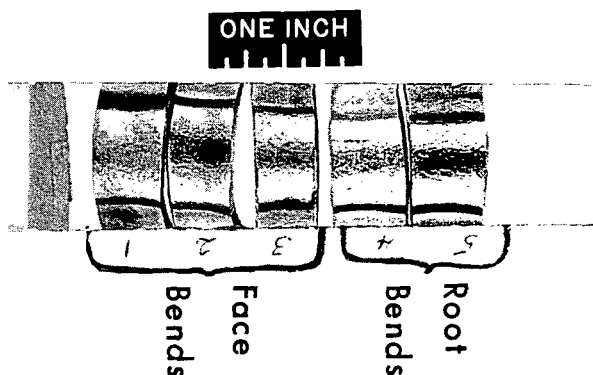
Fig. 89. Titanium A-110AT Weldment Samples After Guided Bend Test. Samples bent on 3T radius.

zirconium with water and with oxygenated uranyl sulfate. The first stage of the investigation under this contract involved the use of the explosion dynamometer.[29] Within the limits of the accuracy of this test, no differences have been found between these two reactions.

Feasibility of Roll Cladding Titanium on Steel

The Armour Research Institute has demonstrated, on an experimental basis, the feasibility of roll cladding titanium on plain carbon steel and on stainless steel.[30] Using total reductions of 80% or more at 850 to 1000°C, titanium-clad carbon steel samples of the order of $3 \times 9\frac{1}{2}$ in. in size were successfully prepared by using an intervening sheet of vanadium as a diffusion barrier. An even better cladding was obtained by employing a double diffusion barrier; a thin layer of copper was incorporated between the vanadium and the carbon steel. Such a composite may be held at temperatures as high as 1000°C without the formation of brittle diffusion zones.

Titanium can be clad on stainless steel by procedures very similar to those employed for plain carbon steel. Whereas the quality of stainless-base clads is not as good as that of their carbon-steel-base counterparts, the stainless clads nevertheless are sound and would be suitable for some applications.

[29]H. M. Higgins and R. D. Schultz, *The Reaction of Metals with Water and Oxidizing Gases at High Temperatures*, IDO-28000 (April 30, 1957).

[30]R. F. Domagala and D. W. Levinson, *The Feasibility of Roll Cladding Titanium on Steel. Summary Rep. Nov. 1, 1955 to Dec. 31, 1956*, AECU-3431.

Flange Bolt, Ferrule, and Nut Failures

Two separate cases of trouble have occurred to HRP flange fasteners in the last year. The first instance involved severe cracking of the bolts at the juncture between bolt head and shank. An investigation revealed these to be quench cracks.[31] A total of 208 bolts, many of which were removed from the HRT, were tested by the magnetic particle method. Five of the bolts showed serious cracks and 13 had surface defects of a less serious nature. A subsequent magnetic particle test which was given to all remaining HRT bolts revealed various degrees of defection.

Subsequent to this time, widespread breakage occurred to bolts as well as to ferrules and nuts which had been in service in the HRP flange test loop. This hardware was of the same lots which had shown quench cracks; however, an investigation pointed to cadmium embrittlement as the cause of failure.[32] The bolts and ferrules were made of AISI-4140, whereas the nuts were of 1040 steel. The bolts had been plated with zinc, and the nuts and ferrules with cadmium. Cadmium under the influence of service stress and a temperature of about 500°F had diffused intergranularly into the metal structure, producing embrittlement. The failures on the bolts invariably occurred in the threaded region where the cadmium-plated nut mated with the bolt.

---

[31]S. E. Beall *et al.*, *HRP Quar. Prog. Rep. Jan. 31, 1957*, ORNL-2272, p 4, esp 9.

[32]G. M. Adamson *et al.*, *HRP Quar. Prog. Rep. April 30, 1957*, ORNL-2331, p 124, esp 134.

APPLIED METALLURGY

J. E. Cunningham

PROCESS METALLURGY

R. J. Beaver

J. H. Erwin   C. F. Leitten
W. J. Kucera   W. C. Thurber
R. C. Waugh

DEVELOPMENT OF FUEL ELEMENTS FOR THE ARMY PACKAGE POWER REACTOR

W. J. Kucera   C. F. Leitten

APPR-1 Fuel Elements

Substitution of Type 347 Stainless Steel for Type 304 in APPR Fuel Elements. — Because of the heat-treatment specifications required in manufacturing APPR-1 fuel elements, an investigation has been conducted for determining the possibilities of substituting a stabilized stainless steel, type 347, for type 304. The processing of 23 plates containing 26 wt % UO_2 and 0.14 wt % B_4C dispersed in type 347 powder and clad with wrought type 347 stainless steel revealed that no appreciable changes in the specifications were required. The green-pressed densification and the densification after sintering and coining were 78.5% and 84.8%, respectively, the same values obtained previously with compacts containing type 304 stainless steel powders. A slight decrease in the core length, after fabrication into composite plates of the nominal thickness specified, indicated a somewhat greater densification in the final product, which may possibly be attributed to the replacement of type 304 stainless steel by type 347.

A longitudinal microscopic cross section of the clad dispersion is shown in Fig. 90 after hot working and in Fig. 91 after a 25% cold reduction followed by annealing at 1125°C. One fuel element containing 18 composite plates in which the steel was of the type 347 variety was brazed within the required tolerances. All the Coast Metals NP—type 347 stainless steel joints appeared to be sound after macroscopic examination.
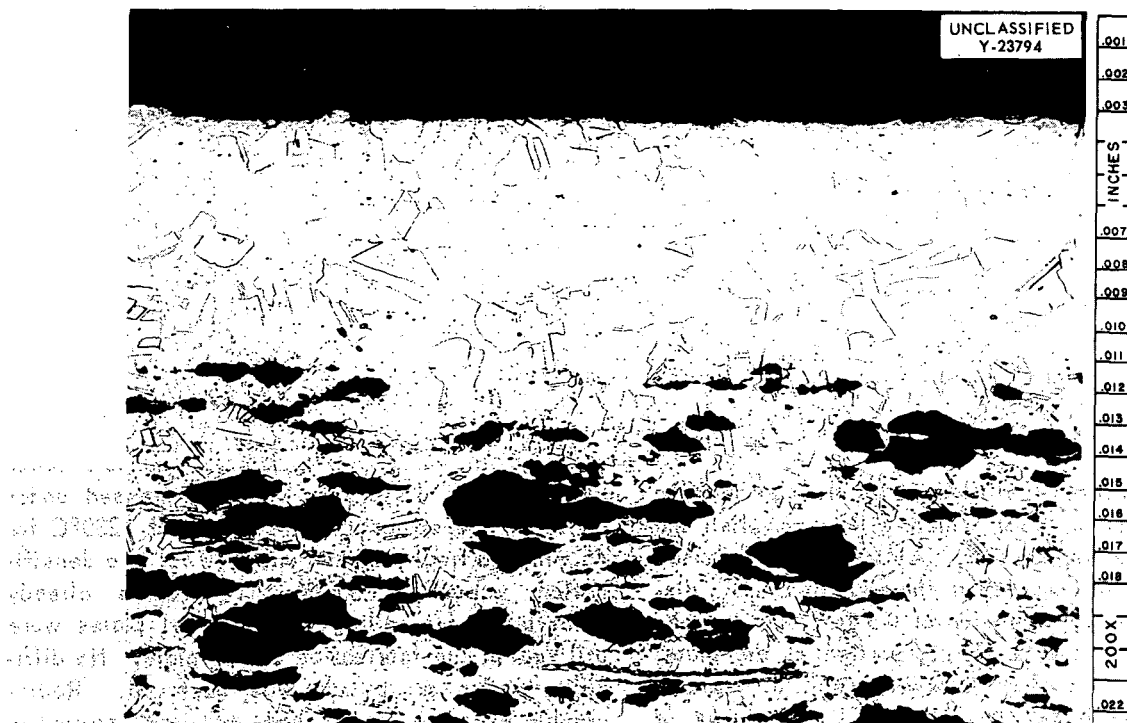
Fig. 90. Photomicrograph of As-Hot-Rolled Fuel Plate Composed of a Dispersion of UO_2, B_4C, and Type 347 Stainless Steel Clad with Type 347 Stainless Steel. Etchant: glyceria regia. Reduced 17%.

133
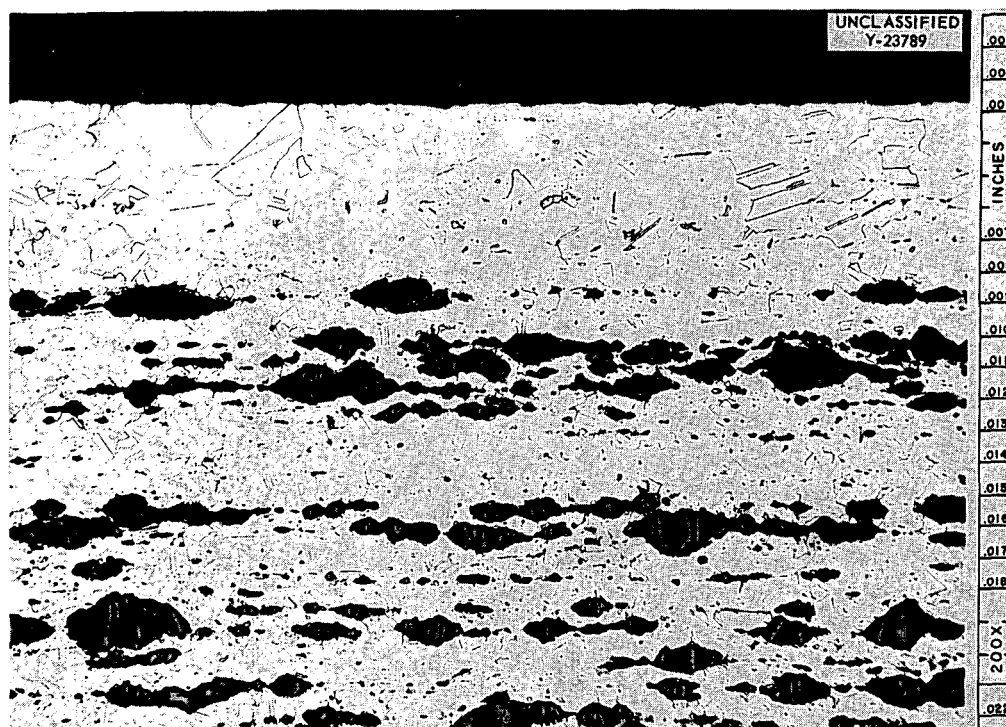
Fig. 91. Photomicrograph of Type 347 Stainless Steel Fuel Plate After 25% Cold Reduction and Anneal at 1125°C. Note degree of fragmentation which has occurred, as compared with Fig. 90. Etchant: glyceria regia. Reduced 17%.

Development of an Internal Flux Suppressor for the APPR Control-Rod Fuel Element. — In the development of the current APPR-1, it became apparent that the gap between the fuel elements and the absorber section in the control rod was sufficiently great to cause adverse flux peaking. This situation was rectified by insertion of Haynes-25 material at this location. However, considerable concern exists in regard to the cobalt activity in the system resulting from corrosion of the Haynes-25. The objective of this investigation is to eliminate this effect by enclosing a dispersion of Eu_2O_3 in stainless steel within the fuel plates of the control-rod fuel element (at the end abutting the absorber section), which will accomplish the desired flux suppression. Alco Products advised that 0.59 g of europium in the form of Eu_2O_3, dispersed along an extension of 0.5 to 1.0 in. beyond the end of the fuel-bearing portion of the plate, might be satisfactory. Development to date has been accomplished by using a Lindsay Mix of rare-earth oxides as a substitute for the highly expensive Eu_2O_3. Calculations, based on a flux

suppressor length of 0.7 in. in the finished plate, revealed that a 17.2 wt % Eu_2O_3–stainless steel dispersion occupying a volume of 0.54 cc would permit the desired europium loading.

The method selected for incorporating this quantity in the desired volume was to prepare a 0.053-in.-thick sheet of the 17.2 wt % dispersion, precision-shear the desired volume of material from the sheet, and insert it in the billet between the core and the frame.

The 17.2% rare-earth–stainless steel dispersion was easily and simply prepared by dry blending of the materials for 3 hr in an oblique blender. After blending, the dispersion was cold-pressed under 33 tsi. The compact was sintered at 1230°C for 45 min, and finally coined under 33 tsi to a densification value of 88.69%. Procedures already established for rolling APPR-1 fuel plates were utilized in the fabrication of the plate. No difficulty during processing was observed. Radiographic examination was made and is illustrated in Fig. 92. The length of the flux suppressor section is approximately $\frac{5}{8}$ in. There is a slight tendency
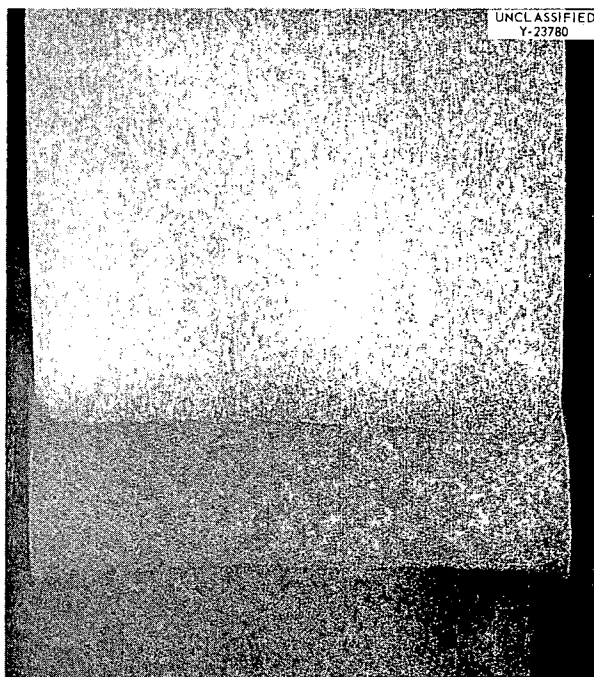
Fig. 92. Photograph Illustrating Radiographic Examination of a Fuel Plate Containing a Flux Suppressor Core of 17.2% Rare-Earth Oxide Dispersed in Stainless Steel.

for the material to tail. The effect shown is representative of five plates. It is felt that this condition can be controlled to the degree shown and is not serious. Figure 93 shows the uniformity of the rare-earth dispersion in the finished plate. Measurements of the cladding on this type of plate revealed that the cladding thickness above the rare-earth section was approximately $\frac{1}{2}$ mil less than the clad thickness above the fuel-bearing section.

All five experimental plates were rolled within tolerance, after adjusting the composition to allow for the greater densification observed with the substitution of type 347 stainless steel. At a plate thickness of 0.030 in., the fuel core length was $21\frac{3}{4}$ in., with a total length, including flux suppressor, of $22\frac{3}{8}$ in. It is proposed to manufacture one depleted fuel element containing the internal Eu_2O_3 flux suppressors, after which a fuel element containing enriched uranium will be prepared for testing in the Alco Critical Facility and later in the APPR-1.
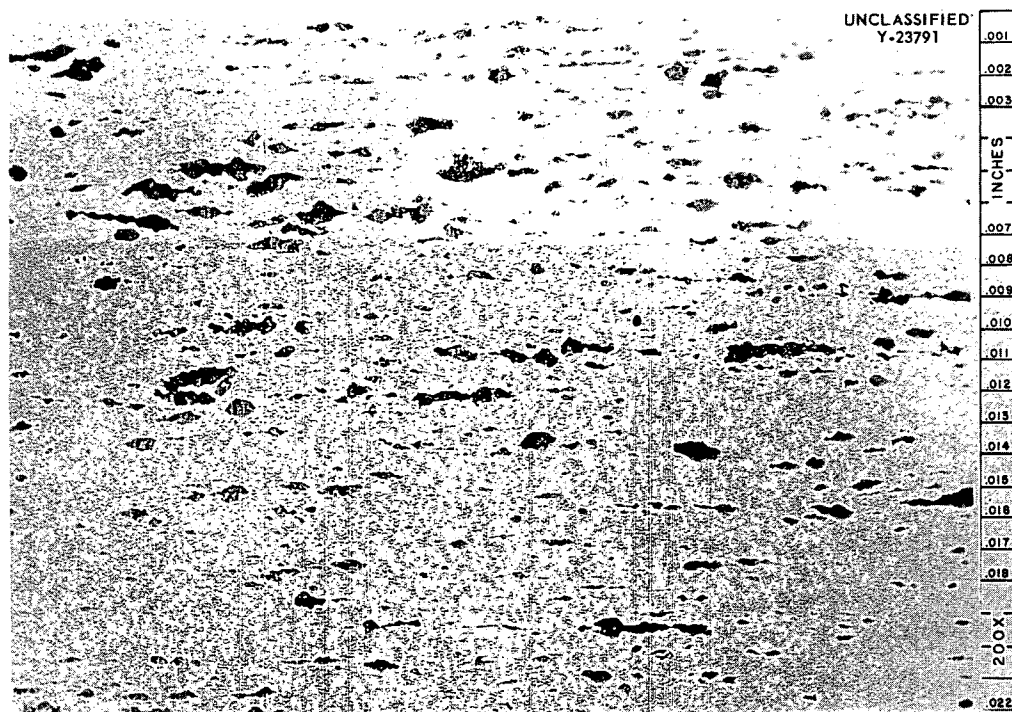
Fig. 93. Rare-Earth Flux Suppressor Dispersion in a Standard Control-Rod Fuel Plate. Note the uniformity of the dispersion. As-polished. Reduced 17%.

DEVELOPMENT OF Eu_2O_3 DISPERSIONS IN IRON-BASE MATERIALS

C. F. Leitten

Because of the uncertainty connected with the extent of irradiation damage to the present boron-bearing absorber section, an investigation has been initiated in order to develop a dispersion of Eu_2O_3 in an iron-base material, clad with stainless steel, as a replacement for the stainless-steel-clad plate containing 3 wt % B^{10} in iron.

Initial investigations were conducted with Lindsay Mix No. 921, a mixture of Sm_2O_3 and Gd_2O_3, since it was felt that this material was chemically similar to the highly expensive Eu_2O_3. Since rare-earth oxides as received from the vendor are extremely fine and porous, it was necessary to agglomerate the oxide by firing it at elevated temperatures.

A temperature of 1700°C was selected as optimum from analyses of stringering and distribution of the rare earth in subsequently fabricated plates. Figure 94 shows the marked stringering in a composite plate containing 30 wt % rare earth in type 302B stainless steel. The rare earth was fired at 1500°C prior to being crushed to −44 μ, blended with −44-μ stainless steel powder, pressed under 31 tsi, and sintered 75 min at 1230°C. Three cores, stacked above each other and separated by 5 mils of stainless steel, were encased in a billet which was evacuated and sealed. The billet was reduced to composite plate at 1150°C by using a 10% reduction in thickness per pass and a total reduction in thickness of 91%. Figure 95 illustrates the marked decrease in stringering of the Eu_2O_3 in a plate fabricated in exactly the same manner, with the exception that the rare earth was prepared by firing at 1700°C.

Direct substitution of Eu_2O_3 for the Lindsay Mix dispersion in type 302B stainless steel resulted in a reaction during sintering which was reflected by an increase in volume instead of the usual shrinkage observed with the Lindsay Mix. The products of this reaction can be seen in Fig. 96, which is an electron micrograph of a 30 wt % Eu_2O_3 dispersion in type 302B stainless steel. Results of compatibility tests of compacts of 30 wt % Eu_2O_3 dispersion in nickel, iron, and various types of stainless steel powders, sintered at various temperatures, are listed in Table 32. The
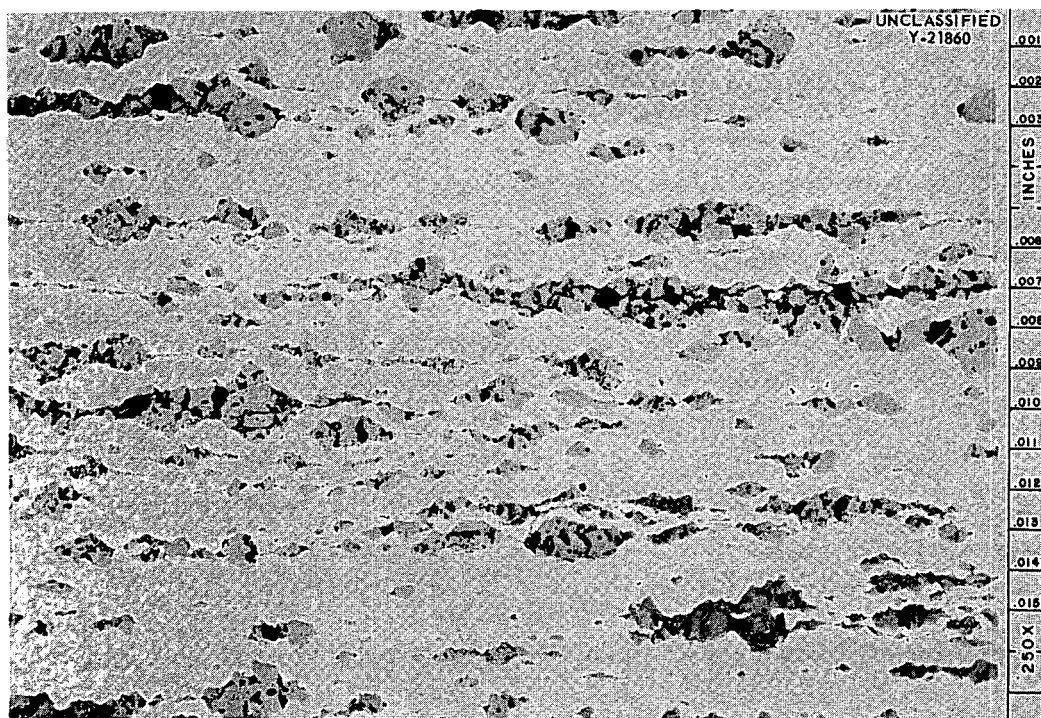
Fig. 94. Longitudinal Section of a Lindsay-Oxide-Bearing Plate Containing Oxide Prefired at 1500°C and Crushed to −325-Mesh Particle Size. As-polished. Reduced 16%.
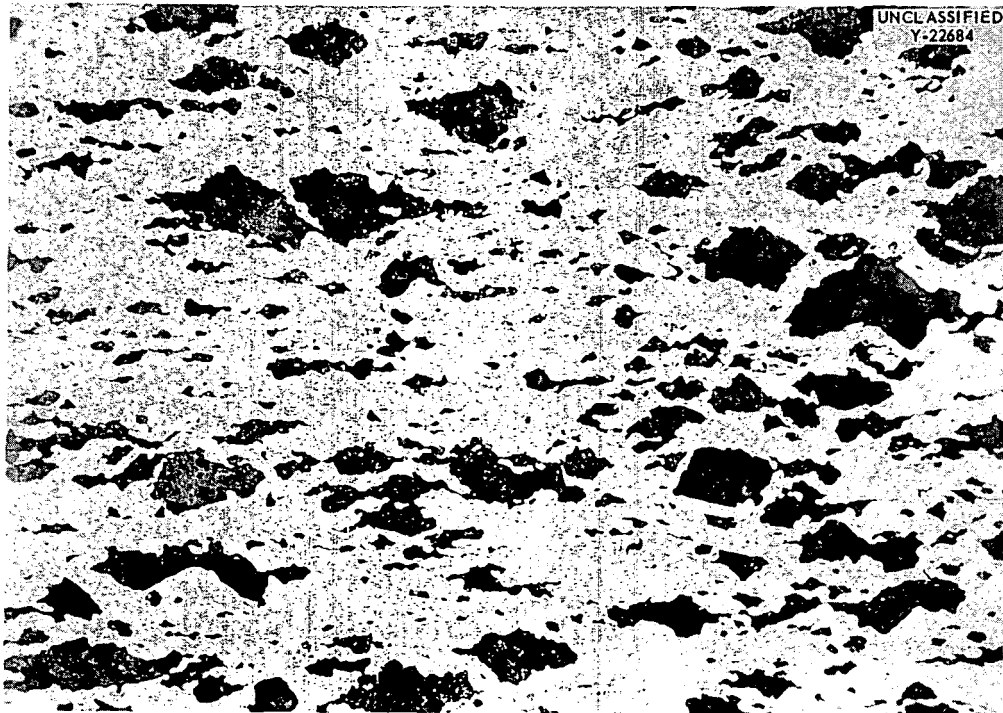
Fig. 95. Longitudinal Section of a Lindsay-Oxide-Bearing Plate Containing Oxide Prefired at 1700°C and Crushed to −325-Mesh Particle Size. As-polished. 500X. Reduced 16%.

Fig. 96. Electron Micrograph of a Compact Containing Eu_2O_3 and Type 302B Stainless Steel. Note reaction ring around stainless steel particle. Replication: Formvar replica, gold-Manganin shadowed. 23,560X. Reduced 33%.

Eu_2O_3 appears to be compatible with iron, nickel, and elemental type 304 stainless steel containing less than 0.2% Si. The results indicate that the reaction is associated with the silicon content of the material.

DEVELOPMENT OF 48% U−3% Si−Al ALLOY

W. C. Thurber

Uranium-aluminum alloys in the range of 45 to 50 wt % U are inherently brittle because of the presence of large amounts of the intermetallic compound, UAl_4. Cast slabs of these materials are difficult to fabricate into flat plates by conventional hot-rolling techniques, and employment of these alloy compositions as cores in composite fuel plates results in the formation of deleterious end effects. These end effects, termed "dog-boning" because of their peculiar shape, result in localized thinning of the cladding at the ends of the fuel core. This dog-boning occurs because the core alloy and the aluminum canning materials have appreciably different yield strengths at the

137

Table 32. Compatibility Studies of Eu_2O_3 and Various Matrix Materials

Matrix Material	Sintering Temperature (°C)	Sintering Time (hr)	Volume Change (%)
302B stainless steel	1230	1½	+6.71
	1120	1½	+6.17
304 stainless steel	1230	1½	+6.22
Electrolytic iron	1150	1½	−2.13
Nickel	1150	1½	−1.52
Chromium (0.6% Si)	1150	1½	+2.15
Silicon	1200	1½	+5.86
Elemental 304 SS (<1% Si)	1200	1½	+0.33
	1175	1½	0.00
Elemental 304 SS (<0.2% Si)	1200	1½	−4.43
	1200	1¼	−0.81

rolling temperature and, consequently, do not deform equally during rolling.

The tendency of 45 to 50 wt % U–Al alloys to drastically crack during hot rolling was minimized by insertion of the cropped casting in an aluminum picture frame to which 0.025-in. aluminum cover sheets were welded. Dog-boning was reduced by substituting high-strength aluminum alloys for the type 1100 aluminum used in conventional manufacturing practice. Neither of these solutions was totally satisfactory, and additional development was directed toward modifications of the uranium-bearing fuel material in order to improve its fabrication qualities.

It was found that the addition of 3 wt % Si to a 48 wt % U–Al alloy was sufficient to completely suppress formation of UAl_4, allowing the primary nucleating intermetallic compound, UAl_3, to be retained as the stable phase at low temperatures. This constitutional modification resulted in an 18% increase in the volume of ductile matrix material, allowing the alloy to be fabricated more readily.

Subsequent developments have revealed that other ternary additions, such as Zr, Sn, Ti, and Ge, will also suppress UAl_4 formation. Table 33 summarizes the effects of 3 wt % additions of

Table 33. Effect of Ternary Alloy Additions on the Suppression of UAl_4 in 48 wt % U–3 wt % X–Al Alloys

Ternary Addition*	Ternary Metal Content (at. %)	Spectrometer Trace (%)		
		$U(Al, X)_3$	UAl_4	Al
Si	5.0	65		35
Ti	3.0	67	8	25
Ge	2.0	60		40
Zr	1.6	70		30
Sn	1.2	70		30
Pb	0.7	20	40	40
In	1.3	35	35	30
Tl	0.7	21	38	41
Fe	2.6	20	38	42
Nb	1.6	24	42	34
**			55	45

*3 wt %.
**No ternary addition (48% U–Al).

several ternary elements on the suppression of UAl_4 in the 48 wt % U—Al alloy.

The 3 wt % Si additions induced rather striking changes in the behavior of the 48 wt % U—Al alloy. These changes are summarized as follows:

1. The macroscopic grain pattern was altered from a completely columnar to a completely equiaxed structure.

2. Hot tearing in cast slabs was eliminated.

3. In castings which are rolled to core plate with a picture frame, the maximum length of edge cracks was reduced by a factor of 2.

4. Rolling of the alloy without picture-framing was permitted.

5. Casting-to-fuel core yields were increased.

6. The room-temperature yield strength of the alloy was reduced by 33%, and the yield strength at the rolling temperature by 19%.

7. The minimum cladding thickness over the core in the worst location was increased from 5 mils to 10 mils for fuel plates encased with alclad 6061 aluminum.

APPLICATION OF URANIUM CARBIDES TO PLATE-TYPE ALUMINUM FUEL ELEMENTS

W. C. Thurber

An evaluation of the stability of aluminum with uranium carbides of varying carbon contents from 4.46 wt % C (below stoichiometric UC) to 9.24 wt % C (above stoichiometric UC_2) was conducted at temperatures required for fuel element manufacture. Studies of dispersions containing 50 wt % of uranium carbides indicate the following:

1. The reaction of uranium carbides with aluminum results in a volume increase.

2. The compounds UAl_3 and UAl_4 are the solid products of the reaction of uranium carbides with aluminum.

3. Hydrogen accelerates the reaction of UC_2 with aluminum.

4. Compacts containing equiweight mixtures of aluminum and uranium carbides of 8.24 to 9.24 wt % C are dimensionally stable for at least 96 hr *in vacuo* at 620°C. Slight amounts of Al-U intermetallic compounds can be detected.

5. Compacts containing equiweight mixtures of aluminum and uranium carbides of 4.46 to 5.75 wt % C grow catastrophically after 10 hr. or less at 620°C *in vacuo*.

Since UC_2 (9.16 wt % C) appeared chemically compatible with aluminum, it was selected for further fabrication studies. Attempts to employ powder metallurgy techniques similar to those used in manufacturing UO_2-Al composite fuel plates for the Geneva Conference Reactor[1] revealed that modifications would be required. Initial experiments entailed heating the assembled billets in air prior to hot rolling. With this method of preheating, more than 50% of the rolled plates were rejected because of blistering during heat treatment. Subsequently, billets were welded on all sides, evacuated for 2 hr at 300°C, and sealed prior to hot rolling at 600°C. The majority of the plates blistered during later heat-treatment. Ultimately, two satisfactory techniques were devised for fabricating blister-free plates. One technique involved evacuation of the assembled billets at 600°C prior to sealing and hot-rolling. The other technique utilized vacuum sintering of the cold-compacted fuel cores for 2 hr at 600°C prior to insertion into picture frames; thus, the necessity for evacuation of billets was eliminated.

It has been hypothesized that the blistering of composite fuel plates containing UC_2-Al cores is caused by the release of gases from the surface of UC_2 particles during heat treatment. These gases may be the result of hydrolytic decomposition of the UC_2 or they may merely be products of surface adsorption.

COMPATIBILITY OF URANIUM OXIDES IN THE MANUFACTURE OF PLATE-TYPE ALUMINUM FUEL ELEMENTS

R. C. Waugh

Investigations were conducted to determine the feasibility of incorporating 56 wt % U_3O_8 and 52 wt % UO_2 in aluminum by powder metallurgy, roll cladding into fuel plates by the picture-frame technique, and brazing into fuel elements. The compound U_3O_8, prepared by calcining $UO_3 \cdot H_2O$, reacts with aluminum at 600°C to form UO_2 and Al_2O_3. Figure 97 shows the rate of UO_2 formation with time at 600°C in plates which had been previously hot rolled at 590°C, flux annealed at 610°C, and cold rolled. The values of UO_2 present were calculated from UO_2/U_3O_8 ratios evaluated from integrated x-ray intensity data. No uranium-aluminum intermetallic compounds were detectable

[1]R. C. Waugh and J. E. Cunningham, *Application of Low-Enrichment Uranium Dioxide to Aluminum Plate-Type Fuel Elements*, ORNL CF-56-8-128 (Aug. 20, 1956).
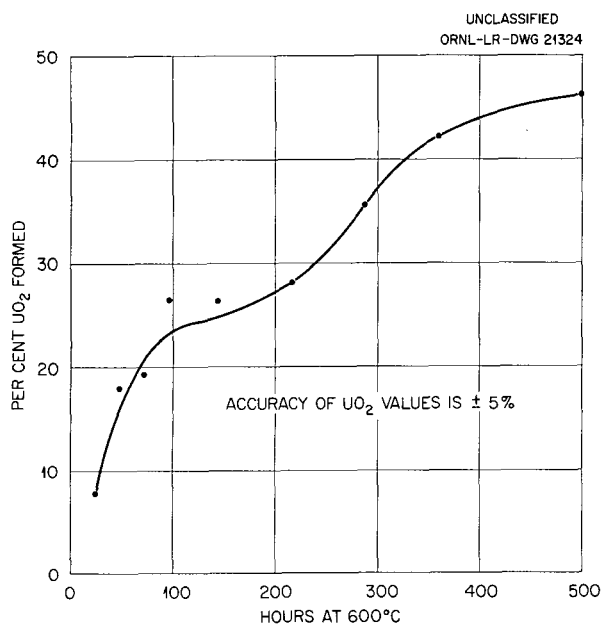
Fig. 97. Uranium Dioxide Formation During Heat Treatment of 56.4 wt % U_3O_8–bal Al Fuel Plate.

Fig. 98. Growth Characteristics of 52.3 wt % UO_2–bal Al Fuel Plates.

by x-ray diffraction. Reaction products were not revealed by metallographic examination.

The U_3O_8 prepared by calcining $UO_3 \cdot H_2O$ and the UO_2 prepared by several methods were each fabricated into composite fuel plates. They were hot rolled at 590°C, flux annealed at 610°C, and cold rolled prior to heat treatment at 600°C. Volume changes occurring during heat treatment were measured by a water displacement technique. As shown in Fig. 98, the volume of fuel plates containing UO_2 prepared from $UO_3 \cdot H_2O$ in a hydrogen atmosphere increased markedly during heat treatment at 600°C relative to plates containing steam oxidized UO_2. However, as illustrated in Fig. 99, extensive reaction between the UO_2 and aluminum had already occurred prior to heat treatment in the plates containing steam oxidized UO_2. The volume increase associated with this reaction could not be measured. Figure 100 shows that only slight peripheral reaction had occurred in similarly treated plates containing UO_2 prepared by the hydrogen reduction of $UO_3 \cdot H_2O$. The mechanism of the Al-UO_2 reaction and its association to the observed volume increase are not presently understood.

Figure 101 compares volume changes at 600°C of plates containing fused UO_2 and UO_2 prepared from $UO_3 \cdot H_2O$ in helium atmosphere with U_3O_8 prepared by the calcination of $UO_3 \cdot H_2O$. It

is apparent that the composite plates containing these dioxides exhibited significant volume increases in relatively short times at 600°C. The volume changes associated with the U_3O_8-Al combinations are in marked contrast to those observed for plates containing UO_2. Unlike the UO_2, volume changes of this small order of magnitude should offer no deterrent to the manufacture of fuel elements of the Materials Testing Reactor (MTR) type. Fuel plates and a brazed element containing depleted U_3O_8 have been successfully processed.

Pronounced warpage accompanied the volume increase observed in heat-treated UO_2-Al fuel plates, whereas similarly treated plates containing U_3O_8 did not warp.

It should be possible to minimize the UO_2-Al reaction, and the consequent growth of the fuel plates, by a reduction in the plate heat-treatment time at 600°C. Such changes could permit successful fabrication of fuel components by modification of joining techniques presently accepted for aluminum plate type of elements.

DEVELOPMENT OF MANUFACTURING PROCEDURES FOR TOWER SHIELDING REACTOR SPHERICAL LOADING

J. H. Erwin

The proposed second reactor core design for the TSF is based on a spherical configuration in which curved alclad uranium-aluminum fuel plates are arranged in segmental fuel elements which conform with the spherical geometry. The fuel alloy
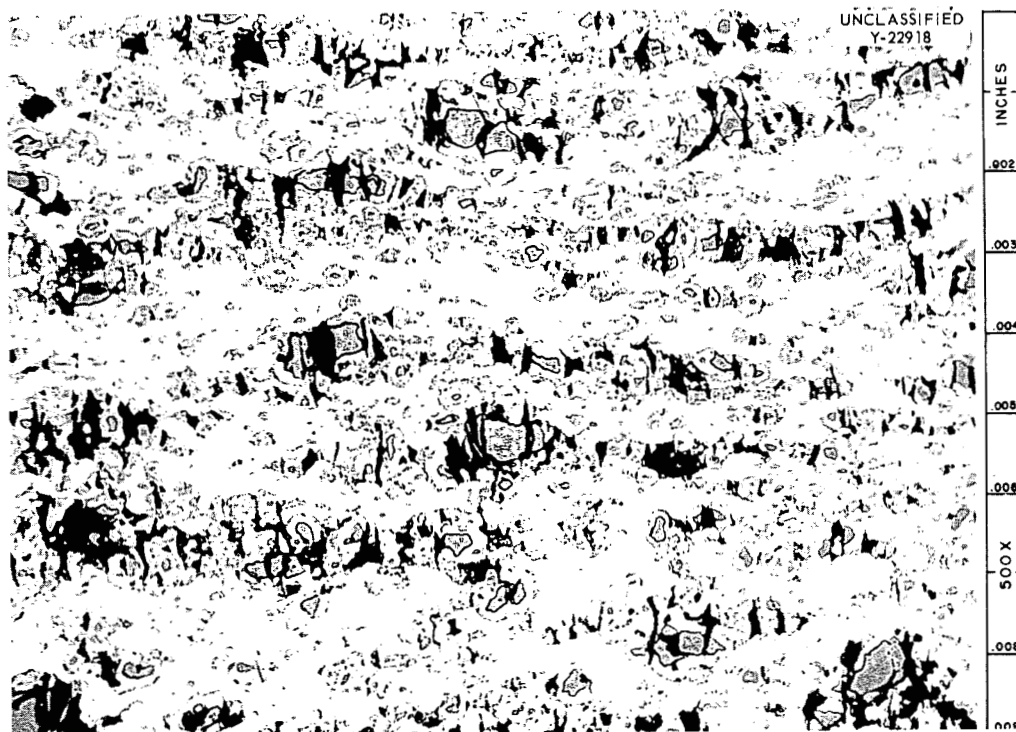
Fig. 99.   As-Polished Section from Heat-Treatment Control Fuel Plate Containing −100 +325 Mesh Steam-Oxidized UO_2. Reduced 17%.

Fig. 100.   As-Polished Section from Heat-Treatment Control Fuel Plate Containing −100 +325 Mesh UO_2 Prepared by Hydrogen Reduction of $UO_3 \cdot H_2O$. Reduced 18%.

141
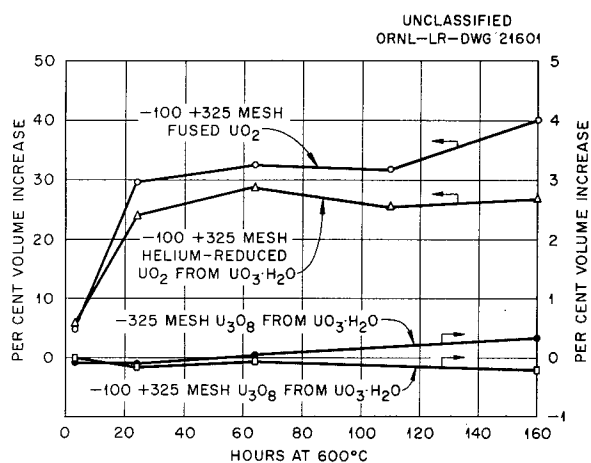
Fig. 101. Growth Characteristics of 52.3 wt % UO_2– and 55.7 wt % U_3O_8–Al Fuel Plates.

contains 20 wt % of highly enriched uranium in aluminum. The core consists of eight internal 90-deg elements and twelve external 30-deg elements. Figure 102 illustrates the general arrangement of the fuel elements which comprise a 90-deg section of the reactor core.

The assembly of these fuel elements involves the use of 72 fuel plates all with different lengths, widths, and radii of curvature, assembled in the two types of elements. The formed fuel-plate radius increases from approximately $1\frac{1}{2}$ in. at the center to $14\frac{1}{2}$ in. at the outer shell. The fuel area and content of the individual plates increase with the plate location from the inside outward.

Development has been directed toward the modification of some procedures presently utilized in the fabrication of composite aluminum plates. The uranium-aluminum alloy was prepared by the
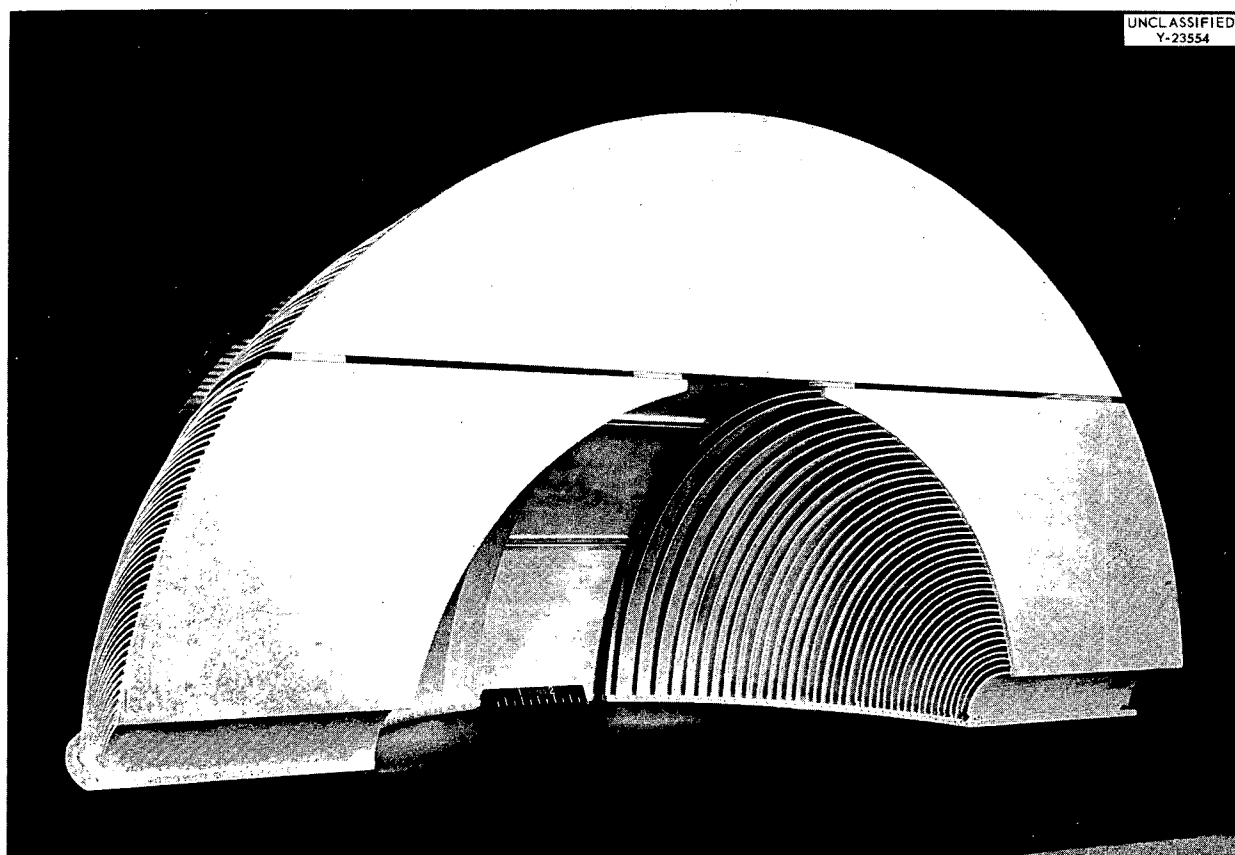
Fig. 102. Ninety-Degree Segment of Spherical Reactor Core Consisting of Two Internal and Three External Fuel Assemblies.

usual procedure as outlined in ORNL-951.[2] The fuel weight was apportioned by punching cores from the U-Al alloy plate which had been rolled to the proper thickness. Six punch and die sets were required and the punched core areas ranged from 0.706 to 6.900 in.[2]. These areas were increased to 10.621 and 120.203 in.[2] by rolling on a 20 × 30 in. two-high mill; a cross-rolling pattern was used to attain the desired fuel dimensions in the finished plate. Alclad type 6951 aluminum was substituted for type 1100 as the frame and cladding material in order to increase the resistance of these elements to damage during handling. The composite plates were bonded by hot rolling at 590°C to a total hot reduction in thickness of 84%.

Press forming to the desired curvatures was not deemed economical, since plates with 72 different radii of curvature were required in the manufacture of the TSF-2 elements. Preliminary forming experiments utilizing 2-in.-dia × 12-in.-long slip forming rolls indicated the feasibility of forming the fuel plates requiring different radii of curvature. Fuel elements manufactured from plates formed with this equipment had plate spacings within 15% of nominal, which was considered acceptable for this reactor design.

Rather than develop brazing procedures for joining plates into the assemblies it was felt that a simpler approach, a combination of a mechanical joint with a tack weld, should be used. Several fuel elements were joined by peening the plates into the grooves of the side plates and securing the plates in position by tack welding. The elements appeared to be sufficiently rigid and were acceptable for this reactor design.

FABRICATION OF ALCLAD CADMIUM PLATES

J. H. Erwin

Standard size Bulk Shielding Facility (BSF) reactor fuel plates have been fabricated with cadmium cores containing 3 to 150 g of cadmium per plate. The cadmium was sealed within a type 1100 aluminum picture frame by roll bonding an evacuated sandwich at 290°C. A weak bond was obtained between the aluminum and the cadmium.

[2]C. D. Smith, F. W. Drosten, and F. Kerze, Jr., *Production of Fuel Assemblies for the Materials Testing Reactor Mock-up Critical Experiments,* ORNL-951 (April 9, 1951).

HIGH-STRENGTH ALUMINUM FUEL ELEMENTS

J. H. Erwin

Static-air-pressure tests were conducted on an MTR-type element containing nineteen 50-mil-thick plates in which type 5050 aluminum was substituted for type 1100. No permanent set was observed at pressures less than 13 psi. Higher pressures produced a permanent set in the concave plate which was only about one-fourth of that which can be produced in the present Mark XI MTR fuel element. However, the concave plate deflection between 0 and 15 psi differential was about twice that of the Mark XI unit.

IRRADIATION TESTING

C. F. Leitten

Miniature Specimens of APPR-1 Absorber Plates Containing 3 wt % Enriched Boron in Electrolytic Iron Clad with Stainless Steel

Results have been obtained on plates which have been irradiated in the MTR to estimated burnup of B^{10} atoms of 11, 32, 41, and 60%. The specimens were measured for dimensional changes after irradiation, heated at 600°F for various periods of time to simulate APPR-plate temperature conditions, and again measured. Dimensional changes were confined to the thickness only. Results are listed in Table 34. The sample which was irradiated to an estimated burnup of 11% of the B^{10} atoms showed no evidence of dimensional changes either after irradiation or after heating at 600°F. The increased thickness in the higher burnup specimen was a result of the separation of core from cladding and the subsequent blister formation. Such a failure of the specimen which was irradiated to an estimated 32% burnup is illustrated in Fig. 103. It is felt that the cladding separated from the core after 48 hr at 600°F. At this time a blister began to form and after 168 hr the blister had increased in size along the entire surface of the specimen directly over the core. The specimen which was irradiated to an estimated 60% burnup was slightly blistered after irradiation and prior to heating at 600°F. No failures in any samples were observed at the clad-frame interface. Further work is being conducted to determine damage to miniature plates which have been irradiated to B^{10} burnup between 11 and 32%.

Table 34. Thickness Changes of Irradiated Phase-I Miniature Samples After Cyclic Annealing at 600°F

Estimated B^{10} Atom Burnup (%)	Preirradiation	Postirradiation (%)	Thickness Change for the Given Annealing Time (%)					
			24 hr	48 hr	120 hr	168 hr	264 hr	312 hr
11	0	0	0	0	0	0	0	0
32	0	1.9	2.6	6.5	9.7	11		
41	0	4.5	6.4	14.7	19.9	21.2		
60	0	34.0	63.0	64.7	69.2	70.5	71.8	72.9
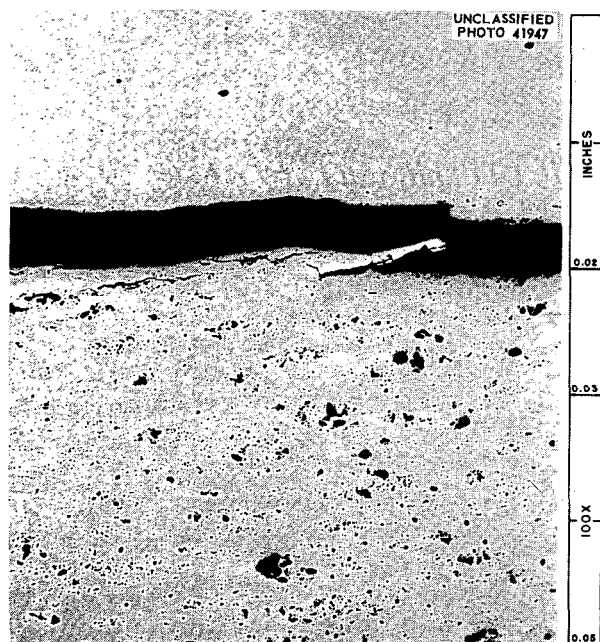
Fig. 103. Core-Clad Separation for Phase I Miniature Sample Irradiated to an Estimated 32% B^{10} Burnup and Cyclic Annealed at 600°F for a Total Time of 312 hr. Reduced 31.5%.

Prototype APPR-1 Absorber Rod, Containing 3 wt % Boron (90% B^{10} Enrichment) in Iron, Tested in the MTR Control Rod

This section, which was very nearly the size of the APPR-1 absorber section, was inserted in the MTR control rod and irradiated as an operating control rod for five MTR cycles without any apparent damage. In removing the section from the control rod for postirradiation examination, the test piece was inadvertently sectioned, and the tip end lost.

Eighteen-Plate MTR Element Containing 20% Enriched Uranium as a 48 wt % U-Al Alloy

This element was irradiated in the active lattice of the MTR to an estimated burnup of 25% of the U^{235} atoms. Postexamination included measurements of actual dimensions of the element and observations of the surfaces of several plates. No damage was apparent.

MANUFACTURING OF REACTOR COMPONENTS

J. H. Erwin

The following fabrications have been accomplished:

1. Eighty partial flat-plate aluminum fuel elements and 750 plates were fabricated for SPERT "B" loading. Type 6061 aluminum was substituted for type 1100, and the components were age-hardened to increase the strength of the material.

2. Fifty-four stainless steel elements containing a dispersion of UO$_2$ and nine stainless steel absorber sections containing 3 wt % boron in iron were manufactured for the first loading of APPR-1.

3. Seventy-two Oak Ridge Research (ORR) reactor fuel elements were brazed.

4. Eighteen Low Intensity Test Reactor (LITR) fuel elements were brazed.

METALLURGICAL MATERIALS AND PROCESSING

E. S. Bomar

R. E. Adams   J. I. Federer

Various metallurgical methods are being examined for conditioning power reactor fuel elements prior to chemical treatments for recovery of unburned uranium. The object of these head-end treatments is to assist chemical methods for recovery of uranium from difficult-to-dissolve fuel elements by retaining inert structural materials as solids for storage or disposal and making the uranium available for nitric acid dissolution. The methods which are being examined are (1) destruction of the corrosion resistance of stainless steel and Nichrome by carburization, (2) liquation of stainless steel to allow a gravity separation of uranium dioxide, and (3) intergranular diffusion of zirconium by magnesium.

TREATMENT OF APPR FUEL MATERIAL BY CARBURIZATION

R. E. Adams

Previous work[1,2] established the feasibility of carburizing APPR-type stainless steel fuel elements to contain up to at least 3.0% carbon and indicated that the uranium dioxide fuel may be exposed and dissolved by two processes: (1) by adding about 2.5% carbon and dissolving the matrix phase and the uranium in dilute nitric acid, or (2) by adding about 0.3% carbon and sensitizing the steel so that intergranular corrosion will expose the uranium to allow it to be dissolved in a subsequent leaching treatment with nitric acid. With process No. 1 about 25% of the stainless steel in the fuel plates is left as an inert solid waste, and with process No. 2 about 85% is left.

Preliminary cost analyses have indicated that treatments based on carburization are likely to be more expensive than those based on complete dissolution in dilute aqua regia, which is presently being developed by the Chemical Technology Division as the Darex process. The costs associated with remote operation and maintenance

of equipment for the high-temperature treatments, with mechanical handling of the fuel elements and solid waste products, and with control of the radioactive fission products possibly released during the high-temperature operations contribute to the high cost of the carburization treatments.

Limited additional research has been done to complete certain phases of the research on carburization processes. This work may be of interest if solutions to certain problems associated with the Darex process are more expensive than anticipated, or if long-range economic considerations emphasize the advantages of permanent storage of reactor wastes as inert solids.

Process Based on Extensive Carburization

A full-size unirradiated APPR fuel element containing normal uranium was previously[3] carburized to contain about 2.2% carbon. J. H. Goode, of the Chemical Technology Division, has reported[4] on a dissolution test made on about 40% of the fuel element. It was reacted in a solution of 2.6 M nitric acid–0.3 M urea at 45 to 55°C for 6.5 hr, but analyses of successive samples of solution indicated that dissolution was completed in 4 to 5 hr. During dissolution, the solution was agitated by air sparging to ensure circulation through the fuel element. The matrix phase of the fuel plates reacted completely, and the remaining carbide network collapsed when the fuel element was removed from the dissolver. The side plates, being thicker than the fuel plates, contained less carbon and did not dissolve completely. They were removed and are shown in Fig. 104 to demonstrate that the edges of the fuel plates reacted completely.

The fuel-plate residue was further treated by boiling in 10 M nitric acid, and essentially all the remaining uranium was dissolved in 1 hr. Of the total amount of uranium recovered, 99.89%

[1]R. E. Adams, *Met. Semiann. Prog. Rep. April 10, 1956*, ORNL-2080, p 181.

[2]R. E. Adams, *Met. Semiann. Prog. Rep. Oct. 10, 1956*, ORNL-2217, p 185.

[3]R. E. Adams, *Met. Semiann. Prog. Rep. Oct. 10, 1955*, ORNL-1988, p 129.

[4]J. H. Goode, *The Preparation of Solvent Extraction Feed from Carburized Stainless Steel Fuel Elements of the APPR Type*, ORNL CF-57-1-157 (Jan. 31, 1957).
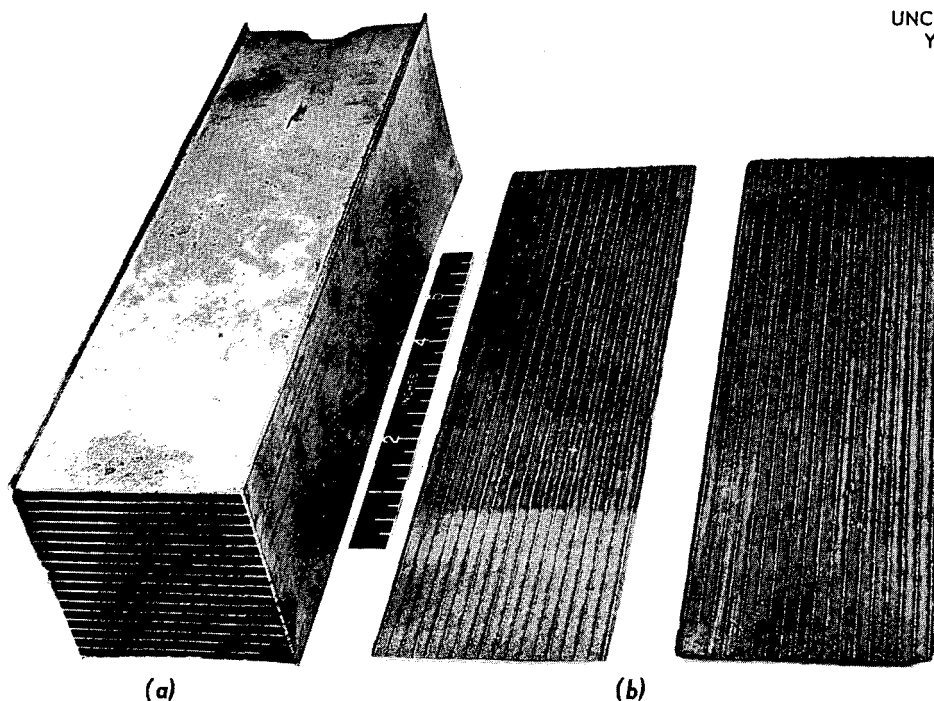
Fig. 104. (a) Carburized and Homogenized Section (Inlet End) of APPR Fuel Element Containing Approximately 2.2% Carbon. (b) Side Plates from Center Section of Same Fuel Element After Dissolution Treatment. Note that uniform attack on all fuel plates extended up to the inside surfaces of the side plates. The front end of one side plate was scrubbed with a fiber brush to indicate ease of removal of the carbide particles.

was in the two nitric acid solutions. The distribution of the uranium and the stainless steel recovered in this test is shown in Table 35.

In most of the dissolution experiments on carburized stainless steel, urea was used to control a passivation effect believed to be caused by the formation of nitrogen oxides and nitrous acid during dissolution in dilute nitric acid. Since urea in combination with nitric acid under certain conditions constitutes an explosion hazard, other methods of controlling passivation were sought. The action of nitric acid on metals has been discussed by Evans,[5] and it appears that stirring or air sparging during dissolution will also prevent passivation.

The use of air to control passivation and the feasibility of recovering uranium from type 347 stainless steel APPR fuel material by extensive carburization were studied in a single test. A

[5]U. R. Evans, *Metallic Corrosion, Passivity and Protection,* 2d ed., Arnold, London, 1946.

specimen was carburized to contain 2.4% carbon, homogenized for 2 hr at 1100°C, and treated in 3 M nitric acid at 50 to 70°C for 5¾ hr. Air was bubbled through the solution continuously. Passivation did not occur, and the solids, after being leached for 1 hr in boiling 10 M nitric acid, contained only 0.014% of the uranium in the specimen.

Process Based on Intergranular Corrosion

Additional experiments were made to investigate the use of intergranular corrosion to expose the uranium in type 347 stainless steel APPR fuel material for subsequent dissolution in nitric acid. These experiments were made on specimens carburized to contain about 0.3% carbon, homogenized for 2 hr at 1150°C, and sensitized for 2 hr at 650°C.

The results of tests in which a copper sulfate and sulfuric acid solution was used to cause intergranular corrosion are shown in Table 36. These results verify that the niobium-stabilized stainless steels are also amenable to treatment by this method. Uranium losses in the corroding

Table 35. Results of Dissolution Test on Carburized APPR Fuel Element

Fuel element data: type 302B stainless steel core containing $\sim$ 18% normal UO_2 and clad with
type 304 stainless steel
carburized for 4 hr at 950°C
homogenized for 2 hr at 1100°C
average carbon content, 2.11%

Recovered in	Per Cent of Fuel Element Material Recovered	
	Stainless Steel	Uranium
Dissolver solution	64.0	93.65
50 liters of 2.61 M nitric acid, 0.3 M urea,		
agitated by air sparging at 45–55°C		
Uranium recovery solution	6.7	6.24
3 liters of 10 M boiling nitric acid		
Solids		
Carbide powder	18.0	0.11
Side plates	11.3	

Table 36. Distribution of Stainless Steel and Uranium from Carburized Type 347 Stainless Steel APPR Fuel Element Material Tested by Intergranular Corrosion and Nitric Acid Leaching

Sample preparation: annealed for $\frac{1}{2}$ hr at 1150°C
carburized for 20 min at 1000°C
homogenized for 2 hr at 1150°C
sensitized for 2 hr at 650°C

Test No.	Per Cent of Fuel Material Recovered in					
	Corroding Solution		Leaching Solution[a]		Solids	
	Uranium	Stainless Steel	Uranium	Stainless Steel	Uranium	Stainless Steel
C-20	0.02[b]	9.1[b]	94.66	9.1	5.32	81.8
C-27	0.006[b]	12.0[b]	99.62	7.4	0.37	80.6
C-30[c]	0.005[b]	7.6[b]	99.30	3.6	0.70	88.8
C-28	99.2[d]	56.5[d]	0.79	1.4	0.01	42.1

[a]Leaching treatment: boiled in 10 M HNO_3 solution for 2 hr.
[b]Corroding treatment: boiled in 1.5 M H_2SO_4–0.4 M $CuSO_4$ solution for 5–6.5 hr.
[c]Specimen annealed for 1 hr at 1200°C prior to carburization.
[d]Corroding treatment: heated at 40–60°C in 4 M HNO_3–2 M HF solution for 2 hr.

solution are desirably low. Uranium losses in the solids are not so low as desired, but the test showing the least loss (0.37% of the uranium present) is promising, and further research might develop methods whereby the uranium recovery could be improved.

The results of a single test (C-28) with a solution of 25% nitric acid and 4% hydrofluoric acid (4 M HNO_3–2 M HF) used to produce intergranular corrosion are also shown in Table 36. This solution caused rapid intergranular attack and also dissolved most of the uranium. In excess of 50% of the stainless steel was dissolved, an indication of the very corrosive nature of the solution. The solids, after being leached with 10 M nitric acid, contained only 0.01% of the uranium, and 42% of the stainless steel was left as a very fine granular powder. Unless similar results can be obtained with much lower concentrations of hydrofluoric acid, this process appears to be undesirable, both because of the corrosive nature of the solution and because the presence of the fluoride ion will complicate the solvent extraction process for recovery of the uranium.

TREATMENT OF NICHROME FUEL MATERIAL BY CARBURIZATION

R. E. Adams

The modified Nichrome V fuel material for the GE-ANP experimental reactor did not respond nearly so well as the APPR fuel material to either of the treatments based on carburization. However, the results of tests in which both the metallurgical and the chemical treatments were slightly modified indicate that methods for processing carburized Nichrome fuel material could probably be developed.

Best results were obtained with specimens carburized to contain about 0.7% or 1% carbon (required ½ or 1 hr at 1000°C for the 0.014-in.-thick specimens) homogenized for 2 hr at 1150°C and sensitized for 2 hr at 650°C. The specimens reacted rapidly in boiling 65% nitric acid; most of the Nichrome and essentially all the uranium dioxide were dissolved. A flaky, friable residue, equivalent in weight to about 10% of the original sample weight, did not dissolve.

The results of two dissolution tests are shown in Table 37. Analysis of samples of the dissolver solution removed after 2 hr indicated that the dissolution reaction was essentially complete at that time. The very low uranium losses in the solids indicate that fuel elements of Nichrome may also be treated successfully by processes based on carburization.

LIQUATION OF TYPE 347 STAINLESS STEEL–URANIUM DIOXIDE FUEL ELEMENTS

J. I. Federer

Liquation of a type 347 stainless steel–uranium dioxide fuel element of the APPR type might result in a gravity concentration of UO_2 particles in the bottom portion of the melt. If a concentration did occur, the portion of the alloy containing the UO_2 could be mechanically separated from the bulk of the stainless steel. Less material would have to be dissolved in acid prior to solvent

Table 37. Results of Dissolution Tests on Nichrome V Fuel Material

Specimen preparation: carburized for ½ or 1 hr at 1000°C
homogenized for 2 hr at 1150°C
sensitized for 2 hr at 650°C
Dissolution treatment: boiled in 65% HNO_3

Test No.	Carbon Content (%)	Dissolution Time (hr)	Per Cent of Total Material Recovered in			
			Dissolver Solution		Solids	
			Uranium	Nichrome	Uranium	Nichrome
01-2	0.7	6	99.98	90.7	0.013	9.3
01-3	1.0	4	99.98	91.2	0.015	8.8

extraction, and much of the stainless steel would be retained in solid form for suitable disposal.

For liquation experiments carbon was added to the stainless steel fuel material to lower the melting temperature. According to the phase diagram for the iron-chromium-carbon system,[6] alloys containing 3% carbon and 18% chromium begin to melt at 1130 to 1260°C. Fuel element samples were gas-carburized at 1100°C in a hydrogen—20% methane atmosphere to contain 4.5 to 5% carbon. Experiments showed that type 347 stainless steel carburized to 5% carbon could be melted at about 1200°C.

Carburized fuel element samples were heated to 1250°C to determine whether a gravity concentration of the —100 +325 mesh UO_2 particles would occur. Figure 105 shows the microstructure of a sample after carburizing to 5% carbon, and Fig. 106 shows a similar specimen which was

homogenized for 1 hr at 1175°C and heated to 1250°C for 5 hr. Microscopic examination of vertical sections of the solidified samples revealed that settling of UO_2 particles did not occur. The presence of numerous carbides, which in Fig. 106 are seen to have increased in size during the time at 1250°C, evidently restricted movement of the UO_2 particles through the molten portion of the sample.

INTERGRANULAR DIFFUSION OF ZIRCONIUM BY MAGNESIUM

J. I. Federer

Solid state diffusion studies at KAPL[7] during fuel element development research revealed that magnesium rapidly diffuses along zirconium grain boundaries. The experiments showed that the rate of penetration for the vapor-solid reaction was approximately the same as for solid-solid

[6]American Society for Metals, *Metals Handbook*, 1948 ed., p 1249, American Society for Metals, Cleveland, 1948.

[7]L. S. DeLuca, H. T. Sumsion, and D. D. Van Horn, *Magnesium-Zirconium Diffusion Studies*, KAPL-1746 (April 1, 1957).
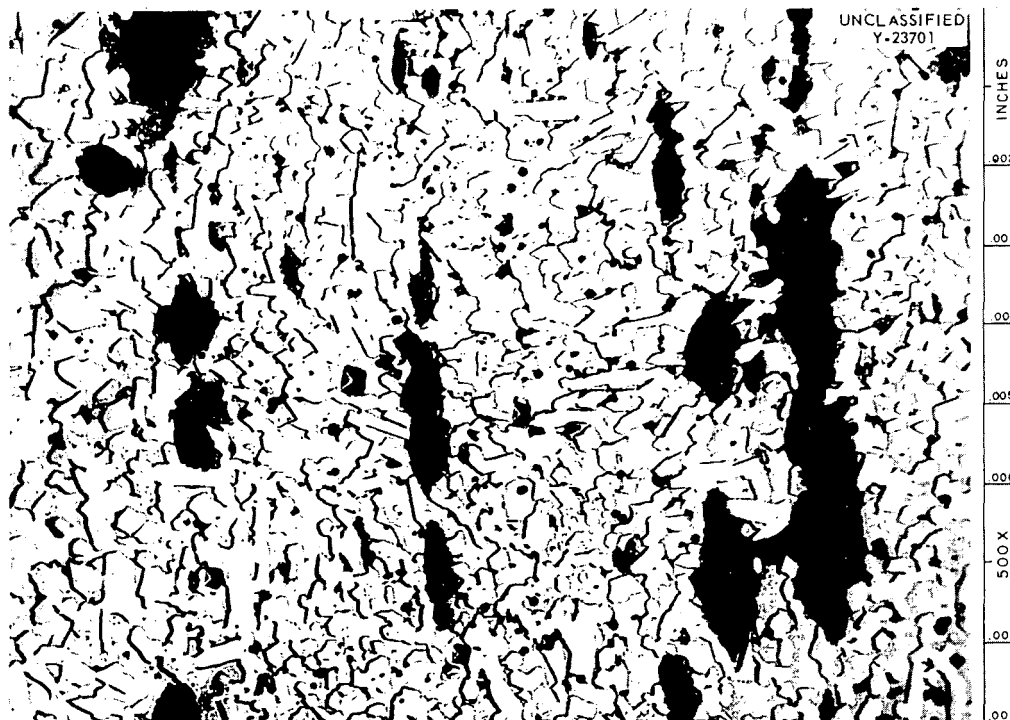
Fig. 105. Type 347 Stainless Steel—Uranium Dioxide Fuel Element Sample Carburized in a Hydrogen—20% Methane Atmosphere for 6.5 hr at 1100°C to 5% C. Large dark particles are uranium dioxide; other particles are carbides. Etchant: glyceria regia. Reduced 17%.
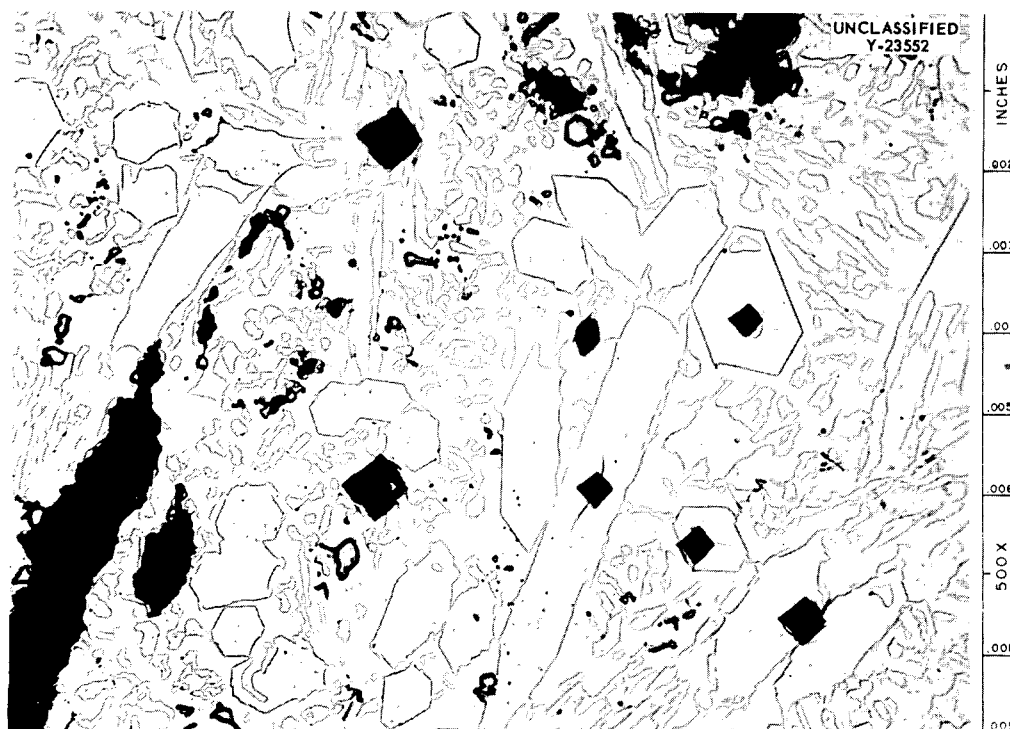
Fig. 106. Type 347 Stainless Steel—Uranium Dioxide Fuel Element Sample Carburized to 5% C, Homogenized at 1175°C, Then Held at 1250°C for 5 hr. Large particles are uranium dioxide; other particles are carbides. The black squares are hardness impressions in the carbide particles and the matrix which yielded values of 1270 and 410 VHN, respectively. Etchant: glyceria regia. Reduced 17%.

diffusion couples at 625°C. The grain-boundary phase resulted in embrittlement of the zirconium.

These results suggested a method for removal of zirconium cladding from reactor fuel elements. If magnesium were diffused into the zirconium cladding, chemical leaching of the grain-boundary material or mechanical deformation of the embrittled zirconium might cause the cladding to break into small pieces and expose the core for dissolution.

Magnesium was diffused into zirconium samples by heating them in contact with magnesium metal or vapor at 625°C. The dependence of magnesium penetration on time is shown in Figs. 107 and 108. In Fig. 107 the grain-boundary penetration was 0.012 in. after 1 hr at 625°C; 3 hr at 625°C resulted in complete penetration through the 0.030-in. specimen as shown in Fig. 108. The grain-boundary phase becomes less continuous with increasing distance from the magnesium, which is on the left in Fig. 108.

Some completely penetrated specimens were heat-treated in attempts to promote greater sensitivity of the grain-boundary material to chemical attack than was observed for as-penetrated specimens. The microstructural changes which occurred during the heat treatments could be observed but not explained, since the phase relationships for zirconium and magnesium have been established for only high-magnesium alloys. Figures 109 and 110 show the microstructures of penetrated specimens subsequently heat-treated for 6 hr at 350 and 500°C, respectively. In both specimens precipitation occurred within the grains rather than at the grain boundaries. In Fig. 110 especially, magnesium has diffused into the grains, resulting in less definition of the grain boundaries.

Samples of as-diffused and heat-treated material were exposed to boiling concentrated nitric acid and MTR dissolving solution[8] in attempts to

[8]A. E. Lindroos and D. B. Stewart, chap. 4.2, p 633, in *Reactor Handbook*, ed. by J. F. Hogerton and R. C. Grass, Technical Information Service, AEC, 1953.
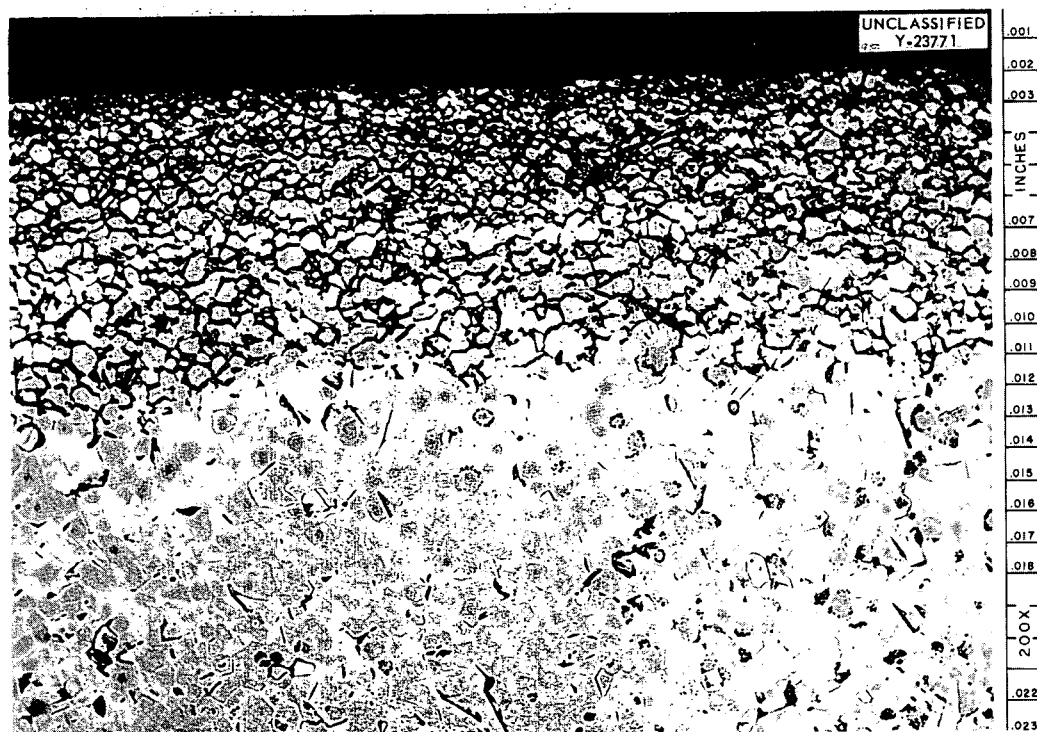
Fig. 107. Zirconium Specimen Which Was in Contact with Magnesium for 1 hr at 625°C. Depth of grain boundary penetration, 0.012 in. Etchant: 46 HNO_3–46 H_2O–8 HF. Reduced 18%.
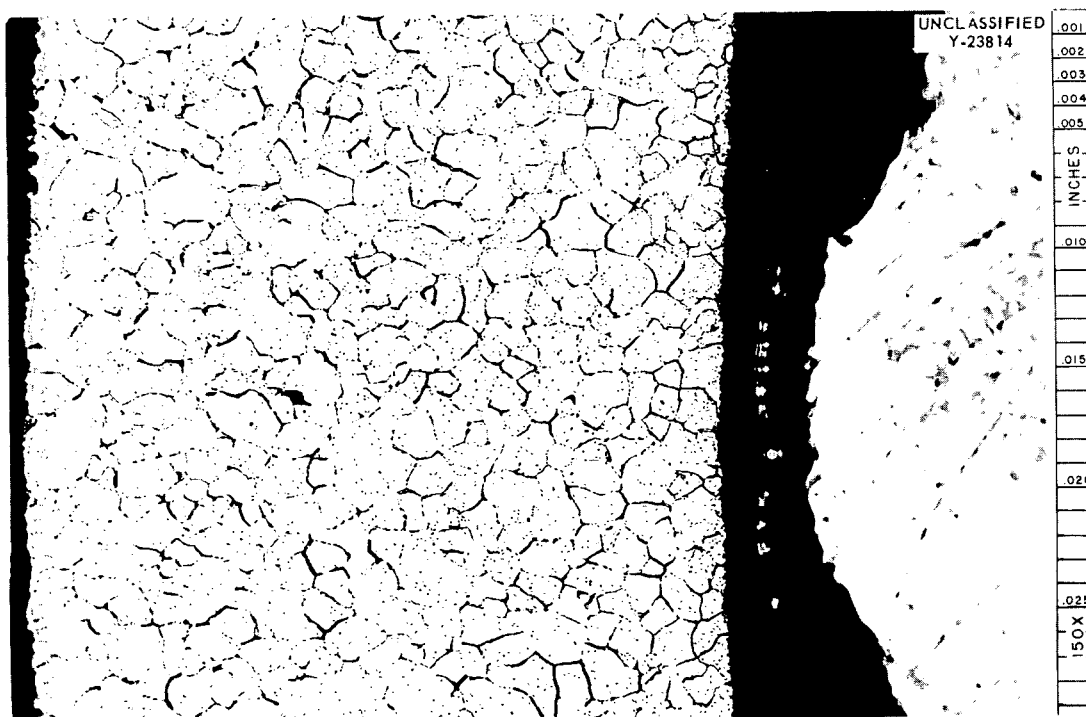
Fig. 108. Zirconium Specimen Which Was in Contact with Magnesium for 3 hr at 625°C. Complete penetration occurred through the 0.030-in. specimen. Etchant: 46 HNO_3–46 H_2O–8 HF. Reduced 15%.

151
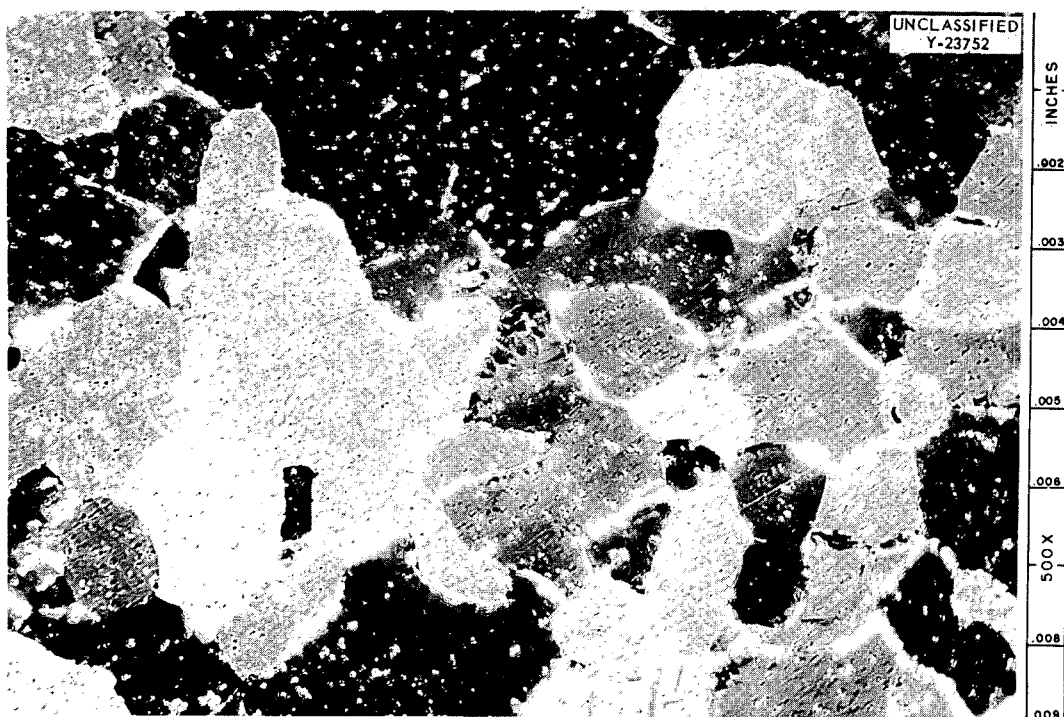
Fig. 109. Zirconium Specimen Completely Penetrated with Magnesium at 625°C; Heat Treated at 350°C for 6 hr. Etchant: 46 HNO_3–46 H_2O–8 HF. Polarized light. Reduced 16%.
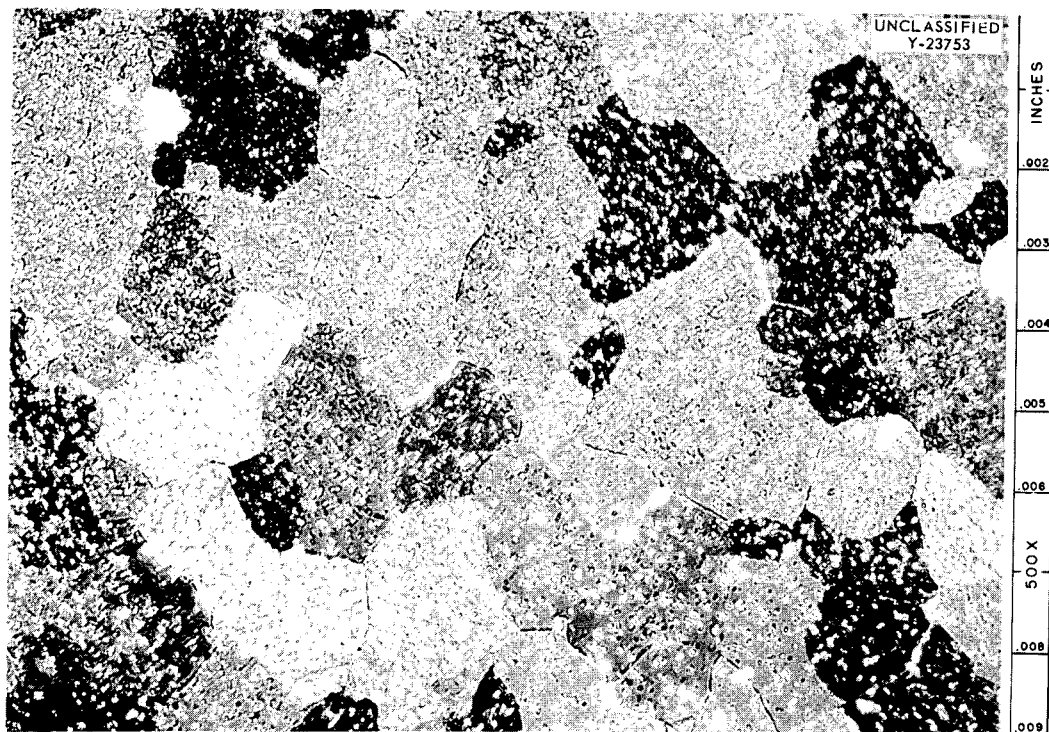
Fig. 110. Zirconium Specimen Completely Penetrated with Magnesium at 625°C; Heat Treated at 500°C for 6 hr. Etchant: 46 HNO_3–46 H_2O–8 HF. Polarized light. Reduced 16%.

dissolve the grain-boundary material. The as-diffused and heat-treated samples were not significantly attacked by either solution on the basis of weight-change measurements. Discoloration of the samples was the only other macroscopic evidence of reaction. Microscopic examination did not reveal any selective attack of the grain-boundary phase.

A section of uranium rod clad with 0.015-in.-thick zirconium was exposed to magnesium at 600 to 650°C and subjected to the bending action imposed by the rolls of a rotary tube and rod straightner. Figure 111 illustrates the effect on the brittle zirconium cladding. The left end of the rod was at a temperature less than 600°C due to a furnace temperature gradient and thus was only partially penetrated by magnesium. Beyond this zone about 90% of the cladding broke away from the core during the operation. Figure 112 is a cross section of the rod showing typical

UNCLASSIFIED
Y-23296
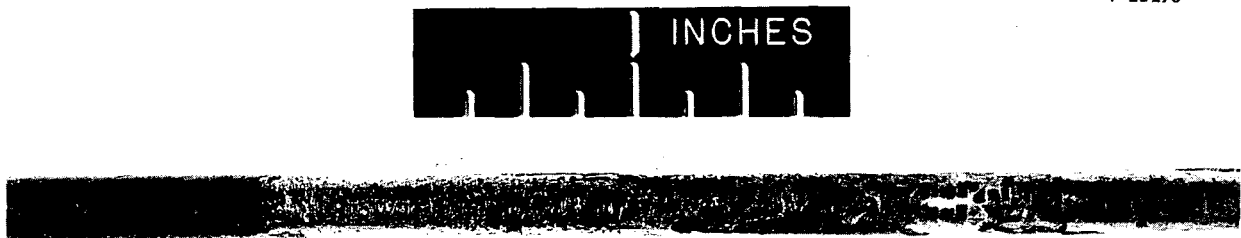
Fig. 111. Zirconium-Clad Uranium Rod Which Was in Contact with Magnesium at 600 to 650°C. Subsequent cold working resulted in breakup of the embrittled zirconium cladding. Due to incomplete penetration, the cladding remained intact on the end of the rod.

UNCLASSIFIED
Y-23320
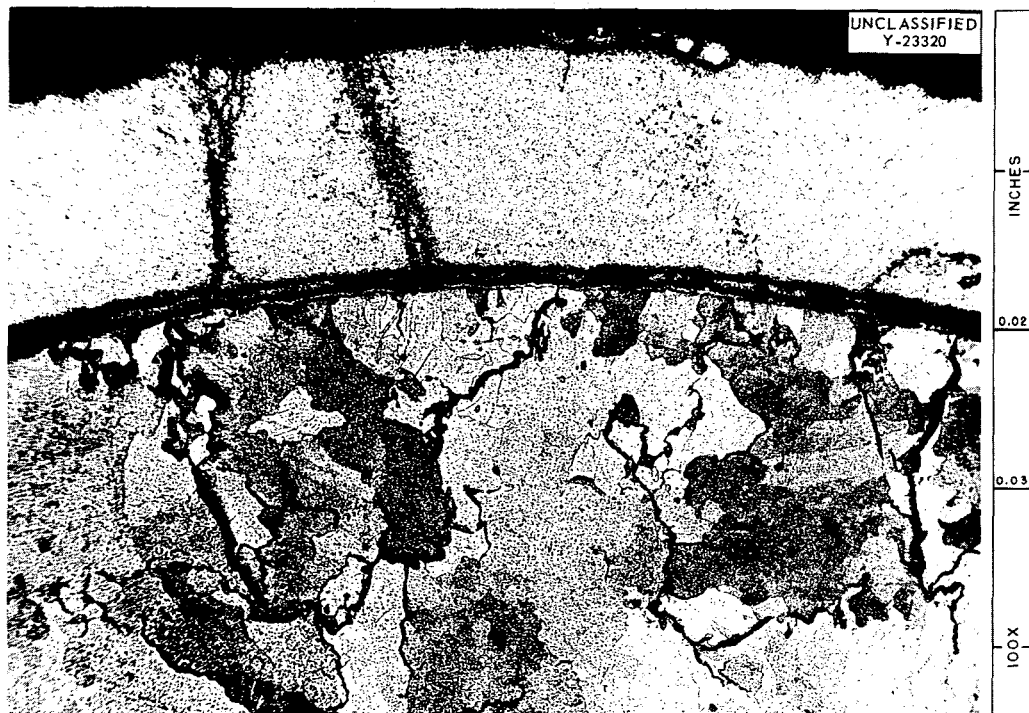
Fig. 112. Cross Section of Magnesium-Diffused, Zirconium-Clad Uranium Rod Showing Typical Cracks After Cold Working. The zirconium cladding (top) is separated from the uranium core by a crack which extends completely around the specimen. Etched cathodically, using 3500 v for 20 min. Reduced 16%.
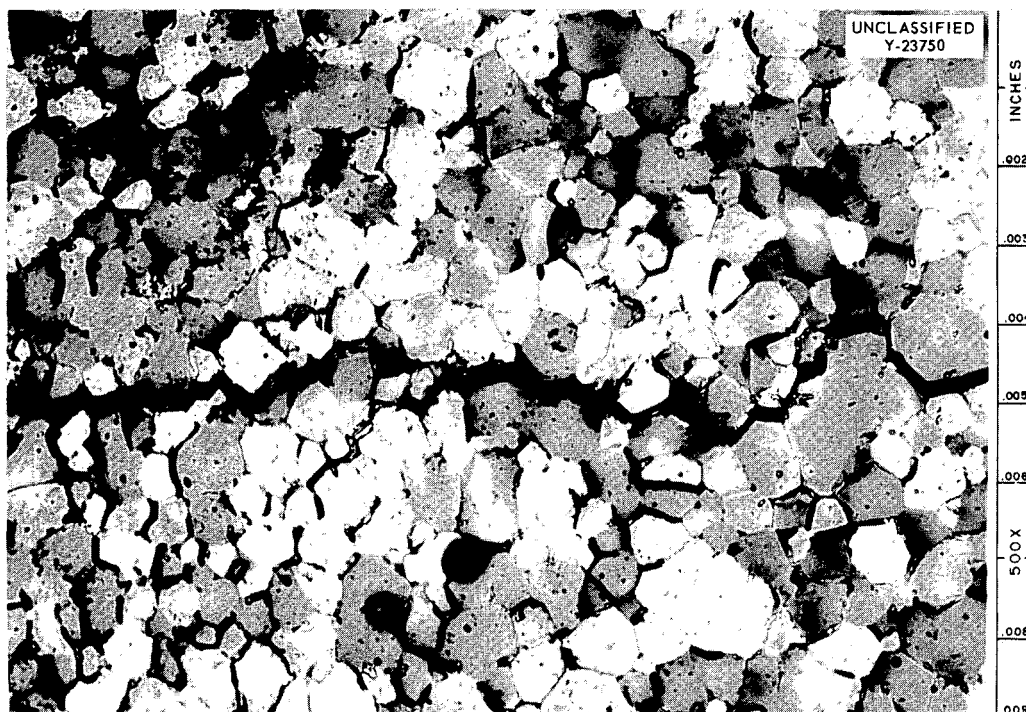
METALLOGRAPHY

R. J. Gray

R. S. Crouse   E. L. Long, Jr.

W. H. Bridges   J. R. Riddle

T. M. Kegley   D. S. Stoneburner

J. E. VanCleve

Almost all the metallographic work for the Metallurgy Division is conducted by the Metallography Group. The following special problems represent primarily the efforts of the technical personnel of the group. The accomplishments of the metallography technicians are reflected through direct metallographic service for other groups of the Metallurgy Division.

METALLOGRAPHIC EXAMINATION OF HEAT EXCHANGERS AND RADIATORS

J. E. VanCleve   R. J. Gray

Radiators

York No. 5. — The radiator failed in service after 1265 hr of operation. Of this time, 223 hr were under nonisothermal conditions. Twenty-seven samples were removed for examination. Table 38 shows the results of the fin-to-tube braze-joint-integrity examination of this radiator compared with three other York Corporation radiators. Table 39 shows the results of the mass-transfer and corrosion examination compared with the same three. The radiator failure was due to the

progression of intergranular cracks caused by creep deformation of the tube walls.

York No. 7. — This radiator did not fail in service after 2574 hr of operation. Of this time, 1544 hr were under nonisothermal conditions. Twenty-seven samples were removed for examination. The results of the fin-to-tube braze-joint-integrity and the mass-transfer and corrosion examinations appear in Tables 38 and 39, respectively. This radiator was the first of a revised design, and grain-boundary voids were found in the tubes between the NaK inlet header and the fin matrix.

York No. 8. — This radiator failed in service after 629 hr of operation, 434 hr of which were under nonisothermal conditions. Twenty-seven samples were removed for examination. The results of the fin-to-tube braze-joint-integrity and the mass-transfer and corrosion examinations appear in Tables 38 and 39, respectively. The radiator failed in the same area in which the grain-boundary voids were found in York No. 7. The failure, in this case, was attributed to the progression of the voids through the tube wall.

Table 38. Comparison of Fin-to-Tube Braze-Joint-Integrity Examinations for Various Radiators

	Radiator			
	York No. 5	York No. 7	York No. 8	ART Test
Number of joint areas examined	3105	2783	2279	2440
Per cent of joint areas having 75–100% adherence	38.4	57	24	41.1
Per cent of joint areas having 50–74% adherence	9.6	7.0	8.0	8.2
Per cent of joint areas having 25–49% adherence	7.0	4.0	6.0	3.1
Per cent of joint areas having 0–24% adherence	45	32	63	47.6
Per cent of joint areas having nonoxidized copper fins	29	17	12	10.2
Per cent of joint areas having slightly oxidized copper fins	13.6	7	45	43.1
Per cent of joint areas having heavily oxidized copper fins	57.4	76	43	46.7

Table 39. Mass-Transfer and Corrosion Data for Various Radiators

	Radiator			
	York No. 5	York No. 7	York No. 8	ART Test
Maximum mass transfer (NaK out, air in), in.	0.0035	0.009	0.005	None
Maximum corrosion (NaK in, air out), in.	0.025	0.004	0.012	None
Total hours of operation	1265	2574	629	870
Hours of nonisothermal operation	223	1544	434	480
Number of samples	27	27	27	44

York No. 16. – This radiator failed in service after 1438 hr of operation, with 1044 hr being under nonisothermal conditions. Fin-to-tube braze-joint-integrity and mass-transfer and corrosion examinations were not performed, since the radiator was heavily damaged by a fire resulting from a gross NaK-to-atmosphere leak. The plugs in five tubes were analyzed and found to contain uranium and zirconium.

ART Test Radiator No. 1. – This radiator failed in service after 870 hr of operation, 480 hr of which were under nonisothermal conditions. Forty-four samples were removed for examination. The results of the fin-to-tube braze-joint-integrity and the mass-transfer and corrosion examinations appear in Tables 38 and 39, respectively. The cause of the failure was not apparent at the conclusion of the examination.

Heat Exchangers

Process Engineering Corp. Heat Exchanger No. 1 (Type SHE-2). – This heat exchanger successfully completed 2574 hr of operation, 1544 of which were under nonisothermal conditions. Fuel No. 30 was used in the test of the heat exchanger, and 31 specimens were removed for examination. The fuel-side corrosion ranged from a minimum of 0.001 in. in the cool area to a maximum of 0.018 in. in the hot area. The NaK-side corrosion ranged from a minimum of a general roughening of the surface to a maximum of 0.007 in.

Process Engineering Corp. Heat Exchanger No. 1 (Type SHE-7). – This heat exchanger successfully completed 1217 hr of operation with fuel No. 30, 571 hr of which were under ART full power conditions. Thirty-seven samples were removed for examination. The fuel-side corrosion ranged from

a minimum of a general roughening of the surface in the cool area to a uniform corrosion of 0.010 in. in the hot area as indicated by subsurface void formation. The NaK-side corrosion ranged from a maximum of a general roughening of the surface in the cool area to 0.010 in. in the hot area at some grain boundaries. In addition to the effect of the uniform fuel-side corrosion and the NaK grain-boundary corrosion in the hot area, there was complete fissuring of the tube wall at some grain boundaries due to strain cycling. A crack 0.006 in. wide was found to have completely extended through the tube wall in the hot area.

Process Engineering Corp. Heat Exchanger No. 2 (Type SHE-7). – This heat exchanger successfully completed 1875 hr of operation with fuel No. 30, 1456 hr of which were under nonisothermal conditions. Thirty-four samples were removed for examination. The fuel-side corrosion ranged from a minimum of 0.001 in. in the cool area to a maximum of 0.010 in. in the hot area as indicated by subsurface void formation. The NaK-side corrosion ranged from a general roughening of the surface to 0.010 in. in the hot area at some grain boundaries. The same condition of complete fissuring in the hot area existed as described above for the No. 1 heat exchanger (SHE-7).

Process Engineering Corp. Heat Exchanger No. 3 (Type SHE-7). – This heat exchanger successfully completed 1438 hr of operation with fuel No. 70, 1044 hr of which were under nonisothermal conditions. Thirty-one samples were removed for examination. The fuel-side corrosion ranged from a minimum of 0.001 in. to a maximum of 0.008 in. in the hot zone as indicated by the subsurface void formation in the hot zone. The NaK-side corrosion ranged from a general roughening of the

surface in the cold zone to 0.005 in. at some grain boundaries in the hot zone. Again there was complete fissuring at some grain boundaries in the hot zone as described above for the No. 1 heat exchanger (SHE-7). A metallic layer was found on the fuel side of the tubes in the hot section. The origin of this deposit is as yet undetermined.

Black, Sivalls & Bryson Heat Exchanger No. 1 (Type IHE-8). – This heat exchanger successfully completed 547 hr of operation under nonisothermal conditions with the NaK entrance temperatures above 1600°F. Sixty-three specimens were removed for examination. The fuel-side corrosion ranged from a minimum of 0.001 in. in the cool zone to a uniform corrosion of 0.012 in. in the hot zone as indicated by subsurface void formation. The NaK-side corrosion ranged from a general roughening of the surface in the cool zone to 0.008 in. in the hot zone at some grain boundaries. There was complete fissuring of the tube wall at some grain boundaries in the hot zone as described above for the No. 1 heat exchanger (SHE-7).

For comparison purpose the depth of corrosion in all the heat exchangers is shown in Table 40.

THERMAL-CONVECTION LOOPS

D. F. Stoneburner

The total number of thermal-convection loops processed during this period was 111. The loops are listed in Table 41 according to the material

and the fluid used. Table 42 presents the metallographic results of three test conditions in more detail.

A special test was conducted on an Inconel loop (No. 1085) to determine the effect of continued temperature and time on the location, size, and character of voids in the absence of a corrosion fluid. The loop was operated for 277 hr at 1500°F in fuel No. 30. It developed subsurface voids to a depth of 0.001 in. and intergranular voids to 0.008 in. A companion loop received the same treatment; then the fuel was drained, and the loop was kept at 1500°F in an inert atmosphere for 750 hr. Investigation revealed the same attack, indicating that time and temperature alone have little or no effect on the void location, size, or character.

Other thermal-convection loops were operated to gain information relative to using fused salts in a civilian power reactor. In one test, in which Inconel was operated for 1000 hr at 1200°F in fuel No. 122, the depth of attack was limited to 0.001 in. Twenty-three loops were operated with Inconel in a special fuel (WR).

Thermal-Cycle Tests

Twenty-nine thermal-cycle tests with 12 specimens per test have been examined. Thermal-cycle tests can be classed as isothermal low frequency (0.01 cps) and high frequency (0.4 cps); some

Table 40. Comparison of Depth of Corrosion in Heat Exchangers

Heat Exchanger	Total Time Tested (hr)	Nonisothermal (hr)	Fuel No.	Number of Samples	Depth of Corrosion (in.)				Remarks
					Fuel Side		NaK Side		
					NaK in Cool	NaK out Hot	NaK in Hot	NaK out Cool	
Process Engineering Corp. No. 1 (SHE-2)	2574	1544	30	31	0.001	0.018			
Process Engineering Corp. No. 1 (SHE-7)	1217	571	30	37	G.R.S.*	0.010	G.R.S.	0.010	Complete fissuring**
Process Engineering Corp. No. 2 (SHE-7)	1658	145	30	34	0.001	0.010	G.R.S.	0.010	Complete fissuring
Process Engineering Corp. No. 3 (SHE-7)	1438	1044	70	31	0.001	0.008	G.R.S.	0.005	Complete fissuring
Black, Sivalls & Bryson No. 1 (IHE-8)	911	547	30	63	NaK in hot 0.012	NaK out cool 0.001	G.R.S.	0.008	Complete fissuring

*General roughening of the surface.
**Complete fissuring is an accumulative effect of fuel corrosion, NaK corrosion, and strain cycling.

Table 41. Summary of the Number of Loops, Materials, and Fluids Tested in Thermal-Convection Loops

Material	Number of Loops Operated						
	Fluid						
	Na	107	30	70	122	WR	Total
Inconel			6	1	1	23	31
Inconel W	2		1				3
Incoloy	2						2
Hastelloy B		1					1
Ni-Mo	18	40					58
Nb clad with type 321 stainless steel*	1	3					4
Hastelloy W with Mo insert*		2					2
Cast Inconel* insert	4		6				10
	27	46	13	1	1	23	111

*See Table 42 for detailed data.

tests were operated at 1.0 cps. For short-time tests with fuel No. 30, there was less attack on the tube wall in the low-frequency test than in the high-frequency test; however, a long-time test indicates little difference.

Thermal-cycle tests have been conducted on Inconel tubing of different grain size and welds. Bend sections have been tested for a comparison of tension and compression areas. Some difference was apparent in the type of attack in small- and large-grained specimens. Attack in the small-grained tubing with a relatively large ratio of grain-boundary area to total area was confined to the grain boundaries. The large-grained tubing with a smaller ratio of grain-boundary area to total area had a more general attack. A comparison of attack in welded and nonwelded areas indicated a relative increase in subsurface voids in the welded area. Tests for compression and tension sections of tubing indicated no difference in attack in the two conditions.

METALLOGRAPHIC EXAMINATIONS FOR THE HOMOGENEOUS REACTOR PROGRAM

T. M. Kegley   R. S. Crouse

The scope of the metallography undertaken for the Homogeneous Reactor Program is indicated in the tabulation given below, which lists micro-

sections that were made during the period September 1, 1956, to August 31, 1957.

	Number of Microspecimens
Materials Research	
Metallurgy	78
Corrosion	241
Engineering Development	
HRT mockup	1
Recombiners	2
Valves and pumps	20
Heat exchangers	77
Engineering Research	
Slurry systems	7
Slurry properties	0
Instrumentation and Controls	
Valves	4
Homogeneous Reactor Test	
Leak detector tubing	157 (600 sections)
High-pressure system flanges	299
Flange bolts and ferrules	41
Other components	23
Total	950

Not reflected in the tabulation is the work involved in macrophotography for the Instrumentation and

Table 42. Metallographic Results of Three Test Conditions

Material	Loop No.	Fluid	Time (hr)	Temperature (°F)	Metallographic Notes	
					Hot Leg	Cold Leg
Hastelloy W with molybdenum insert	1153	107	1000	1500	Surface of molybdenum showed no attack but slight deposit; surface of Hastelloy W was attacked 0.003 in.	
	1154	107	517	1650	No attack at surface of molybdenum but 0.002-in. attack at surface of Hastelloy W	
Niobium clad with type 321 stainless steel	1091	Na	1000	1500	Surface attack of <0.001 in.	Surface attack of 0.002 in.
	1072	107	1664	1500	Surface attack of 0.002 in.	Mass transfer at surface
	1073	107	1000	1500	Surface attack of 0.001 in.	Mass transfer at surface
	1022	107	775	1500	Surface attack of 0.001 in.	No attack nor mass transfer at surface
Inconel with cast Inconel insert	Average of 4 loops	Na	1000	1500	0.001-in. attack in cast section; 0.002-in. attack in wrought section	<0.001-in. attack in both sections
	Average of 6 loops	30	500	1500	0.008- and 0.0085-in. attack in cast and wrought sections, respectively	Mass transfer in both sections

Controls Section, nor the photographic work for slurry research, either for the Materials Research or the Engineering Research Section. The high number of specimens for the Homogeneous Reactor Test reflects the emphasis which was placed on the examination of the HRT leak-detector tubing and flanges during a portion of the year.

Most of the specimens for the metallurgy group of the Materials Research Section were taken from welds of zirconium, titanium, and stainless steel. The specimens from the Engineering Development Section were taken from piping, pump diaphragms, valve seats, poppets, and tube-to-header welds. Most of these specimens were stainless steel, but the valve seats and poppets were of Stellite. The work for the Engineering Research Section consisted in metallographic examinations of a 6-in.-dia type 347 stainless steel pressurized from the slurry mockup, and that for the Instrumentation and Controls section involved bellows of type 347 stainless steel and valve poppets of Stellite. Some of the items from the HRT received for examination included valve bellows, pump diaphragms, piping, and valve poppets.

HOMOGENEOUS REACTOR TEST FLANGE INSPECTION

R. S. Crouse

In February of this year a critical situation developed with the HRT. It was necessary to examine a series of the type 347 stainless steel pipe flanges for stress-corrosion cracking. Some 33 flanges had to be removed from the reactor plumbing and sectioned for metallographic examination. Before sectioning, each flange was dye-checked for possible crack locations. The metallographic samples were then taken from these areas. In all, eight samples were taken from each flange; they were polished and carefully examined and all cracks and other flaws noted. All other work was stopped until these flanges could be examined, since a rapid decision had to be made about the disposition of all the reactor flanges which may have been cracked.

The metallographic examination revealed that the dye-check inspection was unreliable and had not revealed all the cracks existent in the flanges. Of the 33 flanges examined, only 10 showed agreement between the two methods of inspection. Seven of the flanges checked "questionable" or

"acceptable" by the dye-penetrant method were rejected by metallographic inspection, whereas five flanges checked "rejectable" by the dye-penetrant method were acceptable by metallographic inspection. As an example, one of the five flanges is shown in Fig. 114, which reveals the "crack" falsely designated by the dye-penetrant method to actually be a burr in the groove corner. The final decision relative to flange replacement was based primarily on the fact that the two inspection methods did not check each other. It was decided to remove and replace all high-temperature flanges from the system and to remove and replace all other flanges that could not be removed remotely after the reactor goes critical.
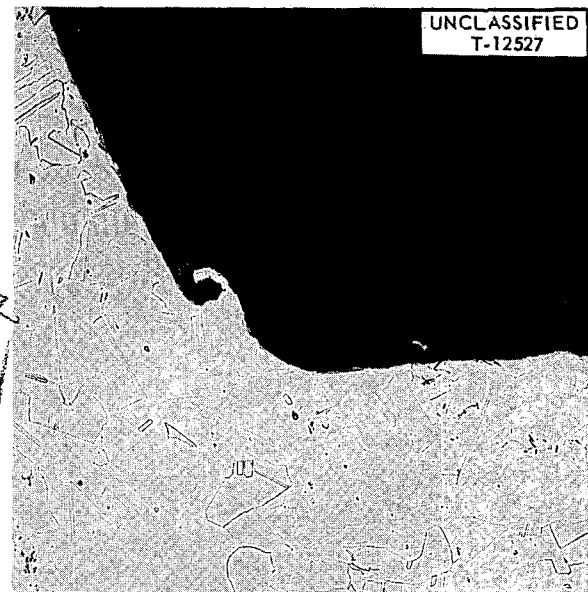
Fig. 114. Machining Burr in Groove Corner. Mistaken for a crack by dye penetrant method. 100X.

Approximately 600 sections of $\frac{1}{4}$-in. type 304 stainless steel heavy-wall tubing from the HRT leak-detector system were examined. The leak-detector tubing connected with flanges in the high-pressure system of the reactor. The sections of leak-detector tubing were examined for inside surface defects and stress-corrosion cracking. The inner surface of defective leak-detector tubing, shown in Fig. 115, exhibited a honeycomb-type surface. The stress-corrosion cracking found in one of the tube sections is given in Fig. 116. Cracking in the tubing and in the flanges previously
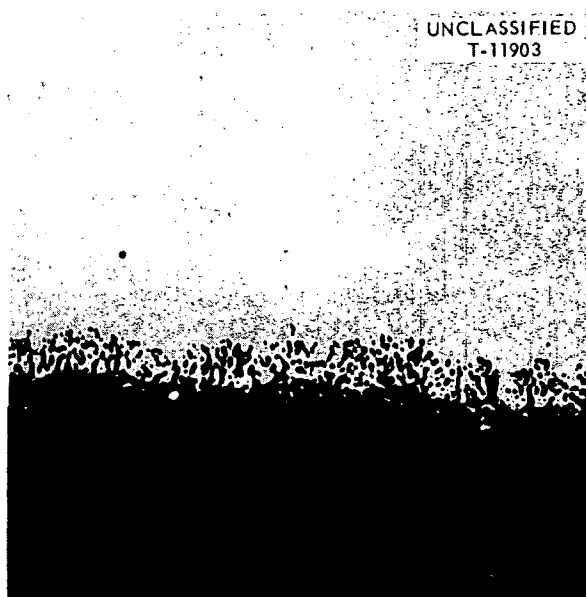
Fig. 115. Inner Surface of Defective HRT Leak Detector Tubing. Unetched. 250X.
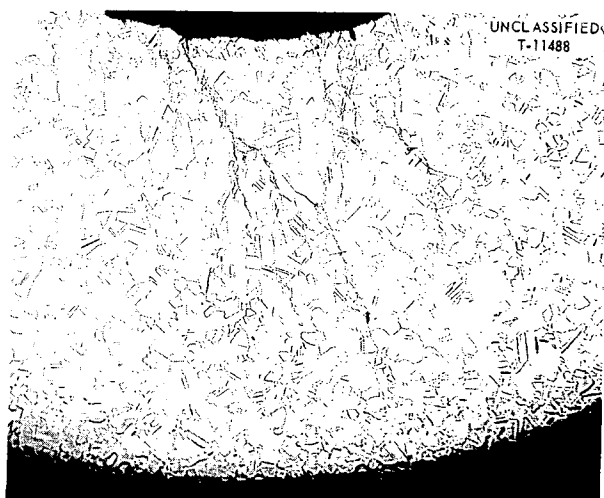
Fig. 116. Stress-Corrosion Cracking in HRT Leak Detector Tubing. Etchant: glyceria regia. 50X. Reduced 26.5%.

mentioned was due to chloride contamination, which was introduced through the use of a contaminated lot of type 304 stainless steel tubing.

STRESS-CORROSION PROBLEM IN HRP

T. M. Kegley

Stress corrosion continues to be a problem in the Homogeneous Reactor Program. Much of the work

submitted to Metallography during the year concerned failures due to stress corrosion.

Stress-corrosion cracking was observed in the HRT mockup. An examination of an end cap of type 347 stainless steel from the 4-in. horizontal header of the mockup showed extensive transgranular cracking (see Figs. 117 and 118) after 3662 hr of exposure to 10 g of uranium per liter of uranyl sulfate. Cracking, not so extensive as that observed in the end cap, was observed in a 6-in.-dia O-ring taken from the mockup. Extensive transgranular cracking was observed in a type 347 stainless steel bellows from the solids-separation loop of the mockup. The bellows in this case had operated for only 183 hr before failure. All these failures by cracking in the HRT mockup were probably due to chloride stress corrosion.

Stress-corrosion cracking was found in stainless steel O-rings taken from slurry loops, which were used to circulate thorium oxide slurries in corrosion tests. The cracking was transgranular and was probably due to chloride contamination introduced through the slurry.

A purge-water condenser from a 200-gpm loop exhibited transgranular cracking near a silver-soldered joint. The condenser was used to condense steam from the pressurizer. Although it had been anticipated that the failure may have been related to the silver-soldered joint, it was found that the silver solder had played no part in the failure. Cracking was most probably due to stress corrosion, although the extensive history of the condenser prevented any definite conclusion from being made.

Intergranular cracking rather than transgranular cracking (Figs. 119 and 120) was found in a 1-in. pipe taken from the high-pressure recombiner loop. The 1-in. pipe had been exposed to superheated steam at 245°C for about 300 hr of intermittent operation. The walls of the pipe were exposed to KOH, possibly as much as 0.5% KOH, due to entrainment. This cracking was believed to have resulted from a form of stress corrosion, possibly due to the caustic environment.

Other Problems in HRP

A set of titanium wear rings and orifice restrictors from slurry corrosion loops was examined. These rings and restrictors, which had been exposed to hydrogenated thorium oxide slurry at 300°C, had absorbed substantial quantities of hydrogen, which was observed in the microstructures of the titanium.

161
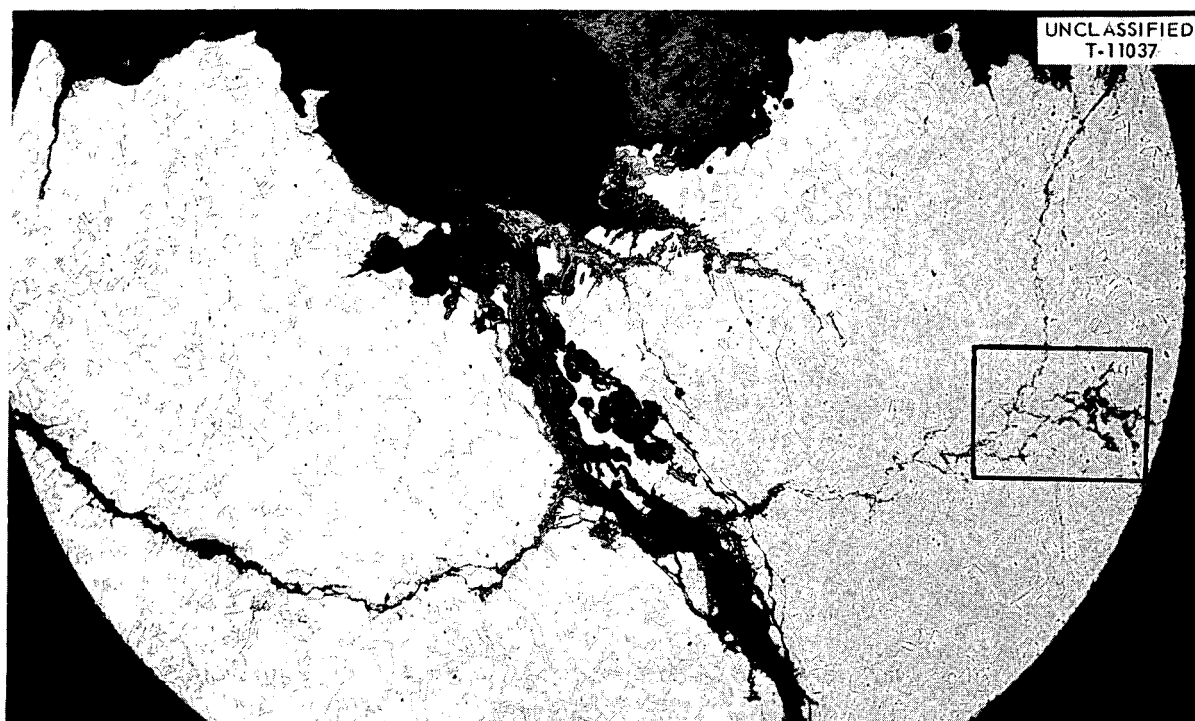
Fig. 117. Stress-Corrosion Cracking in End Cap from 4-in. Horizontal Header of HRT Mockup. Etchant: aqua regia. 50X.
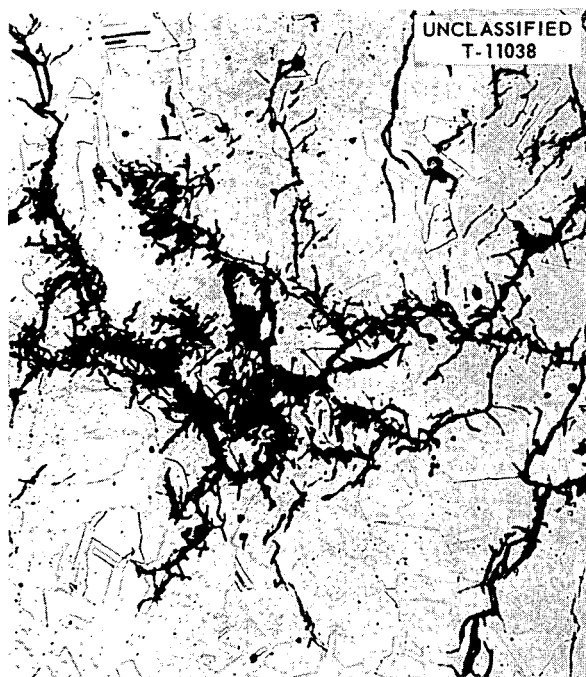
Fig. 118. Stress-Corrosion Cracking. Same area as that outlined in Fig. 117. Etchant: aqua regia. 250X.
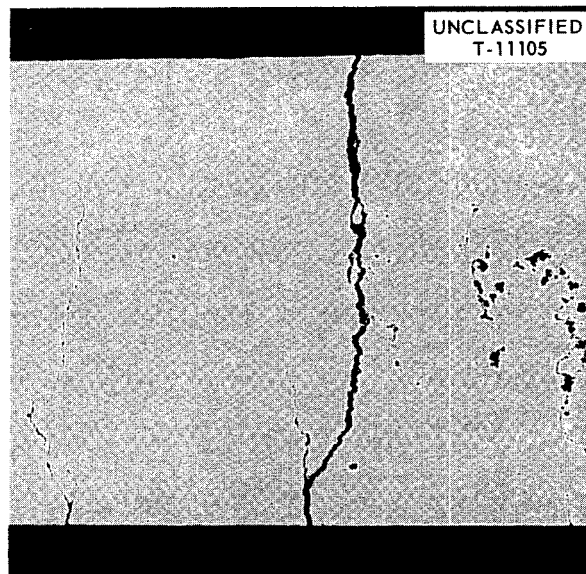
Fig. 119. Cracking in 1-in. Pipe from High-Pressure Recombiner Loop. 14X.
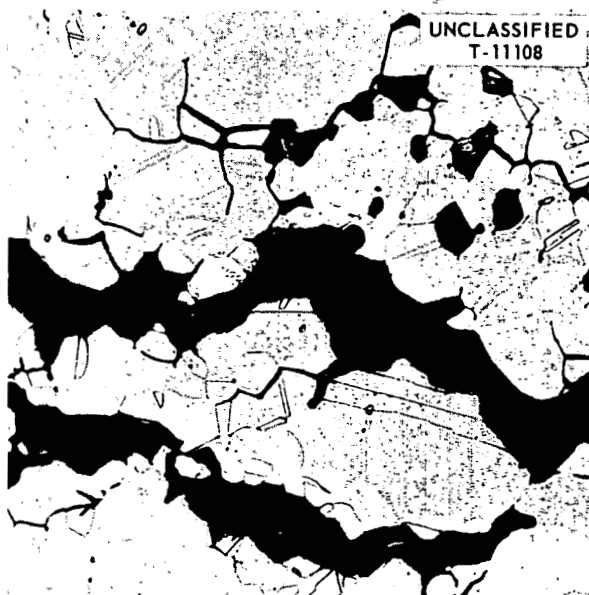
Fig. 120. Intergranular Nature of Cracking in 1-in. Pipe from High-Pressure Recombiner. Etchant: glyceria regia. 250X.

The as-received and after-exposure microstructures of an orifice restrictor of 100A titanium (commercially pure Ti with 100,000-psi yield strength) are shown in Fig. 121.

Flange bolts and ferrules of 4140 steel intended for HRT use exhibited cracks and were examined. Cracks in bolts and ferrules were attributed to quench cracking.

METALLOGRAPHIC EXAMINATION OF PUMP LOOPS

R. S. Crouse

Thirty-eight pump loops have been examined for the Corrosion Group of the Metallurgy Division. These loops were of four different types according to the method of heating and/or the general configuration of the system. Basically, all types consisted of a closed loop with a pump and heating and cooling sections. The following discussion describes each loop type and gives some of the results obtained.

Economizer-Type Loop

This design consisted of a heated loop and a cooling loop connected by a concentric-tube heat economizer or preheater. This method was used to conserve power by using the hot fluid to preheat the fluid from the cold loop.

Most of the loops were constructed of Inconel, and all of them circulated sodium. Other loops were of Hastelloy B, Inconel X, types 304, 347, and 430 stainless steel, and Hastelloy W and were used to check the corrosion and mass-transfer characteristics of these alloys in sodium.

(a)

(b)
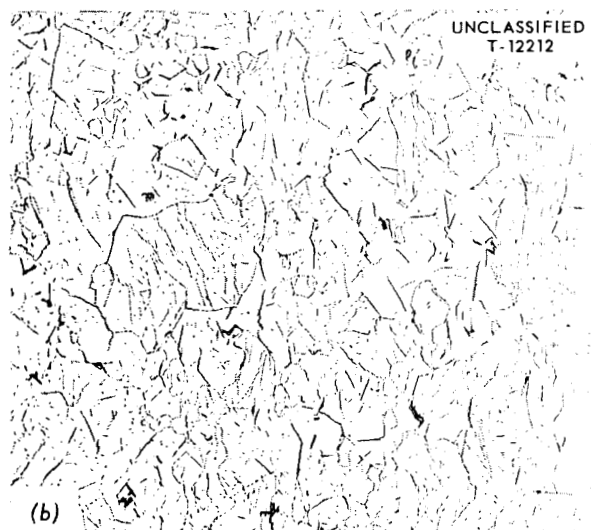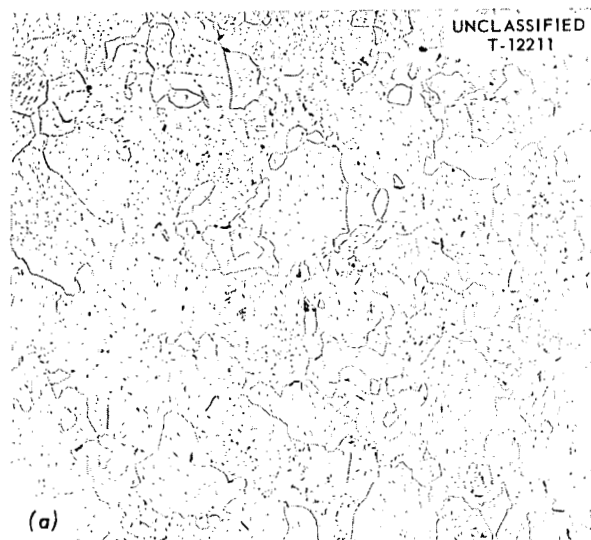
Fig. 121. Hydrogen Absorption in 100A Titanium Orifice Restrictor. (a) As received, 170 ppm H; (b) after exposure to hydrogenated slurry, 400 ppm H. Etchant: 5 HF−10 HNO_3−20 glycerine. 100X. Reduced 11%.

163

In a standard test — 1000 hr at 1500°F with a 300°F ΔT — Inconel showed pitting to 2 mils deep in the hot loop and a metal crystal deposit about 12 mils thick in the economizer. Increasing the time served to increase the deposit, as did the addition of metallic titanium in the hot leg.

The stainless steels had much less attack and mass transfer than did Inconel. Inconel X was about the same as Inconel, and Hastelloy B was erratic, the same conditions producing varying results.

U-Bend Pump Loops

This nomenclature was used because of the general shape of the heated section, which was an elongated U. The heating was done in the legs of the U by electrical resistance; the bend was not heated but was insulated. The heated sections were followed by a finned cooling coil. This type of loop was used primarily to circulate fluorides in Inconel and Hastelloy B.

Inconel showed heavy subsurface void formation 5 to 7 mils deep and very little mass transfer. The tests were for 1000 hr or less at 1500 to 1600°F with fluoride composition No. 30 or No. 70.

Considerable difficulty was experienced in maintaining a leak-free Hastelloy B—fluoride system. It was possible to make some tests successfully, however, and they indicated that the system was a compatible one with little attack but with some tendency for mass transfer.

Gas-Fired Loop

These loops had a coil section in a gas furnace and a finned cooling coil in an air blast. They were capable of higher temperatures and greater temperature differentials with lower power costs and were therefore used primarily for endurance and life tests.

Only four gas-fired loops were examined. Of these, three were of Inconel with sodium, NaK, and fluoride No. 30. The fourth was Hastelloy B with sodium under standard conditions. These tests were not primarily corrosion tests but rather were performance tests, and metallographic examination provided very few meaningful data.

Sodium-Heated Loops

The hot leg of this loop was a straight section of tubing in a sleeve of molten sodium. The sodium was heated by clam-shell heaters. The cooling coil was in an air blast. Only sodium and NaK

were circulated in these loops, and Inconel was the only alloy of which the loops were constructed. High temperature differentials were possible with these loops. It was found that the attack was somewhat heavier and the mass transfer greater than in other sodium-Inconel systems. This was possibly due to the higher temperature differential in these loops.

METALLOGRAPHIC INSPECTION OF REACTOR CORE SHELLS

R. S. Crouse

In conjunction with the Inspection Group, Metallography developed a set of metallographic specifications for the acceptance of core shells for the ART. These specifications dealt primarily with the grain size of the material. With this specification, ten core shells were examined, and about half of them were rejected because of the grain size being too large. Subsequent discussions and investigations indicated that the grain-size specifications were too rigid; therefore dimensional tolerance was used as a guide to acceptance or rejection of core shell.

PREPARATION AND METALLOGRAPHY OF ARC-MELTED URANIUM CARBIDES[1]

R. J. Gray   C. K. H. DuBose
W. C. Thurber[2]

The limitation of 20% enrichment placed on fuel available for export under the Atoms-for-Peace Program has necessitated the replacement of the 10 to 20 wt % enriched U^{235} core in reactor fuel plates with a higher percentage of normal uranium. Under such limitations, a fuel-plate core would require a uranium-aluminum alloy with approximately 50 wt % uranium. An alloy containing this much uranium would impose considerable difficulty due to segregation and would not lend itself to established fabrication procedure.

The high density of uranium carbides (11.7 to 13.6 g/cc) makes them attractive as a fuel material to meet the problem of reactor designs requiring a high uranium investment and lends itself to the picture-frame technique for the fuel-plate fabrication.

---

[1]To be presented at the Second World Metallurgical Congress in Chicago, Nov. 4–8, 1957, and to be published in the *Transactions of the American Society for Metals* for 1958.

[2]Process Metallurgy Group.

Three carbides — the monocarbide (UC) containing 4.80 wt % C, the sesquicarbide (U_2C_3) containing 7.04 wt % C, and the dicarbide (UC_2) containing 9.16 wt % C — have been reported for this binary system. The sesquicarbide cannot be produced directly but, rather, requires a slight amount of stressing to initiate formation from a mixture of UC and UC_2 (ref 3). The sesquicarbide is not included in this investigation.

The carbides UC and UC_2 were produced by inert-gas arc melting of cleaned uranium and varying amounts of spectrographic carbon rod. The melting equipment is shown in Fig. 122. Figure 123 shows a substoichiometric UC with some α-uranium at grain boundaries and as spheroids. Figure 124 shows a matrix of UC with Widmanstätten and grain-boundary precipitates of UC_2. A 50-50 ratio of UC and UC_2 is shown in Fig. 125. The dark and white phases are UC and UC_2, respectively. The dark Widmanstätten precipitate in Fig. 126 is the UC in a matrix of UC_2.

[3] M. W. Mallett, A. F. Gerds, and D. A. Vaughn, *Uranium Sesquicarbide*, AECD-3060 (Jan. 31, 1950).
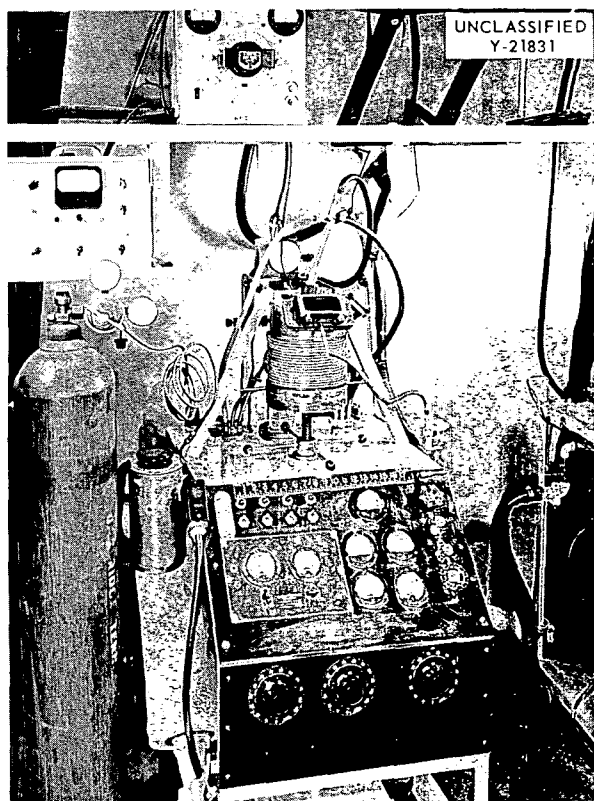
Fig. 122. Inert-Gas Arc-Melting Equipment.

Figure 127 shows a microstructure of 90% UC_2 and 10% UC.

Aluminum-clad fuel plates of aluminum powder and UC_2 have been fabricated as shown in Fig. 128.

PROGRESS AND STATUS OF DEVELOPMENT OF POLISHING TECHNIQUES FOR METALLOGRAPHIC SPECIMENS EMPLOYING VIBRATORY POLISHING MACHINES

E. L. Long, Jr.

In November 1956 a small vibratory lap-polishing machine was purchased for an investigation of its potentialities in preparing metallographic specimens in a metallography laboratory as well as possibly in remote metallography laboratories. The small, 5-in.-dia polisher is shown in Fig. 129. After a test of two months an operation of this nature appeared to be feasible, and an order was placed for three larger vibratory polishing machines. They were received in March 1957, and since then, much effort has been expended in developing good polishing techniques for metallographic specimens.

To date the following materials have been successfully polished in manners that can be classified as routine techniques: Al, Au, Be, B_4O, B_4C, Cd, Cu, Mo, Ni-Mo alloys, Nb, Pt, UO_2, U_3O_8, Zr, Zr alloys, and all stainless steels that have been submitted to this department.

Nickel and Inconel are the only more common metals that are exhibiting any polishing difficulties. However, if an electrolytic etch can be used rather than a chemical etch, excellent results can be obtained without any danger of misinterpretation of structures.

A point that would be pertinent to future considerations for employing this technique in any remote metallography is that inexpensive petroleum mediums, such as mineral oil, can be substituted for water in the alumina abrasive slurries. This substitution serves a twofold purpose: it is possible to polish specimens that would be subject to attack after relatively long exposures to water, and any air-borne contaminants arising from the polishing operation can be controlled by means of normal handling precautions.

The vibratory polishing machines have operated for seven months and have required no maintenance except for occasional changing of polishing cloths, which is a normal procedure in any continued polishing operation. Adaptor plates for "quick-change" polishing bowls were fabricated to
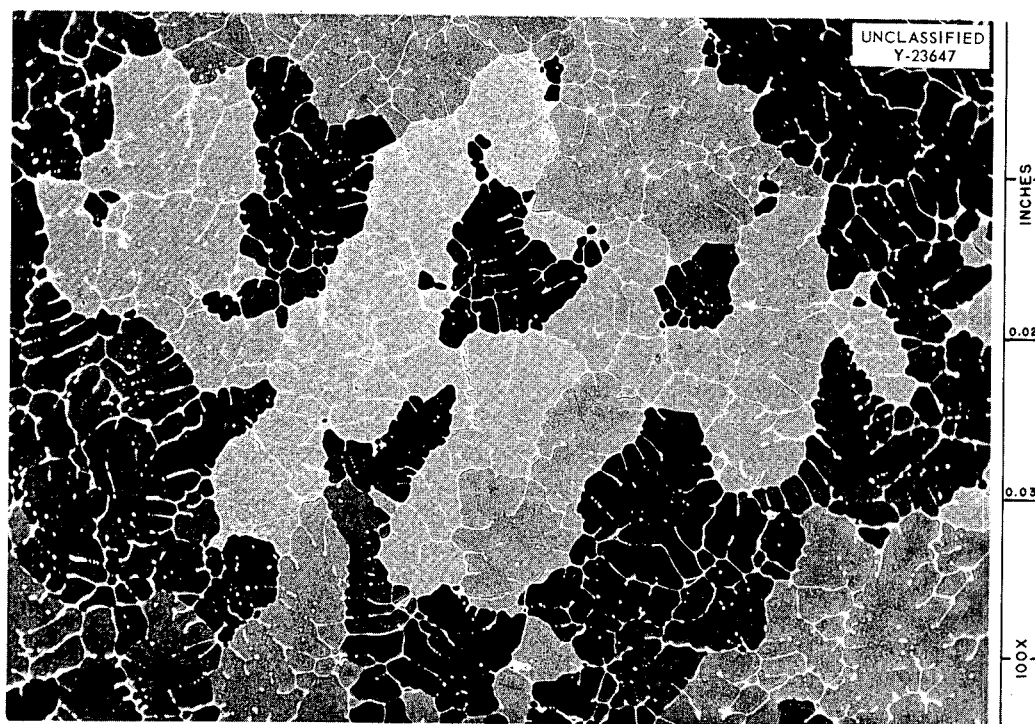
Fig. 123. Photomicrograph of 99% UC Matrix and 1% α-Uranium. Reduced 17%.
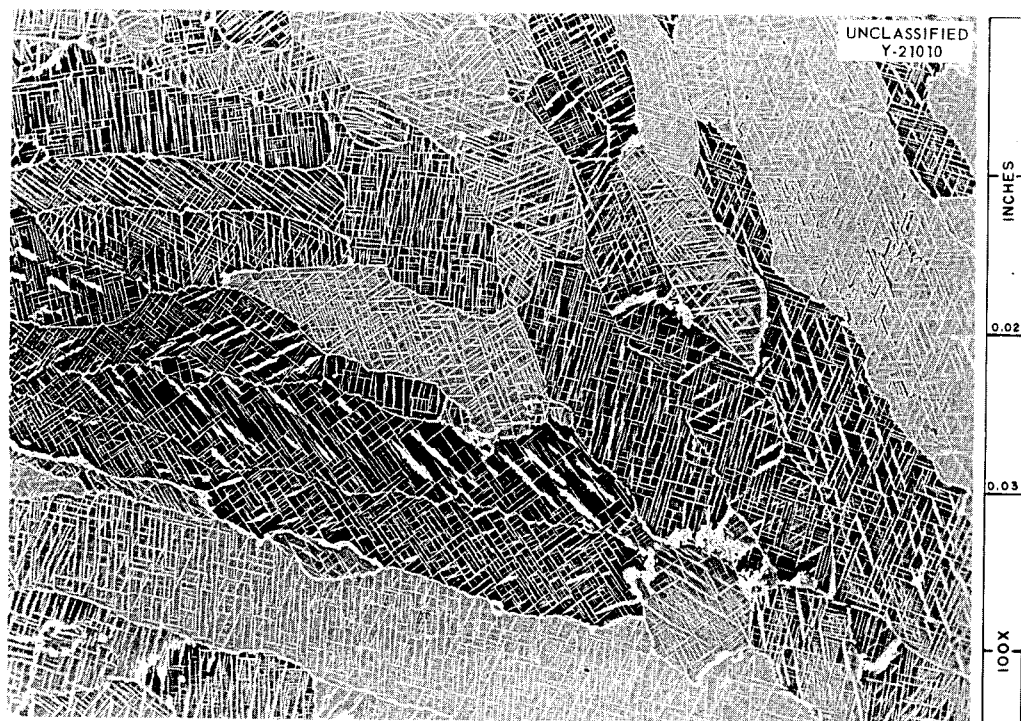
Fig. 124. Photomicrograph of 90% UC Matrix and 10% UC_2. Reduced 18%.
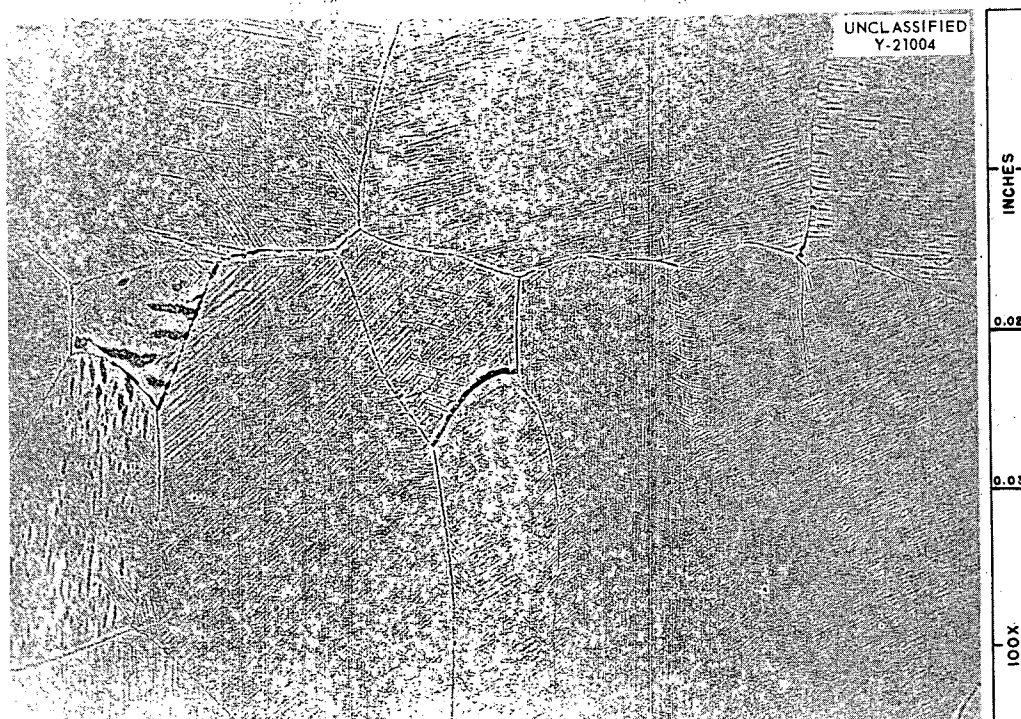
Fig. 125. Photomicrograph of 50% UC and 50% UC_2. Reduced 18%.

Fig. 126. Photomicrograph of 80% UC_2 and 20% UC. Reduced 18%.
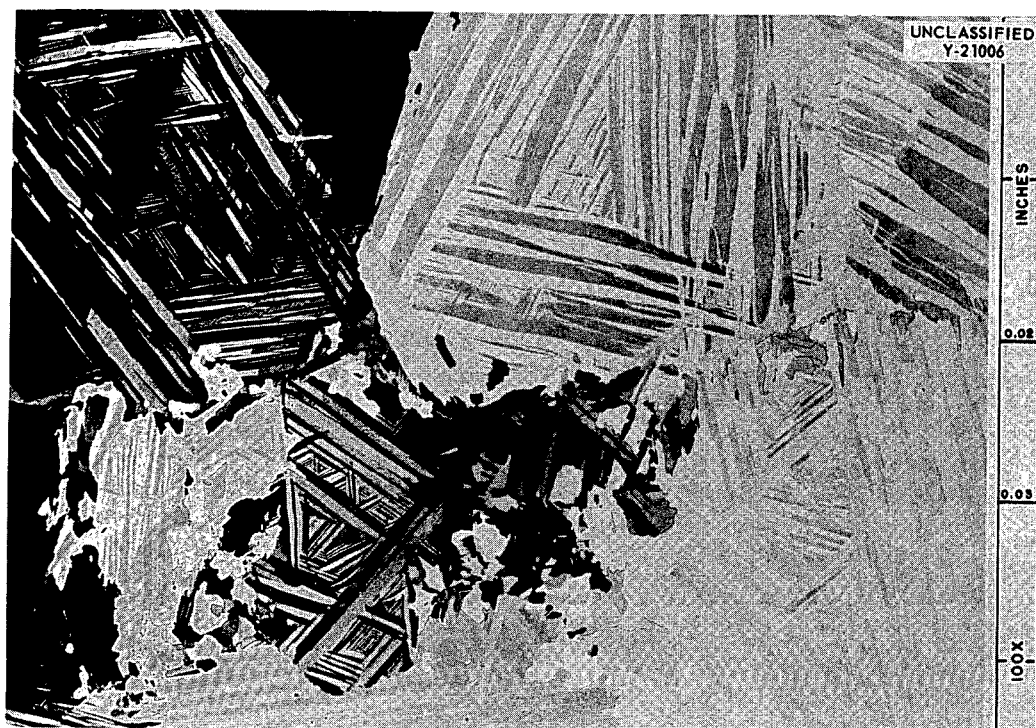
Fig. 127. Photomicrograph of 90% UC$_2$ and 10% UC. Reduced 17%.
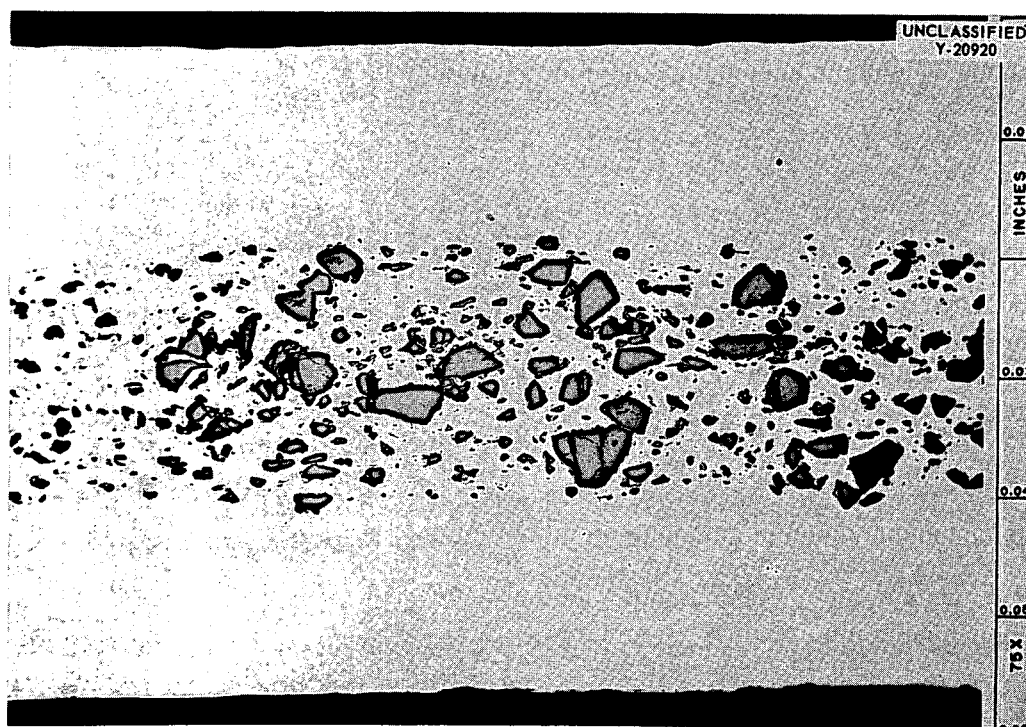
Fig. 128. Transverse View of Completed Fuel Plate with Uranium Dicarbide–Aluminum Core. Reduced 17%.

Vibratory Polishing Equipment

Fig. 129. Small Vibratory Polisher (5-in.-dia Bowl) Employed in Initial Investigation.

facilitate washing out spent abrasive, collected contaminants, etc.; this also allows the operators to keep bowls containing various abrasives on hand. Additional sample holders were fabricated also. The above fabrications increased the maximum daily output from approximately 20 to 25 samples to triple this number. Figure 130 shows the larger vibratory polishers with the adaptors for "quick-change" bowls.

Although there are many advantages in employing the vibratory polishers whenever possible, only a few of the major ones shall be mentioned. The main advantage is that polished surfaces comparable to, and in many instances better surfaces than, those obtained by hand-polishing can be achieved; in addition, the operator or technician is free to carry out other duties during the polishing operation. As an example, approximately 12 to 24 platinum gage strips are submitted periodically for polishing.

An 8-hr work period is required for one operator to hand-polish 12 strips; this time is reduced to approximately 1 hr with the vibratory polisher, and the actual time charged to the requestor is reduced from 8 hr to approximately 20 min.

A typical example of one of the more difficult samples to polish by hand that was polished on the vibratory polishers is shown in Fig. 131. This specimen is an Ni-V-Ag junction that had been silver soldered. Normally, excessive rounding and/or relief polishing would occur from hand polishing before a scratch-free surface could be obtained.

The schematic sketch in Fig. 132 gives the various parts of the vibratory polisher, as well as a simplified vectorial diagram illustrating the principle of operation. In essence the vibratory polisher consists of a base unit, which houses the springs and magnet assembly, and a bowl

169
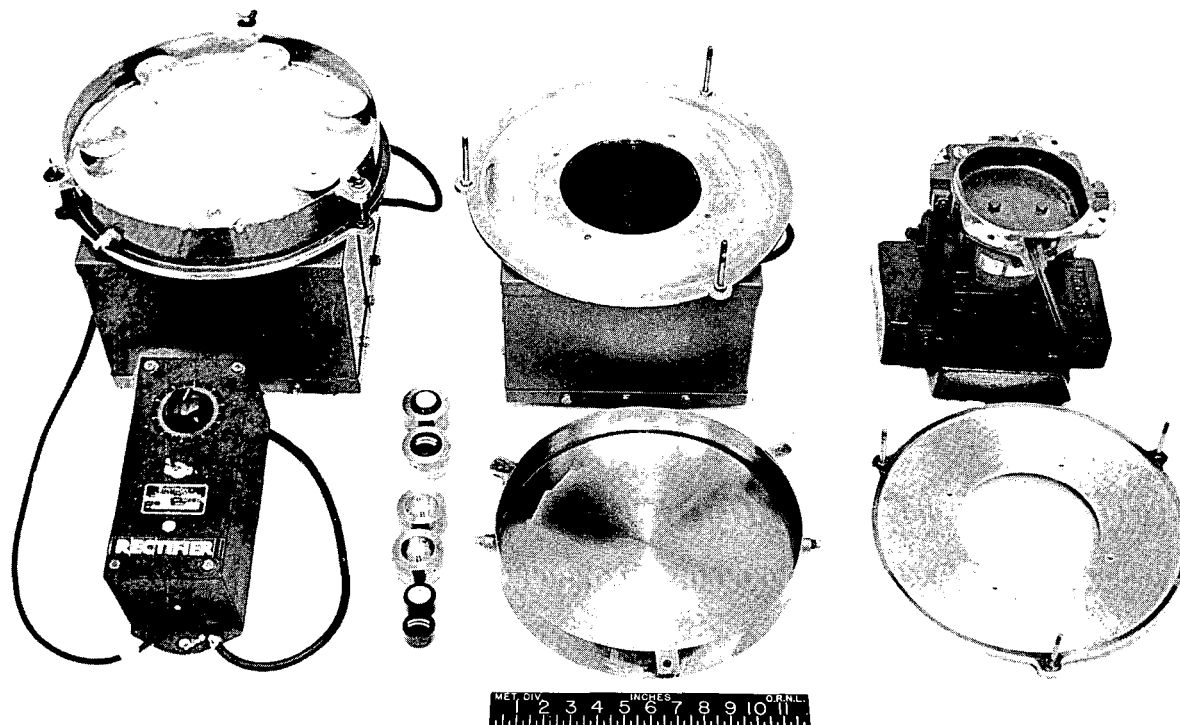
VIBRATORY POLISHERS WITH ADAPTORS FOR QUICK-CHANGE BOWLS

Fig. 130. Vibratory Polishers with Adaptors for Quick-Change Bowls.

containing a flat plate covered with a selected polishing cloth or abrasive paper. The principle of operation is based on the tuned spring system. The magnet is energized by pulsating current. The springs are arranged in a circle and mounted at such an angle that the vertical pull of the magnet causes the bowl to vibrate vertically and in an arc. The positive action of vibratory polishing machines in rotating the metallographic specimens around the periphery of the bowl is due mainly to energization of the electromagnet by a pulsating current.

Each unit is furnished complete with a separate controller, which can be mounted nearby or for remote work. The controller contains the operation

switch, a dial rheostat for controlling the speed of flow of the material in the bowl, and a rectifier that converts alternating current into pulsating current for energizing the electromagnet.

In conclusion, this new method of polishing metallographic samples has been accepted by all the Metallography personnel, and their general consensus is that the vibratory polishing machines are filling a definite need in metallography, although considerable developmental work remains to be done before specimens can be economically processed by use of the vibratory polishers exclusively. This technique of polishing is showing definite promise for remote metallography.

Fig. 131. Photomicrograph of Ni-V-Ag Junction with Ag Solder Weld. Etchant: 50% KCN–(NH₄)₂S₂O₈ and glycerine. 50X. Reduced 19%.

Fig. 132. Schematic Drawing of Vibratory Polisher.

ELECTRON MICROSCOPY

Development of Operational Technique

W. H. Bridges   E. L. Long, Jr.

The RCA electron microscope, model EMU-3B, was installed during August 1956, and since then, many varied problems have been undertaken. A few months were devoted to development of basic techniques, which have since been refined so that most metallurgical samples can be successfully replicated and examined.

A great deal of the time with the microscope was spend in studying thin films of oxides in support of work by the High-Temperature-Reactions Group. One replication problem illustrates the frustratingly slow development of technique. The Zircaloys and zirconium-niobium alloys are being investigated by the Homogeneous Reactor Group. As normally treated for light microscopy, a very thin anodized film covers the surface of the sample. The anodized surfaces are easily replicated with Formvar (a dilute solution of polyvinyl formal in chloroform), but with the anodic film present, the fine microstructure of the alloys cannot be resolved. Without the film, Formvar replicas have

171

not been successfully drawn from the specimen. Carbon replication seemed to be a solution to the problem. The procedure calls for evaporating, in vacuum, a thin film of metallic shadowing on the specimen surface and then evaporating carbon over the film. The shadowed carbon film is then removed from the specimen by chemically etching the base metal away from the film, followed by floating the film on water and picking it up on a

microscope grid. The first few attempts were unsuccessful because the violent action of the $HF-H_2SO_4$ etching mixture tore the carbon film to pieces. With the specimen held close to, but not touching, the acid mixture, the vapors attack the base metal sufficiently to allow the film to come loose in water. A typical structure revealed in a zirconium alloy employing the carbon-replication technique is shown in Fig. 133. While the foregoing
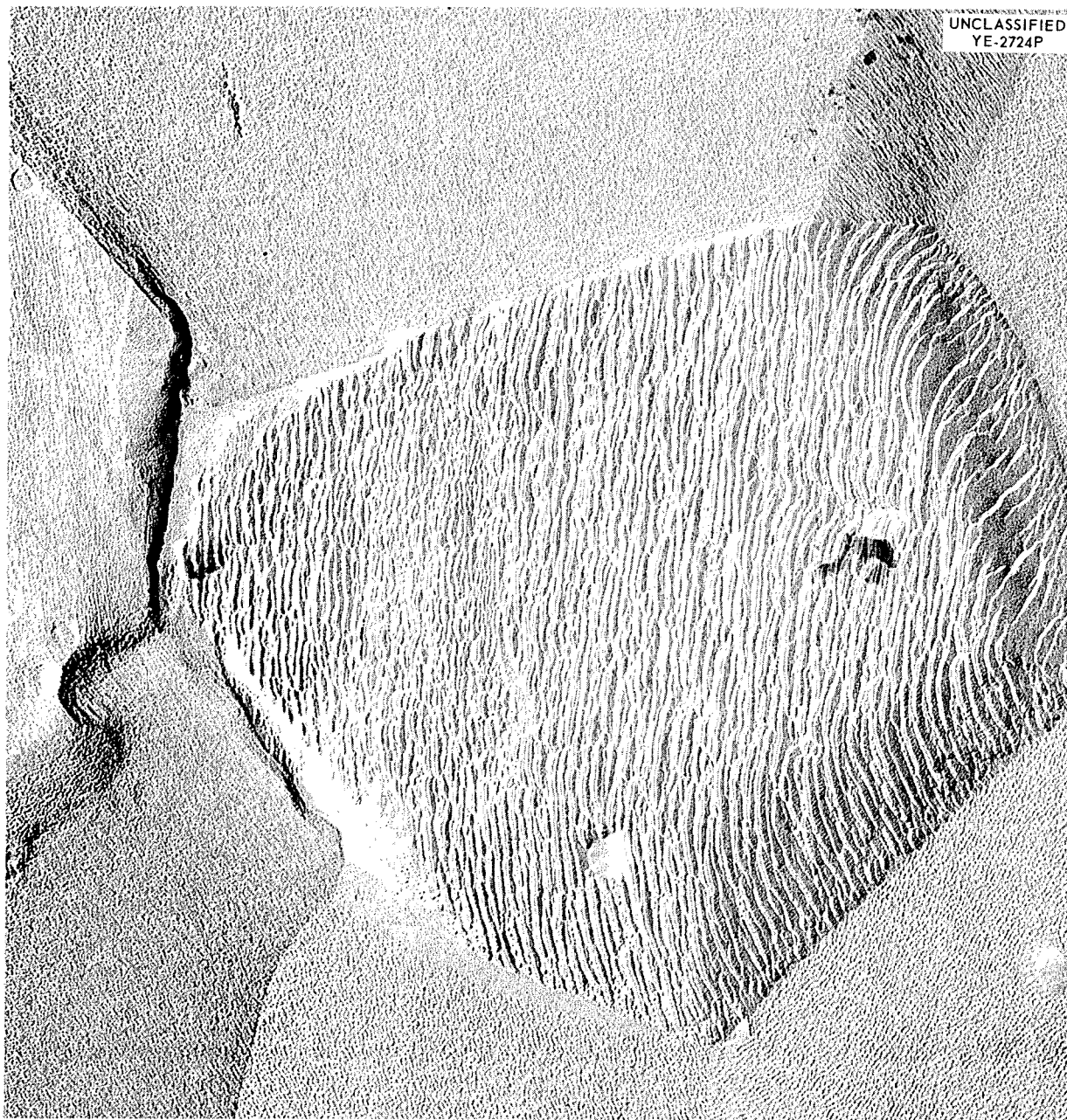
Fig. 133. Zircaloy-2 Cathodically Etched (15 min at 3500 v). Carbon replica shadowed with Pd. 22,560X. Reduced 10%.

method is well noted in the literature, the development of an individual technique is a time-consuming process.

Techniques have been acquired for the replication of specimens containing many voids, such as cermets, powder compacts, and braze metals. For such materials an indirect method is employed. The specimen is pressed into hot sheet plastic, and, when cool, the relatively thick plastic film can be stripped off. The strength of this film is sufficient for it not to tear or be excessively strained. The thick film is then replicated with Formvar, which is stripped, shadowed, and examined.

A few of the many varied samples submitted for examination were powders for particle-size determination and morphological studies, thin films for structure and orientation studies, microstructures of metals and alloys including development alloys of interest to the various reactor programs, and alloys which had undergone a series of various treatments to determine small variations in their structure.

The operation of the electron microscope has been quite satisfactory. During the initial period several difficulties arose which were directly attributed to inexperience. Except for a defective electron gun leaking insulating grease into the microscope, most of the down time was, for routine maintenance.

In the first year of operation approximately 500 specimens were submitted, and approximately 2000 photographs of record have been made.

The Microstructure of Inconel

E. L. Long, Jr.   W. H. Bridges
J. E. VanCleve

For some time doubt has existed as to whether certain microfeatures, which appeared to develop in definite crystallographic arrays in Inconel annealed at relatively high temperatures, were real or were an etching artifact. As the Electron Microscopy Section was only recently activated, they felt that the resolution of such an enigma would provide excellent training in techniques and interpretation. A sample of Inconel was obtained which had been annealed at 2050°F and then used as a stress-relaxation specimen. The sample was polished and electrolytically etched with oxalic acid, one of the usual etchants for metallographic examination in this laboratory. Microscopic observation showed the characteristic microstructure, Fig. 134. The sample was then replicated with Formvar solution (0.75% polyvinyl
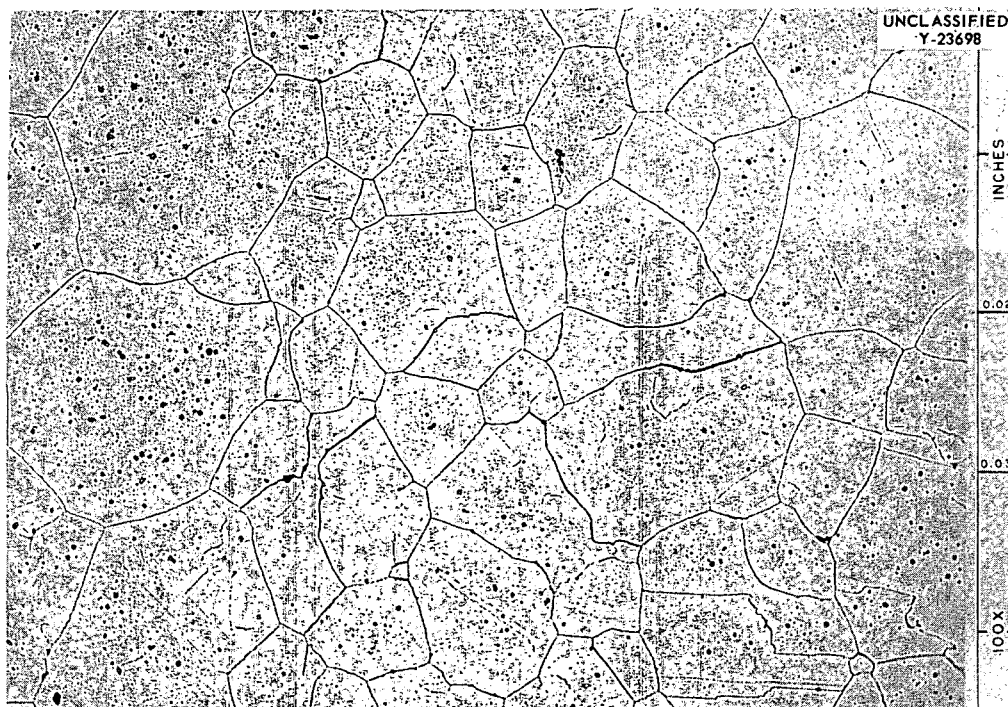
Fig. 134. Inconel Etched Electrolytically with 10% Oxalic Acid Electrolyte. Reduced 16%.

formal [Shawinigan 15/95] in chloroform) and shadowed with gold-Manganin alloy. The replica was then examined in the electron microscope, Fig. 135 being representative. The same sample was repolished and electrolytically etched with sulfuric acid. Formvar replicas, shadowed as before, were examined, and Fig. 136 is a typical electron micrograph.

Another common etchant, nitric acid–hydrochloric acid–glycerin (Glyca regia) mixture, was used. This etch does not usually reveal the characteristic aligned features. When the specimen is replicated, shadowed, and examined in the electron microscope, however, the aligned features are present (Fig. 137) but show one major difference — instead of being pits in the original surface, they are standing above the surface. This was proved by placing very small polystyrene latex spheres (2580 ± 30 Å diameter) on the surface of the replica before it was shadowed. From the direction of the shadows with reference to the shadow of the sphere, it can now be definitely determined during the examination whether or not the features of interest are elevated or depressed. As illustrated in Fig. 138, the

sphere and its shadow are quite evident, and the shadow pattern of the triangular features is reversed. As the sphere is known to be above the surface of the replica, the point of the triangles must be below the surface. As the replica is negative to the original specimen surface, the original feature must stand above the surface.

After being repolished, the specimen was vacuum-cathodic etched in argon. After replicating and shadowing, the electron micrograph (Fig. 139) still shows the characteristic features, and again they are pits in the original surface.

Mahla and Nielsen[4] observed such a phenomenon and developed a method for extracting extremely minute particles from the material for electron studies. With the thought that the structure observed here might be a fine $M_{23}C_6$ precipitate developing along the preferred crystallographic directions, it was decided to attempt the extraction techniques. The specimen was repolished and then etched with 7.5% bromine in methyl alcohol.

---

[4]E. M. Mahla and N. A. Nielsen, *Trans. Am. Soc. Metals* 43, 290 (1951).

UNCLASSIFIED
YE-2025
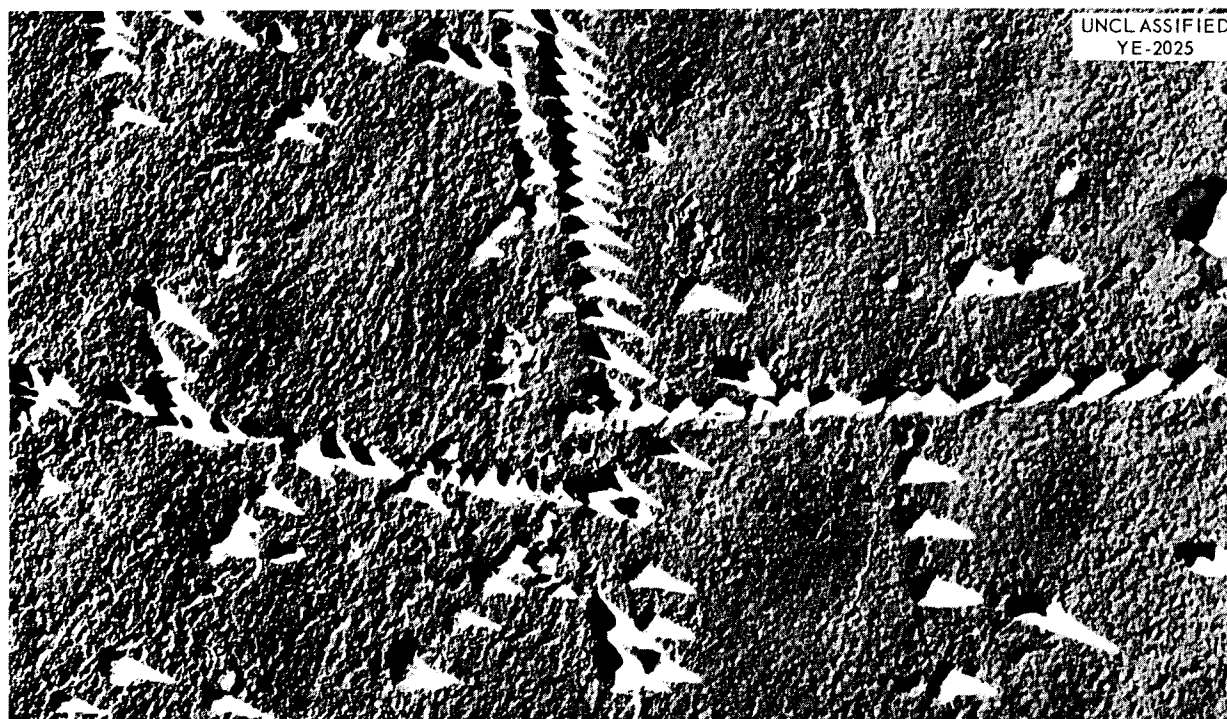
Fig. 135. Inconel Etched Electrolytically with 10% Oxalic Acid Electrolyte. Formvar replica heavily shadowed with gold-Manganin alloy. Note that shadow face of each precipitate triangle appears to be oriented in same direction. 9300X.
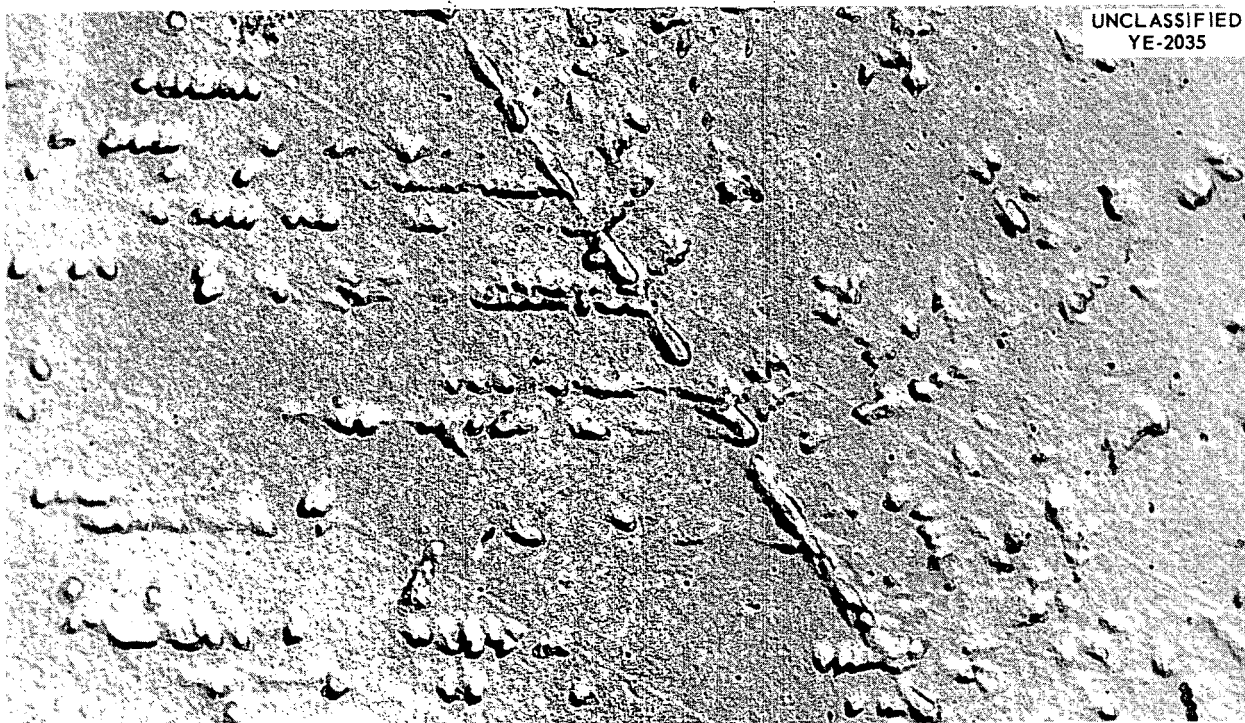
Fig. 136. Inconel Etched Electrolytically with $\frac{1}{2}\%$ H_2SO_4 Electrolyte. Formvar replica shadowed with gold-Manganin alloy. Note alignment of precipitate. 9300X.
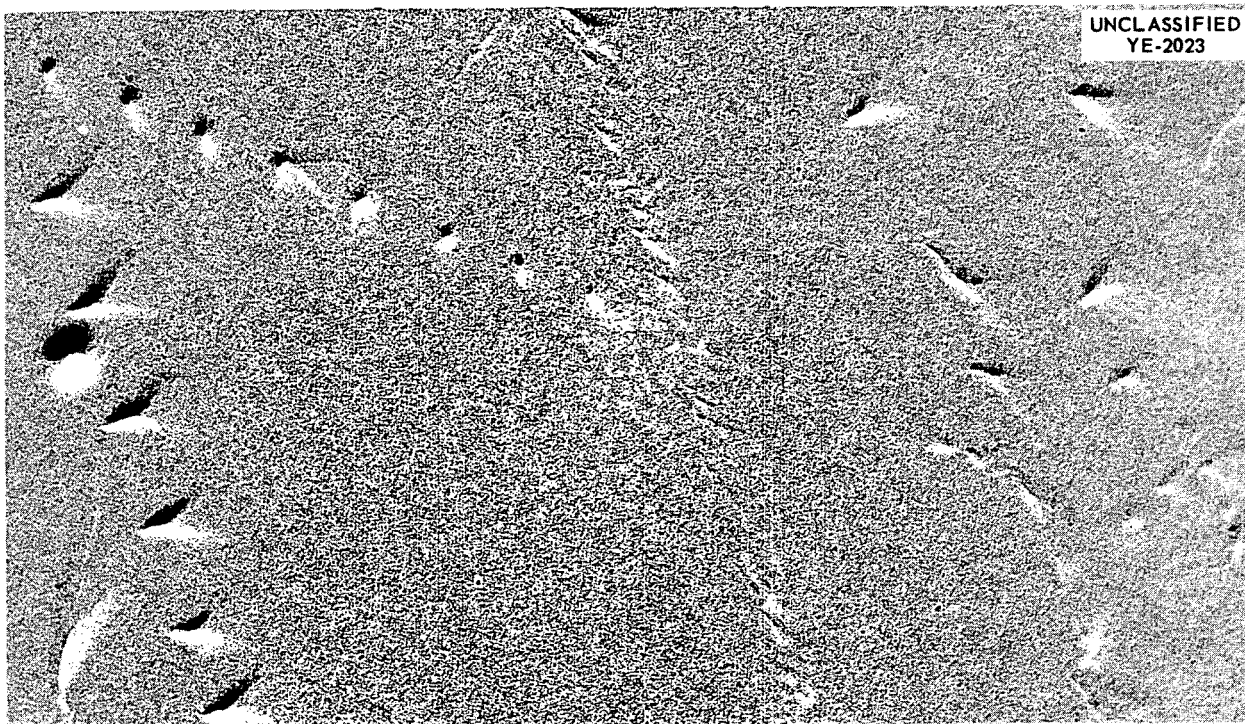
Fig. 137. Inconel Etched with Glyceria Regia. Formvar replica shadowed with gold-Manganin Alloy. "Shark tooth" precipitate is characteristically aligned. 22,500X.

175

Fig. 138. Inconel Etched with Glyceria Regia. Sphere placed on surface to determine shadowing direction. Formvar replica shadowed with gold-Manganin alloy. Same replica as in Fig. 137. Shadows cast by "sharks teeth" can be correlated with shadow of ball. 90,000X.

Fig. 139. Inconel Cathodically Etched in Vacuum. Formvar replica shadowed with gold-Manganin alloy. While not obvious here, lower magnification shows the characteristic alignment of the precipitate. 22,500X.

The surface was then replicated and shadowed. An electron photomicrograph of a typical specimen is shown in Fig. 140.

While the bromine–methyl alcohol etch produced a dramatic surface, the first attempt did not yield any particles for study, probably as the result of too vigorous washing after etching. The procedure was tried again, and this time particles did adhere to the replica. Unfortunately, the diffraction patterns from them were not interpretable. The

UNCLASSIFIED
YE-2291
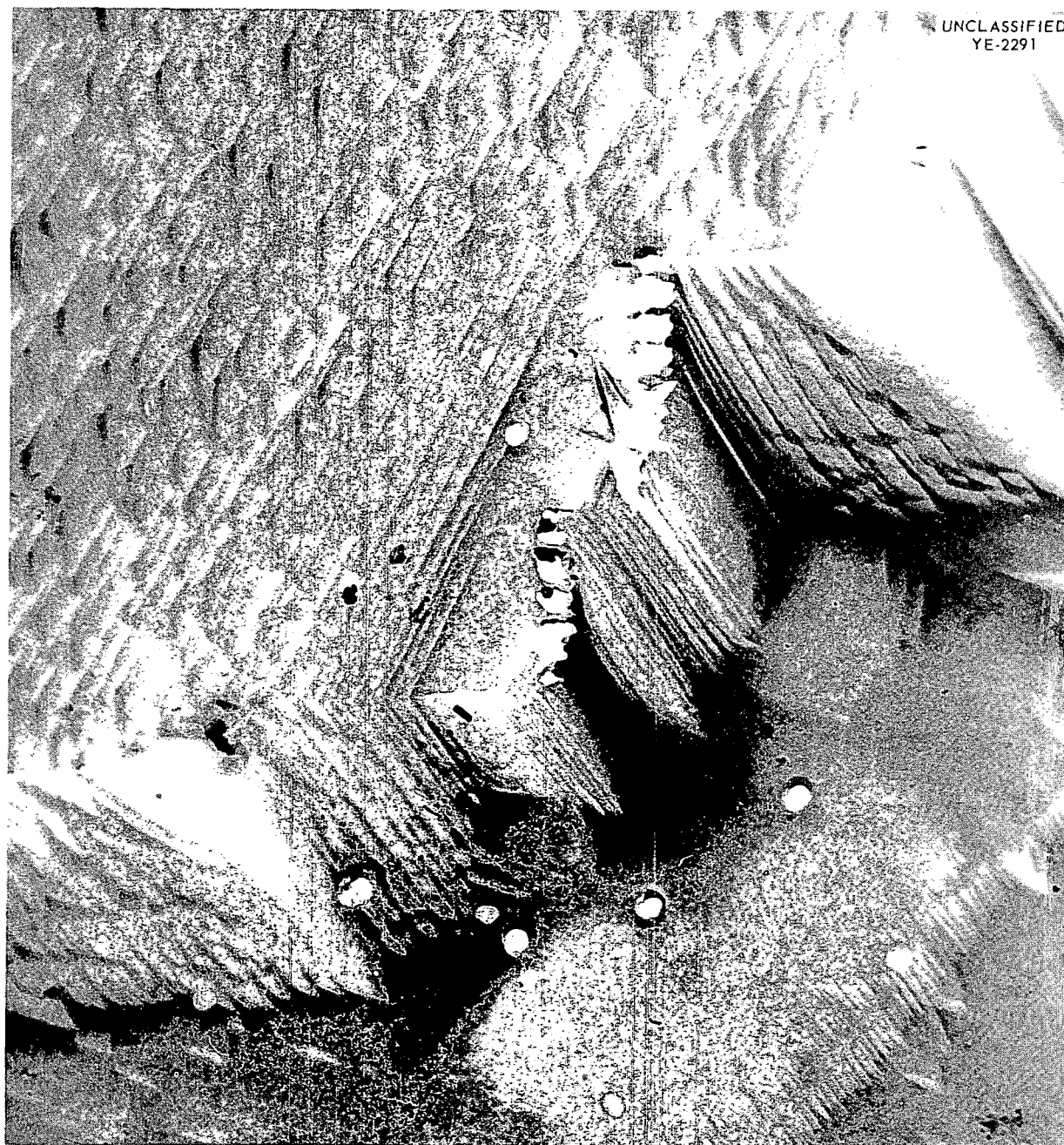
Fig. 140. Inconel Etched with 7.5% Br in Methyl Alcohol. Formvar replica shadowed with gold-Manganin alloy. The bright dots along the top of the "cliff" are small tears in the replica. The small black specks are probably the precipitate in the grain boundary which came off with the replica. 12,000X. Reduced 4%.

Formvar replica was sufficiently thick to cause a large diffuse central area, and so few spots were definitely measurable that the results would be completely unreliable.

As a result of this short, preliminary study, much valuable experience was gained; but most important, it has been definitely established that the microstructure in question is real and not an artifact.

DILATOMETRY

J. R. Riddle

The direct-reading, quartz differential dilatometer of the Metallography Section has been altered so that specimens can now be heated in a vacuum or in an argon atmosphere. The temperature programmer on the dilatometer has also been modified so that power input is supplied by a pneumatically operated Variac which is geared to the programmer. This system eliminates the temperature oscillations formerly encountered under the condition of low temperatures and high voltage. With these modifications in effect, the dilatometer has been used to determine the linear thermal expansion characteristics of 24 metals and alloys.

METALLOGRAPHY OF HASTELLOY B

J. R. Riddle

A metallographic study[5] of isothermally heat-treated Hastelloy B has been expanded to include a series of electron micrographs and will soon be

published as an ORNL report entitled "Metallography of Isothermally Heat-Treated Hastelloy B."

HOT-STAGE MICROSCOPY

T. J. Scheutz[6]   J. R. Riddle

A Unitron hot-stage microscope is being assembled to offer a new service to the Metallurgy Division. This unit should be completed in November 1957, and is expected to operate under a wide range of conditions. Heating rates can be adjusted to meet any desired conditions up to a maximum temperature of 1100°C. The specimen and furnace will be contained in an all-metal vacuum system employing a diffusion pump and a cold trap. At present the system can be evacuated to 1×10^{-5} mm Hg. Specimens under vacuum can be quenched by the system being flooded with argon. Specimens which cannot readily be heated under a vacuum can be heated in argon to a maximum pressure of 3 atm. Lighting for the hot-stage microscope may be furnished either by a filament lamp or a carbon arc. A movie camera is being fitted to the unit to record the transformations occurring at elevated temperatures.

[5]J. R. Riddle and R. J. Gray, *Met. Semiann. Prog. Rep. Oct. 10, 1956*, ORNL-2217, p 199.

[6]Summer employee.

CERAMICS RESEARCH

L. M. Doney

C. E. Curtis	L. A. Harris	T. N. McVay[1]
S. D. Fulkerson	R. A. Potter	T. S. Shevlin[1]
A. G. Tharp	G. D. White	E. D. Lynch[2]
A. J. Taylor	M. P. Haydon	G. C. Robinson[3]
R. L. Hamner	J. M. Kerr	J. A. Griffin
	F. P. Jeffers	

THERMODYNAMIC AND STRUCTURAL PROPERTIES OF SOME HIGH-MELTING COMPOUNDS

A. G. Tharp

Preparation and Identification of Some Rare-Earth Silicides

The knowledge of the phases present and of their properties is extremely meager for most of the high-melting rare-earth compounds. There are several reasons why the oxides, carbides, silicides, and nitrides of selected rare earths are of interest.

Gadolinium, samarium, and europium are of interest in reactor technology because of their high thermal-neutron absorption cross sections. Europium and ytterbium are known to have atomic radii which are considerably larger than those of the elements occurring before and after them in order of atomic number. This fact, coupled with the facts that the rare earths exhibit a normal and continuous contraction in size and that they in general have the same number of outer electrons, makes the rare-earth group unique in the periodic system of the elements. Except for the relatively large atomic radii of the two elements mentioned above, the rare-earth elements are very similar to the actinide series of elements.

Klemm[4] has shown that the atomic radii of the rare earths have not affected the molecular volumes of the rare-earth sesquioxides to any marked extent. Brauer and Haag[5] have published results indicating that the disilicides of lanthanum, cerium, praseodymium, neodymium, and samarium are isostructural with the disilicides of thorium, uranium, and

plutonium, and that these disilicides show a normal lanthanide contraction. The question of interest is whether or not the so-called intermetallic compounds, specifically the silicides and carbides, will show an abnormal molecular volume for those elements that do not exhibit the normal lanthanide contraction. It is postulated that europium and ytterbium silicides and carbides would have larger space requirements than their neighboring elements if there is a significant degree of metallic bonding present in these compounds.

This study is concerned with the preparation and identification of the various silicides of samarium, gadolinium, and europium in order to study the molecular volume requirements of the phases or compounds formed. It is also of interest to compare structurally the compounds of the rare earths with those of the actinide series of elements. Structural data and thermodynamic data will enable the formulation of an idea concerning the type of bonding prevalent in the high-melting compounds.

Since the metals samarium, europium, and gadolinium are not readily available at moderate cost, an effort was made to prepare the silicides by means other than that of combining the elements directly. Mixtures of samarium chloride, calcium hydride, and silicon were heated in the 900-to-1400°C temperature range. Some silicide was formed, but purification was not possible. When mixed with water, the entire mass would react.

Samarium oxide was heated to 1500°C with an excess of pure silicon. Presumably the silicon would reduce the oxide, volatilize SiO gas, and leave the samarium silicide as the remaining product. After three heatings at temperatures in the 1400-to-1500°C temperature range a relatively clean, metallic-appearing product remained. A like procedure gave similar results with gadolinium oxide but was unsuccessful with europium oxide. When europium sesquioxide was heated with excess silicon, most of the europium was volatilized.

[1] Consultant.

[2] Summer research participant, University of Illinois.

[3] Summer research participant, Clemson College.

[4] W. Klemm, *Z. anorg. u. allgem. Chem.* **184**, 345 (1929).

[5] G. Brauer and H. Haag, *Z. anorg. u. allgem. Chem.* **267**, 198 (1952).

Although no effort has as yet been made to identify the volatile europium compound, the most probable assumption is that the silicon reduces Eu_2O_3 to EuO, and at the temperature where the reduction occurs EuO is stable and is very volatile. This phenomenon will be investigated further, since it is of potential importance in the fabrication and use of Eu_2O_3 ceramic bodies.

An x-ray analysis of the product of the reaction between Sm_2O_3 and excess silicon resulted in the identification of a phase which gives a diffraction pattern similar to that for α-USi_2 and α-$ThSi_2$ (refs 6,7). This phase, which will be designated α-$SmSi_2$, gave a very poor diffraction pattern which contained some diffraction lines for an unidentified phase. The strong reflections were indexed well on the assumption that the phase is isostructural with tetragonal α-USi_2 and α-$ThSi_2$. Although reliable cell parameters cannot as yet be reported, there is considerable discrepancy between those found by this author and those reported by Brauer and Haag.[5]

Further heating at about 1500°C and volatilization of silicon from the α-$SmSi_2$ phase gave a phase whose diffraction pattern is very similar to that for β-USi_2 and β-$ThSi_2$. The fact that volatilization of silicon was necessary to form the β-$SmSi_2$ phase is evidence that β-$SmSi_2$ contains less silicon than is indicated by the formula. Further

work will be carried out in order to positively identify the α-$SmSi_2$ and β-$SmSi_2$ phases, as well as other phases formed from samarium and silicon.

Heating of Gd_2O_3 with excess silicon gave products similar to those mentioned above for samarium. The diffraction patterns for α-$GdSi_2$ were very poor, and no attempt has been made to calculate structural data for this phase. The diffraction pattern for the β-$GdSi_2$ phase contained what appeared to be only a few weak, extraneous diffraction lines. The diffraction lines were measured with a Norelco film-measuring apparatus, and the $\sin^2\theta$ values were calculated for the interplanar spacings. Relative intensities were calculated by use of the formula

$$ I \propto F^2 \; \frac{1 + \cos^2 2\theta}{\sin^2 \theta \cos \theta} \; p \; , $$

where F is the structure factor and p is the multiplicity factor. The results of these measurements and calculations are shown in Table 43. The agreement between the observed intensities and interplanar spacings and the calculated values is, in general, quite good. There are some rather marked discrepancies, and these are believed to be caused by the presence of a second phase which has some interplanar spacings coincident with those for β-$GdSi_2$.

The structure is hexagonal, space group $P6/mmm$, and contains one molecule per unit cell.

Twenty grams each of samarium and gadolinium metal have been obtained from the Ames Laboratory. Ten grams of europium metal has been ordered.

[6] W. H. Zachariasen, *Acta Cryst.* 2, 94 (1949).

[7] G. Brauer and A. Mitius, *Z. anorg. u. allgem. Chem.* 249, 325 (1942).

Table 43. Crystallographic Data for β-$GdSi_2$

Copper $K\alpha$ Radiation

hkl	$\sin^2\theta$ (Observed)	$\sin^2\theta$ (Calculated)	Intensity (Observed)*	Intensity (Calculated)
001	0.0340	0.0342	W$^+$	13.9
100	0.0527	0.0527	S$^-$	42.8
101	0.0869	0.0869	VS	89.8
002	0.1372	0.1368	S$^-$	10.6
110	0.1580	0.1581	M$^+$	25.3
102	0.1897	0.1875	M$^-$	13.8
111	0.1918	0.1923	W$^+$	8.2
200	0.2108	0.2108	W$^-$	5.8

Table 43 (continued)

hkl	$\sin^2\theta$ (Observed)	$\sin^2\theta$ (Calculated)	Intensity (Observed)*	Intensity (Calculated)
201	0.2445	0.2450	M^+	18.7
112	0.2944	0.2949	M^+	18.3
003	Absent	0.3078		0.6
202	0.3466	0.3476	W^-	4.9
103	0.3605	0.3605	W	9.7
210	0.3692	0.3689	W^-	4.5
211	0.4029	0.4031	M^+	16.0
113	0.4648	0.4659	W	1.8
300	0.4735	0.4743	W^{--}	4.3
212	0.5047	0.5046	W	5.8
301	Absent	0.5084		1.7
203	0.5173	0.5173	W	5.9
004	0.5480	0.5456	W^-	1.2
104	Absent	0.5982		2.6
302	0.6103	0.6098	W	7.0
220	0.6350	0.6312	W	2.6
221	Absent	0.6653		1.6
213	0.6748	0.6751	W	10.5
310	Absent	0.6838		2.6
114	0.7040	0.7034	W^{--}	7.0
311	0.7174	0.7179	W	10.9
204	Absent	0.7560		2.9
222	0.7669	0.7676	W^-	7.7
303	Absent	0.7803		1.8
312	0.8201	0.8202	W	6.6
400	Absent	0.8416		1.8
005	Absent	0.8525		0.4
401	0.8749	0.8757	W^-	7.6
105	0.9051	0.9051	W^{--}	8.8
214	0.9134	0.9138	W	9.7
223	0.9375	0.9381	W^-	3.7
402	0.9770	0.9780	W^-	9.5
313	0.9905	0.9907	W^+	55.6

*VS = very strong, S = strong, M = medium, W = weak.

It is hoped that preparations with the pure elements will enable more accurate and complete results to be obtained.

Transition Temperature of Europium Oxide

Quill[8] has reported that Eu_2O_3 goes from the cubic to the monoclinic structure at about 1350°C. The same structure transition occurs for several of the rare earth sesquioxides, except that the temperature varies.

Since the cubic structure is similar to the CaF_2-type structure with oxygen vacancies, this writer felt that the cubic form might be metastable, and furthermore, in attempting to fabricate oxide bodies, it is important to know at what temperature a transformation takes place.

Several grams of monoclinic Eu_2O_3 was dissolved in dilute nitric acid and precipitated with a saturated solution of oxalic acid. The precipitate was calcined at 800°C for 4 hr in order to decompose the oxalate. The product was a white, fine powder which gave an x-ray pattern for cubic Eu_2O_3.

The cubic Eu_2O_3 has been heated at 800, 900, 950, and 1000°C for periods up to four days. When heated at 1000°C for four days, the cubic oxide transformed completely into the monoclinic oxide. When both the monoclinic and cubic forms were heated simultaneously for three days at 950°C, no change in structure was observed for either structural form of the oxide. Therefore the transformation is established to take place at some temperature between 950 and 1000°C. When the temperature range is narrowed, an effort will be made to determine whether or not the transformation is reversible. This will also be done for Gd_2O_3 and Sm_2O_3.

Thermodynamic Properties of High-Melting Compounds of Thorium and of Uranium

Due to several breakdowns and leakage difficulties in the high-frequency induction vacuum furnace, no reliable work has been done with thorium and uranium. All necessary equipment has finally been constructed, and satisfactory results are expected shortly. The details of the Knudsen vapor pressure cell, furnace, and cell holder will be given in the next report.

---

[8]L. L. Quill, *Record Chem. Progr. (Kresge-Hooker Sci. Lib.)* **11**, 151 (1950).

DIFFUSION OF CALCIUM IN TITANIUM DIOXIDE

G. D. White

Diffusion studies in which the activation energy and the frequency factor have been determined are reported in the literature for metals and alkali halides; however, the literature contains very little information of this type for refractory oxides or other high-melting compounds. In view of this dearth of information on diffusion for the more typically ceramic materials and the value of such information in relation to solid-state reactions and electrical properties, an investigation was begun in the Ceramic Laboratory to determine data for the diffusion of calcium in the oxides of the elements titanium and thorium.

The diffusion of calcium in titanium dioxide was chosen for initial investigation because of the availability of high-purity material, both powder and large single crystals, and the likelihood that the diffusion coefficient would be relatively large at easily obtainable temperatures. By determining diffusion data first with the use of polycrystalline compacts with coarse crystal sizes and then with single crystals, it could be determined whether internal diffusion data are obtainable with polycrystalline compacts.

If internal diffusion data are obtainable in this manner, the method would be valid only with isotropic compounds; however, values of diffusion constants obtained in this manner on anisotropic compounds would be approximate averages of the direction-dependent constants for single crystals.

Fabrication and firing techniques were determined for diffusion compacts made of pure titanium dioxide and for compacts made of 98 mole % titanium dioxide plus 2 mole % calcium oxide. Pure titania compacts which were to be used as diffusion "solvent" were produced by calcining Baker Analyzed reagent titanium dioxide for 4 hr at 1000°C, crushing the calcined product to pass an 80-mesh sieve, hydrostatically pressing compacts from this material, and firing the compacts at 1400°C for 96 hr. This procedure produced a specimen with 96% of the x-ray density and with rutile crystals ranging from 60 to 100 μ in size.

Compacts of titanium dioxide containing 2 mole % calcium oxide, fabricated and fired by the same procedure as above, had much lower densities and contained rutile crystals with average size greater than 200 μ. Compacts of the same composition

heated to 1400°C with no time at temperature had densities and crystal sizes similar to the calcium-free titania compacts. Specimens prepared in this manner were used as a calcium source in the diffusion determinations. The lowering in density with increasing crystal size during sintering of this material is not normal for polycrystalline oxide compacts. On the contrary, the crystals usually tend to grow into the voids, thus increasing the bulk density of the compact. This behavior of the titania-calcia compact strongly suggests a preferred direction of crystal growth. Naturally occurring rutile has a distinctly elongated crystal habit, the elongation being parallel to the c-axis. It will be interesting to determine whether the crystals in the compacts have a similar habit. Thin sections are being prepared for this determination, which can be done with a petrographic microscope.

The procedure for obtaining the diffusion data was as follows. A compact of pure titania and a compact of titania plus 2 mole % calcia were placed one on top of the other in a resistance furnace and heated at the selected temperatures for a certain period of time. The surfaces in contact were finely polished to allow maximum area of contact, and the specimens were set on platinum during heating to prevent contamination. After diffusion had taken place, samples for analysis were taken by grinding on a lathe. The samples were taken by beginning at the interface and proceeding away from the calcium-rich side. Slices a few hundredths of a centimeter thick were ground off for each sample. Careful measurements were made of specimen length before and after each sample was taken. Samples obtained in this manner were analyzed for calcium spectrographically by comparing the films taken with the unknowns with a standard on a densitometer. This procedure was followed to obtain a rough approximation of the diffusion rate equation. More elaborate equipment and procedure will have to be used for exact, reproducible determinations.

The diffusion coefficient, D, is variable with concentration; however, if the concentration difference in the diffusion system is kept very small, D changes very little with concentration and can be treated as a constant. Under this circumstance Fick's second law of diffusion, which is for diffusion in one direction in an infinite system, will apply. The diffusion equation derived by Jost from Fick's second law for a system like the one described in the procedure is:

$$c(x,t) = \frac{c_0}{2}\left(1 - \text{erf}\,\frac{x}{2\sqrt{Dt}}\right),$$

in which

c = concentration of "solute",

c_0 = initial concentration of "solute," in the "solute"-containing compact,

t = time in seconds,

x = distance in centimeters from interface and is positive in the direction of diffusion,

D = diffusion coefficient.

The function erf x is Gauss' error function, which can be taken from a table. The initial concentration distribution for this system at $t = 0$ is:

$$c = c_0 \text{ for } x < 0 ,$$
$$c = 0 \text{ for } x > 0 .$$

This diffusion equation applies to a finite system so long as the concentration changes at the boundaries are negligible. By determining the concentration of "solute," c, vs distance from interface, x, and substituting these values into the equation, a value of D, the diffusion coefficient, can be calculated for a single temperature. If D is determined for several temperatures and the logarithm of D is plotted vs $1/T$, a straight line results. From this plot the activation energy and frequency factor can be determined for the diffusion rate equation,

$$D = D_0 \exp(-Q/RT) ,$$

in which Q is the activation energy and D_0 is the frequency factor.

Concentration distributions for two temperatures are listed in Table 44. The distance from the interface is midway between the distance before and after the sample was ground off. From the data at 1250 and 1300°C, the coefficients of diffusion were calculated to be 3.69×10^{-11} cm^{2}sec^{-1} and 1.78×10^{-7} cm^{2}sec^{-1}, respectively. The data for 1350°C indicate that diffusion reached the boundaries of the system; therefore, no attempt was made to calculate a coefficient from these data.

The diffusion coefficient for 1250°C was calculated on the basis of the data for the first sample. Since the other concentration values are constant, they must represent calcium present in the original material.

Table 44. Concentration Distribution of Calcium in Titanium Dioxide After Diffusion

Diffusion at 1250°C		Diffusion at 1300°C	
Distance from Interface (cm)	Calcium Concentration (wt %)	Distance from Interface (cm)	Calcium Concentration (wt %)
$\times 10^{-2}$		$\times 10^{-2}$	
2.79	0.2	1.5	0.4
7.24	0.1	4.06	0.4
10.29	0.1	5.96	0.5
12.19	0.1	7.74	0.4
13.97	0.1	9.77	0.3
16.00	0.1	12.44	0.2
17.91	0.1	14.47	0.2
20.27	0.1	16.12	0.15
22.66	0.1		

These determinations indicate that diffusion measurements should be made from specimens heated in the temperature range from 1000 to 1350°C.

PRELIMINARY INVESTIGATION OF THE SYSTEM ThO_2-SiO_2

L. A. Harris

The investigation of the system ThO_2-SiO_2 was undertaken due to the interest displayed in both fertile materials and high-melting refractories. A belief that $ThSiO_4$ could be of use as a slurry in the breeder reactor was based upon the lower density of the compound, in comparison with that of thorium oxide, and the good suspension qualities associated with other silicates, for example, $ZrSiO_4$. Furthermore, the thorium silicate compound revealed definite indications of making a good intermediate-temperature refractory.

A preliminary diagram (Fig. 141) illustrates the general phase equilibrium relationships observed to date. The techniques used in this study involved the quenching method, which is in general service for silicate systems, and examination of all samples by means of both the polarizing microscope and the x-ray diffractometer unit. All samples were fabricated by pressing powders of thoria and amorphous silica (which were mixed in a glass tube on a small roller-type mill for a period
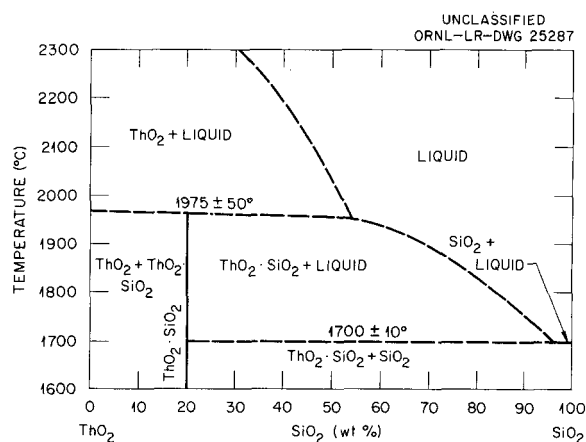
Fig. 141. The System ThO_2-SiO_2.

of 24 hr) in a steel die at a pressure of 10,000 psi into small pellets ($\frac{1}{2}$ in. in diameter). These pellets were next placed in the closed end of a zirconia tube ($4\frac{1}{2}$ in. long $\times$ $\frac{7}{8}$ in. in diameter) which was then positioned in an oxygen-acetylene furnace so that the open end of the tube was flush against the furnace lining and aligned with the sight tube (see Fig. 142). The above arrangement of the tube eliminated burning gases from the line of sight, assuring accurate temperature readings because of the excellent black-body conditions. After the desired temperature was reached, the
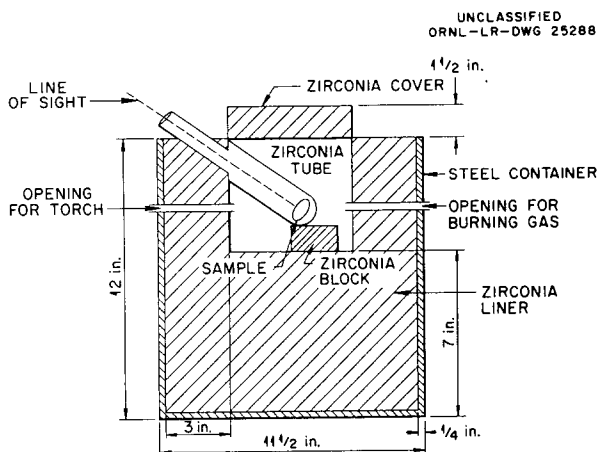
Fig. 142. Cross Section of Oxyacetylene Furnace with Zirconia Tube Positioned.

torch was closed, the zirconia tube was removed, and the pellet was placed in an alumina tray to air-cool.

Once the samples were cooled, they were crushed and sieved through a –325-mesh screen in order to standardize all the x-ray samples and ensure that the data would be comparable. A fraction of the sample not used for x-ray study was placed under the petrographic microscope for phase identification. Due to the sluggishness of reactions in silicate systems it was necessary to rework the samples repeatedly, as many as five times, before equilibrium could be attained.

A survey of the literature revealed that there are two known crystalline forms of $ThSiO_4$ found in nature, namely, tetragonal and monoclinic. The monoclinic form has been synthesized numerous times by solid-state reaction, while no tetragonal structure has been achieved by this method. Pabst[9] observed when heating (in air) thorite samples obtained from widely different locales that the tetragonal mineral crystallized initially; as the temperature was increased, only the monoclinic phase was present. The compositional and structural relationship between these two forms is vague. No experimental data pertaining to the melting point and the type of melting (congruent or incongruent) were available before this report.

Solid-state reactions carried out at this laboratory in the synthesizing of thorium silicate can be summarized by Fig. 143, which presents a series

---

[9]A. Pabst, *Am. Mineralogist* **37**, 137–149 (1952).
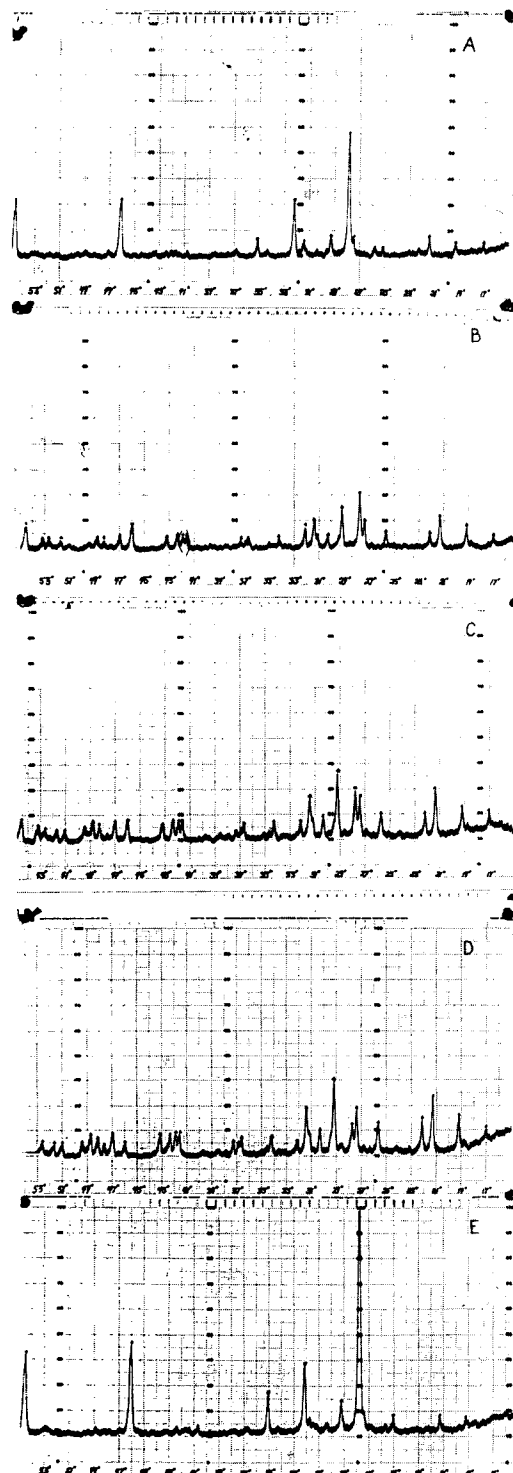
Fig. 143. X-ray Spectrometer Patterns of Samples Composed of 50-50 Mole Percentages of ThO_2 and SiO_2 Showing Crystal Growth of $ThSiO_4$.

of x-ray spectrometer patterns taken of samples quenched at successively higher temperatures. It can readily be observed that the monoclinic thorium silicate peaks become progressively more intense from 1750 ± 25°C (Fig. 143a) to 1925 ± 50°C (Fig. 143d). At this temperature, as indicated by the x-ray data and confirmed by petrographic analysis, the sample was almost pure monoclinic $ThSiO_4$. At 2000 ± 50°C (Fig. 143e) the silicate compound dissociated into ThO_2 and glass, with a small amount of $ThSiO_4$ still present. It is therefore concluded that monoclinic $ThSiO_4$ is an incongruently melting compound whose dissociation temperature is approximately 1975 ± 50°C.

Two samples were prepared by following the method previously described; each was heated in a resistor-type furnace for a period of 1000 hr at 1000°C and 1250°C, respectively. Examination of the sample fired at 1000°C showed absolutely no formation of any thorium silicate, while at 1250°C monoclinic $ThSiO_4$ started to crystallize. Although this experiment is not conclusive, it does imply that the tetragonal $ThSiO_4$ probably cannot be synthesized at low temperatures in air.

Further studies pursued to determine the composition and melting points of both the eutectic and peritectic are not complete. Initial tests appear to give a eutectic temperature of about 1700 ± 10°C at a composition of more than 95 wt % silica. Future experiments which are to be done will help complete the diagram and the synthesis of the tetragonal phase.

BERYLLIUM OXIDE

R. L. Hamner

The beryllium oxide program may be divided generally into two phases: (1) the fabrication of beryllium oxide shapes now required from commercial grades of beryllium oxide where the technology is sufficiently extensive to require a minimum of development work and (2) the confirmation and/or extension of the technology of other promising material(s) which appear advantageous with respect to fabrication to fulfill future requirements.

Beryllium Oxide Fabrication: Commercial Grades

The major effort of this phase of the beryllium oxide program was directed toward fabricating high-density, high-purity shapes for various moderator materials testing programs. Since it has

been well established that low densities result from cold-pressed or extruded bodies of such materials, these shapes were necessarily fabricated by hot-pressing at high temperatures.

Two commercial grades of beryllium oxide were considered, both supplied by the Brush Beryllium Company, designated Luckey S.P. and G.C. grades, respectively. The two grades are made by treating $Be(OH)_2$ to form $BeSO_4$, a different process being used for each grade. The beryllium sulfate is then calcined to the oxide at 1100–1200°C. The Luckey S.P. grade is composed of soft agglomerates, is practically non-dusting, and has a purity of 99.5%. The G.C. grade is a fine, dusty powder referred to as "fluorescent grade"; it is about 99.3% pure.

For the purpose of selecting one material to be used in fabricating test specimens, a cursory survey was made of these materials by hot-pressing approximately 1-in. right solid cylinders at temperatures ranging from 1750 to 1950°C. Similar fabrication characteristics of these materials were noted:

1. The material began to give under pressure at about 1500°C.
2. At 1750°C the finished piece was comparatively white, but the density achieved was only about 80% of theoretical.
3. With increase in temperature to 1950°C, densification was increased to about 95%, the material becoming gray due to carbon pickup.

The Luckey S.P. grade was selected for the following reasons:

1. Its fabrication characteristics were comparable to those of the G.C. grade.
2. Its non-dusting property was desirable from the standpoint of health hazard.
3. The G.C. grade material that was received contained a small quantity of some foreign material which appeared as black specks and which could not readily be identified.

From Luckey S.P. grade material, beryllium oxide shapes were fabricated for testing or for use as component parts of test apparatus as noted.

MTR Specimens. — Two groups of four beryllium oxide solid cylinders approximately 1 × 1 in., having 95% density, were submitted for testing in the MTR. These specimens, to be canned in Inconel, were to be tested primarily for thermal shock characteristics.

Physical Property Measurements. – The hot-pressed BeO and BeO-UO$_2$ specimens listed below were fabricated for physical tests to be conducted by Atomics International as a part of studies involving a nuclear-powered ram-jet missile. Such tests are to include modulus of rupture, elastic modulus, internal friction, thermal expansion, thermal conductivity, total emissivity, and erosion at temperatures up to 1650°C. In addition, UO$_2$-BeO diffusion studies are to be made.

1. Five BeO cylinders 2 in. $\times$ 2 in. $\times$ $\frac{1}{4}$-in. ID, 97% density

2. Four BeO blocks $3 \times 4 \times 1$ in. with four $\frac{1}{4}$-in. holes running longitudinally, 95% density

3. One BeO block $1 \times 1 \times 6\frac{1}{2}$ in., 80% density

4. One BeO block $1 \times \frac{5}{8} \times 6\frac{1}{2}$ in., 90% density

5. One BeO block $1 \times \frac{1}{2} \times 6\frac{1}{2}$ in., 90% density

6. One BeO cylinder $2\frac{1}{2}$ in. OD $\times$ $\frac{3}{8}$ in. ID $\times$ $2\frac{1}{2}$ in., 80% density

7. Nine inches total length of bars containing 50 mole % UO$_2$–50 mole % BeO, $\frac{5}{16} \times \frac{7}{16}$ in., 97% density

8. Four BeO bars $\frac{5}{16} \times \frac{7}{16} \times 6$ in., 95% density

9. Four BeO bars $\frac{1}{8} \times \frac{3}{16} \times 6$ in., 95% density

ETR Specimens. – Three beryllium oxide blocks having 95% density were fabricated as stock material for 27 high-density cylindrical specimens to be canned in Inconel and irradiated in the ETR.

Thermocouple Holder. – Specially designed beryllium oxide thermocouple inserts and shells for determining volume temperature fluctuations in the ART half-scale core model are being fabricated under the supervision of the Ceramic Laboratory. This involves hot-pressing of beryllium oxide blocks to be cut and ground to cylindrical configurations for twelve inserts which are to be fitted into cylindrical beryllium oxide shells with a closed end hole. Holes for the shells will be made by the Cavitron technique, and parallel grooves 180 deg apart will be made in the same manner along the periphery of the inserts for holding the thermocouple leads. For good thermal contact, the base of the shell and the mating surface of the insert are to be platinized.

Beryllium Oxide Development Work

A development program directed toward obtaining high-density beryllium oxide shapes by hot-pressing and by cold-pressing and/or extrusion followed by sintering was begun. According to the literature[10,11] the particle size of the beryllium oxide powder is the major variable involved, and, if the pure powder is sufficiently fine, densities 95% of theoretical or greater may be obtained by either of these methods and at a much lower temperature (*ca* 1500°C). This powder should be so fine that it is not identifiable under the microscope. To produce such a starting material, beryllium sulfate or beryllium hydroxide is calcined to the oxide at temperatures high enough for decomposition but low enough to prevent crystal growth.

A quantity of high-purity BeSO$_4$·nH$_2$O was received from the Brush Beryllium Company for experimentation in the Ceramic Laboratory. This material was calcined at 1000°C for $1\frac{1}{2}$ hr. The following characteristics were noted:

Description	Very fluffy white powder
Weight loss	86%
X-ray examination	BeO plus an unidentified phase, not the sulfate or carbonate
Petrographic examination	No BeO crystals seen with oil immersion objective

Refiring to 1000°C for 1 hr apparently did not change the material.

Quantities of this material were hot-pressed at 1525, 1425, and 1325°C under a pressure of 2000 psi for 15 min. The material began to shrink at about 1300°C – approximately 200°C lower than did the previously used commercial grades. The final densities obtained were 96, 92, and 91%, respectively. It was noted that this material, as pressed, looked very similar to commercial grades pressed at 1950°C, that is, it was gray in color, indicating that it picked up carbon at much lower temperatures than did the commercial grades.

---

[10]*Summary Progress Report on an Investigation of the Manufacture of High-Density Beryllium Oxide Parts by The Brush Beryllium Company*, PWAC-167 (April 5, 1957).

[11]C. Hyde, J. F. Quirk, and W. H. Duckworth, *Preparation of Dense Beryllium Oxide*, BMI-1020 (July 21, 1955).

187

In the future, work will be directed, first, toward establishing conditions for obtaining the most sinterable powder, with x-ray and surface-area measurements as the principal material control factors, then toward establishing optimum conditions for fabricating by hot-pressing, cold-pressing, and extrusion.

gaskets. Billets 4 × 12 in. in size can be treated in a clean hydrogen atmosphere maintained by a gas purification train servicing both furnaces. Temperature measurements at different positions within the retorts can be made and recorded by a Brown-Honeywell 12-point recorder. The pressure is controlled by a Fisher constant-pressure diaphragm-type valve over the range from zero to 5 psig.

METAL HYDRIDES

R. A. Potter

Hydriding System

Work was completed on a furnace system (shown in Fig. 144) for the hydriding of zirconium and yttrium metals. The system includes two hydriding furnaces, one capable of attaining 1800°F and the other 2300°F. The furnace retorts are of $\frac{1}{4}$-in. Inconel and are equipped with water-cooled, flanged covers packed with neoprene O-ring

Zirconium Hydride

The initial hydriding work has been done only on massive, reactor-grade zirconium, as the yttrium metal is not yet readily available. However, the process is similar for both metals, the differences being in the temperature and possibly the pressure that must be used for obtaining the desired amount of hydriding.

Fig. 144. Hydriding Equipment. (Secret with caption)

To establish a process for treating yttrium, zirconium samples have been hydrided to various levels of hydrogen content by two different methods, designated A and B.

In method A (closed system), samples cleaned with ethanol are set on molybdenum foil and heated *in vacuo* to the desired hydriding temperature. Purified hydrogen is then allowed to enter the retort, but no outlet is provided. In this manner the sample can become hydrogen-saturated at any given temperature and pressure within the capability limits of the apparatus. When the saturation point is reached, as indicated by the cessation of gas flow, the retort is flushed with helium and cooled in a helium atmosphere.

Method B (gas through) is being tried because of the physical limitations of the Inconel retort under a vacuum at the higher temperatures necessary for hydriding yttrium metal. The samples are heated in an atmosphere of helium passing through the retort at a constant pressure of 1 psig. When the hydriding temperature is reached, hydrogen is introduced into the retort with the helium at a ratio of approximately 1:1 by volume. The hydrogen-saturation point can be noted by taking readings of the temperature at two places within the retort, one very close to the sample and the other at some distance farther from the specimen. As the metal absorbs hydrogen, the temperature rise and eventual return to normal are recorded and serve as an indication of saturation for the given temperature and pressure. Hydrogen flow is then discontinued, and the sample is cooled in helium.

To establish the two methods, it was necessary to hydride many samples of zirconium metal. Among these was a systematic series of nine groups (two to a group) processed by method A. These samples ranged in hydrogen content from 0.19 to 1.15 wt % (calculated on the basis of weight change), and were rod shaped, approximately 3 in. in length by $\frac{1}{2}$ in. in diameter.

A second series of ten samples was treated by method A, and density and expansion measurements were taken. These samples ranged from 1.10 to 1.17 wt % hydrogen. The bulk density ranged from 5.94 to 5.90 g/cc, and the linear expansion was 2.93 to 3.25% (based on the final length).

Two samples for in-pile testing[12] were inserted within open-end molybdenum capsules ($\frac{1}{2}$-in. OD by 3-in. length) and hydrided *in situ* to an N_H of 3.7 ($N_H \times 10^{22}$ = number of hydrogen atoms per cubic centimeter). The samples were iron-plated (1.75 mil) zirconium metal rods, 0.460 in. in diameter and 2.750 in. in length. A $\frac{1}{8}$-in.-dia. hole had been drilled lengthwise through the rods. The assemblies were fired *in vacuo* to 1700°F, hydrogen was introduced, and the retort temperature was dropped to 1650°F, where it was held until the zirconium was hydrogen-saturated.

An attempt was made to hydride *in situ* two samples similar to those above but without the hole through the center. The maximum amount of hydrogen that could be put into the pieces was 0.73% in one and 0.76% in the other. As this was an insufficient amount of hydrogen, the method was abandoned.

Using method B, the gas-through technique, two of the largest samples to date were hydrided simultaneously to a hydrogen content of 1.147 and 1.155%, respectively; a small fissure in the second sample possibly accounts for the difference in hydrogen content. The pieces were rod-shaped, 3 in. in length by $1\frac{1}{4}$ in. in diameter, and had a combined weight of 832 g. Helium gas was passed through the retort until a 1650°F soak temperature was attained. Hydrogen was then mixed with the helium, and the temperature, taken $\frac{1}{8}$ in. from the samples, rose by 63°F in a period of approximately 30 min. The temperature then began to decrease, and after 1 hr it had returned to 1650°F. Hydrogen was allowed to flow until the retort had cooled to 1600°F. The flow of hydrogen was then discontinued, and the pieces were cooled to room temperature in flowing helium.

FUEL ELEMENT DEVELOPMENT

A. J. Taylor

SiC-Si

The main problem in the development of the SiC-Si fuel element remains that of fueling. No satisfactory and reproducible method has been devised to incorporate more than small amounts (7%)

[12] R. A. Potter, R. E. McDonald, and T. Hikido, *ANP Quar. Prog. Rep. March 31, 1957*, ORNL-2274 (Parts 1-5), p 192-193.

of UO_2 in the core of this element. The heart of the problem is the reaction between UO_2 and silicon. This reaction requires a very high temperature if it is to proceed with any rapidity, and this temperature is provided by the rapid exothermic reaction between silicon and carbon to form SiC. The reaction between UO_2 and silicon, if allowed to proceed to any great extent, can be violent, resulting in a complete disruption of the fuel element. If the reaction is largely controlled, as can be done by any of several techniques, the reaction is not violent, but a small amount of USi_3 is formed. A small amount of USi_3 is not bad in itself, provided that it remains in the core; however, USi_3 tends to wash along through the element with the molten silicon and migrate into the skin, which in effect lessens the cladding thickness. If USi_3 washes on through to the surface and leaves the fuel element, unknown amounts of uranium can be lost. Also, the purpose of the cladding, which is to retain fission products, is defeated.

The use of large (−70 +100 mesh), dense particles of UO_2, having a low ratio of surface to volume, is of considerable help in controlling the reaction between UO_2 and silicon, since the Si-C reaction front can pass by the rather inert UO_2 grains before any extensive reaction between UO_2 and silicon can take place. As the UO_2 grains are left behind the Si-C reaction front, they can no longer react with the silicon, because the required heat is rapidly dissipated to the melt.

Since the use of large, dense particles of UO_2 is in itself insufficient to prevent the formation of some USi_3, other techniques have been devised. None have been completely successful, but neither has sufficient work been done to eliminate any of them as being of little value. Basically, these techniques involve some means of keeping the temperature from rising excessively in the vicinity of the UO_2. This is to be accomplished by additions to the core which will shield the UO_2 particles from either the heat or the silicon, or which will absorb the excess heat in a fusion or other type of reaction.

Two methods are being evaluated in attempting to shield the UO_2 particles. To shield the UO_2 from the silicon, it is hoped to put a thin, dense coating of graphite on the UO_2 particles entering into the core. The Si-C reaction cannot proceed in dense graphite, since the silicon cannot penetrate the graphite rapidly to become available for

reaction. The dense graphite coating would not only keep the silicon from the UO_2 grains but, with its good thermal conductivity at high temperatures, it should tend to raise the over-all thermal conductivity in the core. The other method being evaluated for shielding the UO_2 consists of using a mixture of SiC and UO_2 for the core, or of enclosing a monolayer of UO_2 in SiC for the core. Since the amount of carbon binding the SiC grains together is very low, the exothermic heat of the Si-C reaction in the core should be insufficient to raise the temperature to that required for the UO_2-Si reaction.

In attempting to absorb the heat of the Si-C reaction, cores are being made which consist of a mixture of UO_2 and finely divided silicon. The heat absorbed by the silicon on melting may keep the temperature low enough to prevent the UO_2-Si reaction.

Some success and many failures have been obtained with the fueling techniques described above. Most of the failures have been traced to forming techniques and material compositions which gave unmatched shrinkages or poor green strength, or which caused the cores to be too dense for impregnation. Where the cores have been impregnated, either wholly or partially, there have been definite indications of advantages over the monolayer technique of fueling the plates. In general the UO_2 grains have not been so severely attacked, and consequently there has been considerably less USi_3 formed. In general, however, the USi_3 has not been restricted to the core. If any of these new fueling techniques are successful they will certainly enhance the chances of bringing the fuel content of the fuel plates up to the desired 15–18% UO_2.

The Engineering Properties Section of the Solid State Division has been making a study of the irradiation behavior of the SiC-Si fuel element. Uncooled fuel plates canned in helium, containing sufficient enriched UO_2 to heat them to 1000°C, have been given short exposures in the LITR. The longest exposure has been 3.5×10^{19} *nvt*, corresponding to over 500 hr at 1000°C, and involved 19 thermal cycles. The heat flux from these samples was approximately 120 w/in.^{2}. The burnup from these short exposures has been negligible, perhaps 2%. No damage has been observed as a result of the short irradiations, and it is expected that the material will be stable under intense irradiation, because, as in the case

of graphite, damage is largely annealed out at the temperature at which the material will operate.

An autoradiograph of the particular specimen mentioned above, made by means of the gamma radiation from the fission products, shows exactly the same core configuration as did a radiograph of the core before irradiation. This is a very clear indication that there has been little, if any, diffusion of the fission products into the skin.

Al_2O_3-Cr

The Al_2O_3-Cr cermet has been considered as a fuel-element possibility for quite some time, but it has not received as much attention as has SiC-Si because of its higher neutron cross section (2.1 barns) and lower thermal conductivity (0.04 $cal \cdot sec^{-1} \cdot °C^{-1} \cdot cm^{-2} \cdot cm$ at room temperature).

As a cermet, Al_2O_3-Cr has been known for some time. Fabrication techniques and physical properties were worked out when it was being developed as a high-temperature turbine-bucket material. Being a cold-formed and sintered cermet, it is not difficult to fuel, and putting moderately large amounts of fuel (up to 20%) into this material should be no particularly large problem.

While the cermet has a cross section that is moderately high (although lower than that of most of the better known cermets), it has the advantage of being oxidation resistant at elevated temperatures. Alumina was selected as the oxide because of its availability and known desirable properties, and chromium was the best of a number of metals tried. It is a refractory metal and forms a refractory oxide. It is resistant to oxidation at elevated temperatures and is used in many of the better high-temperature alloys. The oxide, Cr_2O_3, has the same crystal form and unit cell size as Al_2O_3 and goes into solid solution with Al_2O_3 in all proportions. In small amounts Cr_2O_3 goes into solid solution with Al_2O_3, without apparently detracting from the properties of the Al_2O_3.

Several Al_2O_3-Cr plates, both fueled and unfueled, were sent to the Nuclear Development Corporation of America for a series of tests at 2500°F. The test program included interaction between fuel and cladding, diffusion of fuel, and diffusion of fission products. The testing is to be done in a helium atmosphere.

Plates of Al_2O_3-Cr containing sufficient enriched fuel to heat them to 1000°C are currently being irradiated in the LITR. This study will give information on the irradiation stability of the cermet, as well as information on its ability to retain fission products at high temperatures. As with the SiC-Si, the irradiation will be of low intensity and of short duration, but it should supply enough information to make possible a better evaluation of the cermet as a high-temperature fuel-element material.

Other Materials

Several other materials which offer good possibilities for use in high-temperature fuel elements are being either worked with or considered. Of these, graphite would be the ideal material if retention of fission gases did not have to be considered. Experiments indicate that it may be possible to put an SiC-Si coating on graphite which would be capable of retaining fission products reasonably well. Several pieces of graphite were coated by first making the surface porous with an oxidizing furnace treatment and then immersing the piece in molten silicon at 1800°C. This put a thin (approximately 10 mils) nonporous, very adherent coating of SiC-Si on the graphite. The density of the graphite used was not high, 1.54 g/cc, nor was the coating uniform in thickness, but the experiment indicates the possibility of providing graphite with a reasonably gas-tight, oxidation-resistant coating for the temperature range suitable to SiC-Si.

Magnesium oxide has never been considered to be material which would be a suitable cladding for high-temperature fuel elements. It has all of the disadvantages of most ceramic oxides (brittleness, low thermal conductivity, low tensile strength, etc.) and, until recently, the added disadvantage that it had not been fabricated into very high density shapes. The Battelle Memorial Institute[13] was able to fabricate dense MgO (density up to 96.9% of theoretical) by experimenting with types of MgO and calcination temperatures. This Laboratory has made MgO crucibles with densities 97% of theoretical. With the ability to fabricate dense shapes, it should be possible, by fabricating shapes less prone to fail in thermal shock, to make fuel elements of MgO which would be serviceable in the temperature range 1600–1800°C. Magnesium oxide and uranium dioxide form no compounds, and

---

[13]A. G. Allison et al., Sintering of High-Purity Magnesia, BMI-931 (Aug. 2, 1954).

there is no solid solution in any proportion up to 1850°C. Magnesium oxide has an extremely low cross section for thermal neutrons and should lend itself well to the possibility of breeding. Experiments are presently being conducted to determine the best fabrication techniques, sintering temperatures, and sintering atmospheres for making thin plates ($\frac{1}{8}$ in.) of MgO fueled with UO_2. The MgO chosen (its history presently unknown) sinters so tightly and rapidly that it may be possible to sinter the fueled MgO in an oxidizing atmosphere. One plate, $1\frac{3}{8} \times \frac{9}{16} \times \frac{3}{16}$ in., containing 0.75 g of UO_2 (approximately 18%), has been fired to 1650°C in an oxidizing atmosphere and looks very good. Some other fueled MgO plates, which developed cracks early in the firing cycle, showed extensive diffusion of the fuel into the skin. In the case of bars fired in helium, there is no diffusion at temperatures as high as 1850°C, even in bars developing cracks. The only advantage which would be gained by using a gas-fired furnace (oxidizing atmosphere) would be the saving in time. There are good indications that MgO will be stable under irradiation; this observation is based on the KAPL pin-type fuel element, where an MgO core in contact with an annular ring of UO_2 was undamaged after very high (>50%) burnup of the uranium atoms.

A possibility has been opened for fabricating a high-density SiC fuel element by a process used in making some pure β-SiC. Past work had shown that it was impossible to fabricate SiC-Si plates by sintering either a mixture of SiC and silicon or powdered SiC-Si shapes. Any attempt to sinter at temperatures even slightly above the melting point of silicon resulted in a complete loss of silicon and a soft, powdery SiC residue. In making some β-SiC for neutron damage experiments, some uncrushed SiC-Si plates were heat-treated. The result was a strong consolidation of the SiC and an almost complete removal of the silicon. The center of the piece was composed almost completely of dense SiC with some large (0.25-cm) SiC crystals. This graded to a very porous SiC skeleton toward the edges. The silicon content of the sample had been reduced from approximately 25% to approximately 2%. Since the heat treatment can be at a temperature as low as 1500°C, at which there would be no possibility of a reaction between UO_2 and Si or SiC, the possibility is opened of forming high-density SiC fuel elements if the SiC-Si can be fueled with the desired amount

of UO_2 and if the open pores can be successfully filled. One possibility for filling the pores was investigated, namely, to carry on the heat treatment in a silicon melt. The number of pores was markedly reduced, although pores still remained. This indicates, however, that with further work a definite possibility exists for producing a dense SiC shape that might be fueled.

Another material which might find use as a cladding for high-temperature fuel elements is magnesium zirconate ($MgO \cdot ZrO_2$). This material was studied as a summer project, and the results will be reported in detail in a separate report. However, the material sinters to a fairly dense body at 1650°C and has been fueled with UO_2 with no evidence of diffusion of UO_2 into the cladding.

Another cermet being investigated is Al_2O_3-Ni. Presently the work is limited to achieving extremely fine dispersions of the components; this powder should then be fabricable by any of the conventional ceramic forming methods.

HIGH-TEMPERATURE MATERIALS

R. A. Potter   A. J. Taylor

Zirconium Disilicide by Thermite Reaction

A small sample of $ZrSi_2$ was produced by means of a thermite reaction in order to determine the feasibility of the method in producing this silicide and others of interest, for example, those of the elements tantalum or tungsten, both refractory materials reported to melt in the range of 2200°C. The reaction was carried out in a graphite crucible heated with an induction coil. The batch composition, in weight per cent, was as follows: sulfur flowers, 10; silica sand (20 mesh), 50; aluminum metal dust, 35; and zirconium oxide (-325 mesh), 5. The mixture was heated by the external source until the thermite reaction began to take place, at which time the power was turned off and the reaction was allowed to continue to completion. For the removal of free aluminum and silicon, the resultant mixture was leached successively with HCl and with NaOH. Zirconium disilicide (substantiated by an x-ray diffraction pattern) was present in the form of macrocrystals.

Tantalum Diboride

A kerosene-saturated mixture of 80% Ta_2O_5, 10% B_4C, and 10% graphite was fired in a graphite

crucible heated by an induction coil to an undetermined temperature. The escaping gases were ignited, and a visual observation was made of the flame colors. The reaction was assumed to be completed upon the disappearance of excess boron. The reaction product was a metallic regulus, at the bottom of the crucible, consisting of approximately 85% TaB_2 (determined by x-ray analysis). After comminution to –325 mesh, the material was cold-pressed into a block approximately $1 \times 1 \times \frac{1}{2}$ in. and was heated in a helium atmosphere to a pyrometrically determined temperature of 2380°C, at which point fusion just commenced. The resultant piece was quite machinable and had a bulk density of 9.8 g/cc. Since tantalum boride has been suggested as a possible crucible material in which to melt uranium, the sample will be placed in contact with molten uranium metal and its resistance to attack will be determined.

Zirconium Diboride

In order to establish a process for producing borides, ZrB_2 was made by reacting the following materials: 75% zircon sand (60 mesh), 10% graphite, 15% B_4C (100 mesh). The batch was mixed, saturated with kerosene, and fired in a graphite crucible to approximately 2100°C. An x-ray analysis of the resultant metallic spheres showed the predominant phase to be ZrB_2.

Boron Nitride: Fabrication

R. L. Hamner   A. J. Taylor

A number of BN specimens were requested from the Ceramic Laboratory for radiation damage studies. Information in the literature was sparse to the extent that conditions for fabrication had to be established by the laboratory. The technique of hot-pressing was employed. Both Norton and Carborundum grades of boron nitride were used; the Norton grade was pure white and extremely fluffy, whereas the Carborundum grade was gray in color and had a much higher powder density than the Norton grade.

At 1900°C and 2000 psi the structure for both materials was badly laminated and cracked. At 2000°C little improvement was noted. At 2100°C the Norton material pressed into a strong body with a density of 1.75 g/cc; a temperature of 2190°C was required for compacting the Carborundum material to an equivalent product.

Other cylindrical shapes of boron nitride were successfully pressed under these conditions for use as component parts of special test apparatus.

Zirconium Oxide: Fabrication by Hot-Pressing

R. L. Hamner

Attempts were made to fabricate a block of high-density pure ZrO_2 by hot-pressing to 2000 psi at 2000°C. In the hot-pressing operation the material seemed to be compacted well, but in all cases the billets were badly cracked throughout, presumably due to the inversion from the tetragonal form to the monoclinic at about 1050°C during cooling.

Hafnium Carbide

R. L. Hamner

A small quantity of high-purity HfC was produced for use as refractory probes. This was accomplished by first compacting stoichiometric amounts of HfO_2 and graphite with a Bakelite resin, firing the compacts to 1800°C in helium, then fusing in an arc furnace.

RARE-EARTH CERAMICS

C. E. Curtis

Yttrium Oxide

A paper entitled "Properties of Yttrium Oxide Ceramics" was published.[14]

Samarium Oxide and Gadolinium Oxide

A paper entitled "Ceramic Properties of Samarium Oxide and Gadolinium Oxide, X-ray Studies of Other Rare Earth Oxides" was published.[15]

Europium Oxide

The crystal structure of the Eu_2O_3 as received was body-centered cubic at room temperature with $a_0 = 10.860 \pm 0.006$ Å, and the index of refraction was 1.87. After the oxide was fired at 1400°C, the crystal structure was judged to be monoclinic with $a = 13.944$ Å, $b = 3.581$ Å, $c = 8.676$ Å, and $\beta = 98°30'$, and the index of refraction was 2.03. The 1400°C product disintegrates in boiling water at atmospheric pressure, forming an apparently

[14]C. E. Curtis, *J. Am. Ceram. Soc.* **40**, 274–278 (1957).

[15]C. E. Curtis and J. R. Johnson, *J. Am. Ceram. Soc.* **40**, 15–19 (1957).

rhombohedral product which can be dehydrated at about 500°C.

A study of the inversion temperature from the cubic to the monoclinic form of europium oxide indicates that the figure given in the literature (1350°C) is too high by 350°C. An article on europium oxide which will include data bearing on the subject of inversion is being prepared by C. E. Curtis and A. G. Tharp.

Europium oxide specimens sintered at 1300°C in air for 2 hr were 29.7% porous; fired at 1700°C for 2 hr, the specimens were only 10% porous and had a density of 6.88 g/cc (theoretical density = 7.34). The modulus of elasticity of the latter specimens was 4.1×10^6 psi. Other properties determined were: thermal expansion, room temperature to 1200°C, 10.7×10^{-6} in./in./°C; mean specific heat, 0–800°C, 0.0947 cal/g/°C.

Rare-Earth-Oxide Mixture

Specimens were made by dry-pressing from the Lindsay Chemical Company's "rare earth oxide code 330," which has a composition of 45% CeO_2, 22.5% La_2O_3, 17.9% Nd_2O_3, and smaller percentages of other rare-earth oxides. These specimens were light brown when fired at 1100°C (in air) and changed to black at 1500°C. The 1500°C specimens had a density of 5.64 g/cc and a porosity of 10.3% and were rather strong.

ZIRCONIUM OXIDE FURNACE

C. E. Curtis

The Ceramic Laboratory staff loaned materials and equipment and experience to the HRP Blanket Development Group in producing two portable oxyacetylene-fueled furnaces. These furnaces are zirconia-insulated and are similar to that described previously.[16]

ZIRCONIUM NIOBATE CERAMICS

C. E. Curtis

It has been proposed that a compound consisting of 6 molecules of ZrO_2 to one of Nb_2O_5, recently described in the literature, might have unusually good resistance to corrosion under irradiation. A stoichiometric mixture of the respective oxides, when dry-pressed into bars and fired at 1400°C,

---

[16]C. E. Curtis, *A Small High Temperature Laboratory Furnace*, ORNL CF-56-8-133 (Aug. 17, 1956).

contained approximately 95% of the compound, 6 $ZrO_2 \cdot Nb_2O_5$. The bars were rather porous (37%) but could be fired no higher because of the loss of Nb_2O_5 by volatilization at temperatures above 1400°C. The specimens have been sent to the HRP Metallurgy Section for testing under irradiation.

ZIRCONIUM OXIDE–CALCIUM OXIDE COMPOSITIONS

C. E. Curtis

Specimens $\frac{1}{2}$ in. square and $\frac{1}{16}$ in. thick of ZrO_2 and of two compositions containing CaO (2 and 10%, respectively) have been pressed, fired, and machined for irradiation corrosion testing. The estimated compositions after firing were 100% monoclinic, 30% monoclinic (and 70% cubic), and 10% monoclinic ZrO_2, respectively.

THORIUM OXIDE CALCINATION METHODS

C. E. Curtis

Electric and Gas-Fired Furnace Operations

A considerable number of calcinations of ThO_2 from different sources have been made at temperatures from 1000 to 1900°C for different departments of ORNL. At temperatures up to 1600°C, the usual procedure was to heat the material in platinum vessels in a resistor type of furnace. At higher temperatures, alumina containers and a gas-fired furnace were generally employed. The firing operation is periodic and is followed by a pulverization procedure.

Other Calcining Methods

It has been thought that calcined particles with desirable characteristics for use in a slurry blanket might be produced from the ThO_2 as received in one operation by a brief exposure to a very high temperature (3000°C). Among the hoped-for properties are a very fine size (1 μ or less) and rounded corners which should reduce the abrading action. Heat sources considered for this purpose were the oxyacetylene torch, the electric arc, and the induction furnace. Preliminary tests of the first two methods were made.

Flame-Spray Calcination of Thorium Oxide

For the oxyacetylene calcination, a metallizing gun (Metco Flame Spray), which employs a gravity feed, was found to be best. However, ThO_2 (from the oxalate process) tended to pack and was

passed through the gun with difficulty, even when the gun was vibrated strongly. On the second pass there was much less difficulty.

Thorium oxalate and thorium formate offered less difficulty than the oxide. A thorium oxide–acetyl-acetone complex was unsatisfactory in the oxy-acetylene flame-spray gun, apparently because it has a low melting temperature. Under the given conditions three successive passes through the gun seemed necessary for complete conversion of the oxalate and formate to cubic ThO_2. The product from the oxide, formate, or oxalate con-sisted of fine grains which, in part, clung together in agglomerates approximately 0.5 mm in diameter; these were very easily crushed to powder. In the case of thorium oxalate and formate there was a notable volume decrease during the first passage through the gun.

Samples of flame-spray-calcined thorium oxide, formate, and oxalate have been submitted to the HRP Blanket Development Group for tests (in toroids) of abrasive properties and resistance to particle degradation.

Electric Arc Calcination of ThO_2

The apparatus consisted of graphite electrodes $\frac{1}{2}$ in. in diameter extending into the center of a vertical refractory tube 5 in. in diameter. The powdered materials were fed through the arc by means of a vertical zircon tube which was kept in vibration.

The product of one passage through the arc of either the oxide, formate, or oxalate contained some rather perfect spheres of ThO_2, 0.1 to 0.3 mm in diameter; many of these were transparent, iri-descent, hollow bubbles which floated on water and were carried upward by air currents; they were very fragile. Many solid opaque spheres of about the same size were formed also and appeared to be agglomerates of finer particles; they were resistant to crushing.

After three passes through the arc the product of each of the three compounds consisted mostly of spheres and was made up of about equal proportions of the transparent hollow type and the solid opaque type (see Figs. 145 and 146).

It was concluded that the arc process produced, under the given conditions, an unsuitable product for the HRT blanket because of the comparatively large size of the spheres produced. It is con-ceivable that refinements in the apparatus might lead to the production of the submicron-sized rounded grains desired. Uses for the transparent bubbles of ThO_2 are being sought.

THORIUM OXIDE SLURRY: ELECTRICAL PRECIPITATION

C. E. Curtis

Small sheets (15 in.^{2} in total submerged area) of zirconium and of stainless steel were dipped into a slurry consisting of 20 g/liter of LO-12 thorium oxide in distilled water and were connected together through a microammeter. Voltaic action began at once, producing a current of approximately 20 μa. The thorium oxide began almost immediately to settle out of suspension, and precipitation was almost complete in 15 min. A similar suspension with electrodes unconnected showed no settling in the same period (see Fig. 147).

THORIUM OXIDE: KNOOP HARDNESS

C. E. Curtis

The hardness of a piece of thorium oxide previ-ously fused in an electric arc furnace was tested for the Ceramic Laboratory by the Metallography Group of the Metallurgy Division. Under a 100-g load the hardness number was 985.

URANIUM DIOXIDE: HARDNESS OF SINTERED SPECIMENS

C. E. Curtis

Specimens of UO_2 which had been dry-pressed and fired in hydrogen at 1750°C gave a Knoop hardness number of 570. The density of the speci-mens was 10.56 g/cc and the porosity was zero.

UO_2-ThO_2 COMPOSITIONS: DENSITY, MODULUS OF ELASTICITY, AND RESISTANCE TO OXIDATION

C. E. Curtis

A series of compositions of UO_2 and ThO_2 was made up from fine-grain-sized material in proportions from 100% UO_2 to 100% ThO_2 in 10% increments by weight. Dry-pressed flat bars of these compo-sitions were fired in a hydrogen atmosphere for 2 hr at 1750°C.

With increasing ThO_2 content, the color changed from black to green (pure ThO_2 was white), the porosity varied from 0.7 to 2.0% with no certain trends, and the density decreased gradually from 10.0 g/cc for pure UO_2 to 8.9 g/cc for pure ThO_2.
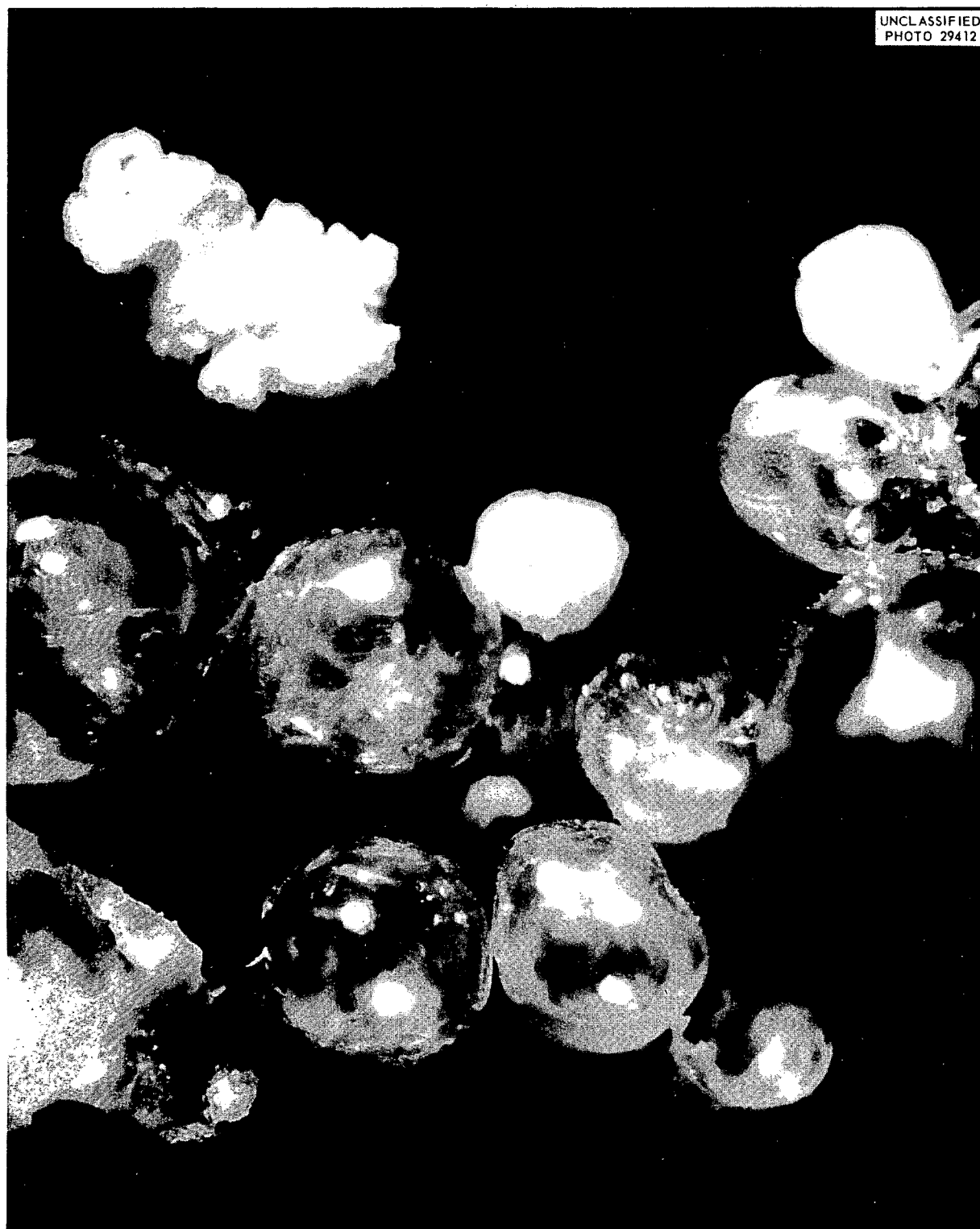
Fig. 145. Thorium Oxide Spheres from Arc Calcination of ThO_2. Largest spheres are approximately 0.3 mm in dia. Note transparent spheres (lower left) and opaque spherical agglomerates (upper right). 140X. Reduced 15%.

Fig. 146. Thorium Oxide Spheres from Thorium Oxalate Calcination. Transparent spheres, opaque spheres, and irregularly shaped agglomerates are visible. Largest spheres are approximately 0.3 mm in dia. 140X. Reduced 17%.
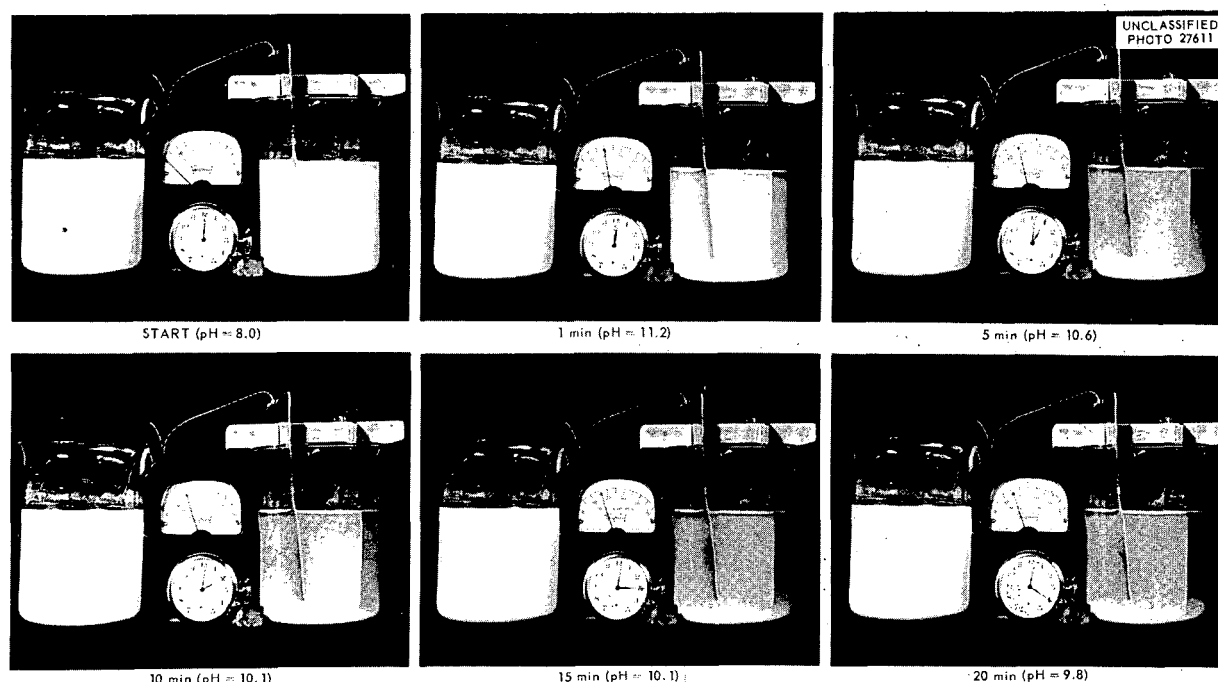
UNCLASSIFIED
PHOTO 27611

START (pH = 8.0)   1 min (pH = 11.2)   5 min (pH = 10.6)

10 min (pH = 10.1)   15 min (pH = 10.1)   20 min (pH = 9.8)

Fig. 147. Effect of Zr—Stainless Steel Voltaic Cell on Settling Rate of ThO_2 Suspension. The suspension in the beaker at left is the control. In the right-hand beaker the electrode at left is stainless steel, the one at the right is zirconium.

The sonic modulus of elasticity for pure UO_2 was 25×10^6 psi and that for ThO_2 was 30×10^6 psi. The values for the mixtures of the two oxides ranged from 16×10^6 to 28×10^6 psi with no certain trends.

Selected portions of the UO_2-ThO_2 specimens ($1\frac{1}{2} \times \frac{3}{8} \times \frac{1}{8}$ in.) containing 10, 30, 50, 70, 90, and 100% ThO_2, respectively, were refired in air (oxyacetylene furnace) to 1800°C with no soaking time. Under these conditions no protection to the UO_2 was obtained by the addition of 10% of ThO_2, and the bar disintegrated; with 20% or more of ThO_2, weight losses in fractions of a per cent were obtained.

SPHEROIDIZING OF ZIRCONIA, ZIRCON, HAFNIA, AND ALUMINA

C. E. Curtis

Fine (−200 mesh) powders of zirconia, zircon, hafnia, and alumina formed spheres when dropped through the electric arc (graphite electrodes). Part of the spheres were transparent and fragile and were light enough to be carried upward by air currents. Others were solid, opaque, and resistant to crushing. Diameters ranged from 0.1 to 0.3 mm.

Apparently the amount, size, and strength of the spheres can be controlled by varying the particle size and/or the amount of agglomeration of the powder used and also the speed of travel of the particles through the arc. Such spheres might be found useful for their high heat insulating value or in operations in which a free-flowing high-calcined powder is necessary. Whether their transparency to visible light can be found useful remains to be seen.

WASTE DISPOSAL: SIMULATED HOPE WASTE SOLUTION EXPERIMENTS

J. M. Kerr

Low-Activity Mixes

Investigations on the retention of fission products (without prior separation) in fired ceramic bodies have been carried out during the past year. Naturally occurring materials such as ball clays, bentonites, phosphate slimes, shales, and atta-pulgites have been utilized, with the best results having been obtained from shale and attapulgite.

Attapulgite is a hydrated magnesium aluminum silicate. The particle shape is very unusual,

198

somewhat resembling a piece of macaroni in that each particle is a long hollow tube. These tubes agglomerate to form bundles which require high shear stresses for separation into the individual particles. Both the single particles and the agglomerates may be seen in Fig. 148. Several of these clays, processed by the Minerals and Chemicals Corporation of America, have been dried so as to contain varying degrees of moisture. The notations LVM, RVM, and HVM denote low volatile matter, regular volatile matter, and high volatile matter, respectively. The LVM clay had been heat-treated at 1800°F for a short period of time, and all of the mechanically held water and most of the chemically held water had been volatilized.

Previous work had been carried out by using single isotopes as tagging isotopes for the Hope solution, which is a mixture of 1.6 M $Al(NO_3)_3$, 0.16 M HNO_3, and 0.02 M H_2SO_4. It had been decided to eliminate the use of the single isotopes and to use mixed fission products in tagging the solutions. Tests were carried out on 81 mixes made with Hope solution tagged with mixed fission products. The results of leach tests from six of the best of these mixes may be seen in Table 45. These had been fired to the three different temperatures indicated. With the exception of mix 15, these mixes contained only 50 g of solid to 250 ml of Hope solution. Mix 15 was so successful in retaining the activity that it should be included among the best mixes, although it contained three times as much dry material, per 250 ml of Hope solution, as the other five mixes.

A new technique for determining the volatility of tagged mixes of clay with Hope solution during the various stages in drying, fuming, and firing was initiated by M. P. Haydon, R. L. Hamner, and J. M. Kerr. Data showing that the volatility of mixed fission products in Hope solution was negligible up to 638°C may be seen in Fig. 149. The general increase in total counts per minute

Fig. 148. Electron Photomicrograph of Attapulgite Particles. (From *Clay Mineralogy*, by Ralph E. Grim, McGraw-Hill, New York, 1953, by permission.)

Table 45. Leach Test Results for Low-Activity Mixes

Mix Number	Composition*	Activity in Lixivium (counts/min/ml)		
		Fired at 426°C	Fired at 638°C	Fired at 800°C
36	Zeogel, 50 g	267	0	16
87	Phosphate slime, 50 g	51	36	8
101	Permagel, 50 g	22	7	2
104	Attasorb LVM, 50 g	34	12	0
107	Attasorb RVM, 50 g	26	10	20
15	Shale, 100 g; limestone, 30 g; soda ash, 30 g		1	3

*Mixed with 250 ml of Hope solution tagged with mixed fission products to a count of between 20,000 and 40,000 counts/min/ml.
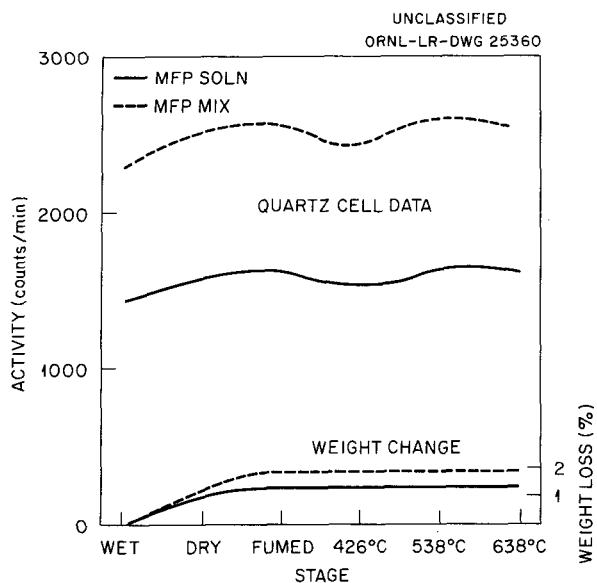

UNCLASSIFIED
ORNL-LR-DWG 25360

Fig. 149. Mixed Fission Products Solution — One Run Only. 100 g of Milwhite Texas bentonite was used to 250 ml of aluminum nitrate solution.

as the temperature was increased and water was removed can be attributed to the decreased shielding of beta particles by the water, and thus does not indicate an increase in the total radioactivity.

High-Activity Mixes

Several mixtures of clay and Hope solution have been made and tagged to a count of roughly 200,000 counts/min/ml. These contain of the order of

seven times as much radioactivity as the previously mentioned mixtures. Because of the excellent results with attapulgite clays in the low-activity ranges, they were used in the high-activity mixes. Four mixes were made up, and results showed that a higher firing temperature was necessary in order to fix the activity. These results may be seen in Table 46. Evidently there was a saturation point beyond which a given weight of clay could not retain more activity. By increasing the temperature of firing, or by increasing the clay content with a given amount of solution, an increased amount of activity may be retained.

Further Work

A nitrogen gas adsorption system has been built and is in working order. This apparatus will be used for surface area determinations in an effort to correlate retention of activity with the surface area of the clays used in the past year.

A small colloid mill has been obtained and will be used to obtain better dispersion of the clay in an effort to reduce the amount of clay necessary to tie up a given amount of radioactivity.

WASTE DISPOSAL: SIMULATED PUREX SOLUTION EXPERIMENTS

M. P. Haydon

Fifty-eight different compositions of clay sinter mixes have been studied. Some of these were tagged with the Cs^{137}-Ba^{137} isotopes, others were tagged with mixed fission products. All were

Table 46. Leach Test Results for High-Activity Mixes

Mix compositions: 50 g of clay

250 ml of Hope solution tagged with mixed fission products
to a count of 200,000 counts/min/ml

Mix Number	Clay	Activity in Lixivium (counts/min/ml)				
		Fired at 426°C	Fired at 638°C	Fired at 800°C	Fired at 1000°C	Fired at 1200°C
109	Attasorb LVM	1806	736	493	104	23
116	Attasorb RVM	1612	436	907	80	60
117	Attasorb HVM	1418	502	1242	80	20
118	Permagel	1114	117	22	144	38

mixed with a simulated reactor waste solution known as Purex, a 2.2 M HNO_3 solution with added carriers.

The sinter mixes were fired to 430, 540, 650, and 870°C; a few of them were fired to 1000, 1200, and 1400°C. They were then soaked for various periods of time in water which was sampled for radioactivity counts. Results of the static leach tests indicate that retention of radioactive material in most of the sinters tagged with mixed fission products and containing no limestone was very good at the levels used in these experiments, namely, 6,000 to 30,000 counts/min of beta particles. Decontamination factors of 10^5 were noted.

Thin films of the sinter mixes spread on silica glass dishes were weighed and counted at each stage of the process of fuming, drying, and firing to successively higher temperatures to determine whether the lowering of the beta activity of the lixivium was due to volatilization of the radioactive material from the sinter or to some change in the sinter itself.

Physical properties of the sinter mixes which may be helpful in the engineering of the disposal of reactor wastes and in the determination of the mechanism of retention in sinters, including volume reduction from wet mix to fired cake, porosity, bulk density, pH of lixivium, and mixing characteristics, have been examined briefly. The details of the experiments will be included in a forthcoming ORNL report.

WASTE DISPOSAL: POROUS CERAMICS AND POROUS CONCRETE STUDIES

G. C. Robinson

In this series of investigations it was desired to determine how effectively porous ceramic bodies and porous concretes can tie up radioactive waste (Hope type). Two methods of attack were considered. The first was to use small vermiculite bricks and to soak up the waste solution, dry it to a salt in the piece, then soak up more liquid, and repeat this process until the maximum amount of waste liquid was retained as dry salts. The second method was to use the waste liquid as the makeup liquid in a concrete, as was suggested briefly in the papers given in Cincinnati in 1955.

Results from the first method show that it is possible to pick up 14.4 gal of waste liquid per cubic foot of vermiculite brick. When fired, this 1 cu ft of brick would shrink to $\frac{1}{2}$ cu ft; hence, on a fired basis, 1 cu ft of vermiculite brick could contain 3.8 cu ft of waste liquor, or 40 lb of the dried salt.

Results from the second method were rather variable, apparently depending on sample size variations and on the surface appearance of the sample. The problem of concrete disintegration could be corrected in two ways: first, a concrete may be prepared that would contain certain ceramic substances which would promote sintering as the hydraulic bond is destroyed; second, a light-weight

concrete would be prepared which would keep the radioactive particles at a greater distance from each other than would be possible in heavy concrete.

From leach tests it may be seen that activity in the leach liquor decreases with increasing firing temperature in the concretes. A temperature above 1100°C is recommended for firing.

It was found that losses in radioactivity when mixtures were fired to as high as 990°F were due solely to losses in ruthenium. This isotope was nearly completely volatilized at the highest temperature.

FLUORIDE FUEL INVESTIGATIONS

L. A. Harris

Phase determinations in the fluoride fuel research program have been made by petrography. Typical systems studied were $NaF-LiF-BeF_2$, $LiF-ThF_2-BeF_2$, $RbF-NaF-BeF_2$, and $KF-BeF_2$. The results have been reported elsewhere.[17-20]

THERMAL ANALYSIS AND THERMAL EXPANSION DETERMINATIONS

S. D. Fulkerson

Perhaps the most important of the services rendered to various departments is that of differential thermal analysis (DTA). For the Health Physics Division's Waste Disposal Program a series of DTA's on the attapulgite clays and clay-flux mixtures was made. Quite a number of DTA's were conducted for the Y-12 Production Division on various UO_2 samples made by different processes. In the ceramics research program on the rare-earth oxides some DTA was done.

Next in importance by way of services rendered are the determinations of linear thermal expansion.[21] A series of nine determinations was carried out for the Metallurgy Division on their Coast Metals brazing alloy program, as well as on INOR-8 alloy.

[17]C. J. Barton *et al.*, *ANP Quar. Prog. Rep. Dec. 31, 1956*, ORNL-2221 (Parts 1–5), p 109.

[18]C. J. Barton *et al.*, *ANP Quar. Prog. Rep. March 31, 1957*, ORNL-2274 (Parts 1–5), p 91.

[19]C. J. Barton *et al.*, *ANP Quar. Prog. Rep. June 30, 1957*, ORNL-2340 (Parts 1–5), p 119.

[20]C. J. Barton *et al.*, *ANP Quar. Prog. Rep. Sept. 30, 1957*, ORNL-2387 (in press).

[21]S. D. Fulkerson, *Apparatus for Determining Linear Thermal Expansions of Material in Vaccum or Controlled Atmospheres*, ORNL CF-57-7-123 (July 30, 1957).

For the ANP program, thermal expansion determinations were made on zirconium hydride. For the Chemistry Division, a determination was made of the thermal expansion of UF_4. In the Ceramics Laboratory some determinations were made on the rare-earth oxides, as well as a series of Be + BeO determinations.

Another branch of services rendered, and perhaps the most time consuming, is that of preparation of samples for various physical property tests which have to be diamond-machined to exact finished dimensions. In a cooperative effort between the Engineering Tests Section of the Solid State Division and the Ceramics Laboratory, numerous siliconized silicon carbide fuel-element plates for in-pile tests were prepared by diamond surface grinding.

There were other services such as modulus of elasticity determinations by sonic means made for other departments, for all of which samples had to be specially prepared.

DESIGN AND BUILDING OF LABORATORY TESTING EQUIPMENT

S. D. Fulkerson

Much time was consumed in the design and building of a new vacuum or controlled-atmosphere recording dilatometer for materials that cannot be heated in air. A report descriptive of this apparatus has been published.[21]

Work is in the advanced stage on the building of a vacuum hot sonic modulus apparatus for the determination of the modulus of elasticity of materials at elevated temperatures.

FABRICATION STUDIES

J. A. Griffin

The first in a proposed series of spherical shells of rare-earth oxides for the Physics Division was produced. This shell of samarium oxide consists of two mated hemispheres approximately $3\frac{1}{2}$ in. OD and 3 in. ID. The parts were formed by isostatic pressing and were then sintered. The final tolerances and finish were obtained by machining. This assembly is shown in Figs. 150 and 151.

Disks of various ceramic materials requested by the Critical Experiments Group were supplied.
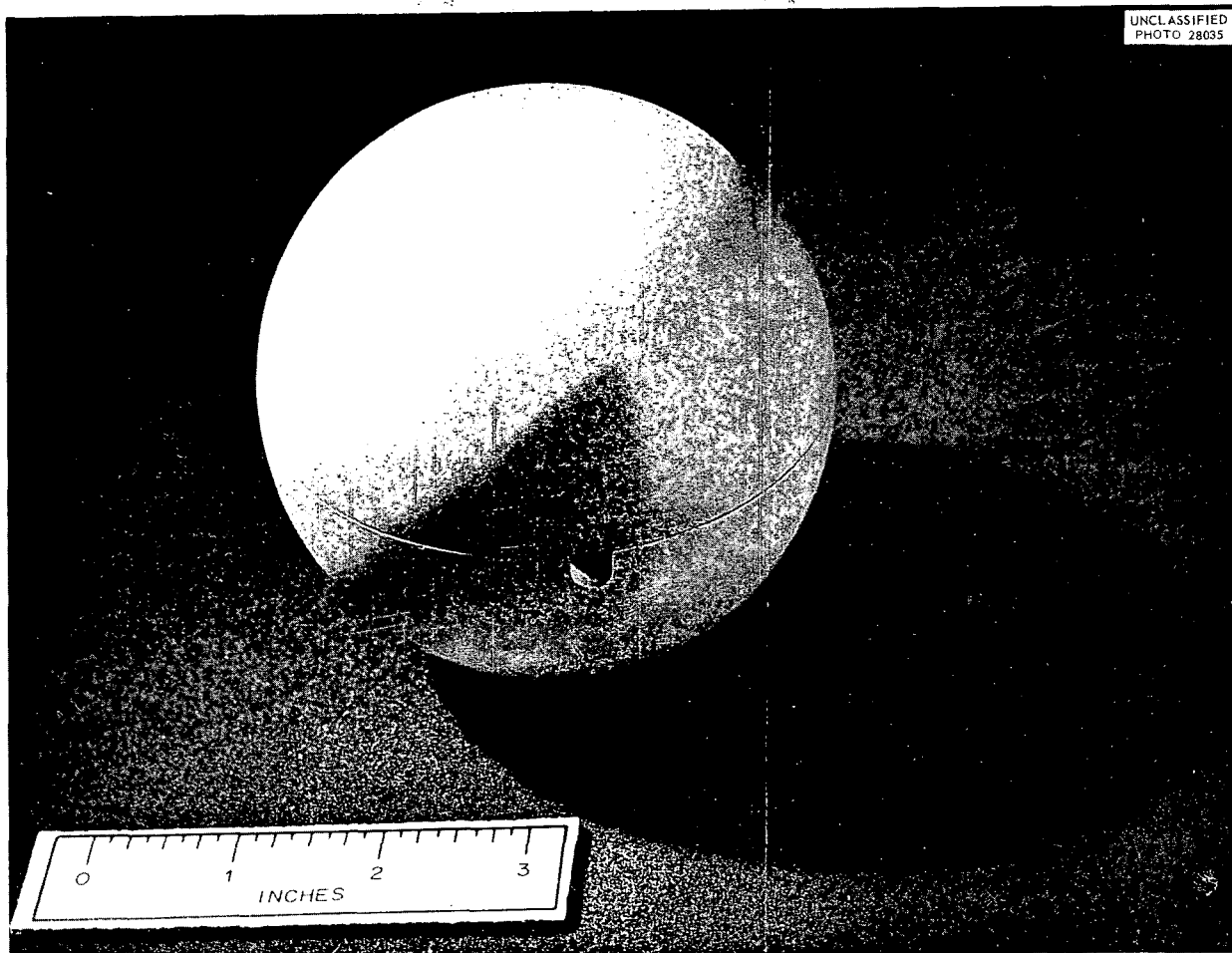
Fig. 150. Spherical Shells.

These included aluminum oxide, calcium fluoride, cadmium oxide, beryllium oxide, and sulfur.

Studies of materials resistant to attack by molten uranium and its alloys were carried out. The effects of the history of the starting material, grain size, and fabrication techniques on the fired density of crucibles and tubes of uranium dioxide, thorium oxide, zirconium oxide, and magnesium oxide were studied. The effects of firing temperatures and atmospheres were also noted. Small crucibles of magnesium oxide with above 95% of theoretical density have been produced. Uranium dioxide crucibles of similar size had 97% of theoretical density.

THERMAL DIFFUSIVITY

G. C. Robinson

A survey of the literature on thermal diffusivity has been made. This will be issued as a CF memo in the future.

CLAYS AS SUSPENDING AGENTS FOR THORIA SLURRIES

E. D. Lynch

The suspending power of several clays was investigated to ascertain their ability to prevent the settling of thoria slurries. The results of this work are contained in a CF memo having the above title, which is to be issued shortly.
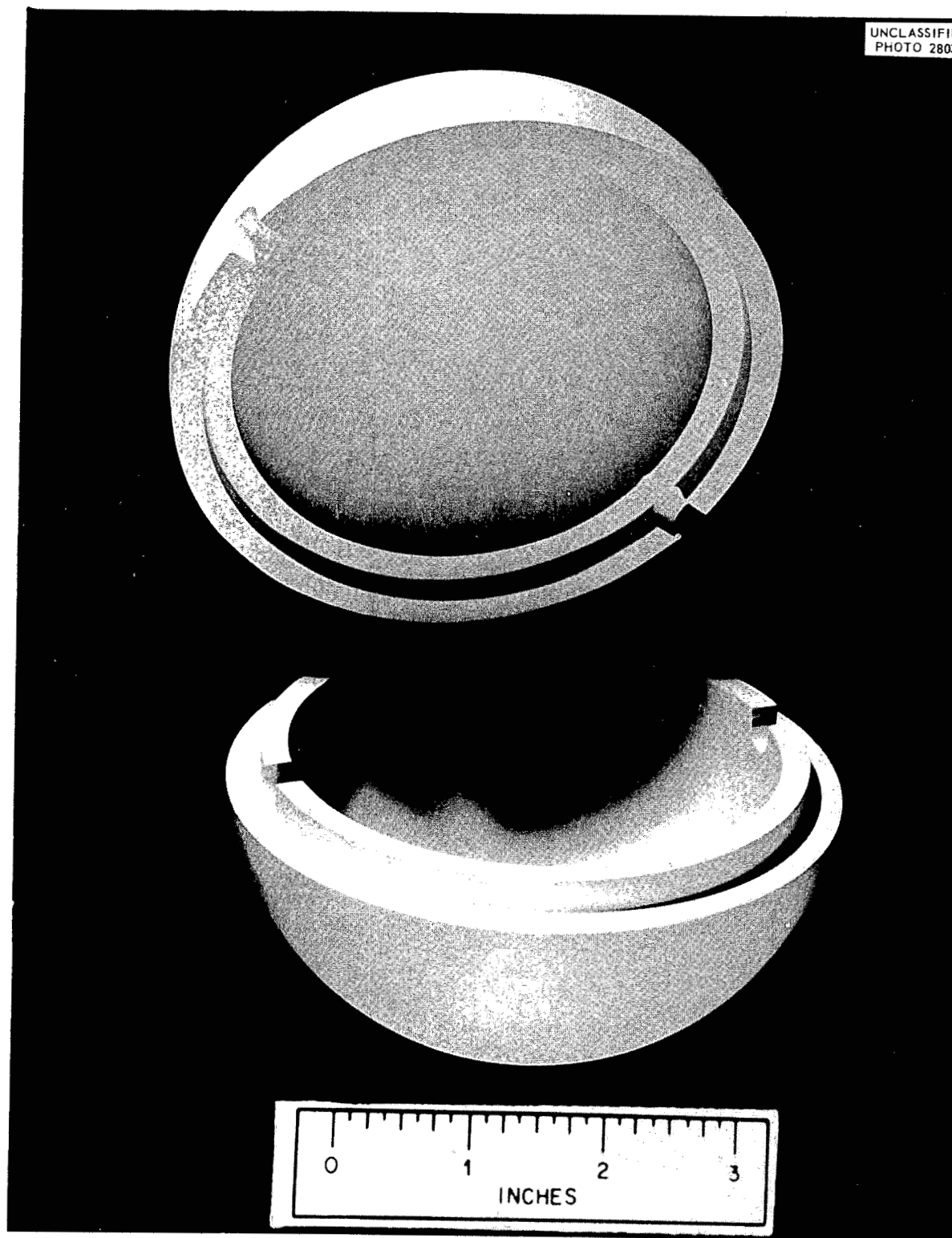
Fig. 151. Spherical Shells.

FUNDAMENTAL METALLURGY

PHYSICOMETALLURGICAL RESEARCH

L. K. Jetter

C. J. McHargue   G. D. Kneip, Jr.
J. C. Ogle   D. S. Easton
J. O. Betterton, Jr.   J. O. Scarbrough
        E. B. Nunn (co-op student)
        D. O. Welch (co-op student)

ALLOTROPIC MODIFICATIONS IN METALLIC CERIUM

C. J. McHargue   H. L. Yakel, Jr.
            L. K. Jetter

Although it has been known for some time that metallic cerium exists in a number of crystallographic states, there have been no detailed studies made of these states nor of the kinetics of the transformations. Trombe and Foëx[1] reported three modifications for cerium. A face-centered cubic phase was found to be stable above 473°K; a hexagonal close-packed phase was formed by slow cooling from 473°K to room temperature; and a phase of unknown structure was formed upon quenching from 473 to 77°K. Schuch and Sturdivant[2] reported the low temperature phase to be also face-centered cubic with a volume 16.5% smaller than the high temperature face-centered cubic phase. The two cubic phases were reported to coexist at 77°K. Bridgman[3] noted evidence of a phase change in cerium upon application of high pressure, and Lawson and Tang[4] showed by x-ray diffraction that the two face-centered cubic phases were present at 15,000 atm.

The present study has been concerned with details of the crystal structures, kinetics of the transformations, and the effect of such variables as mechanical deformation on the transformations.

High-purity cerium metal received from the Institute for Atomic Studies, Ames, Iowa, was further purified by vacuum melting and degassing. Spectrographic and gas analyses of the ingot indicated a purity of 99.9%. Observations were made between 77 and 450°K on polycrystalline samples of this material using an x-ray diffractometer equipped with a cryostat.

Three crystallographic forms of cerium were observed in the present study. At room temperature, a face-centered cubic structure with $a_0 = 5.15$ Å is stable in a previously uncooled annealed sample. Just below the ice point, transformation to a hexagonal close-packed structure with $a_0 = 3.68$ Å, $c_0 = 11.92$ Å, and $c/a = 3.239$ ($ABAC$ repeat) begins. At still lower temperatures, the remaining face-centered cubic phase transforms into the "collapsed" face-centered cubic form for which $a_0 = 4.85$ Å at 77°K. The hexagonal phase does not, itself, transform on further cooling, and it is possible to have all three modifications present at 77°K. Typical x-ray diffraction traces showing the positions of the lines are shown in Fig. 152.

Older work on the crystal structure of cerium reported the hexagonal close-packed form to have a c/a ratio of about 1.63 rather than the "double" hexagonal structure reported here. It is interesting to note that several other rare-earth metals (lanthanum, praseodymium, and neodymium) have been recently found to have a similar double hexagonal structure.[5]

The volume decrease in the cubic-to-cubic transformation is 16.5%, which is in good agreement with the dilatometric work of Trombe and Foëx[1] and the x-ray results of Schuch and Sturdivant.[2] The volume per atom in the hexagonal phase is approximately the same as that in the normal cubic phase. No collapsed hexagonal phase was ever observed under the conditions of these experiments.

Figure 153 shows in detail the manner in which the various transitions occur in an annealed cerium specimen. The ordinate represents the percentage

[1] F. Trombe and M. Foëx, Ann. chim. (Paris) 19, 417 (1944).

[2] A. F. Schuch and J. H. Sturdivant, J. Chem. Phys. 18, 145 (1950).

[3] P. W. Bridgman, Phys. Rev. 48, 825 (1935).

[4] A. W. Lawson and T. Tang, Phys. Rev. 76, 301 (1949).

[5] F. H. Spedding, A. H. Daane, and K. W. Herrmann, Acta Cryst. 9, 559 (1956).
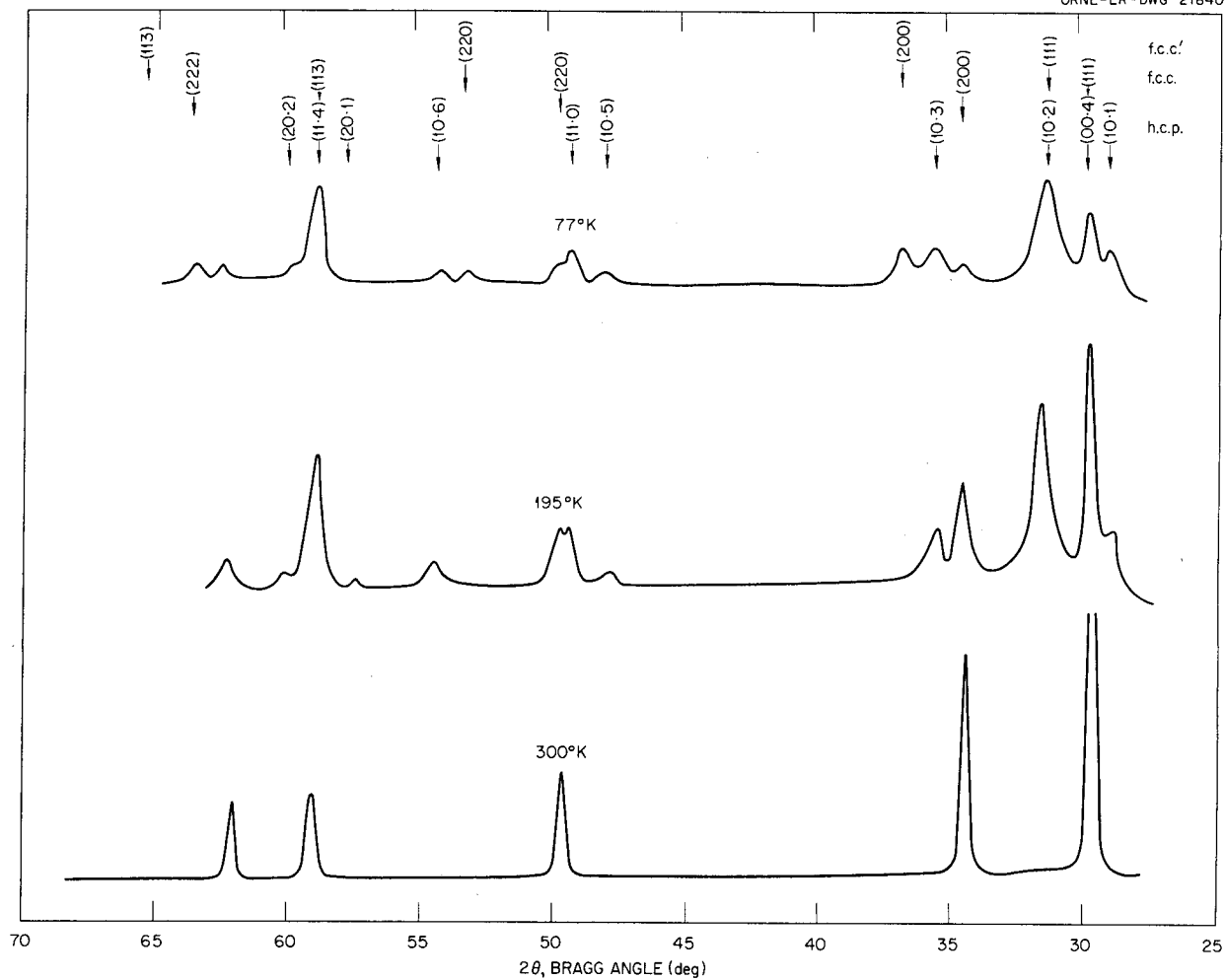
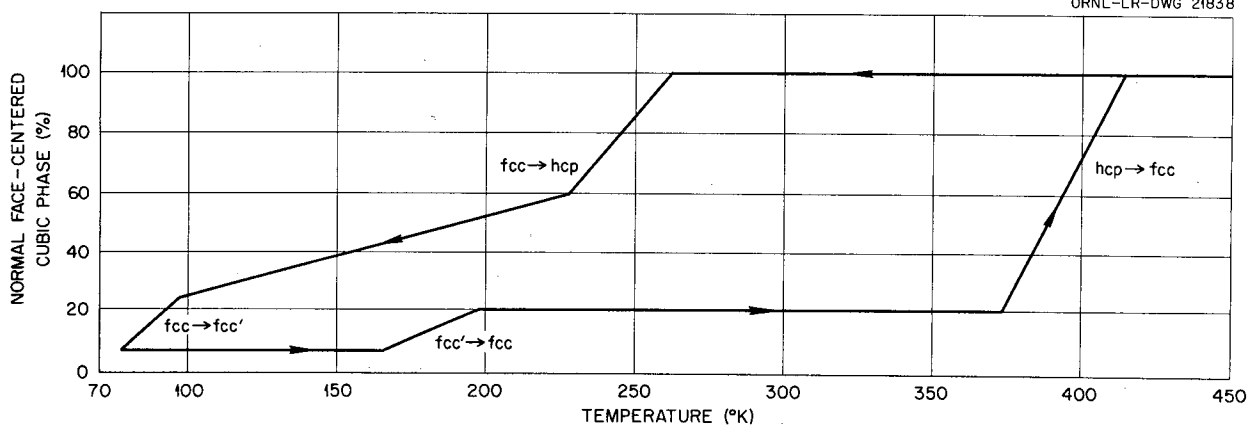Fig. 152. Typical X-Ray Diffraction Traces Showing the Phases Present in Cerium at 300, 195, and 77°K.

Fig. 153. Amount of High-Temperature Face-Centered Cubic Phase Present in an Annealed Specimen of Cerium as a Function of Temperature.

of the normal face-centered cubic phase present. These percentages were obtained from comparison of observed and calculated integrated intensities. No isothermal transformation was ever observed for periods of time ranging from 5 min to 8 hr.

The pronounced knee in the curve representing the transformation of face-centered cubic cerium to hexagonal cerium should be noted. This decrease in transformation rate was reproducible and has been duplicated in a similar curve plotting the percentage of hexagonal phase against temperature. That the cubic-hexagonal transformation is not simple is shown* by the appearance of the (10.2) hexagonal lines in Fig. 154. The disappearance of the lower 2θ component corresponds to the break in the transformation curve of Fig. 153. This behavior is suggestive of a transition phase.

With one exception, the temperatures of transformation appeared to be independent of prior annealing temperatures and times and of prior transformation. The T_s (temperature at start of transformation) for the face-centered cubic to hexagonal transformation was found to be 263 ± 5°K. T_s for the reverse transformation (hexagonal to cubic) was found to be 363 ± 5°K and T_f was 405 ± 5°K. The cubic-to-collapsed-cubic transformation was found to start at 103 ± 5°K. T_s for the collapsed-cubic-to-cubic transformation was 170 ± 5°K and T_f was 200 ± 5°K. The exception to these temperatures is an apparent "memory" effect observed in samples partially transformed to the collapsed-cubic phase and reheated so that all the collapsed phase re-transformed to the normal cubic phase. If the specimen was heated only 20 to 30°C above T_f for the fcc′ —→ fcc reaction and cooled, the fcc —→ fcc′ transformation

started at 123 ± 5°K rather than at 103°K as in specimens cooled from higher temperatures. This effect could be caused by a transformation stress distribution, arrangement of impurities such as a fine precipitate, or an array of dislocations.

If a sample containing only normal cubic cerium is worked at room temperature by rolling or peening and then cooled, transition to the hexagonal phase is suppressed and in some case even eliminated. Figure 155 shows the transformation in a specimen heavily worked at room temperature. It may be noted that the critical temperatures for the collapse transition were the same as in the annealed state.

If a sample which contains some hexagonal cerium from a previous cooling is worked at room temperature, the hexagonal phase tends to revert to the cubic form, and sufficient work may result in 100% reconversion. Subsequent cooling does not produce any more of the hexagonal structure.

Similarly, if an annealed sample is cooled to 195°K and worked, the hexagonal phase which formed on cooling tends to transform back to the normal cubic phase. The cubic structure which is produced in this operation is very faulted as can be seen by the broadened and shifted lines of the diffraction pattern. On cooling below the working temperature of 195°K, the collapse transformation occurs as before.

Working an annealed specimen at 77°K causes an increase in the amount of the collapsed-cubic phase and a decrease in the amount of the other two phases. Figure 156 shows the amount of transformation as a function of deformation. Under the conditions investigated so far, this is the only instance in which the material was entirely transformed to the denser cubic phase.
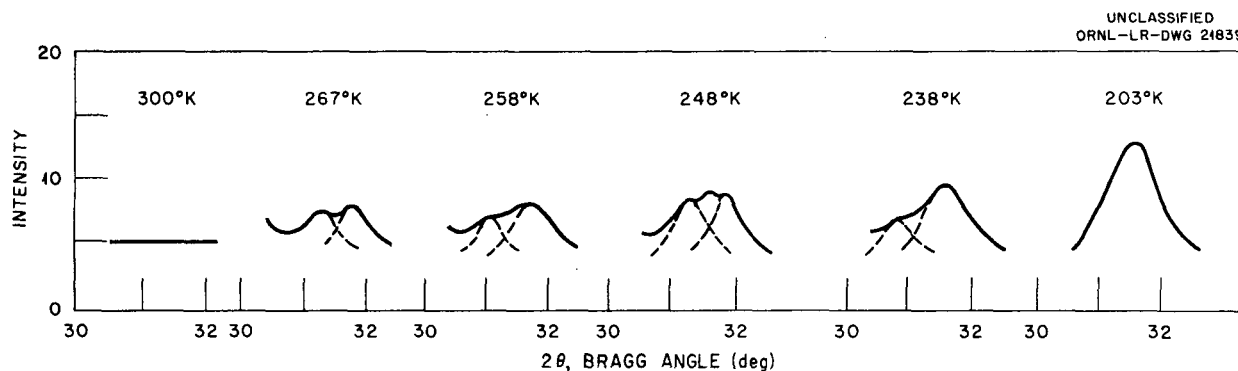
Fig. 154. Appearance of the (10.2) Diffraction Line for the Hexagonal Close-Packed Phase of Cerium.

209
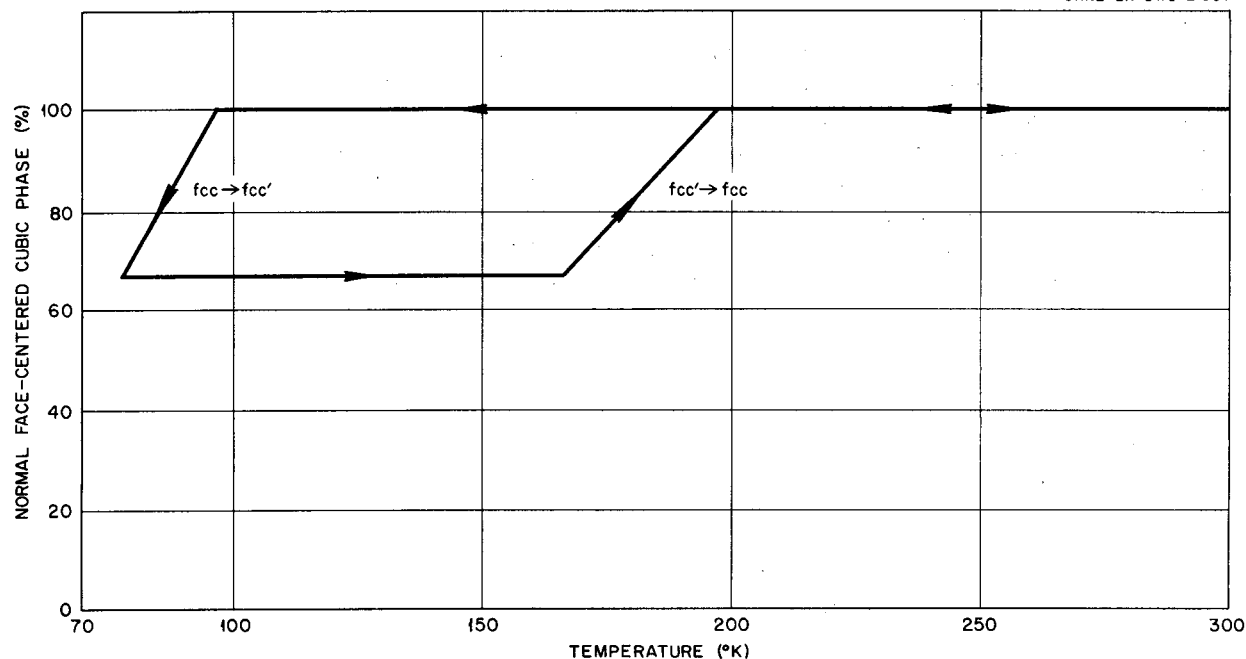
Fig. 155. Amount of High-Temperature Face-Centered Cubic Phase Present in a Deformed Specimen of Cerium as a Function of Temperature. The cubic-to-hexagonal transformation has been completely suppressed.
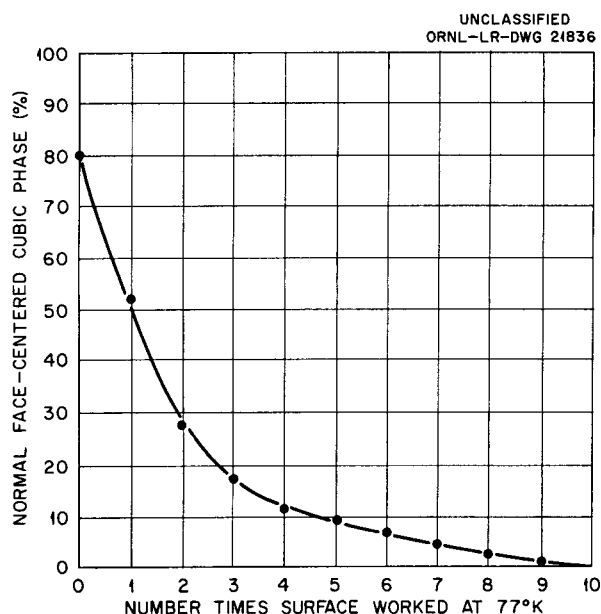
Fig. 156. Amount of Cubic Transformation in Cerium as a Function of Deformation at 77°K.

It seems certain that the hexagonal phase is unstable under deformation at any temperature. The behavior of cerium in this respect is different from that normally expected in martensitic transformation in which stress applied to polycrystalline specimens favors the formation of the lower temperature phase. On the other hand, deformation of the normal cubic phase below 105°K causes more collapse phase to form as shown in Fig. 156.

Figure 157 is a photomicrograph of a specimen cooled to 77°K and examined at room temperature. All the hexagonal phase is retained, whereas the denser cubic phase has transformed back to the normal cubic phase. The original grain diameter was of the order of 0.005 in. The structure shows grains of hexagonal phase in a matrix of cubic which shows considerable distortion.

There are several features of both transitions in cerium which are suggestive of martensitic character. In each, there is no isothermal transformation, the amount of transformation product is a function only of the temperature, and large hysteresis is associated with them.

Fig. 157. Cerium Specimen After Having Been Cooled to 77°K and Reheated to 293°K. Specimen lightly etched in dilute HNO_3. *Reduced 17%.*

In the case of the cubic-to-hexagonal transformation, the mechanism for such a displacive transformation might be similar to those proposed by Burgers,[6] and Sebilleau and Bibring.[7] However, the situation is not exactly the same since the hexagonal structure has the *ABAC*-repeat sequence rather than the simple *ABAB* repeat.

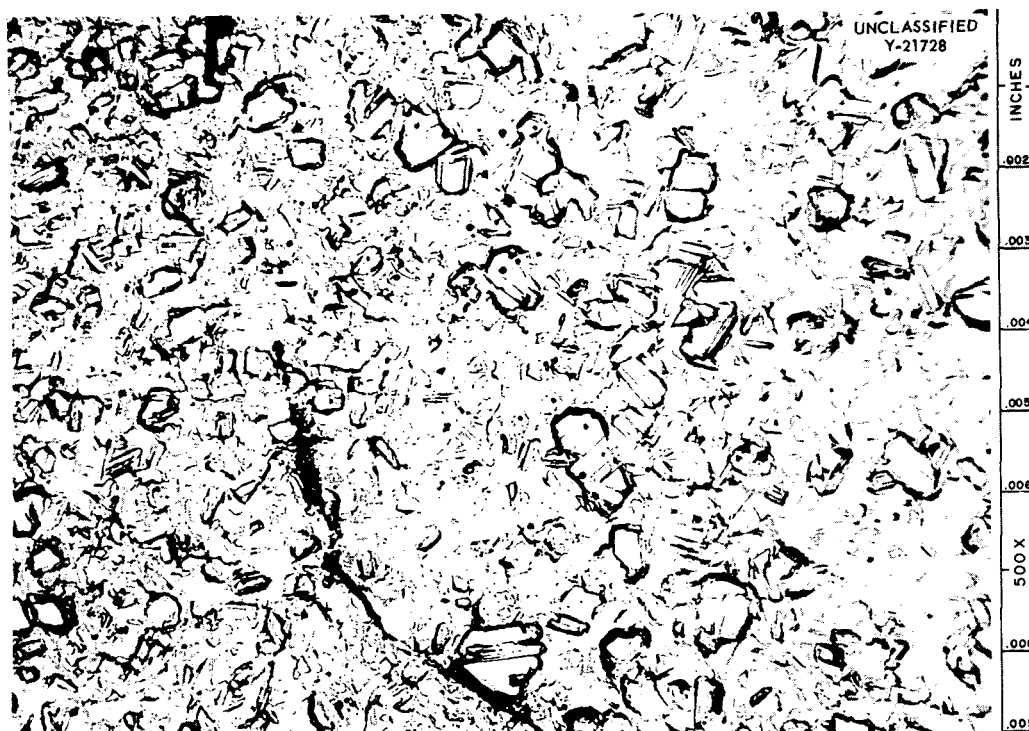There are other features of the cubic-to-hexagonal transformation which suggest a more complicated behavior. The knee in the transformation curve (Fig. 153) and the possible transition phase (Fig. 154) have already been mentioned. Moreover, the hexagonal phase appears in Fig. 157 as grains with markings inside them. The behavior of the hexagonal phase under the influence of deformation is also unique inasmuch as an apparently thermally stable phase can be made to revert to its parent phase by deformation.

In the case of the collapse transformation, the close structural relation between the two phases raises certain problems with respect to a martensitic transition. This type of transformation implies a more-or-less well defined habit plane and a unique plane of zero distortion. Since the linear shrinkage is only about 5% and since the symmetry remains the same, any plane should be an equally good matching plane and the selection of any unique plane of zero distortion becomes doubtful. The hysteresis and the apparent dependence of the amount of transformation on temperature might be due to transformation stresses in the polycrystalline material.

There have been at least two proposals for the fundamental cause of the collapse transformation in cerium. Pauling[8] and Zachariasen[9] suggested that the decrease in atomic volume is caused by promotion of a $4f$ electron to the $5d$ state or a bonding orbital. Recently Varley[10] proposed that

---

[6]W. G. Burgers, *Physica* 1, 561 (1934).

[7]H. Bibring and F. Sebilleau, *Rev. Mét.* 52, 569 (1955).

[8]Personal communication cited by A. F. Schuch and J. H. Sturdivant, *J. Chem. Phys.* 18, 145 (1950).

[9]Personal communication cited by A. W. Lawson and T. Tang, *Phys. Rev.* 76, 301 (1949).

[10]J. H. O. Varley, *Phil. Mag.* 2, Series 8, 384 (1957).

certain factors affecting the volume expansions of pure metals may lead to two isomorphous states differing in volume.

The present work is to be continued by an examination of the crystal structures down to 4°K by x-ray diffraction, a study of the magnetic structure by neutron diffraction, a more detailed metallographic study, determination of the heats of transformation, and a calculation of the band structure in an effort to understand the fundamental cause of the isomorphous transformation.

Temperature of Container and Billet (°F)	Extrusion Speed (fpm)
850	0.3
850	738
650	0.2
650	659
450	0.1
450	615
250	0.2
250	368
75	0.07
75	490

PREFERRED ORIENTATION IN EXTRUDED ALUMINUM ROD

C. J. McHargue   L. K. Jetter

The nature of the structure and its variation are among the important problems associated with the production of extruded products. Smith,[11] Hardy,[12] and Locke[13] have summarized data on the flow of aluminum and aluminum alloys. Depending on the composition and fabricating conditions (temperature, extrusion ratio, and extrusion speed), the product may be unrecrystallized, partially recrystallized, or completely recrystallized. Moreover, there may be variations in the structure from the surface to the center and from front to back of the extrusion. Any inhomogeneity in grain structure and preferred orientation may affect both the mechanical properties of the extruded section and its response to subsequent heat treatment.

The present study has been concerned with the variation of texture with fabricating conditions and with the nature of the texture components in extruded rod which is 99.99% aluminum.

Extrusion billets were chill-cast in cast-iron molds and machined to 3-in.-dia, 5-in.-long cylinders. They were upset to 3.125 in. and extruded through a flat-face 0.890-in. die. The rods were quenched by a water spray at the die face. Extrusion conditions are listed below:

[11]C. Smith, *J. Inst. Metals* **76**, 429 (1950).

[12]H. K. Hardy, *Metallurgia* **30**, 240 (1944).

[13]D. H. Locke, *Metallurgia* **50**, 268 (1954).

Sections approximately 18 in. long were cut from the front and back of each rod, and specimens for x-ray and metallographic studies were taken from the front, middle, and back of the center section. Spherical x-ray specimens 0.200 in. in diameter were machined from the center section and electropolished to 0.190 in. Axis distribution charts were determined by the method of Jetter, McHargue, and Williams.[14]

Variation of Texture with Position

Fiber axis distributions were determined for specimens taken from the front, middle, and back of rods extruded at a slow speed at 75, 450, and 650°F and at a fast speed at 450°F. A duplex $<111> - <001>$ texture was observed in each specimen. The data, summarized in Table 47,

[14]L. K. Jetter, C. J. McHargue, and R. O. Williams, *J. Appl. Phy.* **27**, 368 (1956).

Table 47. Variation of Texture with Position

Temp (°F)	Speed (fpm)	Texture		
		Front	Middle	Back
75	0.07		76% <111>	65% <111>
			24% <001>	35% <001>
450	0.1	65% <111>	48% <111>	33% <111>
		35% <001>	52% <001>	67% <001>
450	615	88% <111>	84% <111>	49% <111>
		12% <001>	16% <001>	51% <001>
650	0.2	44% <111>	30% <111>	22% <111>
		56% <001>	70% <001>	78% <001>

showed that the amount of <001> component increased from front to back while the amount of <111> component showed a corresponding decrease. It can be seen that the relative amount of a given component may vary by a factor of two in the same rod.

The amount of recrystallized material also increased from front to back, and it has already been shown that the <001> component is associated with recrystallized grains and the <111> component is associated with deformed grains.[15]

Such changes in structure are not unexpected since both the amount of deformation and the temperature increase from front to back during extrusion. Smith[11] and Locke[13] have noted the changes in properties of an aluminum alloy extrusion as the microstructure varied from that of cast metal at the front to that of severely worked metal at the back. Mueller[16] reported that the temperature of aluminum billets may increase by 125 to 150°F during extrusion. The faster the extrusion speed the higher is the temperature rise since there is less time for the heat generated to be dissipated to the air and the container and die walls.

Variation of Texture with Extrusion Temperature

For a given position in the rod and a slow extrusion speed, the amount of recrystallization which occurred during deformation, and hence the amount of <001> texture, varied with temperature in the manner shown in Fig. 158. This is a rather surprising relationship since it implies a linear relationship between the amount of recrystallization during deformation and the temperature of deformation. The spread in Fig. 158 is probably due to relatively small deviations in temperature, speed, and relative position in the rods.

In the rods extruded at fast speeds there was no simple relationship between temperature and texture over the whole range. For extrusion temperatures up to 450°F, duplex <111> − <001> textures were produced with not much variation in the relative amount of each component. At 650°F a duplex 3% <111> − 97% <115> texture was developed and at 850°F, a single <118>

---

[15]L. K. Jetter and C. J. McHargue, *Met. Semiann. Prog. Rep. April 10, 1955,* ORNL-1911, p 7.

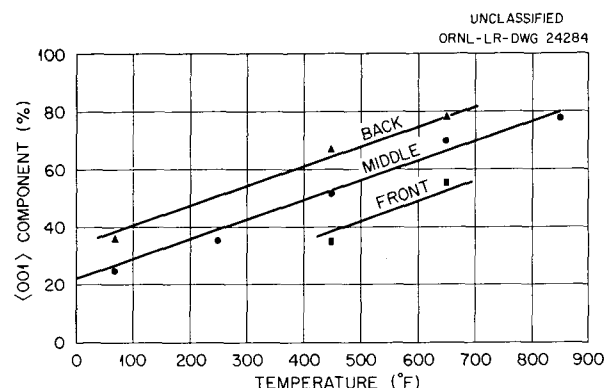[16]A. J. Mueller, *Metal Prog.* 71(2), 76 (1957).

UNCLASSIFIED
ORNL-LR-DWG 24284

Fig. 158. Amount of <001> Texture Component Developed in Aluminum as a Function of Extrusion Temperature.

texture. The position of <115> is 5 deg from <118>. Figure 159 shows the textures obtained in the middle sections of fast extrusions at 450, 650, and 850°F billet temperatures.

The <115> and <118> components are recrystallized components developed at relatively high temperatures. It has been found that an aluminum rod containing <111> − <001> texture develops a <118> component upon annealing for 5 min at 1000°F (ref 15). Because of the speed of extrusion it is not unreasonable for the rod temperature to have been 1000°F for a billet and container temperature of 850°F.

Variation of Texture with Extrusion Speed

The effect of extrusion speed on texture is in part a temperature effect since the faster the speed the greater is the temperature rise in the material being deformed. Another factor which affects texture is the time-at-temperature during and just after deformation. In the present study, extrusions were die-quenched and speeds of 0.1 to 700 fpm were used. At lower temperatures the time effect is probably unimportant, but it may become important at higher temperatures where the rates of recrystallization are much higher. Another possible cause of texture change is strain rate; however, nothing is now known regarding its influence on the development of preferred orientations.

The data of Table 48 summarize the textures found in the middle sections of rods extruded at slow and fast speed in the temperature range 75

213

to 850°F. At temperatures below 450°F, duplex < 111> − <001> textures were developed for each speed with more <001> component occurring in the slow extrusion than in the fast one. As the temperature increased, the difference between the amount of <001> in the slow extrusion and that in the fast one also increased. This appears to be the effect of time at deformation temperature, since the rate of recrystallization is slow.

At temperatures of 150°F and above, duplex < 111> − <001> textures were developed in the slow extrusions, whereas very different textures were developed in the fast ones. As discussed in the previous section, the temperatures of the fast extrusions were higher than the temperatures of the slow ones, as is to be expected. Therefore, the rate of recrystallization would be expected to be very high, and the fast extrusions underwent more recrystallization than the slow ones even though they were at temperature for a shorter length of time. In fact, these components may be due to secondary recrystallization.

LOW-TEMPERATURE SPECIFIC HEATS OF ZIRCONIUM AND A ZIRCONIUM−8% INDIUM ALLOY

G. D. Kneip, Jr.   J. O. Betterton, Jr.

A calorimeter has been constructed for the measurement of the specific heats of zirconium alloys at liquid helium temperatures. At sufficiently low temperatures the specific heat can be considered to depend upon two terms:[17] a term which arises from the lattice vibrations and is proportional to T^3, and a term associated with the conduction electrons which is proportional to the temperature. This electronic part of the specific heat is a measure of the density of states at the Fermi surface. If it is assumed that the solute contributes its valence electrons to the zirconium valence band without altering its shape, then the variation of the electronic heat capacity with solute concentration will be a measure of the density of states at the Fermi surface as a function of the electron concentration in the band.[18]
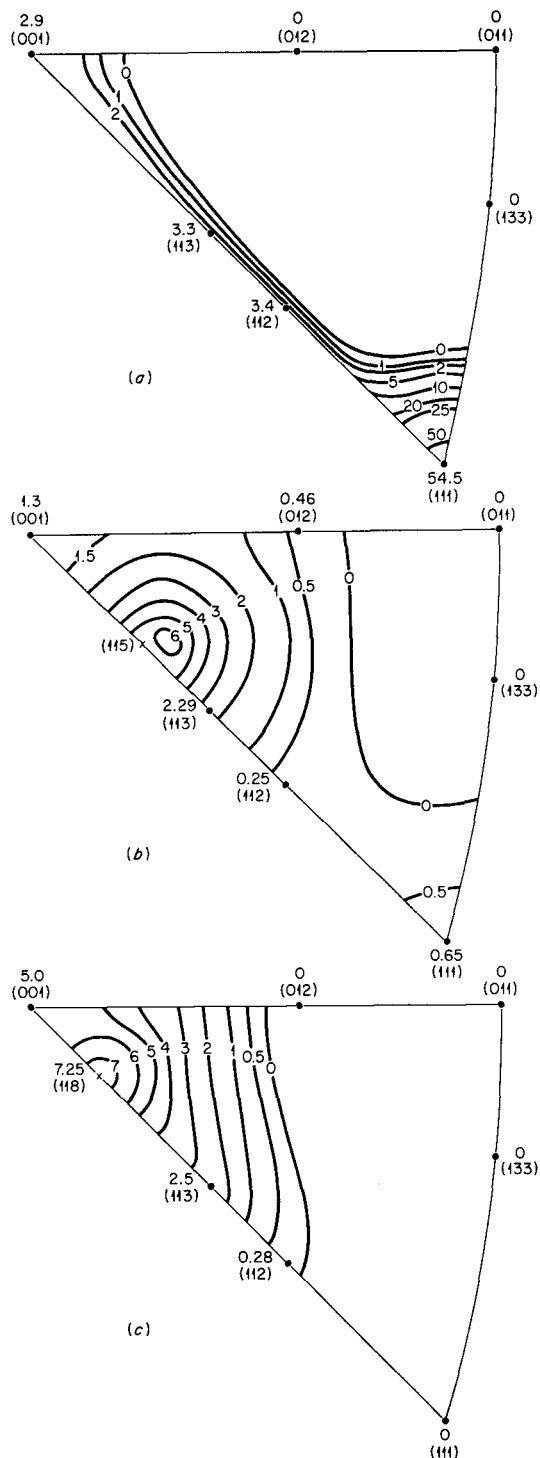
Fig. 159. Fiber Axis Distribution Charts Showing the Textures Developed in the Middle Section of Aluminum Rods Extruded at Fast Speeds at (*a*) 450°F, (*b*) 650°F, and (*c*) 850°F.

[17]F. Seitz, *The Modern Theory of Solids*, p 100, McGraw-Hill, New York, 1940.

[18]N. F. Mott and H. Jones, *The Theory of the Properties of Metals and Alloys*, Clarendon Press, Oxford, 1936.

Table 48. Variation of Texture with Extrusion Speed

Temperature (°F)	Texture	
	Slow	Fast
75	76% <111> + 24% <001>	80% <111> + 20% <001>
250	65% <111> + 35% <001>	75% <111> + 25% <001>
450	48% <111> + 52% <001>	84% <111> + 16% <001>
650	30% <111> + 70% <001>	3% <111> + 97% <115>
850	22% <111> + 78% <001>	<118>

The specific heats of zirconium and titanium alloys are of particular interest since phase diagram studies have shown that of the four outer electrons in these elements only two appear to be important with respect to the allotropic transformation temperatures of the alloys.[19] It was supposed that two of the electrons were of d type and existed only in the zirconium atomic cells of the alloy, while the other two electrons were in a normal collective electron band. Axial ratios of hexagonal zirconium and titanium vary with alloying and have been interpreted in terms of Brillouin Zone overlaps.[20,21] The specific heat measurements will provide a test of these interpretations as well as of the general alloying model involved.

The liquid helium part of the apparatus is shown schematically in Fig. 160 and is similar to others described in the literature.[22,23] In order to evaluate the contribution of the specimen thermometer and heater to the measured specific heat, the carbon thermometer and a 1500-ohm Manganin heater were cemented to a tapered zirconium plug which fits into a mating hole in the specimen. The current and potential leads for the heater

and thermometer are brought through the helium bath to the platinum-lead-to-glass seal[24] to reduce the conduction of heat to the specimen. From the seal a pair of 2-mil superconducting niobium leads are run to the thermometer and a similar

[19]J. O. Betterton, Jr., J. H. Frye, Jr., and D. S. Easton, *Phase Diagram Studies of Zirconium with Silver, Indium, and Antimony*, ORNL-2344 (Aug. 12, 1957).

[20]J. M. Denney, *A Study of Electron Effects in Solid Solution Alloys of Titanium. Sixth Technical Report to the Office of Naval Research.* California Institute of Technology (Jan. 1955).

[21]J. O. Betterton, Jr., *Met. Semiann. Prog. Rep. April 10, 1956*, ORNL-2080, p 228.

[22]W. S. Corak et al., *Phys. Rev.* 98, 1699 (1955).

[23]F. J. Webb and J. Wilks, *Proc. Roy. Soc. (London)* A230, 549—559 (1955).

[24]J. E. Kunzler, T. H. Geballe, and G. W. Hull, *Rev. Sci. Instr.* 28, 96 (1957).

UNCLASSIFIED
ORNL-LR-DWG 25289
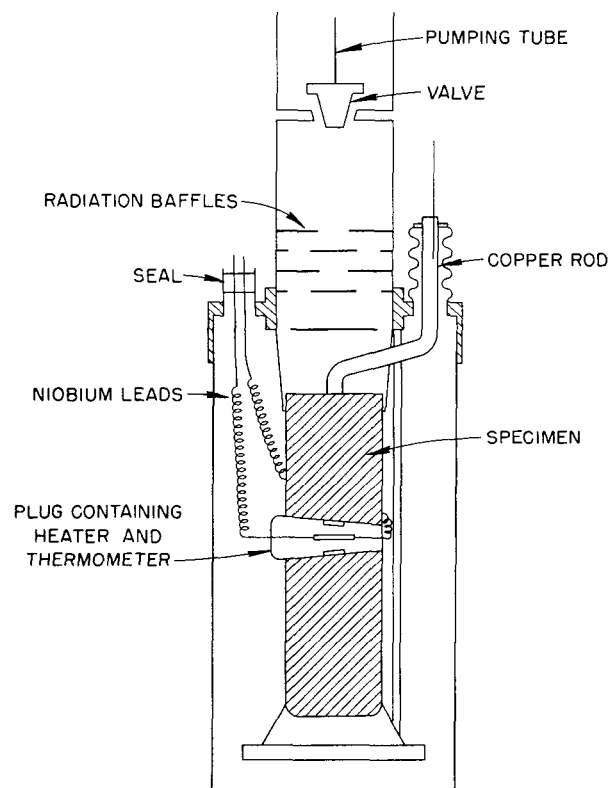
Fig. 160. Low-Temperature Portion of Calorimeter.

pair to the heater. This combination reduces the number of leads run through the high-vacuum walls of the calorimeter to a minimum and yet removes the uncertainties of lead-wire resistances from the measurements. The valve and baffles in the pumping tube were found to be necessary in order to limit the amount of energy incident on the specimen from room temperature radiation and from hot gas molecules.

Both helium exchange gas and the mechanical switch shown in the figure have been used to cool the specimen to the bath temperature. The mechanical switch has been found to be superior in that the thermal connection to the bath is immediately reduced to a very small value when the switch is opened. Stray energy inputs to the specimen (for instance, conduction through the lead wires, vibration of the specimen on the nylon thread, measuring current in the thermometer, etc.) of as little as 40 ergs/min are not unusual with a 1°C temperature differential to the bath.

A pumping system on the helium bath makes temperatures down to 1.5°K attainable.

Figure 161 is a simplified schematic diagram of the external electrical circuits for the thermometer. Although the measuring currents are from 1 to 5 μa, a 12-v source is used with sufficient resistance in the circuit to limit the current to the desired value in order to stabilize the measuring current against thermometer resistance changes. Figure 162 is the schematic diagram of the external electrical circuits for the heater. In order to avoid sudden changes in the battery current, the current is switched between a dummy

Fig. 162. Heater Circuit.

resistance and the heater by a relay. Simultaneously, another relay energizes the clutch of a Standard Electric Time Company clock which is capable of measuring the duration of the heating pulse to ± 0.005 sec.

The carbon-resistance thermometer was calibrated against the vapor pressure of the helium bath on the basis of the 1955 helium vapor pressure–temperature scale, using helium exchange gas to ensure temperature equilibrium between the bath and the specimen. The vapor pressure of the helium bath was measured with a mercury manometer above the lambda point of liquid helium and an Octoil S manometer below the lambda point. Both manometers are equipped with verniers permitting the column heights to be measured to 0.05 mm. Above the lambda point the observed vapor pressure at the surface of the bath was corrected for the difference in hydrostatic head between the specimen and the surface of the bath, and, in order to ensure liquid-vapor equilibrium throughout the bath, heat was supplied to the bottom of the bath at a rate of 40 to 60 Mw. The thermometer resistance was found to fit the Clement[25] relation

$$\frac{\log R}{T} = (a + b \log R)^2 .$$

Errors in the determination of the thermometer sensitivity result in errors in the specific heat

Fig. 161. Thermometer Circuit.

[25]J. R. Clement, J. K. Logan, and J. Gaffney, *An Examination of the 1948 Liquid Helium Vapor Pressure-Temperature Scale*, NRL-4542 (April 25, 1955).

proportional to the error in the thermometer sensitivity. Estimates of this error from the thermometer calibration curves indicate that it is less than $\frac{1}{2}\%$.

Specific heat measurements were made in the customary manner by obtaining the temperature of the specimen as a function of time before and after a heating pulse of known energy input and then extrapolating the temperature drift curves to the center of the heating pulse to obtain the difference in temperature due to the heating pulse. The average specific heat over the temperature interval ΔT is then

$$C_p = \frac{eit}{m\Delta T} - \frac{c_a}{m} ,$$

where e and i are the heater emf and current respectively, t is the time of the heating pulse, m is the specimen mass, and c_a is the heat capacity of the plug containing the thermometer and heater. The heating pulse was chosen to give ΔT's between 0.03 and 0.05°C so that the error introduced by calculating the specific heat from a finite temperature interval is less than 0.1%. Each of the quantities except c_a and ΔT in the above expression are easily measurable to an accuracy of at least 1 part in 5000, and, since the second term is much smaller than the first, the accuracy of the specific heat determination depends mainly upon the precision with which ΔT can be measured. As mentioned above, the accuracy with which ΔT may be determined depends upon the precision with which the thermometer sensitivity is known as well as the extrapolation of the temperature drift curves to the center of the heating pulse. The over-all accuracy of the measurement of the ΔT's is thought to be approximately 1%.

Figure 163 shows a typical heating curve as observed on the recorder. The ΔT can be calculated from the observed deflections extrapolated to the center of the heating period from the emf's observed across the thermometer.

The specific heats at constant pressure and constant volume are related by

$$C_p - C_v = \frac{VT\alpha^2}{X} ,$$

where V is the volume per mole, α the coefficient of thermal expansion, and X the compressibility;
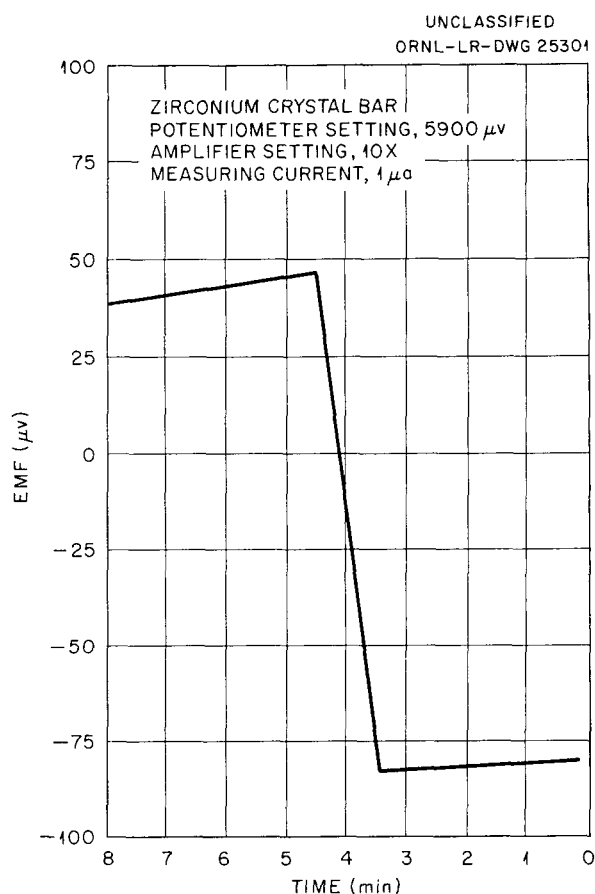
Fig. 163. Typical Heating Curve.

thus the error involved by using C_p and C_v interchangeably may be evaluated. Although the low temperature quantities are not known for zirconium, they may be estimated from the room temperature values. When this is done by assuming that the thermal expansion coefficient is proportional to the temperature, and that the compressibility and atomic volume do not change appreciably with temperature, it is found that the difference between C_p and C_v is of the order of 1 erg·mole^{-1}·(°C)$^{-1}$ at 10°K or about 1 part in 30,000 of the measured C_p. For this reason the measured values will be called the specific heat at constant volume in this discussion because of its greater theoretical interest.

Figure 164 shows the results of the measurements of C_v/T as a function of the square of the temperature for zirconium and for a zirconium–8 at. % indium alloy. The alloy was prepared

217
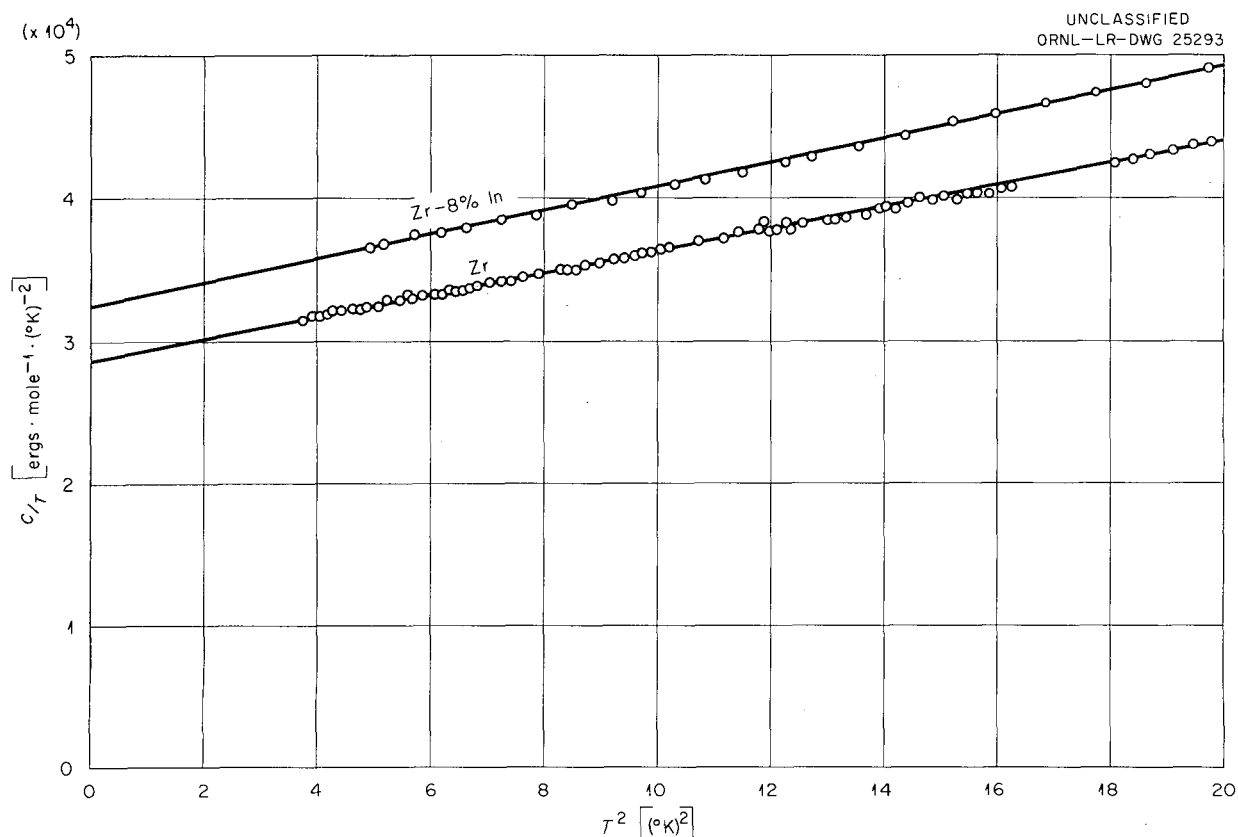
Fig. 164. Temperature Dependence of the Specific Heats of Zirconium and a Zirconium—8% Indium Alloy.

from the same iodide zirconium as was used for the pure specimen. The zirconium was of 99.95% purity. Both specimens were carefully outgassed and annealed in the alpha-phase region. As the heat capacity of the plug has not yet been measured, its value was estimated and subtracted from the observed specific heat. The data plotted in this manner show that the specific heats can be separated into linear and third power temperature terms. The intercepts in this case are the coefficients of the specific heat terms which are linear with temperature and hence are related to the density of states of the valence electrons. As can be seen from the figure, the addition of indium to zirconium increases the coefficient of the linear term, and hence the density of states at the Fermi surface is higher for the alloy than for the pure metal. The alloying addition can be seen to produce little change in the slope of the C_v/T vs T^2 plot and hence little change in the Debye temperature. Since the heat capacity of the plug has not yet been measured, no great

significance should be placed on the numerical values of the electronic contribution coefficient and the Debye temperatures, but it may be observed that the increase in the electronic term, corresponding to an increase in the density of states, agrees with the observed expansion of c/a with electron additions and with increasing temperature. The change in the Debye temperature is considerably smaller than that predicted by the Kopp rule.

THE CADMIUM-ZIRCONIUM SYSTEM

D. S. Easton   J. O. Betterton, Jr.

For full consistency in the valency relations observed in the α/β boundaries of Zr-Ag, Zr-In, and Zr-Sn systems, the effect of cadmium on the transition temperature of zirconium should be essentially negligible. Earlier work[26] on this system had shown that at least two intermediates with

---

[26] D. S. Easton and J. O. Betterton, Jr., *Met. Semiann. Prog. Rep. April 10, 1956*, ORNL-2217, p 216.

the approximate compositions Zr_2Cd and $ZrCd_2$ exist in this system, both with simple face-centered cubic structures. It was not possible to prepare alloys by arc-casting, but specimens were made by diffusion inside a closed zirconium container. Little indication was found of appreciable solid solubility of cadmium in zirconium at that time, but upon increase of the diffusion time and temperature up to 25 to 30 days at 1050 to 1100°C, homogeneous beta-phase alloys have now been prepared up to 15 at. % Cd. Several of the zirconium containers leaked cadmium vapor into the silica capsule, and as no indication could be found of silica contamination of the alloys or of reaction of the cadmium with the silica, recent alloys have been prepared simply by wrapping iodide zirconium with tantalum foil and inserting the cadmium in the bottom of the capsule. (Three analyses of Zr-Cd alloys showed 5 ppm, 5.4 ppm, and 10 ppm silicon. The first two results were obtained by the neutron activation method and and the last value by optical spectroscopy.)

After the higher temperature anneal the alloys were re-annealed at lower temperatures in the vicinity of the α/β transition in zirconium. The partial phase diagram, determined in this way, is shown in Fig. 165. This diagram is as yet incomplete, but the gradual rise of the $(\alpha + \beta)$ region with increased cadmium and the existence of solid solution in both phases is clearly indicated. The effect of cadmium on the α/β boundaries is compared to that of indium and

silver in Fig. 166, where it may be seen that a reasonable agreement with the position predicted by the valency rule was obtained.

An unusual partitioning of the alloy compositions occurred upon annealing with the $(\alpha + \beta)$ region. For example, an alloy with an average composition of 3.8 at. % Cd separated into a central layer of alpha phase (5.82 at. % Cd) and two outer layers of beta phase (2.42 at. % Cd) at 879.3°C. The reason for this behavior is not understood although it could be related to an unfavorable beta grain-nucleation rate in this system. With respect to the phase boundary determination, this phenomenon had the effect of restricting the bracketing data to homogeneous alloys on either side of the $(\alpha + \beta)$ region.

Another feature of the Cd-Zr investigation was that the increase in diffusion temperatures had raised pressures inside the quartz capsules close to the rupture strength of the capsules. It was desirable to obtain information about the pressure-composition-temperature relationships in order to choose safe annealing temperatures.

A program of measuring the cadmium pressure over the zirconium-rich alloys was therefore started using the Hargreaves method.[27] If sufficiently

[27]R. Hargreaves, *J. Inst. Metals*, **64**, 115 (1939).
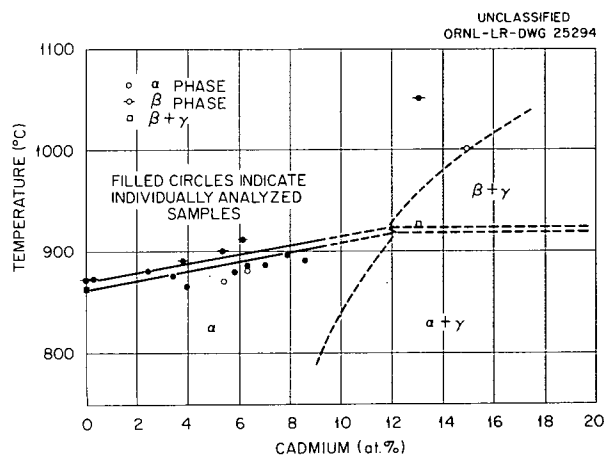

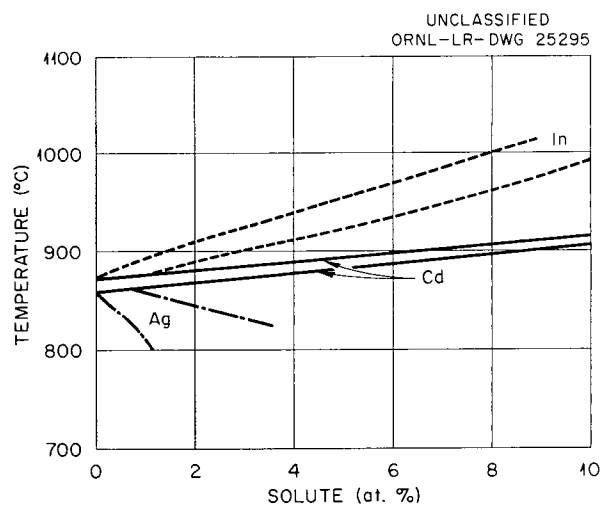Fig. 165. Zirconium-Rich Portion of the Cd-Zr System in the Region 850 to 1100°C.

Fig. 166. The $\alpha/(\alpha + \beta)$ and $\beta/(\alpha + \beta)$ Phase Boundaries of Zr-Cd (Solid Lines) Compared with the Same Boundaries of Zr-In (Dotted Lines) and Zr-Ag (Dashed Lines).

accurate, this investigation would also provide information about the nature of the thermodynamic properties of the α and β phases of Zr-Cd which could then be compared with the thermodynamic approximations which were used for calculation of the α/β-phase boundaries. In the present experiment, a zirconium-cadmium alloy is held isothermally at the hotter end of a temperature gradient while the temperature of condensation of the cadmium vapor is observed at the cooler end of the same gradient.

The vapor pressure of pure zirconium is less than 10^{-8} atm at 1700 to 1800°C so that it is reasonable to neglect the partial pressure of zirconium in the gaseous phase over the alloy. There was no evidence, such as a systematic drift of the results with time at the highest temperatures, of a reaction of the cadmium vapor with the silica tube or of the specimen with the protective tantalum foil. (A slight amount of tantalum would normally be expected to diffuse into the specimen surface at the points of contact, but after sufficient time for cadmium equilibrium these localized spots on the surface should have the same cadmium pressure as the unaffected part of the alloy.) Droplets of the condensate were examined by x-ray diffraction and the spacings corresponded to within 1 part in 8,000 with those measured for high-purity cadmium.

The cadmium pressure of an alloy containing approximately 7.5 at. % Cd in the beta-phase region is shown in the upper part of Fig. 167 for the temperature range 950 to 1050°C. A graph of the activity of the cadmium constituent in this alloy relative to pure liquid cadmium is given in the lower part of this figure. At temperatures lower than 925°C and at times up to 20 days, equilibrium was not obtained with the lump-type specimen which was used in the present work. However, it is hoped that the temperature range can be extended into the alpha-phase region by use of foil or thin-sheet type specimens.

From pressure measurements on this alloy it is apparent that temperatures above 1150°C would be impractical in silica capsules. The partial molar free energy, heat, and entropy of formation, relative to pure liquid cadmium, of this alloy are given below.

Partial Molal Properties of Zr + 7.5% Cd

ΔF	-5600 ± 100 calories/mole
ΔH	-4200 ± 1000 calories/mole
ΔS	$+1.1 \pm 0.5$ calories mole^{-1}·(°C)$^{-1}$

The significance of these numbers will be more obvious when sufficient alloys have been measured to permit integration of the data, and the plotting of the integral properties of these alloys.
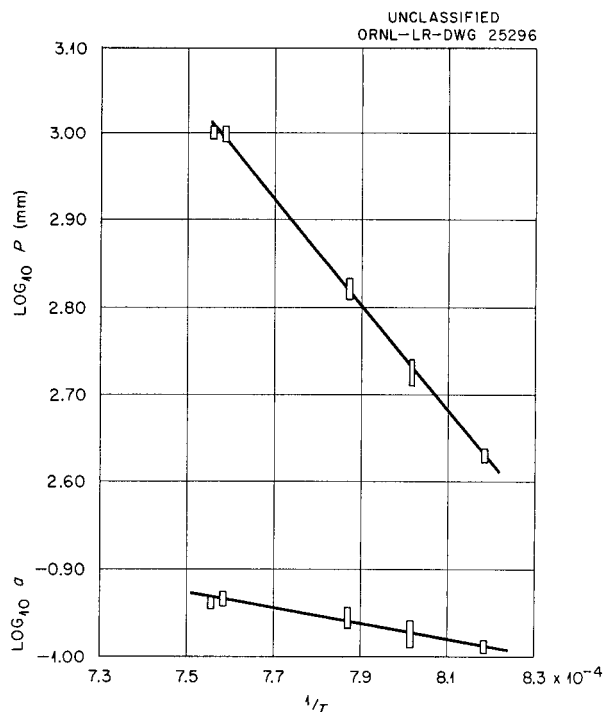

Fig. 167. Cadmium Vapor Pressure and Activity of a Zr–7.5 at. % Cd Alloy in the Beta-Phase Region.

X-RAY DIFFRACTION

H. L. Yakel, Jr.

R. M. Steele   J. C. Richter

X-RAY DIFFRACTION SERVICE PROBLEMS

H. L. Yakel, Jr.

R. M. Steele   J. C. Richter

During the past year, over 1200 x-ray diffraction patterns of nearly as many samples have been recorded by the X-Ray Laboratory in the course of its routine service operations. Such samples have been submitted by members of the Metallurgy, Physics, and Chemical Technology Divisions. A summary of the types of problems encountered, together with some of the more interesting results, follows. More extensive discussions of several problems, whose nature raised them above the routine classification, will be given elsewhere in this report.

The majority of service problems handled by this laboratory may be roughly classified as one of the following: (1) phase identification (alloys, corrosion products, etc.), (2) verification of purity and structure, (3) lattice parameter measurements, (4) semiquantitative analysis of mixtures, (5) crystallite size determinations (primarily ThO_2), and (6) crystal orientation measurements.

Typical phase identification problems submitted during this year included the study of reaction products of various metal inserts in contact with liquid metals and fused salts at high temperatures, the study of the corrosion of an HRT bellows, and an examination of the reaction products of Eu_2O_3 and type 347 stainless steel proposed for use in control rods. Problems involving phase identification in alloy systems included Zr-Cd, Zr-Nb, and Ni-Mo binary mixtures.

The Physics Division submitted a large number of samples for purity checks and parameter measurement. These compounds included trifluorides of Cr, Mn, Fe, Co, and Mo; dibromides of Mn and Co; $Cr(Se_xTe_{1-x})$; $(Fe_xCo_{1-x})Cl_2$; NdI_3. In the case of NdI_3, a new orthorhombic phase with parameters $a_0 = 13.96$ Å, $b_0 = 4.30$ Å, and $c_0 = 9.97$ Å has been tentatively identified.

Samples of rare-earth oxides subjected to various heat treatments were submitted for examination by the Fuel Element Development Section. The "B

forms" (monoclinic) of Sm_2O_3 (ref 1) and Eu_2O_3 were identified in samples heated at 1400 to 1800°C and at 1800°C, respectively. The lattice parameters are as follows:

$$Sm_2O_3: \quad a_0 = 14.18 \text{ Å} ,$$
$$b_0 = 3.633 \text{ Å} ,$$
$$c_0 = 8.85 \text{ Å} ,$$
$$\beta = 100.0 \text{ deg} ,$$
$$Eu_2O_3: \quad a_0 = 13.94 \text{ Å} ,$$
$$b_0 = 3.58 \text{ Å} ,$$
$$c_0 = 8.68 \text{ Å} ,$$
$$\beta = 98.5 \text{ deg} .$$

A new hydrated oxide of Eu_2O_3 was also found during this investigation and was tentatively indexed on the basis of a rhombohedral unit cell with $a_0 = 7.024$ Å, $\alpha = 102.6$ deg. The degree of hydration is uncertain.

In the development of new reactor fuel plates the problem of the reaction of components of the plates during rolling or heat treating is often serious. In particular, the partial reduction of U_3O_8 to UO_2 in U_3O_8-Al fuel plates and the reactions of elementary uranium with aluminum, silicon, and carbon in others have been observed. Semiquantitative measurements of relative amounts of various uranium compounds in such systems were made from accurate counts of areas under selected diffraction maxima. The results of these measurements are given in "Compatibility of Uranium Oxides in the Manufacture of Plate-Type Aluminum Fuel Elements," this report.

THE CRYSTAL STRUCTURE OF GROUP IVA HYDRIDES

H. L. Yakel, Jr.

Structure of hydrides of the Group IVA elements may be related to normal close-packed or body-centered cubic lattices characteristic of metals,

---

[1] R. M. Douglass and E. Staritzky, *Anal. Chem.* **28**, 552 (1956).

in which hydrogen atoms are located interstitially. This is true not only at low hydrogen concentrations, where the interstitial hydrogen merely expands the lattices of the pure elements, but also at high hydrogen concentrations where so-called hydride "compounds" may be formed. These "compounds" are unique in that, for a given Group IV metal–hydrogen system, wide departures from stoichiometry are observed, while compositional and allotropic transformations between phases may be of a high thermodynamic order.[2-4]

In order to further elaborate the structures and transformations of the hydride "compounds," a series of high- and low-temperature x-ray crystallographic experiments on the higher hydrides of the Group IVA metals has been initiated. To date, single-phase hydrides of analyzed compositions $TiH_{1.98}$, $TiD_{1.98}$, $TiH_{1.87}$, $TiH_{1.79}$, and $ZrH_{1.92}$ have been studied. The alloys were prepared by controlled additions of purified hydrogen to cold-rolled crystal-bar titanium or zirconium foil at temperatures from 300 to 500°C. The hydrided foils generally retained their original form and luster, but were easily crushed to black powders. Metallographic examination of the larger crushed particles showed, in the case of $TiH_{1.87}$, an even surface structure except for many small pits scattered in an indefinite pattern. No optical birefringence was noted. A similar surface pattern was noted for $ZrH_{1.92}$, but here a slight birefringence was observed. Chemical analysis for hydrogen was carried out by complete oxidation followed by gravimetric determination of the water evolved. Uncertainties in the analyses are reflected in uncertainties of ±0.02 in the hydrogen subscripts of the formulas.

The x-ray diffraction apparatus[5] used in the low-temperature investigations is a simple cryostat adapted to a standard Norelco high-angle goniometer

(Fig. 168). Copper filings were mixed with the hydride samples for the purpose of angle calibration. High-temperature x-ray diffraction experiments were performed with a 19-cm Unicam S.150 camera. Copper filings were again mixed with the samples, but for the purpose of temperature calibration. In no instance was a high-temperature experiment carried beyond a temperature at which dissociation would affect hydride composition, although in the case of $ZrH_{1.92}$ this normal range was extended by the use of an artificial hydrogen overpressure. Copper K radiation ($\lambda_{K\alpha} = 1.5418$ Å) was used throughout.

Experimental results have confirmed that the crystal structures of the higher hydrides of titanium and zirconium are based on a cubic close packing of metal atoms with hydrogen atoms in tetrahedral interstices. The ideal lattice is isotypic with the cubic fluorite structure. (X-ray diffraction methods are not sufficiently sensitive to determine hydrogen atom positions in the presence of relatively heavy metal atoms; the symmetrical location of hydrogen atoms in the tetrahedral holes at all temperatures was demonstrated by neutron diffraction.) The reported tetragonal distortion of this ideal lattice in higher zirconium hydrides at room temperature has also been observed.[6]

A previously unreported tetragonal distortion of the ideal lattice in the titanium-hydrogen system was found in $TiH_{1.98}$, $TiD_{1.98}$, and $TiH_{1.87}$. The degree of distortion is temperature-dependent below critical temperatures (T_c) near 315°K. Comparisons of the thermal variations of the lattice parameters and axial ratios of $TiH_{1.98}$, $TiH_{1.87}$, and $TiH_{1.79}$ are shown in Figs. 169 and 170. It may be seen that while the lattice distortion, as measured by the axial ratio, is greater for $TiH_{1.98}$ at low temperatures, there is a cross-over at about 265°K above which the distortion for $TiH_{1.87}$ is greater. The increase of T_c from 308°K in $TiH_{1.98}$ to 317°K in $TiH_{1.87}$ should also be noted.

The variation of structure with composition at low temperatures observed in the higher titanium hydrides is similar to that reported by Vaughan and Bridge[7] in the higher zirconium hydrides at room temperature. The assumption that the thermal

[2] S. S. Sidhu and J. C. McGuire, *J. Appl. Phy.* **23**, 1257 (1952).

[3] D. A. Vaughan and J. R. Bridge, *Trans. Am. Inst. Mining Met. Petrol. Engrs.* **206**, 528 (1956).

[4] H. L. Yakel, Jr., *Apparent Second-Order Phase Transformations in TiH_2 and TiD_2*, paper presented at the Thirteenth Annual Pittsburgh Diffraction Conference, Pittsburgh, Pa., November 1955.

[5] L. K. Jetter, C. J. McHargue, R. O. Williams, and H. L. Yakel, Jr., paper submitted to *Rev. Sci. Instr.*

[6] R. E. Rundle, C. G. Shull, and E. O. Wollan, *Acta Cryst.* **5**, 22 (1952).

[7] D. A. Vaughan and J. R. Bridge, *Trans. Am. Inst. Mining Met. Petrol. Engrs.* **206**, 528 (1956).

ASSEMBLY

STAINLESS STEEL CHAMBER

VACUUM SEAL

COPPER SAMPLE HOLDER

BERYLLIUM WINDOW
0.020- TO 0.035-in. THICK

ELECTRICAL LEADS

RADIATION BAFFLE
0.003- TO 0.005-in. NICKEL

STAINLESS STEEL FLASK

COPPER INSERT

RADIATION BAFFLE, 0.003- TO 0.005-in. NICKEL SHEET

"O"-RING SEAL

STAINLESS STEEL COVER

SCALE IN INCHES
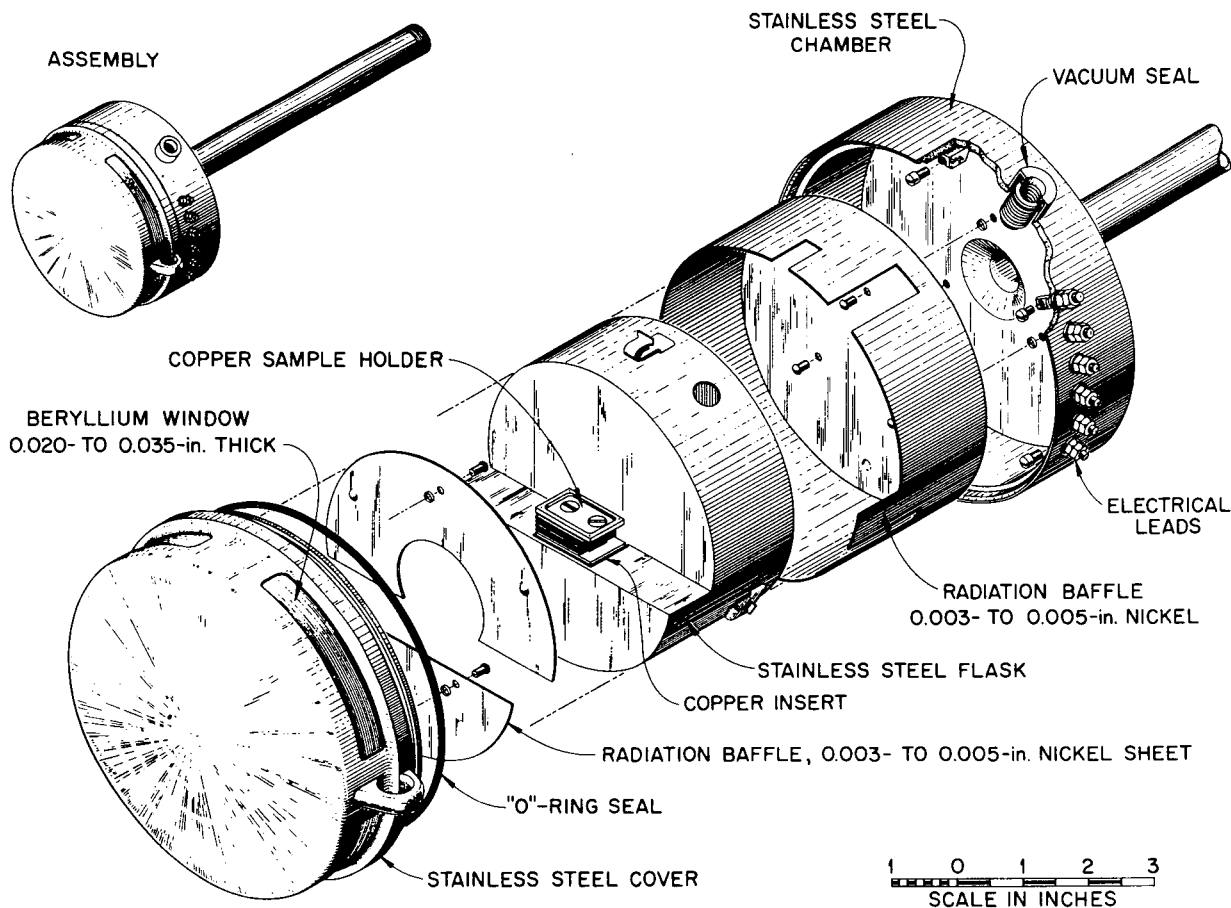
Fig. 168. Exploded View of the Low-Temperature Cryostat Designed for Use with a Norelco Diffractometer.

variations in structure at constant composition observed in titanium hydrides would be observed in zirconium hydrides at high temperatures is therefore reasonable. The results of the high-temperature study of $ZrH_{1.92}$ shown in Fig. 171 verify this assumption, although the critical temperature of the distortion could not be attained iso-compositionally.

The causes of the distortional transformations achieved in $TiH_{1.98}$ and $TiH_{1.87}$ and approached in $ZrH_{1.92}$ are not clear. Their net result is to shorten, in the low-temperature form, 8 of the 12 nearest metal-metal contacts, and Rundle, Shull, and Wollan[6] have attributed the stability of the tetragonal phase to the increased metallic bonding thus produced. Neutron-diffraction experiments have failed to reveal magnetic ordering in these hydrides and, as noted above, show no asymmetrical
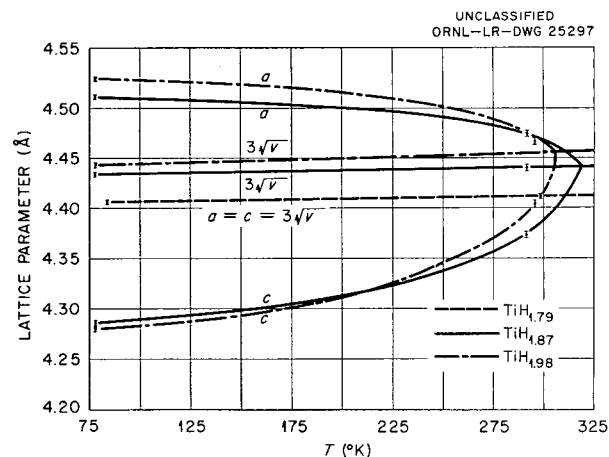
Fig. 169. Variation of Lattice Parameters and Unit Cell Volumes of $TiH_{1.98}$, $TiH_{1.87}$, and $TiH_{1.79}$ Between 78 and 325°K.

223

Fig. 170. Variation of Axial Ratios of $TiH_{1.98}$, $TiH_{1.87}$, and $TiH_{1.79}$ Between 78 and 325°K.

Fig. 171. Variations of Lattice Parameters, Axial Ratio, and Unit Cell Volume of $ZrH_{1.92}$ as a Function of Temperature. Open circles represent low-temperature data; closed circles represent high-temperature data.

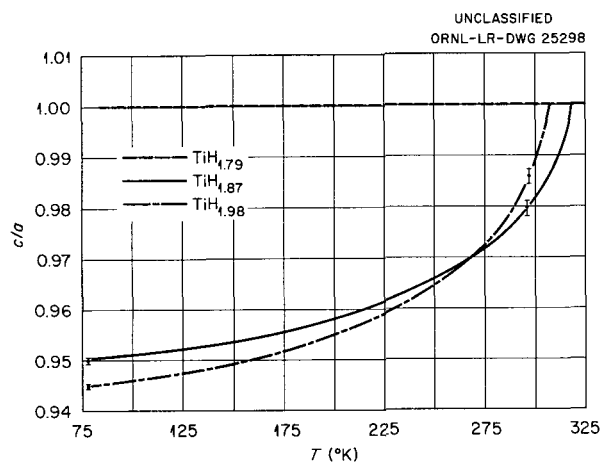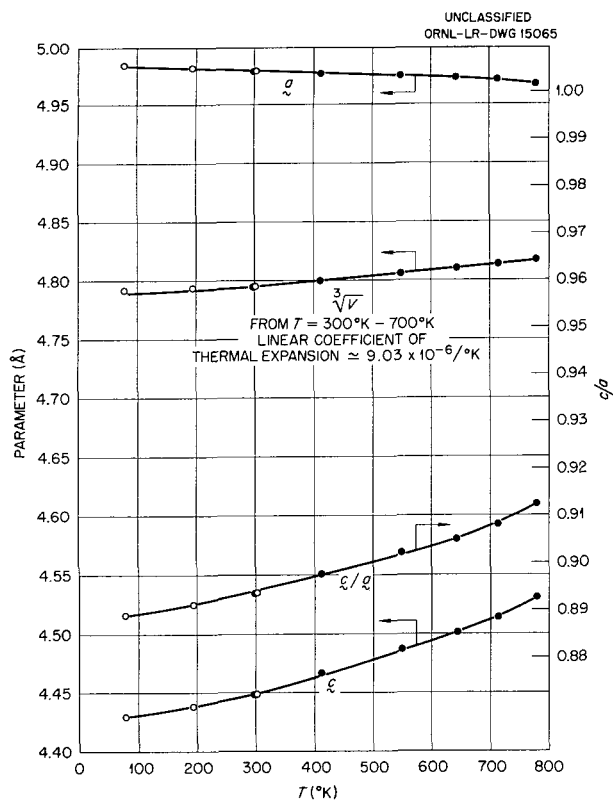displacement of the hydrogen atoms above or below the critical temperatures. The absence of any observable discontinuity in volume or the temperature derivative of volume at T_c is suggestive of a higher-order transformation.[8] The cooperative phenomena, such as magnetic, electric, and atomic ordering, usually associated with such transitions do not appear applicable to the hydride systems, however.

A possible clue to the mechanism of hydride formation in titanium and zirconium was found during examination of the uncrushed $TiH_{1.79}$ foil. Diffractometer scans of this foil showed a marked orientation of normal directions perpendicular to {110} and {311} planes of the face-centered cubic hydride. Similar study of the unhydrided beta-treated titanium foil showed a concentration of normal directions perpendicular to {10.3} and {11.4} planes of the hexagonal cell [the usual rolling texture of hexagonal close-packed (hcp) metals]. From the proposed mechanism for the hcp → bcc (body-centered cubic) transition in zirconium,[9] the normal direction texture of a body-centered cubic phase resulting from a transformation from a hexagonal phase with a [10.3] [11.4] normal direction texture would be predicted as near [111] or [211]. However, these directions become [110] and [311] directions in the face-centered cubic (fcc) hydride if the bcc (solid solution of H) → fcc (hydride) transformation produces small rotations about [110] directions in the body-centered cubic phase. The hypotheses on which the analysis explaining the observed hydride texture is based are as follows:

1. The transformation α (hcp solid solution of H) → β (bcc solid solution of H) involves a diffusionless mechanism analogous to that in the pure metal. From the phase diagrams of the Ti-H and Zr-H systems, a diffusion-controlled clustering of hydrogen in regions which later transform must also occur.

2. The transformation β (bcc solid solution of H) → γ (fcc hydride) involves a diffusionless mechanism. A clustering of hydrogen must again be proposed as a preliminary step.

[8] P. S. Epstein, *Textbook of Thermodynamics*, p 128ff, Wiley, New York, 1937.

[9] W. G. Burgers, *Physica* 1, 561 (1934).

The hydride samples used in these experiments were prepared by M. L. Picklesimer, P. J. Jones, and D. E. LaValle. Analyses were performed by J. H. Edgerton, W. R. Laing, and D. E. LaValle. Neutron-diffraction data were made available by M. K. Wilkinson and C. G. Shull.

THE SODIUM NICKELATE(III) TRANSFORMATION

H. L. Yakel, Jr.

Recent high-temperature diffraction experiments on the monoclinic rhombohedral transition in $NaNiO_2$ have been reported.[10]

This work has confirmed the martensitic character of the transition first suggested by microscopic studies.[11,12] In addition to a well-defined hysteresis, a memory effect involving heating and/or cooling rates was also noted. These transitions are now one of the more clearcut examples of martensitic phase transitions in inorganic materials.

STRUCTURES AND PHASE TRANSITIONS IN PEROVSKITE-TYPE COMPOUNDS

H. L. Yakel, Jr.

Mixed oxides having the general formula ABO_3, where A is a rare-earth element and B a transition metal, frequently crystallize in perovskite-like lattices which may be distorted from cubic symmetry depending on the ionic radii of the elements involved. Investigations of these compounds have been directed toward a detailed description of the atomic coordinates in the distorted structures,[13,14] a description of the ferromagnetic and antiferromagnetic ordering frequently observed at low temperatures,[15,16] and the relation of the lattice distortions and the magnetic behavior.[17,18]

It has been found that the lattice distortions in several compounds which show magnetic ordering are temperature-dependent and that the transition temperatures which mark changes in lattice distortion are usually many degrees above the Néel temperatures of the magnetic transitions.[15] The gradual nature of the crystallographic transformations, suggestive of a cooperative mechanism, has led to the hypothesis that these transformations are due to an ordering of covalent bonds involving transition metal ions. This hypothesis also leads to a logical interpretation of the magnetic properties found on further cooling below the Néel point.[15,18]

During the past year, room-temperature x-ray diffraction studies in these systems have been extended to the orthoferrites of neodymium, holmium, and erbium and to the orthomanganites of neodymium and erbium. High-temperature x-ray diffraction studies of lanthanum orthomanganite and orthocobaltate and of holmium orthoferrite have also been completed.

Room-temperature powder photographs were prepared with conventional techniques using chromium $K\alpha$ radiation ($\lambda = 2.2909$ Å). High-temperature experiments were made with the aid of a Unicam S.150 camera described in another section of this report. Chromium $K\alpha$ radiation was used here also.

A summary of the room-temperature results is given in Table 50. Within the uncertainties inherent in the powder method, the structures of neodymium, holmium, and erbium orthoferrite and neodymium orthomanganite are isomorphous with the orthorhombic gadolinium orthoferrite structure (a distorted perovskite) derived by Geller.[13] In the case of neodymium orthoferrite an attempt has been made to fix the neodymium ion parameters from the observed powder-diffraction intensities. This analysis is not complete, but it is clear that the neodymium ion displacement from the ideal perovskite position is not given by a simple atomic number interpolation between the analogous displacements in $GdFeO_3$ and $LaFeO_3$.

The measured parameters of $NdFeO_3$, $HoFeO_3$, and $ErFeO_3$ are combined with the data for other rare-earth orthoferrites[19,20] and plotted as a

[10]H. L. Yakel, Jr., J. J. McBride, and G. P. Smith, Jr., "A Martensitic Phase Transformation in Sodium Nickelate (III)," p 106, *Fourth International Congress of the International Union of Crystallography, Montreal, Canada, July 10–19, 1957.*

[11]J. J. McBride, *Met. Semiann. Prog. Rep. April 10, 1956,* ORNL-2080, p 135.

[12]C. R. Boston et al., *Met. Semiann. Prog. Rep. Oct. 10, 1954,* ORNL-1875, p 143, esp 156.

[13]S. Geller, *J. Chem. Phys.* 24, 1236 (1956).

[14]M. A. Gilleo, *Acta Cryst.* 10, 161 (1957).

[15]E. O. Wollan and W. C. Koehler, *Phys. Rev.* 100, 545 (1955).

[16]W. C. Koehler and E. O. Wollan, *Phys. and Chem. Solids* 2, 100 (1957).

[17]H. L. Yakel, Jr., *Acta Cryst.* 8, 394 (1955).

[18]J. B. Goodenough, *Phys. Rev.* 100, 564 (1955).

[19]S. Geller and E. A. Wood, *Acta Cryst.* 9, 563 (1956).

[20]F. Bertaut and F. Forrat, *J. phys. radium* 17, 129 (1956).

Table 50. Crystallographic Data on New ABO_3 Compounds

Compound	Lattice Symmetry	Lattice Parameters (Å)*	Probable Space Group	Remarks
$NdFeO_3$	Orthorhombic	$a_0 = 5.450$ $b_0 = 5.587$ $c_0 = 7.761$	*Pbnm*	Structure probably isomorphous with $GdFeO_3$**
$HoFeO_3$	Orthorhombic	$a_0 = 5.282$ $b_0 = 5.592$ $c_0 = 7.606$	*Pbnm*	Structure probably isomorphous with $GdFeO_3$
$ErFeO_3$	Orthorhombic	$a_0 = 5.252$ $b_0 = 5.576$ $c_0 = 7.579$	*Pbnm*	Structure probably isomorphous with $GdFeO_3$
$NdMnO_3$	Orthorhombic	$a_0 = 5.414$ $b_0 = 5.836$ $c_0 = 7.552$	*Pbnm*	Structure probably isomorphous with $GdFeO_3$
$ErMnO_3$	Hexagonal	$a_0 = 6.115$ $c_0 = 11.411$	$P6_3cm$	$Z = 6$; new ABO_3 structure (see Table 51)

*Probable errors in all lattice parameters are ± 0.001 Å.

**S. Geller, *J. Chem. Phys.* 24, 1236 (1956).

function of atomic number in Fig. 172 (monoclinic pseudocell parameters as well as true orthorhombic parameters are shown). The behavior of the orthorhombic b axis is unique in that it shows an inversion at gadolinium. The significance of this inversion is not apparent but should be related to changes in atomic displacements.

The diffraction pattern of $ErMnO_3$ does not correspond to any known ABO_3 structure even though the tolerance factor[21] is 0.85. The powder pattern was indexed by the method of successive differences of $\sin^2\theta$ and is presented in Table 51. The observed extinctions are $hh0l$ when l is odd, $hki0$ when $h - k \neq 3 n$, and $hkil$ when l is odd and $h - k \neq 3 n$. The pycnometrically determined density, with the measured cell parameters, indicates a value of 5.94 formula weights of $ErMnO_3$ per cell. Chemical analysis gives 21.2% total manganese, with less than 0.5% Mn^{4+}, which may be compared with 20.3% Mn^{3+} expected from $ErMnO_3$. The space group cannot be determined unambiguously from powder data. The most likely

group at this time is $P6_3cm$. The number of systematic non-space-group absences in the pattern is remarkable and provides important assistance in the structure determination which is now in progress.

The results of the high-temperature studies of $LaMnO_3$ and $LaCoO_3$ are shown in Figs. 173 and 174. In the case of lanthanum orthomanganite the monoclinic pseudocell parameters are shown. On being heated to successively higher temperatures, $LaMnO_3$ shows a slow decrease in lattice distortion until, at 750°K, a transition to an apparently undistorted lattice is made. Superlattice lines are also vanishingly weak on photographs made above 750°K so that an ideal perovskite structure seems to have been achieved. The transition is completely reversible. This crystallographic transition is about 650°K above the Neél point.

Geller[22] has recently argued that such an orthorhombic $\longrightarrow$ cubic transition is not possible, but that the high-temperature phase must be rhombohedral. Again the ambiguities of the powder method

[21]V. M. Goldschmidt *et al.*, *Skrifter Norske Videnskaps-Akad. Oslo. I. Mat. Naturv. Kl.* No. 8, 7–156 (1926).

[22]S. Geller, *Acta Cryst.* 10, 243 (1957).
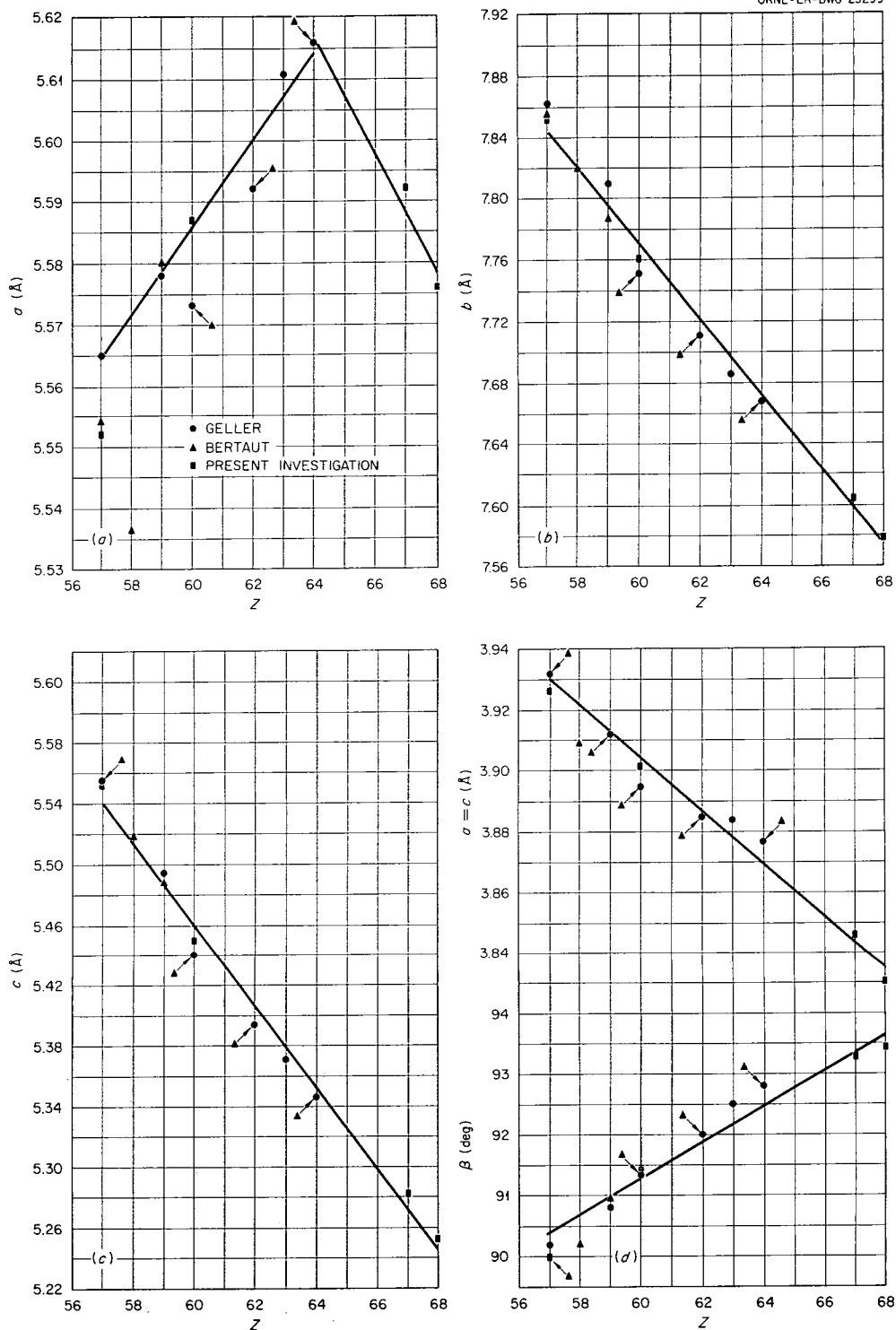
Fig. 172. Variation of Orthorhombic (a-c) and Monoclinic (d) (Pseudo Cell) Parameters of Rare-Earth Ortho-ferrites as a Function of Atomic Number. Least-square straight lines have been drawn through the data points. In (a), Bertaut's and Yakel's points for La, Bertaut's point for Ce, and Geller and Bertaut's points for Nd have been neglected in the least-squares fit.

Table 51. Bragg Spacings and Observed and
Calculated $\sin^2\theta$ Values for $ErMnO_3$
(Cr $K\alpha$, $\lambda = 2.2909$ Å Radiation)

$hk\cdot l$	d_{obs} (Å)	$\sin^2\theta$		I_{obs} *
		Observed	Calculated	
00.2	5.695	0.04045	0.04031	S
10.2	3.876	0.08731	0.08709	M
11.0	3.052	0.14088	0.14035	S
11.1	2.952	0.15061	0.15043	MS
00.4	2.850	0.16154	0.16124	MS
11.2	2.690	0.18129	0.18066	VS
10.4	2.509	0.20848	0.20802	M
20.2	2.399	0.22797	0.22745	MW
11.3	2.378	0.23203	0.23105	M—
11.4	2.083	0.30243	0.30159	S
20.4	1.938	0.34919	0.34837	M
21.2	1.886	0.36880	0.36780	MW
11.5	1.827	0.39299	0.39229	M
10.6	1.787	0.41091	0.40957	M+
30.0	1.764	0.42159	0.42106	S
30.2	1.685	0.46222	0.46137	MS—
21.4	1.637	0.48944	0.48873	M
11.6	1.613	0.50414	0.50314	MS
20.6	1.544	0.55073	0.54992	M
22.0	1.528	0.56192	0.56141	M+
22.1	1.514	0.57205	0.57149	W
30.4	1.500	0.58328	0.58229	S
22.2	1.476	0.60252	0.60172	MS+
11.7	1.438	0.63486	0.63414	W
00.8	1.425	0.64601	0.64495	W
31.2	1.421	0.64985	0.64850	W—
21.6 / 10.8	1.378	0.69133	0.69100	MS
22.4	1.347	0.72304	0.72265	MS
31.4	1.3052	0.77018	0.76943	MW
30.6 / 11.8	1.2923	0.78564	0.78457	M
22.5	1.2698	0.81373	0.81334	W
20.8	1.2556	0.83224	0.83208	M+
40.4	1.2009	0.90978	0.90978	W
22.6	1.1914	0.92435	0.92419	S
32.2	1.1880	0.92965	0.92921	W—
31.6	1.1624	0.97105	0.97098	S
21.8	1.1619	0.97188	0.97244	S
41.0	1.1556	0.98246	0.98247	S
41.1	1.1497	0.99262	0.99254	M

*Intensities estimated visually.
VS, very strong; S, strong; MS, medium strong; M,
medium; MW, medium weak; W, weak.
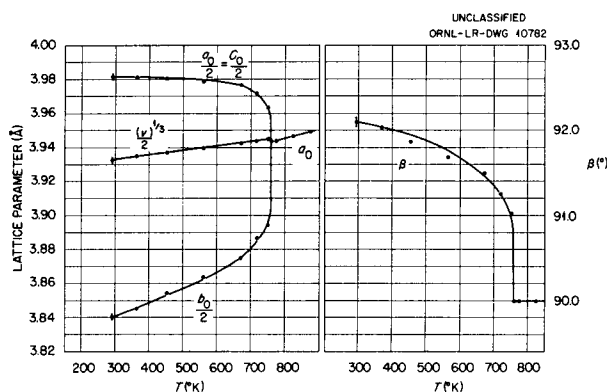VS > S > MS+ > MS > MS— > M+ > M > MW > W > W—.

Fig. 173. Thermal Variation of the Monoclinic
(Pseudo Cell) Lattice Parameters of $LaMnO_3$ from 292
to 875°K. The structure above 750°K is apparently a
simple cubic perovskite.
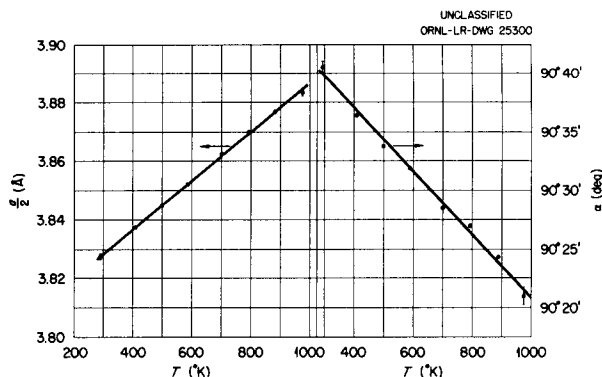
Fig. 174. Thermal Variations of the Rhombohedral
Lattice Parameters of $LaCoO_3$ from 292 to 875°K.
Closure of the rhombohedral distortion would be pre-
dicted at ∼ 1800°C by extrapolation of the α vs T line.

make an accurate determination of lattice symmetry
impossible, but it is certain that if the high-
temperature form of $LaMnO_3$ is rhombohedral, the
lattice distortion is less than 5 min of angle.

The thermal behavior of rhombohedral $LaCoO_3$,
which does not exhibit magnetic ordering at any
temperature,[23] is similar to that observed in lan-
thanum, praseodymium, and neodymium aluminate.[24]
The variations of the $\frac{1}{2}a$ and α parameters of the
face-centered rhombohedral pseudocell are shown
in Fig. 174. The rate of decrease of the angle α

[23]W. C. Koehler and E. O. Wollan, *Phys. and Chem.
Solids* 2, 100 (1957).

[24]S. Geller and V. B. Bala, *Acta Cryst.* 9, 1019 (1956).

with temperature is roughly twice as great in $LaCoO_3$ as in $PrAlO_3$.[24]

Diffraction patterns of $HoFeO_3$ up to 917°K showed only normal thermal expansion but no anomalous decrease in lattice distortion.

This work was performed in cooperation with E. O. Wollan and W. C. Koehler of the Physics Division who provided materials for the x-ray diffraction experiments. Chemical analyses were performed by A. D. Horton.

PRECISION DETERMINATION OF LATTICE PARAMETERS

H. L. Yakel, Jr.   R. M. Steele

The significance of variations of alpha-solid-solution lattice parameters in showing solubility limits and valence effects in zirconium alloys has been presented in a previous report.[25] Since the analysis of these variations depends on the accuracy of the parameter determinations as given from x-ray diffraction data, a partial investigation of the ultimate precision of such data has been undertaken.

The three stages of practical lattice-parameter measurement in which the ultimate precision of the result may be affected are specimen preparation and x-ray diffraction technique, measurement of diffraction photograph or diffractometer trace, and analysis of diffraction data. A detailed discussion of each of these points is given elsewhere.[26] Some of the more important alternatives at each stage and the particular alternative selected for the zirconium-alloy parameter problem are outlined in Table 52.

The results of the parameter determinations in the zirconium-silver system have been discussed.[25] The probable errors in the hexagonal parameters a_0 and c_0 are usually near 1 part in 100,000 and 1 part in 40,000, respectively (from least-squares

[25]D. S. Easton and J. O. Betterton, Jr., *Met. Semiann. Prog. Rep. April 10, 1956,* ORNL-2080, p 218.

[26]H. P. Klug and L. E. Alexander, *X-Ray Diffraction Procedures for Polycrystalline and Amorphous Materials,* chap. 8, Wiley, New York, 1954.

Table 52. Techniques Used in Zirconium Alloy Parameter Measurements

Problems	Alternatives	Choice and Remarks
Diffraction technique	Diffractometer Back-reflection focusing camera Debye-Scherrer camera (Straumanis geometry)	Debye-Scherrer camera
Specimen preparation	Annealed filings Annealed wire (<0.020-in. dia)	Annealed wire (less chance of contamination of sample)
X radiation	Cu, Cr, or Mo target Filtered or unfiltered radiation	Unfiltered Cu K radiation is the only possibility which gives lines in the back-reflection region which depend on c_0
Measurement of films	Nonmagnifying comparator Magnifying comparator Microphotometer	Magnifying Gaertner comparator

Analysis of data	Graphical extrapolation
	Analytic extrapolation
	Choice of extrapolation function
	  Hesse (back-reflection shrinkage)
	  Absorption
	  Bradley-Jay (eccentricity)
	  Cohen (combination of absorption and eccentricity)
	  Nelson-Riley (absorption and focal spot profile)
		Analytic Hesse extrapolation (see text)

analysis using the Hesse back-reflection shrinkage extrapolation). Several duplicate measurements of the same diffraction photograph by the same or another observer have shown substantial agreement within about 1 part in 30,000 for a_0 and 1 part in 20,000 for c_0.

A systematic study of the possible effect of the extrapolation function on the final parameters has been carried out for a single measurement of 20 back-reflection lines on the pattern of sample DSE X/47 (pure zirconium). Least-squares fits of the data extrapolated against the back-reflection shrinkage (Hesse) correction, the absorption correction, the eccentricity (Bradley-Jay) correction, the Cohen function (eccentricity and absorption), and the Nelson-Riley function (absorption and systematic observational error) were calculated with the aid of the Oracle. A variety of weighting factors 1, $1/\sin \phi$, $1/\sin^2\phi$ were used with each extrapolation, and a calculation with and without an additional subjective weight (denoted as "S" in Table 53) for each diffraction line was made for each objective weighting factor. The results are shown in Table 53.

It may be seen that, for a given weighting scheme, the Nelson-Riley extrapolation agrees more nearly with the Hesse extrapolation, rather than the absorption correction extrapolation. This is unexpected, since the large diameter of the sample DSE X/47 ($\sim$0.030 in.) would indicate an important absorption correction. The Cohen extrapolation, on the other hand, which takes both absorption and eccentricity corrections into account explicitly, gives results intermediate between the pure absorption correction and the pure eccentricity correction.

The effect of using purely objective weights 1, $1/\sin \phi$, and $1/\sin^2\phi$ is practically negligible within the standard deviations of the results (about 1 part in 50,000 for a_0 and 1 part in 20,000 for c_0). The effect of adding a subjective weight to the objective weight is also small except in the case of the Cohen extrapolation, where, with 1 and $1/\sin \phi$ plus subjective weighting, the result for c_0 is significantly lower (by 1 part in 7000) than the result without subjective weighting. The results have been verified by recalculation and are quite unusual. Additional calculations with data from other films will be made to further explore this behavior.

The general conclusion which may be drawn from this study at the present date is that maximum uniformity is necessary at all stages of the parameter measurement. This uniformity must extend from the diffraction-sample preparation through the final-data analysis. Such procedure should lead to relatively significant lattice parameters, with a good expectation of finding the true parameter values within the ranges given by the probable errors.

Diffraction samples for this work were prepared and submitted by J. O. Betterton, Jr., and D. S. Easton. Oracle calculations were made by B. Osborne.

Table 53. Extrapolated Lattice Parameters for Sample DSE X/47

Hesse		Absorption		Bradley-Jay		Cohen		Nelson-Riley		Weighting Factors
a_0	c_0	a_0	c_0	a_0	c_0	a_0	c_0	a_0	c_0	
3.23246	5.14777	3.23232	5.14731	3.23250	5.14793	3.23237	5.147848	3.23246	5.14775	1
3.23238	5.14776	3.23230	5.14740	3.23239	5.14787	3.23231	5.14745	3.23237	5.14775	$1/\sin \phi$
3.23236	5.14780	3.23230	5.14748	3.23238	5.14788	3.23233	5.14767	3.23236	5.14779	$1/\sin^2\phi$
3.23250	5.14757	3.23237	5.14714	3.23253	5.14772	3.23224	5.14672	3.23250	5.14775	S, 1
3.23230	5.14765	3.23223	5.14723	3.23232	5.14766	3.23219	5.14706	3.23230	5.14755	S, $1/\sin \phi$
3.23227	5.14765	3.23221	5.14737	3.23229	5.14772	3.23224	5.14750	3.23227	5.14764	S, $1/\sin^2\phi$

X-RAY DIFFRACTION STUDY OF AGING IN ZIRCONIUM-NIOBIUM ALLOYS

H. L. Yakel, Jr.   R. M. Steele

M. L. Picklesimer

The improved corrosion resistance of certain zirconium-niobium alloys makes their application in reactor systems particularly attractive. The unusual aging properties of those alloys near 15% niobium are discussed on the basis of microstructure and hardness evidence in "HRP Metallurgy," this report.

X-ray diffraction studies of zirconium-niobium alloys after various heat treatments have been initiated. From the data now available, tentative identification of phases may be made and mechanisms of possible aging transformations suggested.

The preparation of wire specimens suitable for diffraction experiments with the Debye-Scherrer technique has been described.[27] The grain size in these specimens was sufficiently large to give quite spotty powder diffraction patterns which were useful in establishing orientation relationships between the various phases observed. Specimens in which grain size is large enough to give easily recognized single-crystal patterns are currently being investigated. Copper K radiation ($\lambda_{K\alpha} = 1.5418$ Å) is being used in all diffraction experiments.

A summary of observations to date is presented in Table 54. The phase which is identified as omega in this table appears in as-quenched and partially aged alloys. The structure of this phase is uncertain, although a general correspondence with the results of Robinson *et al.* on Zr-Mo and Zr-Nb alloys was noted.[28] At this time, a gamma-brass-type structure seems most likely.

The amount of omega relative to retained body-centered cubic beta (β_r) increases with decreasing niobium concentration in alloys water-quenched from 900°C. A Zr–5% Nb sample showed only diffraction lines of a hexagonal close-packed alpha structure in the as-quenched condition, indicating that the transition $\beta_r \rightarrow \omega \rightarrow \alpha$ could not be suppressed by quenching in this case. No distinctive effect of ternary alloying additions on this behavior was noted.

The omega diffraction pattern tended to disappear when the alloys were aged for successively longer times at 400 to 500°C. In 85% Zr–15% Nb alloys this effect was most noticeable on the aging temperature being raised from 400 to 500°C.

Diffraction patterns from large-grained specimens of Zr–15% Nb and Zr–15% Nb–2% Pd aged for 3 and 24 hr at 400°C suggest that the structures, as noted in Table 54, may be a single "modulated" structure of the type observed in gold-platinum[29] and copper-nickel-iron alloys.[30] In such a structure, periodic variations of lattice spacing and/or structure factor (alloy concentration) occur along certain directions in the parent lattice, the whole lattice, modulated and unmodulated, scattering coherently. At a later stage in the precipitation process, regions of independently scattering products are formed.

In the Zr-Nb system, the modulated β_r structure would dissociate into two body-centered cubic lattices, one (β), rich in zirconium, with a larger lattice spacing than the other (β''), rich in niobium. The point at which the modulated structure dissociates is ill defined. It may be assumed that, in the case of Zr–15% Nb and Zr–15% Nb–2% Pd alloys, the structure is modulated after 3- and 24-hr aging at 400°C. In the case of Zr–15% Nb–2% Mo alloys aged at 400°C, modulation is not observed after 3 hr but is present after 24 hr. Specimens aged for longer periods at 400°C will be studied to determine whether the dissociation of the modulated structure can be obtained at that temperature.

At an aging temperature of 500°C, 4 hr is sufficient to produce a dissociated ($\beta - \beta''$) structure of Zr–15% Nb alloys. After 24 hr, part of the Zr-rich β phase has evidently transformed to α (hcp), leaving a β'' phase more rich in niobium. After one week at 500°C, the $\beta \rightarrow \alpha$ transition is complete, and the β'' lattice has contracted until its parameter qualitatively agrees with the expected limiting concentration of zirconium in niobium, β'. It is not known whether the contraction of β' is continuous or discontinuous. The aging of Zr–15% Nb–2% Pd alloys at 500°C is similar to that of Zr–15% Nb alloys at 600°C as shown by

[27]G. M. Adamson *et al.*, *HRP Quar. Prog. Rep. July 31, 1957,* ORNL-2379, p 122.

[28]H. A. Robinson *et al.*, *J. Metals* **8**, 1544 (1956).

[29]T. J. Tiedema, J. Bouman, and W. G. Burgers, *Acta Met.* **5**, 310 (1957).

[30]M. E. Hargreaves, *Acta Cryst.* **4**, 301 (1951).

Table 54. A Summary of Data on Zr-Nb Alloys

Composition (wt %)	Aging Temperature* (°C)	Aging Time	Phases Present
85 Zr–15 Nb	As-quenched		Predominantly retained β_r (a_0 = 3.5468 ± 0.001 Å); small amount of ω
90 Zr–10 Nb	As-quenched		Predominantly retained β_r (a_0 = 3.5545 ± 0.001 Å); moderate amount of ω
92.5 Zr–7.5 Nb	As-quenched		Retained β_r (a_0 = 3.5577 ± 0.001 Å); ω present in roughly equal amounts
95 Zr–5 Nb	As-quenched		Alpha (hexagonal close-packed) Zr-Nb solid solution
83 Zr–15 Nb–2 Pd	As-quenched		Predominantly retained β_r (a_0 = 3.5396 ± 0.001 Å); small amount of ω
83 Zr–15 Nb–2 Mo	As-quenched		Predominantly retained β_r (a_0 = 3.5396 ± 0.001 Å); small amount of ω
85 Zr–15 Nb	400	3 hr	Modulated β_r and ω (a_0 = 10.72 ± 0.06 Å) in roughly 2:1 ratio
85 Zr–15 Nb	400	24 hr	Modulated β_r and ω in roughly 2:1 ratio
83 Zr–15 Nb–2 Pd	400	3 hr	Modulated β_r and ω in roughly 2:1 ratio
83 Zr–15 Nb–2 Pd	400	24 hr	Modulated β_r and ω in roughly 2:1 ratio
83 Zr–15 Nb–2 Mo	400	2 hr	Predominantly retained β_r (a_0 = 3.5388 ± 0.001 Å); small amount of ω
83 Zr–15 Nb–2 Mo	400	24 hr	Modulated β_r (may be dissociated) and a small amount of ω
85 Zr–15 Nb	500	4 hr	β (a_0 = 3.5617 ± 0.001 Å) and β'' (a_0 = 3.5256 Å) with a small amount of ω (a_0 = 10.65 ± 0.06 Å)
85 Zr–15 Nb	500	24 hr	Predominantly α (a_0 = 3.224 ± 0.004 Å; c_0 = 5.152 ± 0.006 Å) with small amounts of β and β''
85 Zr–15 Nb	500	1 week	α (a_0 = 3.230 ± 0.004 Å; c_0 = 5.146 ± 0.006 Å) and β' (a_0 = 3.31 ± 0.01 Å) in roughly 3:1 ratio
83 Zr–15 Nb–2 Pd	500	4 hr	Predominantly retained β_r (a_0 = 3.521 ± 0.004 Å) with a small amount of α
83 Zr–15 Nb–2 Pd	500	24 hr	Retained β_r (a_0 = 3.516 ± 0.004 Å) and α in roughly equal amounts
83 Zr–15 Nb–2 Pd	500	1 week	α (a_0 = 3.230 ± 0.004 Å; c_0 = 5.142 ± 0.006 Å) and β' (a_0 = 3.33 ± 0.01 Å) in roughly 3:1 ratio
85 Zr–15 Nb	600	1 hr	Predominantly retained β_r (a_0 = 3.549 ± 0.002 Å) with a small amount of α
85 Zr–15 Nb	600	1 week	Predominantly retained β_r (a_0 = 3.528 ± 0.002 Å) with a moderate amount of α
83 Zr–15 Nb–2 Pd	600	1 hr	Predominantly retained β_r (a_0 = 3.5387 ± 0.001 Å)
83 Zr–15 Nb–2 Pd	600	1 week	Predominantly retained β_r (a_0 = 3.5280 ± 0.001 Å) with a small amount of α

*All samples previously heat-treated at 900°C for 3 hr before aging.

similar diffraction patterns. The partial transition of $\beta_r \to \alpha$ had apparently begun after 4 hr in this case.

The aging process at 600°C probably does not involve a modulated structure. This may be seen in the observation that, after 1 hr at 600°C, a Zr–15% Nb alloy contained only an α (hcp) phase and one β_r phase. After one week at temperature, a greater amount of the hexagonal phase was present, and the lattice parameter of the β_r phase had shifted to a smaller value indicative of a higher niobium content. Since α seems to form directly from one β_r phase at this temperature, the entire aging mechanism would seem to be different from that at 400 or 500°C. Additional experiments with shorter aging times at 600°C should clarify this problem.

The aging process at 400 and 500°C in these alloys may then be postulated as following the sequence

1. β_r (as-quenched) $\to$ modulated β_r,
2. modulated $\beta_r \to \beta + \beta''$ ($a_\beta > a_{\beta''}$),
3. $\beta \to \alpha + Nb$; $\beta'' + Nb \to \beta''$ (richer in Nb),
4. $\beta_c'' \to \alpha + \beta'$ (equilibrium solid solution of Zr in Nb).

The symbol β_c'' represents a hypothetical critical concentration of niobium in β'' above which dissociation to α and β' occurs. Whereas at 400°C the rate of the second reaction is presumably so slow as to produce no observable dissociation of the modulated structure after 24 hr, the rate of the same reaction is fast enough at 500°C to produce complete dissociation after 4 hr. The effect of ternary additions of 2% Mo and Pd seems to be more pronounced for molybdenum, which, at 400°C,

seems to suppress the rate of the first reaction considerably.

The aging process at 600°C may be postulated as following the pattern (1) β_r (as-quenched) $\to \alpha + \beta_r$ (niobium rich), (2) $\beta_c^r \to \alpha + \beta'$ (equilibrium solid solution of Zr in Nb). The continual enrichment in niobium of a single β_r phase may be assumed here to be the first reaction; its rate is evidently slow enough to keep the niobium concentration in β_r below the critical composition β_c^r through an aging period of one week. Note that in both aging sequences the formation and resolution of omega are neglected.

If the hardness curves (see "HRP Metallurgy," this report) of these alloys are examined in the light of the structural evidence, it must be concluded that the age-hardening constituent is the modulated β_r structure. Hargreaves[30] has explained the hardening effect in modulated structures as due to coherency strains. As soon as these strains are removed, the hardness tends to disappear. These results seem to be in semi-quantitative agreement with the observed over-aging effects at 500 and 600°C.

It should be emphasized that the results discussed above are only preliminary. Indications of the need for clarifying experiments at several temperatures have been given. In particular, refined single-crystal or very large-grained polycrystal diffraction experiments would be most rewarding and are currently in preparation.

This program is being carried out in cooperation with the Homogeneous Reactor Project Metallurgy Group. Alloy and diffraction sample preparations were made by M. L. Picklesimer and P. L. Rittenhouse of that group.

SECRET   **UNCLASSIFIED**

SECRET